

Uniwersytet Śląski w Katowicach
Wydział Nauk Ścisłych i Technicznych
Instytut Chemii

mgr inż. KAROLINA KOWALSKA

**Wpływ stężenia TiO_2 na budowę i właściwości szkieł germanianowych
emitujących promieniowanie w zakresie podczerwieni**

ROZPRAWA DOKTORSKA

w formie spójnego tematycznie cyklu dwunastu artykułów
opublikowanych w czasopismach naukowych

Promotor:
prof. dr hab. Wojciech A. Pisarski

Katowice, 2024



Badania przeprowadzone na potrzeby niniejszej pracy doktorskiej zrealizowano
w ramach projektu badawczego finansowanego przez
Narodowe Centrum Nauki (OPUS16) nr 2018/31/B/ST8/00166
*„Szkła tytanowo-germanianowe i ich zastosowania jako włókna optyczne emitujące
promieniowanie w zakresie bliskiej i średniej podczerwieni”*



Kierownik projektu: prof. dr hab. Wojciech A. Pisarski.

*Prezentowana rozprawa doktorska przygotowana została pod opieką Pana **prof. dr hab. Wojciecha A. Pisarskiego**, któremu składam największe podziękowania oraz okazuję wdzięczność za możliwość realizacji doktoratu w Zespole Spektroskopii i Materiałów Luminescencyjnych. Dziękuję za opiekę naukową, nieocenioną pomoc merytoryczną udzielaną podczas wykonywanych badań oraz sugestie, które wpłynęły na ostateczny kształt tej pracy, jak również za zaangażowanie i życzliwość okazane mi podczas kilkuletniej opieki naukowej w trakcie studiów doktoranckich*

*Wyrażam także słowa podziękowania dla Pana **prof. dr hab. Marcina Kochanowicza**, który podczas stażu naukowego wprowadził mnie do świata Laboratorium Technologii Światłowodów, ze szczególnym uwzględnieniem otrzymywania preform światłowodowych metodą MCVD-CDS domieszkowanych jonami ziem rzadkich oraz wyciągania z nich włókien światłowodowych. Dziękuję również pozostałym pracownikom Katedry Fotoniki, Elektroniki i Techniki Świetlnej, Wydziału Elektrycznego, Politechniki Białostockiej za dyskusje naukowe, w miłej atmosferze*

Dziękuję Współautorom artykułów naukowych oraz pozostałym Pracownikom Zespołu Spektroskopii i Materiałów Luminescencyjnych, Instytutu Chemii Uniwersytetu Śląskiego

Spis treści

1. Cel pracy	5
2. Forma pracy	7
3. Streszczenie rozprawy doktorskiej	9
4. Abstract of doctoral dissertation	11
5. Część teoretyczna	13
6. Literatura	19
7. Część eksperymentalna (Badania własne)	26
7.1. Synteza i charakterystyka szkieł tytanowo-germanianowych	27
[P1] Novel multicomponent titanate-germanate glasses: synthesis, structure, properties, transition metal, and rare earth doping	33
[P2] EPR and optical spectroscopy of Cr ³⁺ ions in barium gallo-germanate glasses containing B ₂ O ₃ /TiO ₂	47
[P3] Raman and infrared spectroscopy of barium-gallo germanate glasses containing B ₂ O ₃ /TiO ₂	57
[P4] Influence of titanium dioxide concentration on thermal properties of germanate based glasses	77
7.2. Wpływ stężenia TiO ₂ na właściwości szkieł germanianowych emitujących promieniowanie w zakresie podczerwieni	89
[P5] Nd ³⁺ doped titanate-germanate glasses for near-IR laser applications	98
[P6] Influence of TiO ₂ concentration on near-infrared luminescence of Er ³⁺ ions in barium gallo-germanate glasses	114
[P7] Enhanced mid-IR luminescence of Er ³⁺ ions at 2.7 μm in TiO ₂ -GeO ₂ -BaO-Ga ₂ O ₃ glasses	127
[P8] Optical properties of titanate-germanate glasses containing Ho ³⁺ ions	133
[P9] Experimental and theoretical studies on NIR luminescence of titanate-germanate glasses doped with Pr ³⁺ and Tm ³⁺ ions	143
[P10] Thulium-doped titanate-germanate glasses for infrared photonics	157
[P11] Near-IR luminescence of rare-earth ions (Er ³⁺ , Pr ³⁺ , Ho ³⁺ , Tm ³⁺) in titanate-germanate glasses under excitation of Yb ³⁺	171
[P12] The impact of pair Er ³⁺ /Yb ³⁺ on titanate-germanate glasses: Physicochemical and near-infrared luminescence investigations	185
8. Podsumowanie	195
9. Załączniki	198
9.1. Dorobek naukowy	198
9.2. Oświadczenia	204

1. Cel pracy

W dziedzinie fotoniki oraz zaawansowanych materiałów optycznych znacznym zainteresowaniem cieszą się szkła nieorganiczne domieszkowane jonami ziem rzadkich, które wykazują wydajną emisję promieniowania związaną z głównymi przejściami laserowymi w zakresie podczerwieni. Takie materiały ugruntowały swoją pozycję w zastosowaniach między innymi w technice laserowej oraz w konstrukcji światłowodów i wzmacniaczy optycznych pracujących na przykład w zakresie tzw. okien telekomunikacyjnych. Nadal poszukuje się jednak materiałów do produkcji światłowodów, dla których w zakresie III okna telekomunikacyjnego obserwuje się najmniejszą tłumienność sygnału. Działające wzmacniacze światłowodowe EDFA (ang. *Erbium Doped Fiber Amplifier*) oparte na komercyjnych szklach krzemianowych domieszkowanych jonami Er^{3+} charakteryzują się stosunkowo małą szerokością pasma emisyjnego. Rozwój telekomunikacji optycznej wymaga również zwiększenia przepuszczalności materiałów do zakresu podczerwieni, w którym następuje transmisja sygnału optycznego. Trwają także poszukiwania wydajnych układów emitujących promieniowanie w zakresie średniej podczerwieni. Obecność w szklach grup OH^- , które skutecznie wygaszają luminescencję oraz ograniczają przepuszczalność światła w obszarze 2,7 – 3,0 μm stanowi jedno z ważniejszych wyzwań technologicznych, wpływających na ograniczenie wykorzystania szkieł w zastosowaniach laserowych. Grupy hydroksylowe wpływają również na zmniejszenie wydajności kwantowej szkła, ponieważ emisja promieniowania jonów ziem rzadkich jest wygaszana przez centra pułapkowe utworzone przez te jony. Problem ten jest szczególnie dotkliwy w przypadku szkieł domieszkowanych jonami Er^{3+} , które są atrakcyjne ze względu na emisję promieniowania przy długości fali 2,7 μm .

Próba rozwiązania wymienionych powyżej problemów natury technologicznej i wyzwań naukowych dotyczących szkieł optycznych stanowiły główną motywację do podjęcia problematyki rozprawy doktorskiej. Otrzymanie nowych szkieł nieorganicznych domieszkowanych jonami ziem rzadkich, wykazujących szerokie pasma emisyjne w zakresie podczerwieni oraz długi czas życia luminescencji, przy bardzo niskiej zawartości grup hydroksylowych, aby ograniczyć maksymalnie tłumienie sygnału optycznego było głównym celem podjętych badań.

Przyjęto wstępne założenie, że pasma emisyjne jonów ziem rzadkich w zakresie podczerwieni w szklach tytanowo-germanianowych ulegną znacznemu poszerzeniu oraz wzmocnieniu w wyniku obecności tlenku tytanu(IV). Otrzymanie szkieł optycznych z niską zawartością grup hydroksylowych będzie możliwe przy zachowaniu rygorystycznych warunków technologicznych podczas wszystkich etapów syntezy.

Głównym celem pracy było **wykazanie wpływu stężenia dwutlenku tytanu (TiO_2) na budowę oraz właściwości nowych wieloskładnikowych szkieł tytanowo-germanianowych emitujących promieniowanie w zakresie podczerwieni**. Szczegółowy zakres rozprawy doktorskiej obejmował następujące problemy naukowo-badawcze:

- opracowanie technologii syntezy nowych wieloskładnikowych szkieł tytanowo-germanianowych w układzie $\text{TiO}_2\text{-Ga}_2\text{O}_3\text{-BaO-Ga}_2\text{O}_3$, jako matrycy dla jonów domieszek optycznie aktywnych (jony ziem rzadkich i/lub jony metali przejściowych),
- analizę budowy wewnętrznej otrzymanych szkieł przy użyciu rentgenowskiej analizy fazowej (XRD), spektroskopii elektronowego rezonansu paramagnetycznego (EPR), spektroskopii Ramana i w podczerwieni (FT-IR),
- określenie właściwości termicznych szkieł przy użyciu skaningowej kalorymetrii różnicowej (DSC) w celu wyznaczenia temperatur charakterystycznych oraz parametrów stabilności termicznej,
- analizę właściwości optycznych szkieł tytanowo-germanianowych aktywowanych wybranymi jonami ziem rzadkich i/lub jonami metali przejściowych, obejmującą pomiary widm absorpcyjnych, widm emisji oraz kinetyki zaniku luminescencji,
- wykazanie wpływu zawartości TiO_2 na otrzymywanie szkieł oraz parametry spektroskopowe oraz laserowe, a także wyjaśnienie procesów relaksacji promienistej i niepromienistej oraz ich mechanizmów zachodzących pomiędzy jonami aktywnymi,
- wskazanie układów o najlepszych właściwościach luminescencyjnych, pod kątem potencjalnych zastosowań w podczerwonej fotonice, jak szerokopasmowe wzmacniacze optyczne pracujące w zakresie bliskiej podczerwieni oraz źródła laserowe emitujące promieniowanie w zakresie średniej podczerwieni.

2. Forma pracy

Niniejsza rozprawa doktorska jest przygotowana w postaci tematycznego zbioru dwunastu publikacji P1-P12.

[P1] Wojciech A. Pisarski, **Karolina Kowalska**, Marta Kuwik, Justyna Polak, Ewa Pietrasik, Tomasz Goryczka, Joanna Pisarska, Novel multicomponent titanate-germanate glasses: synthesis, structure, properties, transition metal, and rare earth doping, *Materials* 13 (2020) 4422, IF = 3,400, MNiSW = 140 pkt

[P2] **Karolina Kowalska**, Marta Kuwik, Justyna Polak, Joanna Pisarska, Wojciech A. Pisarski, EPR and optical spectroscopy of Cr³⁺ ions in barium gallo-germanate glasses containing B₂O₃/TiO₂, *Journal of Luminescence* 245 (2022) 118775, IF = 3,600, MNiSW = 100 pkt

[P3] **Karolina Kowalska**, Marta Kuwik, Joanna Pisarska, Maciej Sitarz, Wojciech A. Pisarski, Raman and infrared spectroscopy of barium-gallo germanate glasses containing B₂O₃/TiO₂, *Materials* 16 (2023) 1516, IF = 3,400, MNiSW = 140 pkt

[P4] **Karolina Kowalska**, Ewa Pietrasik, Marta Kuwik, Joanna Pisarska, Tomasz Goryczka, Wojciech A. Pisarski, Influence of titanium dioxide concentration on thermal properties of germanate based glasses, *Journal of Thermal Analysis and Calorimetry* (2024), <https://doi.org/10.1007/s10973-024-12998-9>, IF = 3,000, MNiSW = 100 pkt

[P5] Wojciech A. Pisarski, **Karolina Kowalska**, Marta Kuwik, Joanna Pisarska, Jan Dorosz, Jacek Żmojda, Marcin Kochanowicz, Dominik Dorosz, Nd³⁺ doped titanate-germanate glasses for near-IR laser applications, *Optical Materials Express* 12 (2022) 2912-2926, IF = 2,800, MNiSW = 100 pkt

[P6] **Karolina Kowalska**, Marta Kuwik, Joanna Pisarska, Magdalena Leśniak, Dominik Dorosz, Marcin Kochanowicz, Jacek Żmojda, Jan Dorosz, Wojciech A. Pisarski, Influence of TiO₂ concentration on near-infrared luminescence of Er³⁺ ions in barium gallo-germanate glasses, *Journal of Materials Research and Technology* 21 (2022) 4761-4772, IF = 6,400, MNiSW = 100 pkt

[P7] Wojciech A. Pisarski, **Karolina Kowalska**, Marta Kuwik, Joanna Pisarska, Dominik Dorosz, Marcin Kochanowicz, Jacek Żmojda, Jan Dorosz, Enhanced mid-IR luminescence of Er³⁺ ions at 2.7 μm in TiO₂-GeO₂-BaO-Ga₂O₃ glasses, *Journal of Luminescence* 265 (2024) 120227, IF = 3,600, MNiSW = 100 pkt

[P8] Joanna Pisarska, **Karolina Kowalska**, Marta Kuwik, Jan Dorosz, Marcin Kochanowicz, Jacek Żmojda, Dominik Dorosz, Wojciech A. Pisarski, Optical properties of titanate-germanate glasses containing Ho³⁺ ions, *Materials Research Bulletin* 166 (2023) 112353, IF = 5,400, MNiSW = 100 pkt

[P9] Marta Kuwik, **Karolina Kowalska**, Joanna Pisarska, Wojciech A. Pisarski, Experimental and theoretical studies on NIR luminescence of titanate-germanate glasses doped with Pr³⁺ and Tm³⁺ ions, *Journal of the American Ceramic Society* 106 (2022) 7460-7472, IF = 3,900, MNiSW = 100 pkt

[P10] **Karolina Kowalska**, Marta Kuwik, Joanna Pisarska, Wojciech A. Pisarski, Thulium-doped titanate-germanate glasses for infrared photonics, *Journal of Luminescence* 272 (2024) 120649, IF = 3,600, MNiSW = 100 pkt

[P11] **Karolina Kowalska**, Marta Kuwik, Joanna Pisarska, Wojciech. A. Pisarski, Near-IR luminescence of rare-earth ions (Er^{3+} , Pr^{3+} , Ho^{3+} , Tm^{3+}) in titanate-germanate glasses under excitation of Yb^{3+} , *Materials* 15 (2022) 3660, IF = 3,400, MNiSW = 140 pkt

[P12] **Karolina Kowalska**, Marta Kuwik, Tomasz Goryczka, Joanna Pisarska, Wojciech A. Pisarski, The impact of pair $\text{Er}^{3+}/\text{Yb}^{3+}$ on titanate-germanate glasses: Physicochemical and near-infrared luminescence investigations, *Materials Science and Engineering: B* 301 (2024) 117117, IF = 3,600, MNiSW = 100 pkt

3. Streszczenie rozprawy doktorskiej

Rosnące od wielu lat zapotrzebowanie na różnego typu układy elektroniczne i optyczne powoduje, z jednej strony wzrost zapotrzebowania na komercyjnie dostępne materiały, a z drugiej strony ciągłe poszukiwanie nowych. Jednym z najważniejszych materiałów konstrukcyjnych stosowanych dotychczas w układach optycznych są szkła nieorganiczne. Szczególne znaczenie mają w tym przypadku szkła tlenkowe domieszkowane jonami lantanowców, w których składnikiem szklotwórczym jest tlenek SiO_2 , GeO_2 , B_2O_3 lub P_2O_5 . Charakteryzują się one wieloma bardzo korzystnymi właściwościami fizykochemicznymi, które pozwalają na wykorzystanie ich w układach optycznych, ale posiadają również pewne wady i ograniczenia. Czas życia luminescencji jonów Nd^{3+} w szklach krzemianowych jest stosunkowo długi, ale charakteryzują się małym przekrojem czynnym na emisję wymuszoną. Dużym przekrojem czynnym na emisję wymuszoną charakteryzują się szkła fosforanowe, ale wadą jest w ich przypadku krótki czas życia luminescencji. Z powodu silnych drgań między atomami boru i tlenu występującymi w matrycy szkła boranowego nie obserwuje się w nich niektórych przejść laserowych jonów ziem rzadkich w zakresie podczerwieni. Do niskofononowych szkieł tlenkowych można zaliczyć szkła germanianowe, które są szczególnie interesujące ze względu na dobrą przepuszczalność w zakresie podczerwieni, co daje możliwości zastosowania ich między innymi w technologiach światłowodowych. Intensywny rozwój technologii operujących w zakresie podczerwieni sprawia, że dużym zainteresowaniem cieszą się wieloskładnikowe szkła tlenkowe oparte na układzie $\text{GeO}_2\text{-BaO-Ga}_2\text{O}_3$, o wyróżniających się charakterystykach termicznych, strukturalnych i optycznych, w których tlenek germanu zostaje częściowo zastąpiony innymi tlenkami szklotwórczymi lub modyfikującymi w celu uzyskania wydajnego promieniowania w pożądanym zakresie spektralnym. Tlenek tytanu(IV) jako jeden z nielicznych tlenków może pełnić rolę zarówno składnika szklotwórczego jak i modyfikatora w zależności od jego stężenia w składzie matrycy. Dotychczasowe wyniki badań przedstawione w dostępnej literaturze pokazują, że tlenek tytanu(IV) pełnił najczęściej rolę składnika modyfikującego. Jednym z założeń naukowych niniejszej rozprawy jest opracowanie nowych wieloskładnikowych szkieł tytanowo-germanianowych, w których TiO_2 będzie pełnić rolę składnika szklotwórczego. Oczekiwanym efektem jest znaczące poszerzenie szerokości pasma emisyjnego jonów ziem rzadkich w zakresie podczerwieni. Postawione zadanie badawcze

wymaga dogłębnej analizy wpływu stosunku ilościowego $\text{TiO}_2:\text{GeO}_2$ na budowę chemiczną szkieł, uniknięcia procesu krystalizacji oraz osiągnięcie jak najbardziej korzystnych parametrów spektroskopowych jonów ziem rzadkich.

W ramach rozprawy doktorskiej dokonano charakterystyki nowych szkieł tytanowo-germanianowych dla podczerwonej fotoniki, opartej na zbiorze dwunastu tematycznie powiązanych artykułów naukowych opublikowanych w recenzowanych czasopismach naukowych o zasięgu międzynarodowym.

W przypadku materiałów optycznych jednym z podstawowych problemów naukowych i technologicznych jest synteza. Punktem wyjścia w badaniach nad szklami tytanowo-germanianowymi było otrzymanie oraz charakterystyka wieloskładnikowych szkieł barowo-galowo-germanianowych modyfikowanych TiO_2 . Przeprowadzona analiza rentgenowska potwierdziła w pełni amorficzny charakter otrzymanych szkieł zawierających wysokie stężenia TiO_2 . W celu wykazania korelacji pomiędzy charakterem wiązań uczestniczących między jonami aktywatora a jego najbliższym otoczeniem zastosowano trójwartościowe jony metali przejściowych (Cr^{3+}) oraz jony ziem rzadkich (Eu^{3+}), pełniące niezwykle ważną rolę sondy spektroskopowej. Przeprowadzona została również charakterystyka termiczna w celu sprawdzenia stabilności termicznej szkieł.

W kolejnej części pracy uwagę skoncentrowano na analizie wpływu stężenia TiO_2 na właściwości szkieł germanianowych emitujących promieniowanie w zakresie podczerwieni. Zbadano kompleksowo szkła domieszkowane wybranymi jonami ziem rzadkich w celu otrzymania pełnej charakterystyki ich właściwości spektroskopowych oraz laserowych w funkcji stężenia tlenku tytanu(IV). Na podstawie przeprowadzonej analizy wyników teoretycznych i eksperymentalnych dokonano wyboru szkła tytanowo-germanianowego o najlepszych właściwościach optycznych w zakresie podczerwieni. Właściwości luminescencyjne otrzymanych szkieł tytanowo-germanianowych domieszkowanych jonami ziem rzadkich potwierdziły możliwość ich zastosowania jako szerokopasmowych wzmacniaczy optycznych pracujących w zakresie bliskiej podczerwieni oraz źródeł laserowych emitujących promieniowanie w zakresie średniej podczerwieni. Badane w ramach rozprawy doktorskiej zagadnienia mają charakter interdyscyplinarny i łączą aspekty z dziedziny chemii, technologii i inżynierii materiałowej, niezwykle istotne dla rozwoju współczesnej fotoniki.

4. Abstract of doctoral dissertation

Influence of TiO₂ concentration on the structure and properties of germanate glasses emitting infrared radiation

The variety of applications of laser technology with developing and improving methods of standardizing material properties is reflected in the growing number of glasses as engineering materials used in the construction of optical systems. Oxide glasses based on network-forming oxides such as SiO₂, GeO₂, B₂O₃, and P₂O₅ have been extensively studied as glass host matrices for rare earth ions. In silicate glasses, the luminescence lifetime of Nd³⁺ ions is relatively long, but is associated with a small emission cross section. In contrast, a large emission cross section can be obtained in phosphate glasses, however, the disadvantage is a short luminescence lifetime. Interestingly, due to the strong vibrations between boron and oxygen atoms occurring in the borate-based glass host, some laser transitions of rare earth ions in the infrared range are not observed. Meanwhile, the low phonon glass family includes a germanate-based host valued for its good transmittance in the infrared region, which qualifies it as a material for optical fibers.

Especially taking into account the intensive development of infrared technology, multicomponent modifications of the GeO₂-BaO-Ga₂O₃ glass host with unique thermal, structural, and optical characteristics are being sought, in which other glass-network formers or glass-network modifiers replace the germanium (IV) oxide to obtain efficient radiation in the desired spectral range. Titanium (IV) oxide is one of the few oxides that plays the role of glass-modifier or glass-former, depending on its concentration in the chemical composition of glass. Previous results documented in the literature clearly indicate that titanium (IV) oxide acted only as a network-modifier. The novelty, which is the subject of this doctoral dissertation, is the fabricated of multicomponent titanate-germanate glasses where TiO₂ will also act as a network-former. The advantage of the approach is the possibility of significantly broadening the emission band of selected rare earth ions in the infrared range. To carry out this task, it is necessary to analyze the effect of the TiO₂:GeO₂ molar ratio on the chemical structure of glasses without the crystallization phenomenon and, on the other hand, to obtain the best laser parameters. The methodology of glass synthesis using a specialized glove box is also an interesting research problem.

On the pages of this doctoral dissertation, the characterization of titanate-germanate glasses for infrared photonics is presented based on a series of twelve thematically related articles published in international scientific journals.

An introduction to research issues involving the problem of material properties is the synthesis and characterization of multicomponent barium gallo-germanate glasses modified by TiO₂. X-ray analysis confirmed the fully amorphous nature of the obtained glasses containing a relatively high concentration of TiO₂. Trivalent transition metal ions (Cr³⁺) and rare earth ions (Eu³⁺) playing the role of useful spectroscopic probes were used to demonstrate the correlation between the nature of the bonds involved between the activator ions and their nearest environment. Characterization was carried out to demonstrate that the materials obtained have high stability with special attention to the glass transition temperature T_g.

In the second part, the issues necessary for the functional evaluation of the obtained glasses are presented, with special emphasis on demonstrating the influence of the TiO₂ concentration on the properties of germanate-based glasses emitting radiation in the infrared range. Noteworthy in this part of the research is the presentation of a large range of subjects on the luminescence properties of selected rare earth ions, including numerous spectroscopic and laser parameters as a function of titanium (IV) oxide concentration. Theoretical and experimental results determined the suitable chemical compositions of titanate-germanate glasses for rare earth ions. The luminescence properties of the fabricated optical glasses doped with rare earth ions clearly confirmed their suitability as broadband optical amplifiers operating in the near-infrared range and laser sources emitting radiation in the mid-infrared range. The chosen scientific and cognitive aspects of the interdisciplinary research fit in with the developments in chemical sciences, technologies of optical glasses and their properties, and modern photonics.

5. Część teoretyczna

Szkło jest materiałem amorficznym, charakteryzującym się brakiem uporządkowania dalekiego zasięgu. Jest jednym z najważniejszych optycznych materiałów konstrukcyjnych [1], charakteryzującym się przezroczystością w szerokim zakresie, izotropowością, jednorodnością, dobrą jakością optyczną przejawiającą się brakiem pęcherzy i naprężeń, satysfakcjonującymi właściwościami mechanicznymi oraz dużą odpornością chemiczną i na działanie wilgoci. Bardzo ważnym etapem w rozwoju technologii produkcji szkieł na potrzeby nowoczesnej aparatury optycznej były prace badawcze Ottona Schotta [2]. Współcześnie możemy również obserwować bardzo szybki postęp w dziedzinie szkieł optycznych. Organizacja Narodów Zjednoczonych ogłosiła rok 2022 Międzynarodowym Rokiem Szkieł. O roli szkieł nieorganicznych w rozwoju współczesnej techniki możemy przeczytać w wielu opracowaniach naukowych, między innymi do tej tematyki nawiązują prace J. Ballato [3, 4].

Opracowanie wielu nowych składów szkieł nieorganicznych przyczyniło się do znaczącego postępu w technologii otrzymywania szkieł, w zakresie materiałoznawstwa optycznego oraz optoelektronicznego. Na początku lat pięćdziesiątych XX wieku rozpoczęto badania nad szkami optycznymi wykazującymi luminescencję w zakresie podczerwieni. Od demonstracji akcji laserowej w szkłe domieszkowanym jonami Nd^{3+} dokonanej przez Snitzera w 1961 roku, poczyniono wiele prób domieszkując szkła różnymi jonami ziem rzadkich w celu uzyskania pożądaných przejść laserowych, przyczyniając się tym samym do wzrostu zainteresowania materiałami amorficznymi, na których w dużej mierze opiera się fotonika [5]. Akcję laserową można uzyskać w szkłe spełniającym warunek czystości optycznej, a także dzięki zastosowaniu odpowiedniego domieszkowania jonami ziem rzadkich, które posiadają odpowiednie usytuowanie poziomów energetycznych, między którymi istnieje duże prawdopodobieństwo przejść promienistych oraz emisji promieniowania laserowego [6, 7].

Jednymi z najbardziej znanych i powszechnie stosowanych szkieł nieorganicznych stosowanych m.in. do wyciągania włókien optycznych do celów długodystansowej transmisji sygnału są szkła krzemianowe [8-11]. Tłumienność światłowodów krzemianowych dla optymalnej długości fali w zakresie podczerwieni przy około $1,55 \mu\text{m}$ (${}^4\text{I}_{13/2} \rightarrow {}^4\text{I}_{15/2}$) wynosząca $0,1 \text{ dB/km}$ jest dużo mniejsza niż dla innych szkieł optycznych. W tym zakresie spektralnym emisję promieniowania wykazują

również erbowe wzmacniacze światłowodowe EDFA (*ang. Erbium Doped Fibre Amplifier*) [12-15], znajdujące zastosowanie w trzecim oknie telekomunikacyjnym.

Mimo wielu niewątpliwych zalet szkła krzemianowe posiadają również pewne wady, co skłania do poszukiwań innych rodzajów szkieł. Duża siła wiązań Si-O-Si powoduje, że szkło krzemianowe wykazuje ograniczoną rozpuszczalność pierwiastków ziem rzadkich, a powyżej pewnego granicznego stężenia obserwuje się powstawanie klasterów, co skutkuje zwiększeniem udziału oddziaływań międzyjonowych, czego efektem jest spadek intensywności emisji [16, 17]. Kolejną konsekwencją silnego wiązania kowalencyjnego między tlenem i krzemem jest wysoka energia fononowa ($\sim 1100 \text{ cm}^{-1}$) powodująca wzrost prawdopodobieństwa przejść niepromienistych, a co za tym idzie pogorszenie właściwości optycznych. Uwidacznia się to na przykład w trudnościach związanych z uzyskaniem emisji przy $1,3 \mu\text{m}$ w szklach domieszkowanych jonami prazeodymu [18, 19]. Komercyjnie dostępne erbowe wzmacniacze światłowodowe oparte na szklach krzemianowych wykazują stosunkowo niedużą szerokość pasma [20], co znacząco ogranicza transmisję sygnału w zakresie podczerwieni. Jest to kolejny powód poszukiwania szkieł nieorganicznych domieszkowanych jonami ziem rzadkich wykazujących wydajną luminescencję w szerokim zakresie aż do podczerwieni.

Oprócz szkieł krzemianowych w optoelektronice stosuje się również inne rodzaje szkieł. Sporym zainteresowaniem cieszą się szkła germanianowe, posiadające budowę wewnętrzną podobną do szkieł krzemianowych [21]. Wiązba szkła germanianowego składa się z przypadkowo rozłożonych trójwymiarowych wiązań Ge-O-Ge [22]. Tlenek germanu jest także popularnym dodatkiem do szkła krzemianowego, stosowanym w celu zwiększenia współczynnika załamania światła [23, 24]. Z licznych źródeł literaturowych wynika, że szczególną uwagę poświęcono różnym modyfikacjom wieloskładnikowych szkieł germanianowych. Do tej interesującej rodziny szkieł nieorganicznych można zaliczyć wieloskładnikowy układ $\text{BaO-GeO}_2\text{-Ga}_2\text{O}_3$ określany często w literaturze jako BGG (*ang. Barium Gallo-Germanate Glasses*) [25-31]. Szkła $\text{BaO-Ga}_2\text{O}_3\text{-GeO}_2$ zaliczane są do układów stabilnych chemicznie oraz termicznie. Charakteryzują się niską energią fononową, wykazują względnie szeroki obszar szkłotwórczy, a także są cenione za dobrą przepuszczalność w zakresie podczerwieni, co sprawia, że są obiecującym materiałem do zastosowań laserowych. Dane dotyczące właściwości emisyjnych trójwartościowych jonów ziem rzadkich w szklach barowo-galowo-germanianowych są obecnie dobrze opisane i dostępne w literaturze.

Dotyczą w szczególności spektroskopii jonów Nd^{3+} [32], Er^{3+} [33], Pr^{3+} [34], Tm^{3+} [35], Ho^{3+} [36], $\text{Yb}^{3+}/\text{Er}^{3+}$ [37], $\text{Yb}^{3+}/\text{Ho}^{3+}$ [38], $\text{Er}^{3+}/\text{Ho}^{3+}$ [39], $\text{Tm}^{3+}/\text{Ho}^{3+}$ [40], analizowanych głównie pod kątem możliwości wykorzystania w zakresie podczerwieni oraz formowania z nich włókien szklanych. Analiza spektroskopowa szkieł barowo-galowo-germanianowych wykazała znaczny wpływ modyfikatorów tlenkowych i fluorkowych na otrzymywanie szkieł i właściwości strukturalne oraz luminescencyjne [41, 42]. Wprowadzenie Al_2O_3 (do 15% mol) do matrycy barowo-galowo-germanianowej sprzyja polepszeniu właściwości spektroskopowych jonów Tm^{3+} . Wprowadzenie wyższego stężenia Al_2O_3 (20 i 25% mol) wpływa na polepszenie właściwości emisyjnych jonów Ho^{3+} [43]. Badania wykazały również, że wprowadzenie fluorków do matrycy szkła barowo-galowo germanianowego pozwala na wprowadzenie większego stężenia jonów ziem rzadkich niż w przypadku szkła krzemianowego [44]. Połączenie stosunkowo niskiej energii fononowej tlenkowo-fluorkowego szkła germanianowego z możliwością większej separacji centrów optycznie aktywnych w tej matrycy, umożliwiło efektywne wzmocnienie oraz poszerzenie pasm emisyjnych jonów erbu. Niestety wadą włókien fluorkowych jest niska stabilność chemiczna i mechaniczna, co jest niekorzystne z aplikacyjnego punktu widzenia. Jak wynika z powyższych doniesień literaturowych kluczowego znaczenia nabierają badania dotyczące modyfikacji składu chemicznego matrycy szkieł barowo-galowo-germanianowych, które dzięki domieszkowaniu jonami ziem rzadkich mogą się stać dobrym ośrodkiem aktywnym w układach emitujących wydajne promieniowanie w zakresie podczerwieni. Zakres ten uważany za nieszkodliwy dla wzroku „*eye-safe*” jest szczególnie interesujący, o czym świadczy znaczący wzrost liczby publikacji dotyczący tej rodziny szkieł optycznych i przytaczanych możliwości zastosowania w dziedzinie telekomunikacji, medycyny, czy metrologii.

Ciekawym rozwiązaniem jest synteza szkieł modyfikowanych TiO_2 [45]. Doniesienia literaturowe pokazują, że tlenek tytanu(IV) (TiO_2) wchodzi w skład podstawowych materiałów optycznych, na przykład cienkich warstw ferroelektrycznych tytanianu baru (BaTiO_3) [47, 48]. Dużego znaczenia nabierają badania warstw BaTiO_3 aktywowanych jonami ziem rzadkich, np. jonami Eu^{3+} [49], Nd^{3+} [50], Er^{3+} [51], $\text{Ho}^{3+}/\text{Yb}^{3+}$ [52], czy $\text{Er}^{3+}/\text{Yb}^{3+}$ [53]. Cechą wyróżniającą tych materiałów optycznych są unikalne właściwości, dzięki którym znajdują zastosowanie między innymi w biofotonice. Zainteresowanie tlenkiem tytanu w materiałach optycznych wynika z jego specyficznych właściwości. Na szczególną uwagę zasługują szkła, w których jony tytanu

mogą występować na trzecim lub czwartym stopniu utlenienia. Udowodniono doświadczalnie, że obecność jonów Ti^{3+} i Ti^{4+} oraz wzajemny stosunek Ti^{3+}/Ti^{4+} ściśle zależą od rodzaju szkła, składu chemicznego matrycy szklistej oraz technologicznych warunków otrzymywania [54-56]. Tlenek tytanu może pełnić rolę zarówno składnika modyfikującego lub szkłotwórczego w zależności od jego stężenia w składzie chemicznym szkła. Wpływ TiO_2 i jego stężenia na lokalną strukturę i właściwości przelazowano w boranowych szklach nieorganicznych [57, 58], szklach fosforanowych [59, 60] oraz szklach krzemianowych [61, 62]. Badania naukowe dotyczące właściwości spektroskopowych jonów ziem rzadkich w szklach zawierających TiO_2 skupiają się głównie na niskofononowych szklach tellurowych oraz mieszanych fluorkowych szklach tellurowych, w których TiO_2 pełnił rolę modyfikatora. Przelazowano właściwości spektroskopowe oraz luminescencyjne jonów Tm^{3+} w szklach $80TeO_2-5TiO_2-15Nb_2O_3$ (% wag) w zakresie podczerwieni [63]. Dla tego samego układu przelazowano właściwości jonów Nd^{3+} [64]. Stwierdzono, że szkła tellurowe zawierające TiO_2 mogą być obiecującym materiałem do emisji w zakresie bliskiej podczerwieni oraz akcji laserowej związanej z przejściem $^4F_{3/2} \rightarrow ^4I_{11/2}$ jonów Nd^{3+} . Korzystny wpływ TiO_2 na właściwości spektroskopowe jonów Nd^{3+} wykazano dla szkieł na bazie $PbO-B_2O_3-TiO_2-AlF_3$, w których stężenie dwutlenku tytanu pełniącego rolę modyfikatora więźby szklanej nie przekraczało 10% mol [65]. Interesujące rezultaty otrzymano również dla szkieł krzemianowych na bazie $X_2O-SiO_2-TiO_2$ ($X = Na$ lub K) o wysokiej zawartości TiO_2 (40 i 45% mol) [66]. Rentgenowska analiza fazowa tych układów wykazała jednak, że wysokie stężenie TiO_2 przyczynia się do formowania tytanowych faz krystalicznych, czyli zjawiska niekorzystnego z punktu widzenia włókien światłowodowych. Podobne efekty zaobserwowano w przypadku szkieł $K_2O-TiO_2-GeO_2$, gdzie zarejestrowane rentgenogramy XRD wykazały obecność refleksów pochodzących od fazy krystalicznej $K_2TiGe_3O_9$ [67]. Kolejne badania wykazały, że materiał na bazie $BaO-TiO_2-GeO_2$ zawierający 20% mol TiO_2 wykazuje obecność fazy krystalicznej $Ba_2TiGe_2O_8$ [68]. Z tego względu badania zmierzające do zaprojektowania i syntezy materiału optycznego, który charakteryzuje się w pełni amorficznym charakterem nabierają szczególnego znaczenia. Na podstawie analizy dostępnej literatury naukowej można stwierdzić, że nie zbadano dotychczas wpływu TiO_2 na budowę i właściwości szkieł germanianowych emitujących promieniowanie w zakresie podczerwieni.

Źródła laserowe wykazujące emisję promieniowanie w zakresie średniej podczerwieni 2 - 5 μm mogą być wykorzystywane do celów metrologicznych, bezpieczeństwa oraz innych zastosowań przemysłowych [69]. W tym samym zakresie spektralnym (2,7 μm - 3,0 μm) występują drgania rozciągające grup hydroksylowych. Obecność grup hydroksylowych skutecznie tłumi emisję promieniowania oraz przyczynia się do skrócenia czasu życia stanu wzbudzonego jonów ziem rzadkich [70]. Stąd tak bardzo istotnym wyzwaniem technologicznym jest ograniczenie grup OH⁻ w materiałach optycznych. Szczególne warunki technologiczne podczas wszystkich etapów syntezy szkieł, od przygotowania surowców, syntezy, aż do wyciągania włókien muszą zapewnić brak dostępu wilgoci atmosferycznej. W tym celu stosuje się czyste surowce, a przygotowanie surowców i syntezę prowadzi w atmosferach ochronnych. Warunki takie są szczególnie ważne w przypadku szkieł domieszkowanych jonami Er³⁺, emitujących promieniowanie przy około 2,7 μm związane z głównym przejściem laserowym $^4I_{11/2} \rightarrow ^4I_{13/2}$ [71, 72]. Podobne, bardzo rygorystyczne wymagania dotyczące warunków syntezy znajdziemy w literaturze dotyczącej wieloskładnikowych szkieł fluorkowych domieszkowanych np. jonami Er³⁺ [73-77].

Znając mechanizm krystalizacji, który został opisany w literaturze dla układu germanianowego o składzie 20BaO-10Ga₂O₃-70GeO₂ (% mol) [78] oraz rolę TiO₂ w różnych szklach, wyraźnie widać jak bardzo ważna jest optymalizacja składu chemicznego układu oraz parametrów technologicznych, aby przezwyciężyć silną tendencję do krystalizacji. W rozprawie doktorskiej przeanalizowano dokładnie wpływ stężenia TiO₂ na możliwość otrzymania oraz właściwości szkieł tytanowo-germanianowych emitujących promieniowanie w zakresie podczerwieni, w których dwutlenek tytanu TiO₂ może pełnić podwójną rolę zarówno składnika modyfikującego (TiO₂<30% mol) jak i składnika uczestniczącego w tworzeniu więźby szkła (szkłotwórczego) (TiO₂>30% mol). Przeprowadzona analiza termiczna, strukturalna oraz spektroskopowa wykazała znaczący wpływ wzajemnego ilościowego stosunku TiO₂:GeO₂ na syntezę szkieł, optymalizację parametrów technologicznych oraz właściwości fizykochemiczne i luminescencyjne. Do badań z zastosowaniem spektroskopii optycznej wybrano szkła domieszkowane wybranymi jonami ziem rzadkich, emitującymi w zakresie podczerwieni. Wyboru dokonano uwzględniając potencjalne możliwości wyciągania na ich bazie włókien światłowodowych działających w tym zakresie spektralnym. Na podstawie przeprowadzonych badań wyselekcjonowano układy charakteryzujące się najlepszymi parametrami spektroskopowymi oraz

laserowymi jonów ziem rzadkich. Zagadnienia analizowane w ramach niniejszej rozprawy doktorskiej mogą wnieść wkład w rozwój wiedzy na temat technologii szkieł specjalnych i włókien optycznych oraz zaawansowanej spektroskopii optycznej.

6. Literatura

- [1] W. Blanc, Y.G. Choi, X. Zhang, M. Nalin, K.A. Richardson, G.C. Righini, M. Ferrari, A. Jha, J. Massera, S. Jiang, J. Ballato, L. Petit, The past, present and future of photonic glasses: A review in homage to the United Nations International Year of glass 2022, *Prog. Mater. Sci.* 134 (2023) 101084.
- [2] U. Fotheringham, U. Petzold, S. Ritter, W. James, Optical glass and optical design: Otto Schott's role in the entangled development, *Opt. Mater. Express* 12 (2022) 3171-3186
- [3] J. Ballato, U. Fotheringham, M. Hubert, S. Nolte, L. Petit, K.A. Richardson, Celebrating Optical Glass - the International Year of Glass (2022): feature issue introduction, *Opt. Mater. Expr.* 12 (2022) 4660-4664
- [4] J. Ballato, A. Seddon, A. Clare, L. Petit, J. Hu, K. Richardson, Future of optical glass education, *Opt. Mater. Expr.* 12 (2022) 2626-2634
- [5] E. Snitzer, Optical maser action of Nd^{3+} in a barium crown glass, *Phys. Rev. Lett.* 7 (1961) 444-446
- [6] H. Takebe, Y. Nageno, K. Morinaga, Compositional Dependence of Judd-Ofelt parameters in silicate, borate, and phosphate glasses, *J. Am. Ceram. Soc.* 78 (1995) 1161-1168
- [7] B. R. Judd, Optical Absorption Intensities of Rare-Earth Ions, *Phys. Rev.* 127 (1962) 750-761
- [8] L. Salavcova, A. Mackova, J. Oswald, B. Svecova, S. Janakova, J. Spirkova, Martin Mika, Erbium doping into silicate glasses to form luminescent optical layers for photonics applications, *J. Phys. Chem. Solids* 68 (2007) 891-895
- [9] A. Shearer, B. Hauke, M. Montazerian, J. C. Mauro, A critical review of infrared transparent oxide glasses, *Opt. Mat. X* 20 (2023) 100258
- [10] S. Ali, Y. Iqbal, M. Ajmal, F. Gonella, E. Cattaruzza, A. Quaranta, Field-driven diffusion of transition metal and rare-earth ions in silicate glasses, *J. Non Cryst. Solids* 405 (2014) 39-44
- [11] J. Du, L. Kokou, Europium environment and clustering in europium doped silica and sodium silicate glasses, *J. Non Cryst. Solids* 357 (2011) 2235-2240
- [12] S. Tanabe, Rare-earth-doped glasses for fiber amplifiers in broadband telecommunication, *Compt. Rend. Chim.* 5 (2002) 815-824
- [13] J.D.B. Bradley, M. Pollnau, Erbium-doped integrated waveguide amplifiers and lasers, *Las. Opt. Rev.* 5 (2011) 368-403
- [14] Q. Chen, H. Wang, Q. Wang, Q. Chen, Structural study of the origin of the largest 1.5 μm Er^{3+} luminescence band width in multicomponent silicate glass, *J. Non Cryst. Solids* 404 (2014) 145-150

- [15] G. Devarajulu, G. Lakshminarayana, P. Venkateswara Rao, Dong-Eun Lee, Jonghun Yoon, Taejoon Park, Er³⁺-doped SiO₂-based glasses - an exploration of structural, visible, chromatic, and NIR fluorescence characteristics, *Mater. Res. Bull.* 147 (2022) 111634
- [16] Y. Yamasaki, R. Azuma, Y. Kagebayashi, K. Fujioka, Y. Fujimoto, Optical properties of Er³⁺ heavily doped silica glass fabricated by zeolite method, *J. Non Cryst. Solids* 543 (2020) 120149
- [17] B. Dussardier, W. Blanc, G. Monnom, Luminescent ions in silica-based optical fibers, *fiber and integrated optics* 27 (2008) 484-504
- [18] K.M.S. Dawngliana, A.L. Fanai, S. Rai, Structural and optical studies of Sm³⁺-doped silica glass along with TiO₂ nanoparticles for photonic applications, *J. Non Cryst. Solids* 607 (2023) 122226
- [19] S. Tanabe, Optical transitions of rare earth ions for amplifiers: how the local structure works in glass, *J. Non Cryst. Solids* 259 (1999) 1-9
- [20] J.D.B. Bradley, M. Pollnau, Erbium-doped integrated waveguide amplifiers and lasers. *Laser Photonics Rev.* 5 (2011) 368-403
- [21] S. S. Bayya, G. D. Chin, J. S. Sanghera, and I. D. Aggarwal, Germanate glass as a window for high energy laser systems, *Opt. Express* 14 (2006) 11687-11693
- [22] A. C. Hannon, D.D. Martino, L.F. Santos, R. M. Almeida, A model for the Ge–O coordination in germanate glasses, *J. Non Cryst. Solids* 353 (2007) 1688-1694
- [23] O.V. Butov, K.M. Golant, A.L. Tomashuk, M.J.N. van Stralen, A.H.E. Breuls, Refractive index dispersion of doped silica for fiber optics, *Opt. Commun.* 213 (2002) 301-308
- [24] J. W. Fleming, Dispersion in GeO₂-SiO₂ glasses, *Appl. Opt.* 23 (1984) 4486
- [25] T. Guerineau, C. Strutynski, T. Skopak, S. Morency, A. Hanafi, F. Calvazara, Y. Ledemi, S. Danto, T. Cardinal, Y. Messaddeq, and E. Fargini, Extended germano-gallate fiber drawing domain: from germanates to gallates optical fibers, *Opt. Mater. Expr.* 9 (2019) 2437-2445
- [26] M. Kochanowicz, J. Zmojda, P. Miluski, A. Baranowska, M. Leich, A. Schwuchow, M. Jäger, M. Kuwik, J. Pisarska, W. A. Pisarski, and D. Dorosz, Tm³⁺/Ho³⁺ co-doped germanate glass and double-clad optical fiber for broadband emission and lasing above 2 μm, *Opt. Mater. Express* 9 (2019) 1450-1458
- [27] S.S. Bayya, G.D. Chin, J.S. Sanghera, I.D. Aggarwal, Germanate glass as a window for high energy laser systems, *Opt. Expr.* 14 (2006) 11687-11693
- [28] S. Zhang, M. Xu, X. Chen, Y. Zhang, L. Calvez, X. Zhang, Y. Xu, Y. Huai, Y. Jin, Enhanced thermostability, thermo-optics, and thermomechanical properties of barium gallo-germanium oxyfluoride glasses and glass-ceramics *J. Am. Ceram. Soc.* 96 (2013) 2461-2466

- [29] J.P. Berube, A. Le Camus, S.H. Messaddeq, Y. Petit, Y. Messaddeq, L. Canioni, R. Vallee, Femtosecond laser direct inscription of mid-IR transmitting waveguides in BGG glasses, *Opt. Mater. Expr.* 7 (2017) 3124-3135
- [30] R. Jadach, J. Żmojda, M. Kochanowicz, P. Miluski, J. Pisarska, W.A. Pisarski, M. Sołtys, M. Leśniak, M. Sitarz, D. Dorosz, Investigation of the aluminium oxide content on structural and optical properties of germanium glasses doped with RE ions. *Spectrochim Acta A Mol Biomol Spectrosc.* 201 (2018) 143-152
- [31] A. Le Camus, Y. Petit, J.P. Bérubé, M. Bellec, L. Canioni, R. Vallée, Direct-laser-written integrated mid-IR directional couplers in a BGG glass, *Opt. Expr.* 29 (2021) 8531-8541
- [32] J. Pisarska, M. Sołtys, A. Górny, M. Kochanowicz, J. Zmojda, J. Dorosz, D. Dorosz, M. Sitarz, W. A. Pisarski, Rare earth-doped barium gallo-germanate glasses and their near-infrared luminescence properties, *Spectrochim. Acta Part A: Mol. Biomol. Spectrosc.* 201 (2018) 362-366
- [33] W. A. Pisarski, J. Pisarska, D. Dorosz, J. Dorosz, Towards lead-free oxyfluoride germanate glasses singly doped with Er^{3+} for long-lived near-infrared luminescence, *Mat. Chem. Phys.* 148 (2014) 485-489
- [34] J. Pisarska, M. Kowal, M. Kochanowicz, J. Zmojda, J. Dorosz, D. Dorosz, W. A. Pisarski, Influence of BaF_2 and activator concentration on broadband near-infrared luminescence of Pr^{3+} ions in gallo-germanate glasses, *Opt. Expr.* 24 (2016) 2427-2435
- [35] G. Tang, X. Wen, K. Huang, G. Qian, W. Lin, H. Cheng, L. Jiang, Q. Qian, Z. Yang, Tm^{3+} -doped barium gallo-germanate glass single-mode fiber with high gain per unit length for ultracompact 1.95 μm laser, *Appl. Phys. Express* 11 (2018) 032701
- [36] J. Pisarska, M. Kuwik, A. Górny, J. Dorosz, M. Kochanowicz, J. Żmojda, M. Sitarz, D. Dorosz, W.A. Pisarski, Influence of transition metal ion concentration on near-infrared emission of Ho^{3+} in barium gallo-germanate glasses, *J. Alloys Compd.* 793 (2019) 107-114
- [37] X. P. Jiang, Z. M. Yang, T. Liu, S. H. Xu, Energy transfer between Yb^{3+} and Er^{3+} in barium gallogermanate glass, *J. Appl. Phys.* 105 (2009) 103113
- [38] M. Kochanowicz, J. Żmojda, P. Miluski, A. Baranowska, T. Ragin, J. Dorosz, M. Kuwik, W. A. Pisarski, J. Pisarska, M. Leśniak, D. Dorosz, 2 μm emission in gallo-germanate glasses and glass fibers co-doped with $\text{Yb}^{3+}/\text{Ho}^{3+}$ and $\text{Yb}^{3+}/\text{Tm}^{3+}/\text{Ho}^{3+}$, *J. Lumin.* 211 (2019) 341-346
- [39] G. Tang, X. Wen, Q. Qian, T. Zhu, W. Liu, M. Sun, X. Chen, Z. Yang, Efficient 2.0 μm emission in $\text{Er}^{3+}/\text{Ho}^{3+}$ co-doped barium gallo-germanate glasses under different excitations for mid-infrared laser, *J. All. Compd.* 664 (2016) 19-24

- [40] M. Kochanowicz, J. Zmojda, P. Miluski, A. Baranowska, M. Leich, A. Schwuchow, M. Jäger, M. Kuwik, J. Pisarska, W. A. Pisarski, D. Dorosz, Tm³⁺/Ho³⁺ co-doped germanate glass and double-clad optical fiber for broadband emission and lasing above 2 μm, *Opt. Mat. Expr.* 9 (2019) 1450-1458
- [41] M. Leśniak, G. Mach, B. Starzyk, K. Sadowska, T. Ragiń, J. Żmojda, M. Kochanowicz, M. Kuwik, P. Miluski, G.L. Jimenez, A. Baranowska, J. Dorosz, W. Pisarski, J. Pisarska, Z. Olejniczak, D. Dorosz, The effect of fluorides (BaF₂, MgF₂, AlF₃) on structural and luminescent properties of Er³⁺-doped gallo-germanate glass, *Materials* 15 (2022) 5230
- [42] S. Aouji, T. Guérineau, R. Zaiter, E. Fargin, Y. Messaddeq, T. Cardinal, The key role of yttrium oxide on devitrification resilience of barium gallo-germanate glasses: Physicochemical properties and crystallization study, *J. Non Cryst. Solids* 619 (2023) 122546
- [43] R. Jadach, J. Zmojda, M. Kochanowicz, P. Miluski, J. Pisarska, W.A. Pisarski, M. Sołtys, M. Lesniak, M. Sitarz, D. Dorosz, Investigation of the aluminum oxide content on structural and optical properties of germanium glasses doped with RE ions, *Spectrochim. Acta Part A: Mol. Biomol. Spectrosc.* 201 (2018) 143-152
- [44] J. Fan, B. Tang, D. Wu, Y. Fan, R. Li, J. Li, D. Chen, L. Calveza, X. Zhang, L. Zhang, Dependence of fluorescence properties on substitution of BaF₂ for BaO in barium gallo-germanate glass, *J. Non Cryst. Solids* 357 (2011) 1106-1109
- [45] S. Le Boiteux, P. Segonds, L. Canioni, L. Sarger, T. Cardinal, C. Duchesne, E. Fargin, G. Le Flem, Nonlinear optical properties for TiO₂ containing phosphate, borophosphate, and silicate glasses, *J. Appl. Phys.* 81 (1997) 1481-1487
- [46] P.F. Moulton, Spectroscopic and laser characteristics of Ti:Al₂O₃, *J. Opt. Soc. Am B* 3 (1986) 125
- [47] A. Karvounis, F. Timpu, V. V. Vogler-Neuling, R. Savo, R. Grange, Barium Titanate Nanostructures and Thin Films for Photonics, *Adv. Opt. Mat.* 8 (2020) 2001249
- [48] D. Mewada, Barium titanate (BaTiO₃): A study of structural, optical and dielectric properties, *Mat. Proc.* 54 (2022) 923-926
- [49] K.T. Lee, R.A.M. Osman, P. Poopalan, Optical characteristics and luminescence of amorphous BaTiO₃ thin films doped with Eu³⁺, *J. Non Cryst. Solids* 553 (2021) 120515
- [50] Ch. Sameera Devi, G.S. Kumar, G. Prasad, Spectroscopic and electrical studies on Nd³⁺, Zr⁴⁺ ions doped nano-sized BaTiO₃ ferroelectrics prepared by sol-gel method, *Spectrochim. Acta Part A Mol. Biomol. Spectrosc.*, 136 (2015) 366-372
- [51] D. Kumar Singh, J. Manam, Efficient dual emission mode of green emitting perovskite BaTiO₃: Er³⁺ phosphors for display and temperature sensing applications, *Ceram. Int.* 44 (2018) 10912-10920

- [52] M. K. Mahata, K. Kumar, V. K. Rai, Structural and optical properties of Er³⁺/Yb³⁺ doped barium titanate phosphor prepared by co-precipitation method, *Spectrochim. Acta Part A Mol. Biomol. Spectrosc.*, 124 (2014) 285-291
- [53] J.L. Clabel H., Kelly T. Paula, M.A. Pereira-da-Silva, J.D. Vollet-Filho, Filipe A. Couto, E. Marega J., C.R. Mendonça, Femtosecond laser-induced crystallization in Er/Yb:BaTiO₃ perovskite films: Effects on the optical and electrical properties, *Appl. Surf. Sci.* 642 (2024) 158634
- [54] L. H. C. Andrade, S. M. Lima, A. Novatski, A. M. Neto, A. C. Bento, M. L. Baesso, F. C. G. Gandra, Y. Guyot, G. Boulon, Spectroscopic assignments of Ti³⁺ and Ti⁴⁺ in titanium-doped OH⁻ free low-silica calcium aluminosilicate glass and role of structural defects on the observed long lifetime and high fluorescence of Ti³⁺ ions, *Phys. Rev. B* 78 (2008) 224202
- [55] L. H. C. Andrade, S. M. Lima, A. Novatski, P. T. Udo, N. G. C. Astrath, A. N. Medina, A. C. Bento, M. L. Baesso, Y. Guyot, G. Boulon, Long fluorescence lifetime of Ti³⁺-doped low silica calcium aluminosilicate glass, *Phys. Rev. Lett.* 100 (2008) 027402
- [56] B. Peng, T. Izumitani, Spectroscopic investigation of Ti³⁺-doped silicate glasses, *Rev. Laser Eng.* 22 (1993) 823-827
- [57] M.A. Marzouk, F.H. ElBatal, H.A. ElBatal, Effect of TiO₂ on the optical, structural and crystallization behavior of barium borate glasses, *Opt. Mat.* 57 (2016) 14-22
- [58] R. Shafaghi, O. Rodriguez, Sunjeev Phull, E. H. Schemitsch, P. Zalzal, S.D. Waldman, M. Papini, M. R. Towler, Effect of TiO₂ doping on degradation rate, microstructure and strength of borate bioactive glass scaffolds, *Mat. Sci. Eng. C* 107 (2020) 110351
- [59] M. Kaur, A. Singh, V. Thakur, L. Singh, Effect of TiO₂ substitution on optical and structural aspects of phosphate glasses, *J. Mol. Struct.* 1089 (2015) 95-101
- [60] G. Novajra, C. Vitale-Brovarone, J.C. Knowles, G. Maina, V. Aina, D. Ghigo, L. Bergandi, Effects of TiO₂-containing phosphate glasses on solubility and in vitro biocompatibility. *J. Biomed. Mater. Res. Part A* 99 (2011) 295-306
- [61] H. Hidaka, N. Iwamoto, N. Umesaki, T. Fukunaga, K. Suzuki, Structural analysis of sodium silicate glasses containing TiO₂ by pulsed neutron scattering, *J. Mat. Sci.* 20 (1985) 2497-2502
- [62] M. Abdel-Baki, F. El-Diasty, F. A. Abdel Wahab, Optical characterization of xTiO₂-(60-x)SiO₂-40Na₂O glasses: II. Absorption edge, Fermi level, electronic polarizability and optical basicity, *Opt. Comm.* 261 (2006) 65-70
- [63] R. Balda, J. Fernández, S. García-Revilla, J. M. Fernández-Navarro, Spectroscopy and concentration quenching of the infrared emissions in Tm³⁺-doped TeO₂-TiO₂- Nb₂O₅ glass, *Opt. Expr.* 15 (2007) 6750-6761

- [64] R. Balda, J. Fernández, M A Arriandiaga, J.M. Fernández-Navarro, Spectroscopy and frequency upconversion in Nd³⁺-doped TeO₂-TiO₂-Nb₂O₅ glass, *J. Phys. Condens. Matter* 19 (2007) 086223
- [65] B.C. Jamalaiah, T. Suhasini, L. Rama Moorthy, I.G. Kim, D.S. Yoo, K. Jang, Structural and luminescence properties of Nd³⁺-doped PbO-B₂O₃-TiO₂-AlF₃ glass for 1.07 μm laser applications, *J. Lumin.* 132 (2012) 1144-1149
- [66] S. Karlsson, L.G. Back, P. Kidkhunthod, K. Lundstedt, L. Wondraczek, Effect of TiO₂ on optical properties of glasses in the soda-lime-silicate system, *Opt. Mat. Expr.* 6 (2016) 1198
- [67] T. Fukushima, Y. Benino, T. Fujiwara, V. Dimitrov, T. Komatsu, Electronic polarizability and crystallization of K₂O-TiO₂-GeO₂ glasses with high TiO₂ contents, *J. Solid State Chem.* 179 (2006) 3949
- [68] H. Masai, T. Fujiwara, Y. Benino, T. Komatsu, Large second-order optical nonlinearity in 30BaO-15TiO₂-55GeO₂ surface crystallized glass with strong orientation. *J. Appl. Phys.* 100 (2006) 023526
- [69] J. Hu, L. Mawst, S. Moss, L. Petit, D. Ting, Feature issue introduction: mid-infrared optical materials and their device applications, *Opt. Mater. Express* 8 (2018) 2026-2034
- [70] B. Huang, C. Xu, Z. Zhang, C.Y. Zang, L. Sun, Removal of hydroxyl routes enhancing 2.85 μm mid-infrared luminescence in oxyfluorotellurite glass with high ZnF₂ content, *J. Non Cryst. Solids* 502 (2018) 97-105
- [71] F. Qi, F. Huang, T. Wang, R. Ye, R. Lei, Y. Tian, J. Zhang, L. Zhang, S. Xu, Highly Er³⁺-doped fluorotellurite glass for 1.5 μm broadband amplification and 2.7 μm microchip laser applications, *J. Lumin.* 202 (2018) 132-135
- [72] W. Ding, X. Zhang, L. Li, Q. Ding, S. Wu, S. Yu, J. Zhang, Enhanced mid-infrared emission of erbium-doped fluoro-bromozirconate glass, *Appl. Opt.* 57 (2018) 5380-5384
- [73] F. Qi, F. Huang, T. Wang, R. Ye, R. Lei, Y. Tian, J. Zhang, L. Zhang, S. Xu, Highly Er³⁺-doped fluorotellurite glass for 1.5 μm broadband amplification and 2.7 μm microchip laser applications, *J. Lumin.* 202 (2018) 132-135
- [74] F. Zhang, W.J. Zhang, J. Yuan, D.D. Chen, Q. Qian, Q.Y. Zhang, Enhanced 2.7 μm emission from Er³⁺-doped oxyfluoride tellurite glasses for a diode-pump mid-infrared laser, *AIP Adv.* 4 (2014) 047101
- [75] J. Yu, M. Zhang, X. Lu, Y. Du, G. Brambilla, S. Jia, S. Wang, P. Wang, Broadband 2.7 μm mid-infrared emissions in Er³⁺-doped PbO-PbF₂-Bi₂O₃-Ga₂O₃ glasses, *Opt. Lett.* 45 (2020) 4638-4641
- [76] R. Wang, X. Meng, F. Yin, Y. Feng, G. Qin, W. Qin, Heavily erbium-doped low-hydroxyl fluorotellurite glasses for 2.7 μm laser applications, *Opt. Mater. Express* 3 (2013) 1127-1136

[77] F. Huang, Y. Guo, Y. Tian, S. Xu, J. Zhang, Intense 2.7 μm emission in Er^{3+} doped zinc fluoride glass, *Spectrochim. Acta Part A: Mol. Biomol. Spectrosc.* 179 (2017) 42-45

[78] B. Tang, Y. Yang, Y. Fan, L. Zhang, Barium gallogermanate glass ceramics for infrared applications, *J. Mater. Sci. Technol.* 26 (2010) 558-563

7. Część eksperymentalna (Badania własne)

Przedmiotem badań prowadzonych w ramach rozprawy doktorskiej są szkła nieorganiczne do zastosowań w podczerwonej fotonice. Tematyka badawcza związana jest z otrzymaniem i zbadaniem właściwości fizykochemicznych wieloskładnikowych szkieł tytanowo-germanianowych, ze szczególnym uwzględnieniem właściwości luminescencyjnych w zakresie podczerwieni w funkcji stężenia TiO_2 .

Praca doktorska składa się z dwóch części.

W części pierwszej pt. „Synteza i charakterystyka szkieł tytanowo-germanianowych” opisano metodykę przeprowadzonych badań, których celem było otrzymanie w pełni amorficznego i stabilnego termicznie nowego, wieloskładnikowego szkła tytanowo-germanianowego. W pracach **P1-P4** przedstawiono najważniejsze aspekty technologiczne związane z syntezą opracowanych, nowych wieloskładnikowych szkieł tytanowo-germanianowych i badaniem ich właściwości strukturalnych oraz termicznych. Weryfikację wstępnych założeń dotyczących projektowanych szkieł tytanowo-germanianowych przeprowadzono wykorzystując wybrane jony metali przejściowych i ziem rzadkich, pełniące rolę sond spektroskopowych.

W drugiej części pracy pt. „Wpływ stężenia TiO_2 na właściwości szkieł germanianowych emitujących promieniowanie w zakresie podczerwieni” zaprezentowano właściwości optyczne wytworzonych szkieł, wyselekcjonowano układy o najkorzystniejszych parametrach spektroskopowych oraz laserowych, wskazano możliwości aplikacyjne w postaci źródeł laserowych lub szerokopasmowych wzmacniaczy optycznych stanowiących istotny element sieci światłowodowych. Przedstawiono właściwości luminescencyjne nowych szkieł tytanowo-germanianowych pojedynczo (Nd^{3+} , Er^{3+} , Pr^{3+} , Tm^{3+} , Ho^{3+}) oraz podwójnie ($\text{Yb}^{3+}/\text{Er}^{3+}$, $\text{Yb}^{3+}/\text{Ho}^{3+}$, $\text{Yb}^{3+}/\text{Tm}^{3+}$, $\text{Yb}^{3+}/\text{Pr}^{3+}$) domieszkowanych jonami ziem rzadkich w zakresie bliskiej oraz średniej podczerwieni. Szczegóły zaprezentowano w pracach **P5-P12**.

7.1. Synteza i charakterystyka szkieł tytanowo-germanianowych

Omówiony w części teoretycznej aktualny stan wiedzy wskazuje, że obecnie najbardziej interesującym zagadnieniem jest otrzymanie materiału optycznego wykazującego wydajną emisję promieniowania w zakresie podczerwieni. Emisja w zakresie podczerwieni ma kluczowe znaczenie w technice laserowej oraz dla układów telekomunikacyjnych. W pracy P1 pt.: „*Novel multicomponent titanate-germanate glasses: synthesis, structure, properties, transition metal, and rare earth doping*” przedstawiono syntezę oraz charakterystykę właściwości nowych wieloskładnikowych szkieł tytanowo-germanianowych pojedynczo domieszkowanych jonami ziem rzadkich (Eu^{3+}) oraz jonami metali przejściowych (Cr^{3+}). Otrzymano szkła w wyniku topienia surowców wyjściowych w wysokich temperaturach o relatywnie wysokim stężeniu TiO_2 (30% mol), w których wzajemny ilościowy stosunek $\text{GeO}_2:\text{TiO}_2$ wynosił 1:1. Szkła zawierające TiO_2 wykazują bardzo dużą skłonność do krystalizacji, dlatego charakterystykę ich właściwości rozpoczęto od badań lokalnej struktury z wykorzystaniem rentgenowskiej analizy fazowej. Na dyfraktogramie XRD dla układu $30\text{TiO}_2\text{-}30\text{GeO}_2\text{-}30\text{BaO}\text{-}10\text{Ga}_2\text{O}_3$ (%mol) widoczne są jedynie dwa szerokie pasma, co świadczy o amorficznym charakterze otrzymanego materiału. Wąskich linii dyfrakcyjnych, charakterystycznych dla materiałów krystalicznych, nie zaobserwowano również na dyfraktogramach zarejestrowanych dla szkieł tytanowo-germanianowych domieszkowanych jonami optycznie aktywnymi. Pozwoliło to na jednoznaczne wnioskowanie, że opracowane szkło wykazuje zdolność do domieszkowania bez zmiany całkowicie amorficznego charakteru. Kolejnym zagadnieniem bardzo istotnym z punktu widzenia zastosowań szkieł była charakterystyka termiczna wytworzonych materiałów. Na podstawie charakterystyk otrzymanych z zastosowaniem różnicowej kalorymetrii skaningowej wykazano, że szkła tytanowo-germanianowe charakteryzują się wystarczająco wysoką wartością parametru stabilności termicznej ΔT . Wprowadzenie TiO_2 spowodowało wzrost temperatury transformacji w stosunku do wyjściowego szkła. Temperatura transformacji szkła tytanowo-germanianowego wynosiła 690°C . Bardzo ważnym aspektem analizowanym w ramach rozprawy było zbadanie bezpośredniej korelacji między budową wewnętrzną a właściwościami optycznymi. Przeprowadzono badania strukturalne przy użyciu spektroskopii w podczerwieni, które potwierdziły obecność w badanych układach charakterystycznych drgań, tj. pasm pochodzącego od zginających drgań wiązań Ge-O-Ge i Ge-O-Ga (w zakresie $400\text{-}600\text{ cm}^{-1}$) oraz

asymetrycznych rozciągających drgań Ge-O-Ge i symetrycznych rozciągających drgań Ge-O/Ga-O (w zakresie 700-900 cm^{-1}). Wprowadzenie TiO_2 do szkła barowo-galowo-germanianowego spowodowało spadek intensywności charakterystycznych pasm oraz przesunięcie położenia tych pasm w kierunku większych częstości. Prawdliwość ta została potwierdzona również z zastosowaniem spektroskopii Ramana. O silnym wpływie TiO_2 na więźbę matrycy barowo-galowo-germanianowej świadczy ponadto dodatkowe pasmo położone przy około 650 cm^{-1} . Pasma to przypisano do drgań rozciągających Ti-O. Na podstawie badań stwierdzono, że nawet najmniejsze zmiany strukturalne w otoczeniu aktywatora wywołane modyfikacją składu chemicznego szkła można monitorować spektroskopowo przez trójwartościowe jony metalu przejściowego (Cr^{3+}), których stężenie wynosiło 0,25% mol. Spektroskopia elektronowego rezonansu paramagnetycznego (EPR) wykazała sygnały rezonansowe, to jest niskopolowy ($g = 1,97$) oraz wysokopolowy ($g = 4,8$), potwierdzające obecność jonów chromu na trzecim stopniu utlenienia. Właściwości luminescencyjne wytworzonego materiału są zdeterminowane przez pasma emisyjne przy długości fali 730 nm i 1030 nm, które odpowiadają przejściu ${}^4T_2 \rightarrow {}^4A_2$ jonów Cr^{3+} zajmujących pozycje oktaedryczną oraz tetraedryczną. Zaobserwowano także spadek intensywności zmierzonych pasm emisji jonów Cr^{3+} dla układu zawierającego w składzie chemicznym TiO_2 . W dalszej kolejności przeprowadzono charakterystykę wytworzonego materiału zawierającego 0,5% mol Eu_2O_3 w celu określenia stopnia uporządkowania otoczenia jonów ziem rzadkich. W tym celu zarejestrowano widma wzbudzenia, widma emisji oraz przeprowadzono badania kinetyki zaniku luminescencji. Matryca szkła $\text{GeO}_2\text{-BaO-Ga}_2\text{O}_3$ należy do rodziny niskofononowych szkieł tlenkowych. Na podstawie pomiarów pasma fononowego PSB widocznego na widmie wzbudzenia wykazano, że wprowadzenie TiO_2 powoduje obniżenie maksymalnej energii fononowej matrycy z 790 cm^{-1} do 765 cm^{-1} . Warto w tym miejscu nadmienić, że szkła aktywowane jonami Eu^{3+} wykorzystywane w optyce jako emiterzy czerwone, zostały także dogłębnie przebadane pod kątem emisji promieniowania, która odpowiada przejściom ${}^5D_0 \rightarrow {}^7F_J$ (gdzie $J = 1$ i 2). Szkło zawierające TiO_2 charakteryzowało się znacznie bardziej intensywnym pasmem emisji promieniowania odpowiadającym przejściu ${}^5D_0 \rightarrow {}^7F_2$ (emisja czerwona), które charakteryzuje się dużą wrażliwością na zmiany otoczenia. Wzajemny stosunek intensywności przejścia dipolowo-elektrycznego ${}^5D_0 \rightarrow {}^7F_2$ do intensywności przejścia dipolowo-magnetycznego ${}^5D_0 \rightarrow {}^7F_1$ (emisja pomarańczowa) określany współczynnikiem intensywności fluorescencji R/O, stanowi istotne narzędzie

w określeniu lokalnej symetrii w otoczeniu jonów Eu^{3+} . Po wprowadzeniu TiO_2 do matrycy barowo-galowo-germanianowej współczynnik ten zwiększył się z 3,54 do 4,10. Świadczy to o wzroście lokalnej asymetrii wokół domieszki optycznie aktywnej, a także wzroście kowalencyjnego charakteru wiązania Eu-otoczenie. Analiza kinetyki zaniku luminescencji wskazuje, że TiO_2 wpływa na obniżenie wartości czasu życia poziomu $^5\text{D}_0$ jonów Eu^{3+} z 1,26 ms do 0,78 ms.

W celu szczegółowego przeanalizowania właściwości spektroskopowych jonów chromu w otrzymanym szkłe zaproponowano zastąpienie składnika szkłotwórczego GeO_2 przez inne tlenki metali - praca **P2** pt. „*EPR and optical spectroscopy of Cr^{3+} ions in barium gallo-germanate glasses containing $\text{B}_2\text{O}_3/\text{TiO}_2$* ”. Otrzymano szkło tlenkowe w układzie $\text{GeO}_2\text{-TiO}_2\text{-BaO-Ga}_2\text{O}_3$, gdzie wzajemny ilościowy stosunek $\text{GeO}_2\text{:TiO}_2$ wynosił 5:1 (10% mol TiO_2), 1:1 (30% mol TiO_2) oraz 1:5 (50% mol TiO_2). Wymienione powyżej układy domieszkowano 0,25% mol Cr_2O_3 . Zmierzone widma z wykorzystaniem elektronowego rezonansu paramagnetycznego (EPR) dla wszystkich układów potwierdziły obecność dwóch sygnałów rezonansowych. Pierwszy sygnał rezonansowy ($g = 4,8$) wynika z obecności izolowanych jonów Cr^{3+} . Drugi sygnał rezonansowy ($g = 1,97$) informuje o sprzężonych parach $\text{Cr}^{3+}\text{-Cr}^{3+}$. Przeprowadzona analiza dowiodła, że niezależnie od ilościowej relacji $\text{GeO}_2\text{:TiO}_2$ jony chromu występują na trzecim stopniu utlenienia. Zarejestrowane widma absorpcji charakteryzują się typowym dla jonów chromu szerokim pasmem absorpcji z maksimum położonym przy 630 nm, które związane jest z przejściem $^4\text{A}_2 \rightarrow ^4\text{T}_2$. Na zboczu szerokiego pasma absorpcji przy długości fali około 680 nm zidentyfikowano dodatkowo przejście $^4\text{A}_2 \rightarrow ^2\text{E}$, które przesuwają się w kierunku dłuższych długości fali wraz ze wzrostem stężenia TiO_2 . Widma wzbudzenia wykazały obecność dwóch pasm odpowiadających przejściom ze stanu podstawowego $^4\text{A}_2$ do wyżej położonych stanów wzbudzonych $^4\text{T}_1$ oraz $^4\text{T}_2$ jonów chromu. Interesujące jest, że jony metali przejściowych w zależności od składu chemicznego matrycy szklistej zajmują miejsca o różnej sile pola krystalicznego. Z tego powodu przeprowadzone pomiary wykorzystano do obliczenia istotnego parametru Dq/B . Przyjmując kryterium opisywane w literaturze obliczony parametr spełnia warunek $2,1 < \text{Dq/B} < 2,3$ oraz $\text{Dq/B} > 2,3$, co pozwala na stwierdzenie, że jony chromu w wytworzonych układach znajdują się w pośrednim i/lub silnym polu krystalicznym. Ze względu na nieuporządkowaną budowę wewnętrzną szkła, przeprowadzona charakterystyka wykazała, że zmiana ilościowego stosunku $\text{GeO}_2\text{:TiO}_2$ przyczyniła się do modyfikacji właściwości optycznych jonów chromu. Dowodem mogą

być zarejestrowane widma luminescencji obejmujące dwa zakresy spektralne. Szczególnie interesujące zmiany związane z profilem pasm luminescencyjnych zaobserwowano dla przejścia ${}^4T_2 \rightarrow {}^4A_2$ w zakresie 630 – 900 nm. Wykazano, że wraz ze wzrostem stężenia TiO_2 następuje znaczące przesunięcie maksimum tego pasma w kierunku krótszych długości fali. Układ o stosunku molowym $GeO_2:TiO_2 = 1:5$, w którym TiO_2 pełni rolę składnika szkłotwórczego, charakteryzuje się pasmem luminescencyjnym, które przypisano przejściu ${}^2E \rightarrow {}^4A_2$ (tzw. linia R) jonów chromu. Obecność tego przejścia potwierdza, że jony Cr^{3+} znajdują się w silnym polu krystalicznym. Domieszkowanie wytworzonego szkła jonami chromu pozwoliło również na uzyskanie szerokopasmowej emisji promieniowania podczerwonego obejmującego zakres od 950 nm do 1500 nm, którą można przypisać przejściom ${}^4T_2 \rightarrow {}^4A_2$ (Cr^{3+}) oraz ${}^3T_2 \rightarrow {}^3A_2$ (Cr^{4+}). Wykazano, że zmiana składu chemicznego szkła przyczyniła się do znaczących zmian intensywności zarejestrowanych pasm. W analizowanym przypadku wzmocnioną emisję wykazuje układ, w którym rolę składnika szkłotwórczego pełni GeO_2 ($GeO_2:TiO_2 = 5:1$).

Wyniki uzyskane dla szkieł tytanowo-germanianowych domieszkowanych jonami metali przejściowych oraz jonami metali ziem rzadkich pełniących rolę sondy spektroskopowej stanowiły główną motywację do szczegółowego przeanalizowania lokalnej struktury wytworzonego materiału. W pracy **P3** pt. „*Raman and Infrared Spectroscopy of Barium-Gallo Germanate Glasses Containing B_2O_3/TiO_2* ” zaprezentowano wyniki badań eksperymentalnych dla matrycy barowo-galowo-germanianowej modyfikowanej TiO_2 bez domieszek optycznie aktywnych. Na podstawie przeprowadzonej rentgenowskiej analizy fazowej i zarejestrowanych dyfraktogramów XRD dla materiałów z układu $GeO_2-TiO_2-BaO-Ga_2O_3$ stwierdzono, że zarówno szkła zawierające tlenek tytanu pełniący rolę składnika modyfikującego ($TiO_2 < 30\%$ mol) jak i szkłotwórczego ($TiO_2 > 30\%$ mol) są w pełni amorficzne. Charakterystyka właściwości optycznych wykazała, że na zarejestrowanych widmach absorpcji wraz ze wzrostem stężenia TiO_2 krawędź absorpcji przesuwa się w kierunku dłuższych długości fali. W ramach zaplanowanych badań wchodzących w zakres pracy doktorskiej otrzymano również próbki szkła zawierające bardzo niskie stężenie TiO_2 . Na zarejestrowanym widmie absorpcji wysokiej rozdzielczości dla szkła zawierającego 0,005% mol TiO_2 obserwuje się pasmo przy długości fali 700 nm, które związane jest z obecnością par $Ti^{3+}-Ti^{4+}$. Szkło tytanowo-germanianowe po wzbudzeniu falą o długości 345 nm wykazuje interesujące właściwości optyczne. Na widmie emisyjnym można

zaobserwować znaczące zmiany intensywności pasma luminescencyjnego spowodowane zmianą składu chemicznego matrycy szklistej. Szkło zawierające najmniejsze stężenie TiO_2 charakteryzuje się pasmem emisji przy długości fali 450 nm, które przypisano obecności jonów Ti^{4+} . Przy większym stężeniu TiO_2 w matrycy barowo-galowo-germanianowej zaobserwowano pasmo emisji przy długości fali 550 nm, które przypisano obecności jonów Ti^{3+} . W kolejnym etapie badań przeprowadzono analizę właściwości strukturalnych wytworzonego materiału. Zestawienie widm Ramana oraz FT-IR pozwoliło na wykazanie zmian w budowie wewnętrznej szkła w funkcji zmian ilościowego stosunku $\text{GeO}_2:\text{TiO}_2$. Zarejestrowane na widmach Ramana oraz FT-IR pasma przy około 450 cm^{-1} oraz 800 cm^{-1} odpowiadają drganiom pochodzącym od grup germanianowych, których intensywność maleje w przypadku wzrostu stężenia tlenku tytanu w składzie szkła. Pasma te nie są widoczne na widmie FT-IR dla układu, w którym stosunek $\text{GeO}_2:\text{TiO}_2$ wynosi 1:5. Dla tego samego układu na widmie Ramana widoczne jest pasmo przy około 650 cm^{-1} odpowiedzialne za drgania rozciągające Ti-O.

Kolejny problem badawczy podjęty w pracy **P4** pt. „*Influence of titanium dioxide concentration on thermal properties of germanate-based glasses*” dotyczył analizy termicznej wytworzonych szkieł oraz parametrów stabilności termicznej w funkcji stężenia TiO_2 w matrycy barowo-galowo-germanianowej. Zbadanie parametrów termicznych szkieł jest bardzo istotne pod kątem potencjalnych zastosowań w postaci włókien optycznych. Na podstawie charakterystyk termicznych z użyciem różnicowej kalorymetrii skaningowej (DSC) wyznaczone zostały temperatury charakterystyczne dla szkieł. Dla szkła zawierającego największe stężenie TiO_2 (50% mol) wartość temperatury zeszklenia była największa – 708°C . Dla porównania dla szkieł nie zawierających TiO_2 w składzie wynosiła 620°C . Parametry stabilności termicznej również ulegają zmianie dla szkieł tytanowo-germanianowych. Parametr stabilności termicznej ΔT dla szkieł wynoszący powyżej 100°C daje nadzieję na wyciągnięcie dobrej jakości włókien. Na podstawie temperatur charakterystycznych określonych z krzywych DSC obliczono parametry stabilności termicznej ($\Delta T = T_x - T_g$, parametry zaproponowane przez Hruby'ego, Saad-Poulaina, Weinberga i Lu/Liu) dla szkieł tytanowo-germanianowych. Badania cieplne z zastosowaniem metody DSC jednoznacznie wykazały, że co prawda stabilność termiczna maleje ze wzrostem stężenia TiO_2 w składzie szkła, ale jest wciąż wystarczająca z punktu widzenia wyciągania włókien optycznych dla układów ($\Delta T > 100^\circ\text{C}$ dla stężenia $\text{TiO}_2 \leq 30\%$ mol), w których dwutlenek tytanu pełni rolę składnika

modyfikującego. Najlepsze wyniki parametru ΔT otrzymano dla wieloskładnikowych układów tytanowo-germanianowych o znacznym stężeniu GeO_2 (60% mol - 187°C, 50% mol - 150°C, 40% mol - 120°C oraz 30% mol - 115°C). Wybór matrycy szkła tytanowo-germanianowego jest zatem pewnym kompromisem między stabilnością termiczną niezbędną do wyciągania włókna optycznego a właściwościami optycznymi i laserowymi jonów ziem rzadkich.

Kolejnym interesującym problemem naukowym były badania kinetyki krystalizacji szkła zawierającego 30% mol TiO_2 ($\text{GeO}_2:\text{TiO}_2 = 1:1$) przy różnej prędkości ogrzewania (od 5°C/min do 20°C/min). Otrzymane wyniki porównano z wynikami dla wyjściowego szkła. Zaobserwowano, że wraz ze wzrostem prędkości ogrzewania wzrasta intensywność pików oraz przesuwały się one w kierunku wyższych temperatur. Energia aktywacji jest parametrem określającym tendencję do krystalizacji szkła. Korzystając z uproszczonego równania Kissingera obliczono, że energia aktywacji wynosi 223 kJ/mol (bez TiO_2) oraz 377 kJ/mol (z TiO_2).

Określono również wpływ procesu wygrzewania na budowę i właściwości szkieł tytanowo-germanianowych. Znajomość budowy wewnętrznej szkła jest bardzo ważna, ponieważ decyduje ona o właściwościach fizykochemicznych i użytkowych. Pojawienie się faz krystalicznych w wyniku wygrzewania wywołuje także zmianę właściwości optycznych. Zarejestrowane dyfraktogramy XRD potwierdziły obecność wąskich linii dyfrakcyjnych po 4 oraz 5 godzinach obróbki termicznej szkła, wskazując na pojawienie się w układzie faz krystalicznych $\text{Ba}_2\text{TiGe}_2\text{O}_8$, $\text{Ga}_2\text{Ge}_2\text{O}_7$, $\text{Ba}_3\text{Ga}_2\text{O}_6$, BaO oraz Er_2O_3 . Zmiany otoczenia wokół optycznie aktywnego jonu Er^{3+} w wyniku procesu wygrzewania potwierdzono również na podstawie zmierzonych widm absorpcyjnych (analizując między innymi przejście nadczułe $^4\text{I}_{15/2} \rightarrow ^2\text{H}_{11/2}$). Dowodem spektroskopowym potwierdzającym wzrost uporządkowania wokół optycznie czynnej domieszki jest zmniejszenie szerokości pasma emisji związanego z przejściem $^4\text{I}_{13/2} \rightarrow ^4\text{I}_{15/2}$ w bliskiej podczerwieni przy 1,5 μm oraz wydłużenie czasu życia luminescencji z poziomu $^4\text{I}_{13/2}$ jonów Er^{3+} . Obserwowane zmiany są związane z transformacją szkła do materiału szklano-ceramicznego w wyniku procesu wygrzewania. Zagadnienia te wykraczają jednak poza zakres niniejszej pracy doktorskiej i otwierają nowy ciekawy rozdział badań.

P1

Wojciech A. Pisarski, Karolina Kowalska, Marta Kuwik, Justyna Polak, Ewa Pietrasik,
Tomasz Goryczka, Joanna Pisarska,

**Novel multicomponent titanate-germanate glasses: synthesis, structure, properties,
transition metal, and rare earth doping**

Materials 13 (2020) 4422

Article

Novel Multicomponent Titanate-Germanate Glasses: Synthesis, Structure, Properties, Transition Metal, and Rare Earth Doping

Wojciech A. Pisarski ^{1,*}, Karolina Kowalska ¹, Marta Kuwik ¹, Justyna Polak ¹, Ewa Pietrasik ¹, Tomasz Goryczka ² and Joanna Pisarska ¹

¹ Institute of Chemistry, University of Silesia, Szkolna 9 Street, 40-007 Katowice, Poland; k.kowalska119@gmail.com (K.K.); marta.kuwik88@gmail.com (M.K.); justyna.polak@us.edu.pl (J.P.); ewa.pietrasik@us.edu.pl (E.P.); joanna.pisarska@us.edu.pl (J.P.)

² Institute of Materials Science, University of Silesia, 75 Pułku Piechoty 1A Street, 41-500 Chorzów, Poland; tomasz.goryczka@us.edu.pl

* Correspondence: wojciech.pisarski@us.edu.pl

Received: 13 August 2020; Accepted: 29 September 2020; Published: 4 October 2020



Abstract: Novel multicomponent titanate-germanate glasses singly doped with transition metal (Cr^{3+}) and rare earth ions (Eu^{3+}) were synthesized and the glass transition temperatures and thermal stability parameters were determined using DSC measurements. X-ray diffraction analysis confirmed fully amorphous nature of the received samples. Their structural and optical properties were compared with germanate glasses without TiO_2 . Correlation between local structure and optical properties in titanate-germanate glasses is well evidenced by FT-IR, Raman, EPR, and luminescence spectroscopy. In particular, luminescence spectra and their decays are examined for glass samples, where GeO_2 was partially substituted by TiO_2 .

Keywords: glasses; structure-property relationship; Cr^{3+} ; Eu^{3+} ; spectroscopic parameters

1. Introduction

Since 1986 the formation of TiO_2 containing glasses has been investigated in detail [1–8]. Unfortunately, most of titanate glass systems are partly crystallized. The obtained systems possess crystalline phases mainly because of different titanates and their thermal stability parameters are relatively low, which makes them unsuitable for optical-fiber applications. In fact, it is difficult to prepare thermally stable and fully amorphous systems with relatively high titanium oxide content. On the other hand, germanate glasses have quite strong chemical and mechanical stability useful for optical fiber drawing and belong to low-phonon glass family. Compared to other low-phonon glass systems such as tellurite glasses, germanate based glass-host matrices have relatively large glass-forming region. In particular, thermal stability parameter referred to as a difference between crystallization onset T_x and glass transition temperature T_g is considerably higher for germanate-based glass with $\Delta T = 155\text{ }^\circ\text{C}$ [9] than tellurite based glass with $\Delta T = 27\text{ }^\circ\text{C}$ [10]. Quantum efficiencies for $^4\text{F}_{3/2} \rightarrow ^4\text{I}_{11/2}$ (Nd^{3+}) and $^4\text{I}_{13/2} \rightarrow ^4\text{I}_{15/2}$ (Er^{3+}) transitions of rare earth ions in germanate glasses based on $\text{GeO}_2\text{-BaO-Ga}_2\text{O}_3$ are close to 80% [11] and 71% [12], respectively. Their values are also larger compared to main near-infrared laser transitions of Nd^{3+} ($\eta = 68\%$) and Er^{3+} ($\eta = 46\%$) ions in glasses based on $\text{TeO}_2\text{-ZnO}$ [13,14]. Various glass-modifiers were tested in order to obtain thermally stable and amorphous systems with excellent luminescence properties. Systematic studies clearly indicate that the effect of modifier oxides on emission properties of rare earth ions in different glass matrices is significant [15]. Influence of modifier oxides M_2O where M denotes Li, Na, K, Rb, Cs [16], MO where $\text{M} = \text{Ca, Sr, Ba}$ [17,18], M_2O_3 where $\text{M} = \text{Al or Ga}$ [19] and MO_2 where $\text{M} = \text{Te, Ge, Si}$ [20] on local

structure of glasses and their multifunctional properties and potential applications has been presented and discussed. Special attention has been paid to germanate glasses with different glass-modifiers. High niobium oxide content in alkali germanate glasses was evidenced by the optical absorption, DSC and XRD analysis, FT-IR, and Raman spectroscopy. Marcondes et al. [21] suggest that high niobium oxide content causes an increase in the glass-host network and strongly modifies thermal, structural, and optical properties of alkali germanate glasses. These structural and optical aspects for Eu^{3+} doped germanate glasses modified by MO/MF_2 where M denotes Ca, Sr, Ba, have been also studied [22]. In particular, the influence of the oxide and fluoride glass-modifiers on local structure of germanate glasses has been examined using X-ray diffraction analysis. The experimental results clearly demonstrate that samples with modifiers MO/MF_2 ($\text{M} = \text{Ca}$ or Sr) are crystalline, whereas samples with BaO and/or BaF_2 are fully amorphous. Further studies revealed that modification of germanate glasses by P_2O_5 allows control of their local structure and visible luminescence. The increase of P_2O_5 content leads to the reduction of spectral linewidth and the shift of emission band of Eu^{3+} ions in germanate glass to shorter wavelengths [23]. The effect of the spectroscopic properties of Tm^{3+} ions for different compositions with varying $\text{Nb}_2\text{O}_5/\text{La}_2\text{O}_3$ ratios has been studied and the optical concentration of glass components for efficient 1.8 μm near-infrared laser applications was determined [24]. Rare earth-doped germanate glasses modified by Bi_2O_3 [25], Y_2O_3 and Nb_2O_5 [26] have been also analyzed for mid-infrared emission. These aspects were not yet examined for germanate-based glass in the presence of titanium dioxide.

In the present work, multicomponent glasses based on $\text{TiO}_2\text{-GeO}_2\text{-BaO-Ga}_2\text{O}_3\text{-M}_2\text{O}_3$ (M —rare earth or transition metal) were successfully synthesized using conventional high-temperature melting and their structure and properties are presented and compared to the glasses in the absence of TiO_2 . Local structure and properties of multicomponent glasses containing two glass-network formers GeO_2 and TiO_2 were characterized using various experimental techniques: X-ray diffraction (XRD), differential scanning calorimetry (DSC), electron paramagnetic resonance (EPR), Raman and Fourier-transform infrared spectroscopy (FT-IR), absorption and luminescence spectroscopy. Transition metal (Cr^{3+}) and rare earth (Eu^{3+}), commonly known as spectroscopic probe, were used as the optical dopants. Our new preliminary results for titanate-germanate glasses are presented and discussed in relation to potential visible (Eu^{3+}) and near-infrared (Cr^{3+}) luminescence applications. In particular, luminescence spectra and decay curves were examined for glass samples, where germanium dioxide was substituted by titanium dioxide and the relative molar ratio of these two main glass-former components is equal to $\text{GeO}_2:\text{TiO}_2 = 1:1$. In previous work TiO_2 was substituted by GeO_2 in multicomponent germanoniobophosphate glass system allowing the glass stabilization against devitrification and the improvement of photoluminescence behavior, but amount of titanium dioxide playing the role as glass-network modifier did not exceed 15 molar % [27].

2. Materials and Methods

Multicomponent glasses undoped and doped with transition metal or rare earth were prepared: $30\text{TiO}_2\text{-}30\text{GeO}_2\text{-}30\text{BaO-}10\text{Ga}_2\text{O}_3$ (referred as TiGe), $30\text{TiO}_2\text{-}30\text{GeO}_2\text{-}30\text{BaO-}9.75\text{Ga}_2\text{O}_3\text{-}0.25\text{Cr}_2\text{O}_3$ (TiGe-Cr), $30\text{TiO}_2\text{-}30\text{GeO}_2\text{-}30\text{BaO-}9.75\text{Ga}_2\text{O}_3\text{-}0.5\text{Eu}_2\text{O}_3$ (TiGe-Eu) and their structure and properties were compared to glass samples without titanium dioxide $60\text{GeO}_2\text{-}30\text{BaO-}10\text{Ga}_2\text{O}_3$ (referred as Ge), $60\text{GeO}_2\text{-}30\text{BaO-}9.75\text{Ga}_2\text{O}_3\text{-}0.25\text{Cr}_2\text{O}_3$ (Ge-Cr), and $60\text{GeO}_2\text{-}30\text{BaO-}9.75\text{Ga}_2\text{O}_3\text{-}0.5\text{Eu}_2\text{O}_3$ (Ge-Eu). The concentrations of components are given in molar %. Titanate-germanate glasses were synthesized using high-temperature melt quenching-technique. The appropriate amounts of glass components (metal oxides of high purity 99.99%, Aldrich Chemical Co., St. Louis, MO, USA) were mixed and melted (1200 °C/0.45 h).

The amorphous nature of samples was confirmed by X-ray diffraction measurements (X'Pert Pro diffractometer, Panalytical, Almelo, The Netherlands) with $\text{Cu K}\alpha_1$ radiation ($\lambda = 1.54056 \text{ \AA}$). The Cu X-ray tube operating at 40 kW/30 mA was used. Diffraction patterns were measured in step-scan mode with a step size of 0.05° and time per step of 10 s. The glass samples were characterized

by a SETARAM Labsys thermal analyzer (SETARAM Instrumentation, Caluire, France) using the DSC method. The DSC curves were acquired with heating rate of 10 °C /min.

The electron paramagnetic resonance spectra were performed using Bruker EMX EPR spectrometer (Bruker-Biospin, Karlsruhe, Germany) working at X-band frequency (9.8 GHz). The EPR instrument parameters are as follows: central field 3480 G, modulation amplitude 2.0 G, time constant 40.96, gain 1×10^4 G, and microwave power 20.12 mW. The infrared spectra using the ATR technique were recorded over the frequency range of 1000–350 cm^{-1} using a Nicolet™ iS™ 50 FT-IR spectrometer (Thermo Fisher Scientific, Waltham, MA, USA) with a diamond attenuated total reflectance (ATR) module. The Raman spectra using a Thermo Fisher Scientific™ DXR™2xi Raman Imaging Microscope and laser working as the source (24 mW power) with excitation wavelength 780 nm were measured. The laser was directly focused on the glass sample with an Olympus long-working-distance microscope objective (50×).

Next, the glass samples were characterized using absorption (Varian Cary 5000 UV-VIS-NIR spectrophotometer, Agilent Technology, Santa Clara, CA, USA) and luminescence spectroscopy (laser equipment, which consists of PTI QuantaMaster QM40 spectrofluorometer, tunable pulsed optical parametric oscillator (OPO), Nd:YAG laser (Opotek Opolette 355 LD, Carlsbad, CA, USA), double 200 mm monochromators, multimode UVVIS PMT R928 and Hamamatsu H10330B-75 detectors (Hamamatsu, Bridgewater, NJ, USA), PTI and ASOC-10 USB-2500 oscilloscope). Resolution for spectral measurements was ± 0.1 nm, whereas decay curves with accuracy ± 0.5 μs were acquired.

3. Results and Discussion

3.1. Undoped Titanate-Germanate Glasses

Titanate-germanate glasses were successfully synthesized and their structure and properties were examined using XRD, DSC, FT-IR, and Raman spectroscopy. Figure 1 shows XRD patterns (a, b), DSC curves (c, d), FT-IR (e), and Raman (f) spectra for titanate-germanate glasses referred as TiGe. They are compared to the results obtained for glass samples without titanium dioxide (Ge).

The received glass samples (TiGe and Ge) reveal X-ray diffraction patterns characteristic for amorphous systems and narrow diffraction lines typical for crystalline materials are not observed. Moreover, any significant structural changes in the XRD patterns have been observed for glass samples after transition metal (TiGe-Cr) or rare earth (TiGe-Eu) doping. It clearly indicates that titanate-germanate glasses are able to accommodate transition metal or rare earth ions and the samples are still fully amorphous. Our previous studies for lead borate glasses demonstrated that rare earth oxides influence on the resistance to crystallization. In contrast to sample with Nd_2O_3 , several crystalline peaks due to the ErBO_3 phase are present after addition of Er_2O_3 to the base lead borate glass, suggesting the increased tendency toward crystallization [28]. From DSC curves measured for glass samples (TiGe and Ge), the glass transition temperature T_g and thermal stability parameter ($\Delta T = T_x - T_g$) were determined. In contrast to germanate glass (Ge), the additional exothermic peak representing the crystallization of the glass can be observed for glass sample with the presence of TiO_2 . It is well evidenced that the thermal stability parameter is reduced where GeO_2 is partially replaced by TiO_2 . The glass transition temperature T_g increases from 620 °C to 690 °C suggesting less open glass structure [29]. These thermal parameters T_g and ΔT are also schematized on Figure 1c. The Raman and FT-IR spectra between 350 cm^{-1} and 1000 cm^{-1} frequency region consists of two main bands centered at about 500 cm^{-1} and 800 cm^{-1} . Similar to previous reports for germanate-based glasses [30,31], the low-frequency band located from 400 cm^{-1} to 600 cm^{-1} is assigned to bending vibration involving Ge-O-Ge and Ge-O-Ga bridges, whereas the high-frequency band between 700 cm^{-1} and 900 cm^{-1} is attributed to asymmetric stretching vibrations of Ge-O-Ge bonds and symmetric stretching of Ge-O/Ga-O bonds. In general, Raman and FT-IR bands are shifted to lower frequency region in the presence of TiO_2 . Kamitsos et al. [31] observed similar effects for germanate glasses in function of Rb_2O . In the 630–700 cm^{-1} frequency region, the additional band located near 650 cm^{-1} is quite well observed

for glass sample with titanium dioxide. This band is due to the stretching vibration of Ti-O in TiO_6 unit [32].

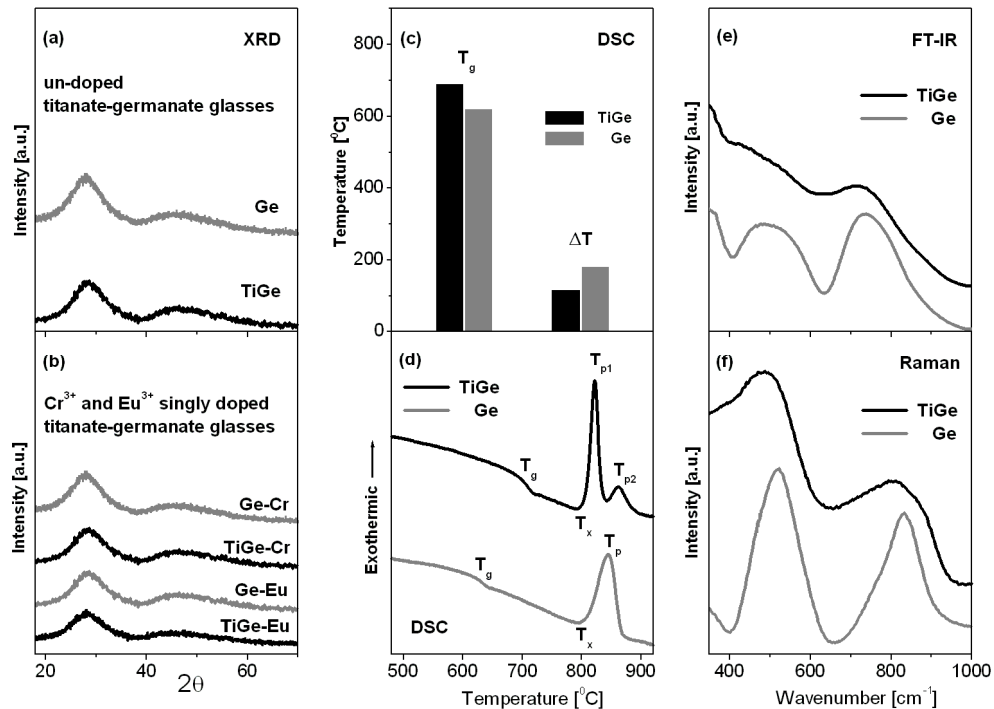


Figure 1. X-ray diffraction patterns (a,b), thermal parameters T_g and ΔT (c) and DSC curves (d), FT-IR (e) and Raman (f) spectra measured for titanate-germanate glasses (TiGe) and compared to glass samples without TiO_2 (Ge).

3.2. Titanate-Germanate Glasses Doped with Chromium Ions

Figure 2 shows results for titanate-germanate glasses doped with chromium ions, which were characterized using EPR (a), absorption (b), and luminescence (c–f) spectroscopy. Independently on samples with the presence (TiGe-Cr) or absence (Ge-Cr) of TiO_2 , the EPR spectra show two resonant signals at about $g = 4.8$ and $g = 1.97$, which evidently proves the 3+ valence state for chromium ions and the octahedral coordination. The similar effects were observed earlier for trivalent chromium ions in lead niobium germanosilicate glasses [33] and antimony phosphate glasses [34]. These two resonance signals may be quite well interpreted. They are related to the isolated Cr^{3+} ions ($g = 4.8$) and the exchange coupled pairs $\text{Cr}^{3+}\text{-Cr}^{3+}$ ($g = 1.97$) [35]. The presence of chromium ions at trivalent state in the studied glass systems was also confirmed by the absorption spectra measurements. The spectra measured in 550–800 nm ranges show characteristic broad absorption band, which consist of three overlapped peaks due to transitions originating from 4A_2 ground state to the 4T_2 , 2T_1 , and 2E excited states of trivalent chromium, respectively. Comparing to sample Ge-Cr, the $^4A_2 \rightarrow ^2E$ transition of Cr^{3+} ions is shifted to longer wavelengths in the presence of titanium dioxide (TiGe-Cr). At this moment, it should be also noticed that the second absorption band associated to the $^4A_2 \rightarrow ^4T_1$ transition of Cr^{3+} ions is located at about 430 nm. This band has not been observed for several glasses, because it is masked by strong UV-vis absorption of the host or lies on the tail of absorption edge. However, both absorption bands of chromium ions were successfully measured by us for barium gallo-germanate glass. Thus, some important spectroscopic parameters were calculated owing to the Tanabe-Sugano diagram for d^3 electronic configuration suggesting that chromium ions in barium gallo-germanate glass are in an intermediate octahedral ligand field environment ($2.1 < Dq/B < 2.3$).

The crystal field parameters, the Racah parameters, and the related ligand field parameters are as follows: $Dq = 1557 \text{ cm}^{-1}$, $B = 732 \text{ cm}^{-1}$, $C = 2991 \text{ cm}^{-1}$, and $Dq/B = 2.13$ [36].

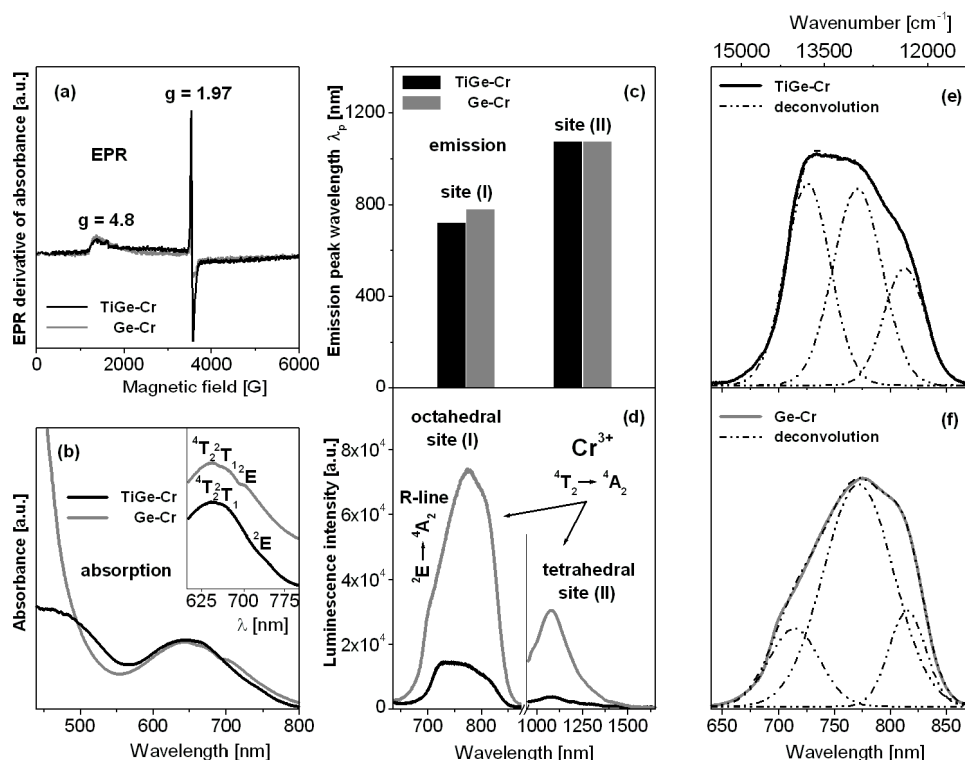


Figure 2. EPR (a), absorption (b), and luminescence (c,d) spectra measured for titanate-germanate glasses doped with chromium ions (TiGe-Cr) and compared to glass samples without TiO_2 (Ge-Cr). Deconvoluted emission bands for both glass samples TiGe-Cr (e) and Ge-Cr (f) are also given.

The near-infrared luminescence spectra of chromium ions revealed two emission bands, but both well observed lines are assigned to the transition originating from the 4T_2 excited state to the 4A_2 ground state. According to the excellent paper published recently, the near-infrared emission bands centered at about 730 nm and 1030 nm are related to the $^4T_2 \rightarrow ^4A_2$ transitions in octahedral sites (I) and tetrahedral sites (II) of chromium ions [37]. Further spectroscopic analysis indicates that the intensities of luminescence bands are stronger for chromium ions located at octahedral site (I) than tetrahedral site (II). The maximum of emission peak wavelength for the $^4T_2 \rightarrow ^4A_2$ transition of chromium ions in octahedral sites (I) is changed from 730 nm (Ge-Cr) to 775 nm in the presence of titanium dioxide (TiGe-Cr) in contrast to tetrahedral site (II), where both peak maxima are the same. Furthermore, the profiles of emission bands associated to transition of chromium ions in site (I) are completely different. It is especially evidenced for the $^2E \rightarrow ^4A_2$ transition commonly known as R-line, which is overlapped with the $^4T_2 \rightarrow ^4A_2$ transition of chromium ions in octahedral site (I). The maximum of R-line is shifted to longer wavelength from 715 nm (Ge-Cr) to 727 nm (TiGe-Cr). In order to further study the structural changes occurring in the arrangement around Cr^{3+} , the emission bands were successfully deconvoluted into three Gaussian components. The luminescence band ascribed to the $^4T_2 \rightarrow ^4A_2$ transition was well divided into the red and the blue components, confirming the coexistence of two completely different site distributions for chromium ions. During the deconvolution procedure, peak wavenumber (ν), linewidth ($\Delta\nu$), the energy gap between both 4T_2 and 2E excited states $\Delta E = E(^2E) - E(^4T_2)$, and the relative integrated emission line intensities $I(^2E)/I(^4T_2) = A_{\text{R-LINE}}/(A_{\text{RED}} + A_{\text{BLUE}})$ and $I(^2E)/I_{\text{TOTAL}} = A_{\text{R-LINE}}/(A_{\text{RED}} + A_{\text{BLUE}} + A_{\text{R-LINE}})$ were estimated. The $A_{\text{RED}} + A_{\text{BLUE}} + A_{\text{R-LINE}}$ denotes the integrated

emission intensities of the red and the blue components of 4T_2 as well as 2E (R-line), respectively. The relative integrated intensities of the bands were measured in order to monitor the equilibrium position between the 4T_2 and 2E excited states of chromium. The results are summarized in Table 1.

Table 1. Spectroscopic parameters for chromium ions in glasses TiGe-Cr and Ge-Cr.

Spectroscopic Parameter	TiGe-Cr	Ge-Cr
$\nu_{\text{RED}} ({}^4T_2)$ (cm $^{-1}$)	12,326	12,266
$\nu_{\text{BLUE}} ({}^4T_2)$ (cm $^{-1}$)	12,963	12,981
$\nu_{\text{R-LINE}} ({}^2E)$ (cm $^{-1}$)	13,755	13,986
ΔE (cm $^{-1}$)	792	1005
$d\nu_{\text{RED}} ({}^4T_2)$ (cm $^{-1}$)	518	480
$d\nu_{\text{BLUE}} ({}^4T_2)$ (cm $^{-1}$)	711	900
$d\nu_{\text{R-LINE}} ({}^2E)$ (cm $^{-1}$)	838	1082
$I({}^2E)/I({}^4T_2)$	0.63	0.21
$I({}^2E)/I_{\text{TOTAL}}$	0.39	0.17

Our calculations give interesting results. The energy gap between the 4T_2 and 2E excited states of chromium ions increases significantly from 792 cm $^{-1}$ (TiGe-Cr) to 1005 cm $^{-1}$ in the glass sample with the absence of titanium dioxide (Ge-Cr). The relative integrated emission line intensities denoted as A_{RED} , A_{BLUE} , and $A_{\text{R-LINE}}$ due to the ${}^4T_2 \rightarrow {}^4A_2$ and ${}^2E \rightarrow {}^4A_2$ transitions of chromium ions are also drastically changed. Thus, the relative integrated line intensity ratios of $I({}^2E)/I({}^4T_2)$ and $I({}^2E)/I_{\text{TOTAL}}$ are increased with the presence of TiO $_2$ in glass composition. The appropriate relative integrated line intensity ratios increase from 0.21 to 0.63 ($I({}^2E)/I({}^4T_2)$) and from 0.17 to 0.39 ($I({}^2E)/I_{\text{TOTAL}}$), when GeO $_2$ was partially substituted by TiO $_2$, respectively. It suggests that chromium ions occupy higher crystal-field sites in germanate glasses in the presence of TiO $_2$. Completely different situation was observed previously for chromium ions in lead borate glass. The energy gap between 4T_2 and 2E states was changed from 1055 cm $^{-1}$ (PbO:B $_2$ O $_3$ = 1:1) to 770 cm $^{-1}$ (PbO:B $_2$ O $_3$ = 4:1). In this case, the same Gaussian-fitting procedure was applied to evaluate spectroscopic parameters. The relative integrated line intensity ratios were nearly twice reduced, suggesting the presence of chromium ions in lower crystal-field sites with increasing PbO concentration [38].

Spectroscopic results for the studied glasses suggest that photoluminescence properties of chromium ions depend critically on titanium dioxide. For germanate glass in presence of TiO $_2$ (TiGe-Cr), the Cr $^{3+}$ ions are located in the higher crystal field and, thus, the emission of sharp R-line arising from the spin-forbidden ${}^2E \rightarrow {}^4A_2$ transition is more intense. When the Cr $^{3+}$ ions are located in the lower crystal field, broadband emission originating from the spin-allowed ${}^4T_2 \rightarrow {}^4A_2$ transition is dominated (Ge-Cr). There is in a good agreement with the results obtained previously for fluoride-sulfophosphate glasses, which are promising hosts for broadband optical amplification through transition metal activators [39].

3.3. Titanate-Germanate Glasses Doped with Europium Ions

Excitation (Figure 3a) and emission (Figure 3b) spectra, and decay curves (Figure 3c) measured for titanate-germanate glasses doped with europium ions (TiGe-Eu) are presented in Figure 3. The results are compared to glass samples without TiO $_2$ (Ge-Eu). All changes are also schematized on Figure 3d–f.

The excitation spectrum consists of several bands, which originate from the 7F_0 ground state to the higher-lying 5D_2 , 5D_3 , 5L_6 , 5L_7 , 5G_1 , and 5D_4 excited states of europium ions. The most intense bands are due to ${}^7F_0 \rightarrow {}^5L_6$ (near 390 nm) and ${}^7F_0 \rightarrow {}^5D_2$ (near 460 nm) transitions. The later transition is known as the pure electronic transition (PET). In this spectral region, the phonon sideband (PSB) is also located and associated with the pure electronic transition (PET). The difference between the positions of both PSB and PET bands is well-known as the phonon energy of the host. Our studies indicate that the phonon energy of the glass host is reduced from 790 cm $^{-1}$ (Ge-Eu) to 765 cm $^{-1}$ with the presence of TiO $_2$ (TiGe-Eu). From phonon sideband measurements [40–42], the electron–phonon

coupling strength g can be also estimated, which is due to the intensity ratio of the PSB ($\int I_{\text{PSB}} d\nu$) to the PET ($\int I_{\text{PET}} d\nu$), respectively. The results are given in Table 2.

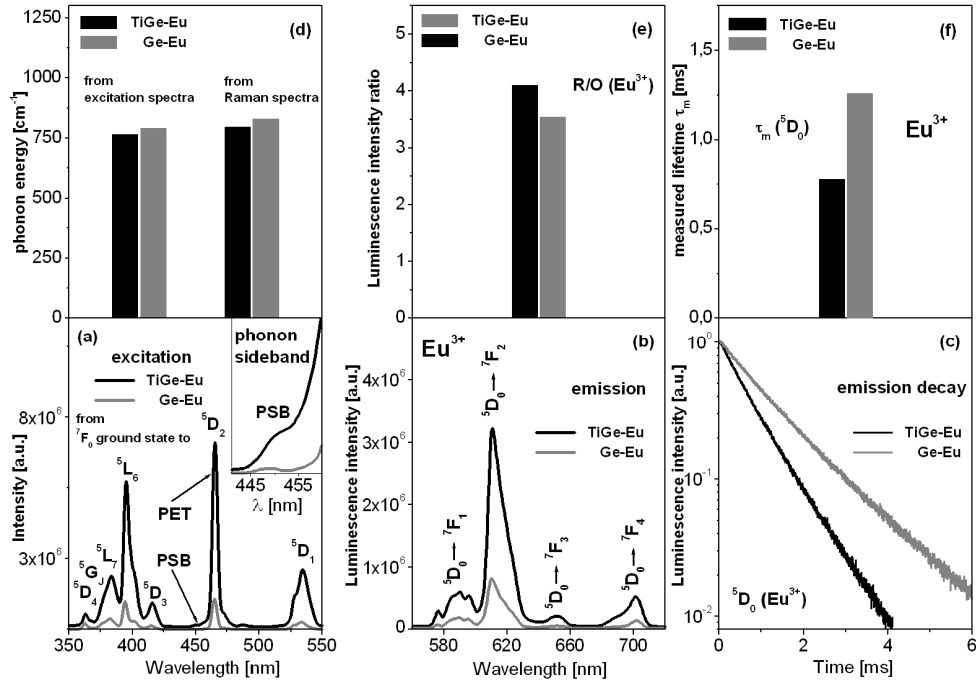


Figure 3. Excitation (a) and emission (b) spectra, and decay curves (c) for titanate-germanate glasses doped with europium ions (TiGe-Eu) and compared to glass samples without TiO_2 (Ge-Eu). All changes are also schematized (d–f).

Table 2. Spectroscopic parameters for europium ions in glasses TiGe-Eu and Ge-Eu.

Spectroscopic Parameter	TiGe-Eu	Ge-Eu
PSB-PET (cm^{-1})	765	790
Electron-phonon coupling strength g ($\times 10^{-3}$)	1.7	5.2
Non-radiative relaxation rate $W_p(T)/W_0(0)$ (s^{-1})		
from ${}^5\text{D}_1$ state	6.85×10^{-7}	1.37×10^{-5}
from ${}^5\text{D}_2$ state	4.87×10^{-10}	3.66×10^{-8}

Finally, the multiphonon relaxation rate $W_p(T)$ depending on the electron–phonon coupling strength and phonon energy of the glass host can be determined as follows $W_p(T) = W_0(0)\exp(-\alpha\Delta E)$, where $W_0(0)$ is the transition probability extrapolated to zero energy gap, ΔE denotes the energy gap between neighboring energy states and the values of ${}^5\text{D}_1$ – ${}^5\text{D}_0$ and ${}^5\text{D}_2$ – ${}^5\text{D}_1$ energy gaps of Eu^{3+} ions are equal nearly to 1750 cm^{-1} and 2500 cm^{-1} , respectively. In this relation the α parameter is close to $(\ln(p/g)-1)/h\omega$, where $h\omega$ represents the phonon energy, g —the electron-phonon coupling strength, and p as the phonon number is equal to $\Delta E/h\omega$. In some cases, the multiphonon relaxation rate is given as $W_p(T)/W_0(0)$ [43]. Our spectroscopic calculations presented in Table 2 clearly indicate that the electron-phonon coupling strength and multiphonon relaxation rates from the ${}^5\text{D}_1$ and ${}^5\text{D}_2$ states of europium ions are significantly smaller for glass sample with the presence of titanium dioxide.

Further experimental investigations shown on Figure 3 suggest that titanate-germanate glass demonstrates the efficient reddish-orange emission independently on the excitation wavelengths at 390 nm (${}^5\text{L}_6$ state) or 460 nm (${}^5\text{D}_2$ state) and its intensity is considerably higher in comparison to the

glass sample without titanium dioxide. The emission bands correspond to the electronic transitions originating from the 5D_0 state to the 7F_J ($J = 1-4$) states of europium ions, respectively.

In order to evaluate the glass asymmetry and the strength of bonding (covalent/ionic character) between europium ions and their surroundings, the ratio of integrated band intensity of $^5D_0 \rightarrow ^7F_2$ transition to that of the $^5D_0 \rightarrow ^7F_1$ transition, well-known in literature as red-to-orange factor R/O (Eu^{3+}), was calculated. It is generally accepted that the value of R/O (Eu^{3+}) starts to increase with increasing local asymmetry and covalent bonding. This phenomenon is just observed for our glass sample with the presence of titanium dioxide. For the studied systems, the fluorescence intensity ratio R/O (Eu^{3+}) was changed from 3.54 (Ge-Eu) to 4.10 (TiGe-Eu).

Based on decay curve measurements, the luminescence lifetimes for the 5D_0 state of europium ions were also determined. In general, the multiphonon relaxation rates decrease with decreasing phonon energy of the glass-host and consequently the lifetimes measured for excited states of rare earths are usually enhanced. Completely opposite situation is observed for europium ions, because the energy gap between 5D_0 state and lower-lying 7F_6 state of europium ions is very large. Its value seems to be nearly $12,500 \text{ cm}^{-1}$. In this case, several phonons are needed to bridge energy gap and radiative relaxation is a dominant transition. For low-phonon glass systems containing europium ions, the non-radiative relaxation rate is negligibly small in contrast to the radiative relaxation rate. Thus, the nonradiative relaxation rate can be ignored. In a practice, the radiative relaxation rate represents total relaxation rate. The spectroscopic consequence is reduction of luminescence lifetime (as an inverse of total radiative relaxation rate) for the 5D_0 state of europium ions with decreasing phonon energy of the glass-host. These phenomena were presented and discussed in our previous published work [44]. The analysis of luminescence decay curves for glass samples with the presence and absence of titanium dioxide confirms the hypothesis given above. The measured lifetime τ_m for the 5D_0 state of europium ions is reduced from 1.26 ms (Ge-Eu) to 0.78 ms (TiGe-Eu), when the phonon energy decreases from 790 cm^{-1} to 765 cm^{-1} for glass sample with the presence of TiO_2 . It suggests that the influence of titanium dioxide on spectroscopic parameters of europium ions is significant. The changes of phonon energy, fluorescence intensity ratio R/O, and 5D_0 measured lifetime of Eu^{3+} ions in function of TiO_2 are also schematized in Figure 3d–f.

The effects of TiO_2 on luminescence behavior of germanate glass depend greatly on the kind of active dopants (transition metal or rare earth). Luminescence properties of germanate glasses in the presence of TiO_2 are completely different for europium ions than chromium ions discussed in previous Part 3.2. In particular, the intensities of luminescence bands of the optically active ions are changed drastically, when GeO_2 was substituted by TiO_2 in the glass composition. The intensities of luminescence bands of chromium ions are reduced, whereas the emission band intensities of europium ions increase significantly in the presence of TiO_2 . Compared to the results for similar glass-hosts published recently [45–48], we postulate that our multicomponent titanate-germanate glass doped with Eu^{3+} ions is suitable as red-emitting component for LED applications.

First of all, the significant advantage of our systems is the lower phonon energy of the host in comparison to other oxide glasses such as borate ($\sim 1400 \text{ cm}^{-1}$), phosphate ($\sim 1200 \text{ cm}^{-1}$), and silicate ($\sim 1050 \text{ cm}^{-1}$) systems [49–51]. It is assumed that glasses with low phonon energy are more suitable as host materials for rare earth ions because of less probable non-radiative relaxation process, which may result in a higher lifetime of the excited state. According to experimental results presented in Table 3, the luminescence lifetime for 5D_0 excited state evaluated for glass samples (Ge-Eu and TiGe-Eu) is similar to the values obtained for various germanate systems doped with europium ions [52–60]. However, as has already been discussed for low-phonon glass-hosts containing Eu^{3+} ions, the non-radiative relaxation process can be neglected. Thus, the luminescence lifetime as an inverse of total radiative relaxation rate reduces with decreasing phonon energy of the glass-host. Therefore, the value of lifetime for 5D_0 state in glass sample Ge-Eu (790 cm^{-1}) is longer than the value of lifetime for systems with titanium oxide (765 cm^{-1}), lead oxide (775 cm^{-1}), and bismuth oxide (770 cm^{-1}) [51–53]. Moreover, it was stated that the fluorescence intensity ratio R/O (Eu^{3+}) was

increased from 3.54 (Ge-Eu) to 4.10 (TiGe-Eu) for the glass samples and the value of this spectroscopic parameters is significantly higher than those of lead germanate glasses [52,57] antimony [55] and tellurium [56] oxides-modified germanate systems. The obtained value of the ratio R/O indicates the higher local asymmetry around the Eu^{3+} ions in the glass host. It is worth noting that this factor confirms that the addition of a high concentration of titanium dioxide to the germanate matrix does not prompt the crystallization process, although TiO_2 can be a nucleating agent in glass host. Taking this issue into consideration, further research is needed to determine if a thermally stable and fully amorphous system with relatively high titanium oxide content is a good candidate for optical materials, that may find potential use in photonic devices such as optical fibers and amplifiers.

Table 3. Comparison of spectroscopic parameters of Eu^{3+} -doped germanate glasses.

Glass Composition	R/O	τ_m (ms)	References
Ge-Eu	3.54	1.26	present work
TiGe-Eu	4.10	0.78	present work
PbO-GeO ₂ -Ga ₂ O ₃	3.06	1.11	[52]
Bi ₂ O ₃ -GeO ₂	3.94	1.03	[53]
GeO ₂ -Nb ₂ O ₅ -Li ₂ O	6.50	0.81	[54]
GeO ₂ -Nb ₂ O ₅ -Na ₂ O	9.00	0.76	[54]
GeO ₂ -Ga ₂ O ₃ -BaO-Sb ₂ O ₃	1.94	-	[55]
GeO ₂ -Ga ₂ O ₃ -BaO-TeO ₂	2.49	-	[56]
PbO-GeO ₂	2.86	-	[57]
Sb ₂ O ₃ -GeO ₂ -B ₂ O ₃ -Al ₂ O ₃ -Na ₂ O	1.80	-	[58]
GeO ₂ -B ₂ O ₃ -Al ₂ O ₃ -Lu ₂ O ₃ -Gd ₂ O ₃	-	1.43	[59]
GeO ₂ -PbO	-	1.10	[60]

4. Conclusions

Multicomponent titanate-germanate glasses undoped and doped with transition metal (Cr^{3+}) and rare earths (Eu^{3+}) were prepared and then characterized using various experimental techniques: DSC, XRD, EPR, FT-IR, Raman, and luminescence spectroscopy. X-ray diffraction analysis revealed that all received samples are fully amorphous. Thermal and structural studies indicate that the glass transition temperature increases and thermal stability factor is reduced, whereas the Raman and FT-IR bands are shifted to lower frequency region in the presence of TiO_2 . The EPR spectra show typical signals confirming the presence of Cr^{3+} ions at trivalent state and the octahedral coordination. From the excitation spectra (phonon sideband analysis) of Eu^{3+} , the phonon energy of the glass-host, the electron-phonon coupling strength, and the multiphonon relaxation rate were also determined.

In particular, luminescence spectra have been examined for glass samples, where germanium dioxide was substituted by titanium dioxide as well as the relative molar ratio of two glass-former components is equal to $\text{GeO}_2:\text{TiO}_2 = 1:1$. Near-infrared luminescence spectra of chromium ions show two emission bands near 730 nm and 1030 nm, which correspond to the ${}^4\text{T}_2 \rightarrow {}^4\text{A}_2$ transitions in octahedral and tetrahedral sites, respectively. Further spectral analysis suggests that chromium ions occupy higher crystal-field sites in germanate glass with the presence of titanium dioxide. Visible luminescence spectra of europium ions present characteristic emission bands associated to ${}^5\text{D}_0 \rightarrow {}^7\text{F}_j$ ($j = 1-4$) transitions. The red-to-orange fluorescence intensity ratio R/O and the luminescence lifetime for the ${}^5\text{D}_0$ state of europium were determined. The later parameter, i.e., the measured ${}^5\text{D}_0$ lifetime was reduced from 1.26 ms (Ge-Eu) to 0.78 ms (TiGe-Eu). This behavior is quite well correlated with the phonon energy, which decreases from 790 cm^{-1} to 765 cm^{-1} with the presence of titanium dioxide. The factor R/O was changed from 3.54 (Ge-Eu) to 4.10 (TiGe-Eu) suggesting the increase of local asymmetry and stronger covalent character of bonding between europium ions and their nearest surroundings in glass sample in the presence of TiO_2 .

Our spectroscopic studies clearly indicate that luminescence properties of multicomponent titanate-germanate glasses are completely different for transition metal ions than rare earth ions.

The intensities of emission bands of chromium ions are reduced, whereas the emission band intensities of europium ions increase drastically in the presence of TiO₂. The obtained results demonstrate that titanate-germanate glass doped with Eu³⁺ ions is a promising candidate for red luminescence applications.

Author Contributions: Conceptualization, W.A.P.; methodology, M.K., J.P. (Justyna Polak), E.P., and T.G.; formal analysis, W.A.P. and J.P. (Joanna Pisarska); investigation, M.K., K.K., J.P. (Justyna Polak), E.P., T.G., and J.P. (Joanna Pisarska); writing—original draft preparation, W.A.P.; writing—review and editing, W.A.P.; project administration, W.A.P.; funding acquisition, W.A.P. All authors have read and agreed to the published version of the manuscript.

Funding: This research was funded by National Science Centre (Poland), grant number 2018/31/B/ST8/00166.

Conflicts of Interest: The authors declare no conflict of interest.

References

- Chen, J.; Wei, C. Formation and structure of titanate glasses. *J. Non-Cryst. Solids* **1986**, *80*, 135–140.
- Fukushima, T.; Benino, Y.; Fujiwara, T.; Dimitrov, V.; Komatsu, T. Electronic polarizability and crystallization of K₂O–TiO₂–GeO₂ glasses with high TiO₂ contents. *J. Solid State Chem.* **2006**, *179*, 3949–3957. [[CrossRef](#)]
- Masai, H.; Fujiwara, T.; Benino, Y.; Komatsu, T. Large second-order optical nonlinearity in 30BaO–15TiO₂–55GeO₂ surface crystallized glass with strong orientation. *J. Appl. Phys.* **2006**, *100*, 023526. [[CrossRef](#)]
- Toloman, D.; Suci, R.; Leostean, C.; Regos, A.; Ardelean, I. The influence of TiO₂ concentration in some calcium-phosphate glasses. *Physica B* **2014**, *438*, 84–87. [[CrossRef](#)]
- Kirchhof, J.; Unger, S.; Dellith, J.; Scheffel, A. Diffusion in binary TiO₂–SiO₂ glasses. *Opt. Mater. Express* **2014**, *4*, 672–680. [[CrossRef](#)]
- Slavov, S.S.; Dimitriev, Y.B. Glass formation in the system Bi₂O₃–TiO₂–SiO₂. *J. Chem. Technol. Metall.* **2016**, *51*, 536–546.
- ElBatal, F.H.; Marzouk, M.A.; ElBatal, H.A. Optical and crystallization studies of titanium dioxide doped sodium and potassium silicate glasses. *J. Mol. Struct.* **2016**, *1121*, 54–59. [[CrossRef](#)]
- Freschi, C.D.; Gouveia, J.T.; Marcondes, L.; Ferrari, J.L.; Cassanjes, F.C.; Poirier, G. Crystallization of anatase TiO₂ in niobium potassium phosphate glasses. *Mater. Res.* **2017**, *20*, 502–508. [[CrossRef](#)]
- Pisarska, J.; Kowal, M.; Kochanowicz, M.; Zmojda, J.; Dorosz, J.; Dorosz, D.; Pisarski, W.A. Influence of BaF₂ and activator concentration on broadband near-infrared luminescence of Pr³⁺ ions in gallo-germanate glasses. *Opt. Express* **2016**, *24*, 2427–2435. [[CrossRef](#)]
- Walas, M.; Lewandowski, T.; Synak, A.; Lapiński, M.; Sadowski, W.; Kościelska, B. Eu³⁺ doped tellurite glass ceramics containing SrF₂ nanocrystals: Preparation, structure and luminescence properties. *J. Alloys Compd.* **2017**, *696*, 619–626. [[CrossRef](#)]
- Pisarska, J.; Sołtys, M.; Górny, A.; Kochanowicz, M.; Zmojda, J.; Dorosz, J.; Dorosz, D.; Sitarz, M.; Pisarski, W.A. Rare earth-doped barium gallo-germanate glasses and their near-infrared luminescence properties. *Spectrochim. Acta A* **2018**, *201*, 362–366. [[CrossRef](#)] [[PubMed](#)]
- Zur, L.; Janek, J.; Sołtys, M.; Pisarska, J.; Pisarski, W.A. Effect of BaF₂ content on luminescence of rare-earth ions in borate and germanate glasses. *J. Am. Ceram. Soc.* **2016**, *99*, 2009–2016. [[CrossRef](#)]
- Uppendra Kumar, K.; Prathyusha, V.A.; Babu, P.; Jayasankar, C.K.; Joshi, A.S.; Speghini, A.; Bettinelli, M. Fluorescence properties of Nd³⁺-doped tellurite glasses. *Spectrochim. Acta A* **2007**, *67*, 702–708. [[CrossRef](#)] [[PubMed](#)]
- Jaba, N.; Ben Mansour, H.; Kanoun, A.; Brenier, A.; Champagnon, B. Spectral broadening and luminescence quenching of 1.53 μm emission in Er³⁺-doped zinc tellurite glass. *J. Lumin.* **2009**, *129*, 270–276. [[CrossRef](#)]
- Ratnakaram, Y.C.A.; Balakrishna, A.; Rajesh, D. Effect of modifier oxides on absorption and emission properties of Eu³⁺ doped different lithium fluoroborate glass matrices. *Physica B* **2012**, *407*, 4303–4307. [[CrossRef](#)]
- O’Shaughnessy, C.; Henderson, G.S.; Nesbitt, H.W.; Bancroft, G.M.; Neuville, D.R. The influence of modifier cations on the Raman stretching modes of Qⁿ species in alkali silicate glasses. *J. Am. Ceram. Soc.* **2020**, *103*, 3991–4001. [[CrossRef](#)]

17. Yusub, S.; Rajyasree, C.; Ramesh Babu, A.; Vinaya Teja, P.M.; Krishna Rao, D. Influence of alkaline earth oxides (R = Ca, Sr and Ba) on spectroscopic and dielectric studies of iron doped RO–Na₂O–B₂O₃ glasses. *J. Non-Cryst. Solids* **2013**, *364*, 62–68. [[CrossRef](#)]
18. Janek, J.; Sołtys, M.; Żur, L.; Pietrasik, E.; Pisarska, J.; Pisarski, W.A. Luminescence investigations of rare earth doped lead-free borate glasses modified by MO (M = Ca, Sr, Ba). *Mater. Chem. Phys.* **2016**, *180*, 237–243. [[CrossRef](#)]
19. Sołtys, M.; Żur, L.; Pisarska, J.; Goryczka, T.; Pisarski, W.A. Selective oxide modifiers M₂O₃ (M = Al, Ga) as crystallizing agents in Er³⁺-doped lead phosphate glass host. *Ceram. Int.* **2015**, *41*, 4334–4339. [[CrossRef](#)]
20. Pisarski, W.A.; Pisarska, J.; Żur, L.; Goryczka, T. Structural and optical aspects for Eu³⁺ and Dy³⁺ ions in heavy metal glasses based on PbO–Ga₂O₃–XO₂ (X = Te, Ge, Si). *Opt. Mater.* **2013**, *35*, 1051–1056. [[CrossRef](#)]
21. Marcondes, L.M.; Maestri, S.; Sousa, B.; Goncalves, R.R.; Cassanjes, F.C.; Poirier, G.Y. High niobium oxide content in germanate glasses: Thermal, structural, and optical properties. *J. Am. Ceram. Soc.* **2018**, *101*, 220–230. [[CrossRef](#)]
22. Żur, L.; Janek, J.; Sołtys, M.; Goryczka, T.; Pisarska, J.; Pisarski, W.A. Structural and optical investigations of rare earth doped lead-free germanate glasses modified by MO and MF₂ (M = Ca, Sr, Ba). *J. Non-Cryst. Solids* **2016**, *431*, 145–149. [[CrossRef](#)]
23. Żmojda, J.; Kochanowicz, M.; Miluski, P.; Golonko, P.; Baranowska, A.; Ragiń, T.; Dorosz, J.; Kuwik, M.; Pisarski, W.A.; Pisarska, J.; et al. Luminescent studies on germanate glasses doped with europium ions for photonic applications. *Materials* **2020**, *13*, 2817. [[CrossRef](#)] [[PubMed](#)]
24. Peng, Y.-P.; Yuan, X.; Zhang, J.; Zhang, L. The effect of La₂O₃ in Tm³⁺-doped germanate-tellurite glasses for ~2 μm emission. *Sci. Rep.* **2014**, *4*, 5256. [[CrossRef](#)]
25. Ragiń, T.; Baranowska, A.; Kochanowicz, M.; Żmojda, J.; Miluski, P.; Dorosz, D. Study of mid-infrared emission and structural properties of heavy metal oxide glass and optical fibre co-doped with Ho³⁺/Yb³⁺ ions. *Materials* **2019**, *12*, 1238. [[CrossRef](#)]
26. Wei, T.; Chen, F.; Tian, Y.; Xu, S. Efficient 2.7 μm emission and energy transfer mechanism in Er³⁺ doped Y₂O₃ and Nb₂O₅ modified germanate glasses. *J. Quant. Spectrosc. Radiat.* **2014**, *133*, 663–669. [[CrossRef](#)]
27. de Mello, L.B.; Sigoli, F.A.; Mazali, I.O. Structural and optical properties of erbium and ytterbium codoped germanoniobophosphate glasses. *J. Am. Ceram. Soc.* **2014**, *97*, 2462–2470. [[CrossRef](#)]
28. Pisarski, W.A.; Goryczka, T.; Wodecka-Duś, B.; Płońska, M.; Pisarska, J. Structure and properties of rare earth-doped lead borate glasses. *Mater. Sci. Eng. B* **2005**, *122*, 94–99. [[CrossRef](#)]
29. Grujić, S.; Blagojević, N.; Tošić, M.; Živanović, V.; Božović, B. The effect of TiO₂ on the structure and devitrification behavior of potassium titanium germanate glass. *J. Therm. Anal. Cal.* **2006**, *83*, 463–466. [[CrossRef](#)]
30. Guerineau, T.; Strutynski, C.; Skopak, T.; Morency, S.; Hanafi, A.; Cazavara, F.; Ledemi, Y.; Danto, S.; Cardinal, T.; Messaddeq, Y.; et al. Extended germano-gallate fiber drawing domain: From germanates to gallates optical fibers. *Opt. Mater. Express* **2019**, *9*, 2437–2445. [[CrossRef](#)]
31. Kamitsos, E.I.; Yiannopoulos, Y.D.; Karakassides, M.A.; Chryssikos, G.D.; Jain, H. Raman and infrared structural investigation of xRb₂O-(1-x)GeO₂ glasses. *J. Phys. Chem.* **1996**, *100*, 11755–11765. [[CrossRef](#)]
32. Lu, M.; Wang, F.; Liao, Q.; Chen, K.; Qin, J.; Pan, S. FTIR spectra and thermal properties of TiO₂-doped iron phosphate glasses. *J. Mol. Struct.* **2015**, *1081*, 187–192. [[CrossRef](#)]
33. Narendrudu, T.; Suresh, S.; Chinna Ram, G.; Veeraiah, N.; Krishna Rao, D. Spectroscopic and structural properties of Cr³⁺ ions in lead niobium germanosilicate glasses. *J. Lumin.* **2017**, *183*, 17–25. [[CrossRef](#)]
34. De Vicente, F.S.; Santos, F.A.; Simões, B.S.; Dias, S.T.; Siu Li, M. EPR, optical absorption and luminescence studies of Cr³⁺-doped antimony phosphate glasses. *Opt. Mater.* **2014**, *38*, 119–125. [[CrossRef](#)]
35. Murali, A.; Rao, J.L. Electron paramagnetic resonance and optical absorption spectra of Cr³⁺ ions in fluorophosphate glasses. *J. Phys. Condens. Matter* **1999**, *11*, 1321–1331. [[CrossRef](#)]
36. Pisarska, J.; Kuwik, M.; Górný, A.; Dorosz, J.; Kochanowicz, M.; Żmojda, J.; Sitarz, M.; Dorosz, D.; Pisarski, W.A. Influence of transition metal ion concentration on near-infrared emission of Ho³⁺ in barium gallo-germanate glasses. *J. Alloys Compd.* **2019**, *793*, 107–114. [[CrossRef](#)]
37. Li, Y.; Ye, S.; Zhang, Q. Ultra-broadband near-infrared luminescence of ordered–disordered multi-sited Cr³⁺ in La₃Ga_{5.5}Nb_{0.5}O₁₄:Cr³⁺. *J. Mater. Chem. C* **2014**, *2*, 4636–4641. [[CrossRef](#)]

38. Pisarski, W.A.; Pisarska, J.; Dominiak-Dzik, G.; Ryba-Romanowski, W. Transition metal (Cr^{3+}) and rare earth (Eu^{3+} , Dy^{3+}) ions used as a spectroscopic probe in compositional-dependent lead borate glasses. *J. Alloys Compd.* **2009**, *484*, 45–49. [[CrossRef](#)]
39. Wang, W.C.; Le, Q.H.; Zhang, Q.Y.; Wondraczek, L. Fluoride-sulfophosphate glasses as hosts for broadband optical amplification through transition metal activators. *J. Mater. Chem. C* **2017**, *5*, 7969–7976. [[CrossRef](#)]
40. Ramachari, D.; Rama Moorthy, L.; Jayasankar, C.K. Phonon sideband spectrum and vibrational analysis of Eu^{3+} -doped niobium oxyfluorosilicate glass. *J. Lumin.* **2013**, *143*, 674–679. [[CrossRef](#)]
41. Manasa, P.; Jayasankar, C.K. Luminescence and phonon side band analysis of Eu^{3+} -doped lead fluorosilicate glasses. *Opt. Mater.* **2016**, *62*, 139–145. [[CrossRef](#)]
42. Rajesh, M.; Reddy, G.R.; Sushma, N.J.; Devarajulu, G.; Deva Prasad Raju, B. Phonon sideband analysis, structural and spectroscopic properties of Eu^{3+} ions embedded $\text{SiO}_2\text{-B}_2\text{O}_3\text{-CaF}_2\text{-NaF-Na}_2\text{O}$ glasses. *Opt. Mater.* **2020**, *107*, 110038. [[CrossRef](#)]
43. Vijaya Prakash, G.; Jagannathan, R. Fluorescence properties of Eu^{3+} doped lead bearing fluoro-chloro phosphate glasses. *Spectrochim. Acta A* **1999**, *55*, 1799–1808. [[CrossRef](#)]
44. Pisarski, W.A.; Żur, L.; Kowal, M.; Pisarska, J. Enhancement and quenching photoluminescence effects for rare earth - doped lead bismuth gallate glasses. *J. Alloys Compd.* **2015**, *651*, 565–570. [[CrossRef](#)]
45. Aryal, P.; Kim, H.J.; Khan, A.; Saha, S.; Kang, S.J.; Kothan, S.; Yamsuk, Y.; Kaewkhao, J. Development of Eu^{3+} -doped phosphate glass for red luminescent solid-state optical devices. *J. Lumin.* **2020**, *227*, 117564. [[CrossRef](#)]
46. Roy, J.S.; Messaddeq, Y. Photoluminescence study of Eu^{3+} doped zinc-tungsten-antimonite glasses for red LED applications. *J. Lumin.* **2020**, *228*, 117608. [[CrossRef](#)]
47. Lakshminarayana, G.; Wagh, A.; Kamath, S.D.; Dahshan, A.; Hegazy, H.H.; Marzec, M.; Kityk, I.V.; Lee, D.-E.; Yoon, J.; Park, T. Eu^{3+} -doped fluoro-telluroborate glasses as red-emitting components for W-LEDs application. *Opt. Mater.* **2020**, *99*, 109555. [[CrossRef](#)]
48. Maity, A.; Jana, S.; Ghosh, S.; Sharma, S. Spectroscopic investigation on europium (Eu^{3+}) doped strontium zinc lead phosphate glasses with varied ZnO and PbO compositions. *J. Non-Cryst. Solids* **2020**, *550*, 120322. [[CrossRef](#)]
49. Vázquez, G.V.; Muñoz, H.G.; Camarillo, I.; Falcony, C.; Caldiño, U.; Lira, A. Spectroscopic analysis of a novel Nd^{3+} -activated barium borate glass for broadband laser amplification. *Opt. Mater.* **2015**, *46*, 97–103. [[CrossRef](#)]
50. Mazurak, Z.; Bodył, S.; Lisiecki, R.; Gabryś-Pisarska, J.; Czaja, M. Optical properties of Pr^{3+} , Sm^{3+} and Er^{3+} doped $\text{P}_2\text{O}_5\text{-CaO-SrO-BaO}$ phosphate glass. *Opt. Mater.* **2010**, *32*, 547–553. [[CrossRef](#)]
51. Pisarska, J.; Zur, L.; Pisarski, W.A. Optical spectroscopy of Dy^{3+} ions in heavy metal lead-based glasses and glass-ceramics. *J. Mol. Struct.* **2011**, *993*, 160–166. [[CrossRef](#)]
52. Zur, L. Structural and luminescence properties of Eu^{3+} , Dy^{3+} and Tb^{3+} ions in lead germanate glasses obtained by conventional high-temperature melt-quenching technique. *J. Mol. Struct.* **2013**, *1041*, 50–54. [[CrossRef](#)]
53. Gökçe, M. Development of Eu^{3+} doped bismuth germanate glasses for red laser applications. *J. Non-Cryst. Solids* **2019**, *505*, 272–278. [[CrossRef](#)]
54. Guedes, L.F.N.; Marcondes, L.M.; Evangelista, R.O.; Batista, G.; Mendoza, V.G.; Cassanjes, F.C.; Poirier, G.Y. Effect of alkaline modifiers on the structural, optical and crystallization properties of niobium germanate glasses and glass-ceramics. *Opt. Mater.* **2020**, *105*, 109866. [[CrossRef](#)]
55. Szal, R.; Zmojda, J.; Kochanowicz, M.; Miluski, P.; Dorosz, J.; Leśniak, M.; Jeleń, P.; Starzyk, B.; Sitarz, M.; Kuwik, M.; et al. Spectroscopic properties of antimony modified germanate glass doped with Eu^{3+} ions. *Ceram. Int.* **2019**, *45*, 24811–24817. [[CrossRef](#)]
56. Jadach, R.; Zmojda, J.; Kochanowicz, M.; Miluski, P.; Leśniak, M.; Sołtys, M.; Pisarska, J.; Pisarski, W.A.; Lukowiak, A.; Sitarz, M.; et al. Spectroscopic properties of rare earth doped germanate glasses. *Proc. SPIE* **2018**, *10683*, 1068316.
57. Wachtler, M.; Speghini, A.; Gatterer, K.; Fritzer, H.P.; Ajò, D.; Bettinelli, M. Optical Properties of Rare-Earth Ions in Lead Germanate Glasses. *J. Am. Ceram. Soc.* **1998**, *81*, 2045–2052. [[CrossRef](#)]
58. Zmojda, J.; Kochanowicz, M.; Miluski, P.; Baranowska, A.; Pisarski, W.A.; Pisarska, J.; Jadach, R.; Sitarz, M.; Dorosz, D. Structural and optical properties of antimony-germanate-borate glass and glass-fiber co-doped Eu^{3+} and Ag nanoparticles. *Spectrochim. Acta A* **2018**, *201*, 1–7. [[CrossRef](#)]

59. Wang, X.; Huang, L.; Zhao, S.; Xu, S. Eu^{3+} doped heavy germanate scintillating glasses. *J. Lumin.* **2018**, *196*, 256–258. [[CrossRef](#)]
60. Bensalem, C.; Mortier, M.; Vivien, D.; Diaf, M. Thermal and optical investigation of EuF_3 -doped lead fluorogermanate glasses. *J. Non-Cryst. Solids* **2010**, *356*, 56–64. [[CrossRef](#)]



© 2020 by the authors. Licensee MDPI, Basel, Switzerland. This article is an open access article distributed under the terms and conditions of the Creative Commons Attribution (CC BY) license (<http://creativecommons.org/licenses/by/4.0/>).

P2

Karolina Kowalska, Marta Kuwik, Justyna Polak, Joanna Pisarska,

Wojciech A. Pisarski,

**EPR and optical spectroscopy of Cr³⁺ ions in barium gallo-germanate glasses
containing B₂O₃/TiO₂**

Journal of Luminescence 245 (2022) 118775



Contents lists available at ScienceDirect

Journal of Luminescence

journal homepage: www.elsevier.com/locate/jlumin

EPR and optical spectroscopy of Cr³⁺ ions in barium gallo-germanate glasses containing B₂O₃/TiO₂

Karolina Kowalska^{*}, Marta Kuwik, Justyna Polak, Joanna Pisarska, Wojciech A. Pisarski^{**}

Institute of Chemistry, University of Silesia, Szkolna 9 Street, 40-007, Katowice, Poland

ARTICLE INFO

Keywords:

Glasses
Transition metal ions
Spectroscopy
Structural properties
Near-infrared luminescence

ABSTRACT

The remarkable variety of glasses doped with transition metal ions is a major reason for the growing popularity of spectroscopic studies to identify their optical properties. This study presents interesting results of analyzing the relationship between structural and optical properties of multicomponent germanate glass systems doped with Cr³⁺ ions. The chemical composition of the developed glasses was changed as a function of boron oxide and titanium oxide. EPR studies showed that each glass system exhibits two resonance signals in the low and high magnetic fields, respectively. The optical properties of the fabricated glasses were analyzed by recording optical absorption, excitation, and emission spectra. The calculated spectroscopic parameters showed very well the changes of the crystal field strength around Cr³⁺ ions. The used approach perfectly demonstrates the changes in the profile of the recorded luminescence bands related to the ⁴T₂ → ⁴A₂ and ²E → ⁴A₂ transitions of trivalent chromium ions. These findings set a new direction in infrared photonics because show a way to effectively tune the unique optical properties of Cr³⁺ ions from the change of the chemical composition of the germanate glassy matrix.

1. Introduction

Inorganic glasses containing transition metal oxides have generated considerable recent research interest. This phenomenon is primarily advanced research undertaken by a broad group of scientists, presenting exciting correlations between the type of matrix and the spectroscopic properties of transition metal ions [1–3]. Particulars of interest are phosphate, silicate, or borate glasses. The last ones exhibit dielectric properties, while doped with V₂O₅ increases their semi-conducting nature [4]. The same transition metal oxide determines the thermal properties of tellurite glasses [5]. Studies of the effects of transition metal oxides on the local structure and properties of glasses are the fundamentals for the development of materials that are used in radiometric thermometry [6], cathode materials [7], and optical device applications [8,9].

It was published an excellent paper in 1996 by van Walree et al. [10] in which followed interesting changes in the luminescence decay of excited energy levels ⁴T₂ and ²E of Cr³⁺ ions in glasses whose main network-former component was germanium dioxide. Germanate glass belonging to the low-phonon glass family is characterized mainly by a

wide transparency window and a relatively high refractive index [11, 12]. Its additional advantage is also quite a high solubility of transition metal ions [13], hence it can be successfully used as starting material for optical applications. On the other hand, Cr³⁺ ions are one of the extremely sensitive activators used in inorganic glasses, being the main reason for the popularization of near-infrared device technology [14].

The different glass systems have distinct properties, however, it should be noted that each is characterized by the absence of long-range order. The trivalent chromium ions in the glassy phase occupy sites with different crystal field strengths [15]. From a scientific perspective, these aspects are the main motivation to undertake the analysis of the properties of chromium ions using appropriate research tools. The variation of the intensity, as well as the shifts of the resonance signals on the electron paramagnetic resonance (EPR) spectra, make it possible to determine the structural changes. When chromium ions playing an important role as paramagnetic ions are introduced into glass matrices, the EPR spectra exhibit two resonance signals in low and high magnetic fields, respectively. Effective g values equal to about 6 and 2 are assigned to isolated Cr³⁺ centers located in the strongly distorted octahedral sites, Cr³⁺ centers in cubic sites, and Cr³⁺ - Cr³⁺ paired centers

^{*} Corresponding author.

^{**} Corresponding author.

E-mail addresses: karolina.kowalska@us.edu.pl (K. Kowalska), wojciech.pisarski@us.edu.pl (W.A. Pisarski).

<https://doi.org/10.1016/j.jlumin.2022.118775>

Received 23 August 2021; Received in revised form 3 February 2022; Accepted 5 February 2022

Available online 7 February 2022

0022-2313/© 2022 Elsevier B.V. All rights reserved.

coupled by magnetic dipolar interaction [16–18].

Glasses intended directly to optical materials emitting infrared radiation must meet the criterion of the correct selection of an optically active dopant for the glassy matrix [19]. It is phenomenally presented by the NIR emission spectra of the fluorogermanate glass samples doped with Cr^{3+} , Ho^{3+} , and $\text{Cr}^{3+}/\text{Ho}^{3+}$ ions, respectively [20]. Controlling the unique luminescent properties of Cr^{3+} ions enable the modification of the content of network-former and network-modifier. R. Lachheb et al. [21] showed that the optical alkalinity of glasses strongly affects the increase in the intensity of the ${}^4\text{T}_2 \rightarrow {}^4\text{A}_2$ transition of Cr^{3+} . In the performed analysis of spectroscopic parameters for Cr^{3+} ions, the value of Dq/B is also a key issue [22]. Its value exceeding 2.3 may be the main reason for the appearance of the characteristic NIR emission line of Cr^{3+} so-called R-line. Actually, $\text{PbO-Nb}_2\text{O}_5\text{-GeO}_2\text{-SiO}_2$ based glass doped with 0.1 and 0.2 %mol Cr_2O_3 [23] is a quite good example of a material which emission is dominated by a narrow band corresponding to the ${}^2\text{E} \rightarrow {}^4\text{A}_2$ transition of Cr^{3+} . In this context, it is worth mentioning that Cr^{3+} ions, due to their emission in a surprisingly long wavelength range, are active components of laser medium and tunable solid-state laser medium. Thus, the synthesis and studies of chromium ions in amorphous materials are very attractive from both the scientific and application point of view. To summarize the discussion so far, the main aim of our work is to improve the knowledge of the structural and luminescence properties of chromium ions in germanate glasses containing TiO_2 and B_2O_3 .

In this paper, the Authors report the results of oxide glasses in $\text{GeO}_2\text{-B}_2\text{O}_3\text{-BaO-Ga}_2\text{O}_3$ and $\text{GeO}_2\text{-TiO}_2\text{-BaO-Ga}_2\text{O}_3$ compositions singly doped with Cr^{3+} ions, which were prepared using a high-temperature melt quenching technique. The resonance signals on the EPR spectra provided information about the local environment around the Cr^{3+} ions. The research issues highlighted in the next chapter are focused on the optical properties of the received glasses. It was presented and discussed based on the optical absorption, excitation, and emission spectra. In particular, emission properties of glasses have been investigated in the near-infrared range.

2. Experimental

Germanate glasses singly doped with chromium ions were synthesized using a high-temperature melt quenching-technique. It was assumed that the basic oxides in the developed glasses would be GeO_2 , TiO_2 , and B_2O_3 . The chemical composition and quantitative relationships of individual metal oxides are presented in Table 1. High-purity starting materials (99.99%, Aldrich Chemical Co.) were used for the synthesis. The appropriate amounts of metal oxides were mixed in an agate mortar, put into a corundum crucible, and then subjected to thermal treatment. The temperature of glass melting in an electric furnace was 1250 °C. The samples were melted for 1 h in the air atmosphere and, next, cooled to room temperature. Additionally, each glass sample was polished for optical measurements. As a result of the procedure, $\text{GeO}_2\text{-B}_2\text{O}_3\text{-BaO-Ga}_2\text{O}_3\text{-Cr}_2\text{O}_3$ and $\text{GeO}_2\text{-TiO}_2\text{-BaO-Ga}_2\text{O}_3\text{-Cr}_2\text{O}_3$ glass systems characterized by an intense green color were obtained.

Table 1

Molar compositions of the barium gallo-germanate glasses containing $\text{B}_2\text{O}_3/\text{TiO}_2$.

Glass code	% GeO_2	% B_2O_3	% TiO_2	% BaO	% Ga_2O_3	% Cr_2O_3
GBCr1	50	10	–	30	9.75	0.25
GBCr2	30	30	–	30	9.75	0.25
GBCr3	10	50	–	30	9.75	0.25
GTCr1	50	–	10	30	9.75	0.25
GTCr2	30	–	30	30	9.75	0.25
GTCr3	10	–	50	30	9.75	0.25

Electron paramagnetic resonance measurements of all samples were performed using a Bruker EMX EPR spectrometer (Bruker - Biospin, Karlsruhe, Germany) operating at X-band frequency (9.8 GHz). Next, an optical study of the glass samples was conducted. Absorption spectra in the wavelength range 400–800 nm were recorded using a Cary 5000 UV-VIS-NIR spectrophotometer (Agilent Technology Santa Clara, CA, USA). Measurements of excitation and emission spectra in the near-infrared range were carried out with the use of laser equipment, which consists of PTI QuantaMaster QM40 spectrofluorometer, tunable pulsed optical parametric oscillator (OPO), Nd:YAG laser (Opotek Opolette 355 LD, Carlsbad, CA, USA), double 200 mm monochromators, multimode UUVIS PMT R928 and Hamamatsu H10330B-75 detectors (Hamamatsu, Bridgewater, NJ, USA).

3. Results and discussion

3.1. Electron paramagnetic resonance studies

Investigations of glasses doped with transition metal ions using electron paramagnetic resonance spectroscopy (EPR) provide information on the effect of the individual components on the microstructure around the d-electron metal ions [24], which in the presented work consists of chromium ions. The EPR research is significant because the environment and the strength of the crystal field around the chromium ions change as a result of differences in binding to the ligands. The experimental EPR spectra of germanate glasses containing different concentrations of TiO_2 and B_2O_3 doped with Cr_2O_3 presented in Fig. 1 show resonance signals with two special features.

In the part of the spectrum corresponding to low magnetic field values, a centered asymmetric broad signal at $g = 4.8$ was registered. A second narrow, intense resonance signal with an effective g value = 1.97 was detected in the high magnetic field. Taking into account the signal intensity in the low magnetic field, it was observed that it is greater in germanate glasses containing boron oxide. On the other hand, germanate glasses with titanium dioxide show more intense resonance in the high magnetic field. Thus, it has been reported that the recorded two EPR signals as a function of the quantitative $\text{GeO}_2\text{:TiO}_2$ and $\text{GeO}_2\text{:B}_2\text{O}_3$ relationships indicate the occurrence of Cr^{3+} ions in different crystal field environments. Numerous scientific reports of EPR signals at $g = 4.8$ and $g = 1.97$ suggest that they only come from Cr^{3+} ions. The occurrence in the phosphate, silicate, and borate, glasses of a broad resonance signal in a low magnetic field is justified by the presence of isolated Cr^{3+} ion centers at strongly distorted octahedral sites only [25–27]. The devoted reports on the high field portion ($g = 1.97$) are attributed to the exchange-coupled pairs of anti-ferromagnetic $\text{Cr}^{3+} - \text{Cr}^{3+}$ [28,29]. However, the same resonance signal may be also due to Cr^{3+} isolated at the axially distorted octahedral site [30,31]. Further experiments indicate that the oxidation states of chromium ions present in the studied glass samples can be quite well detected using the EPR method. The EPR spectra recorded for silica glasses show two well-defined signals near $g = 1.97$ assigned to Cr^{3+} and Cr^{4+} ions and it was also confirmed by the absorption spectra measurements [32].

3.2. Optical studies

The optical absorption spectra for Cr^{3+} doped systems revealed two main bands near 430 nm and 600 nm, which correspond to ${}^4\text{A}_2 \rightarrow {}^4\text{T}_1$ (blue region) and ${}^4\text{A}_2 \rightarrow {}^4\text{T}_2$ (red region) transitions, respectively. For Cr^{4+} doped systems, two main absorption bands are located at about 500 nm and 1000 nm. They are assigned to ${}^3\text{A}_2 \rightarrow {}^3\text{T}_1$ (VIS) and ${}^3\text{A}_2 \rightarrow {}^3\text{T}_2$ (NIR) transitions of Cr^{4+} . All absorption transitions are quite well observed for $\text{Cr}^{3+}/\text{Cr}^{4+}$ co-doped systems [33,34]. In our case, the absorption spectra for barium gallo-germanate glasses containing B_2O_3 or TiO_2 present broad band characteristics for the d-d transition of chromium ions at a trivalent oxidation state. Fig. 2 (on left) shows the optical absorption spectra of Cr^{3+} -doped germanate glasses containing different

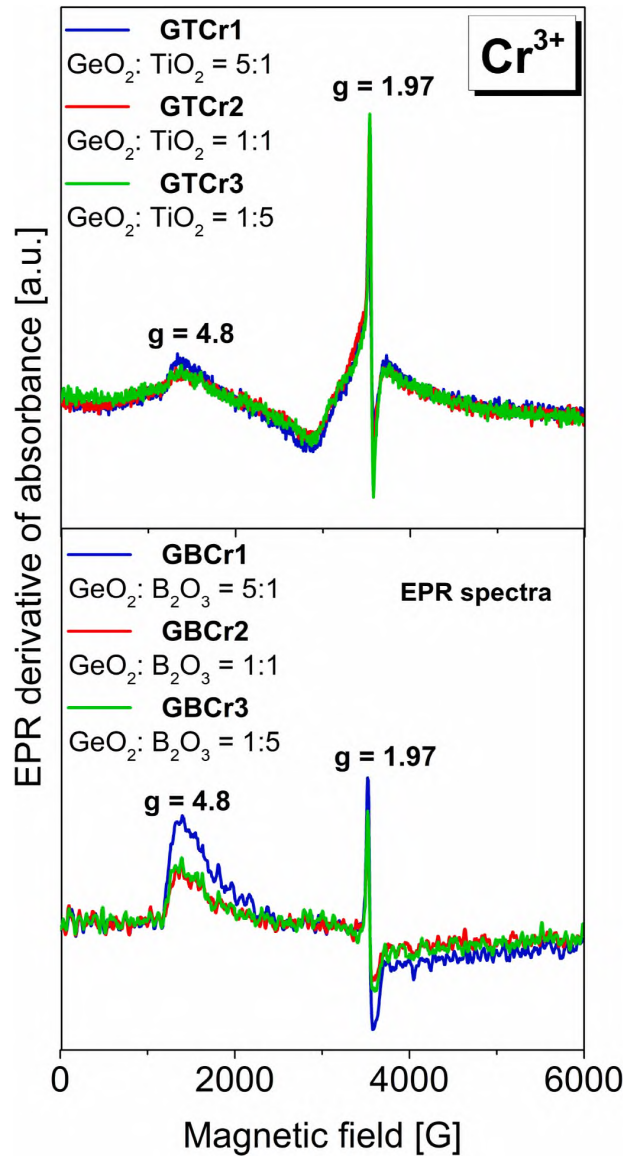


Fig. 1. EPR spectra as a function of $\text{TiO}_2/\text{B}_2\text{O}_3$ content for germanate glasses doped with chromium ions.

concentrations of titanium dioxide (GTCr) and boron oxide (GBCr). In the present study, the absorption spectra of all glasses recorded in the 400–800 nm range show a broad band. The registered absorption band corresponds to the transition ${}^4\text{A}_2 \rightarrow {}^4\text{T}_2$ of chromium ions.

Further spectroscopic analysis suggests the presence of a poorly resolved absorption band, which is attributed to the transition ${}^4\text{A}_2 \rightarrow {}^2\text{E}$ of Cr^{3+} ions. It was well demonstrated in Fig. 2 (on right). When B_2O_3 and TiO_2 were introduced to the base barium gallo-germanate glass, the absorption spectra are drastically changed. The changes in positions and spectral profiles of absorption bands are completely different for B_2O_3 than TiO_2 . For the GBCr glass series, the main broad absorption band due to transition ${}^4\text{A}_2 \rightarrow {}^4\text{T}_2$ of Cr^{3+} is shifted to higher wavenumbers with increasing B_2O_3 content. Independently on B_2O_3 concentration, the absorption band corresponding to transition ${}^4\text{A}_2 \rightarrow {}^2\text{E}$ of Cr^{3+} ions is located near 700 nm. The absorption spectra measurements for the GTCr glass series give interesting and rather unexpected results. In contrast to the GBCr series, the position of the broad absorption band due to

transition ${}^4\text{A}_2 \rightarrow {}^4\text{T}_2$ is nearly independent on glass-host, whereas the spin-forbidden transition ${}^4\text{A}_2 \rightarrow {}^2\text{E}$ of Cr^{3+} ions is shifted to higher wavenumbers with increasing TiO_2 content. It indicates that the absorption spectra measured for GTCr glass series are more complex and the observed changes may be due to so-called Fano resonance effect. Thus, the ${}^4\text{T}_2$ state can be lower-lying than the ${}^2\text{E}$ state of Cr^{3+} , when the concentration of TiO_2 is relatively high. This situation is rather rarely observed. It was demonstrated earlier for Cr^{3+} ions in crystals $\text{Cs}_2\text{NaScCl}_6$ [35] and $\text{Sc}_2(\text{MoO}_4)_3$ [36]. The spectral shift of transition ${}^4\text{A}_2 \rightarrow {}^2\text{E}$ (Cr^{3+}) varying with modification of chemical composition was presented and discussed for chloride and bromide fluorozirconate glasses [37]. However, based on the absorption spectra measured for several oxide and fluoride glass systems it is generally accepted that the ${}^2\text{E}$ state is energetically below the ${}^4\text{T}_2$ state of Cr^{3+} . In some cases, the maxima of absorption bands due to ${}^4\text{A}_2 \rightarrow {}^4\text{T}_2$ and ${}^4\text{A}_2 \rightarrow {}^2\text{E}$ transitions of Cr^{3+} ions lie close to each other and characteristic dips corresponding to Fano antiresonances were obtained for fluoride-based glasses [38,39].

The conducted analysis of the studied glasses shows the presence of absorption bands corresponding to the transitions characteristic for the octahedral symmetry of the Cr^{3+} crystal field. Generally speaking, only two bands due to ${}^4\text{A}_2 \rightarrow {}^4\text{T}_2$ and ${}^4\text{A}_2 \rightarrow {}^2\text{E}$ transitions are observed in the presented absorption spectra, while optical research of glasses doped with Cr^{3+} ions show also the additional band located around 450 nm. It was assigned to transition ${}^4\text{A}_2 \rightarrow {}^4\text{T}_1$ of Cr^{3+} ions [40,41]. Moreover, our results indicate that with increasing titanium dioxide content, the spectra in the short-wavelength region are masked by strong absorption of the glass host. On the other hand, the absorption edge gradually shifts towards shorter wavelengths in the GBCr glass series as the boron oxide content increases. It should be emphasized here that the tendency to obscure the spin-allowed ${}^4\text{A}_2 \rightarrow {}^4\text{T}_1$ transition of Cr^{3+} through the absorption edge was also observed in fluoroborophosphate [42] and calcium borosilicate [43] glasses, clearly suggesting that it is caused by strong absorption of the glass host. In these cases, the excitation spectra are usually applied to measure all bands necessary to calculate Racah parameters of Cr^{3+} ions [44–46].

The excitation spectra of germanate glasses containing $\text{TiO}_2/\text{B}_2\text{O}_3$ were recorded by monitoring at an emission wavelength of 780 nm (Fig. 3).

The bands that contain between spectral range 550 and 870 nm (transitions ${}^4\text{A}_2 \rightarrow {}^4\text{T}_2$ and ${}^4\text{A}_2 \rightarrow {}^2\text{E}$) show similar features to the analyzed bands of the optical absorption spectra. Importantly, a well-separated band was found at shorter wavelengths around 480 nm. This relatively intense band was attributed to the transition from the ${}^4\text{A}_2$ ground level to the higher-lying energy level ${}^4\text{T}_1$ of Cr^{3+} ions [47]. Its presence is significant, and, in particular, the value of its energy makes it possible to perform appropriate theoretical calculations. With the Tanabe-Sugano diagram for the d^3 configuration of trivalent chromium ions in octahedral symmetry [48], the following parameters 10Dq , B , and Dq/B were calculated using equations (1)–(3) presented below. The calculated values of these parameters for germanate glasses containing B_2O_3 are given in Table 2.

$$\text{Dq} = \frac{1}{10} [E({}^4\text{T}_2) - E({}^4\text{A}_2)] \quad (1)$$

$$\frac{\text{Dq}}{B} = \frac{[15(x - 8)]}{[x^2 - 10x]} \quad (2)$$

$$x = \frac{1}{\text{Dq}} [E({}^4\text{T}_1) - E({}^4\text{T}_2)] \quad (3)$$

The interatomic repulsion strength of Cr^{3+} ions expressed by the parameter B in the developed glasses was in the range 733 cm^{-1} - 661 cm^{-1} (GBCr glass series). Compared with the standard interelectron repulsion value for the free ion ($B = 918 \text{ cm}^{-1}$) [49], a decrease in the value of this parameter was found by 28% in the GBCr3 glass sample suggesting the relatively strong covalent nature of the bond between

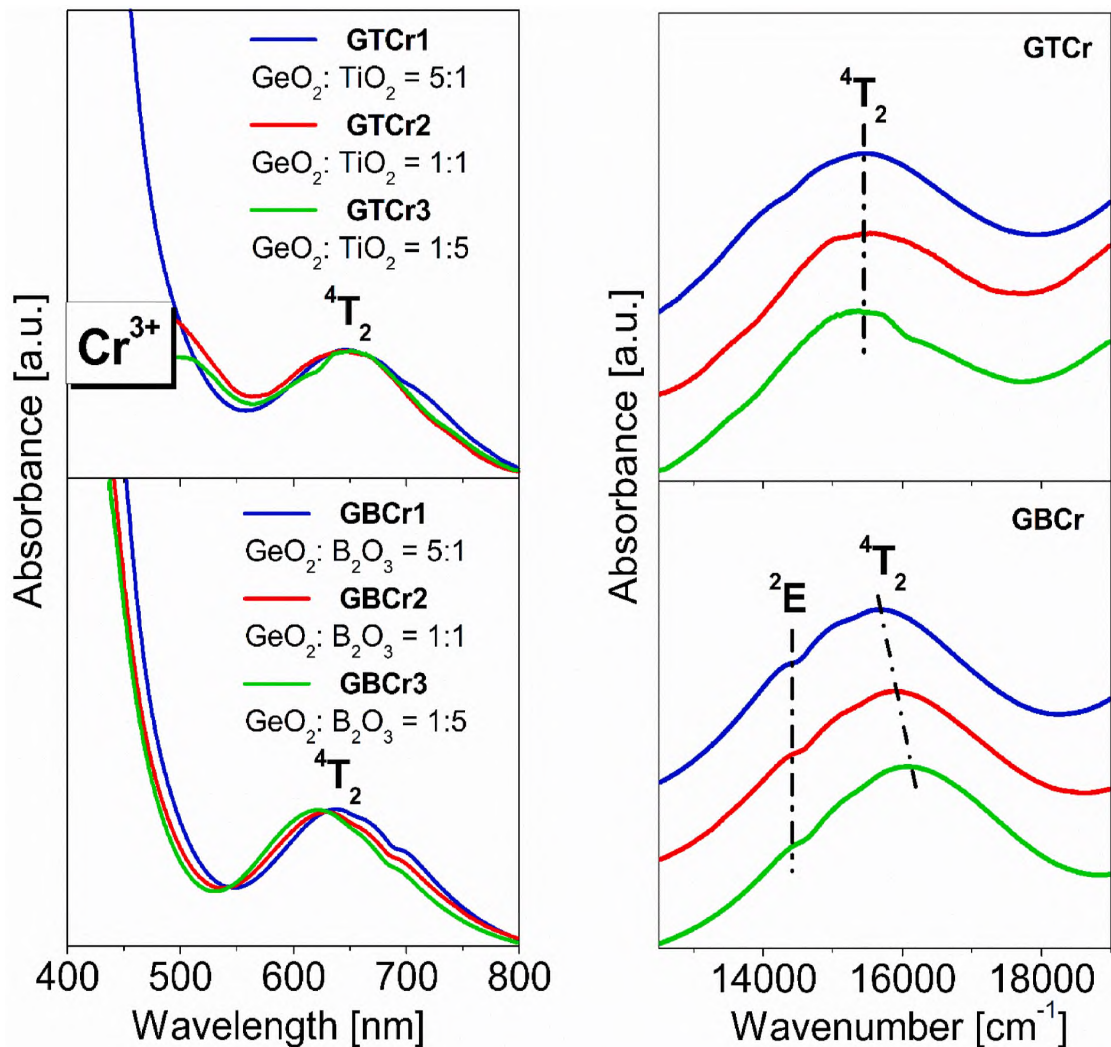


Fig. 2. Optical absorption spectra of germanate glasses with TiO_2 (GTCr) and B_2O_3 (GBCr) doped with chromium ions.

Cr^{3+} ions and surrounding ligands and the effective protection of the d shell electrons of chromium ions [50]. Next, it was important to obtain information on the crystal field strength of the chromium ions contained in the glasses. From the spectroscopic point of view, the Dq/B ratio provides information about the strength of the crystal field. Literature data indicate that the value of the spectroscopic parameter Dq/B for most oxide glass systems [51–53] is within three ranges: $Dq/B < 2.3$ (weak crystal field), $2.1 < Dq/B < 2.3$ (intermediate crystal field), and $Dq/B > 2.3$ (strong crystal field).

For Cr^{3+} doped barium gallo-germanate glass, the value of Dq/B is close to 2.13 [54] suggesting an intermediate octahedral ligand field environment ($2.1 < Dq/B < 2.3$), which separate the low-field (${}^4\text{T}_2$ state) and high-field (${}^2\text{E}$ state) sites. When B_2O_3 was introduced to the germanate based glass, the nearest surrounding of Cr^{3+} ions is changed in direction to a stronger crystal field. The value of Dq/B increases from 2.15 (GBCr1) to 2.29 (GBCr2) and 2.44 (GBCr3) within increasing B_2O_3 content. A similar situation was also observed for Cr^{3+} ions in borate based glasses [55–57]. In contrast to the GBCr glass series, the positions of absorption bands of Cr^{3+} , except the spin-forbidden transition ${}^4\text{A}_2 \rightarrow {}^2\text{E}$, depend slightly on TiO_2 content. Considering $Dq = 1550 \text{ cm}^{-1}$ and $B = 658 \text{ cm}^{-1}$, factor Dq/B for GTCr glass series is nearly close to 2.35 independently on TiO_2 concentration. It suggests that Cr^{3+} ions are

located in the intermediate/strong crystal field confirming the results obtained previously for some Cr^{3+} doped titanate compounds [58]. Undoubtedly, the spectroscopic parameters obtained from the excitation spectra indicate that the glass components B_2O_3 and TiO_2 influence significantly on the strength of the crystal field of Cr^{3+} ions in germanate based glass. For that reason, special attention has been paid to the luminescence properties of Cr^{3+} ions in barium gallo-germanate glasses containing $\text{B}_2\text{O}_3/\text{TiO}_2$ in the next part of the manuscript.

It is well known that Cr^{3+} ions in amorphous materials act as a useful paramagnetic spectroscopic probe [59]. Previous studies of glasses have presented different positions and intensities of luminescence bands of Cr^{3+} ions. If the ${}^4\text{T}_2$ level is below the ${}^2\text{E}$ level, the emission spectrum shows only a broad band located in the 700–870 nm range corresponding to the ${}^4\text{T}_2 \rightarrow {}^4\text{A}_2$ transition of Cr^{3+} ions [60]. In another case, the main luminescence band centered around 680 nm is attributed to the ${}^2\text{E} \rightarrow {}^4\text{A}_2$ transition of Cr^{3+} ions [61]. As shown in Fig. 4 registered the emission spectra of Cr^{3+} ions in GTCr and GBCr glass series, which were measured under direct excitation with 600 nm line.

Spectral analysis of all the studied glass samples shows that Cr^{3+} ions are very sensitive to the change in the quantitative relationship of the individual oxides and thus are affected by different crystal field strengths. Comparative analysis shows different spectral profiles of Cr^{3+}

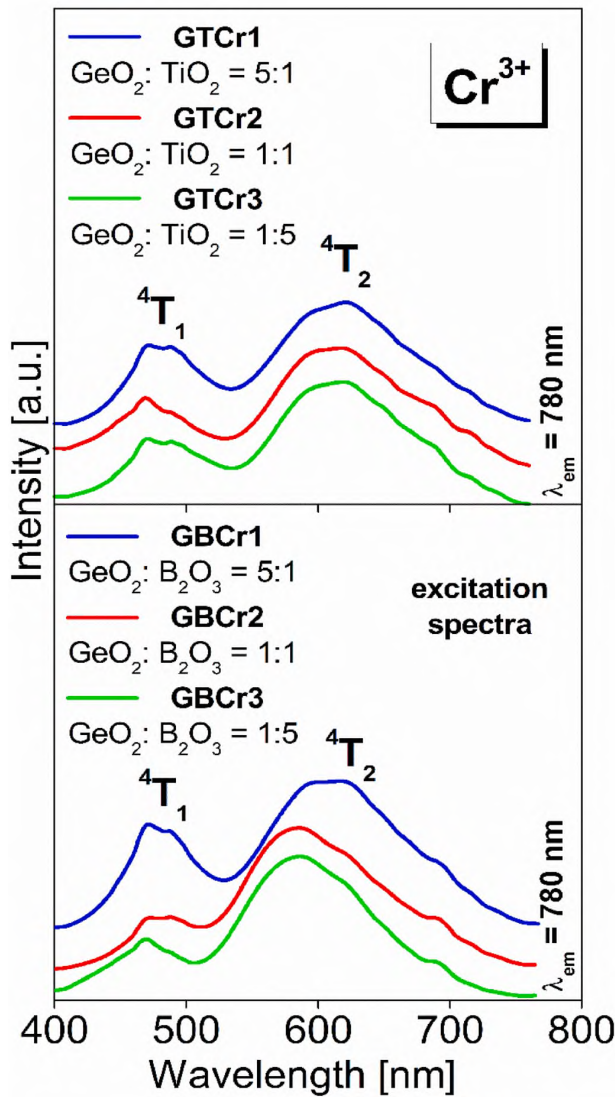


Fig. 3. Excitation spectra of germanate glasses with TiO_2 (GTCr) and B_2O_3 (GBCr) doped with chromium ions ($\lambda_{\text{exc}} = 780 \text{ nm}$).

Table 2
Spectral parameters for Cr^{3+} ions in germanate glasses containing B_2O_3 .

Glass code	Molar ratio	Dq [cm^{-1}]	B [cm^{-1}]	Dq/B
	$\text{GeO}_2: \text{B}_2\text{O}_3$			
GBCr1	5 : 1	1571	733	2.15
GBCr2	1 : 1	1593	697	2.29
GBCr3	1 : 5	1615	661	2.44

ions for both germanate glass systems containing TiO_2 and B_2O_3 .

Firstly, the Authors' followed the luminescence properties of Cr^{3+} ions in germanate based glass samples with TiO_2 referred to as GTCr1, GTCr2, and GTCr3. In general, independent of the relative molar ratio of $\text{GeO}_2:\text{TiO}_2$, each glass system is characterized by a broad luminescence band, which confirms that Cr^{3+} ions in an octahedral symmetry environment occur [62]. However, the detailed analysis confirmed well-defined broad emission band consists of two overlapping emission lines of Cr^{3+} ions. Their relative positions and intensities strongly depend on oxides as the network-former or network-modifier depending

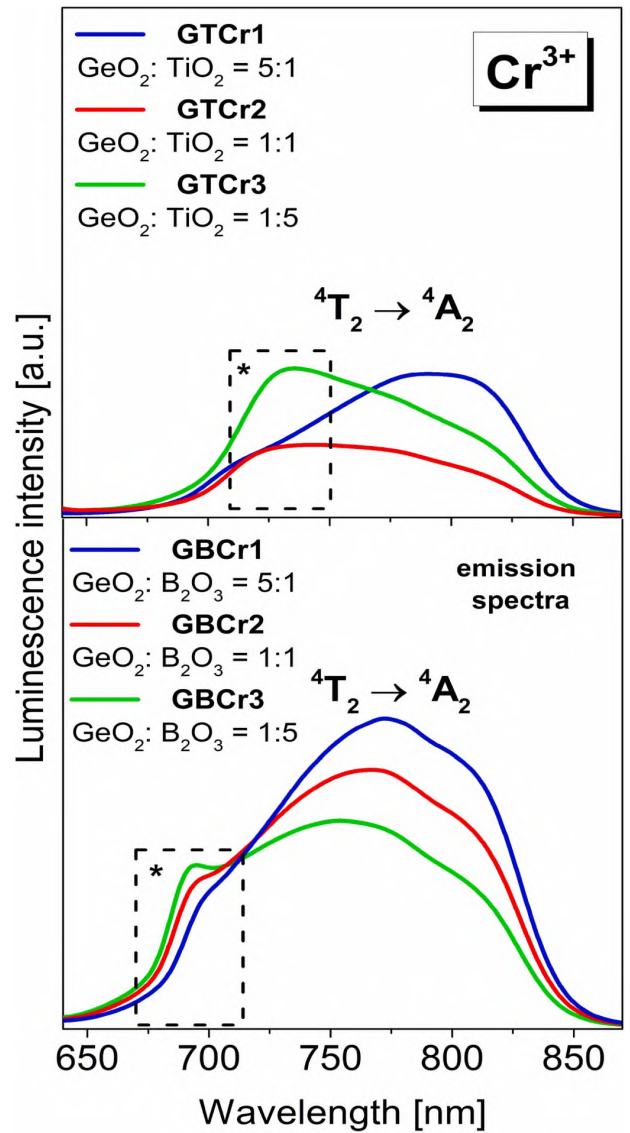


Fig. 4. Luminescence spectra of germanate glasses with TiO_2 (GTCr) and B_2O_3 (GBCr) doped with chromium ions ($\lambda_{\text{exc}} = 600 \text{ nm}$). The spectra were measured in the 640–875 nm range.

on its concentration. The luminescence spectrum for glass samples containing predominantly germanium dioxide (GTCr1) is dominated by the broad band corresponding to the spin-allowed ${}^4\text{T}_2 \rightarrow {}^4\text{A}_2$ transition of Cr^{3+} ions. The maximum emission band is significantly shifted towards shorter wavelengths with increasing TiO_2 content. From this point of view, the key aspect is the spectral range marked as (*). Luminescence band centered at about 730 nm is related to the characteristic so-called R-line [63,64] and corresponds to the ${}^2\text{E} \rightarrow {}^4\text{A}_2$ transition of Cr^{3+} ions. For the GTCr2 glass sample ($\text{GeO}_2:\text{TiO}_2 = 1:1$), the intensities of emission bands related to ${}^4\text{T}_2 \rightarrow {}^4\text{A}_2$ and ${}^2\text{E} \rightarrow {}^4\text{A}_2$ transitions are comparable. The profile of the emission band is completely different for the GTCr3 glass sample, where the ${}^2\text{E} \rightarrow {}^4\text{A}_2$ transition is dominant. Similar changes in spectral profiles of emission bands corresponding to both ${}^4\text{T}_2 \rightarrow {}^4\text{A}_2$ and ${}^2\text{E} \rightarrow {}^4\text{A}_2$ transitions of chromium were observed for tetraborate glasses with $\text{KLiB}_4\text{O}_7:\text{Cr}$ and $\text{Li}_2\text{B}_4\text{O}_7:\text{Cr}$ compositions [61]. Interestingly, the emission spectra of Cr^{3+} ions in glasses, where titanium dioxide was replaced by boron oxide, are completely different. In the GBCr

glass series, the quantitative relationship of the individual oxides did not significantly affect the position of the broadband luminescence. However, detectable changes are related to the intensity of the broad emission band, which is reduced from GBCr1 via GBCr2 to GBCr3 with increasing B_2O_3 content. An inverse emission intensity dependence is observed for glass samples by changing the molar ratio of GeO_2 to B_2O_3 from 5:1 to 1:5. It is noted that the narrow, poorly separated emission band corresponding to the ${}^2E \rightarrow {}^4A_2$ transition of Cr^{3+} (R-line) and presented by the insert marked as (*), becomes more evident as a result of introducing higher content of boron oxide. It is quite well evidenced that the intensity of broadband luminescence due to the ${}^4T_2 \rightarrow {}^4A_2$ transition of Cr^{3+} ions decrease but still dominated, whereas the intensity of R-line increases with increasing B_2O_3 content. The mutual relation of these two emission lines allows us to explain that a significant part of the Cr^{3+} ions in germanate glasses containing boron oxide is located in the stronger field sites. It quite well collaborates with the results obtained from the absorption/excitation measurements and calculation of spectroscopic parameter Dq/B which its value increases with increasing B_2O_3 content.

Finally, near-infrared luminescence properties of Cr^{3+} ions in glass series GTCr and GBCr have been also examined in the 950–1500 nm range. In this spectral range, two NIR emission bands corresponding to the octahedrally coordinated Cr^{3+} ions in $3d^3$ configuration and the tetrahedrally coordinated Cr^{4+} ions in $3d^2$ configuration can be observed for numerous amorphous and crystalline materials [65]. These emission bands are located usually at NIR I (ranging up to about 1200 nm) and NIR II (1200–1600 nm) regions and they are assigned to ${}^4T_2 \rightarrow {}^4A_2$ (Cr^{3+}) and ${}^3T_2 \rightarrow {}^3A_2$ (Cr^{4+}) transitions of chromium. Compared to Cr^{3+} , near-infrared luminescence of Cr^{4+} ions in glasses, transparent glass-ceramics, and other crystalline phosphors are shifted to longer wavelengths [66,67]. Especially, it is well evidenced for Cr^{3+}/Cr^{4+} co-doped systems, where the coexistence of chromium ions at trivalent and tetravalent oxidation states was confirmed by absorption/excitation and emission spectra measurements [68,69].

Fig. 5 shows near-infrared luminescence spectra measured in the 950–1500 nm region under excitation with the 600 nm line.

Irrespective of the glass composition, both glass series GTCr and GBCr are characterized by a single broad near-infrared luminescence band centered at about 1050 nm. In general, the intensities of bands are reduced independently on B_2O_3 or TiO_2 concentration increase, whereas luminescence band profiles are practically not changed. The results for NIR luminescence that existed above 1000 nm in numerous Cr^{3+} doped compounds are quite well documented in the literature. The presence of two emission bands at 730 nm and 1030 nm for $La_3Ga_5Nb_{0.5}O_{14}:Cr^{3+}$ phosphors is ascribed to trivalent chromium ions in disordered octahedral (site I) sites and tetrahedral sites (site II), respectively [70]. Also, further studies demonstrate some chromium doped NIR phosphors, i.e. $Cs_2AgInCl_6:Cr^{3+}$ [71] and $LiScGeO_4:Cr^{3+}$ [72] with peak emission wavelength longer than 1000 nm, which correspond to the spin-allowed ${}^4T_2 \rightarrow {}^4A_2$ transition of Cr^{3+} .

In our case, we also observe for both glass series GTCr and GBCr the near-infrared emission bands centered near 1050 nm. The excitation spectra measurements under various monitoring emission wavelengths 680 nm and 1050 nm (Fig. 6) confirm the presence of two main ${}^4A_2 \rightarrow {}^4T_1$ and ${}^4A_2 \rightarrow {}^4T_2$ transitions of chromium ions at trivalent oxidation state. However, the positions of maxima of excitation bands measured under two monitoring VIS ($\lambda_{em} = 680$ nm) and NIR ($\lambda_{em} = 1050$ nm) emission wavelengths are different. The maxima of the 4T_2 bands are located at a longer wavelength for $\lambda_{em} = 1050$ nm than $\lambda_{em} = 680$ nm. These phenomena could be explained by the presence of two types of octahedral Cr^{3+} ions with slightly different crystal field strengths, i.e., isolated Cr^{3+} ions evidenced by the visible emission, and another Cr^{3+} ions which transfer successfully their excitation energy to nearby tetrahedral chromium ions giving the near-infrared emission. The investigations are in a progress.

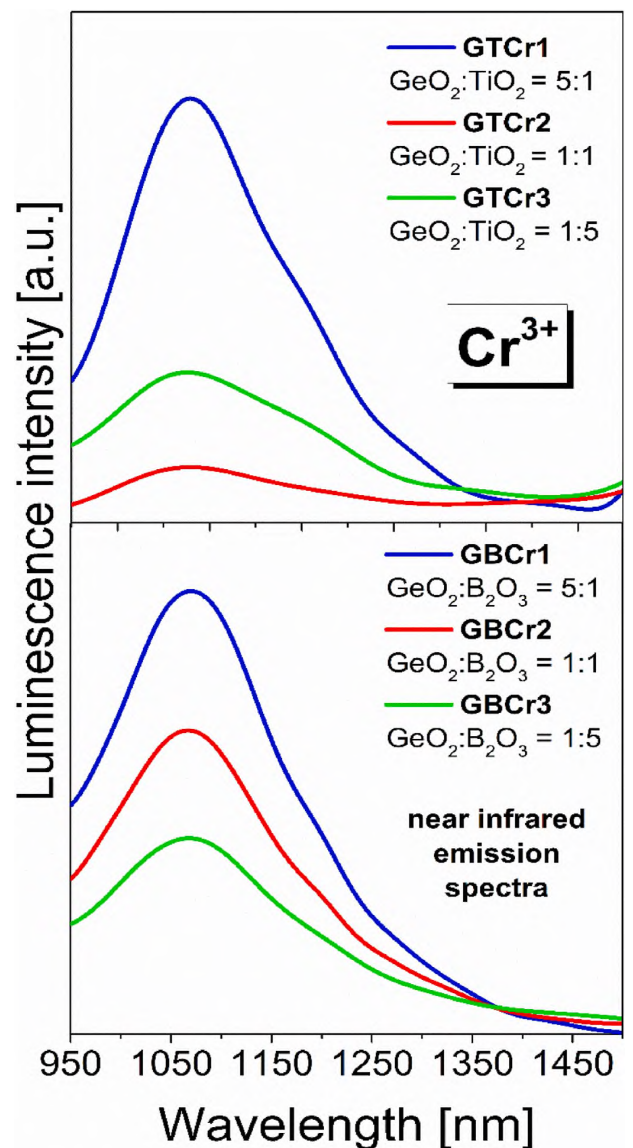


Fig. 5. Near-infrared luminescence spectra of germanate glasses with TiO_2 (GTCr) and B_2O_3 (GBCr) doped with chromium ions ($\lambda_{exc} = 600$ nm). The spectra were measured in the 950–1500 nm range.

4. Conclusion

In this paper, chromium-doped germanate glass matrices ($GeO_2-B_2O_3-BaO-Ga_2O_3-Cr_2O_3$ and $GeO_2-TiO_2-BaO-Ga_2O_3-Cr_2O_3$) were successfully synthesized and studied using EPR and luminescence spectroscopy. The author's strategy was based on a prepared series of glass samples with different $GeO_2:B_2O_3$ and $GeO_2:TiO_2$ molar ratios. Using this approach, the Authors' managed to obtain interesting spectroscopic results. The received materials were studied using EPR spectroscopy to confirm chromium ions occur in the trivalent oxidation state. The optical absorption spectra consist of two characteristic transitions of Cr^{3+} ions: ${}^4A_2 \rightarrow {}^4T_2$ and ${}^4A_2 \rightarrow {}^2E$. Moreover, an interpretation of the results concerning parameters Dq/B obtained from excitation spectra allows us to state that the Cr^{3+} ions are located in an intermediate/strong crystal field. Further analysis of the obtained glasses perfectly has proven that the quantitative relationship of metal oxides determines the luminescent

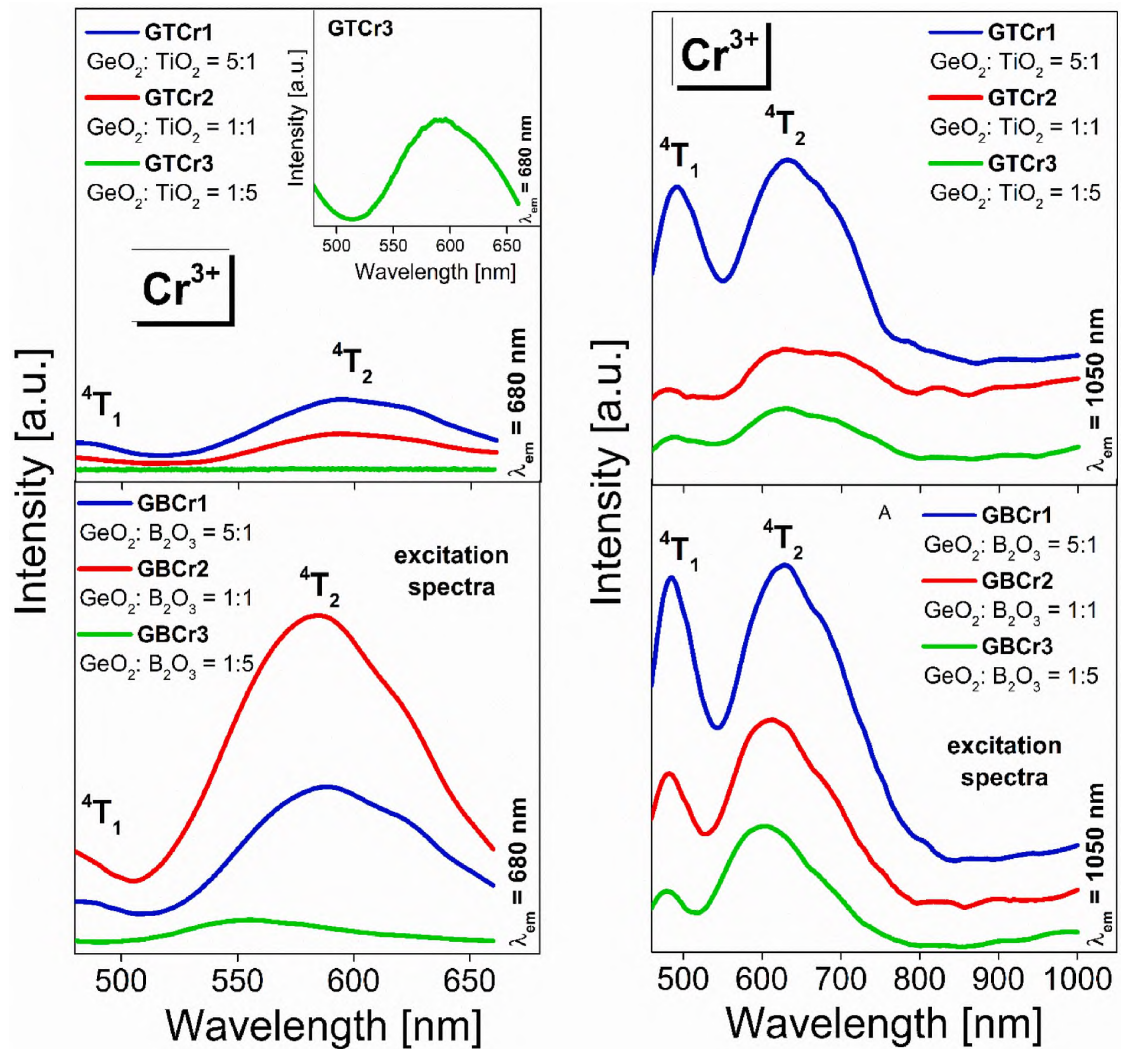


Fig. 6. Excitation spectra of germanate glasses with TiO_2 (GTCr) and B_2O_3 (GBCr) measured under various monitoring emission wavelengths $\lambda_{\text{em}} = 680$ nm and 1050 nm.

properties of Cr^{3+} ions. The glasses show evident differences in the profile of the recorded emission band associated with the ${}^4\text{T}_2 \rightarrow {}^4\text{A}_2$ transition of Cr^{3+} ions. Simultaneously, it was revealed that the content of individual oxides allows identifying the R-line characteristic for trivalent chromium ions. The presented results may be important in terms of potential application because suggest new approaches tailored to the needs of developing an optical material. Concluding our research showed that trivalent chromium ions are very sensitive to modification chemical compositions of germanate glasses that can be applied in many optoelectronic devices emitting radiation in the wide near-infrared spectral range.

Credit author statement

Karolina Kowalska: Investigation, Writing - Original Draft, Visualization
Marta Kuwik: Investigation
Justyna Polak: Investigation
Joanna Pisarska: Conceptualization
Wojciech A. Pisarski: Conceptualization, Writing - Review & Editing, Visualization.

Declaration of competing interest

The authors declare that they have no known competing financial interests or personal relationships that could have appeared to influence the work reported in this paper.

Acknowledgment

The National Science Centre (Poland) supported this work under research project 2018/31/B/ST8/00166.

References

- [1] M. Karimi, A. Mehdizadeh, M. Hossein Hekmatshoar, S. Vafaei, A new method for controlling structural, electrical, and optical properties of phosphate glasses, containing transition metal ions (TMIs), *J. Non-Cryst. Solids* 525 (2019), <https://doi.org/10.1016/j.jnoncrysol.2019.119693>. Article 119693.
- [2] A.A. Abul-Magd, H.Y. Morshidy, A.M. Abdel-Ghany, The role of NiO on structural and optical properties of sodium zinc borate glasses, *Opt. Mater.* 109 (2020), <https://doi.org/10.1016/j.optmat.2020.110301>. Article 110301.
- [3] E.M. Abou Hussein, A.M. Madbouly, F.M. Ezz Eldin, N.A. ElAlaily, Evaluation of physical and radiation shielding properties of $\text{Bi}_2\text{O}_3\text{-B}_2\text{O}_3$ glass doped transition

- [52] N. Luewarasirikul, Y. Ruangthaweeep, J. Kaewkhao, Preparation and spectroscopic studies of Cr³⁺-doped aluminium calcium sodium borate glasses, *Mater. Today Proc.* 17 (2019) 1831–1836, <https://doi.org/10.1016/j.matpr.2019.06.220>.
- [53] K. Jyothi Raju, B. Lakshmana Rao, S.V.G.V.A. Prasad, P. Rajani Kanth, Y. Gandhi, The structural investigations of PbO-Sc₂O₃-P₂O₅ glasses with Cr₂O₃ as additive by means of spectroscopic studies, *Mater. Today Proc.* 5 (2018) 26255–26262, <https://doi.org/10.1016/j.matpr.2018.08.075>.
- [54] J. Pisarska, M. Kuwik, A. Gorny, J. Dorosz, M. Kochanowicz, J. Zmojda, M. Sitarz, D. Dorosz, W.A. Pisarski, Influence of transition metal ion concentration on near-infrared emission of Ho³⁺ in barium gallo-germanate glasses, *J. Alloys Compd.* 793 (2019) 107–114, <https://doi.org/10.1016/j.jallcom.2019.04.154>.
- [55] C.R. Kesavulu, R.P.S. Chakradhar, C.K. Jayasankar, J. Lakshmana rao, EPR, optical, photoluminescence studies of Cr³⁺ ions in Li₂O-Cs₂O-B₂O₃ glasses - an evidence of mixed alkali effect, *J. Mol. Struct.* 975 (2010) 93–99, <https://doi.org/10.1016/j.molstruc.2010.03.091>.
- [56] K. Chandra Sekhar, B. Srinivas, N. Narsimlu, M. Narasimha Chary, Md Shareefuddin, The role of halides on a chromium ligand field in lead borate glasses, *Mater. Res. Express* 4 (2017), <https://doi.org/10.1088/2053-1591/aa8d7e>. Article 150203.
- [57] R. Nagaraju, B. Devaiah, L. Haritha, K. Chandra Sekhar, Md Shareefuddin, M. A. Sayed, G. Lalitha, K. Vijaya Kumar, Influence of CaF₂ on spectroscopic studies of lead fluoro bismuth borate glasses doped with Cr³⁺ ions, *J. Non-Cryst. Solids* 560 (2021), <https://doi.org/10.1016/j.jnoncrysol.2021.120705>. Article 120705.
- [58] M. Gaft, R. Reisfeld, G. Panczer, *Modern Luminescence Spectroscopy of Minerals and Materials*, Springer, 2015.
- [59] G. El-Damrawi, A.M. Abdelghany, A.H. Oraby, M.A. Madshal, Structural and optical absorption studies on Cr₂O₃ doped SrO-P₂O₅ glasses, *Spectrochim. Acta Mol. Biomol. Spectrosc.* 228 (2020), <https://doi.org/10.1016/j.saa.2019.117840>. Article 117840.
- [60] L.N. Rao, M.V.S. Rao, Ch Tirupataiah, V. Aruna, M.N. Lakshmi, Influence of chromium ions on photonic applicability of Na₂O-Bi₂O₃-B₂O₃-SiO₂ glass system, *Opt Commun.* 480 (2021), <https://doi.org/10.1016/j.optcom.2020.126496>. Article 126496.
- [61] B.V. Padhyak, W. Ryba-Romanowski, R. Lisiecki, V.T. Adamiv, YaV. Burak, I. M. Teslyuk, Synthesis, EPR and optical spectroscopy of the Cr-doped tetraborate glasses, *Opt. Mater.* 34 (2012) 2112–2119, <https://doi.org/10.1016/j.optmat.2012.06.014>.
- [62] M.A.F.M. da Silva, I.C.S. Carvalho, N. Cella, H.N. Bordallo, L.P. Sosman, Evidence of broad emission band in the system MgGa₂O₄-Ga₂O₃ doped with Cr³⁺ ions, *Opt. Mater.* 35 (2013) 543–546, <https://doi.org/10.1016/j.optmat.2012.10.008>.
- [63] D. Chen, Z. Wan, Y. Zhou, Z. Ji, Cr³⁺-doped gallium-based transparent bulk glass ceramics for optical temperature sensing, *J. Eur. Ceram. Soc.* 35 (2015) 4211–4216, <https://doi.org/10.1016/j.jeurceramsoc.2015.08.005>.
- [64] V. C Costa, F.S. Lameiras, M.V.B. Pinheiro, D.F. Sousa, L.A.O. Nunes, Y.R. Shen, K. L. Bray, Laser spectroscopy and electron paramagnetic resonance of Cr³⁺ doped silicate glasses, *J. Non-Cryst. Solids* 273 (2000) 209–214, [https://doi.org/10.1016/S0022-3093\(00\)00170-8](https://doi.org/10.1016/S0022-3093(00)00170-8).
- [65] Kück, Laser-related spectroscopy of ion-doped crystals for tunable solid-state lasers, *Appl. Phys. B* 72 (2001) 515–562, <https://doi.org/10.1007/s003400100540>.
- [66] A.M. Malyarevich, Yu V. Volk, K.V. Yumashev, V.K. Pavlovskii, S.S. Zapalova, O. S. Dymshits, A.A. Zhilin, Absorption, emission and absorption saturation of Cr⁴⁺ ions in calcium aluminate glass, *J. Non-Cryst. Solids* 351 (2005) 3551–3555, <https://doi.org/10.1016/j.jnoncrysol.2005.08.030>.
- [67] Y. Zhuang, S. Tanabe, J. Qiu, Wavelength tailorability of broadband near-infrared luminescence in Cr⁴⁺-activated transparent glass-ceramics, *J. Am. Ceram. Soc.* 97 (2014) 3519–3523, <https://doi.org/10.1111/jace.13128>.
- [68] Z. Wang, F. Huang, Q. Yang, Y. Hua, J. Zhang, R. Ye, S. Xu, Efficient controllable NIR-MIR luminescence conversion in optical nanostructured silicate glasses, *J. Phys. Chem. C* 123 (2019) 14662–14668, <https://doi.org/10.1021/acs.jpcc.9b02943>.
- [69] X. Wang, Z. Wang, M. Zheng, J. Cui, Y. Yao, L. Cao, M. Zhang, H. Suo, P. Li, A dual-excited and dual near-infrared emission phosphor Mg₁₄Ge₅O₂₄:Cr³⁺, Cr⁴⁺ with a super broad band for biological detection, *Dalton Trans.* 50 (2021) 311–322, <https://doi.org/10.1039/D0DT03554H>.
- [70] Y. Li, S. Ye, Q. Zhang, Ultra-broadband near-infrared luminescence of ordered-disordered multi-sited Cr³⁺ in La₃Ga_{5.5}Nb_{0.5}O₁₄:Cr³⁺, *J. Mater. Chem. C* 2 (2014) <https://doi.org/10.1039/C4TC00243A>. Article 4636.
- [71] F. Zhao, Z. Song, J. Zhao, Q. Liu, Double perovskite Cs₂AgInCl₆:Cr³⁺-broadband and near-infrared luminescent materials, *Inorg. Chem. Front.* 6 (2019) 3621–3628, <https://doi.org/10.1039/C9QI00905A>.
- [72] S. Miao, Y. Liang, Y. Zhang, D. Chen, X.J. Wang, Broadband short-wave infrared light-emitting diodes based on Cr³⁺-doped LiScGeO₄ phosphor, *ACS Appl. Mater. Interfaces* 13 (2021) 36011–36019, <https://doi.org/10.1021/acsami.1c10490>.

P3

Karolina Kowalska, Marta Kuwik, Joanna Pisarska, Maciej Sitarz,

Wojciech A. Pisarski,

**Raman and infrared spectroscopy of barium-gallo germanate glasses
containing B₂O₃/TiO₂,**

Materials 16 (2023) 1516

Article

Raman and Infrared Spectroscopy of Barium-Gallo Germanate Glasses Containing B₂O₃/TiO₂

Karolina Kowalska ^{1,*} , Marta Kuwik ¹ , Joanna Pisarska ¹, Maciej Sitarz ²  and Wojciech A. Pisarski ¹

¹ Institute of Chemistry, University of Silesia, Szkolna 9 Street, 40-007 Katowice, Poland

² Faculty of Materials Science and Ceramics, AGH University of Science and Technology, 30 Mickiewicza Av., 30-059 Kraków, Poland

* Correspondence: karolina.kowalska@us.edu.pl

Abstract: Modified barium gallo-germanate glass hosts are still worthy of attention in studying structure–property relationships. In this work, two different series of glass systems based on (60-x)GeO₂-xTiO₂-30BaO-10Ga₂O₃ and (60-x)GeO₂-xB₂O₃-30BaO-10Ga₂O₃ (x = 10, 30, 50 mol%) were synthesized, and their properties were studied using spectroscopic techniques. X-ray diffraction (XRD) patterns revealed that all fabricated glasses were fully amorphous material. The absorption edge shifted toward the longer wavelengths with a gradual substitution of GeO₂. The spectroscopic assignments of titanium ions were performed with excitation and emission spectra compared to the additional sample containing an extremely low content of TiO₂ (0.005 mol%). On the basis of Raman and FT-IR investigations, it was found that increasing the TiO₂ content caused a destructive effect on the GeO₄ and GeO₆ structural units. The Raman spectra of a sample containing a predominantly TiO₂ (50 mol%) proved that the band was located near 650 cm⁻¹, which corresponded to the stretching vibration of Ti-O in TiO₆ unit. The deconvoluted IR results showed that the germanate glass network consisted of the coexistence of two BO₃ and BO₄ structural groups. Based on the experimental investigations, we concluded that the developed materials are a promising candidate for use as novel glass host matrices for doping rare-earth and/or transition metal ions.

Keywords: barium gallo-germanate glasses; boron trioxide; titanium dioxide; vibrational raman and infrared spectroscopies; structure–property relationship



Citation: Kowalska, K.; Kuwik, M.; Pisarska, J.; Sitarz, M.; Pisarski, W.A. Raman and Infrared Spectroscopy of Barium-Gallo Germanate Glasses Containing B₂O₃/TiO₂. *Materials* **2023**, *16*, 1516. <https://doi.org/10.3390/ma16041516>

Academic Editors: M.I. Sayyed and Mengge Dong

Received: 20 November 2022

Revised: 2 February 2023

Accepted: 9 February 2023

Published: 11 February 2023



Copyright: © 2023 by the authors. Licensee MDPI, Basel, Switzerland. This article is an open access article distributed under the terms and conditions of the Creative Commons Attribution (CC BY) license (<https://creativecommons.org/licenses/by/4.0/>).

1. Introduction

Glass, according to the definition, is a supercooled liquid and exhibits an amorphous nature. It should be noted that the common specific feature of all oxide glasses is the lack of long-range ordering. In the last few years, much research has been focused on explaining the relationship between the content of network formers and network modifiers and the stretching or bending vibrations occurring in the glasses. Special attention has been paid to the attractive infrared range characterizing the local structure of glassy systems using vibration analysis such as Raman and FTIR spectroscopy. There are extremely useful experimental techniques in investigating the structural properties of inorganic glasses [1–3]. Although there are well-documented scientific reports, the interpretation of the vibrations of glass host structural units occurring in oxide glasses is still a subject of ongoing scientific debate.

The above vibrational spectroscopies were successfully applied to examine the local structure of borate [4,5], phosphate [6,7], tellurite [8,9], silicate [10,11], and germanate [12–16] glass-host matrices. Studies in the last decade have shown that basic glass composition can be realized by adding several oxides and/or fluoride additives [17,18]. The main goal is to develop materials with excellent thermal, chemical, structural, and spectroscopic properties and various potential applications. Among those mentioned above, germanate glass is a promising starting material. First observed by Ivanov and Evstropiev [19], the coordination of Ge would continuously change from GeO₄

to GeO_6 with the addition of alkali oxides. Recently, the structural properties of germanate-based glasses have been examined in $\text{Na}_2\text{O-GeO}_2\text{-TeO}_2$ [20], $\text{Li}_2\text{O-GeO}_2\text{-TeO}_2$ [20], $\text{MnO-GeO}_2\text{-PbO}_2$ [21], $\text{TeO}_2\text{-GeO}_2\text{-PbO}$ [22], $\text{Na}_2\text{CO}_3\text{-CaO-GeO}_2$ [23], and $\text{Ga}_2\text{O}_3\text{-GeO}_2\text{-BaO}$ [24]. Among the reported germanate-based glasses, the barium gallo-germanate matrix has received the most attention due to its excellent properties, i.e., relatively large glass-forming region, high transmittance in a wide wavelength region, superior chemical durability, and thermal stability [25,26]. The structural properties of the BGG glass system modified by boron trioxide are less documented in the literature. Borate-based glass has excellent properties among the common glass-forming agents due to its high bond strength, coordination geometry, and maximum phonon energy ($\sim 1400\text{ cm}^{-1}$). The transformation of the coordination environment of boron, in terms of the equilibrium of the structural changes related to the conversion between BO_3 and BO_4 , has been extensively studied [27]. Meanwhile, titanium oxide (TiO_2) is one of the important constituents of luminescent glass, which acts as both network formers and network modifier [28]. Depending on the glass type, titanium can exhibit both trivalent and tetravalent valence states. The first attempts in this area were made by Cheng J. and Chen W. [29], who showed that stable titanate glasses could be obtained without adding glass network components (SiO_2 , B_2O_3). However, the formation of titanium ions in glasses has been reported, but most of the glass systems are partially crystallized. Up to now, fully amorphous barium gallo-germanate glasses containing higher TiO_2 contents (10–50 mol%) were not obtained. It is well known that metal oxides such as B_2O_3 and TiO_2 can be added to germanate-based glass to modify their optical and structural properties. The effect of the spectroscopic properties of properties for $\text{SrO-BaO-B}_2\text{O}_3\text{-SiO}_2$ glass ceramics [30] with different $\text{TiO}_2/\text{B}_2\text{O}_3$ ratios has been studied. Consequently, the fraction in the form of TiO_4 and TiO_6 increased when the fraction of BO_3 decreased. For this reason, it is important to broaden our knowledge of the structural properties of the $\text{GeO}_2\text{-BaO-Ga}_2\text{O}_3$ glass system modified by $\text{TiO}_2/\text{B}_2\text{O}_3$.

In our previous work [31], Cr^{3+} ions were used in multicomponent germanate glasses as a spectroscopic probe. We observed that GeO_2 and $\text{TiO}_2/\text{B}_2\text{O}_3$ strongly influenced the profiles of luminescence bands and their relative intensity of trivalent chromium ions in the visible and infrared range. The calculated spectroscopic parameters from the Tanabe–Sugano diagram indicated that Cr^{3+} ions in the $\text{GeO}_2\text{-BaO-Ga}_2\text{O}_3$ glassy phase occupied the intermediate (sample with B_2O_3) and strong (sample with TiO_2) crystal field, respectively. It is assumed that adding glass formers such as TiO_2 and B_2O_3 to the BGG network changes the local structure. We have extended this experimental approach to the analysis structural properties of undoped $\text{GeO}_2\text{-TiO}_2\text{-BaO-Ga}_2\text{O}_3$ and $\text{GeO-B}_2\text{O}_3\text{-BaO-Ga}_2\text{O}_3$ systems. Structural changes in the studied glasses were examined by XRD, FT-IR and Raman spectroscopy. Our study intends to present the role of titanium ions in germanate glass-host matrices based on excitation and emission spectra compared to the glass sample containing an extremely low content of TiO_2 . Another aspect worth exploring is a mathematical procedure of spectral decomposition as the possibility of determining the component bands resulting from matrix vibrations for the $\text{GeO}_2\text{-B}_2\text{O}_3\text{-BaO-Ga}_2\text{O}_3$ glass system.

2. Materials and Methods

In the presented procedure, multicomponent germanate-based glass systems modified by $\text{TiO}_2/\text{B}_2\text{O}_3$ were prepared using the conventional melt quench technique. The high purity chemicals such as (>99.99%) germanium oxide (GeO_2), boron trioxide (B_2O_3), titanium oxide (TiO_2), barium oxide (BaO), and gallium trioxide (Ga_2O_3) (Sigma Aldrich Chemical Co., St. Louis, MO, USA) were used to synthesize the glass samples. The glass samples were entitled as GT1 ($\text{GeO}_2:\text{TiO}_2 = 5:1$), GT2 ($\text{GeO}_2:\text{TiO}_2 = 1:1$), GT3 ($\text{GeO}_2:\text{TiO}_2 = 1:5$) and GB1 ($\text{GeO}_2:\text{B}_2\text{O}_3 = 5:1$), GB2 ($\text{GeO}_2:\text{B}_2\text{O}_3 = 1:1$), and GB3 ($\text{GeO}_2:\text{B}_2\text{O}_3 = 1:5$), where the first letters refer of the GeO_2 , TiO_2 , and B_2O_3 metal oxides. The chemical compositions of the $\text{GeO}_2/\text{TiO}_2$ and $\text{GeO}_2/\text{B}_2\text{O}_3$ molar ratios and nomenclature are listed in Tables 1 and 2. The glass components were taken in appropriate proportions and mixed using agate-made mortar and pestle in a glove box in an inert atmosphere to constitute a 5 g batch. The

homogenized mixtures were melted in a crucible (Łukasiewicz Research Network, Institute of Ceramics and Building Materials, Cracow, Poland) at a temperature of 1250 °C for 60 min in an electric furnace (CZYLOK Company, Jastrzębie-Zdrój, Poland). The molten glass sample was taken out of the electric furnace, cast on a porcelain plate, and cooled down to room temperature. At the end of the procedure, the glass samples were polished (semiautomatic grinding and polishing LaboPol-5 Struers, Denmark) in the desired shape. Finally, we fabricated glass samples of dimensions 15 mm × 15 mm and thickness ± 3 mm for the following optical and structural measurements. Figures 1 and 2 show images of the polished samples GT2 and GB2.

Table 1. Nominal composition (mol%) and GeO₂/TiO₂ ratio of glass samples.

Chemical Composition of BGG Glass with TiO ₂ (mol%)					
Sample Code	GeO ₂	TiO ₂	BaO	Ga ₂ O ₃	GeO ₂ :TiO ₂
GT1	50	10	30	10	5:1
GT2	30	30	30	10	1:1
GT3	10	50	30	10	1:5

Table 2. Nominal composition (mol%) and GeO₂/B₂O₃ ratio of glass samples.

Chemical Composition of BGG Glass with B ₂ O ₃ (mol%)					
Sample Code	GeO ₂	B ₂ O ₃	BaO	Ga ₂ O ₃	GeO ₂ :B ₂ O ₃
GB1	50	10	30	10	5:1
GB2	30	30	30	10	1:1
GB3	10	50	30	10	1:5



Figure 1. Photographs of the obtained glass sample: 30GeO₂-30TiO₂-30BaO-10Ga₂O₃ (GT2).

An XRD spectrum for prepared samples was recorded with an X'Pert Pro diffractometer with CuK α radiation with a $\lambda = 1.54056$ Å wavelength supplied by PANalytical (Almelo, The Netherlands) in the range 20–70°. The diffraction patterns were measured in step-scan mode with a step size of 0.050 and a time per step of 10 s. The UV-VIS spectrophotometer (Varian Cary 5000, Agilent Technology, Santa Clara, CA, USA) was used to measure the optical absorption spectra. The excitation and luminescence spectra of the glasses in a range of 260–650 nm were registered using a laser system that consisted of a PTI Quanta-Master 40 UV/VIS Steady State Spectrofluorometer (Photon Technology International, Birmingham, NJ, USA) coupled with a tunable pulsed optical parametric oscillator (OPO) pumped by the third harmonic of an Nd:YAG laser (Opotek Opolette 355 LD, OPOTEK, Carlsbad,

CA, USA). The laser system was coupled with a Xe lamp (75 W). The resolution for the excitation and luminescence spectra was ± 0.25 nm.



Figure 2. Photographs of the obtained glass sample: $30\text{GeO}_2\text{-}30\text{B}_2\text{O}_3\text{-}30\text{BaO}\text{-}10\text{Ga}_2\text{O}_3$ (GB2).

In the next step, the structural investigations for the obtained materials were evaluated. The bonding vibrations were determined via a Fourier Transform Infrared (FTIR) measurement in the region $1600\text{-}400\text{ cm}^{-1}$ (Nicolet™ iS™ 50, Thermo Fisher Scientific, Waltham, MA, USA) with a diamond attenuated total reflectance (ATR) module. The complementary structural characterization of the obtained glass samples was verified using Raman spectroscopy (Thermo Scientific, Waltham, MA, USA). The appropriate laser source with an excitation wavelength of 780 nm was used to obtain the Raman spectra. The laser was directly focused on the sample with an Olympus long-working-distance microscope objective ($50\times$). The Raman and IR spectra were normalized and deconvoluted using Origin Pro 9.1 software. All the measurements were performed at room temperature.

3. Results

The aim of this work is to evaluate the effect of a boron trioxide (B_2O_3) and titanium dioxide (TiO_2) substitution on the properties of barium gallo-germanate (BGG) glasses. Firstly, to emphasize the potential of titanium-rich glasses and boron-rich BGG glasses, X-ray diffraction (XRD) was used to verify the local structure of the studied glass systems. Absorption spectroscopy is a very useful technique for characterizing the optical properties within the range of 200–800 nm of fabricated glasses. The assignment of the titanium ions' emission bands that were derived from the spectroscopic results allowed us to confirm the Ti^{3+} ions in barium gallo-germanate glass systems. Secondly, a thorough analysis of the structural properties was performed by means of FT-IR and Raman spectroscopy. In those pioneering works, the properties of barium gallo-germanate systems were studied for possible applications in low-loss fiber optics and optical components [32–34]. The morphology of barium germanate glasses was reported by Shelby [35]. It should be noted that the barium gallo-germanate system shows a broad glass-forming region [36]. The properties of these systems can also be modified by adding or substituting other components. The effect of various substitutions in the barium gallo-germanate glasses was studied by Jewell et al. [37]. As a result, gadolinium is a typical modifier ion because of its large field strengths. Next, aluminum acts as an intermediate with AlO_4^- substituting directly for Ga_2O_4^- units. In the presence of GeO_2 , gallium atoms tend to reinforce the glass network as observed in $\text{BaO}\text{-Ga}_2\text{O}_3\text{-GeO}_2$ glass compositions, where the corners bind GaO_4 and GeO_4 tetrahedra. Consequently, depending on the content of various components, their role can change from network modifier to network former. To the best of our knowledge, these phenomena were not yet examined for B_2O_3 , one of the typical covalent network formers that meet Zachariasen's rules for glass formation, and TiO_2 ,

whose role can change from glass network modifier to glass network former depending on its amount in the glass.

3.1. Glass Characterization

In order to examine the amorphous or crystalline state of the fabricated glasses, a phase analysis was conducted with the use of X-ray diffraction (XRD). Figure 3a,b present representative X-ray diffraction patterns measured of the barium gallo-germanate glasses with the varying content of TiO_2 and B_2O_3 (from 10 to 50 mol%). According to the literature data [38], the barium gallo-germanate glass system can exhibit a tendency toward surface crystallization. However, it is well known that bulk crystallization can be made possible in various glass systems by phase separation followed by nucleation and crystal growth. It needs to be stressed that TiO_2 was an effective crystal nucleating agent in various glass systems. Systematic studies clearly indicate that the crystallization of TiO_2 in glass systems depends on several factors, e.g., ionic size, ionic chance, and the ability to be conditional glass former ions [39,40]. The main drawbacks of TiO_2 content are related to decreasing the viscosity of the glasses at a high temperature process and importantly promoting glass liquid–liquid phase separation, which provides more phase interfaces. Mingshen et al. [41] exhibited the role of TiO_2 (5–10 wt%) in the process of the phase separation, nucleation, and crystallization of $\text{CaO-MgO-Al}_2\text{O}_3\text{-SiO}_2\text{-Na}_2\text{O}$ system glasses. Importantly, they showed that the number of the main crystalline phase increased with temperature and time. Our results indicated that this phenomenon was not observed in the fabricated glass system using the traditional high-temperature melt-quenching method. For this reason, for the structural analysis, we started using X-ray diffraction measurements.

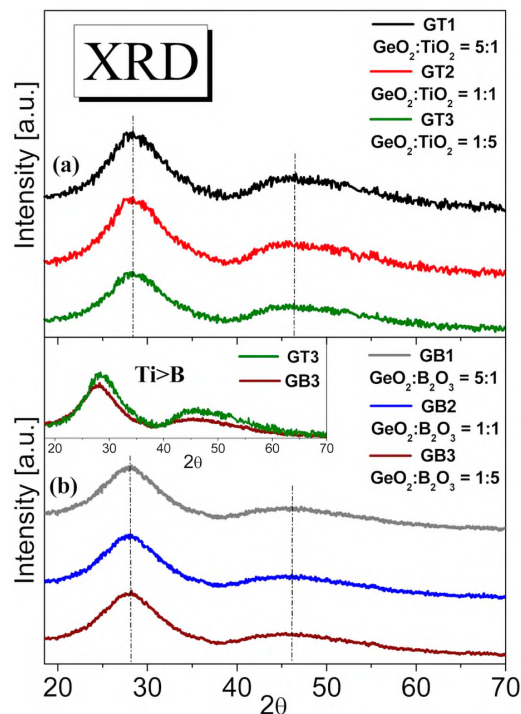


Figure 3. XRD profiles of barium gallo-germanate glasses containing various molar ratios TiO_2 (a) and B_2O_3 (b). Insets show the X-ray diffraction intensity for GT3 ($\text{GeO}_2:\text{TiO}_2 = 1:5$) and GB3 ($\text{GeO}_2:\text{B}_2\text{O}_3 = 1:5$) glass samples.

Figure 3 shows the XRD patterns of the GT and GB precursor glasses. The titanate–germanate samples revealed only a broad diffuse scattering at different angles instead of narrow lines typical for crystalline materials, confirming a long-range structural disorder

characteristic of the amorphous glassy network. The same behavior was observed in the case of a glass sample where GeO_2 was partially substituted by B_2O_3 from Figure 3b. The broad low intense peak at the angles $20\text{--}30^\circ$ confirmed the amorphous nature of the GB1, GB2, and GB3 samples. Additionally, the hump's maximum did not shift, corroborating the absence of the evolution to a lower degree of the order of the local structure of the studied glasses with wide $\text{GeO}_2\text{:TiO}_2$ and $\text{GeO}_2\text{:B}_2\text{O}_3$ molar ratios. Moreover, the GT3 glass sample containing 50 mol% TiO_2 showed a higher peak intensity than the glass sample with predominantly boron trioxide content GB3. This phenomenon met the requirement that the higher the atomic number of an element ($\text{Ti} > \text{B}$), the higher the X-ray diffraction intensity shown in the inset of Figure 3.

Figure 4 illustrates the optical UV–visible absorption spectra for fabricated germanate glasses modified by titanium dioxide (Figure 4a) and boron trioxide (Figure 4b). It should be noted that the characteristic of both series of $\text{GeO}_2\text{-TiO}_2\text{-BaO-Ga}_2\text{O}_3$ and $\text{GeO}_2\text{-B}_2\text{O}_3\text{-BaO-Ga}_2\text{O}_3$ glass matrices is the absorption edge which was shifting towards the longer wavelength with increasing TiO_2 and B_2O_3 content. Following that, the UV cut-off wavelength, referred to as the intersection between the zero-base line and the extrapolation of the absorption edge, was estimated. The inset in Figure 4a,b presents the absorption edge for the GT1, GT2, GT3 and GB1, GB2, GB3 glasses. From absorption spectra, it is clear that with the increasing $\text{TiO}_2/\text{B}_2\text{O}_3$ concentration, the absorption edges were shifted to longer wavelengths.

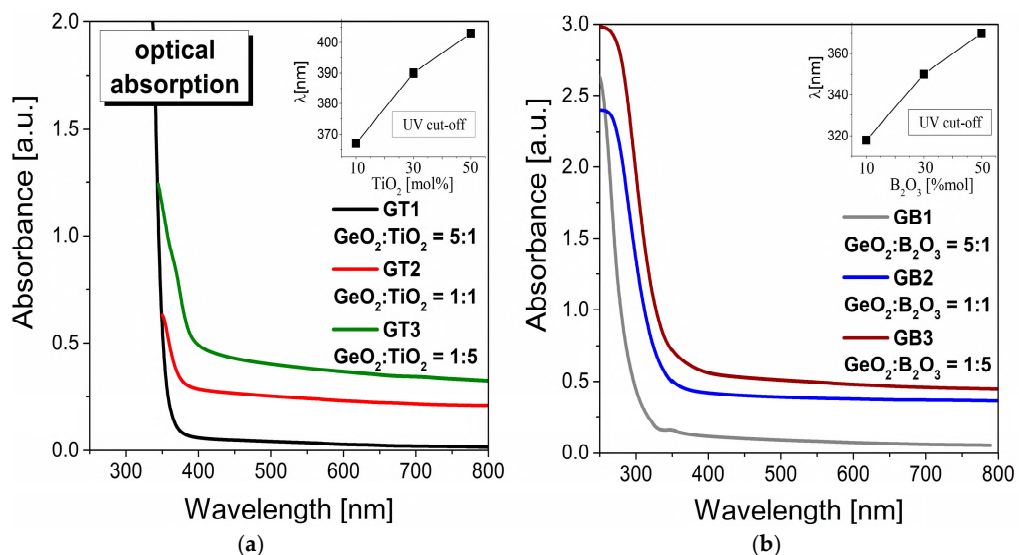


Figure 4. UV–visible optical absorption spectra for glass systems modified by TiO_2 (a) and B_2O_3 (b). Insets show the variation in UV cut-off as a function of TiO_2 and B_2O_3 concentration.

According to the literature [42,43], titanium ions are also accepted to exist in glasses in various oxidation states. For this reason, we extended our experimental approach in optical research by designing and preparing a glass sample doped with an extremely low concentration of TiO_2 (0.005 mol% TiO_2). We registered the optical absorption spectrum for the spectroscopic characterization of titanium states in the glass sample (Figure 5a). Rao et al. [44] suggest that the intense and very broad absorption in the visible region was a result of superimposed bands from Ti^{3+} and Ti^{4+} ions. In the silica calcium aluminosilicate system, the band of about 310 nm corresponded to the Ti^{4+} ions [45]. However, this band was strongly masked by the absorption edge for titanium-doped germanate glass, which was significantly shifted toward longer wavelengths. Moreover, in the case of a fabricated sample doped with titanium ions, the inset of Figure 5a displays the high-resolution optical absorption spectrum in the 675–730 nm range. The low intense absorption band centered at 700 nm may be quite well interpreted and related to the $\text{Ti}^{3+}\text{--Ti}^{4+}$ ion pair interactions [45].

Based on it, it was stated that the presented experiment constitutes the next step toward measurements with different emission wavelengths

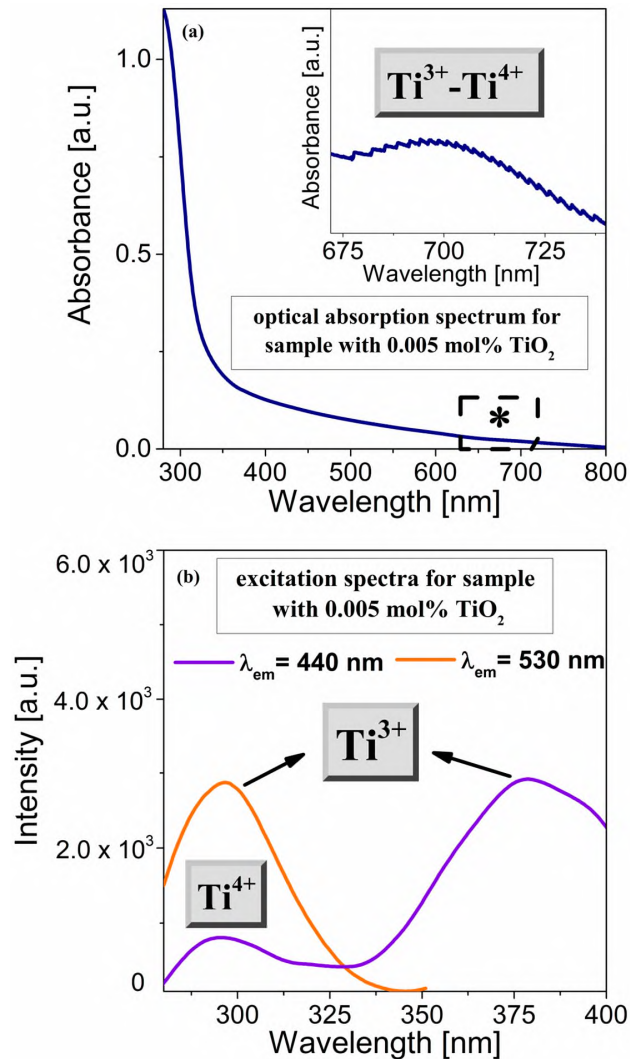


Figure 5. Optical absorption spectrum (a) and excitation spectra (b) of the sample containing extremely low titanium dioxide content. The excitation spectra are monitored at 440 nm and 530 nm. The inset shows $Ti^{3+}-Ti^{4+}$ pair's interaction in the range 675–730 nm (*) recorded with high resolution.

To analyze the emission spectra for the prepared glasses, it is necessary to know the excitation wavelengths of titanium ions. For this purpose, Figure 5 shows combined excitation spectra for the titanium-doped germanate glass sample (0.005 mol%). Upon excitation at 440 nm, the band at 270 nm might be identified as Ti ions in a tetravalent oxidation state [44,45]. On the other hand, our experimental investigations demonstrated the excitation band by monitoring the emission at 530 nm. The spectrum exhibited a relatively intense band at about 300 nm, which could be related to the Ti^{3+} ions [44, 45].

We performed the same procedure for the GT1, GT2, and GT3 glass samples (Figure 6). Obviously, changing the chemical glass composition leads to changes in the positions and intensities of the relevant excitation bands of the titanium species. Within the VIS range, the excitation spectra consisted of a characteristic band centered at 390 nm (Figure 6a). The relatively highest intensity of these excitation band glasses suggests a larger Ti^{3+} ions concentration in these samples. Notably, the band associated with titanium ions on

the tetravalent valence state was very weakly detectable. Further analysis demonstrated notable changes in the excitation spectra ($\lambda_{em} = 530$ nm) dependent on the TiO_2 content. To evaluate a full picture of the optical properties of the titanate–germanate glass system, we performed a luminescence experiment using the direct excitation wavelength between two excitation bands ($\lambda_{exc} = 345$ nm).

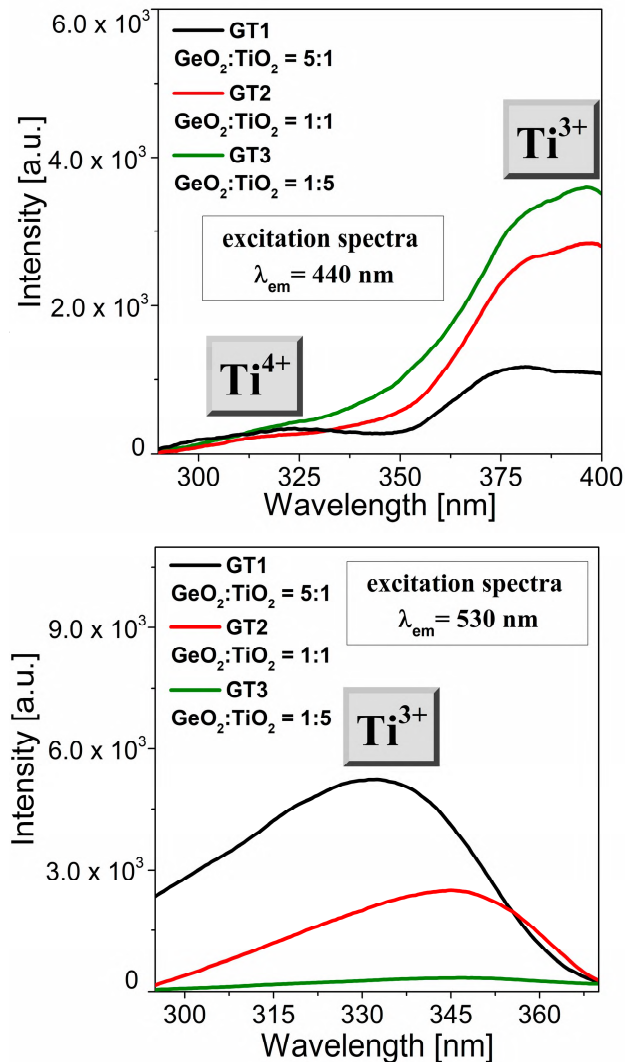


Figure 6. Excitation spectra ($\lambda_{em} = 440$ nm and $\lambda_{em} = 530$ nm) for GT1, GT2, GT3 samples.

The emission properties of GeO_2 - TiO_2 - BaO - Ga_2O_3 glass systems with different GeO_2 : TiO_2 molar ratios were investigated under the 345 nm excitation wavelength and recorded in the 400–650 nm range, as shown in Figure 7. The asterisk (*) refers to the extremely low titanium dioxide concentration of the glass samples. For the fabricated titanate–germanate glasses (GT1, GT2, GT3), the intensities of the recorded band at 560 nm increased with the increasing GeO_2 : TiO_2 molar ratio. Interestingly, for the sample with the highest GeO_2 : TiO_2 molar ratio (1:5), the concentration quenching of the emission of the Ti^{3+} ions was observed. Our research phenomenally demonstrated that the successive replacement of germanium dioxide by titanium dioxide shifts the redox equilibrium Ti^{3+} - Ti^{4+} to obtain optically detectable amounts of Ti^{3+} ions. Hence, a sample with a 10 mol% concentration of TiO_2 is preferable for achieving a high luminescence emission of

Ti³⁺ ions. Broadband, low-intensity emission with a maximum of 440 nm is characteristic of the Ti⁴⁺ valence state [44,45].

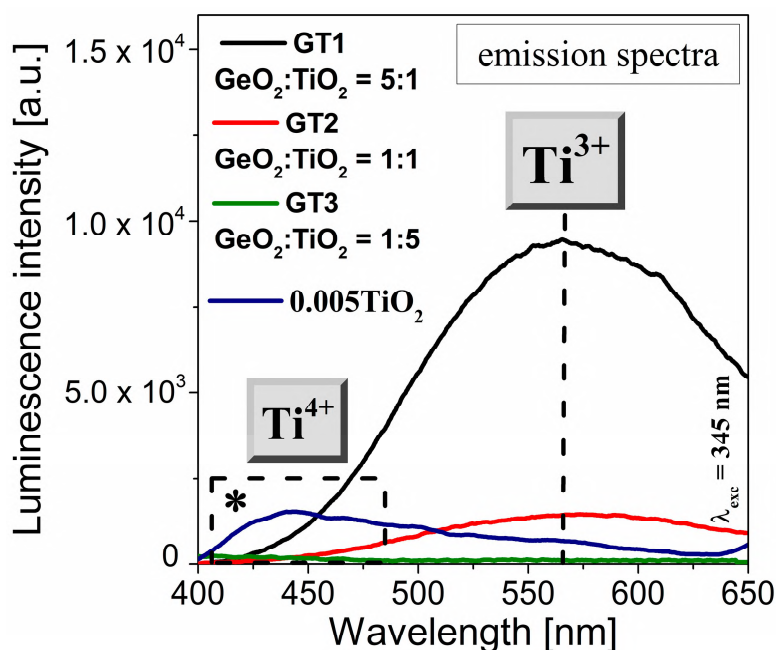


Figure 7. Visible emission spectra ($\lambda_{\text{exc}} = 345 \text{ nm}$) for GT1, GT2, and GT3 samples. The asterisk (*) refers to glass containing an extremely low titanium dioxide concentration.

The absorption, excitation, and luminescence results showed that titanium dioxide caused variations in the valence state of the titanium ions in the germanate glass network that may produce structural modifications and local-field variations in the structure. For this reason, this work discusses the IR and Raman spectroscopy of germanate-based glass systems modified by TiO₂/B₂O₃.

3.2. Raman and FT-IR Spectroscopy of Barium Gallo-Germanate Glasses Containing TiO₂/B₂O₃

Previous reports showed that many types of germanate glass had been studied using vibrational spectroscopy [46–49]. Initially, the precise determination of the network units characterized by multicomponent germanate matrices was a complicated task due to the character of composed network-forming or network-modifier oxides. The network of germanate glass is formed by tetrahedral GeO₄ structural units, which share their corners, and the Ge atom is covalently bonded to four bridging oxygens. The thermodynamic instability of the GeO₆ octahedral units produces a large concentration of nonbridging oxygen ions. This evolution clearly indicates the conversion of [GeO₄] → [GeO₆] structural units [50]. According to the literature [51], the vibrational spectrum of the germanate glasses is rather remarkable. The germanate matrix is characterized by the structural units' dominant contributions in low- and high-frequency regions. The low-frequency region is mainly characterized by a peak around 560 cm^{−1} and is associated with the bending vibrations of Ge-O-Ge. The high-frequency region is reported to contain a band at approx. 915 cm^{−1}, and low inflections at approx. 1000 cm^{−1} are attributed to the asymmetric vibrations of the Ge-O-(Ge) bridges. These bands occur in a typical infrared spectrum when the glassy germanium oxide is composed of germanium–oxygen tetrahedra with nonbridging oxygens. It was repeatedly demonstrated that changes in the local structure of the germanate network as the alkali concentration [52,53] increased resulted in a systematic shift in the band components associated with the vibrations of the GeO₄ units. This is evidenced by the broken Ge-O bridges at about 750 and 870 cm^{−1} for the Q2 and

Q3 units. Comprehensive studies of germanate glasses have also provided strong evidence regarding the replacement of GeO_4 by other units, including germanate–oxygen octahedra (GeO_6). This strong modification is demonstrated by the appearance of a band at about 715 cm^{-1} in the midinfrared spectrum, evidently involving a change in the coordination number of the germanium ions from four (LK = 4) to six (LK = 6) [54,55]. According to the paper published by McKeon and Marzbacher [56], when the GeO_2 content decreases, the midfrequency envelope shifts to higher frequencies while the high-frequency features shift to lower frequencies. It was interpreted as a reduction in the average ring size, as well as an average lengthening of the T–O (where T is Ge or Ga) band.

Figure 8 shows the measured FT-IR and Raman spectra in the wavelength range of $400\text{--}1600\text{ cm}^{-1}$ of barium gallo-germanate glasses with various $\text{GeO}_2\text{:TiO}_2$ molar ratios. The spectra exhibited two groups of bands (i) in the low-frequency region located from 400 to 600 cm^{-1} and (ii) in the high-frequency region from 700 to 900 cm^{-1} . A single band dominates the first region of $400\text{--}600\text{ cm}^{-1}$ due to the GeO_4 structural units, which share their corners, where the germanium atom bending is covalently bonded to four bridging oxygens. The second high-frequency region, between $620\text{--}900\text{ cm}^{-1}$, is attributed to the GeO_6 structural units, where the central atom is germanium and is surrounded by six oxygen atoms [57,58]. As expected, the molar ratio of TiO_2 strongly affected these structural properties of glasses. As one can see from Figure 8, the intensities of the IR and Raman bands related to the GeO_4 and GeO_6 structural units underwent significant changes by incorporating the TiO_2 content into the germanate glass host. With the introduction of TiO_2 up to 30mol% in the $\text{GeO}_2\text{-BaO-Ga}_2\text{O}_3$ glass network, the intensity band centered at about 450 cm^{-1} and 800 cm^{-1} was observed to significantly decrease with the shifting towards the lower frequency region. However, when the TiO_2 concentration was greater than 30mol%, it was observed that the band due to the GeO_6 structural units was shifted to higher frequencies. The explanation for these results lies in the dual role of titanium dioxide in the glass network. Titanium dioxide acted both as the network modifier and network former, which participated during the formation of the glass network in the form of TiO_4 or existed in the gap outside the network in the form of TiO_6 units [57–60]. In this work, the effect observed with the increased TiO_2 content very well confirms that the doping titanium ions of the germanate matrix generated a strong destruction of germanate tetrahedra and octahedra units caused by the formation of more Ti–O structural units. We considered the Raman spectrum for the $\text{GeO}_2\text{:TiO}_2 = 1\text{:}5$ (GT3) glass sample when titanium dioxide acted as a network former. The main problem with this material is the interpretation of the local structure due to the overlapping bands. The most interesting observation concerning all registered spectra was the presence of a band in the frequency range of $600\text{--}700\text{ cm}^{-1}$. The mentioned band was very detectable with the increase in the amount of titanium ions introduced at the expense of germanium ions, which resulted in a systematic decrease in the amount of GeO_4 tetrahedrons and GeO_6 octahedrons. According to the data, this Raman peak is considered strong evidence of Ti–O stretching vibration connected with the TiO_6 unit. Earlier studies of other glasses containing TiO_2 exhibited a well-resolved band at about $\sim 720\text{ cm}^{-1}$ identified due to the vibration of TiO_4 structural units [61,62].

As a final point of our investigations, we characterized the structural properties of the barium gallo-germanate glass host containing B_2O_3 (Figure 9). As expected, independently, the chemical composition germanate glass structure resulted in the appearance of the spectra, revealing signals from the bending and stretching modes of the GeO_4 and GeO_6 structural units. In contrast to TiO_2 , the addition of boron oxide was found to be a weak scatterer in low-frequency and high-frequency ranges between $400\text{--}1600\text{ cm}^{-1}$. Adding B_2O_3 to glass causes progressive changes in the low and higher frequency range. These changes are accompanied by the decreasing of a strong band at 450 cm^{-1} (almost vanishing at 50 mol% B_2O_3 in the FT-IR spectrum) and the one at 800 cm^{-1} with increasing borate content and shifts to lower frequencies. The obtained results indicated that the Raman shift decreased from 1411 cm^{-1} (glass GeO_2 -rich composition) to 1340 cm^{-1} (glass B_2O_3 -rich composition). A clear correspondence was observed between the bands in the Raman

spectra and the measurements carried out of the infrared spectra for the obtained glasses. In general, in the boron-based glass host, boron is three-coordinated. Moreover, previous studies indicated the presence of trigonal and tetrahedral boron with different ratios and the partial conversion of BO_3 into BO_4 units [63,64].

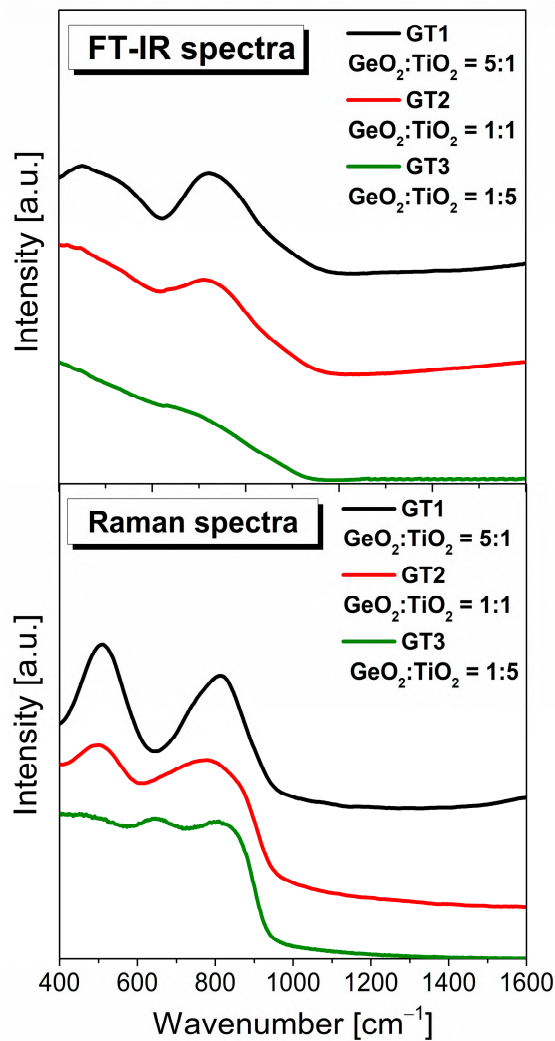


Figure 8. Infrared and Raman spectra of the investigated samples with $\text{GeO}_2/\text{TiO}_2$ ratio (5:1, 1:1, and 1:5).

To better visualize the obtained data, the deconvoluted components infrared bands were separated by a Gaussian deconvolution constructed for each sample GB1, GB2, and GB3 (see Figure 10). From the structural point of view, the most important observation was the change in the shift and the relative intensities of these two deconvoluted components positioned at 1230 cm^{-1} and 1360 cm^{-1} initiated as a function of the quantitative $\text{GeO}_2/\text{B}_2\text{O}_3$ ratio. Hence, in assessing the effect of boron oxide on the barium gallo-germanate glass network, it is useful to analyze the location and mutual intensity of the appropriate deconvoluted bands, which have been previously described in detail in the scientific report of lead-borate glass systems [65].

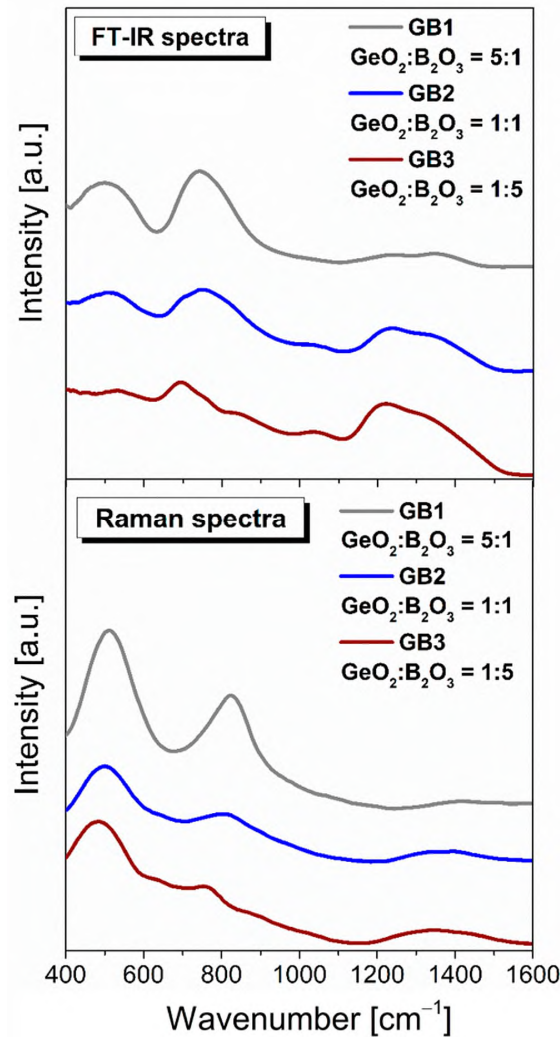


Figure 9. Infrared and Raman spectra of investigated glass samples with $\text{GeO}_2/\text{B}_2\text{O}_3$ ratio (5:1, 1:1, and 1:5).

The peculiar structural properties of borate glasses come from the ability of boron to occur in three or four coordination. In general, the equilibrium of the structural conversion between the BO_3 and BO_4 units in the glass network depends on the chemical composition and the kind of modifiers [66,67]. Moreover, the relative fraction of the BO_3 and BO_4 groups proved to be a sensitive probe of the basic structural units of the network. Calculations were evaluated with the following formula presented in Figure 11, where A_3 and A_4 correspond to the areas of the BO_3 and BO_4 groups. The relative integrated intensity A_3/A_4 of the $\text{GeO}_2\text{-B}_2\text{O}_3\text{-BaO-Ga}_2\text{O}_3$ glass system upon adding oxides GeO_2 and B_2O_3 in three different concentrations of 10%, 30%, and 50% each drastically reduced from 1.03 (glass sample GB1) to 0.38 (glass sample GB3), respectively. We can conclude that the incorporation of B_2O_3 changed the local structure of the barium gallo-germanate glasses, and the low polymeric states containing the BO_3 units constantly transformed into the high polymerized network units that mainly consisted of BO_4 . Interestingly, the group Mogus-Milankovic et al. [68] noted results for the quaternary $\text{Li}_2\text{O-B}_2\text{O}_3\text{-P}_2\text{O}_5\text{-Ge}_2\text{O}_3$ glass system. With the addition of lower GeO_2 content, the dominant borate unit was BO_4 , whose charge was more delocalized and enhanced the ion transport. In contrast, the formation of neutral BO_3 units at a higher GeO_2 concentration could break the conduction pathways and reduce the mobility of

the ions. According to the literature [69–71], the competition for charge compensation between highly charged cations is the fundamental reason for boron coordination. The field strength of different modifier cations such as Na^+ , Ba^{2+} , and Ca^{2+} [72] affects the enhanced stabilization of tetraborate groups by involving higher field strength cations in NBO-rich glasses. A similar effect of Na^+ in sodium borate glasses has been recently found for the highly charged state of lanthanide ions (which act as modifiers) [73], which boosts the formation of negatively charged tetrahedral boron.

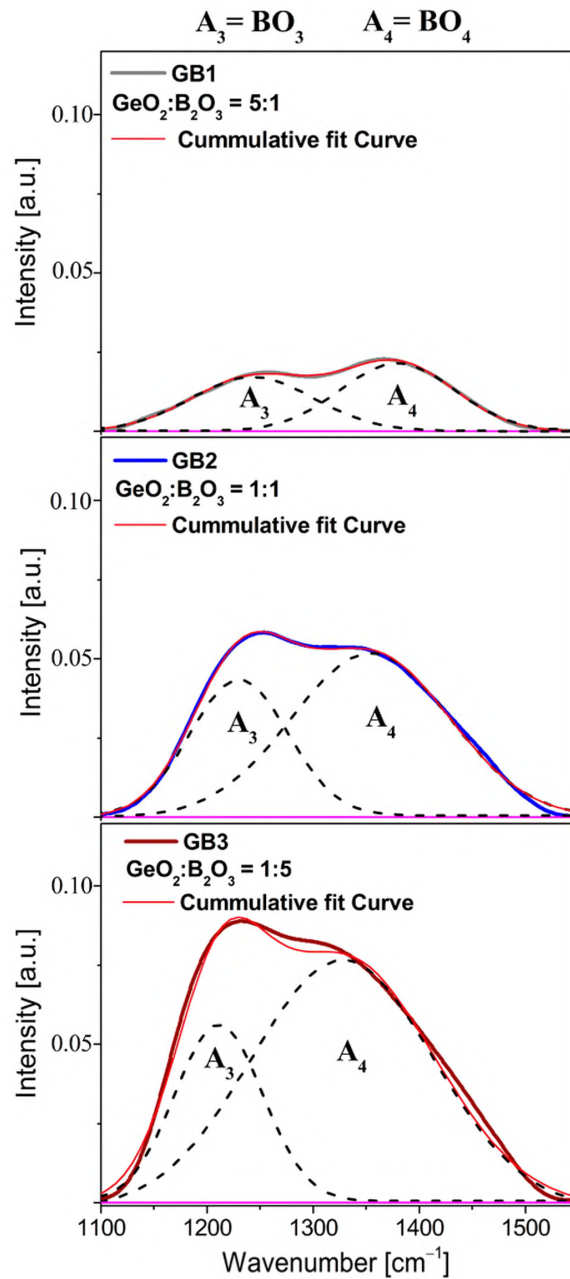


Figure 10. Deconvoluted infrared bands of series glass samples (GB1, GB2, GB3) as a function of GeO_2 and B_2O_3 concentration in spectra range $1100\text{--}1550\text{ cm}^{-1}$.

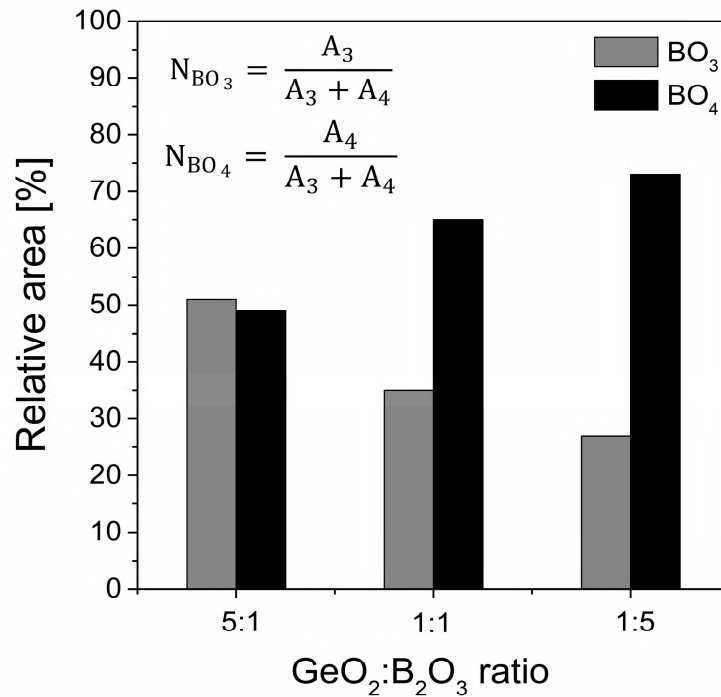


Figure 11. Change with composition of the calculated total fraction of BO₃ and BO₄ units versus the GeO₂/B₂O₃ molar ratio.

4. Discussion

The properties of precursor glasses were characterized using various experimental techniques to fulfill laser sources emitting midinfrared radiation and broadband optical amplifiers operating at near-IR range requirements. The obtained novel titanate–germanate and borogermanate glasses with a TiO₂ and B₂O₃ content of up to 50 mol% were transparent and exhibited a fully amorphous nature. The luminescence studies of the GeO₂-TiO₂-BaO-Ga₂O₃ glasses perfectly confirmed the oxidation state of titanium ions in the function of the GeO₂:TiO₂ molar ratio. In the case of the GT series of glasses, the titanium acted as a glass network and a network modifier in the barium gallo-germanate network. It was proven that the incorporation of two various metal oxides in the barium-gallo germanate glass host influenced their structural GeO₄ and GeO₆ units. Indeed, this effort led to the better identification of the structural building blocks and the evolution of the Raman and FT-IR spectra of the BaO-Ga₂O₃-GeO₂ glass system containing TiO₂/B₂O₃ in the lower and higher frequency, respectively. It is well known that in glasses doped with lanthanide ions, the highest-energy phonons exercise the most influence in nonradiative relaxations because multiphonon decay occurs with the fewest number of phonons required to bridge the energy gap between two manifolds. On the other hand, the lower phonon energy of the glass host can reduce the probability of nonradiative relaxation and enable the higher quantum efficiency of photoluminescence and/or a higher luminescence lifetime of the excited state of lanthanide ions [74,75]. Moreover, we indicated [76] that the highest phonon energy for glass with GeO₂:TiO₂ equal to 1:1 decreased to 765 cm⁻¹, which was smaller than that of the pure barium gallo-germanate glass reported (845 cm⁻¹) [77]. For this reason, in the field of developing the glass structure system by embedding optically active ions to enhance their optical characteristics, titanium dioxide is a very useful component. Our systematic investigations demonstrated that barium gallo-germanate glasses containing TiO₂ can be successfully used for near-IR laser applications at 1.06 μm through Nd³⁺ doping. The same glass systems doped with Er³⁺ ions are suitable for near-IR luminescence at 1.5 μm and could be useful for near-infrared broadband optical amplifiers. However,

the optimal molar ratios of $\text{GeO}_2:\text{TiO}_2$ in these glass systems were completely different for Nd^{3+} [78] than Er^{3+} [79] ions. The further characterization of barium gallo-germanate glasses with TiO_2 and their energy transfer processes between Yb^{3+} and Ln^{3+} ions ($\text{Ln} = \text{Pr}, \text{Er}, \text{Tm}, \text{Ho}$) [80] allowed us to demonstrate that the measured lifetimes decreased with an increasing TiO_2 content, while changes in the energy transfer efficiency seemed to be nonlinear. To extend the optical applications of barium gallo-germanate glasses, the effect of B_2O_3 on structural modifications in the higher frequency range was observed, suggesting the important role of the molar ratio of $\text{GeO}_2:\text{B}_2\text{O}_3$ in the formation of the glass host. In general, borate glasses are striking hosts because they are highly transparent, thermally stable, and show an appreciable solubility of lanthanide ions [81]. In the part of this work devoted to the results the Raman band near 1300 cm^{-1} was very well observed after B_2O_3 incorporation. This Raman band was related to the maximal phonon energy of the borate glass host, which caused emission quenching and the suppression of radiative emissions, especially in the near-IR spectral range. For that reason, barium gallo-germanate glasses containing relatively higher B_2O_3 concentrations are rather useless for near-IR luminescence applications, but they are interesting glass materials for the emission of visible light. These glass systems doped with Dy^{3+} ions emitted an intense greenish light, which was changed to yellowish light with an increasing $\text{GeO}_2:\text{B}_2\text{O}_3$ molar ratio [82]. Interestingly, increasing B_2O_3 concentrations in barium gallo-germanate glasses did not negatively affect the reddish–orange luminescence and experimental lifetimes of Eu^{3+} ions despite their relatively high phonon energy [83]. This suggests evidently that barium gallo-germanate glass can be an excellent candidate for visible or near-IR luminescence depending on the glass modifiers (TiO_2 or B_2O_3) and lanthanide doping.

5. Conclusions

Undoped germanate-based glasses modified by $\text{TiO}_2/\text{B}_2\text{O}_3$ were studied experimentally using XRD, luminescence, FT-IR, and Raman spectroscopy. The results led to the following conclusions:

1. Barium gallo-germanate glass hosts can accommodate 50 mol% TiO_2 and B_2O_3 , and the samples were still fully amorphous. Based on the absorption spectra measurements, the absorption edge was determined. It was proven that the intensities of the excitation and emissions and the position bands of Ti^{3+} and Ti^{4+} strongly depended on the chemical composition of the fabricated materials.
2. Analysis of Raman and FT-IR spectra for the modified barium gallo-germanate glasses showed evidence of GeO_4 and GeO_6 structural units, independently of the $\text{GeO}_2/\text{TiO}_2$ and $\text{GeO}_2/\text{B}_2\text{O}_3$ molar ratio. However, titanium dioxide strongly modified the structure of the glass between the 400 cm^{-1} and 1000 cm^{-1} frequency region, while boron trioxide modified the structure between the 1100 cm^{-1} and 1600 cm^{-1} frequency region. As the titanium dioxide increased, the bands were shifted to a lower frequency region. From the Raman spectra, we observed that the additional band located near 650 cm^{-1} confirmed the presence of the TiO_6 unit. The dependence of the fractions of the BO_3 and BO_4 units on the kind of glass network formers was reduced from 1.03 to 0.38. Therefore, we confirmed such a hypothesis that there was a strict correlation between the local structure and optical properties of the barium gallo-germanate glass system in the function of two various network-former components (TiO_2 and B_2O_3). The presented analysis confirmed that the developed materials are one of the most important classes of matrices for doping optically active ions for photonic applications.

Author Contributions: Conceptualization, J.P. and M.S.; methodology, K.K. and M.K.; formal analysis, K.K. and M.S.; investigation, K.K. and M.K.; writing—original draft preparation, K.K.; writing—review and editing, J.P., M.K., and W.A.P.; visualization, K.K.; project administration, W.A.P.; funding acquisition, W.A.P. All authors have read and agreed to the published version of the manuscript.

Funding: This research was funded by the National Science Centre (Poland), grant number 2018/31/B/ST8/00166.

Institutional Review Board Statement: Not applicable.

Informed Consent Statement: Not applicable.

Data Availability Statement: Not applicable.

Conflicts of Interest: The authors declare no conflict of interest.

References

- Doweidar, H.; El-Egili, K.; Ramadan, R.; Khalil, E. Structural species in mixed-fluoride $\text{PbF}_2\text{-CdF}_2\text{-B}_2\text{O}_3$ borate glasses; FTIR investigation. *Vib. Spectrosc.* **2019**, *102*, 23–30. [[CrossRef](#)]
- Doweidar, H.; El-Damrawi, G.; Mansour, E.; Fetouh, R.E. Structural role of MgO and PbO in $\text{MgO-PbO-B}_2\text{O}_3$ glasses as revealed by FTIR; a new approach. *J. Non-Cryst. Solids* **2012**, *358*, 941–946. [[CrossRef](#)]
- Linda, D.; Dutreilh-Colas, M.; Hamani, D.; Thomas, P.; Mirgorodsky, A.; Duclere, J.R.; Masson, O.; Loukil, M.; Kabadou, A. New glasses within the $\text{Ti}_2\text{O-Ag}_2\text{-TeO}_2$ system: Thermal characteristics, Raman spectra and structural properties. *Mater. Res. Bull.* **2010**, *24*, 1816–1824. [[CrossRef](#)]
- Maniu, D.; Iliescu, T.; Ardelean, I.; Cinta-Pinzaru, S.; Tarcea, N.; Kiefer, W. Raman study on $\text{B}_2\text{O}_3\text{-CaO}$ glasses. *J. Mol. Struct.* **2003**, *651–653*, 485–488. [[CrossRef](#)]
- Pascuta, P.; Pop, L.; Rada, S.; Bosca, M.; Culea, E. The local structure of bismuth borate glasses doped with europium ions evidenced by FT-IR spectroscopy. *J. Mater. Sci.* **2008**, *19*, 424–428. [[CrossRef](#)]
- Ivascu, C.; Timar Gabor, A.; Cozar, O.; Daraban, L.; Ardelean, I. FT-IR, Raman and thermoluminescence investigation of $\text{P}_2\text{O}_5\text{-BaO-Li}_2\text{O}$ glass system. *J. Mol. Struct.* **2011**, *993*, 249–253. [[CrossRef](#)]
- Lai, Y.M.; Liang, X.F.; Yang, S.Y.; Wang, J.X.; Cao, L.H.; Dai, B. Raman and FTIR spectra of iron phosphate glasses containing cerium. *J. Mol. Struct.* **2011**, *992*, 84–88. [[CrossRef](#)]
- Rong, Q.J.; Osaka, A.; Nanba, T.; Takada, J.; Miura, Y. Infrared and Raman spectra of binary tellurite glasses containing boron and indium oxides. *J. Mater. Sci.* **1992**, *27*, 3793–3798. [[CrossRef](#)]
- Lalla, E.A.; Sanz-Arranz, A.; Konstantinidis, M.; Freemantle, J.; Such, P.; Lozano-Gorriñ, A.D.; Lavin, V.; Lopez-Reyes, G.; Rull-Perez, F.; Rodriguez-Mendoza, U.R. Raman-IR spectroscopic structural analysis of rare-earth (RE^{3+}) doped fluorotellurite glasses at different laser wavelengths. *Vib. Spectrosc.* **2020**, *106*, 103020. [[CrossRef](#)]
- Silva, A.M.B.; Queiroz, C.M.; Agathopoulos, S.; Correia, R.N.; Fernandes, M.H.V.; Oliveira, J.M. Structure of $\text{SiO}_2\text{-MgO-Na}_2\text{O}$ glasses by FTIR, Raman and ^{29}Si MAS NMR. *J. Mol. Struct.* **2011**, *986*, 16–21. [[CrossRef](#)]
- Eniu, D.; Gruian, C.; Vanea, E.; Patcas, L.; Simon, V. FTIR and EPR spectroscopic investigation of calcium-silicate glasses with iron and dysprosium. *J. Mol. Struct.* **2015**, *1084*, 23–27. [[CrossRef](#)]
- Baia, L.; Iliescu, T.; Simon, S.; Kiefer, W. Raman and IR spectroscopic studies of manganese doped $\text{GeO}_2\text{-Bi}_2\text{O}_3$ glasses. *J. Mol. Struct.* **2001**, *599*, 9–13. [[CrossRef](#)]
- Sigaev, V.N.; Gregora, I.; Pernice, P.; Champagnon, B.; Smelyanskaya, E.N.; Aronne, A.; Sarkisov, P.D. Structure of lead germanate glasses by Raman spectroscopy. *J. Non. Cryst. Solids* **2001**, *279*, 136–144. [[CrossRef](#)]
- Pascuta, P.; Pop, L.; Rada, S.; Bosca, M.; Culea, E. The local structure of bismuth germanate glasses and glass ceramics doped with europium ions evidenced by FT-IR spectroscopy. *Vib. Spectrosc.* **2008**, *48*, 281–283. [[CrossRef](#)]
- Koroleva, O.N.; Shtenberg, M.V.; Ivanova, T.N. The structure of potassium germanate glasses as revealed by Raman and IR spectroscopy. *J. Non-Cryst. Solids* **2019**, *510*, 143–150. [[CrossRef](#)]
- Hongisto, M.; Danto, S.; Ghena, M.; Iancu, D.; Ighigeanu, D.; Mihai, L.; Jubera, V.; Petit, L. Response of Various Yb^{3+} -Doped Oxide Glasses to Different Radiation Treatments. *Materials* **2022**, *15*, 3162. [[CrossRef](#)]
- Agathopoulos, S.; Tulyaganov, D.U.; Ventura, J.M.G.; Kannan, S.; Saranti, A.; Karakassides, M.A.; Ferreira, J.M.F. Structural analysis and devitrification of glasses based on the CaO-MgO-SiO_2 system with B_2O_3 , Na_2O , CaF_2 , and P_2O_5 additives. *J. Non-Cryst. Solids* **2006**, *352*, 322–328. [[CrossRef](#)]
- Rada, M.; Rus, L.; Rada, S.; Culea, E.; Rusu, T. The network modifier and former role of the bismuth ions in the bismuth-lead-germanate glasses. *Spectrochim. Acta A Mol. Biomol. Spectrosc.* **2014**, *132*, 533–537. [[CrossRef](#)]
- Ivanov, A.O.; Evstropiev, K.S. Structure of simple germanate glass. *Dokl. Akad. Nauk. SSSR* **1962**, *145*, 797.
- Tagiara, N.S.; Chatzipanagis, K.I.; Bradtmuller, H.; Rodrigues, A.C.M.; Moncke, D.; Kamitos, E.I. Network former mixing effects in alkali germanotellurite glasses: A vibrational spectroscopic study. *J. Alloys Compd.* **2021**, *882*, 160782. [[CrossRef](#)]
- Rada, S.; Erhan, R.V.; Bodnarchuk, V.; Barbu-Tudoran, L.; Culea, E. SANS, RAMAN and SEM studies of lead-germanate glasses doped with the manganese oxide. *J. Alloys Compd.* **2021**, *882*, 160721. [[CrossRef](#)]
- Mattos, G.R.S.; Bordon, C.D.S.; Kassab, L.R.P.; Issa, S.A.; AlMisned, G.; Tekin, H.O. Towards obtaining the optimum physical, optical, and nuclear radiation attenuation behaviours of tellurite-germanate glasses through Eu_2O_3 reinforcement: Glass synthesis, experimental and theoretical characterization study. *Ceram. Int.* **2023**, *49*, 986–994. [[CrossRef](#)]
- Pipes, R.S.; Shelby, J.E. Formation and properties of soda lime germanate glasses. *J. Non-Cryst. Solids* **2021**, *553*, 120506. [[CrossRef](#)]
- Falci, R.F.; Guerineau, T.; Delarosbil, J.L.; Messaddeq, Y. Spectroscopic properties of gallium-rich germane gallate glasses doped with Tm^{3+} . *J. Lumin.* **2022**, *249*, 119014. [[CrossRef](#)]

25. Jianga, X.P.; Yang, Z.M.; Liu, T.; Xu, S.H. Energy transfer between Yb^{3+} and Er^{3+} in barium gallogermanate glass. *J. Appl. Phys.* **2009**, *105*, 103113. [[CrossRef](#)]
26. Pisarska, J.; Sołtys, M.; Górny, A.; Kochanowicz, M.; Zmojda, J.; Dorosz, J.; Dorosz, D.; Sitarz, M.; Pisarski, W.A. Rare earth-doped barium gallo-germanate glasses and their near-infrared luminescence properties. *Spectrochim. Acta A* **2018**, *201*, 362–366. [[CrossRef](#)]
27. Edwards, T.; Endo, T.; Walton, J.H.; Sen, S. Observation of the transition state for pressure-induced $\text{BO}_3 \rightarrow \text{BO}_4$ conversion in glass. *Mater. Sci.* **2014**, *345*, 1261201. [[CrossRef](#)]
28. Farouk, M. Effect of TiO_2 on the structural, thermal, and optical properties of $\text{BaO-Li}_2\text{O-diborate}$ glasses. *J. Non-Cryst. Solids* **2014**, *402*, 74–78. [[CrossRef](#)]
29. Cheng, J.; Chen, W. Formation, and structure of titanate glasses. *J. Non-Cryst. Solids* **1986**, *80*, 135–140.
30. Zhang, B.; He, F.; Cao, X.; Wei, M.; Zheng, C.; Xie, J. The effect of TiO_2 and B_2O_3 on sintering behavior and crystallization behavior of $\text{SrO-BaO-B}_2\text{O}_3\text{-SiO}_2$ glass-ceramics. *Ceram. Int.* **2022**, *48*, 7013–7023. [[CrossRef](#)]
31. Kowalska, K.; Kuwik, M.; Polak, J.; Pisarska, J.; Pisarski, W.A. EPR and optical spectroscopy of Cr^{3+} ions in barium gallo-germanate glasses containing $\text{B}_2\text{O}_3/\text{TiO}_2$. *J. Lumin.* **2022**, *48*, 118775. [[CrossRef](#)]
32. Calzavara, F.; Allix, M.; Dussauze, M.; Jubera, V.; Nalin, M.; Cardinal, T.; Fargin, E. Glass forming regions, structure and properties of lanthanum barium germanate and gallate glasses. *J. Non Cryst. Solids* **2021**, *571*, 121064. [[CrossRef](#)]
33. Leśniak, M.; Mach, G.; Starzyk, B.; Sadowska, K.; Ragiń, T.; Zmojda, J.; Kochanowicz, M.; Kuwik, M.; Miluski, P.; Jimenez, G.L.; et al. The Effect of Fluorides (BaF_2 , MgF_2 , AlF_3) on Structural and Luminescence Properties of Er^{3+} -Doped Gallo-Germanate Glass. *Materials* **2022**, *15*, 5230. [[CrossRef](#)] [[PubMed](#)]
34. Skopak, T.; Calzavara, F.; Ledemi, Y.; Celarie, F.; Allix, M.; Veron, E.; Dussauze, M.; Cardinal, T.; Fargin, E.; Messaddeq, Y. Properties, structure and crystallization study of germane-gallate glasses in the $\text{Ga}_2\text{O}_3\text{-GeO}_2\text{-BaO-K}_2\text{O}$ system. *J. Non Cryst. Solids* **2019**, *514*, 98–107. [[CrossRef](#)]
35. Shelby, J. Properties and Morphology of Barium Germanate Glasses. *J. Am. Ceram. Soc.* **1984**, *67*, 557–560. [[CrossRef](#)]
36. Bayya, S.S.; Chin, G.D.; Sanghera, J.S.; Aggarwal, I.D. Germanate glass as a window for high energy laser systems. *Opt. Express* **2006**, *14*, 11687–11693. [[CrossRef](#)]
37. Jewell, J.M.; Higby, P.L.; Aggarwal, I.D. Properties of $\text{BaO-R}_2\text{O}_3\text{-Ga}_2\text{O}_3\text{-GeO}_2$ ($\text{R}=\text{Y, Al, La, and Gd}$) Glasses. *J. Am. Ceram. Soc.* **1994**, *77*, 698–700. [[CrossRef](#)]
38. Bayya, S.S.; Harbison, B.B.; Sanghera, J.S.; Aggarwal, I.D. $\text{BaO-Ga}_2\text{O}_3\text{-GeO}_2$ glasses with enhanced properties. *J. Non-Cryst. Solids* **1997**, *212*, 198–207. [[CrossRef](#)]
39. ElBatal, F.H.; Marzouk, M.N.; ElBatal, H.A. Optical and crystallization studies of titanium dioxide doped sodium and potassium silicate glasses. *J. Mol. Struct.* **2016**, *1121*, 54–59. [[CrossRef](#)]
40. Raghavaiah, B.V.; Laxmikanth, C.; Veeraiiah, N. Spectroscopic studies of titanium ions in $\text{PbO-Sb}_2\text{O}_3\text{-As}_2\text{O}_3$ glass system. *Opt. Commun.* **2004**, *235*, 341–349. [[CrossRef](#)]
41. Mingshen, M.; Wen, N.; Yali, W.; Zhongjie, W.; Fengmei, L. The effect of TiO_2 on phase separation and crystallization of glass-ceramic in $\text{CaO-MgO-Al}_2\text{O}_3\text{-SiO}_2\text{-Na}_2\text{O}$ system. *J. Non. Cryst. Solids* **2008**, *354*, 5395–5401. [[CrossRef](#)]
42. Drabik, J.; Cichy, B.; Marciniak, L. New Type on Nanocrystalline Luminescent Thermometers Based on $\text{Ti}^{3+}/\text{Ti}^{4+}$ and $\text{Ti}^{4+}/\text{Ln}^{3+}$ ($\text{Ln} = \text{Nd}^{3+}, \text{Eu}^{3+}, \text{Dy}^{3+}$) Luminescence Intensity Ratio. *J. Phys. Chem C* **2018**, *122*, 14928–14936. [[CrossRef](#)]
43. Colak, S.C. Role of titanium ions on the optical and thermal properties of zinc borate glass doped with TiO_2 . *Phys. Chem. Glasses Part B* **2017**, *58*, 41–48. [[CrossRef](#)]
44. Rao, R.B.; Rao, D.K.; Veeraiiah, N. The role of titanium ions on structural, dielectric, and optical properties of $\text{Li}_2\text{O-MgO-B}_2\text{O}_3$ glass system. *Mater. Chem. Phys.* **2004**, *87*, 357–369. [[CrossRef](#)]
45. Andrade, L.H.; Lima, S.M.; Novatski, A.; Neto, A.M.; Bento, A.C.; Baesso, L.M.; Gandra, F.C.G.; Guyot, Y.; Boulon, G. Spectroscopic assignments of Ti^{3+} and Ti^{4+} in titanium-doped OH^- free low-silica calcium aluminosilicate glass and role of structural defects on the observed long lifetime and high fluorescence of Ti^{3+} ions. *Phys. Rev. B* **2008**, *78*, 224202. [[CrossRef](#)]
46. Biswas, K.; Sontakke, A.D.; Annapurna, K. Effect of TiO_2 on thermal, structural and third-order nonlinear optical properties of Ca-La-B-O glass system. *J. Alloys Compd.* **2010**, *489*, 493–498. [[CrossRef](#)]
47. Pernice, P.; Aronne, A.; Catauro, M. Glass transition temperature and devitrification study of barium germanate glasses. *J. Non-Cryst. Solids* **1997**, *210*, 23–31. [[CrossRef](#)]
48. Rojas, S.S.; De Souza, J.E.; Andreeta, M.R.B.; Hernandez, A.C. Influence of ceria addition on thermal properties and local structure of bismuth germanate glasses. *J. Non-Cryst. Solids* **2010**, *356*, 2942–2946. [[CrossRef](#)]
49. Szal, R.; Zmojda, J.; Kochanowicz, M.; Miluski, P.; Dorosz, J.; Lesniak, M.; Jeleń, P.; Starzyk, B.; Sitarz, M.; Kuwik, M.; et al. Spectroscopic properties of antimony modified germanate glass doped with Eu^{3+} ions. *Ceram. Int.* **2019**, *45*, 24811–24817. [[CrossRef](#)]
50. Sahar, M.R.; Wahab, A.; Hussein, M.A.; Hussin, R. Structural characteristic of $\text{Na}_2\text{O-P}_2\text{O}_5\text{-GeO}_2$ glass systems. *J. Non-Cryst. Solids* **2007**, *353*, 1134–1140. [[CrossRef](#)]
51. Zmojda, J.; Kochanowicz, M.; Miluski, P.; Lesniak, M.; Sitarz, M.; Pisarski, W.A.; Pisarska, J.; Dorosz, D. Effect of GeO_2 content on structural and spectroscopic properties of antimony glasses doped with Sm^{3+} ions. *J. Mol. Struct.* **2016**, *1126*, 207–212. [[CrossRef](#)]
52. Di Martino, D.; Santos, L.F.; Marques, A.C.; Almeida, R.M. Vibrational spectra and structure of alkali germanate glasses. *J. Non-Cryst. Solids* **2001**, 293–295, 394–401. [[CrossRef](#)]

53. Alvarado-Rivera, J.; Rodriguez-Carvajal, D.A.; Acosta-Enriquez, M.d.C.; Manzaneres-Martinez, M.B.; Alvarez, E.; Lozada-Morales, R.; Diaz, G.C.; de Leon, A.; Zayas, M.E. Effect of CeO₂ on the Glass Structure of Sodium Germanate Glasses. *J. Am. Ceram. Soc.* **2014**, *97*, 3493–3500. [[CrossRef](#)]
54. Rachkovskaya, G.E.; Zakharevich, G.B. IR spectra of tellurium germanate glasses and their structure. *J. Appl. Spectrosc.* **2007**, *74*, 86–89. [[CrossRef](#)]
55. Henderson, G.S.; Fleet, M.E. The structure of glasses along the Na₂O-GeO₂ join. *J. Non-Cryst. Solids* **1991**, *134*, 259–269. [[CrossRef](#)]
56. McKeown, D.A.; Merzbacher, C.I. Raman spectroscopic studies of BaO-Ga₂O₃-GeO₂ glasses. *J. Non-Cryst. Solids* **1995**, *183*, 61–72. [[CrossRef](#)]
57. Curtis, B.; Hynek, D.; Kaizer, S.; Feller, S.; Martin, S.W. Composition dependence of the short range order structures in 0.2Na₂O+0.9[xBO₃/₂+(1-x)GeO₂] mixed glass formers. *J. Non-Cryst. Solids* **2018**, *500*, 61–69. [[CrossRef](#)]
58. Kukhareenko, S.A.; Shilo, A.E.; Itsenko, P.P.; Kutsai, A.N. The effect of titanium dioxide on the structure of silicate multicomponent glasses. *J. Superhard Mater.* **2010**, *32*, 396–405. [[CrossRef](#)]
59. Klyuev, V.P. Dependences of the dilatometric properties of glasses on their structure: II. Silicate, phosphate, fluorine-containing, and titanium-containing glasses. *Glass Phys. Chem.* **2006**, *32*, 196–205. [[CrossRef](#)]
60. El-Ahafi, N.A.; Morsi, M.M. Optical absorption and infrared studies of some silicate glasses containing titanium. *J. Mater. Sci.* **1997**, *32*, 5185–5189. [[CrossRef](#)]
61. Elsaghier, H.M.; Azooz, M.A.; Zidan, N.A.; Abbas, W.; Okasha, A.; Marzouk, S.Y. The influence of Er³⁺ ions on the spectroscopic and lasing characteristics of alkaline earth titanium borate glasses for photonic applications. *Opt. Mater.* **2022**, *131*, 112624. [[CrossRef](#)]
62. Cernosek, Z.; Chladkova, M.; Holubova, J. The influence of TiO₂ on the structure and properties of sodium-zinc phosphate glasses. *J. Non-Cryst. Solids* **2020**, *531*, 119866. [[CrossRef](#)]
63. Subhadra, M.; Kistaiah, P. Infrared and Raman spectroscopic studies of alkali bismuth borate glasses: Evidence of mixed alkali effect. *Vib. Spectrosc.* **2012**, *62*, 23–27. [[CrossRef](#)]
64. Fajans, K.; Barber, S.W. Properties and Structures of Vitreous and Crystalline Boron Oxide. *J. Am. Chem. Soc.* **1952**, *74*, 2761–2768. [[CrossRef](#)]
65. Pisarski, W.A.; Pisarska, J.; Ryba-Romanowski, W. Structural role of rare earth ions in lead borate glasses evidenced by infrared spectroscopy: BO₃→BO₄ conversion. *J. Mol. Struct.* **2005**, *744–747*, 515–520. [[CrossRef](#)]
66. Huang, S.; Wang, W.; Jiang, H.; Zhao, H.; Ma, Y. Network Structure and Properties of Lithium Aluminosilicate Glass. *Materials* **2022**, *15*, 4555. [[CrossRef](#)]
67. Culea, E.; Ristoiu, T.; Bratu, I. Magnetic and structural behavior of some borate glasses containing holmium ions. *Mater. Sci. Eng.* **1999**, *57*, 259–261. [[CrossRef](#)]
68. Mogus-Milankovic, A.; Sklepik, K.; Mosner, P.; Koudelka, L.; Kalendra, P. Lithium-Ion Mobility in Quaternary Boro-Germano-Phosphate Glasses. *J. Phys. Chem. B* **2016**, *120*, 3978–3987. [[CrossRef](#)]
69. Cormier, L.; Ghaleb, D.; Delaye, J.M.; Calas, G. Competition for charge compensation in borosilicate glasses: Wide-angle X-ray scattering and molecular dynamics calculations. *Phys. Rev. B* **2000**, *61*, 14495. [[CrossRef](#)]
70. Costa-silva, D.L.; Bartolome, J.F.; Silva, A.C.; Mello-Castanho, S. Structural and thermal influence of niobia in aluminoborosilicate glasses. *Ceram. Int.* **2022**, *48*, 18433–18440. [[CrossRef](#)]
71. Yin, H.; Gao, Y.; Guo, H.; Wang, C.; Yang, C. Effect of B₂O₃ Content and Microstructure on Verdet Constant of Tb₂O₃-Doped GBSB Magneto-Optical Glass. *J. Phys. Chem. C* **2018**, *122*, 16894–16900. [[CrossRef](#)]
72. Wu, J.; Stebbins, J.F. Cation Field Strength Effects on Boron Coordination in Binary Borate Glasses. *J. Am. Ceram. Soc.* **2014**, *97*, 2794–2801. [[CrossRef](#)]
73. Fabian, M.; Gergely, F.; Osan, J.; Cendak, T.; Kesari, S.; Rao, R. Structural investigation of borosilicate glasses containing lanthanide ions. *Sci. Rep.* **2020**, *10*, 7835. [[CrossRef](#)] [[PubMed](#)]
74. Xu, R.; Xu, L.; Hu, L.; Zhang, J. Structural Origin and Laser Performance of Thulium-Doped Germanate Glasses. *J. Phys. Chem. A* **2011**, *115*, 14163–14167. [[CrossRef](#)]
75. Ebendorff-Heidepriem, H.; Wang, P. Chapter 3—Oxide Glass and Optical Fiber Fabrication. *Mid-Infrared Fiber Photonics* **2022**, *Chapter 3*, 111–176. [[CrossRef](#)]
76. Pisarski, W.A.; Kowalska, K.; Kuwik, M.; Polak, J.; Pietrasik, E.; Goryczka, T.; Pisarska, J. Novel Multicomponent Titanate-Germanate Glasses: Synthesis, Structure, Properties, Transition Metal, and Rare Earth Doping. *Materials* **2020**, *13*, 4422. [[CrossRef](#)]
77. Wen, X.; Tang, G.; Yang, Q.; Chen, X.; Qian, Q.; Zhang, Q.; Yang, Z. Highly Tm³⁺ doped germanate glass and its single mode fiber for 2.0 μm laser. *Sci Rep.* **2016**, *6*, 20344. [[CrossRef](#)]
78. Pisarski, W.A.; Kowalska, K.; Kuwik, M.; Pisarska, J.; Dorosz, D.; Żmojda, J.; Kochanowicz, M.; Dorosz, D. Nd³⁺ doped titanate-germanate glasses for near-IR laser applications. *Opt. Mater. Express* **2022**, *7*, 2912–2926. [[CrossRef](#)]
79. Kowalska, K.; Kuwik, M.; Pisarska, J.; Leśniak, M.; Dorosz, D.; Kochanowicz, M.; Żmojda, J.; Dorosz, A.; Pisarski, W.A. Influence of TiO₂ concentration on near-infrared luminescence of Er³⁺ ions in barium gallo-germanate glasses. *J. Mater. Res. Technol.* **2022**, *21*, 4761–4772. [[CrossRef](#)]
80. Kowalska, K.; Kuwik, M.; Pisarska, J.; Pisarski, W.A. Near-IR Luminescence of Rare-Earth Ions (Er³⁺, Pr³⁺, Ho³⁺, Tm³⁺) in Titanate-Germanate Glasses under Excitation of Yb³⁺. *Materials* **2022**, *15*, 3660. [[CrossRef](#)]

81. Kaur, S.; Mohan, S.; Singh, D.P. Spectroscopic properties and lasing potentialities of Sm³⁺ doped multi-component borate glasses. *Opt. Commun.* **2021**, *482*, 126523. [[CrossRef](#)]
82. Kuwik, M.; Górny, A.; Pisarski, W.A.; Pisarska, J. Influence of glass formers and glass modifiers on spectral properties and CIE coordinated of Dy³⁺ ions in lead-free borate glasses. *Spectrochim. Acta A* **2022**, *268*, 120693. [[CrossRef](#)]
83. Kowalska, K.; Kuwik, M.; Polak, J.; Pisarska, J.; Pisarski, W.A. Transition Metals (Cr³⁺) and Lanthanides (Eu³⁺) in Inorganic Glasses with Extremely Different Glass-Formers B₂O₃ and GeO₂. *Materials* **2021**, *14*, 7156. [[CrossRef](#)]

Disclaimer/Publisher's Note: The statements, opinions and data contained in all publications are solely those of the individual author(s) and contributor(s) and not of MDPI and/or the editor(s). MDPI and/or the editor(s) disclaim responsibility for any injury to people or property resulting from any ideas, methods, instructions or products referred to in the content.

P4

Karolina Kowalska, Ewa Pietrasik, Marta Kuwik, Joanna Pisarska, Tomasz Goryczka,
Wojciech A. Pisarski,

**Influence of titanium dioxide concentration on thermal properties
of germanate based glasses**

Journal of Thermal Analysis and Calorimetry (2024)

<https://doi.org/10.1007/s10973-024-12998-9>



Influence of titanium dioxide concentration on thermal properties of germanate-based glasses

Karolina Kowalska¹ · Ewa Pietrasik¹ · Marta Kuwik¹ · Joanna Pisarska¹ · Tomasz Goryczka² · Wojciech A. Pisarski¹

Received: 20 July 2023 / Accepted: 18 February 2024
© Akadémiai Kiadó, Budapest, Hungary 2024

Abstract

Influence of titanium dioxide concentration on thermal properties of germanate-based glasses has been studied. Germanate glasses varying with TiO₂ content were examined using DSC methods. The DSC curves exhibit two exothermic peaks, when GeO₂ is substituted by TiO₂. Based on DSC measurements, characteristic temperatures were determined. The studies demonstrate that glass transition temperature increases, whereas thermal stability parameters are reduced with increasing TiO₂ concentration. The DSC curves were also acquired with different heating rates, and the Kissinger method was used to calculate the activation energy. X-ray diffraction analysis for germanate-based glass with TiO₂ indicates that crystallization processes are more complex and several phases are formed during annealing. The absorption and emission spectra of glass samples doped with Er³⁺ ions were also examined before and after annealing process.

Keywords TiO₂ · Germanate glass · Thermal properties · Optical properties

Introduction

Previous results published for inorganic glasses proved that the presence of modifier oxides [1] or rare earths playing the role as the optical activators [2] has an important influence on their thermal properties. Among metal oxides that are components of photonic glasses emitting visible light or infrared radiation, titanium(IV) oxide (TiO₂) deserves particular attention. Several glass systems varying with TiO₂ concentration were synthesized, and their thermal, structural and optical properties have been determined [3–9]. The introduction of titanium dioxide to the glass increases the refractive indices and the radiative transition rates. Thermal investigations demonstrate that glasses with low TiO₂ content exhibit high stability against crystallization. Moreover, small quantities of TiO₂ enhance the glass-forming ability and chemical durability of the glass systems [3]. On the

other hand, multicomponent germanate-based glasses with relatively high TiO₂ concentration are preferred for broad-band near-infrared emission of erbium ions at 1500 nm in the so-called third telecommunication window [10]. Therefore, it is necessary to synthesize thermally stable and fully amorphous precursor systems with relatively high TiO₂ concentrations, which can be applied to optical fiber drawing.

In this work, the influence of TiO₂ concentration on thermal behavior of multicomponent germanate-based glass has been studied using differential scanning calorimetry (DSC). Special attention has been paid to thermal stability parameters, which are important criteria in relation to glass stability and vitrification ability [11–14]. Crystallization kinetics of germanate glasses with the absence and presence of TiO₂ have been evaluated by non-isothermal analysis [15–18]. Here, the results for the following series of glasses TiO₂–GeO₂–BaO–Ga₂O₃ (un-doped samples) and TiO₂–GeO₂–BaO–Ga₂O₃–Er₂O₃ (Er³⁺-doped samples) are shown. Erbium oxide (Er₂O₃) plays the important role as the optically active doping element. It was added to the base glass TiO₂–GeO₂–BaO–Ga₂O₃ in order to study its absorption and emission properties. In particular, luminescence properties of Er³⁺-doped glasses [19] and glass–ceramics [20] have been often examined for applications in the 1.5 μm telecommunication window. Thanks to the favorable positions of energy states, Er³⁺-doped glass systems can be also

✉ Karolina Kowalska
karolina.kowalska@us.edu.pl

✉ Wojciech A. Pisarski
wojciech.pisarski@us.edu.pl

¹ Institute of Chemistry, University of Silesia, Katowice, Poland

² Institute of Materials Engineering, University of Silesia, Chorzów, Poland

applied to optical temperature sensors through up-conversion luminescence processes [21]. Germanate-based glasses containing TiO_2 (30 mol %) and Er_2O_3 (0.5 mol %) were also heat-treated in order to fabricate glass–ceramics. Our previous studies for lead borate glasses and glass–ceramics indicated that the intensities of emission bands related to the main $^4\text{I}_{13/2} \rightarrow ^4\text{I}_{15/2}$ near-infrared laser transition of erbium ions are enhanced and their decays are long-lived after annealing process [22]. Transformation from germanate glass containing TiO_2 to glass–ceramic system was confirmed using the X-ray diffraction. In particular, hypersensitive absorption spectra, near-infrared emission spectra at 1500 nm and their decays have been examined for glass samples before and after annealing. These aspects are also presented and discussed in details.

Experimental

Glasses with the following chemical compositions $x\text{TiO}_2-(60-x)\text{GeO}_2-30\text{BaO}-10\text{Ga}_2\text{O}_3$ and $x\text{TiO}_2-(60-x)\text{GeO}_2-30\text{BaO}-9.5\text{Ga}_2\text{O}_3-0.5\text{Er}_2\text{O}_3$ ($x=0, 10, 20, 30, 40, 45, 50$) were synthesized using melt quenching technique. In these glass compositions, the concentrations of components are given in molar %. Metal oxides of high purity (99.99%, Aldrich Chemical Co.) were used to prepare glass systems. The appropriate amounts of metal oxides were mixed homogeneously together. Next, they were melted at $T=1200^\circ\text{C}$ for 0.45 h.

The samples were characterized by a SETARAM Lab-sys thermal analyzer (SETARAM Instrumentation, Caluire, France) using the DSC method. The DSC curves were acquired with heating rate of 5°C min^{-1} , 7°C min^{-1} , $10^\circ\text{C min}^{-1}$, $12^\circ\text{C min}^{-1}$, $15^\circ\text{C min}^{-1}$ and $20^\circ\text{C min}^{-1}$, respectively. Glass powder samples weighing 50 mg were heated in Al_2O_3 crucibles at the appropriate rates from ambient temperature up to 1300°C in a flowing high-purity argon atmosphere. The values of characteristic temperatures and stability parameters were determined within an accuracy of $\pm 0.5^\circ\text{C}$. At least three tests were performed on each sample to verify reproducibility. The Raman spectra were obtained using a Thermo Scientific™ DXR™2xi Raman imaging microscope. The appropriate laser source with an excitation wavelength of 633 nm was used to collect the data. The nature of samples was examined using by X-ray diffraction measurements (X'Pert Pro diffractometer, Panalytical, Almelo, The Netherlands) with $\text{Cu K}\alpha_1$ radiation ($\lambda=1.54056\text{ \AA}$). Also, glass samples were characterized using absorption (Cary 5000 UV–VIS–NIR spectrophotometer, Agilent Technology, USA) and luminescence spectroscopy. For emission spectra and decays, laser equipment was used: PTI QuantaMaster QM40 spectrofluorometer with a xenon lamp (75W), tunable pulsed optical parametric

oscillator, Nd:YAG laser (OpotekOpolette 355 LD), double 200-mm monochromators, Hamamatsu H10330B-75 detector and PTI ASOC-10 USB-2500 oscilloscope. Resolution for spectral measurements was $\pm 0.1\text{ nm}$. Decay curves were recorded with an accuracy of $\pm 0.5\text{ }\mu\text{s}$.

Results and discussion

Figure 1 presents DSC curves for germanate-based glasses varying with TiO_2 concentration. The DSC curves were measured under standard heating rate of 10°C/min . The inset referred here as (*) shows DSC curves registered for glass samples, where TiO_2 plays the role as glass modifier and its concentration is changed up to 30 molar % ($\text{TiO}_2:\text{GeO}_2=1:1$). Thermal measurements for germanate glass without TiO_2 clearly indicate that only one unsymmetrical exothermic peak corresponding to crystallization of the glassy matrix appears. The DSC curves exhibit two exothermic peaks, when GeO_2 is partially replaced by TiO_2 . The first exothermic peak shifts to lower-temperature region with increasing TiO_2 concentration. The profiles of DSC curves are practically unchanged for glass samples with titanium dioxide playing the role as glass former ($\text{TiO}_2 > 30$ molar%). The presence of two exothermic peaks on the DSC curves suggests more complex crystallization process for our multicomponent $\text{TiO}_2\text{-GeO}_2\text{-BaO-Ga}_2\text{O}_3$ glass. Based on the analysis of glass composition, it is possible to hypothesize explaining the presence of two exothermic peaks on the DSC curves. It could be assumed that the first crystallization peak is responsible for forming phases based on GeO_2 during the crystallization of the germanate glass network. The clear separation of two exothermic peaks with increasing TiO_2 concentration indicates the possibility of crystallizing

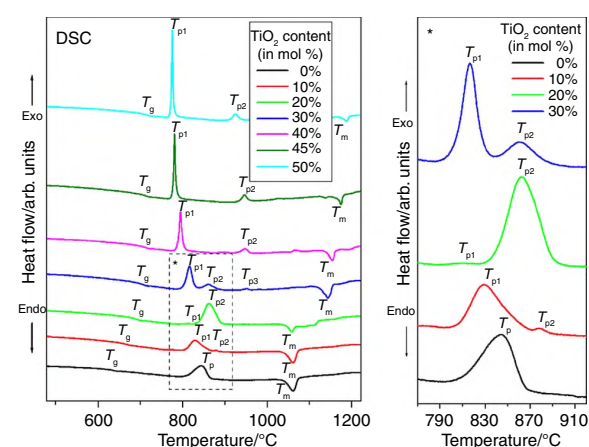


Fig. 1 DSC curves for germanate-based glasses varying with TiO_2 concentration

another phase during annealing at higher temperatures. The results suggest that the second crystallization peak corresponds to the formation of titanate crystalline phases in a glass network. Completely different situation was observed earlier for glass based on $\text{GeO}_2\text{-K}_2\text{O-TiO}_2$ with one exothermic peak contrary to potassium germanate glass without titanium dioxide exhibiting two exothermic peaks [23].

In order to determine correlation between thermal properties of germanate-based glasses varying with titanium dioxide concentration and glass composition, the structural aspects of studied systems were analyzed using Raman spectroscopy. Figure 2 shows Raman spectra registered for germanate glasses with TiO_2 as glass modifier or glass former in $400 \div 1200 \text{ cm}^{-1}$ spectral region. It was observed that spectra exhibit two separate frequency regions independent of titanium dioxide content. The first group of bands (low-frequency region) is mainly attributed to the stretching vibrations of tetrahedral structural units (GeO_4). In contrast, the second group of bands (high-frequency region) originates vibrations of octahedral (GeO_6) and tetrahedral structural units with non-bridging oxygen atoms (NBOs) [24, 25]. According to the literature, the low-frequency region of Raman spectra consists of several overlapped bands. The band located at around 473 cm^{-1} can be assigned to symmetric stretching vibrations of Ge-O-Ge in 4-membered GeO_4 rings. On the other hand, the band corresponding to the symmetric stretching vibrations of Ge-O-Ge in 3-membered GeO_4 rings was registered at 524 cm^{-1} [26]. It is important to note that the high-frequency region of Raman spectra is attributed to symmetric stretching vibrations Ge-O in GeO_6 and asymmetric stretching vibrations Ge-O(Ge) (767 cm^{-1}) [27] as well as tetrahedral structural Q^2 (827 cm^{-1}) and Q^3 (882 cm^{-1}) units with two and

one non-bridging oxygen atoms [28]. It was observed that the decreased intensity of bands in low-frequency regions corresponds to the conversion of GeO_4 to tetrahedral structural units with two or one non-bridging oxygen atoms. The formation of Q^2 and Q^3 units due to the depolymerization of 4- or 3-membered GeO_4 rings is associated with TiO_2 as a glass modifier ($\text{TiO}_2 < 30 \text{ molar\%}$) in the germanate glass host. Moreover, for studied systems where TiO_2 is a glass former ($\text{TiO}_2 > 30 \text{ molar\%}$), the additional band (650 cm^{-1}) due to the stretching vibration of Ti-O in the TiO_6 unit is well observed. Titanium dioxide can exist in the gap outside the glass network as TiO_6 units [29]. On the other hand, TiO_2 can participate in forming the glass network with tetrahedral structural units TiO_4 . The typical Raman band corresponding to the tetrahedral structural unit (TiO_4) linked into the glass network is around 900 cm^{-1} [30]. This band overlaps with the bands related to the GeO_4 and GeO_6 units. To investigate the influence of changes in the glass network on physicochemical properties of the germanate glasses when TiO_2 plays a role as a glass modifier ($\text{TiO}_2 < 30 \text{ molar\%}$) or glass former ($\text{TiO}_2 > 30 \text{ molar\%}$), a comparative analysis of thermal properties and structural properties was performed.

From DSC curves glass transition temperature T_g , crystallization onset T_x , maximum of crystallization peak T_p and melting temperature T_m were evaluated. The thermal stability parameter ΔT referred as $T_x - T_g$ was also calculated. The factors T_g , T_m and ΔT for glass samples varying with TiO_2 concentration are schematized in Fig. 3.

As the TiO_2 content increases in glass composition, the glass transition temperature T_g increases from $620 \text{ }^\circ\text{C}$ (0 mol% TiO_2) to nearly $708 \text{ }^\circ\text{C}$ (50 mol% TiO_2). It suggests that titanium dioxide acts as a glass-network modifier or former, depending on its concentration. According to Grujić et al. [23], the glass transition temperature T_g measured for oxide glass systems depends on bond strength, cross-link density and closeness of packing of the glass. In our case, the glass transition temperature T_g increases with increasing TiO_2 content, which indicates that the glass structure is less open in contrast to germanate glass without titanium dioxide. Moreover, Calzavara et al. [31] stated that the change in the structure of the germanate glass host influences glass transition temperature T_g evaluated from DSC measurements. It was observed that an increase in Ga_2O_3 concentration led to the formation of Ge-O-Ga bonds and polymerization of the germanate glass network. Values of glass transition temperature were increasing at the same time. This phenomenon corresponds to reducing the number of structural units with non-bridging oxygens and forming new gallate units in the glass network. Our studies for germanate-based glasses varying with TiO_2 concentration indicate a similar relation between structural and thermal properties. Analysis of Raman spectra for systems with titanium dioxide content higher than 30 molar% suggests the destruction of germanate

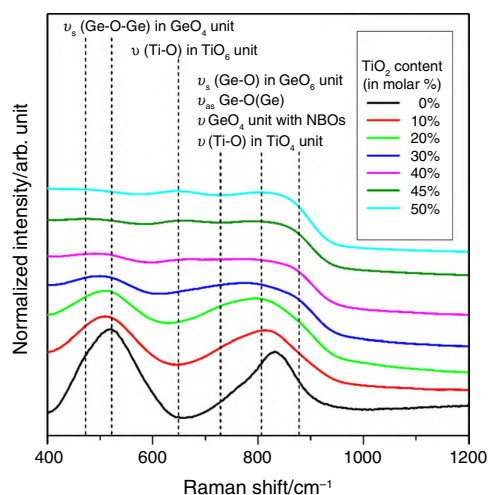


Fig. 2 Raman spectra for germanate-based glasses varying with TiO_2 concentration

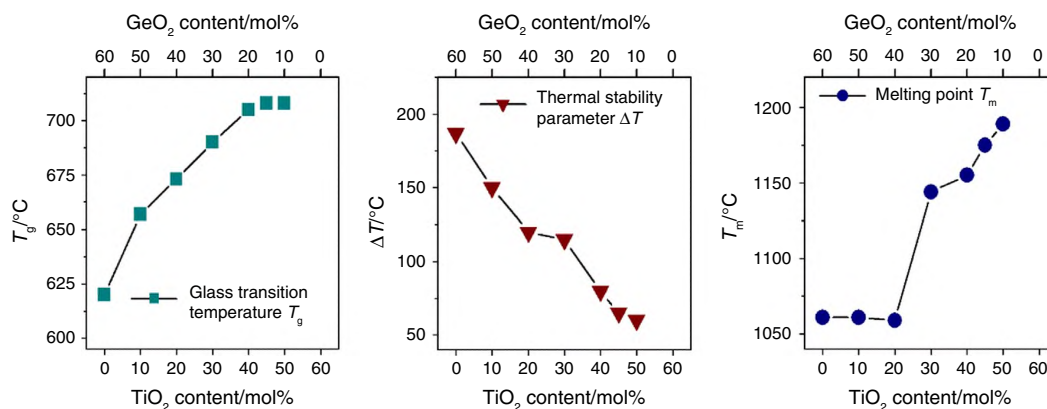


Fig. 3 Glass transition temperature T_g , the melting temperature T_m and the thermal stability parameter ΔT for germanate-based glasses varying with TiO_2 concentration

units, especially tetrahedral structural units with NBOs, and the formation of structural units with Ti–O bond that caused polymerization of glass network. The values of evaluated T_g are higher when the glass network polymerizes, and the structure is less open due to the increasing titanium dioxide content in the glass composition.

The systematic investigations revealed that the glass transition temperatures are usually increased with increasing concentrations of network-modifiers in various glass compositions. Among others, this situation has been observed for glass systems with trivalent element oxides Sb_2O_3 [32] or M_2O_3 , where $M = Sc, Y, La$ and In [33], which behave as glass network modifiers. Further studies demonstrated that the initial addition of B_2O_3 to the phosphate-based glass increases the glass transition temperature, whereas further additions of boron oxide have less effect. In the same work published by Freudenberg et al. [34], no systematic effect of replacement the alkaline earth modifier from CaO to SrO on values of T_g was found. Also, the glass transition temperature is nearly unchanged ($T_g = 377$ °C) after the introduction of BaO into mixed tellurite-phosphate glass composition [35]. In particular, glass systems with the following network modifiers such as SrO, ZnO or V_2O_5 give interesting thermal results. Increase in the SrO content results in a decrease in T_g . This situation was observed for glasses based on $CaO-SiO_2-B_2O_3-Na_2O-ZrO_2$ [36] and $BaO-SrO-SiO_2-B_2O_3$ [37]. Completely different results have been observed for $B_2O_3-P_2O_5-SrO-Li_2O$ glass [38], where values of T_g increase linearly with SrO content. An introduction of ZnO into phosphate [39] and tellurite [40–42]-based glasses results in increase in the glass transition temperature. Contrary to glass systems mentioned above, the values of T_g decrease with increasing ZnO concentration in tellurite glass [43]. Also, different trends of T_g have been observed for glasses with V_2O_5 concentration.

The addition of V_2O_5 induces a decrease of T_g for aluminosilicate [44] and borosilicate [45] glass systems, whereas the glass transition temperature increases with increasing vanadium oxide concentration in $Li_2O-PbO-V_2O_5$ glasses [46]. It clearly suggests that the variation in T_g with concentration of network modifier oxides depends critically on glass compositions.

Further thermal studies demonstrate that the values of melting temperature T_m depend critically on TiO_2 concentration. The values of T_m are considerably higher for glass samples with titanium dioxide playing the role as glass former ($TiO_2 \geq 30$ molar%) than glass modifier ($TiO_2 < 30$ molar%). It should be also noted that the melting temperature for samples with glass modifier TiO_2 is almost unchanged ($T_m = 1060$ °C ± 1 °C), whereas the values of T_m are increased from 1144 °C (30 molar% TiO_2) to 1189 °C (50 molar% TiO_2) with further increasing TiO_2 concentration. Similar phenomena were also observed for barium lithium tetraborate glasses $BaO-TiO_2-Li_2B_4O_7$, where the melting temperature was increased considerably with increasing TiO_2 content up to 20 molar% [47]. Studies for phosphate glasses containing sodium oxide as a glass modifier by Ciecinska et al. indicated that physicochemical properties depend on the structure of the glass. Introducing modifiers into the glass network depolymerizes the glass structure due to forming ionic bonds between non-bridging oxygen atoms and modifiers. At the same time, thermal measurements confirmed that the value of melting temperature T_m was practically unchanged for systems with a low glass modifier content [48]. Based on the structural characterization of our germanate glasses, it can be supposed that the evaluated value of temperature T_m for samples with a low concentration of titanium dioxide modifier ($TiO_2 < 30$ molar%) does not change because TiO_2 plays a role as a glass modifier and causes partially depolymerization of the glass network.

In contrast with the glass transition temperature T_g , the thermal stability parameter ΔT is reduced with increasing TiO_2 concentration in germanate-based glasses (Fig. 3). This situation is completely different compared to $\text{TeO}_2\text{-La}_2\text{O}_3\text{-TiO}_2$ glass, where the thermal stability factor ΔT was found to increase with TiO_2 composition [49]. Here, the thermal stability parameter ΔT is reduced from 187 °C (0 mol% TiO_2) to 150 °C (10 mol% TiO_2), 120 °C (20 mol% TiO_2), 115 °C (30 mol% TiO_2), 80 °C (40 mol% TiO_2), 65 °C (45 mol% TiO_2) and 60 °C (50 mol% TiO_2) in the presence of titanium dioxide in glass composition. This reducing trend with TiO_2 content was confirmed by the Hruby parameter [50], the Saad-Poulain criterion [51] as well as Weinberg [52] and Lu and Liu [53] factors, which were also applied to further evaluate the thermal glass stability. The results are summarized in Table 1.

The thermal stability parameters ΔT are reduced with increasing TiO_2 concentration, which is useless in relation to fabrication of the optical fibers from precursor germanate-based glasses containing titanium dioxide. It is generally accepted that the larger values of ΔT give a larger working range during operations for fiber drawing and glass can be considered as a glass with relatively good thermal ability if ΔT is higher than 100 °C. On the other hand, germanate-based glasses with higher TiO_2 content are strongly recommended from the optical point of view, but their values of ΔT are relatively low. The thermal stability factors ΔT for glass samples with $\text{TiO}_2 \leq 30$ molar% are still higher than 100 °C. It suggests that glasses with TiO_2 content up to 30 molar% exhibit good thermal stability against devitrification, giving quite large working range during operations for fiber drawing. The proper choice of glass-host, which we would like to use for optical fiber drawing, is a compromise between thermal stability factors and spectroscopic/laser parameters of rare earth ions.

Germanate-based glass with 30 molar% titanium dioxide ($\text{TiO}_2\text{:GeO}_2 = 1\text{:}1$) was selected for further non-thermal analysis. A widely used non-isothermal technique is the classical

Kissinger method [54] assuming single activation energy E_a . Also, the Kissinger method was applied to calculate the activation energy for some germanate-based glasses [55]. Matusita and Sakka [56] found criteria on the application of the Kissinger equation based on the surface nucleation and crystallization mechanism in the function of the heating rate for $\text{Li}_2\text{O-SiO}_2$ glass. In this work, we used the simplest form equation throughout the crystallization process as follows:

$$\ln\left(\frac{\beta}{T_p^2}\right) = \left(\frac{-E_a}{RT_p}\right) + \text{const}$$

where T_p is the temperature that corresponds to the position of the rate peak maximum, R is the gas constant, β is the heating rate. The slopes of the linear fit the experimental data from a Kissinger plot of $\ln(\beta/T_p^2)$ versus $1/T_p$, which gives the value of E_a . The activation energy E_a of crystallization that seems to be responsible for the molecular motion and rearrangements of atoms around the glass transition temperature for fabricated material has been evaluated from a set of DSC curves measured under different heating rates. Figure 4 shows the DSC curves for germanate glass with 30 molar% TiO_2 acquired with heating rate of 5 °C min⁻¹, 7 °C min⁻¹, 10 °C min⁻¹, 12 °C min⁻¹, 15 °C min⁻¹ and 20 °C min⁻¹. The results were compared to glass without titanium dioxide. In both cases, with increasing heating rate, we observed a shift to a higher temperature range and an increase in the height of the peak maximum. Previously published work for crystallization kinetics of glass systems gives interesting results. For lithium borate glasses [57], the curves were registered for the pre-annealed, slowly, and quickly quenched samples. Based on this experimental data, Koga et al. [57] clearly suggested that the number of pre-existing nuclei was smaller in the slowly quenched glasses.

The activation energies E_a for glass samples without and with 30 molar% TiO_2 are close to 223 kJ mol⁻¹ and 377 kJ mol⁻¹, respectively. The calculations using the Kissinger method demonstrate the increase in activation energy

Table 1 Thermal stability parameters for glass samples varying with TiO_2

$\text{TiO}_2/\text{mol}\%$	$T_g/^\circ\text{C}$	$\Delta T/^\circ\text{C}$	K_H^*	K_{SP}^{**}	K_W^{***}	K_{LL}^{****}
0	620	187	0.74	11.16	0.21	0.5
10	657	150	0.59	5.25	0.16	0.48
20	673	120	0.45	3.03	0.13	0.47
30	690	115	0.34	1.83	0.11	0.45
40	705	80	0.22	1.13	0.08	0.43
45	708	65	0.16	0.73	0.06	0.42
50	708	60	0.14	0.68	0.06	0.41

*Hruby parameter $K_H = (T_x - T_g)/(T_m - T_x)$

**Saad-Poulain parameter $K_{SP} = (T_p - T_x) \times (T_x - T_g)/T_g$

***Weinberg parameter $K_W = (T_p - T_g)/T_m$

****Lu and Liu parameter $K_{LL} = T_p/(T_g + T_m)$

Fig. 4 DSC curves for germanate glass **a** without and **b** with 30 molar% TiO₂ measured under different heating rates

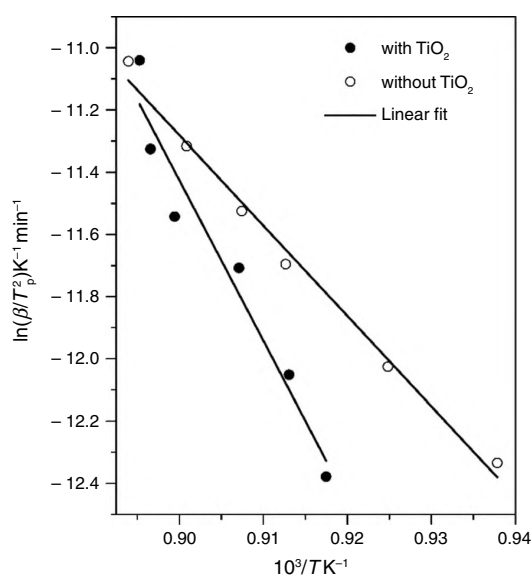
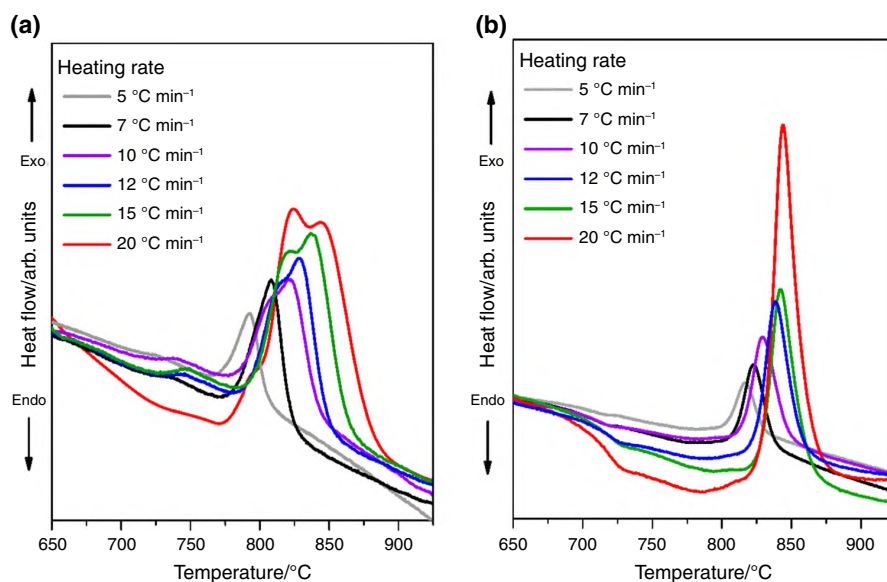


Fig. 5 Kissinger plots for germanate-based glasses without and with 30 molar% TiO₂

E_a with respect to progress of crystallization process of germanate-based glass in the presence of titanium dioxide. The regression coefficients of the linear fitting presented in Fig. 5 are equal to 0.962 (glass with 30 molar% TiO₂) and 0.991 (glass without TiO₂).

Finally, the crystallization processes in germanate-based glasses containing 30 molar% TiO₂ have been examined using the X-ray diffraction and optical methods (absorption and emission spectroscopy). For that reason, the precursor

glasses were heat treated at the appropriate annealing temperature and time. The annealing temperature is usually chosen between the crystallization onset T_x and the glass transition temperature T_g . For germanate-based glass with 30 molar% TiO₂, the values of T_x and T_g are close to 805 °C and 690 °C, respectively. Thus, the annealing temperature $T = 750$ °C was selected to study crystallization processes in germanate-based glasses with titanium dioxide. In our case, the glass samples were annealed from 1 to 5 h.

From literature, it is well known that precursor glasses are partially crystallized during temperature-controlled process, and at consequence, micro-/nanocrystals are formed. They are distributed into amorphous matrices. Thus, new composite materials so-called transparent glass-ceramics (TGC) can be successfully fabricated. Optical changes during structural transformation from glass to glass-ceramic are possible to detect in the studied systems through rare earth doping. In our case, trivalent erbium ions were used as the optical active dopants and they are usually incorporated into crystalline phase present in glass after annealing process. Differences in the optical characteristics (absorption and emission spectra) of erbium ions in glasses before and after annealing can be explained by structural changes in the environment around the optically active dopants.

Figure 6 presents the X-ray diffraction patterns for germanate-based glass with TiO₂ before and after annealing process. The XRD pattern measured for precursor germanate-based glass with 30 molar% TiO₂ (before annealing) suggests that sample is fully amorphous. Further XRD measurements demonstrate that samples after annealing at $T = 750$ °C for 1, 2 and 3 h are still fully amorphous. Situation was completely changed for samples annealed at

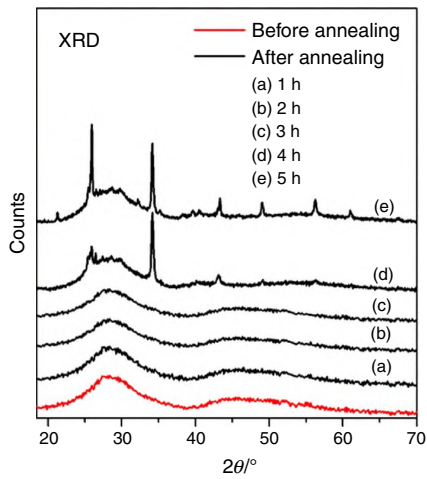


Fig. 6 X-ray diffraction patterns for germanate-based glasses with 30 molar% TiO_2 before and after annealing process

$T = 750$ °C for 4 and 5 h. It is well evident from the XRD measurements that the narrow diffraction lines characteristic for crystalline phases can be observed. It suggests that our glass was partially crystallized. This is the experimental proof that a structural transformation from precursor glasses to glass–ceramics has occurred.

The XRD analysis suggests that crystallization process is more complex than previously studied $\text{BaO-TiO}_2\text{-GeO}_2$ ternary system, where only one crystalline phase $\text{Ba}_2\text{TiGe}_2\text{O}_8$ is successfully formed [58, 59]. In our case, the phase identification is not entirely evident. We suggest that narrow diffraction lines may be assigned to the following crystalline phases: TiO_2 (card no. 01-075-1537), $\text{Ga}_2\text{Ge}_2\text{O}_7$ (card no.

00-035-0387), $\text{Ba}_3\text{Ga}_2\text{O}_6$ (card no. 00-023-1021), BaO (card no. 00-030-0143) and Er_2O_3 (card no. 00-008-0050), but at this moment it should be pointed out that further structural investigations are necessary to identify the nature of these crystalline phases. However, it may be concluded that complex phases consist of many elements that crystallize easier [1]. The results obtained by Laudisio et al. [60] confirmed that the crystallization processes of lithium–titanium–germanate glasses occur in one or more steps into two non-identifiable crystalline phases.

Also, our previous crystallization studies for multi-component germanate glasses without TiO_2 give similar results. The examination of the crystallization processes is quite easy in these glass systems, where only a single phase is growing from nuclei generated during annealing process. Situation is more complicated, when at least two or more crystalline phases are formed in glass systems. These effects are observed for multicomponent germanate glasses, for which the presence of four crystalline phases (BaF_2 , BaO , $\text{Ba}_3\text{Ga}_2\text{Ge}_4\text{O}_{14}$, GeO_2) was verified by the X-ray diffraction measurements [61].

Optical changes for germanate-based glasses containing titanium dioxide after annealing process were verified using the optical spectroscopy. The optical results were limited to the measurements of hypersensitive absorption spectra and near-infrared luminescence spectra of Er^{3+} ions in germanate glasses with TiO_2 before and after annealing. The luminescence decays from the excited state of Er^{3+} ions were also analyzed in details. The absorption and emission spectra as well as luminescence decay curves for erbium ions in germanate-based glasses with TiO_2 before and after annealing process are presented in Figs. 7 and 8, respectively.

Fig. 7 **a** hypersensitive absorption spectra and **b** near-infrared luminescence spectra measured for germanate-based glasses with TiO_2 before and after annealing process

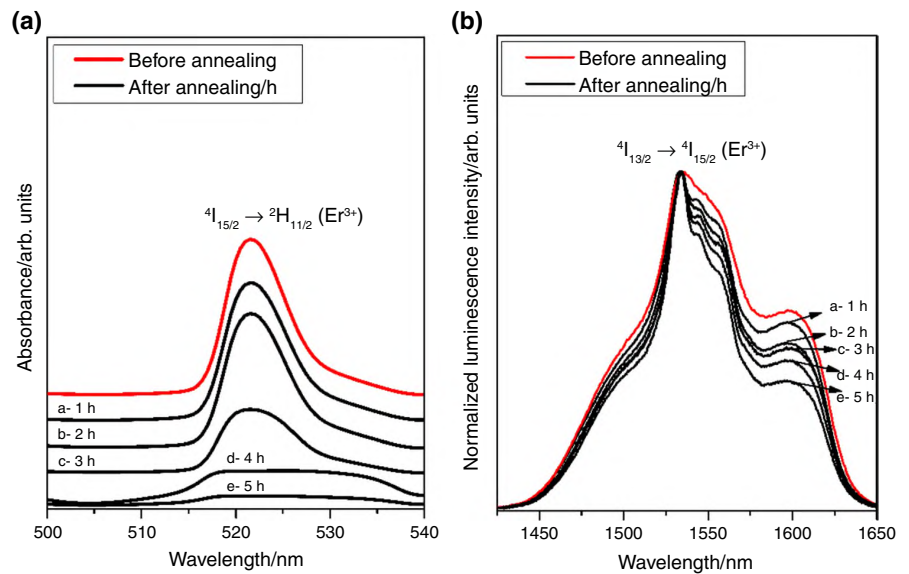
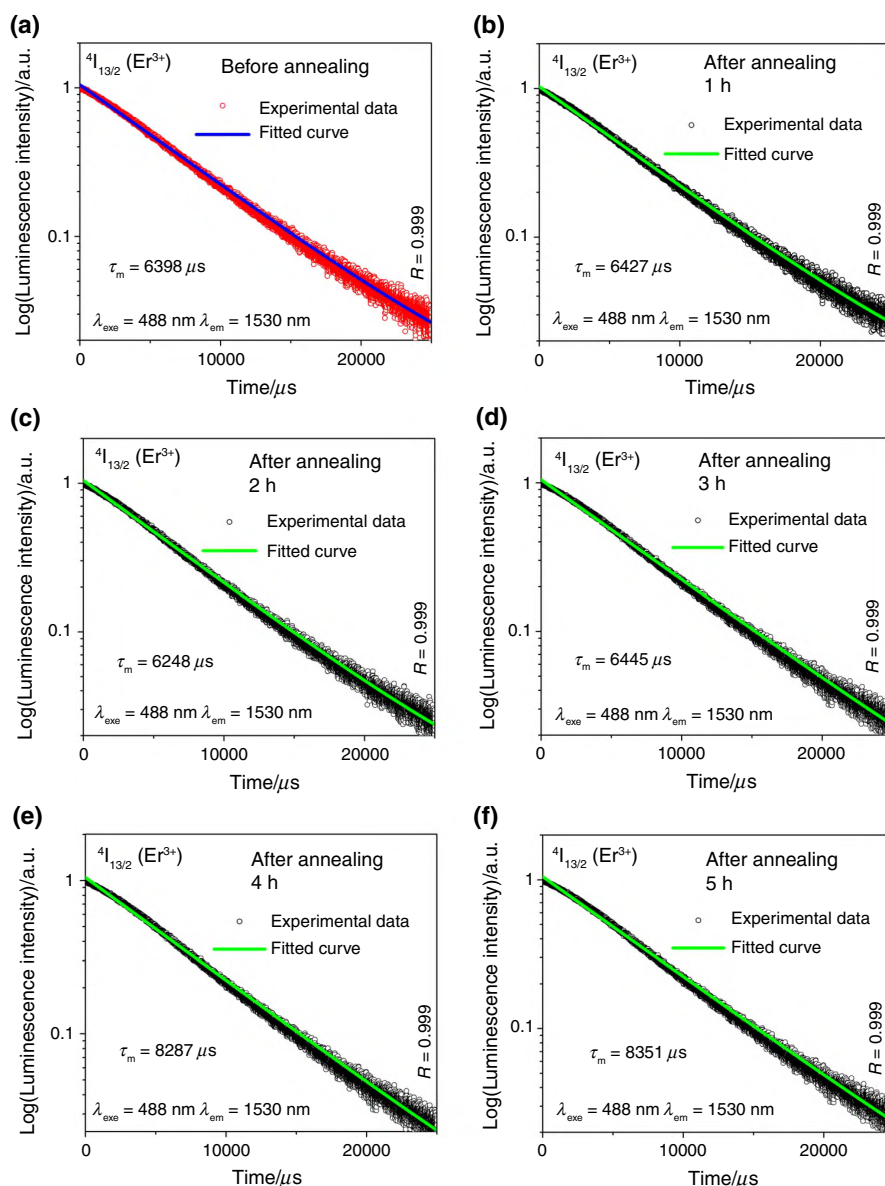


Fig. 8 Luminescence decays from the ${}^4I_{13/2}$ excited state of Er^{3+} ions in germanate-based glasses with TiO_2 **a** before and **b, c, d, e, f** after annealing process



The characteristic band due to hypersensitive ${}^4I_{15/2} \rightarrow {}^2H_{11/2}$ transition of Er^{3+} ions is located in the absorption spectrum between 500 and 540 nm [62]. This absorption band is sensitive to even the slightest structural changes of the glass host. The near-infrared emission spectrum at about 1500 nm consists of band originating to the main laser transition from the ${}^4I_{13/2}$ excited state to the ${}^4I_{15/2}$ ground state of Er^{3+} . The absorption and near-infrared emission measurements presented in Fig. 7 well demonstrate that the spectra are changed after annealing process and these effects are stronger for glass systems heat treated at 750 °C for 4 and 5 h. In particular, luminescence bandwidth for the ${}^4I_{13/2} \rightarrow {}^4I_{15/2}$ near-infrared laser

transition of Er^{3+} referred as full width at half maximum (FWHM) is reduced with annealing time, which is characteristic for semi-crystalline glass-ceramic systems. Luminescence decay curve analysis confirms this hypothesis. To obtain an additional information on the luminescence of Er^{3+} ions in titanate-germanate system, the luminescence decay curves for the ${}^4I_{13/2}$ state were recorded by monitoring the emission and excitation wavelengths at $\lambda_{\text{em}} = 1530$ nm and $\lambda_{\text{exc}} = 488$ nm, respectively. Figure 8 presents the decay profiles of the samples under investigation. All decay curves exhibit a slight deviation from the single-exponential function. Luminescence decays are longer for samples annealed for 4 h (Fig. 8e) and 5 h

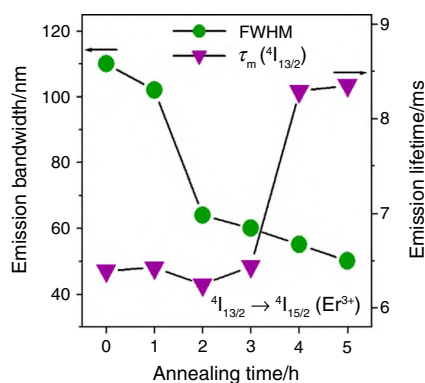


Fig. 9 Near-infrared emission bandwidth for the $^4I_{13/2} \rightarrow ^4I_{15/2}$ transition and the $^4I_{13/2}$ lifetime of Er^{3+} ions varying with annealing time

(Fig. 8f). Based on decay curve measurements, the luminescence lifetimes $^4I_{13/2}$ (Er^{3+}) were calculated by fitting the luminescence decay curves. Their values are relatively higher for samples annealed for 4 and 5 h (above 8000 μs) compared to the glass samples before annealing (Fig. 8a) or samples heat treated (Fig. 8b–d) for shorter time (1 \div 3 h). It evidently illustrates that part of erbium ions is distributed into crystalline phases. The optical changes limited to values of FWHM and the $^4I_{13/2}$ luminescence lifetimes are also schematized in Fig. 9.

Conclusions

Influence of TiO_2 content on thermal properties of germanate-based glasses has been examined in details. The profiles of DSC curves depend critically on titanium dioxide, which plays the role as glass modifier or former, depending on its concentration. The DSC curves exhibit two exothermic peaks, when GeO_2 is partially replaced by TiO_2 . From DSC curve measurements, characteristic temperatures were determined. The glass transition temperature increases, whereas thermal stability parameters are reduced with increasing TiO_2 content. Also, the DSC curves for germanate glass containing TiO_2 were measured under various heating rates in order to determine the activation energy of crystallization. The Kissinger method was applied to calculate the activation energy, which is considerably higher compared to glass without TiO_2 . X-ray diffraction measurements revealed that crystallization processes are more complex and several phases are formed during annealing process of germanate-based glass with TiO_2 at 750 $^{\circ}C$ for 4 and 5 h. Transformation from glass to glass–ceramic was also confirmed for samples doped with Er^{3+} ions using absorption and emission spectroscopy.

Author contributions KK contributed to investigation, data curation, data analysis, writing—original draft. EP contributed to methodology, investigation, data analysis. MK contributed to investigation, data analysis. JP contributed to investigation, data analysis. TG contributed to methodology, investigation, data analysis. WAP contributed to conceptualization, data analysis, writing—original draft, writing—review.

Funding This research was funded by National Science Centre (Poland), grant number 2018/31/B/ST8/00166.

References

- Goj P, Ciecinska M, Szumera M, Stoch P. Thermal properties of $Na_2O-P_2O_5-Fe_2O_3$ polyphosphate glasses. *J Therm Anal Calorim.* 2020;142:203–9.
- Pop L, Bolundut L, Pascuta P, Culea E. Influence of Er^{3+} ions addition on thermal and optical properties of phosphate–germanate system. *J Therm Anal Calorim.* 2019;138:1895–9.
- de Sousa NCA, de Araujo MT, Jacinto C, Vermelho MVD, Dantas NO, Santos CC, Guedes I. The role of TiO_2 in the $B_2O_3-Na_2O-PbO-Al_2O_3$ glass system. *J Solid State Chem.* 2011;184:3062–5.
- Toloman D, Suciur R, Leostean C, Regos A, Ardelean I. The influence of TiO_2 concentration in some calcium–phosphate glasses. *Physica B.* 2014;438:84–7.
- Karlsson S, Grund BL, Kidkhunthod P, Lundstedt K, Wondraczek L. Effect of TiO_2 on optical properties of glasses in the soda–lime–silicate system. *Opt Mater Exp.* 2016;6:1198–216.
- Ali AA, Rammah YS, Shaaban MH. The influence of TiO_2 on structural, physical and optical properties of $B_2O_3-TeO_2-Na_2O-CaO$ glasses. *J Non-Cryst Solids.* 2019;514:52–9.
- Es-soufi H, Bih L. Effect of TiO_2 on the chemical durability and optical properties of Mo-based phosphate glasses. *J Non-Cryst Solids.* 2021;558:120655.
- Pal SG, Singh J, Kaur P, Singh T, Kaur R, Kaur S, Singh DP. Impact of TiO_2 on radiation shielding competencies and structural, physical and optical properties of $CeO_2-PbO-B_2O_3$ glasses. *J Alloys Compd.* 2021;885:160939.
- Rao RB, Rao DK, Veeraiah N. The role of titanium ions on structural, dielectric and optical properties of $Li_2O-MgO-B_2O_3$ glass system. *Mater Chem Phys.* 2004;87:357–69.
- Kowalska K, Kuwik M, Pisarska J, Leśniak M, Dorosz D, Kochanowicz M, Żmojda J, Dorosz J, Pisarski WA. Influence of TiO_2 concentration on near-infrared luminescence of Er^{3+} ions in barium gallo–germanate glasses. *J Mater Res Technol.* 2022;21:4761–72.
- Kozmidis-Petrovic AF. Theoretical analysis of relative changes of the Hruby, Weinberg, and Lu–Liu glass stability parameters with application on some oxide and chalcogenide glasses. *Thermochim Acta.* 2010;499:54–60.
- Kozmidis-Petrovic AF. Sensitivity of the Hruby, Lu–Liu, Fan, Yuan, and Long glass stability parameters to the change of the ratios of characteristic temperatures T_x/T_g and T_m/T_g . *Thermochim Acta.* 2010;510:137–44.
- Kozmidis-Petrovic AF. Which glass stability criterion is the best? *Thermochim Acta.* 2011;523:116–23.
- Kozmidis-Petrovic AF, Sestak J. Forty years of the Hruby glass-forming coefficient via DTA when comparing other criteria in relation to the glass stability and vitrification ability. *J Therm Anal Calorim.* 2012;110:997–1004.
- Cheng K. Evaluation of crystallization kinetics of glasses by non-isothermal analysis. *J Mater Sci.* 2001;36:1043–8.

16. Malek J, Pustkova P, Shanelova J. Kinetic phenomena in non-crystalline materials studied by thermal analysis. *J Thermal Anal Calorim.* 2003;72:289–97.
17. Joseph K, Krishnan RV, Kutty KVG, Rao PRV. Kinetics of non isothermal crystallization of $\text{Cs}_2\text{O}-\text{Fe}_2\text{O}_3-\text{P}_2\text{O}_5$ glasses. *Thermochim Acta.* 2011;512:67–70.
18. Joseph K. Non-isothermal crystallization in $\text{BaO}-\text{Fe}_2\text{O}_3-\text{P}_2\text{O}_5$ glasses: a comparison with iron phosphate and $\text{Cs}_2\text{O}-\text{Fe}_2\text{O}_3-\text{P}_2\text{O}_5$ glasses. *J Therm Anal Calorim.* 2018;131:241–8.
19. Yuliantini L, Djamal M, Hidayat R, Boonin K, Yasaka P, Kothan S, Kaewkhao J. IR emission of Er^{3+} ion-doped fluoroborotellurite glass for communication application. *J Non-Cryst Solids.* 2021;566:120849.
20. Tikhomirov VK, Furniss D, Seddon AB, Ferrari M, Rolli R. Er^{3+} -doped ultra-transparent oxy-fluoride glass-ceramics for application in the 1.54 μm telecommunication window. *J Mater Sci Lett.* 2002;21:293–5.
21. Pisarski WA, Pisarska J, Lisiecki R, Ryba-Romanowski W. Sensitive optical temperature sensor based on up-conversion luminescence spectra of Er^{3+} ions in $\text{PbO}-\text{Ga}_2\text{O}_3-\text{XO}_2$ ($\text{X} = \text{Ge}, \text{Si}$) glasses. *Opt Mater.* 2016;59:87–90.
22. Pisarski WA, Pisarska J, Czopek I, Goryczka T, Lisiecki R, Ryba-Romanowski W. Enhanced and long-lived near-infrared luminescence of Er^{3+} ions in lead borate glass-ceramics containing PbWO_4 nanocrystals. *J Am Ceram Soc.* 2013;96:1685–7.
23. Grujić S, Blagojević N, Tošić M, Živanović V, Božović B. The effect of TiO_2 on the structure and devitrification behavior of potassium titanium germanate glass. *J Therm Anal Calorim.* 2006;83:463–6.
24. Sigaev VN, Gregora I, Pernice P, Champagnon B, Smelyanskaya EN, Aronne A, Sarkisov PD. Structure of lead germanate glasses by Raman spectroscopy. *J Non-Cryst Solids.* 2001;279:136–44.
25. Di Martino D, Santos LF, Marques AC, Almeida RM. Vibrational spectra and structure of alkali germanate glasses. *J Non-Cryst Solids.* 2001;293–295:394–401.
26. Leśniak M, Zeid J, Starzyk B, Kochanowicz M, Kuwik M, Żmojda J, Miluski P, Baranowska A, Dorosz J, Pisarski W, Pisarska J, Dorosz D. Investigation of the $\text{TeO}_2/\text{GeO}_2$ ratio on the spectroscopic properties of Eu^{3+} -doped oxide glasses for optical fiber application. *Materials.* 2022;15:117.
27. Szal R, Żmojda J, Kochanowicz M, Miluski P, Dorosz J, Lesniak M, Jeleń P, Starzyk B, Sitarz M, Kuwik M, Pisarska J, Pisarski WA, Iijima Y, Mori T, Dorosz D. Spectroscopic properties of antimony modified germanate glass doped with Eu^{3+} ions. *Ceram Int.* 2019;45:24811–7.
28. Fernandes RG, Franco DF, Mastelaro VR, Cardinal T, Toulemonde O, Nalin M. Thermal and structural modification in transparent and magnetic germanoborate glasses induced by Gd_2O_3 . *Ceram Int.* 2020;46:22079–89.
29. Lu M, Wang F, Liao Q, Chen K, Qin J, Pan S. FTIR spectra and thermal properties of TiO_2 -doped iron phosphate glasses. *J Mol Struct.* 2015;1081:187–92.
30. Dymshits OS, Zhilin AA, Petrov VI, Tsenter MY, Chuvaeva TI, Shashkin AV, Golubkov VV, Kang UK, Lee K-H. A Raman spectroscopic study of phase transformations in titanium-containing magnesium aluminosilicate glasses. *Glass Phys Chem.* 2002;28:66–78.
31. Calzavara F, Allix M, Dussauze M, Jubera V, Nalin M, Cardinal T, Fargin E. Glass forming regions, structure and properties of lanthanum barium germanate and gallate glasses. *J Non-Cryst Solids.* 2021;571:121064.
32. Soury D, Shahmoradi Y. Calorimetric analysis of non-crystalline $\text{TeO}_2-\text{V}_2\text{O}_5-\text{Sb}_2\text{O}_3$. *J Therm Anal Calorim.* 2017;129:601–7.
33. Branda F, Costantini A, Luciani G, Laudisio G. The role of trivalent element oxides in $\text{CaO}(\text{Na}_2\text{O})-\text{M}_2\text{O}_3-\text{SiO}_2$ glasses from T_g . *J Therm Anal Calorim.* 2001;64:1017–24.
34. Freudenberger PT, Blatt RL, Youngman RE, Brow RK. Network structures and the properties of Na-Ca-Sr-borophosphate glasses. *J Non-Cryst Solids.* 2023;600:121966.
35. Leśniak M, Szal R, Starzyk B, Gajek M, Kochanowicz M, Żmojda J, Miluski P, Dorosz J, Sitarz M, Dorosz D. Influence of barium oxide on glass-forming ability and glass stability of the tellurite-phosphate oxide glasses. *J Therm Anal Calorim.* 2019;138:4295–302.
36. Chhina MK, Mittal R, Kaur S, Singh K. SrO effect on the structure, phase separation and crystallization kinetics of $\text{CaO}-\text{SiO}_2-\text{B}_2\text{O}_3-\text{Na}_2\text{O}-\text{ZrO}_2$ glasses. *J Non-Cryst Solids.* 2022;576:121301.
37. Li X, Groß-Barsnick SM, Baumann S, Koppitz T, Meulenberg WA, Natour G. Thermal properties and joinability investigation of $\text{BaO}-\text{SrO}-\text{SiO}_2-\text{B}_2\text{O}_3$ glasses for oxygen transport membrane application. *Adv Eng Mater.* 2022;24:2200660.
38. Thipperudra A, Manjunatha S, Pushpalatha HL, Prashanth KM. DSC, FTIR studies of borophosphate glasses doped with SrO , Li_2O . *J Phys Conf Ser.* 2021;1921:012110.
39. Li X, Yang H, Song X, Wu Y. Glass forming region, structure and properties of zinc iron phosphate glasses. *J Non-Cryst Solids.* 2013;379:208–13.
40. Linganna K, Park J, Choi JH. Effect of ZnO and MoO_3 addition on thermal and mechanical properties of tellurite glasses. *Phys Stat Sol (a).* 2019;216:1801013.
41. Schwarz J, Ticha H. Thermal expansion and structural properties of some $(\text{PbO})_x(\text{ZnO})_{35-x}(\text{TeO}_2)_{65}$ glasses. *SN Appl Sci.* 2021;3:484.
42. Hrabovsky J, Desevedavy F, Strizik L, Gadret G, Kalenda GP, Frumarova B, Benes L, Slang S, Veis M, Wagner T, Smejtala F. Glass formation and properties of the $\text{TeO}_2-\text{ZnO}-\text{BaO}$ tellurite optical glasses. *J Non-Cryst Solids.* 2022;582:121445.
43. Effendy N, Sidek HAA, Halimah MK, Zaid MHM. Enhancement on thermal, elastic and optical properties of new formulation tellurite glasses: influence of ZnO as a glass modifier. *Mater Chem Phys.* 2021;273: 125156.
44. Cicconi MR, Lu Z, Uesbeck T, van Wüllen L, Brauer DS, de Ligny D. Influence of vanadium on optical and mechanical properties of aluminosilicate glasses. *Front Mater.* 2020;7:161.
45. Lu X, Sun R, Huang L, Ryan JV, Vienna JD, Du J. Effect of vanadium oxide addition on thermomechanical behaviors of borosilicate glasses: Toward development of high crack resistant glasses for nuclear waste disposal. *J Non-Cryst Solids.* 2019;515:88–97.
46. Saddeek YB, Shaaban ER, Aly KA, Sayed IM. Crystallization kinetics of $\text{Li}_2\text{O}-\text{PbO}-\text{V}_2\text{O}_5$ glasses. *Physica B.* 2009;404:2412–8.
47. Farouk M. Effect of TiO_2 on the structural, thermal and optical properties of $\text{BaO}-\text{Li}_2\text{O}-\text{diborate}$ glasses. *J Non-Cryst Solids.* 2014;402:74–8.
48. Ciecńska M, Stoch P, Stoch A, Nocun M. Thermal properties of $60\text{P}_2\text{O}_5-20\text{Fe}_2\text{O}_3-20\text{Al}_2\text{O}_3$ glass for salt waste immobilization. *J Therm Anal Calorim.* 2015;121:1225–32.
49. Stambouli W, Elhouichet H, Ferid M. Study of thermal, structural and optical properties of tellurite glass with different TiO_2 composition. *J Mol Struct.* 2012;1028:39–43.
50. Hrubý A. Evaluation of glass-forming tendency by means of DTA. *Czech J Phys B.* 1972;22:1187–93.
51. Saad M, Poulain M. Glass forming ability criterion. *Mater Sci Forum.* 1987;19–20:11–8.
52. Weinberg MC. An assessment of glass stability criteria. *Phys Chem Glass.* 1994;35:119–23.
53. Lu ZP, Liu CT. A new glass-forming ability criterion for bulk metallic glasses. *Acta Mater.* 2002;50:3501–12.
54. Kissinger HE. Reaction kinetics in differential thermal analysis. *Anal Chem.* 1957;29:1702–6.
55. Laudisio G, Catauro M. The non-isothermal devitrification of $\text{Li}_2\text{O}-\text{TiO}_2-\text{GeO}_2$ glass. *Thermochim Acta.* 1998;320:155–9.

56. Matusita K, Sakka S. Kinetic study of crystallization of glass by differential thermal analysis—criterion on application of Kissinger plot. *J Non-Cryst Solids*. 1980;38–39:741–6.
57. Koga N, Yamaguchi K, Sestak J. Crystallization kinetics of lithium diborate glass by DTA. *J Therm Anal Calorim*. 1999;56:755–61.
58. Yanagida T, Masai H, Okada G, Kawano N, Kawaguchi N. Optical and scintillation properties of $30\text{BaO}-(70-x)\text{TiO}_2-x\text{GeO}_2$ ($x=50, 55, 60$) glass-ceramics. *J Non-Cryst Solids*. 2018;501:106–10.
59. Chakrabarti A, Molla AR. Synthesis of Eu_2O_3 doped $\text{BaO-TiO}_2\text{-GeO}_2$ based glass-ceramics: crystallization kinetics, optical and electrical properties. *J Non-Cryst Solids*. 2019;505:354–66.
60. Laudisio G, Catauro M, Aronne A, Pernice P. Glass transition temperature and devitrification behaviour of lithium-titanium-germanate glasses. *Thermochim Acta*. 1997;294:173–8.
61. Pisarska J, Sołtys M, Janek J, Górny A, Pietrasik E, Goryczka T, Pisarski WA. Crystallization of lead-based and lead-free oxyfluoride germanate glasses doped with erbium during heat treatment process. *J Non-Cryst Solids*. 2018;501:121–5.
62. Pisarska J, Pisarski WA, Goryczka T, Lisiecki R, Ryba-Romanowski W. Thermal analysis and near-infrared luminescence of Er^{3+} -doped lead phosphate glasses modified by PbF_2 . *J Lumin*. 2015;160:57–63.

Publisher's Note Springer Nature remains neutral with regard to jurisdictional claims in published maps and institutional affiliations.

Springer Nature or its licensor (e.g. a society or other partner) holds exclusive rights to this article under a publishing agreement with the author(s) or other rightsholder(s); author self-archiving of the accepted manuscript version of this article is solely governed by the terms of such publishing agreement and applicable law.

7.2. Wpływ stężenia TiO₂ na właściwości szkieł germanianowych emitujących promieniowanie w zakresie podczerwieni

Badania prowadzone w niniejszej rozprawie doktorskiej ukierunkowane były na poszukiwanie nowych niskofononowych szkieł domieszkowanych trójwartościowymi jonami pierwiastków ziem rzadkich, które emitują promieniowanie elektromagnetyczne w zakresie podczerwieni. Powinny się wyróżniać interesującymi właściwościami optycznymi, między innymi intensywnymi i poszerzonymi pasmami emisyjnymi w wymienionym powyżej zakresie spektralnym. W tym celu opracowano nowe składy szkieł, zoptymalizowano parametry technologiczne, przeprowadzono syntezę oraz kompleksową charakterystykę właściwości fizykochemicznych i luminescencyjnych szkieł z układu TiO₂-GeO₂-BaO-Ga₂O₃-Ln₂O₃ (gdzie Ln = Nd, Er, Tm, Pr, Ho), w których tlenek tytanu w zależności od stężenia pełnił rolę szkłotwórczą (TiO₂>30% mol) lub modyfikującą więźbę (TiO₂<30% mol). Otrzymane wyniki badań omówiono szczegółowo w publikacjach **P5-P10**. Podstawowym zadaniem badawczym podjętym w publikacji naukowej **P5** pt.: “*Nd³⁺ doped titanate-germanate glasses for near-IR laser applications*” było określenie wpływu zawartości TiO₂ na właściwości spektroskopowe jonów Nd³⁺ w szklach tytanowo-germanianowych. Przeprowadzono syntezę szkieł pojedynczo aktywowanych jonami Nd³⁺ (1% mol) w układzie TiO₂-GeO₂-BaO-Ga₂O₃, gdzie wprowadzono TiO₂ o stężeniu odpowiednio 10, 20, 30, 40, 45 oraz 50% mol. Na podstawie badań z wykorzystaniem spektroskopii absorpcyjnej stwierdzono, że największą intensywność pasma absorpcyjnego związanego z przejściem nadczułym $^4I_{9/2} \rightarrow ^4G_{5/2}, ^2G_{7/2}$ jonów Nd³⁺ obserwuje się dla układu zawierającego 20% mol TiO₂ (GeO₂:TiO₂ = 2:1). Schemat poziomów energetycznych trójwartościowych jonów Nd³⁺ sprzyja emisji promieniowania w zakresie bliskiej podczerwieni. Szczegółowa charakterystyka właściwości optycznych wykazała, że dla otrzymanego szkła można zaobserwować trzy pasma luminescencyjne przy długości fali około 0,89 μm, 1,06 μm oraz 1,35 μm, które odpowiadają przejściom $^4F_{3/2} \rightarrow ^4I_{J/2}$ (gdzie J = 9, 11, 13) jonów Nd³⁺. Najbardziej intensywne pasmo emisyjne położone przy długości fali 1,06 μm odpowiada głównemu przejściu laserowemu $^4F_{3/2} \rightarrow ^4I_{11/2}$ jonów Nd³⁺, które przesuwana się w kierunku dłuższych długości fal wraz ze wzrostem zawartości TiO₂. Szerokość spektralna głównego przejścia laserowego jonów Nd³⁺ jest niezależna od składu chemicznego szkła i jej wartość została określona na około $41,5 \pm 1$ nm.

Na podstawie badań eksperymentalnych, wykorzystując widma absorpcji, emisji i kinetyki ich zaniku oraz obliczeń z teorii Judda-Ofelta, określono szereg parametrów spektroskopowych i laserowych jonów Nd^{3+} w szklach tytanowo-germanianowych w funkcji stężenia TiO_2 . Najkorzystniejsze parametry decydujące o potencjalnych możliwościach jego zastosowania otrzymano dla szkła zawierającego 20% mol TiO_2 ($\text{GeO}_2:\text{TiO}_2 = 2:1$): przekrój czynny na emisję wymuszoną $\sigma_{\text{em}} = 4,41 \times 10^{-20} \text{cm}^2$, zmierzony czas życia luminescencji $\tau_m = 154 \mu\text{s}$, wydajność kwantowa $\eta = 88\%$, $\sigma_{\text{em}} \times \text{FWHM} = 1,85 \times 10^{-25} \text{cm}^3$ i $\sigma_{\text{em}} \times \tau_m = 67,91 \times 10^{-25} \text{cm}^2\text{s}$. Wykazano, że nowe szkła tytanowo-germanianowe domieszkowane jonami Nd^{3+} , zawierające 20% mol TiO_2 ($\text{GeO}_2:\text{TiO}_2 = 2:1$) emitują wydajne promieniowanie podczerwone przy $1,06 \mu\text{m}$, co daje możliwości zastosowania tych układów na przykład w laserach opartych na ciele stałym.

Możliwość wyciągania włókien ze szkieł optycznych przyczyniła się do rozwoju technologii światłowodowej działającej w zakresie tzw. okien telekomunikacyjnych. W zakresie trzeciego okna telekomunikacyjnego przy długości fali $1,5 \mu\text{m}$ obserwuje się najmniejsze tłumienie w światłowodzie. W ramach rozprawy doktorskiej podjęto badania nad opracowaniem i syntezą tytanowo-germanianowych szkieł aktywnych z jonami Er^{3+} przydatnych dla technologii światłowodowych. Zagadnieniom tym poświęcona jest publikacja naukowa **P6** pt.: *“Influence of TiO_2 concentration on near-infrared luminescence of Er^{3+} ions in barium gallo-germanate glasses”*. Przeprowadzono syntezę oraz badania luminescencyjne nowych szkieł tytanowo-germanianowych aktywowanych jonami Er^{3+} (0,5% mol) emitujących promieniowanie w zakresie bliskiej podczerwieni. Na podstawie badań eksperymentalnych i obliczeń teoretycznych wykorzystujących teorię Judda-Ofelta wyznaczono szereg parametrów spektroskopowych i laserowych. Szerokość spektralna pasma luminescencyjnego związanego z głównym przejściem laserowym ${}^4\text{I}_{13/2} \rightarrow {}^4\text{I}_{15/2}$ jonów Er^{3+} znacząco wzrosła od 48 nm (bez TiO_2) do 119 nm (50% mol TiO_2). Zauważalny wzrost tego parametru spektroskopowego jest bardzo korzystny z punktu widzenia zastosowania otrzymanego materiału do budowy szerokopasmowych podczerwonych laserów przestrajalnych. Czas życia górnego poziomu laserowego ${}^4\text{I}_{13/2}$ (Er^{3+}) maleje wraz ze wzrostem zawartości TiO_2 w matrycy barowo-galowo-germanianowej. Wykorzystując zmierzony i obliczony czas życia wyznaczono wydajność kwantową poziomu wzbudzonego, która osiąga bardzo wysoką wartość (powyżej 90%) dla układu barowo-galowo-germanianowego zawierającego duże stężenia TiO_2 (dla porównania wydajność kwantowa dla szkła bez TiO_2 wynosi 59%). Wyznaczono szereg parametrów zmieniających się w funkcji stężenia tlenku tytanu.

Najkorzystniejsze parametry otrzymano dla szkła zawierającego 40% mol TiO_2 ($\text{GeO}_2:\text{TiO}_2 = 1:2$): $\sigma_{\text{em}} = 6,04 \times 10^{-21} \text{cm}^2$, $\tau_m = 5,04 \text{ms}$, $\sigma_{\text{em}} \times \text{FWHM} = 423 \times 10^{-28} \text{cm}^3$, $\sigma_{\text{em}} \times \tau_m = 30,44 \times 10^{-24} \text{cm}^2 \cdot \text{s}$. Szkła o najkorzystniejszych parametrach spektroskopowych i laserowych jonów Er^{3+} wybrano do dalszej szczegółowej analizy.

W przypadku większości materiałów tlenkowych ze względu na ich stosunkowo duże drgania matrycy oraz znaczny udział przejść niepromienistych nie obserwuje się emisji w zakresie średniej podczerwieni związanej z przejściem z poziomu wzbudzonego $^4\text{I}_{11/2}$ na niżej położony poziom $^4\text{I}_{13/2}$ jonów Er^{3+} . Weryfikację spektroskopowego potencjału otrzymanego szkła tytanowo-germanianowego przedstawiono w publikacji P7 pt.: „*Enhanced mid-IR luminescence of Er^{3+} ions at 2.7 μm in $\text{TiO}_2\text{-GeO}_2\text{-BaO-Ga}_2\text{O}_3$ glasses*”. Charakterystyka termiczna pozwoliła stwierdzić, że temperatura zeszklenia wytworzonego szkła T_g wzrasta z 620°C do 705°C w obecności TiO_2 . Szkło wykazuje ponadto dobrą stabilność termiczną niezbędną do wyciągania włókien optycznych. Dzięki zachowaniu rygorystycznych warunków podczas procesu syntezy szkieł tytanowo-germanianowych w specjalnej komorze, w atmosferze ochronnej otrzymane szkła charakteryzują się bardzo niskim współczynnikiem α_{OH} wynoszącym $< 0,05 \text{cm}^{-1}$. Przeprowadzone badania w zakresie średniej podczerwieni potwierdziły, że niska zawartość grup hydroksylowych korzystnie wpływa na właściwości emisyjne. Uzyskana dla szkła tytanowo-germanianowego emisja promieniowania przy $2,7 \mu\text{m}$ związana z przejściem $^4\text{I}_{13/2} \rightarrow ^4\text{I}_{15/2}$ jonów Er^{3+} jest około czterokrotnie wzmocniona w porównaniu do wyjściowego szkła bez TiO_2 . Przy wprowadzeniu do matrycy 40% mol TiO_2 szerokość spektralna pasma odpowiadającego przejściu $^4\text{I}_{13/2} \rightarrow ^4\text{I}_{15/2}$ zmniejsza się nieznacznie ze 126nm do 118nm . Niżej położony poziom $^4\text{I}_{13/2}$ ulega efektywnej depopulacji niż wyżej położony stan $^4\text{I}_{11/2}$ jonów Er^{3+} . Znalazło to swoje odzwierciedlenie w przeprowadzonej analizie kinetyki zaniku luminescencji. Czas życia poziomu $^4\text{I}_{13/2}$ zmniejsza się z $5,35 \text{ms}$ do $5,04 \text{ms}$, podczas gdy czas życia poziomu $^4\text{I}_{11/2}$ wydłuża się z $69 \mu\text{s}$ do $138 \mu\text{s}$. Przeprowadzone badania jednoznacznie potwierdziły, że szkła tytanowo-germanianowe domieszkowane jonami Er^{3+} są dobrym kandydatem dla źródeł laserowych emitujących promieniowanie nie tylko w zakresie trzeciego okna telekomunikacyjnego, ale również przy długości fali $2,7 \mu\text{m}$. Warto zauważyć, że wartość parametru $\sigma_{\text{em}} \times \text{FWHM}$ wzrosła od $5,17 \times 10^{-26} \text{cm}^3$ do $8,14 \times 10^{-26} \text{cm}^3$, co jest korzystne dla generacji akcji laserowej. Można zatem stwierdzić, że układ o składzie chemicznym $20\text{GeO}_2\text{-}40\text{TiO}_2\text{-}30\text{BaO}\text{-}9.5\text{Ga}_2\text{O}_3\text{-}0.5\text{Er}_2\text{O}_3$ (%mol) jest obiecujący jako materiał emitujący wzmocnione promieniowanie w zakresie średniej podczerwieni.

Wymagania stawiane nowym materiałom optycznym w dziedzinie podczerwonej fotoniki są coraz wyższe. Poszukuje się wydajnych układów emitujących promieniowanie w zakresie podczerwieni od 1,8 μm do 2 μm , ze względu na potencjalne zastosowanie w bezpiecznych dla oczu radarach laserowych lub laserach medycznych stosowanych w chirurgii. Do tych układów można zaliczyć między innymi szkła domieszkowane trójwartościowymi jonami holmu, które wykazują intensywne pasmo emisji w zakresie podczerwonym przy długości fali 2 μm . Do tej problematyki nawiązuje publikacja naukowa **P8** pt.: "*Optical properties of titanate-germanate glasses containing Ho^{3+} ions*", w której uwagę skupiono przede wszystkim na otrzymaniu i zbadaniu właściwości spektroskopowych szkieł tytanowo-germanianowych domieszkowanych jonami Ho^{3+} (0,25% mol). Wyznaczono szereg parametrów spektroskopowych i laserowych zmieniających się w funkcji stężenia TiO_2 (od 10 do 50% mol) w układzie szkła $\text{TiO}_2\text{-GeO}_2\text{-BaO-Ga}_2\text{O}_3\text{-Ho}_2\text{O}_3$. Prawdopodobieństwo przejść promienistych głównego przejścia laserowego $^5\text{I}_7 \rightarrow ^5\text{I}_8$ jonów Ho^{3+} przy 2 μm przyjmuje stosunkowo wysokie wartości od 120 do 140 s^{-1} w szklach, w których tlenek tytanu pełni rolę składnika szkłotwórczego (40-50% mol TiO_2). Dalsze badania również potwierdziły korzystny wpływ wzrostu stężenia TiO_2 na właściwości luminescencyjne jonów Ho^{3+} . Szerokość połówkowa przejścia $^5\text{I}_7 \rightarrow ^5\text{I}_8$ jonów Ho^{3+} przy długości fali 2 μm wzrosła od 160 nm (bez TiO_2) do 175 nm (50% mol TiO_2). Szkła tytanowo-germanianowe zawierające stosunkowo wysokie stężenie TiO_2 (40 i 45% mol) charakteryzują się najwyższymi przekrojami czynnymi na emisję wymuszoną oraz wydajnościami kwantowymi wynoszącymi $\sigma_{\text{em}} = 0,45 \times 10^{-20} \text{ cm}^2$ i $\eta = 48\%$ (układ $\text{GeO}_2\text{:TiO}_2 = 1:2$) oraz $\sigma_{\text{em}} = 0,44 \times 10^{-20} \text{ cm}^2$ i $\eta = 51\%$ (układ $\text{GeO}_2\text{:TiO}_2 = 1:3$). Stosunkowo duży przekrój na emisję wymuszoną i wysoka wydajność kwantowa zwiększają prawdopodobieństwo uzyskania akcji laserowej, co oznacza, że tytanowe szkło barowo-galowo-germanianowe domieszkowane jonami Ho^{3+} , w którym TiO_2 pełni rolę składnika szkłotwórczego jest potencjalnym kandydatem do zastosowań laserowych przy długości fali 2 μm . Badania przedstawione w pracy **P6** jednoznacznie wykazały, że w wieloskładnikowym szkłe tytanowo-germanianowym aktywowanym jonami Er^{3+} o dużym stężeniu TiO_2 (40% mol) jest możliwy znaczny wzrost intensywności pasma emisji przy długości fali 1,5 μm . Podobną zależność zaobserwowano w omawianej pracy **P8**. Analiza otrzymanych wyników wykazała, że szkła tytanowo-germanianowe domieszkowane jonami Ho^{3+} zawierające 40% i 45% mol TiO_2 (układy $\text{GeO}_2\text{:TiO}_2 = 1:2$ i $1:3$) są również atrakcyjnym materiałem, który może być stosowany w zakresie podczerwieni przy 2 μm .

Szczegółową charakterystykę szkieł tytanowo-germanianowych pojedynczo domieszkowanych trójwartościowymi jonami Pr^{3+} i Tm^{3+} przedstawia kolejna publikacja naukowa **P9** pt.: „*Experimental and theoretical studies on NIR luminescence of titanate-germanate glasses doped with Pr^{3+} and Tm^{3+} ions*”. Przeprowadzone badania wykazały, że kierunek zmian właściwości luminescencyjnych jonów ziem rzadkich w otrzymanym materiale zależy nie tylko od składu chemicznego matrycy szklistej, ale również od samego lantanowca, a dokładniej od położenia jonu optycznie aktywnego w szeregu lantanowców (promienia jonowego). Analizując parametry spektroskopowe wyznaczone dla jonów Pr^{3+} i Tm^{3+} w nowych tytanowych szklach barowo-galowo-germanianowych w funkcji stężenia TiO_2 można zauważyć, że różnią się w sposób istotny. Podobnie jak dla układu z jonami Nd^{3+} , szkła tytanowo-germanianowe domieszkowane jonami Pr^{3+} zawierające 20% mol TiO_2 (układ $\text{GeO}_2:\text{TiO}_2 = 2:1$) charakteryzują się najlepszymi parametrami związanymi z głównym przejściem laserowym $^1\text{D}_2 \rightarrow ^1\text{G}_4$ jonów Pr^{3+} przy długości fali 1,5 μm : $\tau_m = 88 \mu\text{s}$, $\sigma_{em} = 1,16 \times 10^{-20} \text{ cm}^2$, $\sigma_{em} \times \text{FWHM} = 233 \times 10^{-27} \text{ cm}^3$ oraz $\sigma_{em} \times \tau_m = 102 \times 10^{-26} \text{ cm}^2\text{s}$. Na podstawie przeprowadzonych badań obejmujących pomiar widm emisji związanych z przejściem $^3\text{F}_4 \rightarrow ^3\text{H}_6$ jonów Tm^{3+} przy długości fali 1,8 μm oraz kinetyki zaniku luminescencji stanu $^3\text{F}_4$ najlepsze parametry otrzymano dla szkła tytanowo-germanianowego zawierającego 40% mol TiO_2 (układ $\text{GeO}_2:\text{TiO}_2 = 1:2$): $\sigma_{em} = 6,05 \times 10^{-21} \text{ cm}^2$, $\tau_m = 1,96 \text{ ms}$, $\eta = 72,1\%$ i $\sigma_{em} \times \text{FWHM} = 138,5 \times 10^{-29} \text{ cm}^3$, podobnie jak w przypadku wcześniej omawianych układów z jonami Er^{3+} lub Ho^{3+} . Na podstawie przeprowadzonych badań emisyjnych w zakresie podczerwieni można zatem stwierdzić, że szkła tytanowo-germanianowe o niższym stężeniu TiO_2 ($\text{GeO}_2:\text{TiO}_2 = 2:1$) preferują jony ziem rzadkich o większym promieniu jonowym z początku szeregu lantanowców (Pr^{3+} , Nd^{3+}). W szklach o większym stężeniu TiO_2 ($\text{GeO}_2:\text{TiO}_2 = 1:2$) obserwuje się sytuację odwrotną: preferowane są jony znajdujące się na końcu szeregu lantanowców (Er^{3+} , Tm^{3+} , Ho^{3+}).

Dalsze badania wykazały, że wzrost stężenia TiO_2 przyczynia się do stopniowego wzrostu intensywności pasma emisyjnego związanego z głównym przejściem laserowym $^3\text{F}_4 \rightarrow ^3\text{H}_6$ jonów Tm^{3+} . Jednym z etapów prowadzonych badań, których wyniki zaprezentowano w publikacji naukowej **P10** pt. „*Thulium-doped titanate-germanate glasses for infrared photonics*” było porównanie właściwości wieloskładnikowych szkieł na bazie $\text{GeO}_2\text{-BaO-GeO}_2$ oraz $\text{TiO}_2\text{-GeO}_2\text{-BaO-Ga}_2\text{O}_3$ domieszkowanych jonami Tm^{3+} o zmiennym stosunku $\text{GeO}_2:\text{TiO}_2$ (od 5:1 do 1:5) i stężeniu aktywatora (jonów Tm^{3+}). Badania te potwierdziły wpływ składu chemicznego matrycy szklistej, ze szczególnym

uwzględnieniem ilościowego stosunku $\text{GeO}_2:\text{TiO}_2$, na właściwości luminescencyjne szkieł w zakresie stężeń od 0,05 - 1% mol jonów Tm^{3+} . Analiza widm luminescencji próbek szkieł barowo-galowo-germanianowych wykazała, że największą intensywność pasma emisyjnego związanego z przejściem ${}^3\text{F}_4 \rightarrow {}^3\text{H}_6$ jonów Tm^{3+} wykazuje układ zawierający 0,3% mol Tm_2O_3 . Wyższe stężenie powodowało wygaszanie luminescencji na skutek znanego dla jonów Tm^{3+} bezpromienistego procesu przekazywania energii na drodze relaksacji krzyżowej (*ang. cross-relaxation*, CR). Potwierdzeniem tego jest malejący czas życia stanu ${}^3\text{F}_4$ w funkcji stężenia domieszki optycznie aktywnej (Tm^{3+}). Wydajność kwantowa zmniejsza się drastycznie od 50% do 4% wraz ze wzrostem stężenia jonów aktywatora. Krawędź absorpcji w zakresie widzialnym ściśle zależy od stosunku $\text{GeO}_2:\text{TiO}_2$. Dla układu $\text{GeO}_2\text{-BaO-Ga}_2\text{O}_3$ wynosi 290 nm. Wprowadzenie 10% mol TiO_2 ($\text{GeO}_2:\text{TiO}_2 = 5:1$) spowodowało znaczne przesunięcie krawędzi w stronę dłuższych fal do 350 nm. Zmiany otoczenia jonów Tm^{3+} wywołane wzrostem stężenia TiO_2 w matrycy barowo-galowo-germanianowej powodują zmianę położenia pasma nadczułego ${}^3\text{H}_6 \rightarrow {}^3\text{F}_4$ jonów Tm^{3+} . Wzrost stężenia TiO_2 spowodował przesunięcie położenia pasma w stronę dłuższych fal od 1640 nm do 1685 nm, co świadczy o wzroście kowalencyjnego charakteru wiązania $\text{Tm}^{3+}\text{-O}$ w funkcji stężenia TiO_2 w szkłe. Znaczącą część badań w niniejszej pracy poświęcono właściwościom luminescencyjnym szkieł tytanowo-germanianowych, w których TiO_2 odgrywa rolę składnika szkłotwórczego ($\text{TiO}_2 > 30\%$ mol) lub składnika modyfikującego ($\text{TiO}_2 < 30\%$ mol), zawierających różne stężenie jonów tulu. W każdym analizowanym przypadku wykazano, że intensywność pasma związanego z przejściem ${}^3\text{F}_4 \rightarrow {}^3\text{H}_6$ jonów Tm^{3+} jest prawie 5-krotnie zwiększona w wyniku wprowadzenia 50% mol TiO_2 , a jego maksymalna szerokość spektralna wynosi 253 nm. Obliczona na podstawie eksperymentalnych czasów życia z krzywych zaniku luminescencji oraz radiacyjnych czasów życia z teorii Judda-Ofelta wydajność kwantowa dla stanu ${}^3\text{F}_4$ jonów Tm^{3+} osiągnęła wartość powyżej 70% dla układów, w których stosunek GeO_2 do TiO_2 wynosił 1:1, 1:2 oraz 1:3. Dla wszystkich otrzymanych układów korzystając z modelu Inokuti-Hirayama wykazano, że wygaszanie podczerwonej emisji zmniejsza się wraz ze wzrostem stężenia TiO_2 w próbkach szkieł domieszkowanych wysokim stężeniem jonów Tm^{3+} . Prowadzone badania poszerzono o wyjaśnienie korelacji między właściwościami emisyjnymi a zmieniającym się uporządkowaniem bliskiego zasięgu w funkcji stężenia TiO_2 z wykorzystaniem spektroskopii Ramana. Optymalne stężenie TiO_2 w szklach tytanowo-germanianowych domieszkowanych jonami Tm^{3+} ustalono na: 30% mol ($\text{GeO}_2:\text{TiO}_2 = 1:1$), 40% mol ($\text{GeO}_2:\text{TiO}_2 = 1:2$) oraz

45% mol ($\text{GeO}_2:\text{TiO}_2 = 1:3$). Uzyskane wyniki potwierdziły unikalne właściwości szkieł tytanowo-germanianowych jako matryc dla podczerwonej fotoniki. Pozwalają one także stwierdzić, że kolejnym interesującym kierunkiem badań poświęconym jonom Tm^{3+} w szklach tytanowo-germanianowych, będzie analiza widma emisyjnego przy długości fali 2,3 μm związanego z przejściem ${}^3\text{H}_4 \rightarrow {}^3\text{H}_5$, które wykorzystywane jest między innymi w zastosowaniach takich jak bezinwazyjny pomiar poziomu glukozy we krwi.

Przeprowadzone w niniejszej rozprawie doktorskiej badania potwierdziły niezwykle korzystny wpływ dwutlenku tytanu TiO_2 w wieloskładnikowych szklach tytanowo-germanianowych pojedynczo domieszkowanych jonami ziem rzadkich na właściwości luminescencyjne w zakresie podczerwieni. Możliwość badania wydajnej emisji promieniowania podczerwonego nie ogranicza się jednak tylko do szkieł pojedynczo domieszkowanych jonami ziem rzadkich. W publikacji naukowej **P11** pt.: *“Near-IR luminescence of rare-earth ions (Er^{3+} , Pr^{3+} , Ho^{3+} , Tm^{3+}) in titanate-germanate glasses under excitation of Yb^{3+} ”* określono wpływ TiO_2 na właściwości luminescencyjne w zakresie podczerwieni, analizując zjawisko przekazywania energii wzbudzenia od Yb^{3+} do Ln^{3+} ($\text{Ln} = \text{Er}, \text{Pr}, \text{Ho}, \text{Tm}$). Wykorzystano w tym celu układy szkieł tytanowo-germanianowych, w których stężenie jonów Yb^{3+} wynosiło 0,5% mol, natomiast jonów Er^{3+} , Pr^{3+} , Ho^{3+} i Tm^{3+} wynosiło 0,1% mol. Na podstawie analizy widm luminescencji zaobserwowano nieliniową zależność zmiany intensywności głównych przejść laserowych ${}^1\text{G}_4 \rightarrow {}^3\text{H}_5$ (Pr^{3+}), ${}^4\text{I}_{13/2} \rightarrow {}^4\text{I}_{15/2}$ (Er^{3+}), ${}^3\text{F}_4 \rightarrow {}^3\text{H}_6$ (Tm^{3+}) oraz ${}^5\text{I}_7 \rightarrow {}^5\text{I}_8$ (Ho^{3+}) w funkcji stężenia TiO_2 . Na przykładzie szkła aktywowanego parą jonów $\text{Yb}^{3+}/\text{Er}^{3+}$ zauważono, że intensywność przejścia ${}^4\text{I}_{13/2} \rightarrow {}^4\text{I}_{15/2}$ (Er^{3+}), które jest wykorzystywane w telekomunikacji optycznej, najpierw maleje w funkcji zmiany ilościowego stosunku $\text{GeO}_2:\text{TiO}_2$ od 5:1 do 1:2, a następnie wzrasta. Z kolei jego szerokość spektralna wzrasta nieznacznie od 38 nm ($\text{GeO}_2:\text{TiO}_2 = 5:1$) do 55 nm ($\text{GeO}_2:\text{TiO}_2 = 1:5$). Obserwuje się ponadto znaczne skrócenie czasów zaniku luminescencji ze stanu ${}^2\text{F}_{5/2}$ jonów Yb^{3+} przy wzroście stężenia TiO_2 . W układach szkieł tytanowo-germanianowych podwójnie domieszkowanych czas życia ${}^2\text{F}_{5/2}$ (Yb^{3+}) maleje z 0,63 ms do 0,40 ms (układ podwójnie aktywowany $\text{Yb}^{3+}/\text{Pr}^{3+}$), z 0,65 ms do 0,49 ms (układ podwójnie aktywowany $\text{Yb}^{3+}/\text{Er}^{3+}$), z 0,70 ms do 0,48 ms (układ podwójnie aktywowany $\text{Yb}^{3+}/\text{Tm}^{3+}$) i z 0,83 ms do 0,52 ms (układ podwójnie aktywowany $\text{Yb}^{3+}/\text{Ho}^{3+}$). Maksymalne wartości wydajności transferu energii dla układów tytanowo-germanianowych wynoszą odpowiednio: 53% ($\text{Yb}^{3+}/\text{Pr}^{3+}$), 48% ($\text{Yb}^{3+}/\text{Er}^{3+}$), 49%, ($\text{Yb}^{3+}/\text{Tm}^{3+}$) i 40% ($\text{Yb}^{3+}/\text{Ho}^{3+}$).

W nawiązaniu do wcześniejszych badań w celu poszerzenia wiedzy na temat podwójnego domieszkowania otrzymanego materiału, porównano jak wzrost stężenia jonów Er^{3+} i Yb^{3+} wpływa na właściwości emisyjne szkieł tytanowo-germanianowych. W ramach badań przedstawionych w ostatniej publikacji naukowej **P12** wchodzącej do cyklu rozprawy pt. ” *The impact of pair $\text{Er}^{3+}/\text{Yb}^{3+}$ on titanate-germanate glasses: Physicochemical and near-infrared luminescence investigations*” przeprowadzono syntezę szkieł w układzie tlenkowym $\text{GeO}_2\text{-BaO-Ga}_2\text{O}_3$ oraz $\text{TiO}_2\text{-GeO}_2\text{-BaO-Ga}_2\text{O}_3$ ($\text{GeO}_2:\text{TiO}_2 = 1:1$) podwójnie domieszkowanych jonami Er^{3+} (0,1; 0,25; 0,5% mol) oraz Yb^{3+} (0,5; 1,25; 2,5% mol). Przy wzbudzeniu falą o długości 980 nm otrzymane szkła wykazywały charakterystyczną emisję dla jonów Er^{3+} , z maksimum przy długości fali około 1,5 μm (przejście $^4\text{I}_{13/2} \rightarrow ^4\text{I}_{15/2}$). Intensywność głównego przejścia laserowego jonów Er^{3+} jest prawie dwukrotnie zwiększona w porównaniu do szkła bez TiO_2 . Zaobserwowano również wyraźne zmiany szerokości spektralnej, której wartość dla układu $30\text{TiO}_2\text{-}30\text{GeO}_2\text{-}30\text{BaO-}7\text{Ga}_2\text{O}_3\text{-}0.5\text{Er}_2\text{O}_3\text{-}2.5\text{Yb}_2\text{O}_3$ (% mol) wynosi 65 nm, natomiast dla układu $60\text{GeO}_2\text{-}30\text{BaO-}7\text{Ga}_2\text{O}_3\text{-}0.5\text{Er}_2\text{O}_3\text{-}2.5\text{Yb}_2\text{O}_3$ (% mol) jest blisko dwukrotnie mniejsza (31 nm). Na podstawie krzywych zaniku luminescencji określono wydajność transferu energii wzbudzenia od jonów Yb^{3+} do jonów Er^{3+} , która wraz ze wzrostem stężenia Er_2O_3 oraz Yb_2O_3 w matrycy barowo-galowo-germanianowej wzrasta od 22% do 73%. Dla układów tytanowo-germanianowych zaobserwowano odwrotną zależność. Wydajność kwantowa wzrasta od 24% do 39%, a następnie maleje osiągając wartość 36%. Zmiany stężenia jonów Er^{3+} i Yb^{3+} mogą również wpływać na zmianę właściwości strukturalnych otrzymanego materiału, co pokazały wyraźnie badania przeprowadzone przy pomocy dyfrakcji rentgenowskiej, spektroskopii Ramana oraz spektroskopii absorpcyjnej i luminescencyjnej. Na podstawie analizy pasma nadczułego związanego z przejściem $^4\text{I}_{15/2} \rightarrow ^2\text{H}_{11/2}$ jonów Er^{3+} w układzie tytanowo-germanianowym zawierającym największe stężenie jonów ziem rzadkich można zauważyć występowanie rozszczepień Starkowskich. Efekt ten obserwowany również na widmie Ramana świadczy niewątpliwie o zmianie lokalnej struktury (zmianie bezpośredniego otoczenia jonów ziem rzadkich). Przeprowadzona rentgenowska analiza fazowa (XRD) wykazała, że wprowadzenie do matrycy tytanowo-germanianowej małego stężenia Er_2O_3 i Yb_2O_3 (0,1/0,5 oraz 0,25/0,5% mol) nie powoduje zmiany lokalnej struktury. Układ przestaje być w pełni amorficzny w przypadku wprowadzenia jonów ziem rzadkich o znacznie większym stężeniu. Obecność charakterystycznych wąskich linii dyfrakcyjnych, świadczących o obecności fazy krystalicznej $\text{Yb}_2\text{Ti}_2\text{O}_7$ i $\text{Er}_2\text{Ti}_2\text{O}_7$, stwierdzono dla układu

tytanowo-germanianowego zawierającego największe stężenia jonów domieszek optycznie aktywnych. Badania spektroskopowe dowodzą, że optymalne stężenie jonów donora i akceptora w szkle, gdzie stosunek molowy składników $\text{GeO}_2:\text{TiO}_2 = 1:1$, wynosi odpowiednio 0,25% mol jonów Er^{3+} oraz 1,25% mol jonów Yb^{3+} .

Problematyka badawcza podjęta w ramach rozprawy doktorskiej i przedstawiona w omówionych publikacjach naukowych (**P5-P12**) wnosi swój wkład do poszerzenia wiedzy na temat szkieł nieorganicznych oraz możliwości ich zastosowań w dziedzinie podczerwonej fotoniki. Szczegółowa i dokładna analiza właściwości luminescencyjnych otrzymanego materiału, ze szczególnym uwzględnieniem składu chemicznego matrycy szklistej (stosunek molowy $\text{GeO}_2:\text{TiO}_2$) oraz optymalnego stężenia domieszek optycznie aktywnych, pozwala na dobór szkieł tytanowo-germanianowych wyróżniających się najlepszymi parametrami spektroskopowymi i laserowymi jonów ziem rzadkich. Interesujące właściwości optyczne szkieł tytanowo-germanianowych pozwalają na ich potencjalne wykorzystanie w technologii elementów optycznych, źródeł laserowych emitujących promieniowanie w zakresie średniej podczerwieni oraz szerokopasmowych wzmacniaczy optycznych pracujących w zakresie bliskiej podczerwieni.

P5

Wojciech A. Pisarski, Karolina Kowalska, Marta Kuwik, Joanna Pisarska, Jan Dorosz,
Jacek Żmojda, Marcin Kochanowicz, Dominik Dorosz,

Nd³⁺ doped titanate-germanate glasses for near-IR laser applications

Optical Materials Express 12 (2022) 2912-2926



Nd³⁺ doped titanate-germanate glasses for near-IR laser applications

WOJCIECH A. PISARSKI,^{1,*} KAROLINA KOWALSKA,¹ MARTA KUWIK,¹ JOANNA PISARSKA,¹ JAN DOROSZ,² JACEK ŻMOJDA,² MARCIN KOCHANOWICZ,²  AND DOMINIK DOROSZ³

¹University of Silesia, Institute of Chemistry, Szkolna 9 Street, 40-007 Katowice, Poland

²Bialystok University of Technology, Faculty of Electrical Engineering, Wiejska 45D Street, 15-351 Bialystok, Poland

³AGH University of Science and Technology, Faculty of Materials Science and Ceramics, Mickiewicza Avenue, 30-059 Cracow, Poland

*wojciech.pisarski@us.edu.pl

Abstract: In current work, spectroscopic properties of Nd³⁺ ions in titanate-germanate glasses have been studied for near-IR luminescence and laser applications. Near-IR luminescence at 1.06 μm due to ⁴F_{3/2} → ⁴I_{11/2} laser transition of Nd³⁺ ions has been examined in the function of TiO₂ concentration. Based on theoretical calculations and experimental investigations, several spectroscopic and laser parameters for Nd³⁺ ions in titanate-germanate glasses were determined and compared to the previous results published for similar glass systems. Our systematic studies indicate that Nd³⁺ doped glass with molar ratio GeO₂:TiO₂ = 2:1 presents excellent near-IR luminescence properties and could be successfully applied to laser technology.

© 2022 Optica Publishing Group under the terms of the [Optica Open Access Publishing Agreement](#)

1. Introduction

The first laser action in glass was developed over sixty years ago [1] and initiated successfully the era of laser glass technology. The laser oscillations observed in the near-infrared (NIR) spectral range at about 1.06 μm are associated with the main ⁴F_{3/2} → ⁴I_{11/2} transition of Nd³⁺. Further experiments well demonstrated that spectroscopic parameters for the ⁴F_{3/2} → ⁴I_{11/2} NIR laser transition of Nd³⁺ ions such as stimulated emission cross section, peak fluorescence wavelength, effective fluorescence bandwidth, calculated and measured lifetimes, transition probabilities, fluorescence branching ratios, and quantum efficiency of excited state varying strongly on glass-host composition [2]. Since then, many excellent papers have been published on optical and near-IR laser properties of Nd³⁺ ions in numerous inorganic glass systems [3–6]. In particular, near-IR luminescence properties of Nd³⁺ ions in borate [7–13], phosphate [14–20], silicate [21–23], germanate [24–28], tellurite [28–35], as well as mixed borotellurite [36–38], borogermanate [39] and borobismuthate [40–42] glasses have been examined in details. Special attention has been devoted to non-oxide glasses containing Nd³⁺ ions [43–46].

Among amorphous matrices, barium gallo-germanate glass belonging to low-phonon oxide glass family presents some advantages, i.e. relatively large glass-forming region, good thermal stability parameters, quite strong chemical and mechanical stability useful for optical fiber drawing and enhanced luminescence properties. It was proposed as a window for high energy laser systems [47]. Moreover, barium gallo-germanate glasses doped with rare earth ions are excellent candidate for optical waveguides [48,49] and solid-state lasers [50,51] operated in the near-IR ranges. Current work is focused on spectroscopic and laser properties of Nd³⁺ ions in barium gallo-germanate glasses, where GeO₂ was partially substituted by TiO₂. Their thermal and structural properties were evidenced by differential scanning calorimetry (DSC), X-ray diffraction (XRD), electron paramagnetic resonance (EPR), Raman and infrared spectroscopy in

our previously published work [52]. Here, several spectroscopic and laser parameters for Nd^{3+} ions were determined in function of TiO_2 content. The results are presented and discussed for glass samples, where $\text{GeO}_2:\text{TiO}_2$ molar ratio was changed from 5:1 to 1:5. Titanium dioxide plays the role of glass-modifier or glass-former, depending on its concentration. Until now, emission properties of rare earth ions in inorganic glasses with a high content of TiO_2 have not been yet studied, to the best of our knowledge. Recently, near-IR emission properties of Nd^{3+} have been examined in $\text{GeO}_2\text{-PbO-TiO}_2$ [53], $\text{TeO}_2\text{-TiO}_2\text{-Nb}_2\text{O}_5$ [54], $\text{TeO}_2\text{-TiO}_2\text{-WO}_3$ [55], $\text{TeO}_2\text{-TiO}_2\text{-ZnO}$ [56] and multicomponent $\text{PbO-B}_2\text{O}_3\text{-TiO}_2\text{-AlF}_3$ [57] glasses, where amount of titanium dioxide playing the role as glass-network modifier did not exceed 10 molar %. Here, the purpose of our work concerns on the enhanced near-IR luminescence of Nd^{3+} ions in multicomponent germanate glasses in the presence of TiO_2 .

2. Experimental details

Glasses with the following chemical compositions $x\text{TiO}_2\text{-(60-x)GeO}_2\text{-30BaO-9Ga}_2\text{O}_3\text{-1Nd}_2\text{O}_3$ (where $x = 0, 10, 20, 30, 40, 45$ and 50) were prepared using melt quenching technique. The concentrations of components are given in molar %. The appropriate amounts of metal oxides of high purity (99.99%, Aldrich Chemical Co.) were mixed homogeneously together and then melted at 1200°C for 0.45h. Each Nd^{3+} -doped sample was polished for optical measurements.

In the next step, the Metricon 2010 prism coupler was applied to determine the refractive index of the glass-host at a wavelength of 632.8 nm. Glass samples were then characterized using absorption (Cary 5000 UV-VIS-NIR spectrophotometer, Agilent Technology, USA) and luminescence spectroscopy. For luminescence spectra and decay curve measurements laser equipment was used, which consists of PTI QuantaMaster QM40 spectrofluorometer, tunable pulsed optical parametric oscillator (OPO), Nd:YAG laser (Opotek Opolette 355 LD), double 200 mm monochromators, Hamamatsu H10330B-75 detector and PTI ASOC-10 USB-2500 oscilloscope. Resolution for spectral measurements was ± 0.1 nm. Decay curves were recorded and stored by a PTI ASOC-10 [USB-2500] oscilloscope with an accuracy of ± 0.5 μs .

3. Results and discussion

Previously published works for titanate glasses [58–60] revealed that they are partly crystallized and present relatively low thermal stability. These glass systems possess crystalline phases usually assigned to different titanates. In particular, it is quite difficult to synthesize thermally stable and fully amorphous systems with high TiO_2 concentration. In our case, multicomponent glasses with various molar ratios $\text{GeO}_2:\text{TiO}_2$ from 5:1 to 1:5 were successfully prepared. It is interesting to notice that glass-forming region for the studied compositions is relatively broad. All studied samples are fully amorphous, which was verified by X-ray diffraction. Typical X-ray diffraction patterns for selected glass samples with the absence and presence of titanium dioxide ($\text{GeO}_2:\text{TiO}_2 = 1:1$) are shown in Fig. S1. Further DSC experiments shown in Fig. S2 indicate that the glass transition temperature increases in the presence of TiO_2 suggesting less open glass-structure for titanate-germanate glass samples. On the other hand, thermal stability parameter ($\Delta T = T_x - T_g$) is reduced for glass sample, where GeO_2 is partially replaced by TiO_2 (for more details please refer to Table S1). However, ΔT factor is still above 100°C exhibiting good thermal stability against devitrification and quite large working range during operations for fiber drawing.

Another key parameter is the infrared absorption coefficient α_{OH} for band near 3400 cm^{-1} assigned to the stretching vibrations of hydroxyl groups (Fig. S3). In general, glass systems with extremely low content of OH^- groups are necessary to fabricate active near-IR emitting optical fibers. According to the previous excellent results published for Tm^{3+} doped barium gallo-germanate glass single-mode fibers [50], the value of α_{OH} is reduced drastically from 3.05 cm^{-1} for sample melted in air to 0.19 cm^{-1} for precursor glass prepared under the optimized

Reaction Atmosphere Procedure (RAP). In our case, the OH- absorption coefficients are low, because samples were prepared under rigorous technological conditions in special glove-box, in a protective atmosphere of dried argon of high purity. The infrared absorption coefficient for titanate-germanate glass sample is close to 0.23 cm^{-1} (Table S2) and its value is similar to the results obtained earlier for germanate based glasses [61–63]. Further investigations indicate that titanium ions at trivalent oxidation state are present in the studied glass samples (Fig. S4). It was also confirmed for $\text{Ti}^{3+}/\text{Ti}^{4+}$ doped calcium aluminosilicate glasses [64].

3.1. Absorption spectra and refractive index of the glass-host

Figure 1 shows absorption spectra of Nd^{3+} ions in glasses with various molar ratios $\text{GeO}_2:\text{TiO}_2$. The following glass parameters, i.e. UV cut-off wavelength, bonding parameter δ and refractive index of the glass-host n in function of TiO_2 concentration are also indicated.

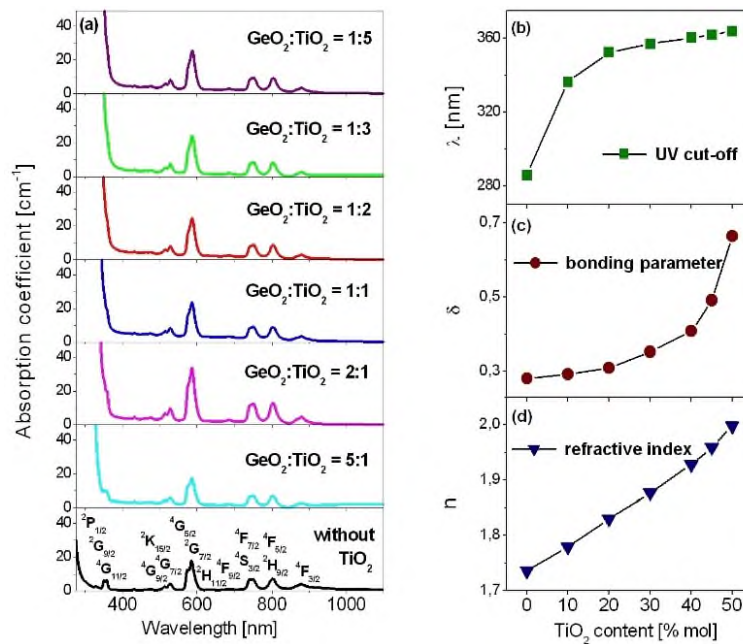


Fig. 1. Absorption spectra of Nd^{3+} -doped titanate-germanate glasses (a), UV cut-off (b), bonding parameter (c) and refractive index of glass-host (d) in function of TiO_2 content.

The absorption spectra consist of the inhomogeneously broadened lines characteristic for $4f^3-4f^3$ electronic transitions of Nd^{3+} ions. They are located in the 300–950 nm spectral range. Absorption bands of Nd^{3+} ions correspond to transitions originating from the $^4\text{I}_{9/2}$ ground state to the higher-lying $^4\text{F}_{3/2}$, $^4\text{F}_{5/2}$, $^2\text{H}_{9/2}$, $^4\text{F}_{7/2}$, $^4\text{S}_{3/2}$, $^4\text{F}_{9/2}$, $^2\text{H}_{11/2}$, $^4\text{G}_{5/2}$, $^2\text{G}_{7/2}$, $^4\text{G}_{7/2}$, $^2\text{K}_{15/2}$, $^4\text{G}_{11/2}$, $^2\text{G}_{9/2}$ and $^2\text{P}_{1/2}$ excited states, respectively. Among observed absorption lines, the $^4\text{I}_{9/2} \rightarrow ^4\text{G}_{5/2}$, $^2\text{G}_{7/2}$ transition of Nd^{3+} located near 600 nm, so-called hypersensitive transition, is the most intense. It follows well the selection rules: $|S| = 0$, $|\Delta L| \leq 2$ and $|\Delta J| \leq 2$. Its position and intensity is very sensitive to small changes of environment around Nd^{3+} ions. The absorption measurements for Nd^{3+} ions clearly indicates that the intensity of this band is the highest for glass with $\text{GeO}_2:\text{TiO}_2$ molar ratio equal to 2:1. Furthermore, the UV cut-off wavelength defined as the intersection between the zero base line and the extrapolation of absorption edge was determined. The absorption edge for titanate-germanate glass is shifted to longer wavelengths with increasing TiO_2 concentration.

From the optical absorption spectra measured for Nd^{3+} ions in titanate-germanate glasses, bonding parameters (β and δ) were also calculated using the expression $\delta = [(1 - \beta)/\beta] \times 100\%$, where $\beta = \sum_N = \beta^*/N$ and $\beta^* = \nu_c/\nu_a$ [65]. In this expression, β is the shift of energy level position (Nephelauxetic effect), N - number of levels used for calculation of β -values, ν_c and ν_a are energies of the corresponding transitions in the investigated complex and free-ion [66]. Positive or negative sign for the values of δ suggests covalent or ionic bonding between Nd^{3+} ions and surrounding ligands. Our calculations indicate that bonding parameter δ increase from 0.281 (glass without TiO_2) to 0.665 (glass with molar ratio $\text{GeO}_2:\text{TiO}_2 = 1:5$). It suggests that titanate-germanate glasses exhibit more covalent character in comparison to lead borate glass doped with Nd^{3+} , for which the bonding parameter δ was found to be -0.210 [67]. The results are well correlated with the refractive index, which increases from 1.736 (glass without TiO_2) to 1.998 (glass with molar ratio $\text{GeO}_2:\text{TiO}_2 = 1:5$) with increasing TiO_2 concentration. Details are given in Table 1.

Table 1. Glass composition, TiO_2 content, Nd^{3+} ion concentration, UV cut-off, bonding parameter (δ) and refractive index of glass-host (n).

Glass composition [mol %]	TiO_2 content [% mol]	$\text{GeO}_2:\text{TiO}_2$	Nd^{3+} $N \times 10^{20}$ [g/cm ³]	UV cut-off [nm]	δ	n
60 GeO_2 -30 BaO -9 Ga_2O_3 -1 Nd_2O_3	0	-	4.30	286	0.281	1.736
50 GeO_2 -10 TiO_2 -30 BaO -9 Ga_2O_3 -1 Nd_2O_3	10	5 : 1	4.34	336.5	0.293	1.779
40 GeO_2 -20 TiO_2 -30 BaO -9 Ga_2O_3 -1 Nd_2O_3	20	2 : 1	4.39	352.5	0.309	1.830
30 GeO_2 -30 TiO_2 -30 BaO -9 Ga_2O_3 -1 Nd_2O_3	30	1 : 1	4.43	355	0.363	1.877
20 GeO_2 -40 TiO_2 -30 BaO -9 Ga_2O_3 -1 Nd_2O_3	40	1 : 2	4.49	359	0.409	1.928
15 GeO_2 -45 TiO_2 -30 BaO -9 Ga_2O_3 -1 Nd_2O_3	45	1 : 3	4.58	361.5	0.442	1.969
10 GeO_2 -50 TiO_2 -30 BaO -9 Ga_2O_3 -1 Nd_2O_3	50	1 : 5	4.64	364	0.665	1.998

3.2. Judd-Ofelt calculations

The standard Judd-Ofelt theory [68,69] was used to calculate radiative transition probabilities for excited states of Nd^{3+} ions in titanate-germanate glasses. The calculation procedure was carried out using the software OriginPro. According to the standard procedure, the x-axis of absorption spectrum was converted to wavenumbers given in cm^{-1} . Then, the baseline was fitted individually to the each absorption band and the integrated area was calculated. The intensities of bands shown in Fig. 1 are estimated by measuring the areas under the absorption lines using the Eq. (1):

$$P_{\text{meas}} = 4.318 \times 10^{-9} \int \epsilon(\nu) d\nu. \quad (1)$$

In this equation $\epsilon(\nu) = A/cl$, $\int \epsilon(\nu)$ represents the area under the absorption line, A indicates the absorbance, c is the concentration of Nd^{3+} ions in $\text{mol} \times \text{l}^{-1}$ and l denotes the optical path length.

The measured oscillator strengths of transitions were obtained from the absorption bands of Nd^{3+} ions. The theoretical oscillator strengths for each transition of Nd^{3+} , within $4f^3$ electronic configuration, were calculated using the following relation (2):

$$P_{\text{calc}} = \frac{8\pi^2 mc(n^2 + 2)^2}{3h\lambda(2J + 1) \cdot 9n} \times \sum_{t=2,4,6} \Omega_t (\langle 4f^N J || U^t || 4f^N J' \rangle)^2 \quad (2)$$

where m is the mass of the electron, c is the velocity of light, h is the Planck constant and λ is the mean wavelength of the each transition of Nd^{3+} , n is the refractive index of the glass-host, an $||U^t||^2$ represents the square of the matrix elements of the unit tensor operator U^t connecting the initial and final states. The squared reduced matrix elements $||U^t||^2$ were taken from [66].

Measured and calculated oscillator strengths for Nd^{3+} ions in the studied glasses are given in Table 2 (0, 10, 20 and 30% TiO_2) and Table 3 (40, 45 and 50% TiO_2), respectively. The quality of the fit can be expressed by the magnitude of the root-mean-square (rms) deviation. It is defined by $\Sigma(P_{\text{meas}} - P_{\text{calc}})^2$. The rms values are also given in Tables 2 and 3.

Table 2. Measured and calculated oscillator strengths ($\times 10^{-6}$) for Nd^{3+} ions in titanate-germanate glasses. Transitions are from the $^4I_{9/2}$ ground state to the levels indicated. The rms deviation ($\times 10^{-6}$) is also given.

Levels	Energy [cm^{-1}]	0% TiO_2		10% TiO_2		20% TiO_2		30% TiO_2	
		P_{meas}	P_{calc}	P_{meas}	P_{calc}	P_{meas}	P_{calc}	P_{meas}	P_{calc}
$^4F_{3/2}$	11350	2.430	2.023	1.650	1.531	3.580	3.278	2.220	1.959
$^4F_{5/2}, ^2H_{9/2}$	12450	4.890	5.386	5.170	5.315	9.820	10.187	6.020	6.338
$^4F_{7/2}, ^4S_{3/2}$	13400	5.340	4.977	5.660	5.554	10.430	10.157	6.640	6.403
$^4F_{9/2}$	14620	0.600	0.414	0.510	0.439	0.900	0.818	0.560	0.515
$^2H_{11/2}$	15850	0.170	0.114	0.100	0.119	0.200	0.221	0.150	0.140
$^2H_{11/2}$	17100	21.400	21.392	25.200	25.190	44.900	44.895	31.500	31.491
$^4G_{5/2}, ^2G_{7/2}$									
rms deviation		0.581		0.053		0.308		0.228	

Table 3. Measured and calculated oscillator strengths ($\times 10^{-6}$) for Nd^{3+} ions in titanate-germanate glasses. Transitions are from the $^4I_{9/2}$ ground state to the levels indicated. The rms deviation ($\times 10^{-6}$) is also given.

Levels	Energy [cm^{-1}]	40% TiO_2		45% TiO_2		50% TiO_2	
		P_{meas}	P_{calc}	P_{meas}	P_{calc}	P_{meas}	P_{calc}
$^4F_{3/2}$	11350	2.130	1.914	1.880	1.660	2.090	1.894
$^4F_{5/2}, ^2H_{9/2}$	12450	6.260	6.523	5.920	6.188	6.200	6.439
$^4F_{7/2}, ^4S_{3/2}$	13400	6.930	6.735	6.810	6.612	6.810	6.634
$^4F_{9/2}$	14620	0.580	0.537	0.600	0.520	0.600	0.529
$^2H_{11/2}$	15850	0.150	0.143	0.150	0.140	0.130	0.143
$^2H_{11/2}$	17100	33.500	33.494	33.100	33.096	33.600	33.595
$^4G_{5/2}, ^2G_{7/2}$							
rms deviation		0.156		0.166		0.132	

The three Ω_t ($t = 2, 4, 6$) intensity parameters (J-O) were evaluated from the least-square fit of measured and calculated oscillator strengths for Nd^{3+} ions. They are collected in Table 4.

Table 4. The Judd-Ofelt intensity parameters Ω_t ($t = 2, 4, 6$) $\times 10^{-20} \text{ cm}^2$.

TiO_2 content [% mol]	$\text{GeO}_2 : \text{TiO}_2$	Ω_2	Ω_4	Ω_6	Ω_4/Ω_6
0	-	4.88 ± 0.48	3.74 ± 0.77	2.95 ± 0.31	1.27
10	5 : 1	6.64 ± 0.14	2.47 ± 0.21	3.30 ± 0.09	0.75
20	2 : 1	10.67 ± 0.34	5.31 ± 0.51	5.72 ± 0.20	0.93
30	1 : 1	7.58 ± 0.28	3.01 ± 0.42	3.48 ± 0.17	0.87
40	1 : 2	7.79 ± 0.22	2.75 ± 0.34	3.53 ± 0.13	0.78
45	1 : 3	7.82 ± 0.22	2.21 ± 0.33	3.38 ± 0.13	0.65
50	1 : 5	7.52 ± 0.19	2.57 ± 0.29	3.28 ± 0.12	0.78

The J-O parameters Ω_t ($t = 2, 4, 6$) are quite well correlated with thermal results obtained by DSC method (Fig. S2). The Ω_4 and Ω_6 parameters are found to be a structure-dependent. In contrast to germanate glass without TiO_2 , the Ω_2 and Ω_6 parameters are higher than values of Ω_4 suggesting that titanate-germanate glasses exhibit more rigidity and confirm less open glass structure from DSC measurements. Moreover, the magnitude of Ω_4/Ω_6 named as spectroscopic quality parameter, is found to be less than unity for glasses where the $^4F_{3/2} \rightarrow ^4I_{11/2}$ transition

at 1.06 μm is the intense lasing transition. Glass systems with more than unity of Ω_4/Ω_6 factor demonstrate the intense lasing ${}^4F_{3/2} \rightarrow {}^4I_{9/2}$ transition of Nd^{3+} at 0.89 μm . It was well presented and discussed in details for numerous inorganic glasses containing Nd^{3+} ions [70]. In our case, all values of Ω_4/Ω_6 factor are less than unity, except glass without TiO_2 , which indicate that titanate-germanate glass is promising to achieve lasing condition for the ${}^4F_{3/2} \rightarrow {}^4I_{11/2}$ (Nd^{3+}) near-IR luminescence channel at about 1.06 μm .

The Judd-Ofelt parameter Ω_2 indicates the degree of covalency between Nd^{3+} ions and surrounding ligands. Also, it reflects the asymmetry of the environment around Nd^{3+} ions. It is interesting to see that the Judd-Ofelt parameter Ω_2 for glass with molar ratio $\text{GeO}_2:\text{TiO}_2 = 2:1$ is the highest ($\Omega_2 = 10.67 \times 10^{-20} \text{cm}^2$) than values obtained for other studied Nd^{3+} doped glass samples. It suggests that the bonds between Nd^{3+} ions and ligands existing in glass sample with $\text{GeO}_2:\text{TiO}_2 = 2:1$ are highly covalent in character and the results are comparable to the values Ω_2 equal to $10.43 \times 10^{-20} \text{cm}^2$ obtained for Nd^{3+} ions in $\text{Li}_2\text{O-Ta}_2\text{O}_5\text{-ZrO}_2\text{-SiO}_2$ glasses [71] and $10.26 \times 10^{-20} \text{cm}^2$ for Nd^{3+} doped oxyfluorosilicate glass [72].

In the next step, the values of Ω_t ($t = 2, 4, 6$) were used to calculate the radiative transition probabilities A_J , luminescence branching ratios β and radiative lifetimes τ_{rad} . The radiative transition probabilities A_J for excited states of Nd^{3+} ions from an initial state J to a final ground state J' were calculated using the following expression (3):

$$A_J = \frac{64\pi^4 e^2}{3h(2J+1)\lambda^3} \times \frac{n(n^2+2)^2}{9} \times \sum_{t=2,4,6} \Omega_t (\langle 4f^N J || U^t || 4f^N J' \rangle)^2. \quad (3)$$

The total radiative emission probability A_T involving all the intermediate terms is given by the sum of the A_J terms. Thus, radiative lifetime τ_{rad} of an excited state is the inverse of the total radiative emission probability given by the following relation (4):

$$\tau_{\text{rad}} = \frac{1}{\sum_i A_{Ji}} = \frac{1}{A_T} \quad (4)$$

Luminescence branching ratio β is related to the relative intensities of transitions from the excited state to all lower-lying states of Nd^{3+} and given by expression (5):

$$\beta = \frac{A_J}{\sum_i A_{Ji}} \quad (5)$$

The calculated radiative transition probabilities A_J and the luminescence branching ratios β for Nd^{3+} ions in titanate-germanate glasses are calculated. The results for the studied glass samples are shown in Table 2 (0, 10, 20 and 30% TiO_2) and Table 3 (40, 45 and 50% TiO_2), respectively. In all cases, the luminescence branching ratios for the ${}^4F_{3/2} \rightarrow {}^4I_{11/2}$ transition at 1.06 μm are the highest and the values of β are between 46% to 52%, depending on TiO_2 concentration. The radiative transition probability is the highest for glass with $\text{GeO}_2:\text{TiO}_2 = 2:1$ and its value for the ${}^4F_{3/2} \rightarrow {}^4I_{11/2}$ transition at 1.06 μm is close to $A_J = 2787 \text{ s}^{-1}$.

3.3. Near-IR luminescence spectra and their decays

Figure 2 presents near-IR luminescence spectra of Nd^{3+} ions in titanate-germanate glasses. Luminescence bands at 0.89 μm , 1.06 μm and 1.33 μm correspond to ${}^4F_{3/2} \rightarrow {}^4I_{9/2}$, ${}^4F_{3/2} \rightarrow {}^4I_{11/2}$ and to ${}^4F_{3/2} \rightarrow {}^4I_{13/2}$ transitions of Nd^{3+} . They are schematized on energy level diagram (Fig. 3).

Spectroscopic studies indicate that the intensities of luminescence bands of Nd^{3+} ions are enhanced with increasing TiO_2 concentration in glass composition. The most intense near-IR

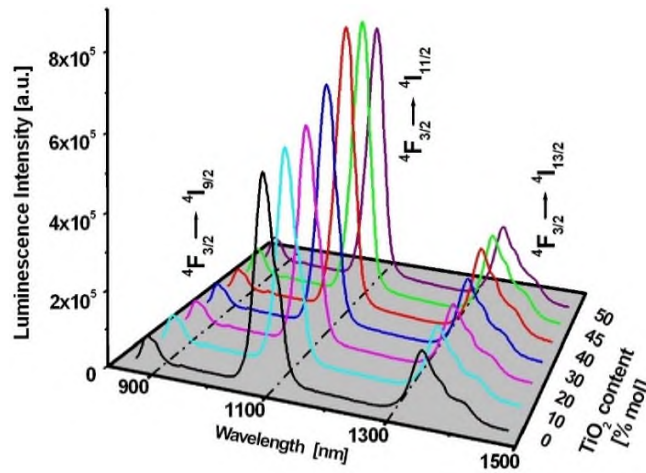


Fig. 2. Near-IR luminescence spectra of Nd³⁺ ions in titanate-germanate glasses.

emission band located near 1.06 μm is related to the main ${}^4F_{3/2} \rightarrow {}^4I_{11/2}$ laser transition of Nd³⁺. It was examined in details in function of TiO₂ concentration. Figure 4 presents near-IR emission band at about 1.06 μm varying with TiO₂ content. Some spectroscopic parameters such as the emission peak wavelength and the emission bandwidth for the ${}^4F_{3/2} \rightarrow {}^4I_{11/2}$ transition of Nd³⁺ are also schematized. It is clearly seen that the ${}^4F_{3/2} \rightarrow {}^4I_{11/2}$ transition of Nd³⁺ ions is shifted to longer wavelengths with increasing TiO₂ content. The near-IR emission band is shifted from 1064 nm (glass without TiO₂) to 1070 nm (glass sample with molar ratio GeO₂:TiO₂ = 1:5), respectively. The luminescence bandwidth referred as full width at half maximum (FWHM) is nearly independent on TiO₂ concentration and its value is close to 41.5 ± 1 nm.

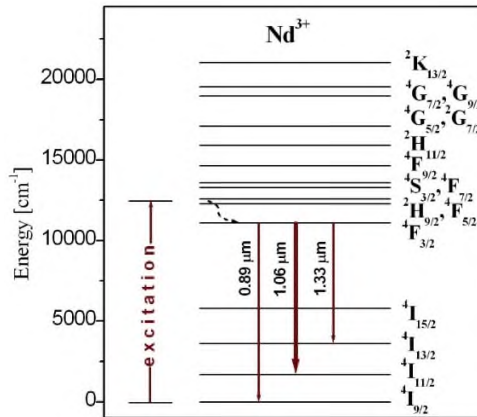


Fig. 3. Energy level diagram for Nd³⁺ ions. Near-IR emission transitions of Nd³⁺ are indicated.

The luminescence bandwidth and the radiative transition probability A_J calculated for the ${}^4F_{3/2} \rightarrow {}^4I_{11/2}$ transition of Nd³⁺ (Tables 5 and 6) were applied to obtain the peak stimulated

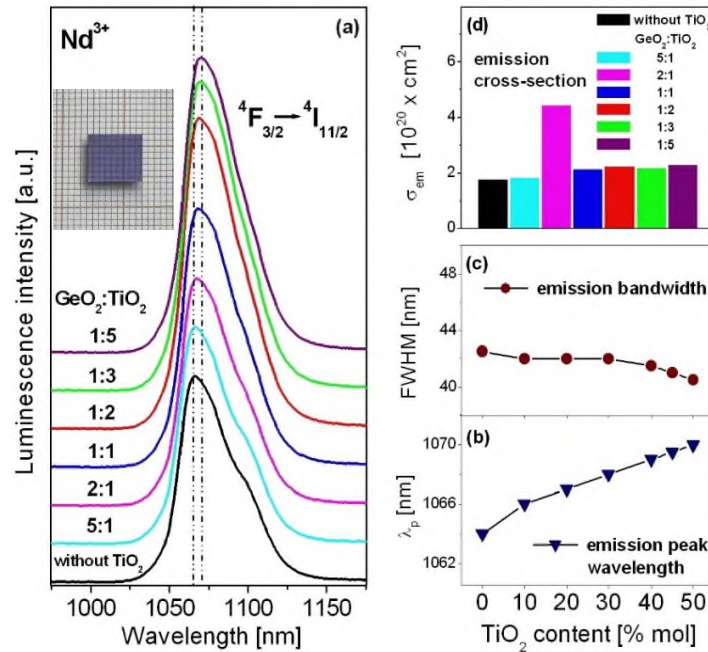


Fig. 4. Near-IR luminescence bands due to ${}^4F_{3/2} \rightarrow {}^4I_{11/2}$ laser transition of Nd^{3+} ions in titanate-germanate glass (a), emission peak wavelength (b), emission bandwidth FWHM (c) and stimulated emission cross-section (d) in function of TiO_2 content.

emission cross-section σ_{em} using the following relation (6):

$$\sigma_{em} = \frac{\lambda_p^4}{8\pi c n^2 \Delta\lambda} A_J \quad (6)$$

where λ_p is the emission peak wavelength, $\Delta\lambda$ is the luminescence bandwidth (FWHM), n is the refractive index and c is the velocity of light.

Table 5. The calculated radiative transition probabilities A_J and luminescence branching ratios β for Nd^{3+} ions in germanate glass without TiO_2 and titanate-germanate glasses (0, 10, 20 and 30% TiO_2).

Transition	Average wavelength [nm]	0% TiO_2		10% TiO_2		20% TiO_2		30% TiO_2	
		A_J [s^{-1}]	β [%]	A_J [s^{-1}]	β [%]	A_J [s^{-1}]	β [%]	A_J [s^{-1}]	β [%]
${}^4F_{32} \rightarrow {}^4I_{9/2}$	890	1127	40	1063	38	2353	41	1480	40
${}^4F_{32} \rightarrow {}^4I_{11/2}$	1060	1317	46	1419	51	2787	49	1823	49.5
${}^4F_{32} \rightarrow {}^4I_{13/2}$	1330	370	13	293	10.5	552	9.5	369	10
${}^4F_{32} \rightarrow {}^4I_{15/2}$	1870	27	1	14	0.5	28	0.5	18	0.5

The peak stimulated emission cross-section σ_{em} belongs to the important spectroscopic parameters, which designate the potential laser performance of the glass-host. The emission cross-section for the ${}^4F_{3/2} \rightarrow {}^4I_{11/2}$ transition of Nd^{3+} is relatively large for glass with molar ratio $GeO_2:TiO_2 = 2:1$ ($\sigma_{em} = 4.41 \times 10^{-20} cm^2$) compared to the other values, which were calculated for the studied glass samples (Fig. 4). Details are also given in Table 7.

In the next step, luminescence decay curves for the upper ${}^4F_{3/2}$ laser state of Nd^{3+} ions were measured and analyzed in function of TiO_2 concentration. Decay curves were quite well fitted to

Table 6. The calculated radiative transition probabilities A_J and luminescence branching ratios β for Nd^{3+} ions in titanate-germanate glasses (40, 45 and 50% TiO_2).

Transition	Average wavelength [nm]	40% TiO_2		45% TiO_2		50% TiO_2	
		A_J [s^{-1}]	β [%]	A_J [s^{-1}]	β [%]	A_J [s^{-1}]	β [%]
${}^4\text{F}_{3/2} \rightarrow {}^4\text{I}_{9/2}$	890	1526	38.5	1384	36.5	1620	38.5
${}^4\text{F}_{3/2} \rightarrow {}^4\text{I}_{11/2}$	1060	1989	50.5	1984	52	2105	50.5
${}^4\text{F}_{3/2} \rightarrow {}^4\text{I}_{13/2}$	1330	412	10.5	425	11	435	10.5
${}^4\text{F}_{3/2} \rightarrow {}^4\text{I}_{15/2}$	1870	19	0.5	20	0.5	20	0.5

Table 7. The emission peak wavelength λ_p , the luminescence bandwidth FWHM, the radiative transition probability A_J for the ${}^4\text{F}_{3/2} \rightarrow {}^4\text{I}_{11/2}$ transition of Nd^{3+} , the stimulated emission cross-section σ_{em} and gain bandwidth $\sigma_{\text{em}} \times \text{FWHM}$ varying with TiO_2 concentration.

TiO_2 content [% mol]	$\text{GeO}_2 : \text{TiO}_2$	λ_p [nm]	FWHM [nm]	A_J [s^{-1}]	σ_{em} [$10^{-20} \times \text{cm}^2$]	$\sigma_{\text{em}} \times \text{FWHM}$ [$10^{-25} \times \text{cm}^3$]
0	-	1064	42.5	1317	1.75	0.74
10	5 : 1	1066	42	1419	1.81	0.76
20	2 : 1	1067	42	2787	4.41	1.85
30	1 : 1	1068	42	1823	2.13	0.90
40	1 : 2	1069	41.5	1989	2.23	0.93
45	1 : 3	1069	41	1984	2.16	0.89
50	1 : 5	1070	40.5	2105	2.29	0.92

nearly single-exponential function given below (7):

$$I(t) = I_0 e^{-\frac{t}{\tau_m}} \quad (7)$$

where I_0 is the intensity at time $t = 0$ and τ_m is a luminescence lifetime.

Figure 5 shows luminescence decays from the ${}^4\text{F}_{3/2}$ state of Nd^{3+} ions in multicomponent titanate-germanate glasses. Luminescence lifetimes and quantum efficiencies varying with TiO_2 content are also schematized. Luminescence decay curve analysis suggests that the ${}^4\text{F}_{3/2}$ lifetimes of Nd^{3+} ions depend slightly on TiO_2 concentration. Their values are shorter compared to glass sample without TiO_2 .

The radiative lifetime τ_{rad} calculated from the Judd-Ofelt theory using Eq. (4) and the measured lifetime τ_m were applied to obtain the quantum efficiency for the ${}^4\text{F}_{3/2} \rightarrow {}^4\text{I}_{11/2}$ laser transition of Nd^{3+} ions using the following expression (8):

$$\eta = \frac{\tau_m}{\tau_{\text{rad}}} \times 100\% \quad (8)$$

Among the studied samples, the quantum efficiency for the ${}^4\text{F}_{3/2} \rightarrow {}^4\text{I}_{11/2}$ transition of Nd^{3+} ions is the highest for glass with $\text{GeO}_2:\text{TiO}_2 = 2:1$ (Fig. 5) and its value is close to $\eta = 88\%$. Details are also given in Table 8.

Based on measurements of luminescence spectra and their decays it can be concluded that glass with molar ratio $\text{GeO}_2:\text{TiO}_2$ equal to 2:1 has the highest stimulated emission cross-section ($\sigma_{\text{em}} = 4.41 \times 10^{-20} \text{cm}^2$) and quantum efficiency ($\eta = 88\%$) for the ${}^4\text{F}_{3/2} \rightarrow {}^4\text{I}_{11/2}$ laser transition of Nd^{3+} ions. It suggests that titanate-germanate glass ($\text{GeO}_2:\text{TiO}_2 = 2:1$) with 1 mol% Nd^{3+} can be successfully used for near-IR laser applications. At this moment, it should be also mentioned that nominal activator concentration is in a good agreement with the actual neodymium content, which was determined from the chemical analysis (Table S3). In particular, the stimulated emission cross-section for the ${}^4\text{F}_{3/2} \rightarrow {}^4\text{I}_{11/2}$ transition of Nd^{3+} in glass with $\text{GeO}_2:\text{TiO}_2 = 2:1$ is comparable with the values σ_{em} ranging between 4 and 4.75 (in 10^{-20}cm^2) obtained for similar inorganic laser glasses [72–80].

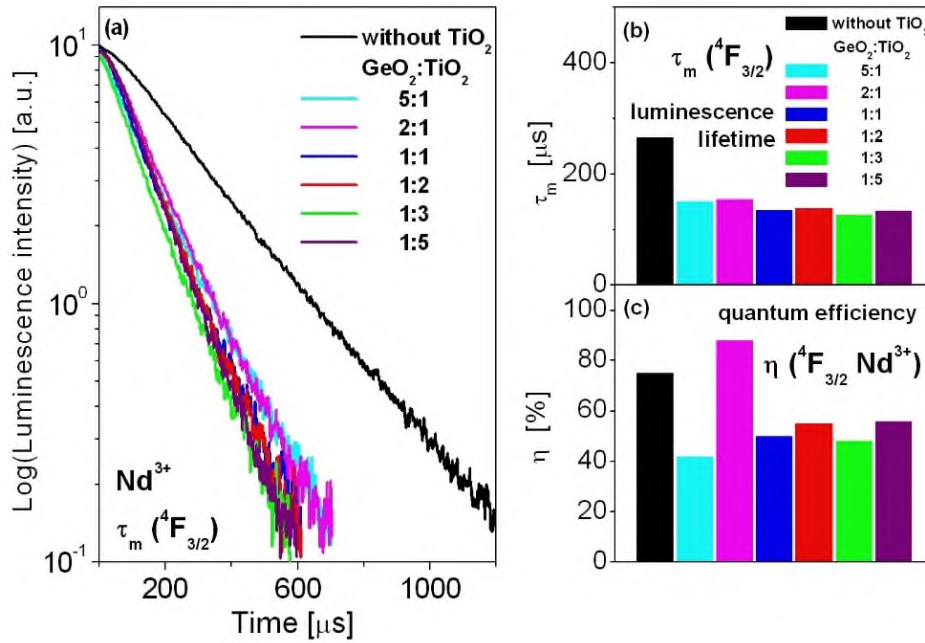


Fig. 5. Luminescence decays from the upper ${}^4F_{3/2}$ laser state of Nd^{3+} ions in multicomponent titanate-germanate glasses (a), measured luminescence lifetime (b) and quantum efficiency (c) in function of TiO_2 content.

Table 8. The calculated radiative lifetime τ_{rad} , the measured lifetime τ_m , the quantum efficiency η , the stimulated emission cross-section σ_{em} and figure of merit $\sigma_{\text{em}} \times \tau_m$ varying with TiO_2 concentration.

TiO ₂ content [% mol]	GeO ₂ : TiO ₂	τ_{rad} [μs]	τ_m [μs]	η [%]	σ_{em} [$10^{-20} \times \text{cm}^2$]	$\sigma_{\text{em}} \times \tau_m$ [$10^{-23} \times \text{cm}^2 \text{s}$]
0	-	352	265	75	1.75	46.37
10	5 : 1	359	151	42	1.81	27.33
20	2 : 1	175	154	88	4.41	67.91
30	1 : 1	271	135	50	2.13	28.75
40	1 : 2	253	139	55	2.23	31.00
45	1 : 3	262	126	48	2.16	27.22
50	1 : 5	239	134	56	2.29	30.69

Finally, the stimulated emission cross-section (σ_{em}), the luminescence bandwidth (FWHM) and the measured lifetime τ_m for the ${}^4F_{3/2} \rightarrow {}^4I_{11/2}$ transition of Nd^{3+} were applied to calculate the laser parameters: gain bandwidth ($\sigma_{em} \times FWHM$) and figure of merit FOM ($\sigma_{em} \times \tau_m$). These laser parameters varying with TiO_2 concentration are presented in Tables 7 and 8, respectively.

From literature data [72–81] it is well-known that the gain bandwidth and the figure of merit are really important to identify the laser glass-host and near-IR broadband amplification. The gain bandwidth is defined as the range of frequencies into which the optical amplification can occur, whereas the laser threshold is evaluated by the figure of merit FOM [82]. In general, high gain medium with low threshold pump power is required. Both parameters $\sigma_{em} \times FWHM$ and $\sigma_{em} \times \tau_m$ exhibiting relatively high values for the ${}^4F_{3/2} \rightarrow {}^4I_{11/2}$ near-IR transition of Nd^{3+} are necessary to generate laser action in inorganic glasses.

Previously published works for Nd^{3+} ions in glass systems containing lead give interesting results [77–79]. For lead tungsten tellurite glass [77] the gain bandwidth is extremely high, but the figure of merit is found to be smaller. The opposite situation is observed for lead phosphate glass [78], where value of $\sigma_{em} \times FWHM$ is found to be rather smaller, but product of $\sigma_{em} \times \tau_m$ known as the figure of merit is relatively higher. For lead fluorosilicate glass [79], both values are large compared with other reported glasses. It clearly suggests that both laser parameters depend significantly on glass composition.

Our near-IR luminescence investigations clearly demonstrate that the highest values of gain bandwidth ($\sigma_{em} \times FWHM = 1.85 \times 10^{-25} \text{ cm}^3$) and figure of merit ($\sigma_{em} \times \tau_m = 67.91 \times 10^{-25} \text{ cm}^2 \text{ s}$) were obtained for Nd^{3+} ions in multicomponent glass with molar ratio $GeO_2:TiO_2 = 2:1$. They are compared to some Nd^{3+} -doped laser glasses published previously [72–81]. The results are summarized in Table 9.

Table 9. Comparison of the stimulated emission cross-section (σ_{em}), gain bandwidth ($\sigma_{em} \times FWHM$) and figure of merit ($\sigma_{em} \times \tau_m$) in different laser glasses doped with Nd^{3+} .

Glass-host	σ_{em} [$10^{-20} \times \text{cm}^2$]	$\sigma_{em} \times FWHM$ [$10^{-25} \times \text{cm}^3$]	$\sigma_{em} \times \tau_m$ [$10^{-25} \times \text{cm}^2 \text{ s}$]	Ref.
$GeO_2:TiO_2 = 2:1$	4.41	1.85	67.91	this work
$Nb_2O_5-K_2O-ZnF_2-LiF-SiO_2$	4.30	1.63	58.05	[72]
$Al(PO_3)_3-RF_2-NaF$ (R = Mg, Ca, Sr, Ba)	4.51	1.29	-	[73]
	4.05	1.13	-	[74]
$P_2O_5-K_2O-SrO-Al_2O_3$	4.20	1.01	66.36	[75]
TeO_2-ZnO	4.18	0.75	63.11	[76]
$B_2O_3-Na_2O-NaF$	4.75	1.98	39.42	[77]
$PbF_2-WO_3-TeO_2$	4.38	0.96	75.34	[78]
$PbO-P_2O_5$	4.11	1.49	98.64	[79]
$PbF_2-SiO_2-K_2O-Na_2O-LiF$	4.41	1.27	86.24	[80]
$P_2O_5-K_2O-MgO-Al_2O_3$	3.69	0.99	88.56	[17]
$P_2O_5-Ng_2O_5-K_2O-Al_2O_3$	3.42	-	81.05	[81]
$P_2O_5-K_2O-CaO-Al_2O_3-CaF_2$				

In our case, the gain bandwidth for the ${}^4F_{3/2} \rightarrow {}^4I_{11/2}$ near-IR transition of Nd^{3+} ions in glass with $GeO_2:TiO_2 = 2:1$ is found to be larger than for other lead-free glasses reported in Table 9. However, the figure of merit (FOM) is smaller compared to oxide and oxyfluoride phosphate based glasses [80–81]. The product $\sigma_{em} \times \tau_m$ for our sample ($GeO_2:TiO_2 = 2:1$) is similar to the values obtained for glasses based on $ZnO-TeO_2$ [75] and $B_2O_3-Na_2O-NaF$ [76], respectively. It can be concluded that both parameters $\sigma_{em} \times FWHM$ and $\sigma_{em} \times \tau_m$ for the ${}^4F_{3/2} \rightarrow {}^4I_{11/2}$ transition of Nd^{3+} are promising and glass ($GeO_2:TiO_2 = 2:1$) could be potentially useful for lasing action compared along with reported laser glasses. Therefore, Nd^{3+} -doped titanate-germanate glass with $GeO_2:TiO_2 = 2:1$ is suitable for near-IR laser gain active media operating at 1.06 μm .

4. Conclusions

In this work, Nd³⁺ doped titanate-germanate glasses have been examined for near-IR laser applications. Multicomponent glasses with different molar ratios GeO₂:TiO₂ were prepared and then studied experimentally using photoluminescence spectroscopy. Theoretical calculations were also obtained using the Judd-Ofelt framework.

Based on absorption and luminescence spectra, and decay curve measurements, several spectroscopic and laser parameters for Nd³⁺ ions in glass varying with TiO₂ concentration were determined. Systematic investigations indicate that Nd³⁺ doped glass with GeO₂:TiO₂ = 2:1 presents strong near-IR luminescence at 1.06 μm corresponding to the ⁴F_{3/2} → ⁴I_{11/2} transition. The spectroscopic and laser parameters for the main ⁴F_{3/2} → ⁴I_{11/2} transition of Nd³⁺ ions are as follows: the stimulated emission cross-section $\sigma_{em} = 4.41 \times 10^{-20} \text{cm}^2$, the measured lifetime $\tau_m = 154 \mu\text{s}$, the quantum efficiency $\eta = 88\%$, the gain bandwidth $\sigma_{em} \times \text{FWHM} = 1.85 \times 10^{-25} \text{cm}^3$ and figure of merit known as $\sigma_{em} \times \tau_m \text{ product} = 67.91 \times 10^{-25} \text{cm}^2\text{s}$, respectively. They are attractive compared with some reported glass systems and commercially-available laser glasses documented in literature. Therefore, we suggest that Nd³⁺-doped titanate-germanate glass with molar ratio GeO₂:TiO₂ equal to 2:1 is suitable for near-IR luminescence at 1.06 μm and could be useful for solid-state laser applications.

Funding. Narodowe Centrum Nauki (2018/31/B/ST8/00166).

Disclosures. The Authors declare no conflict of interest.

Data availability. Data underlying the results presented in this paper are not publicly available at this time but may be obtained from the authors upon reasonable request.

Supplemental document. See [Supplement 1](#) for supporting content.

References

1. E. Snitzer, "Optical maser action of Nd³⁺ in a barium crown glass," *Phys. Rev. Lett.* **7**(12), 444–446 (1961).
2. R. Jacobs and M. Weber, "Dependence of the ⁴F_{3/2} → ⁴I_{11/2} induced-emission cross section for Nd³⁺ on glass composition," *IEEE J. Quant. Soc. Electron.* **12**(2), 102–111 (1976).
3. R. Balda, J. Fernandez, M. Sanz, A. de Pablos, J. M. Fdez-Navarro, and J. Mugnier, "Laser spectroscopy of Nd³⁺ ions in GeO₂-PbO-Bi₂O₃ glasses," *Phys. Rev. B* **61**(5), 3384–3390 (2000).
4. L. R. P. Kassab, S. H. Tatum, C. M. S. Mendes, L. C. Courrol, and N. U. Wetter, "Optical properties of Nd doped Bi₂O₃-PbO-Ga₂O₃ glasses," *Opt. Express* **6**(4), 104–108 (2000).
5. R. Balda, J. Fernandez, I. Iparraguirre, J. Azkargorta, S. Garcia-Revilla, J. I. Pena, R. I. Merino, and V. M. Orera, "Broadband laser tunability of Nd³⁺ ions in 0.8CaSiO₃-0.2Ca₃(PO₄)₂ eutectic glass," *Opt. Express* **17**(6), 4382–4387 (2009).
6. G. Tang, D. Yang, W. Huang, L. Kuang, W. Lin, Y. Zhang, F. Zhang, Z. Nie, D. Chen, Q. Qian, and Z. Yang, "Nd³⁺ doped multi-component phosphate glass multi-material fiber for a 1.05 μm laser," *Opt. Mater. Express* **11**, 1385–1391 (2021).
7. B. Karthikeyan and S. Mohan, "Spectroscopic and glass transition investigations on Nd³⁺ doped NaF-Na₂O-B₂O₃ glasses," *Mater. Res. Bull.* **39**(10), 1507–1515 (2004).
8. J. Pisarska, W. Ryba-Romanowski, G. Dominiak-Dzik, T. Goryczka, and W. A. Pisarski, "Nd-doped oxyfluoroborate glasses and glass-ceramics for NIR laser applications," *J. Alloys Compd.* **451**(1-2), 223–225 (2008).
9. C. N. Santos, D. Mohr, W. F. Silva, A. S. S. de Camargo, H. Eckert, M. S. Li, M. V. D. Vermelho, A. C. Hernandez, A. Ibanez, and C. Jacinto, "Luminescent and thermo-optical properties of Nd³⁺-doped yttrium aluminoborate laser glasses," *J. Appl. Phys.* **106**(2), 023512 (2009).
10. C. M. Reddy, N. Vijaya, and B. D. P. Raju, "NIR fluorescence studies of neodymium ions doped sodium fluoroborate glasses for 1.06 μm laser applications," *Spectrochim. Acta, Part A* **115**, 297–304 (2013).
11. C.R. Kesavulu, H.J. Kim, S.W. Lee, J. Kaewkhao, N. Wantana, E. Kaewnuam, S. Kothan, and S. Kaewjaeng, "Spectroscopic investigations of Nd³⁺ doped gadolinium calcium silica borate glasses for the NIR emission at 1059 nm," *J. Alloys Compd.* **695**, 590–598 (2017).
12. N. Deopa, A. S. Rao, M. Gupta, and G. V. Prakash, "Spectroscopic investigations of Nd³⁺ doped lithium lead alumino borate glasses for 1.06 μm laser applications," *Opt. Mater.* **75**, 127–134 (2018).
13. J. T. James, J. K. Jose, M. Manjunatha, K. Suresh, and A. Madhu, "Structural, luminescence and NMR studies on Nd³⁺-doped sodium-calciumborate glasses for lasing applications," *Ceram. Int.* **46**(17), 27099–27109 (2020).
14. D. Sontakke, K. Biswas, A. K. Mandal, and K. Annapurna, "Concentration quenched luminescence and energy transfer analysis of Nd³⁺ ion doped Ba-Al-metaphosphate laser glasses," *Appl. Phys. B* **101**(1-2), 235–244 (2010).

15. I. Iparraguirre, J. Azkargorta, R. Balda, K. V. Krishnaiah, C. K. Jayasankar, M. Al-Saleh, and J. Fernández, "Spontaneous and stimulated emission spectroscopy of a Nd³⁺-doped phosphate glass under wavelength selective pumping," *Opt. Express* **19**, 19440–19453 (2011).
16. A. L. F. Novais, N. O. Dantas, I. Guedes, and M. V. D. Vermelho, "Spectroscopic properties of highly Nd-doped lead phosphate glass," *J. Alloys Compd.* **648**, 338–345 (2015).
17. P. Manasa, T. Srihari, Ch. Basavapoornima, A. S. Joshi, and C.K. Jayasankar, "Spectroscopic investigations of Nd³⁺ ions in niobium phosphate glasses for laser applications," *J. Lumin.* **211**, 233–242 (2019).
18. M. M. Ismail, I. K. Batisha, L. Zur, A. Chiasera, M. Ferrari, and A. Lukowiak, "Optical properties of Nd³⁺-doped phosphate glasses," *Opt. Mater.* **99**, 109591 (2020).
19. M. Muñoz-Quinero, J. Azkargorta, I. Iparraguirre, R. J. Jiménez-Riobóo, G. Tricot, C. Shao, F. Muñoz, J. Fernández, and R. Balda, "Dehydroxylation processing and lasing properties of a Nd alumino-phosphate glass," *J. Alloys Compd.* **896**, 163040 (2022).
20. M. Kumar and Y. C. Ratnakaram, "Role of TeO₂ coordination with the BaF₂ and Bi₂O₃ on structural and emission properties in Nd³⁺ doped fluoro phosphate glasses for NIR 1.058 μm laser emission," *Opt. Mater.* **112**, 110738 (2021).
21. K. Hauptmanová, J. Pantoflíček, and K. Pátek, "Absorption and fluorescence of Nd³⁺ ion in silicate glass," *Phys. Status Solidi B* **9**(2), 525–537 (1965).
22. K. Zou, H. Guo, M. Lu, W. Li, C. Hou, W. Wei, J. He, B. Peng, and B. Xiangli, "Broad-spectrum and long-lifetime emissions of Nd³⁺ ions in lead fluorosilicate glass," *Opt. Express* **17**(12), 10001–10009 (2009).
23. I. Pal, A. Agarwal, S. Sanghi, M. P. Aggarwal, and S. Bhardwaj, "Fluorescence and radiative properties of Nd³⁺ ions doped zinc bismuth silicate glasses," *J. Alloys Compd.* **587**, 332–338 (2014).
24. C. Hirayama, F. E. Camp, N. T. Melamed, and K. B. Steinbruegge, "Nd³⁺ in germanate glasses: spectral and laser properties," *J. Non-Cryst. Solids* **6**(4), 342–356 (1971).
25. B. J. Chen, L. F. Shen, E. Y. B. Pun, and H. Lin, "Nd³⁺-doped ion-exchanged aluminum germanate glass channel waveguide," *Opt. Mater. Express* **5**(1), 113–123 (2015).
26. T. Wei, Y. Tian, C. Tian, X. Jing, M. Cai, J. Zhang, L. Zhang, and S. Xu, "Comprehensive evaluation of the structural, absorption, energy transfer, luminescent properties and near-infrared applications of the neodymium doped germanate glass," *J. Alloys Compd.* **618**, 95–101 (2015).
27. L. R. P. Kassab, D. M. Silva, J. A. M. Garcia, D. S. da Silva, and C. B. de Araújo, "Silver nanoparticles enhanced photoluminescence of Nd³⁺ doped germanate glasses at 1064 nm," *Opt. Mater.* **60**, 25–29 (2016).
28. C. D. S. Bordon, E. S. Magalhaes, D. M. da Silva, L. R. P. Kassab, and C. B. de Araújo, "Influence of Al₂O₃ on the photoluminescence and optical gain performance of Nd³⁺ doped germanate and tellurite glasses," *Opt. Mater.* **109**, 110342 (2020).
29. M. J. Weber, J. D. Myers, and D. H. Blackburn, "Optical properties of Nd³⁺ in tellurite and phosphotellurite glasses," *J. Appl. Phys.* **52**(4), 2944–2949 (1981).
30. K. Upendra Kumar, V.A. Prathyusha, P. Babu, C.K. Jayasankar, A.S. Joshi, A. Speghini, and M. Bettinelli, "Fluorescence properties of Nd³⁺-doped tellurite glasses," *Spectrochim. Acta, Part A* **67**(3-4), 702–708 (2007).
31. R. Rajeswari, S. Surendra Babu, and C. K. Jayasankar, "Spectroscopic characterization of alkali modified zinc-tellurite glasses doped with neodymium," *Spectrochim. Acta, Part A* **77**(1), 135–140 (2010).
32. S. Surendra Babu, R. Rajeswari, K. Jang, C. E. Jin, K. H. Jang, H. J. Seo, and C. K. Jayasankar, "Spectroscopic investigations of 1.06 μm emission in Nd³⁺-doped alkali niobium zinc tellurite glasses," *J. Lumin.* **130**(6), 1021–1025 (2010).
33. A. Miguel, J. Azkargorta, R. Morea, I. Iparraguirre, J. Gonzalo, J. Fernandez, and R. Balda, "Spectral study of the stimulated emission of Nd³⁺ in fluorotellurite bulk glass," *Opt. Express* **21**(8), 9298–9307 (2013).
34. K. Linganna, R. Narro-García, H. Desirena, E. De la Rosa, Ch. Basavapoornima, V. Venkatramu, and C. K. Jayasankar, "Effect of P₂O₅ addition on structural and luminescence properties of Nd³⁺-doped tellurite glasses," *J. Alloys Compd.* **684**, 322–327 (2016).
35. E. A. Lalla, U. R. Rodríguez-Mendoza, A. D. Lozano-Gorrín, A. Sanz-Arranz, F. Rull, and V. Lavín, "Nd³⁺-doped TeO₂-PbF₂-AlF₃ glasses for laser applications," *Opt. Mater.* **51**, 35–41 (2016).
36. J. Azevedo, J. Coelho, G. Hungerford, and N. S. Hussain, "Lasing transition (4F_{3/2} → 4I_{11/2}) at 1.06 μm in neodymium oxide doped lithium borotellurite glass," *Phys. B (Amsterdam, Neth.)* **405**(22), 4696–4701 (2010).
37. A. Madhu, B. Eraiah, P. Manasa, and N. Srinatha, "Nd³⁺-doped lanthanum lead boro-tellurite glass for lasing and amplification applications," *Opt. Mater.* **75**, 357–366 (2018).
38. K. S. R. K. Reddy, K. Swapna, Sk. Mahamuda, M. Venkateswarulu, and A. S. Rao, "Structural, optical and photoluminescence properties of alkaline-earth boro tellurite glasses doped with trivalent neodymium for 1.06 μm optoelectronic devices," *Opt. Mater.* **111**, 110615 (2021).
39. S. S. Kumar, J. Khatei, S. Kasthuriengan, K. S. R. K. Rao, and K. P. Ramesh, "Optical absorption and photoluminescence studies of Nd³⁺ doped alkali borogermanate glasses," *J. Non-Cryst. Solids* **357**(3), 842–846 (2011).
40. Y. Chen, Y. Huang, M. Huang, R. Chen, Z. Luo, and M. Huang, "Effect of Nd³⁺ on the spectroscopic properties of bismuth borate glasses," *J. Am. Ceram. Soc.* **88**(1), 19–23 (2005).
41. I. D. Sontakke and K. Annapurna, "Spectroscopic properties and concentration effects on luminescence behavior of Nd³⁺ doped zinc-boro-bismuthate glasses," *Mater. Chem. Phys.* **137**(3), 916–921 (2013).

42. G. Gupta, A. D. Sontakke, P. Karmakar, K. Biswas, S. Balaji, R. Saha, R. Sen, and K. Annapurna, "Influence of bismuth on structural, elastic and spectroscopic properties of Nd³⁺ doped zinc-boro-bismuthate glasses," *J. Lumin.* **149**, 163–169 (2014).
43. J. Azkargorta, I. Iparraguirre, R. Balda, J. Fernandez, E. Denoue, and J. L. Adam, "Spectroscopic and laser properties of Nd³⁺ in BiGaZLuTMn fluoride glasses," *IEEE J. Quant. Electron.* **30**(8), 1862–1867 (1994).
44. S. M. Lima, J. A. Sampaio, T. Catunda, A. S. S. de Camargo, L. A. O. Nunes, M. L. Basso, and D. W. Hewak, "Spectroscopy, thermal and optical properties of Nd³⁺-doped chalcogenide glasses," *J. Non-Cryst. Solids* **284**(1-3), 274–281 (2001).
45. T. Suzuki, H. Kawai, H. Nasu, S. Mizuno, H. Ito, K. Hasegawa, and Y. Ohishi, "Spectroscopic investigation of Nd³⁺-doped ZBLAN glass for solar-pumped lasers," *J. Opt. Soc. Am. B* **28**(8), 2001–2006 (2011).
46. J. Azkargorta, I. Iparraguirre, R. Balda, and J. Fernández, "On the origin of bichromatic laser emission in Nd³⁺-doped fluoride glasses," *Opt. Express* **16**(16), 11894–11906 (2008).
47. S. S. Bayya, G. D. Chin, J. S. Sanghera, and I. D. Aggarwal, "Germanate glass as a window for high energy laser systems," *Opt. Express* **14**(24), 11687–11693 (2006).
48. T. Guerneau, C. Strutyński, T. Skopak, S. Morency, A. Hanafi, F. Calvazara, Y. Ledemi, S. Danto, T. Cardinal, Y. Messaddeq, and E. Fargini, "Extended germano-gallate fiber drawing domain: from germanates to gallates optical fibers," *Opt. Mater. Express* **9**(6), 2437–2445 (2019).
49. M. Kochanowicz, J. Zmojda, P. Miluski, A. Baranowska, M. Leich, A. Schwuchow, M. Jäger, M. Kuwik, J. Pisarska, W. A. Pisarski, and D. Dorosz, "Tm³⁺/Ho³⁺ co-doped germanate glass and double-clad optical fiber for broadband emission and lasing above 2 μm," *Opt. Mater. Express* **9**(3), 1450–1458 (2019).
50. X. Wen, G. Tang, J. Wang, X. Chen, Q. Qian, and Z. Yang, "Tm³⁺ doped barium gallo-germanate glass single-mode fibers for 2.0 μm laser," *Opt. Express* **23**(6), 7722–7731 (2015).
51. J. Pisarska, M. Kowal, M. Kochanowicz, J. Zmojda, J. Dorosz, D. Dorosz, and W. A. Pisarski, "Influence of BaF₂ and activator concentration on broadband near-infrared luminescence of Pr³⁺ ions in gallo-germanate glasses," *Opt. Express* **24**(3), 2427–2435 (2016).
52. W. A. Pisarski, K. Kowalska, M. Kuwik, J. Polak, E. Pietrasik, T. Goryczka, and J. Pisarska, "Novel multicomponent titanate-germanate glasses: Synthesis, structure, properties, transition metal, and rare earth doping," *Materials* **13**(19), 4422 (2020).
53. I. Herrera, F. Londono, and N. M. Balzaretta, "Structural and optical properties of Nd³⁺ doped GeO₂-PbO glass modified by TiO₂ for applications in laser and fiber amplifier," *Opt. Mater.* **113**, 110884 (2021).
54. R. Balda, J. Fernandez, M. A. Arriandiaga, and J. M. Fernandez-Navarro, "Spectroscopy and frequency upconversion in Nd³⁺-doped TeO₂-TiO₂-Nb₂O₅ glass," *J. Phys.: Condens. Matter* **19**(8), 086223 (2007).
55. H. Fares, I. Jlassi, S. Hraiech, H. Elhouichet, and M. Férid, "Radiative parameters of Nd³⁺-doped titanium and tungsten modified tellurite glasses for 1.06 μm laser materials," *J. Quant. Spectrosc. Radiat. Transfer* **147**, 224–232 (2014).
56. J. de Clermont-Gallerande, S. Saito, T. Hayakawa, M. Colas, J.-R. Duclère, and P. Thomas, "Optical properties of Nd³⁺-doped TeO₂-TiO₂-ZnO glasses with lower hydroxyl content," *J. Non-Cryst. Solids* **528**, 119678 (2020).
57. B. C. Jamalajah, T. Suhasini, L. R. Moorthy, I.-G. Kim, D.-S. Yoo, and K. Jang, "Structural and luminescence properties of Nd³⁺-doped PbO-B₂O₃-TiO₂-AlF₃ glass for 1.07 μm laser applications," *J. Lumin.* **132**(5), 1144–1149 (2012).
58. J. Chen and C. Wei, "Formation and structure of titanate glasses," *J. Non-Cryst. Solids* **80**(1-3), 135–140 (1986).
59. T. Fukushima, Y. Benino, T. Fujiwara, V. Dimitrov, and T. Komatsu, "Electronic polarizability and crystallization of K₂O-TiO₂-GeO₂ glasses with high TiO₂ contents," *J. Solid State Chem.* **179**(12), 3949–3957 (2006).
60. H. Masai, T. Fujiwara, Y. Benino, and T. Komatsu, "Large second-order optical nonlinearity in 30BaO-15TiO₂-55GeO₂ surface crystallized glass with strong orientation," *J. Appl. Phys.* **100**(2), 023526 (2006).
61. J. Pisarska, M. Kuwik, A. Górny, M. Kochanowicz, J. Zmojda, J. Dorosz, D. Dorosz, M. Sitarz, and W. A. Pisarski, "Holmium doped barium gallo-germanate glasses for near-infrared at 2000nm," *J. Lumin.* **215**, 116625 (2019).
62. K. Han, P. Zhang, S. Wang, Y. Guo, D. Zhou, and F. Yu, "Optical characterization of Tm³⁺ doped Bi₂O₃-GeO₂-Ga₂O₃ glasses in absence and presence of BaF₂," *Sci. Rep.* **6**(1), 31207 (2016).
63. X. Wen, G. Tang, Q. Yang, X. Chen, Q. Qian, Q. Zhang, and Z. Yang, "Highly Tm³⁺ germanate glass and its single mode fiber for 2.0 μm laser," *Sci. Rep.* **6**(1), 20344 (2016).
64. L. H. C. Andrade, S. M. Lima, A. Novatski, A. M. Neto, A. C. Bento, M. L. Baesso, F. C. G. Gandra, Y. Guyot, and G. Boulon, "Spectroscopic assignments of Ti³⁺ and Ti⁴⁺ in titanium-doped OH⁻ free low-silica calcium aluminosilicate glass and role of structural defects on the observed long lifetime and high fluorescence of Ti³⁺ ions," *Phys. Rev. B* **78**(22), 224202 (2008).
65. S. P. Sinha, *Complexes of the Rare Earth* (Pergamon Press, 1966).
66. W. T. Carnall, P. R. Fields, and K. Rajnak, "Electronic energy levels in the trivalent lanthanide aquo ions. I. Pr³⁺, Nd³⁺, Pm³⁺, Sm³⁺, Dy³⁺, Ho³⁺, Er³⁺, and Tm³⁺," *J. Chem. Phys.* **49**(10), 4424–4442 (1968).
67. J. Pisarska, W. A. Pisarski, G. Dominiak-Dzik, and W. Ryba-Romanowski, "Spectroscopic investigations of Nd³⁺ ions in B₂O₃-PbO-Al₂O₃-WO₃ glasses," *J. Mol. Struct.* **792-793**, 201–206 (2006).
68. B. R. Judd, "Optical absorption intensities of rare-earth ions," *Phys. Rev.* **127**(3), 750–761 (1962).
69. G. S. Ofelt, "Intensities of crystal spectra of rare-earth ions," *J. Chem. Phys.* **37**(3), 511–520 (1962).

70. P. Ramprasad, Ch. Basavapoornima, S.R. Depuru, and C.K. Jayasankar, "Spectral investigations of $\text{Nd}^{3+}:\text{Ba}(\text{PO}_3)_2 + \text{La}_2\text{O}_3$ glasses for infrared laser gain media applications," *Opt. Mater.* **129**, 112482 (2022).
71. T. Srikumar, M. G. Brik, Ch. S. Rao, Y. Gandhi, D. K. Rao, V. R. Kumar, and N. Veeraiyah, "Spectral and fluorescent kinetics features of Nd^{3+} ion in Nb_2O_5 , Ta_2O_5 and La_2O_3 mixed lithium zirconium silicate glasses," *Spectrochim. Acta, Part A* **81**(1), 498–503 (2011).
72. D. Ramachari, L. Rama Moorthy, and C.K. Jayasankar, "Optical absorption and emission properties of Nd^{3+} -doped oxyfluorosilicate glasses for solid state lasers," *Infrared Phys. Technol.* **67**, 555–559 (2014).
73. Y. Tian, J. Zhang, X. Jing, and S. Xu, "Optical absorption and near infrared emissions of Nd^{3+} doped fluorophosphate glass," *Spectrochim. Acta, Part A* **98**, 355–358 (2012).
74. K. U. Kumar, P. Babu, K. H. Jang, H. J. Seo, C. K. Jayasankar, and A. S. Joshi, "Spectroscopic and 1.06 μm laser properties of Nd^{3+} -doped K–Sr–Al phosphate and fluorophosphate glasses," *J. Alloys Compd.* **458**(1-2), 509–516 (2008).
75. L. M. Moreira, V. Anjos, M. J. V. Bell, C. A. R. Ramos, L. R. P. Kassab, D. J. L. Doualan, P. Camy, and R. Moncorge, "The effects of Nd_2O_3 concentration in the laser emission of TeO_2 -ZnO glasses," *Opt. Mater.* **58**, 84–88 (2016).
76. R. T. Karunakaran, K. Marimuthu, S. Arumugam, S. S. Babu, S. F. Leon-Luis, and C. K. Jayasankar, "Structural, optical absorption and luminescence properties of Nd^{3+} ions in NaO–NaF borate glasses," *Opt. Mater.* **32**(9), 1035–1041 (2010).
77. M. Venkateswarlu, Sk. Mahamuda, K. Swapna, M. V. V. K. S. Prasad, A. S. Rao, A. M. Babu, S. Shakya, and G. V. Prakash, "Spectroscopic studies of Nd^{3+} doped lead tungsten tellurite glasses for the NIR emission at 1062 nm," *Opt. Mater.* **39**, 8–15 (2015).
78. S. Jana and S. Mitra, "Compositional dependence of the luminescence properties of Nd^{3+} ions in lead phosphate glasses: The efficient laser active materials," *Opt. Laser Technol.* **141**, 107123 (2021).
79. P. Manasa, D. Ramachari, J. Kaewkhao, P. Meejitpaisan, E. Kaewnuam, A.S. Joshi, and C.K. Jayasankar, "Studies of radiative and mechanical properties of Nd^{3+} -doped lead fluorosilicate glasses for broadband amplification in a chirped pulse amplification based high power laser system," *J. Lumin.* **188**, 558–566 (2017).
80. S. S. Babu, P. Babu, C. K. Jayasankar, A. S. Joshi, A. Speghini, and M. Bettinelli, "Luminescence and optical absorption properties of Nd^{3+} ions in K–Mg–Al phosphate and fluorophosphate glasses," *J. Phys.: Condens. Matter* **18**(16), 3975–3991 (2006).
81. K. Linganna, C. S. Dwaraka Viswanath, R. Narro-Garcia, S. Jua, W.-T. Han, C. K. Jayasankar, and V. Venkatramu, "Thermal and optical properties of Nd^{3+} ions in K–Ca–Al fluorophosphate glasses," *J. Lumin.* **166**, 328–334 (2015).
82. G.V. Vázquez, G. Muñoz H, I. Camarillo, C. Falcony, U. Caldiño, and A. Lira, "Spectroscopic analysis of a novel Nd^{3+} -activated barium borate glass for broadband laser amplification," *Opt. Mater.* **46**, 97–103 (2015).

P6

Karolina Kowalska, Marta Kuwik, Joanna Pisarska, Magdalena Leśniak, Dominik Dorosz, Marcin Kochanowicz, Jacek Żmojda, Jan Dorosz, Wojciech A. Pisarski,
**Influence of TiO₂ concentration on near-infrared luminescence of Er³⁺ ions
in barium gallo-germanate glasses**

Journal of Materials Research and Technology 21 (2022) 4761-4772



Available online at www.sciencedirect.com

jmr&t
Journal of Materials Research and Technology

journal homepage: www.elsevier.com/locate/jmrt



Original Article

Influence of TiO₂ concentration on near-infrared luminescence of Er³⁺ ions in barium gallo-germanate glasses



Karolina Kowalska^a, Marta Kuwik^a, Joanna Pisarska^a,
Magdalena Leśniak^b, Dominik Dorosz^b, Marcin Kochanowicz^c,
Jacek Żmojda^c, Jan Dorosz^c, Wojciech A. Pisarski^{a,*}

^a Institute of Chemistry, University of Silesia, Szkolna 9 Street, 40-007 Katowice, Poland

^b AGH University of Science and Technology, 30 Mickiewicza Av., 30-059 Krakow, Poland

^c Białystok University of Technology, Wiejska 45D Street, 15-351 Białystok, Poland

ARTICLE INFO

Article history:

Received 6 September 2022

Accepted 13 November 2022

Available online 17 November 2022

Keywords:

Barium gallo-germanate glasses

TiO₂

Er³⁺ ions

Near-infrared luminescence

ABSTRACT

Erbium (Er)-doped barium gallo-germanate (BGG) glasses modified by TiO₂ have been investigated for near-infrared luminescence applications. Luminescence at 1.5 μm associated to ⁴I_{13/2} → ⁴I_{15/2} transition of Er³⁺ ions has been examined in function of TiO₂ concentration. Several spectroscopic and near-infrared (NIR) laser parameters for Er³⁺ such as stimulated emission cross-section, luminescence bandwidth and lifetime, quantum efficiency, gain bandwidth and figure of merit were determined based on experiments and theoretical calculations using the Judd-Ofelt framework. Our systematic investigations indicate that Er-doped glass with molar ratio GeO₂:TiO₂ = 1:2 shows excellent luminescence properties and could be successfully applied to near-infrared broadband optical amplifiers.

© 2022 The Author(s). Published by Elsevier B.V. This is an open access article under the CC BY-NC-ND license (<http://creativecommons.org/licenses/by-nc-nd/4.0/>).

1. Introduction

Barium gallo-germanate glass referred as BGG is an excellent candidate for high energy laser systems [1]. Systematic studies well demonstrated that BGG glasses present enhanced thermo-stability and thermomechanical properties [2]. They are chemically-stable, non-toxic and exhibit quite high infrared (IR) transparency and improved optical properties. These aspects are also important for the optical fiber drawing

from precursor BGG glass [3]. Further investigations revealed that direct laser writing (DLW) as a powerful tool for the fabrication of integrated electronic devices based on optical waveguides operating in the mid-IR was successfully applied to BGG glass [4,5]. Furthermore, BGG glass can accommodate transition metals and/or rare earths emitting efficient infrared radiation [6–10]. Thus, BGG glass can be used to fabrication of single-mode fibers with high gain per unit length for ultra-compact laser [11], double-clad optical fibers emitting

* Corresponding author. University of Silesia, Institute of Chemistry, Katowice, Poland.

E-mail address: wojciech.pisarski@us.edu.pl (W.A. Pisarski).

<https://doi.org/10.1016/j.jmrt.2022.11.081>

2238-7854/© 2022 The Author(s). Published by Elsevier B.V. This is an open access article under the CC BY-NC-ND license (<http://creativecommons.org/licenses/by-nc-nd/4.0/>).

near-infrared (NIR) radiation [12,13] and up-conversion luminescence temperature sensors [14].

Among trivalent rare earths, Er ions distributed into low-phonon glass-host matrices are attractive for solid-state lasers and tunable NIR optical fiber amplifiers [15]. Lakshminarayana et al. [16] suggest that it could be more conducive to explore rare earth ions in low-phonon environments with optimized host compositions for attaining longer lifetime, wide bandwidth, higher emission cross-section and quantum efficiency in relation to some applications such as NIR lasers and fiber amplifiers. In particular, relatively long decay from the upper laser state ${}^4I_{13/2}$ (Er^{3+}) is required for practical applications in Er-doped fiber amplifiers (EDFAs). For that reason, low-phonon glass matrices are especially favored in contrast to B_2O_3 based glasses, where non-radiative relaxation is dominant and near-infrared luminescence due to the main ${}^4I_{13/2} \rightarrow {}^4I_{15/2}$ transition of Er^{3+} at $1.5 \mu\text{m}$ can be successfully quenched. NIR luminescence properties of Er^{3+} ions have been examined for numerous glass systems like borate [16–19], borosilicate [20], borotellurite [21], antimonate [22–24], silicate [24–28], bismuthate [29], germanate [30–32], tellurite [33–37] as well as heavy metal glasses based on $\text{PbO}-\text{Bi}_2\text{O}_3-\text{Ga}_2\text{O}_3$ [38], $\text{PbO}-\text{PbF}_2-\text{B}_2\text{O}_3$ [39], $\text{PbO}-\text{Ga}_2\text{O}_3-\text{GeO}_2$ [40], $\text{PbO}-\text{P}_2\text{O}_5$ [41,42]. Special attention has been paid to oxide and oxyhalide phosphate based glass systems [43–53]. Our previous investigations indicate that BGG oxyfluoride glass doped with Er^{3+} ions is promising for long-lived near-infrared emission at $1.5 \mu\text{m}$ [54]. Recently, BGG glasses with Er^{3+} ions were modified by fluoride components (BaF_2 , MgF_2 , AlF_3) to improve their luminescence properties [55].

Here, spectroscopic and laser properties of Er^{3+} ions have been studied for BGG, where GeO_2 was partially substituted by TiO_2 . The influence of TiO_2 concentration on near-infrared luminescence properties of Er^{3+} has been examined in details. Thermal and structural properties of BGG glasses modified by TiO_2 were evidenced by differential scanning calorimetry (DSC), X-ray diffraction (XRD), electron paramagnetic resonance (EPR), Raman and FT-IR spectroscopy in our previous work [56]. In this work, several spectroscopic and laser parameters for Er ions in BGG glasses were determined in function of TiO_2 concentration. Theoretical and experimental results are presented and discussed for glass samples, where $\text{GeO}_2:\text{TiO}_2$ molar ratio was changed from 5:1 to 1:5. From literature data it is known that glass component TiO_2 plays the role of network-modifier or network-former, depending on its concentration. However, most of titanate based glasses are partly crystallized. Unfortunately, crystalline phases due to different titanates are usually present in these systems. Thermal stability parameters are also relatively low. It makes them unsuitable for potential fiber applications. In general, preparation of thermally-stable and fully amorphous systems with relatively high TiO_2 concentration is still difficult. These aspects are important from the scientific and technological points of view.

Emission properties of Er^{3+} ions in glass systems containing high content of TiO_2 have not yet been studied, to our knowledge. NIR luminescence of Er^{3+} at $1.5 \mu\text{m}$ has been examined for niobophosphate [57,58], lead borate aluminum [59], borate [60] and multicomponent tellurite based glasses [61–64], where amount of titanium dioxide playing the role as

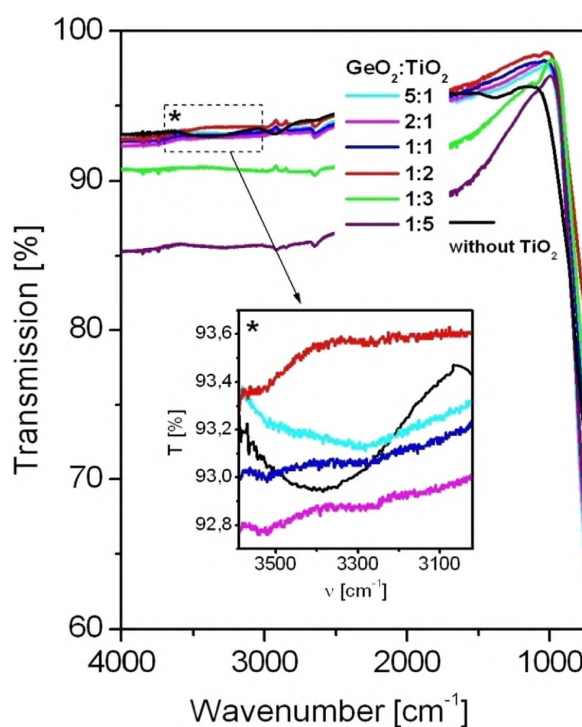


Fig. 1 – Transmittance spectra of barium gallo-germanate glasses modified by TiO_2 . Inset shows transmittance bands related to the stretching vibration of OH^- groups.

glass-network-modifier did not exceed 15 M%. The aim of our work is concerned on the enhanced NIR luminescence of Er^{3+} ions in BGG glasses in the presence of TiO_2 .

2. Experimental

Glasses with the following compositions $x\text{TiO}_2-(60-x)\text{GeO}_2-30\text{BaO}-9.5\text{Ga}_2\text{O}_3-0.5\text{Er}_2\text{O}_3$ (where $x = 0, 10, 20, 30, 40, 45$ and 50) were prepared using melt quenching technique. The concentrations of components are given in molar %. The appropriate amounts of metal oxides of high purity (99.99%, Aldrich Chemical Co.) were mixed homogeneously together and then melted at $1200 \text{ }^\circ\text{C}$ for 0.45 h. Each Er^{3+} -doped sample was polished for optical measurements.

Transmittance spectra were performed on the Nicolet iS50 ATR spectrometer in an infrared frequency region. The refractive index of the glass-host at a wavelength of 632.8 nm was determined using the Metricon 2010 prism coupler. In the next step, glass samples were characterized using absorption (Cary 5000 UV-VIS-NIR spectrophotometer, Agilent Technology, USA) and photoluminescence spectroscopy. For luminescence measurements (spectra and decays) laser equipment was used, which consists of PTI QuantaMaster QM40 spectrofluorometer with a xenon lamp (75 W) as an excitation source, tunable pulsed optical parametric oscillator (OPO), Nd:YAG laser (OpotekOpolette 355 LD), double 200 mm monochromators, Hamamatsu H10330B-75 detector and PTI ASOC-10 USB-2500 oscilloscope. Resolution for spectral

measurements was ± 0.1 nm. Decay curves were recorded with an accuracy of ± 0.5 μ s.

3. Results and discussion

3.1. Transmittance spectra

Systematic investigations of Er^{3+} -doped glasses clearly indicate that only two stretching vibrations of the OH^- groups with their energies of about 3300 cm^{-1} are able to bridge energy gap between the upper $^4\text{I}_{13/2}$ laser state and the $^4\text{I}_{15/2}$ ground state ($\Delta E = 6600\text{ cm}^{-1}$). It is especially important for Er^{3+} -doped glass systems, because the hydroxyl groups can couple to the Er^{3+} ions. Thus, NIR luminescence at $1.5\text{ }\mu\text{m}$ corresponding to the $^4\text{I}_{13/2} \rightarrow ^4\text{I}_{15/2}$ transition of Er^{3+} could be strongly quenched by hydroxyl groups. An effective elimination of OH^- groups was also verified in BGG glasses in the presence of TiO_2 using by transmittance spectra measurements. Fig. 1 shows transmittance spectra measured for BGG glass samples varying with TiO_2 concentration. Inset shows broad absorption bands centered between 3300 and 3400 cm^{-1} , which are attributed to the stretching vibrations of

OH^- groups. Based on spectra measurements we can conclude that glass samples show longer IR transmittance compared to BGG without TiO_2 .

Our previous investigations indicated that BGG glass without TiO_2 presents relatively broad transparency from 0.35 to $8\text{ }\mu\text{m}$ and the light transmission is above 80% at wavelengths nearly up to $8\text{ }\mu\text{m}$ [65]. Here, the light transmission in broad frequency region is above 90% for the studied glass samples. It was changed for glass samples with molar ratios $\text{GeO}_2:\text{TiO}_2$ equal to $1:3$ and $1:5$, for which the light transmission decreased to about 90% and 85% , respectively. Further analysis indicates that the residual absorption of OH^- groups is reduced drastically in BGG glasses with the presence of TiO_2 . The IR absorption coefficient α_{OH} (given in cm^{-1}) was also calculated using the relation $\alpha_{\text{OH}} = (1/L) \ln (T_0/T)$, where: L is the thickness of the glass, T_0 and T are the transmission value of maximum and at $3\text{ }\mu\text{m}$, respectively. The IR absorption coefficient α_{OH} for BGG glass without TiO_2 is close to 0.25 cm^{-1} . The results are comparable to the value of α_{OH} at $3\text{ }\mu\text{m}$ equal to 0.196 cm^{-1} , which was obtained for the $\text{Er}^{3+}/\text{Pr}^{3+}$ co-doped germanate glasses without any hydroxyl removal process [66]. It is also in a good agreement with α_{OH} close to 0.19 cm^{-1} [7], 0.34 cm^{-1} [67] and 0.39 cm^{-1} [68] for similar GeO_2 based glass

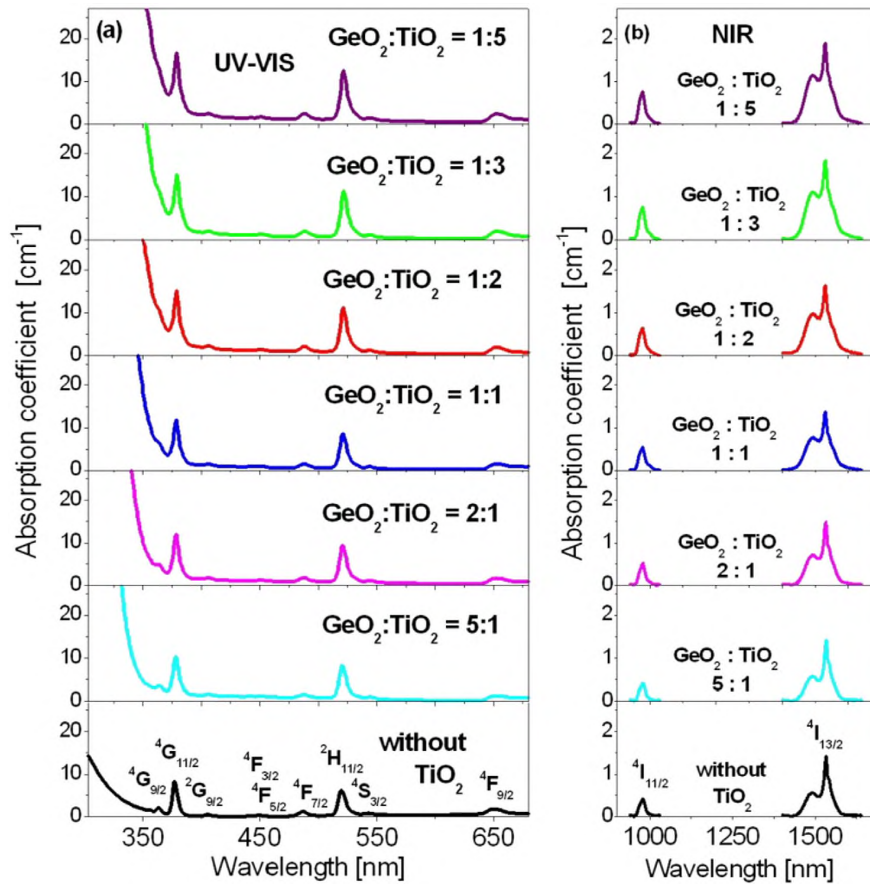


Fig. 2 – Absorption spectra of Er^{3+} ions in barium gallo-germanate glasses modified by TiO_2 .

Table 1 – Glass composition, TiO₂ content, rare earth ion concentration, UV cut-off and refractive index of glass-host.

Glass composition [mol %]	TiO ₂ content [% mol]	GeO ₂ :TiO ₂	N × 10 ²⁰ [ion/cm ³]	UV cut-off [nm]	n
60GeO ₂ –30BaO–9.5Ga ₂ O ₃ –0.5Er ₂ O ₃	0	–	2.17	337	1.736
50GeO ₂ –10TiO ₂ –30BaO–9.5Ga ₂ O ₃ –0.5Er ₂ O ₃	10	5:1	2.18	342	1.779
40GeO ₂ –20TiO ₂ –30BaO–9.5Ga ₂ O ₃ –0.5Er ₂ O ₃	20	2:1	2.20	350	1.830
30GeO ₂ –30TiO ₂ –30BaO–9.5Ga ₂ O ₃ –0.5Er ₂ O ₃	30	1:1	2.22	359	1.877
20GeO ₂ –40TiO ₂ –30BaO–9.5Ga ₂ O ₃ –0.5Er ₂ O ₃	40	1:2	2.25	365	1.928
15GeO ₂ –45TiO ₂ –30BaO–9.5Ga ₂ O ₃ –0.5Er ₂ O ₃	45	1:3	2.30	367	1.969
10GeO ₂ –50TiO ₂ –30BaO–9.5Ga ₂ O ₃ –0.5Er ₂ O ₃	50	1:5	2.33	368	1.998

systems. The IR absorption coefficient α_{OH} is reduced significantly for samples, where GeO₂ was replaced by TiO₂. The value of α_{OH} decreases from 0.25 cm⁻¹ (sample without TiO₂) to 0.16 cm⁻¹ (sample with GeO₂:TiO₂ = 5:1). The infrared absorption coefficients are extremely low (below 0.05 cm⁻¹) for glass samples with higher TiO₂ concentration, but their values are difficult to calculate with good accuracy. Our studies suggest that titanium dioxide influence strongly on the OH⁻ content in glass composition. Multicomponent titanate-germanate glasses appear to be more stable against water absorption probably due to their strengthened network. These effects were also observed for phosphate glasses under the introduction of TiO₂ [69].

Similar phenomena were also documented earlier by us for BGG oxyfluoride glasses, where BaO was substituted by BaF₂ [70]. For these systems, the values of α_{OH} decreased to 0.025 cm⁻¹ (15% BaF₂), 0.020 cm⁻¹ (10% BaF₂) and even below 0.01 cm⁻¹ (5% BaF₂), respectively. The extremely low IR absorption coefficients (α_{OH} less than 0.05 cm⁻¹) are possible to obtain, because all samples were synthesized under rigorous technological conditions in glove-box, in a protective

atmosphere of dried argon of high purity. It suggests that BGG glasses containing TiO₂ are attractive for active optical fibers emitting IR radiation.

3.2. Absorption spectra

Fig. 2 presents optical absorption spectra of Er³⁺ ions in BGG glasses with various molar ratios GeO₂:TiO₂. The spectra consist of the inhomogeneously broadened absorption lines characteristic for 4f¹¹–4f¹¹ electronic transitions of Er³⁺. Absorption bands correspond to transitions originating from the ⁴I_{15/2} ground state to the higher-lying ⁴I_{13/2}, ⁴I_{11/2}, ⁴I_{9/2}, ⁴F_{9/2}, ⁴S_{3/2}, ²H_{11/2}, ⁴F_{7/2}, ⁴F_{5/2}, ⁴F_{3/2}, ²G_{9/2}, ⁴G_{11/2} and ⁴G_{9/2} excited states of Er³⁺.

From the spectra, the ultraviolet (UV) cut-off wavelength defined as the intersection between the zero base line and the extrapolation of absorption edge was determined. The absorption edge for the studied samples is shifted to longer wavelengths with increasing TiO₂ concentration in glass composition. Moreover, the refractive index increases from 1.736 (glass without TiO₂) to 1.998 (glass with molar ratio

Table 2 – Measured and calculated oscillator strengths (× 10⁻⁶) for Er³⁺ ions in barium gallo-germanate glasses modified by TiO₂. Transitions are from the ⁴I_{15/2} ground state to the levels indicated. The rms deviations (× 10⁻⁶) are also given.

States	Energy [cm ⁻¹]	0% TiO ₂		10% TiO ₂		20% TiO ₂		30% TiO ₂	
		P _{meas}	P _{calc}	P _{meas}	P _{calc}	P _{meas}	P _{calc}	P _{meas}	P _{calc}
⁴ I _{11/2}	10,200	0.550	0.588	0.500	0.579	0.660	0.686	0.760	0.709
⁴ F _{9/2}	15,300	1.500	1.510	1.460	1.505	1.720	1.723	2.060	1.894
⁴ S _{3/2}	18,300	0.400	0.385	0.400	0.370	0.430	0.453	0.400	0.501
² H _{11/2}	19,200	11.10	11.65	10.94	10.98	12.63	12.25	11.61	11.16
⁴ F _{7/2}	20,400	1.600	1.511	1.580	1.483	1.840	1.772	1.880	1.956
⁴ F _{3/2} , ⁴ F _{5/2}	22,300	0.700	0.727	0.700	0.715	0.800	0.875	1.000	0.968
² G _{9/2}	24,500	0.650	0.533	0.630	0.554	0.770	0.671	0.800	0.742
⁴ G _{11/2}	26,300	19.70	19.15	19.42	19.37	21.21	21.61	19.20	19.67
⁴ G _{9/2}	27,750	1.700	1.721	1.750	1.665	1.820	1.890	1.340	1.975
rms deviation		0.63		0.36		0.33		0.88	
States	Energy [cm ⁻¹]	40% TiO ₂		45% TiO ₂		50% TiO ₂			
		P _{meas}	P _{calc}	P _{meas}	P _{calc}	P _{meas}	P _{calc}		
⁴ I _{11/2}	10,200	0.800	0.819	0.930	0.853	0.940	0.876		
⁴ F _{9/2}	15,300	2.840	2.700	2.930	2.694	3.090	2.902		
⁴ S _{3/2}	18,300	0.500	0.581	0.400	0.609	0.540	0.622		
² H _{11/2}	19,200	13.65	13.29	13.72	13.49	14.76	14.17		
⁴ F _{7/2}	20,400	2.520	2.452	2.380	2.521	2.490	2.629		
⁴ F _{3/2} , ⁴ F _{5/2}	22,300	1.110	1.122	1.270	1.177	1.180	1.201		
² G _{9/2}	24,500	0.910	0.889	1.080	0.925	1.200	0.952		
⁴ G _{11/2}	26,300	23.06	23.43	23.55	23.78	24.35	24.97		
⁴ G _{9/2}	27,750	2.050	2.704	1.840	2.607	2.210	2.300		
rms deviation		0.73		0.85		0.87			

Table 3 – The Judd-Ofelt intensity parameters Ω_t ($t = 2, 4, 6$) $\times 10^{-20} \text{ cm}^2$ for Er^{3+} ions.

TiO ₂ content [% mol]	GeO ₂ :TiO ₂	Ω_2	Ω_4	Ω_6
0	–	4.77 ± 0.23	1.07 ± 0.29	0.97 ± 0.21
10	5:1	6.47 ± 0.06	0.93 ± 0.09	0.81 ± 0.05
20	2:1	6.92 ± 0.13	0.97 ± 0.19	0.95 ± 0.11
30	1:1	5.94 ± 0.19	1.01 ± 0.28	1.01 ± 0.17
40	1:2	6.53 ± 0.16	1.61 ± 0.24	1.12 ± 0.14
45	1:3	6.44 ± 0.18	1.51 ± 0.27	1.14 ± 0.16
50	1:5	6.56 ± 0.21	1.64 ± 0.32	1.13 ± 0.19

GeO₂:TiO₂ = 1:5) with increasing TiO₂ content. The following glass parameters, the UV cut-off wavelength, Er³⁺ ion concentration and refractive index of the glass-host varying with TiO₂ concentration are given in Table 1.

In the next step, radiative transition probabilities for excited states of Er³⁺ ions in BGG glasses containing TiO₂ were calculated using the Judd-Ofelt theory [71,72]. The intensities of absorption bands shown in Fig. 2 were estimated by measuring the areas under characteristic lines of Er³⁺ ions and then the measured oscillator strengths of transitions were

obtained. Meanwhile, the theoretical oscillator strengths for each transition of Er³⁺, within 4f¹¹ electronic configuration, were calculated using the following relation:

$$P_{\text{calc}} = \frac{8\pi^2 mc(n^2 + 2)^2}{3h\lambda(2J + 1) \cdot 9n} \times \sum_{t=2,4,6} \Omega_t \left(\langle 4f^n J \| U^t \| 4f^n J' \rangle \right)^2 \quad (1)$$

where m is the mass of the electron, c is the velocity of light, h is the Planck constant and λ is the mean wavelength of the each transition of Er³⁺, n is the refractive index of the glass-host, and $\|U^t\|^2$ taken from Ref. [73] represents the squared reduced matrix elements of the unit tensor operator U^t connecting the initial and final states. Measured and calculated oscillator strengths for Er³⁺ ions in BGG glass varying with TiO₂ concentration are given in Table 2.

The quality of the fit shown in Table 2 can be expressed by the magnitude of the root-mean-square (rms) deviation and it is defined by $\Sigma(P_{\text{meas}} - P_{\text{calc}})^2$. The rms deviations for the studied glass systems are in the range 0.33–0.88 ($\times 10^{-6}$). The error is within the acceptable range compared to similar Er-doped glass systems, which were examined using the Judd-Ofelt theory. The three Ω_t ($t = 2, 4, 6$) phenomenological Judd-Ofelt parameters (J-O) were evaluated from the

Table 4 – The calculated radiative transition probabilities A_J and luminescence branching ratios β for Er^{3+} ions in barium gallo-germanate glasses without and with TiO₂.

Transition	Average wavelength [nm]	0% TiO ₂		10% TiO ₂		20% TiO ₂		30% TiO ₂	
		A_J [s ⁻¹]	β	A_J [s ⁻¹]	β	A_J [s ⁻¹]	β	A_J [s ⁻¹]	β
⁴ S _{3/2} → ⁴ F _{9/2}	3175	1	–	1	–	1	–	1	–
⁴ I _{9/2}	1639	65	0.038	62	0.038	78	0.037	90	0.037
⁴ I _{11/2}	1212	40	0.024	35	0.022	45	0.022	52	0.021
⁴ I _{13/2}	844	485	0.287	455	0.281	589	0.281	684	0.282
⁴ I _{15/2}	547	1100	0.651	1067	0.659	1381	0.660	1606	0.660
⁴ F _{9/2} → ⁴ I _{9/2}	3448	9	0.006	8	0.006	10	0.006	9	0.005
⁴ I _{11/2}	1980	81	0.056	76	0.055	95	0.057	105	0.055
⁴ I _{13/2}	1156	70	0.049	67	0.049	80	0.048	87	0.046
⁴ I _{15/2}	654	1280	0.889	1217	0.890	1475	0.889	1695	0.894
⁴ I _{9/2} → ⁴ I _{11/2}	4651	1	0.006	1	0.006	1	0.005	1	0.004
⁴ I _{13/2}	1739	48	0.268	44	0.257	57	0.279	66	0.283
⁴ I _{15/2}	806	130	0.726	126	0.737	146	0.716	166	0.713
⁴ I _{11/2} → ⁴ I _{13/2}	2778	21	0.102	19	0.098	24	0.099	27	0.103
⁴ I _{15/2}	980	184	0.898	174	0.902	218	0.901	236	0.897
⁴ I _{13/2} → ⁴ I _{15/2}	1538	110	1.000	107	1.000	136	1.000	155	1.000
Transition	Average wavelength [nm]	40% TiO ₂		45% TiO ₂		50% TiO ₂			
		A_J [s ⁻¹]	β	A_J [s ⁻¹]	β	A_J [s ⁻¹]	β		
⁴ S _{3/2} → ⁴ F _{9/2}	3175	1	–	1	–	1	–		
⁴ I _{9/2}	1639	121	0.041	130	0.040	140	0.041		
⁴ I _{11/2}	1212	65	0.022	71	0.022	75	0.022		
⁴ I _{13/2}	844	836	0.280	918	0.280	960	0.280		
⁴ I _{15/2}	547	1960	0.657	2153	0.658	2251	0.657		
⁴ F _{9/2} → ⁴ I _{9/2}	3448	11	0.004	12	0.004	13	0.004		
⁴ I _{11/2}	1980	128	0.045	139	0.047	147	0.045		
⁴ I _{13/2}	1156	132	0.047	137	0.046	152	0.047		
⁴ I _{15/2}	654	2555	0.904	2669	0.903	2952	0.904		
⁴ I _{9/2} → ⁴ I _{11/2}	4651	1	0.002	2	0.005	2	0.005		
⁴ I _{13/2}	1739	81	0.220	89	0.233	93	0.217		
⁴ I _{15/2}	806	287	0.778	291	0.762	333	0.778		
⁴ I _{11/2} → ⁴ I _{13/2}	2778	35	0.108	37	0.106	40	0.108		
⁴ I _{15/2}	980	288	0.892	313	0.894	330	0.892		
⁴ I _{13/2} → ⁴ I _{15/2}	1538	197	1.000	209	1.000	215	1.000		

least-square fit of measured and calculated oscillator strengths for Er^{3+} . They are summarized in Table 3.

The Judd–Ofelt intensity parameter Ω_2 indicates the degree of covalency between Er^{3+} ions and surrounding ligands. It reflects the asymmetry of the environment around rare earth ions. It is interesting to see that glass with molar ratio $\text{GeO}_2:\text{TiO}_2 = 2:1$ exhibits the highest value of Ω_2 equal to $6.92 \times 10^{-20} \text{ cm}^2$. It suggests that the bonds between Er^{3+} ions and surrounding ligands existing in glass sample with $\text{GeO}_2:\text{TiO}_2 = 2:1$ are highly covalent in character compared to series of the studied glass samples. It is in a good agreement with the results obtained for Nd^{3+} ions, where the Judd–Ofelt parameter Ω_2 for glass with $\text{GeO}_2:\text{TiO}_2 = 2:1$ was the highest [74]. Next, the values of Ω_t ($t = 2, 4, 6$) were used to calculate the radiative transition probabilities, luminescence branching ratios and radiative lifetimes.

The radiative transition probability A_J for excited states of Er^{3+} ions from an initial state J to a final ground state J' is defined as follows:

$$A_J = \frac{64\pi^4 e^2}{3h(2J+1)\lambda^3} \times \frac{n(n^2+2)^2}{9} \times \sum_{t=2,4,6} \Omega_t \left(\langle 4f^N J \| U^t \| 4f^N J' \rangle \right)^2 \quad (2)$$

The luminescence branching ratio β is related to the relative intensities of transitions from excited state to all terminal states whereas the radiative lifetime τ_{rad} of an excited state is the inverse of the total radiative emission rate A_T involving all the intermediate terms (the sum of the A_J terms). These relations are given below.

$$\beta = \frac{A_J}{\sum_i A_{Ji}} \quad (3)$$

$$\tau_{\text{rad}} = \frac{1}{\sum_i A_{Ji}} = \frac{1}{A_T} \quad (4)$$

The radiative transition probabilities and the luminescence branching ratios for Er^{3+} ions in BGG glasses in function of TiO_2 concentration were calculated. The results are shown in Table 4.

3.3. Luminescence spectra and decays

Fig. 3 shows NIR luminescence spectra of Er^{3+} ions in BGG glasses varying with TiO_2 concentration. The luminescence spectra for glass samples with the absence and presence of TiO_2 were excited by 488 nm line.

Luminescence bands at 1.5 μm correspond to the main ${}^4I_{13/2} \rightarrow {}^4I_{15/2}$ NIR laser transition of Er^{3+} . Spectroscopic studies

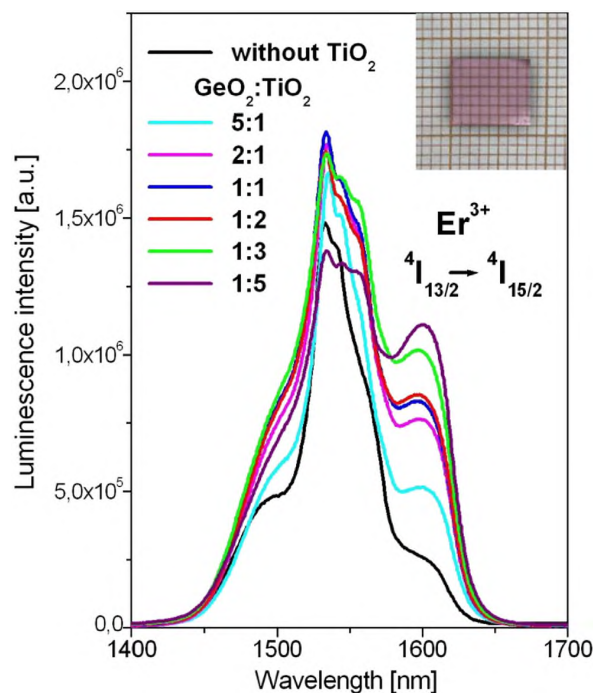


Fig. 3 – Near-infrared luminescence spectra of Er^{3+} ions in barium gallo-germanate glasses modified by TiO_2 . Inset shows the photo of glass with molar ratio $\text{GeO}_2:\text{TiO}_2 = 1:2$.

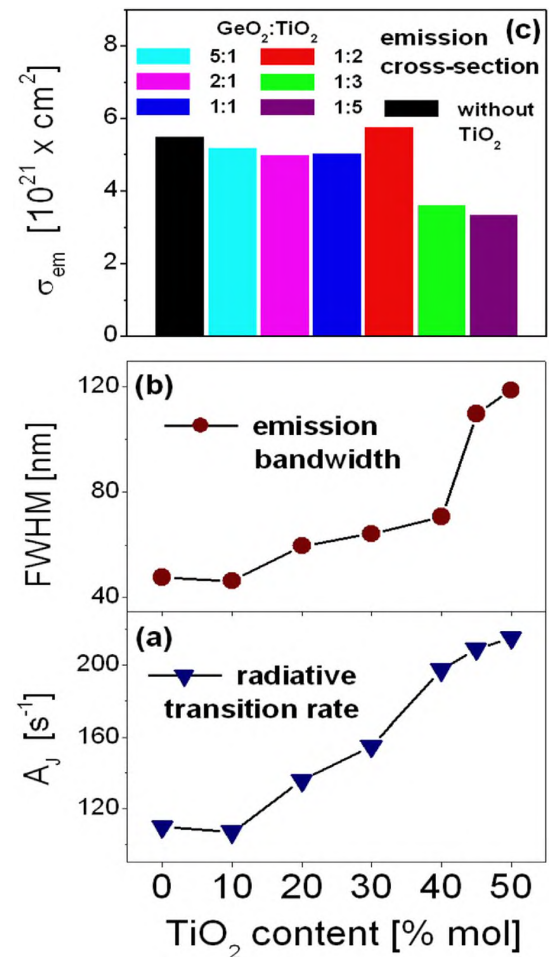


Fig. 4 – Radiative transition rates, luminescence bandwidth and peak stimulated emission cross-section for ${}^4I_{13/2} \rightarrow {}^4I_{15/2}$ transition of Er^{3+} ions varying with TiO_2 concentration.

Table 5 – The emission peak wavelength λ_p , the luminescence bandwidth FWHM, the stimulated emission cross-section σ_{em} , the gain bandwidth $\sigma_{em} \times \text{FWHM}$ and the figure of merit $\sigma_{em} \times \tau_m$ for the ${}^4I_{13/2} \rightarrow {}^4I_{15/2}$ near-infrared transition Er^{3+} ions varying with TiO_2 concentration.

TiO_2 content [% mol]	$\text{GeO}_2:\text{TiO}_2$	λ_p [nm]	FWHM [nm]	σ_{em} [$10^{-21} \times \text{cm}^2$]	$\sigma_{em} \times \text{FWHM}$ [$10^{-28} \times \text{cm}^3$]	$\sigma_{em} \times \tau_m$ [$10^{-24} \times \text{cm}^2\text{s}$]
0	–	1533	48	5.55	270	29.69
10	5:1	1535.5	48	5.17	248	29.88
20	2:1	1534.5	60	4.98	299	27.74
30	1:1	1534	64.5	5.01	323	27.00
40	1:2	1534	70	6.04	423	30.44
45	1:3	1534	110	3.60	396	17.06
50	1:5	1534	119	3.32	395	14.94

indicate that the profiles of emission bands of Er^{3+} ions depend strongly on TiO_2 concentration in glass composition. Some spectroscopic parameters such as the emission bandwidth and the peak stimulated emission cross-section for the ${}^4I_{13/2} \rightarrow {}^4I_{15/2}$ transition of Er^{3+} ions were determined and they are illustrated in Fig. 4.

It is clearly seen that the radiative transition rates calculated from the Judd-Ofeldt framework for the ${}^4I_{13/2} \rightarrow {}^4I_{15/2}$ transition of Er^{3+} are increased with increasing TiO_2 concentration. The same situation is observed for the luminescence bandwidth referred as full width at half maximum (FWHM). The values of FWHM increase with increasing TiO_2 concentration. These effects are especially stronger for glass samples containing higher TiO_2 content. The luminescence bandwidths are changed from 48 nm (glass without TiO_2) to nearly 110 nm ($\text{GeO}_2:\text{TiO}_2 = 1:3$) and 119 nm ($\text{GeO}_2:\text{TiO}_2 = 1:5$), respectively. The radiative transition rate for the ${}^4I_{13/2} \rightarrow {}^4I_{15/2}$ transition of Er^{3+} (Table 4) and the luminescence bandwidth

were applied to calculate the peak stimulated emission cross-section σ_{em} . It is generally accepted that the potential laser performance of the glass-host is characterized by the peak stimulated emission cross-section σ_{em} , which is defined as follows:

$$\sigma_{em} = \frac{\lambda_p^4}{8\pi c n^2 \Delta\lambda} A_{Jl} \tag{5}$$

where λ_p is the peak luminescence wavelength, $\Delta\lambda$ is the luminescence bandwidth (FWHM), n is the refractive index and c is the velocity of light.

The peak stimulated emission cross-section for the ${}^4I_{13/2} \rightarrow {}^4I_{15/2}$ transition of Er^{3+} ions is relatively large for glass with molar ratio $\text{GeO}_2:\text{TiO}_2 = 1:2$ ($\sigma_{em} = 6.04 \times 10^{-21} \text{ cm}^2$) compared to the other values, which were calculated for the studied glass samples (Fig. 4). Details are given in Table 5.

Decay curves for the upper ${}^4I_{13/2}$ laser state of Er^{3+} ions were also measured and examined in function of TiO_2

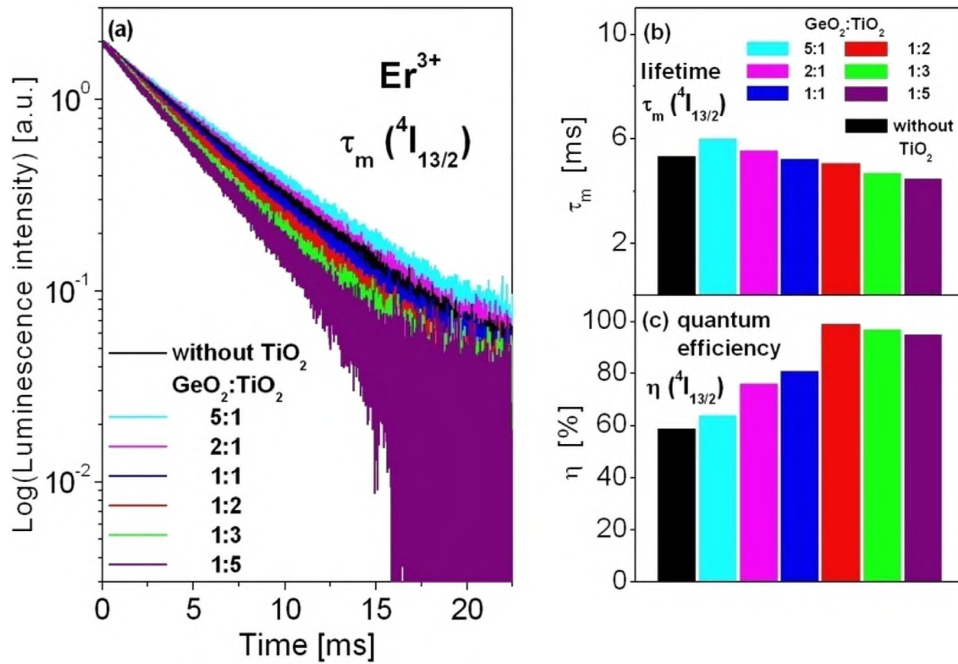


Fig. 5 – Decays from the upper ${}^4I_{13/2}$ laser state of Er^{3+} ions in barium gallo-germanate glasses modified by TiO_2 . Luminescence lifetimes and quantum efficiencies for ${}^4I_{13/2}$ (Er^{3+}) state varying with TiO_2 concentration are also schematized.

Table 6 – The calculated radiative lifetime τ_{rad} , the measured lifetime τ_{m} and the quantum efficiency η for the upper ${}^4I_{13/2}$ laser state of Er^{3+} ions varying with TiO_2 concentration.

TiO_2 content [% mol]	$\text{GeO}_2:\text{TiO}_2$	τ_{rad} [ms]	τ_{m} [ms]	η [%]
0	–	9.09	5.35	59
10	5:1	9.35	5.98	64
20	2:1	7.35	5.57	76
30	1:1	6.45	5.23	81
40	1:2	5.13	5.04	98
45	1:3	4.79	4.65	97
50	1:5	4.64	4.45	96

concentration. Luminescence decays from the ${}^4I_{13/2}$ state of Er^{3+} ions in BGG glasses varying with TiO_2 content are presented in Fig. 5.

Luminescence lifetimes were determined based on decay curves which are single-exponential. Decay curve analysis clearly demonstrated that the luminescence lifetimes ${}^4I_{13/2}$ (Er^{3+}) are reduced with increasing TiO_2 concentration. The measured luminescence lifetimes τ_{m} and the radiative lifetimes τ_{rad} calculated from the Judd-Ofelt theory are necessary to determine the quantum efficiency for the ${}^4I_{13/2} \rightarrow {}^4I_{15/2}$ transition of Er^{3+} given by $\eta = \tau_{\text{m}}/\tau_{\text{rad}} \times 100\%$. Measured luminescence lifetimes and quantum efficiencies varying with TiO_2 concentration are also schematized on Fig. 5. The quantum efficiencies for the ${}^4I_{13/2} \rightarrow {}^4I_{15/2}$ transition of Er^{3+} ions are relatively high (η above 90%) for glass samples containing higher TiO_2 content. They are comparable to the results obtained for Er^{3+} ions in multicomponent oxyhalide glass based on $\text{SrO}-\text{Al}_2\text{O}_3-\text{B}_2\text{O}_3-\text{BaCl}_2-\text{TeO}_2$ ($\eta = 90\%$), $\text{TeO}_2-\text{H}_3\text{BO}_3-\text{PbO}-\text{Bi}_2\text{O}_3-\text{CdO}$ ($\eta = 92\%$) and $\text{TeO}_2-\text{GeO}_2-\text{Na}_2\text{O}-\text{ZnO}$

($\eta = 93\%$), respectively [75–77]. Spectroscopic analysis indicates that glass with molar ratio $\text{GeO}_2:\text{TiO}_2 = 1:2$ exhibits the highest value of η . It suggests that the introduction of TiO_2 to BGG glass is conducive to achieve high quantum efficiency. Details are given in Table 6.

The peak stimulated emission cross-section, the luminescence bandwidth and the measured luminescence lifetime for the ${}^4I_{13/2} \rightarrow {}^4I_{15/2}$ transition of Er^{3+} ions were applied to calculate the laser parameters, i.e. gain bandwidth ($\sigma_{\text{em}} \times \text{FWHM}$) and figure of merit FOM ($\sigma_{\text{em}} \times \tau_{\text{m}}$). The gain bandwidth and the figure of merit are important laser parameters to identify the lasing in glass-hosts and near-infrared broadband amplification. In practice, high gain medium with low threshold pump power is strongly required. It is experimentally proved that both factors $\sigma_{\text{em}} \times \text{FWHM}$ and $\sigma_{\text{em}} \times \tau_{\text{m}}$ exhibiting high values for the ${}^4I_{13/2} \rightarrow {}^4I_{15/2}$ NIR transition of Er^{3+} ions at $1.5 \mu\text{m}$ are necessary to generate laser action in glasses. These laser parameters varying with TiO_2 content are also presented in Table 5. Based on measurements of emission spectra and decays we can conclude that glass with molar ratio $\text{GeO}_2:\text{TiO}_2 = 1:2$ has the highest stimulated emission cross-section ($\sigma_{\text{em}} = 6.04 \times 10^{-21} \text{ cm}^2$), gain bandwidth ($\sigma_{\text{em}} \times \text{FWHM} = 423 \times 10^{-28} \text{ cm}^3$) and figure of merit FOM ($\sigma_{\text{em}} \times \tau_{\text{m}} = 30.44 \times 10^{-24} \text{ cm}^2\text{s}$) for the ${}^4I_{13/2} \rightarrow {}^4I_{15/2}$ transition of Er^{3+} ions. Therefore, BGG glass with $\text{GeO}_2:\text{TiO}_2 = 1:2$ doped with Er^{3+} ions belonging to low-phonon oxide glass family can be successfully used for NIR laser applications.

Finally, the peak stimulated emission cross-section, the gain bandwidth and the figure of merit for the main ${}^4I_{13/2} \rightarrow {}^4I_{15/2}$ near-infrared transition are compared to several Er^{3+} -doped laser glasses published previously [78–93]. The results are summarized in Table 7.

The peak stimulated emission cross-section for glass with $\text{GeO}_2:\text{TiO}_2 = 1:2$ is smaller in comparison to some germanate

Table 7 – Comparison of the stimulated emission cross-section (σ_{em}), the gain bandwidth ($\sigma_{\text{em}} \times \text{FWHM}$) and the figure of merit ($\sigma_{\text{em}} \times \tau_{\text{m}}$) for the ${}^4I_{13/2} \rightarrow {}^4I_{15/2}$ near-infrared transition in different laser glasses doped with Er^{3+} .

Glass-host	σ_{em} [$10^{-21} \times \text{cm}^2$]	$\sigma_{\text{em}} \times \text{FWHM}$ [$10^{-28} \times \text{cm}^3$]	$\sigma_{\text{em}} \times \tau_{\text{m}}$ [$10^{-24} \times \text{cm}^2\text{s}$]	Ref.
$\text{GeO}_2:\text{TiO}_2 = 1:2$	6.04	423	30.44	this work
GeO_2-BaO	7.89	560	16.57	[78]
GeO_2-MgO	8.55	693	38.05	[78]
$\text{GeO}_2-\text{Ga}_2\text{O}_3-\text{Li}_2\text{O}$	7.78	424	–	[79]
$\text{GeO}_2-\text{Ga}_2\text{O}_3-\text{Na}_2\text{O}$	7.58	402	–	[79]
$\text{GeO}_2-\text{Ga}_2\text{O}_3-\text{K}_2\text{O}$	7.62	403	–	[79]
$\text{GeO}_2-\text{PbO}-\text{Na}_2\text{O}$	7.00	364	–	[80]
$\text{Na}_2\text{O}-\text{CaO}-\text{Al}_2\text{O}_3-\text{GeO}_2$	5.70	239	–	[81]
$\text{TeO}_2-\text{WO}_3-\text{Na}_2\text{O}-\text{Nb}_2\text{O}_5$	5.87	376	14.09	[82]
$\text{PbF}_2-\text{TeO}_2-\text{B}_2\text{O}_3$	5.37	466	–	[83]
$\text{Na}_2\text{O}-\text{Al}_2\text{O}_3-\text{P}_2\text{O}_5$	5.50	293	37.40	[84]
$\text{P}_2\text{O}_5-\text{K}_2\text{O}-\text{SrO}-\text{Al}_2\text{O}_3$	6.03	204	–	[85]
$\text{P}_2\text{O}_5-\text{K}_2\text{O}-\text{Al}_2\text{O}_3-\text{PbO}-\text{Na}_2\text{O}$	6.73	310	13.86	[86]
$\text{NaF}-\text{RF}_2-\text{AlF}_3-\text{YF}_3-\text{Al}(\text{PO}_3)_3$	6.77	379	49.80	[87]
$\text{P}_2\text{O}_5-\text{K}_2\text{O}-\text{Al}_2\text{O}_3-\text{CaF}_2$	10.50	704	23.21	[88]
$\text{Nb}_2\text{O}_5-\text{K}_2\text{O}-\text{ZnF}_2-\text{LiF}-\text{SiO}_2$	7.46	694	15.82	[89]
$\text{SiO}_2-\text{GeO}_2-\text{CaO}-\text{BaO}-\text{Nb}_2\text{O}_5-\text{Li}_2\text{O}$	9.55	735	–	[90]
$\text{SiO}_2-\text{Al}_2\text{O}_3-\text{Na}_2\text{CO}_3-\text{SrF}_2-\text{CaF}_2$	9.80	520	37.57	[91]
$\text{SiO}_2-\text{Al}_2\text{O}_3-\text{LiF}-\text{SrF}_2$	11.66	735	–	[92]
$\text{TeO}_2-\text{B}_2\text{O}_3-\text{ZnF}_2-\text{BaO}$	2.94	222	35.80	[93]

based glasses exhibiting σ_{em} above $7 \times 10^{-21} \text{ cm}^2$ [78–80], but the gain bandwidth is similar to the results obtained for $\text{GeO}_2\text{--Ga}_2\text{O}_3\text{--R}_2\text{O}$ glasses, where R denotes Li, Na or K [79]. According to Zhanget al. [79], the larger value of $\sigma_{em} \times \text{FWHM}$, the wider the gain bandwidth and glasses might be promising host materials for broadband fiber amplifiers at $1.5 \mu\text{m}$, when values of $\sigma_{em} \times \text{FWHM}$ are larger than $400 \times 10^{-28} \text{ cm}^3$. The emission cross-section for the ${}^4\text{I}_{13/2} \rightarrow {}^4\text{I}_{15/2}$ transition of Er^{3+} ions in glass with molar ratio $\text{GeO}_2\text{:TiO}_2 = 1:2$ ($\sigma_{em} = 6.04 \times 10^{-21} \text{ cm}^2$) is comparable with the values σ_{em} ranging between 5.3 and 6.8 (in 10^{-21} cm^2) for some inorganic glasses [81–87]. Comparative analysis indicates that the emission cross-sections of Er^{3+} are significantly higher for selected phosphate [88] and silicate [89–92] glasses. For oxyfluoride glasses based $\text{P}_2\text{O}_5\text{--K}_2\text{O--Al}_2\text{O}_3\text{--CaF}_2$ [88] and $\text{SiO}_2\text{--Al}_2\text{O}_3\text{--LiF--SrF}_2$ [92], the values of σ_{em} are equal to even 10.50 and 11.66 ($\times 10^{-21} \text{ cm}^2$). Previous work for Er^{3+} ions in fluoroborotellurite glass gives interesting results, i.e. values of σ_{em} and $\sigma_{em} \times \text{FWHM}$ are found to be rather smaller compared to other reported glass systems (Table 7), but product of $\sigma_{em} \times \tau_m$ known as the figure of merit is relatively high [93]. In our case, the product $\sigma_{em} \times \tau_m$ for the ${}^4\text{I}_{13/2} \rightarrow {}^4\text{I}_{15/2}$ transition of Er^{3+} in BGG glass with TiO_2 ($30.44 \times 10^{-24} \text{ cm}^2\text{s}$) is found to be larger than some other glasses reported in Table 7. The figure of merit (FOM) for our BGG sample with $\text{GeO}_2\text{:TiO}_2 = 1:2$ is similar to glasses based on $\text{GeO}_2\text{--MgO}$ [78], $\text{Na}_2\text{O--Al}_2\text{O}_3\text{--P}_2\text{O}_5$ [84], $\text{NaF--RF}_2\text{--AlF}_3\text{--YF}_3\text{--Al(PO}_3)_3$ (R = Mg, Ca, Sr, Ba) [87], $\text{SiO}_2\text{--Al}_2\text{O}_3\text{--Na}_2\text{CO}_3\text{--SrF}_2\text{--CaF}_2$ [91] and $\text{TeO}_2\text{--B}_2\text{O}_3\text{--ZnF}_2\text{--BaO}$ [93], for which the values $\sigma_{em} \times \tau_m$ are larger than $30 \times 10^{-24} \text{ cm}^2\text{s}$.

Based on theoretical and experimental results we conclude that glass ($\text{GeO}_2\text{:TiO}_2 = 1:2$) could be potentially useful for lasing action compared along with reported laser glasses. Therefore, Er^{3+} -doped BGG glass with $\text{GeO}_2\text{:TiO}_2 = 1:2$ is suitable for broadband NIR laser gain active media operating at $1.5 \mu\text{m}$.

4. Conclusions

In this work, Er-doped BGG glass modified by TiO_2 is proposed as an excellent candidate for NIR luminescence and laser applications. The absorption and luminescence spectroscopy and calculations using the Judd–Ofelt theory were used to examine multicomponent glass with different molar ratios $\text{GeO}_2\text{:TiO}_2$. Several spectroscopic and laser parameters for Er^{3+} ions in glass varying with TiO_2 concentration were determined and compared to similar inorganic glasses and commercial laser glass systems reported well in literature. Our studies clearly indicate that Er-doped glass with $\text{GeO}_2\text{:TiO}_2 = 1:2$ shows strong NIR luminescence. Emission band at $1.5 \mu\text{m}$ corresponds to the ${}^4\text{I}_{13/2} \rightarrow {}^4\text{I}_{15/2}$ NIR transition of Er^{3+} ions. The spectroscopic and laser parameters are as follows: the peak stimulated emission cross-section $\sigma_{em} = 6.04 \times 10^{-21} \text{ cm}^2$, the measured lifetime $\tau_m = 5.04 \text{ ms}$, the quantum efficiency $\eta = 98\%$, the gain bandwidth $\sigma_{em} \times \text{FWHM} = 423 \times 10^{-28} \text{ cm}^3$ and figure of merit known as $\sigma_{em} \times \tau_m$ product = $30.44 \times 10^{-24} \text{ cm}^2\text{s}$, respectively. We suggest that Er^{3+} -doped glass with molar ratio $\text{GeO}_2\text{:TiO}_2 = 1:2$ is suitable for luminescence at $1.5 \mu\text{m}$ and could be useful for NIR broadband optical amplifiers.

CRediT author statement

K. Kowalska: Investigation, Data Curation, Visualization **M. Kuwik:** Investigation, Data Curation, Validation **J. Pisarska:** Methodology, Investigation, Resources, Supervision **M. Leśniak:** Investigation, Validation **D. Dorosz:** Investigation, Formal analysis **M. Kochanowicz:** Investigation **J. Żmojda:** Investigation **J. Dorosz:** Formal analysis **W.A. Pisarski:** Conceptualization, Writing - Original Draft, Writing - review & editing, Project administration, Funding acquisition, Supervision.

Declaration of competing interest

The authors declare that they have no known competing financial interests or personal relationships that could have appeared to influence the work reported in this paper.

Acknowledgment

The National Science Centre (Poland) supported this work under research project 2018/31/B/ST8/00166.

REFERENCES

- [1] Bayya SS, Chin GD, Sanghera JS, Aggarwal ID. Germanate glass as a window for high energy laser systems. *Opt Express* 2006;14:11687–93.
- [2] Zhang S, Xu M, Chen X, Zhang Y, Calvez L, Zhang X, et al. Enhanced thermostability, thermo-optics, and thermomechanical properties of barium gallo-germanium oxyfluoride glasses and glass-ceramics. *J Am Ceram Soc* 2013;96:2461–6.
- [3] Guerneau T, Strutynski C, Skopak T, Morency S, Hanafi A, Calvazara F, et al. Extended germano-gallate fiber drawing domain: from germanates to gallates optical fibers. *Opt Mater Express* 2019;9:2437–45.
- [4] Berube J-P, Le Camus A, Messaddeq SH, Petit Y, Messaddeq Y, Canioni L, et al. Femtosecond laser direct inscription of mid-IR transmitting waveguides in BGG glasses. *Opt Mater Express* 2017;7:3124–35.
- [5] Le Camus A, Petit Y, Bérubé J-P, Bellec M, Canioni L, Vallée R. Direct-laser-written integrated mid-IR directional couplers in a BGG glass. *Opt Express* 2021;29:8531.
- [6] Jiang XP, Yang ZM, Liu T, Xu SH. Energy transfer between Yb^{3+} and Er^{3+} in barium gallo-germanate glass. *J Appl Phys* 2009;105:103113.
- [7] Wen X, Tang G, Wang J, Chen X, Qian Q, Yang Z. Tm^{3+} doped barium gallo-germanate glass single-mode fibers for $2.0 \mu\text{m}$ laser. *Opt Express* 2015;23:7722–31.
- [8] Tang G, Wen X, Qian Q, Zhu T, Liu W, Sun M, et al. Efficient $2.0 \mu\text{m}$ emission in $\text{Er}^{3+}/\text{Ho}^{3+}$ co-doped barium gallo-germanate glasses under different excitations for mid-infrared laser. *J Alloys Compd* 2016;664:19–24.
- [9] Pisarska J, Kowal M, Kochanowicz M, Żmojda J, Dorosz J, Dorosz D, et al. Influence of BaF_2 and activator concentration on broadband near-infrared luminescence of Pr^{3+} ions in gallo-germanate glasses. *Opt Express* 2016;24:2427–35.

- [10] Pisarska J, Kuwik M, Górny A, Dorosz J, Kochanowicz M, Zmojda J, et al. Influence of transition metal ion concentration on near-infrared emission of Ho^{3+} in barium gallo-germanate glasses. *J Alloys Compd* 2019;793:107–14.
- [11] Tang G, Wen X, Huang K, Qian G, Lin W, Cheng H, et al. Tm^{3+} -doped barium gallo-germanate glass single-mode fiber with high gain per unit length for ultracompact 1.95 μm laser. *Appl. Phys. Express* 2018;11:032701.
- [12] Kochanowicz M, Zmojda J, Miluski P, Ragin T, Pisarski WA, Pisarska J, et al. Structural and luminescent properties of germanate glasses and double-clad optical fiber co-doped with $\text{Yb}^{3+}/\text{Ho}^{3+}$. *J Alloys Compd* 2017;727:1221–6.
- [13] Kochanowicz M, Zmojda J, Miluski P, Baranowska A, Leich M, Schwuchow A, et al. $\text{Tm}^{3+}/\text{Ho}^{3+}$ co-doped germanate glass and double-clad optical fiber for broadband emission and lasing above 2 μm . *Opt Mater Express* 2019;9:1450–8.
- [14] Pisarski WA, Janek J, Pisarska J, Lisiecki R, Ryba-Romanowski W. Influence of temperature on up-conversion luminescence in $\text{Er}^{3+}/\text{Yb}^{3+}$ doubly doped lead-free fluorogermanate glasses for optical sensing. *Sens Actuators B* 2017;253:85–91.
- [15] Lin H, Jiang S, Wu J, Song F, Peyghambarian N, Pun EYB. Er^{3+} doped $\text{Na}_2\text{O}-\text{Nb}_2\text{O}_5-\text{TeO}_2$ glasses for optical waveguide laser and amplifier. *J Phys D Appl Phys* 2003;36:812–7.
- [16] Lakshminarayana G, Meza-Rocha AN, Soriano-Romero O, Caldino U, Lira A, Lee D-E, et al. Optical and visible and near-infrared fluorescence aspects of Er^{3+} , Tm^{3+} , and Nd^{3+} -doped B_2O_3 -rich glasses for fiber amplifiers and NIR lasers. *J Mater Res Technol* 2022;18:658–80.
- [17] Lakshminarayana G, Meza-Rocha AN, Soriano-Romero O, Caldino U, Lira A, Lee D-E, et al. Assessment of optical and fluorescence aspects of Er^{3+} -doped multicomponent B_2O_3 glasses as active media for 1.532 μm near-infrared optical amplifiers. *J Mater Res Technol* 2022;18:3457–77.
- [18] Swapna K, Mahamuda Sk, Venkateswarlu M, Rao AS, Jayasimhadri M, Shakya S, et al. Visible, Up-conversion and NIR (~1.5 μm) luminescence studies of Er^{3+} doped zinc alumino bismuth borate glasses. *J Lumin* 2015;163:55–63.
- [19] Mariyappan M, Arunkumar S, Marimuthu K. Effect of Bi_2O_3 on JO parameters and spectroscopic properties of Er^{3+} incorporated sodium fluoroborate glasses for amplifier applications. *J Non-Cryst Solids* 2020;532:119891.
- [20] Jose A, Gopi S, Krishnapriya T, Jose TA, Joseph C, Unnikrishnan NV, et al. Spectroscopic investigations on 1.53 μm NIR emission of Er^{3+} doped multicomponent borosilicate glasses for telecommunication and lasing applications. *Mater Chem Phys* 2021;261:124223.
- [21] Gomes JF, Lima AMO, Sandrini M, Medina AN, Steimacher A, Pedrochi F, et al. Optical and spectroscopic study of erbium doped calcium borotellurite glasses. *Opt Mater* 2017;66:211–9.
- [22] Ouannes K, Lebbou K, Walsh BM, Poulain M, Alombert-Goget G, Guyot Y. New Er^{3+} doped antimony oxide based glasses: thermal analysis, structural and spectral properties. *J Alloys Compd* 2015;649:564–72.
- [23] Asirvadam A, Kumar VR, Nagarjuna M, Raju GN, Prasad PS, Baskaran GS, et al. Optical and luminescence properties of Er^{3+} doped $\text{Sb}_2\text{O}_3-\text{Li}_2\text{O}-\text{MO}$ ($\text{M}=\text{Mg}$, Ca and Sr) glasses. *Opt Mater* 2022;128:112422.
- [24] Zhang W, Lin L, Lan B, Liu J, Chen Y, Zhou G, et al. Er^{3+} -doped antimony-silica glass and fiber for broadband optical amplification. *J Am Ceram Soc* 2021;104:5584–92.
- [25] Xu S, Yang Z, Dai S, Yang J, Hu L, Jiang Z. Spectral properties and thermal stability of Er^{3+} -doped oxyfluoride silicate glasses for broadband optical amplifier. *J Alloys Compd* 2003;361:313–9.
- [26] Serqueira EO, de Moraes RF, Dantas NO. Controlling the spectroscopic parameters of Er^{3+} -doped sodium silicate glass by tuning the Er_2O_3 and Na_2O concentrations. *J Alloys Compd* 2013;560:200–7.
- [27] Chen Q, Wang H, Wang Q, Chen Q. Structural study of the origin of the largest 1.5 μm Er^{3+} luminescence band width in multicomponent silicate glass. *J Non-Cryst Solids* 2014;404:145–50.
- [28] Devarajulu G, Lakshminarayana G, Venkateswara Rao P, Lee Dong-Eun, Yoon Jonghun, Park Taejoon. Er^{3+} -doped SiO_2 -based glasses – an exploration of structural, visible, chromatic, and NIR fluorescence characteristics. *Mater Res Bull* 2022;147:111634.
- [29] Yang J, Dai S, Zhou Y, Wen L, Hu L, Jiang Z. Spectroscopic properties and thermal stability of erbium doped bismuth-based glass for optical amplifier. *J Appl Phys* 2003;93:977–83.
- [30] Wang R, Yang Z, Zhou D, Song Z, Qiu J. Structure and luminescent property of Er^{3+} -doped germanate glasses. *J Non-Cryst Solids* 2014;383:200–4.
- [31] Marcondes LM, Evangelista RO, Goncalves RR, de Camargo ASS, Manzani Danilo, Naline M, et al. Er^{3+} -doped niobium alkali germanate glasses and glass-ceramics: NIR and visible luminescence properties. *J Non-Cryst Solids* 2019;521:119492.
- [32] Marcondes LM, da Cunha CR, de Sousa BP, Maestri S, Gonçalves RR, Cassanjes FC, et al. Thermal and spectroscopic properties studies of Er^{3+} -doped and $\text{Er}^{3+}/\text{Yb}^{3+}$ -codoped niobium germanate glasses for optical applications. *J Lumin* 2019;205:487–94.
- [33] Chen H, Liu YH, Zhou YF, Jiang ZH. Spectroscopic properties of Er^{3+} -doped tellurite glass for a 1.55 μm optical amplifier. *J Alloys Compd* 2005;397:286–90.
- [34] Jaba N, Mansour HB, Kanoun A, Brenier A, Champagnon B. Spectral broadening and luminescence quenching of 1.53 μm emission in Er^{3+} -doped zinc tellurite glass. *J Lumin* 2009;129:270–6.
- [35] Dousti MR, Amjad RJ, Sahar MR, Zabidi ZM, Alias AN, de Camargo ASS. Er^{3+} -doped zinc tellurite glasses revisited: concentration dependent chemical durability, thermal stability and spectroscopic properties. *J Non-Cryst Solids* 2015;429:70–8.
- [36] Sajna MS, Thomas S, Jayakrishnan C, Joseph C, Biju PR, Unnikrishnan NV. NIR emission studies and dielectric properties of Er^{3+} -doped multicomponent tellurite glasses. *Spectrochim. Acta A* 2016;161:130–7.
- [37] Lemiere A, Bondziar B, Aromaki I, Petit L. Study of visible, NIR, and MIR spectroscopic properties of Er^{3+} -doped tellurite glasses and glass-ceramics. *J Am Ceram Soc* 2022;105:7186–95.
- [38] Choi YG, Kim KH. Spectroscopic properties of and energy transfer in $\text{PbO}-\text{Bi}_2\text{O}_3-\text{Ga}_2\text{O}_3$ glass doped with Er_2O_3 . *J Am Ceram Soc* 1999;82:2762–8.
- [39] Kassab LRP, Courrol LC, Seragioli R, Wetter NU, Tatumi SH, Gomes L. Er^{3+} laser transition in $\text{PbO}-\text{PbF}_2-\text{B}_2\text{O}_3$ glasses. *J Non-Cryst Solids* 2004;348:94–7.
- [40] Yamauchi H, Ohishi Y. Spectroscopic properties of Er^{3+} -doped $\text{PbO}-\text{Ga}_2\text{O}_3-\text{GeO}_2$ glass for optical amplifiers. *Opt Mater* 2005;27:679–90.
- [41] Santos CC, Guedes I, Loong C-K, Boatner LA, Moura AL, de Araujo MT, et al. Spectroscopic properties of Er^{3+} -doped lead phosphate glasses for photonic application. *J Phys D Appl Phys* 2010;43:025102.
- [42] Santos CC, Rocha U, Guedes I, Vermelho MVD, Boatner LA, Jacinto C. Thermal lens study of thermo-optical properties and concentration quenching of Er^{3+} -doped lead pyrophosphate-based glasses. *J Appl Phys* 2012;111:123101.
- [43] Jiang S, Myers M, Peyghambarian N. Er^{3+} doped phosphate glasses and lasers. *J Non-Cryst Solids* 1998;239:143–8.
- [44] Babu P, Seo HJ, Jang KH, Balakrishnaiah R, Jayasankar CK, Lim K-S, et al. Optical spectroscopy, 1.5 μm emission, and

- upconversion properties of Er³⁺-doped metaphosphate laser glasses. *J Opt Amer Soc B* 2007;24:2218–28.
- [45] Pradeesh K, Oton CJ, Agotiya VK, Raghavendra M, Vijaya Prakash G. Optical properties of Er³⁺ doped alkali chlorophosphate glasses for optical amplifiers. *Opt Mater* 2008;31:155–60.
- [46] Choi JH, Shi FG, Margaryan A, Margaryan A, van der Veer W. Novel alkaline-free Er³⁺-doped fluorophosphate glasses for broadband optical fiber lasers and amplifiers. *J Alloys Compd* 2008;450:540–5.
- [47] Gonçalves TS, Moreira Silva RJ, de Oliveira Junior M, Ferrari CR, Poirier GY, Eckert H, et al. Structure-property relations in new fluorophosphate glasses singly and co-doped with Er³⁺ and Yb³⁺. *Mater Chem Phys* 2015;157:45–55.
- [48] Linganna K, Suresh K, Ju S, Han W-T, Jayasankar CK, Venkatramu V. Optical properties of Er³⁺-doped K-Ca-Al fluorophosphate glasses for optical amplification at 1.53 μm. *Opt Mater Express* 2015;5:1689–703.
- [49] Pugliese D, Boetti NG, Lousteau J, Ceci-Ginistrelli E, Bertone E, Geobaldo F, et al. Concentration quenching in an Er-doped phosphate glass for compact optical lasers and amplifiers. *J Alloys Compd* 2016;657:678–83.
- [50] Lopez-Isocha P, Petit L, Massera J, Janner D, Boetti NG, Pugliese D, et al. Effect of the addition of Al₂O₃, TiO₂ and ZnO on the thermal, structural and luminescence properties of Er³⁺-doped phosphate glasses. *J Non-Cryst Solids* 2017;460:161–8.
- [51] Kuusela L, Veber A, Boetti NG, Petit L. Impact of ZnO addition on Er³⁺ near-infrared emission, the formation of Ag nanoparticles, and the crystallization of sodium fluorophosphate glass. *Materials* 2020;13:527.
- [52] Shams MS, Marzouk SY, El-Refaey AM, Abdel-Hafez SH, Olarinoye IO, Rammah YS. Fabrication, linear/nonlinear optical properties, Judd-Ofelt parameters and gamma-ray attenuation capacity of Er₂O₃ doped P₂O₅-ZnO-CdO glasses. *J Mater Res Technol* 2021;15:5540–53.
- [53] Shoaib M, Khan I, Chanthima N, Alhuthali Abdullah, Intachai N, Kothan S, et al. Photoluminescence analysis of Er³⁺-ions doped P₂O₅-Gd₂O₃/GdF₃-BaO-ZnO glass systems. *J Alloys Compd* 2022;902:163766.
- [54] Pisarski WA, Pisarska J, Dorosz D, Dorosz J. Towards lead-free oxyfluoride germanate glasses singly doped with Er³⁺ for long-lived near-infrared luminescence. *Mater Chem Phys* 2014;148:485–9.
- [55] Leśniak M, Mach G, Starzyk B, Sadowska K, Ragiń T, Żmojda J. The effect of fluorides (BaF₂, MgF₂, AlF₃) on structural and luminescent properties of Er³⁺-doped gallo-germanate glass. *Materials* 2022;15:5230.
- [56] Pisarski WA, Kowalska K, Kuwik M, Polak J, Pietrasik E, Goryczka T, et al. Novel multicomponent titanate-germanate glasses: synthesis, structure, properties, transition metal, and rare earth doping. *Materials* 2020;13:4422.
- [57] Bozelli JC, de Oliveira Nunes LA, Sigoli FA, Mazali IO. Erbium and ytterbium codoped titanoniobophosphate glasses for ion-exchange-based planar waveguides. *J Am Ceram Soc* 2010;93:2689–92.
- [58] De Mello LB, Sigoli FA, Mazali IO. Structural and optical properties of erbium and ytterbium codoped germanoniobophosphate glasses. *J Am Ceram Soc* 2014;97:2462–70.
- [59] Jamalaih BC, Suhasini T, Moorthy LR, Reddy KJ, Kim I-G, Yoo D-S, et al. Visible and near infrared luminescence properties of Er³⁺-doped LBTAf glasses for optical amplifiers. *Opt Mater* 2012;34:861–7.
- [60] Elsaghier HM, Azooz MA, Zidan NA, Abbas W, Okasha A, Marzouk SY. The influence of Er³⁺ ions on the spectroscopic and lasing characteristics of alkaline earth titanium borate glasses for photonic applications. *Opt Mater* 2022;131:112624.
- [61] Lakshminarayana G, Qiu J, Brik MG, Kumar GA, Kityk IV. Spectral analysis of Er³⁺-, Er³⁺/Yb³⁺- and Er³⁺/Tm³⁺/Yb³⁺-doped TeO₂-ZnO-WO₃-TiO₂-Na₂O glasses. *J Phys Condens Matter* 2008;20:375101.
- [62] Baki SO, Tan LS, Kan CS, Kamari HM, Noor ASM, Mahdi MA. Structural and optical properties of Er³⁺-Yb³⁺ codoped multicomposition TeO₂-ZnO-PbO-TiO₂-Na₂O glass. *J Non-Cryst Solids* 2013;362:156–61.
- [63] Leal JJ, Narro-García R, Flores-De los Ríos JP, Gutierrez-Mendez N, Ramos-Sánchez VH, González-Castillo JR, et al. Effect of TiO₂ on the thermal and optical properties of Er³⁺/Yb³⁺ co-doped tellurite glasses for optical sensor. *J Lumin* 2019;208:342–9.
- [64] Krishnaiah KV, Marques-Hueso J, Suresh K, Venkataiah G, Richards BS, Jayasankar CK. Spectroscopy and near infrared upconversion of Er³⁺-doped TZNT glasses. *J Lumin* 2016;169:270–6.
- [65] Pisarski WA, Janek J, Pisarska J, Lisiecki R, Ryba-Romanowski W. Influence of excitation wavelengths on up-converted luminescence sensing behavior of Er³⁺ ions in lead-free germanate glass. *J Lumin* 2018;193:34–8.
- [66] Xu R, Tian Y, Hu L, Zhang J. Enhanced emission of 2.7 μm pumped by laser diode from Er³⁺/Pr³⁺-codoped germanate glasses. *Opt Lett* 2011;36:1173–5.
- [67] Han K, Zhang P, Wang S, Guo Y, Zhou D, Yu F. Optical characterization of Tm³⁺ doped Bi₂O₃-GeO₂-Ga₂O₃ glasses in absence and presence of BaF₂. *Sci Rep* 2016;6:31207.
- [68] Wen X, Tang G, Yang Q, Chen X, Qian Q, Zhang Q, et al. Highly Tm³⁺ germanate glass and its single mode fiber for 2.0 μm laser. *Sci Rep* 2016;6:20344.
- [69] M. Hongisto, O. Linros, S. Danto, V. Jubera, L. Petit, Impact of Al₂O₃, TiO₂ and ZnO addition on the crystallization of Yb³⁺ doped phosphate glass-ceramic, *Mater Res Bull* 157 (2023) 112032.
- [70] Pisarska J, Kuwik M, Górný A, Kochanowicz M, Żmojda J, Dorosz J, et al. Holmium doped barium gallo-germanate glasses for near-infrared luminescence at 2000 nm. *J Lumin* 2019;215:116625.
- [71] Judd BR. Optical absorption intensities of rare-earth ions. *Phys Rev* 1962;127:750–61.
- [72] Ofelt GS. Intensities of crystal spectra of rare-earth ions. *J Chem Phys* 1962;37:511–20.
- [73] Carnall WT, Fields PR, Rajnak K. Electronic energy levels in the trivalent lanthanide aquo ions. I. Pr³⁺, Nd³⁺, Pm³⁺, Sm³⁺, Dy³⁺, Ho³⁺, Er³⁺, and Tm³⁺. *J Chem Phys* 1968;49:4424–42.
- [74] Pisarski WA, Kowalska K, Kuwik M, Pisarska J, Dorosz J, Żmojda J, et al. Nd³⁺ doped titanate-germanate glasses for near-IR laser applications. *Opt Mater Express* 2022;12:2912–26.
- [75] Sailaja P, Mahamuda Sk, Swapna K, Venkateswarlu M, Gupta M, Rao AS. Broadband NIR emission at 1.53 μm in trivalent erbium ions doped SrO-Al₂O₃-B₂O₃-BaCl₂-10TeO₂ glasses for optical fiber and NIR laser applications. *J Non-Cryst Solids* 2021;567:120937.
- [76] Arunkumar S, Marimuthu K. Spectroscopic properties of Er³⁺-doped bismuth lead telluroborate glasses for 1.53 μm optical amplifiers. *J Alloys Compd* 2015;627:54–68.
- [77] Rivera VAG, Barbosa LC. Spectroscopic properties of Er³⁺-doped sodium-modified tellurite glasses for use as optical amplifiers at 1540 nm. *J Lumin* 2014;156:116–23.
- [78] Wang R, Zhou D, Zhao Z, Yang Z, Song Z, Zhu K, et al. Effect of optical basicity on broadband infrared fluorescence in erbium-doped germanate glasses. *J Alloys Compd* 2012;513:339–42.
- [79] Shi DM, Zhao YG, Wang XF, Liao GH, Zhao C, Peng MY, et al. Effects of alkali ions on thermal stability and spectroscopic properties of Er³⁺-doped gallogermanate glasses. *Physica B* 2011;406:628–32.

- [80] Yang Z, Xu S, Dai S, Yang J, Hu L, Jiang Z. Thermal stability and optical transition of Er^{3+} in sodium-lead-germanate glasses. *J Mater Sci* 2004;39:3641–6.
- [81] Lin H, Pun EYB, Man SQ, Liu XR. Optical transitions and frequency upconversion of Er^{3+} ions in $\text{Na}_2\text{O}\cdot\text{Ca}_3\text{Al}_2\text{Ge}_3\text{O}_{12}$ glasses. *J. Opt. Amer. Soc. B* 2001;18:602–9.
- [82] Zheng S, Zhou Y, Yin D, Xu X, Qi Y, Peng S. The 1.53 μm spectroscopic properties and thermal stability in $\text{Er}^{3+}/\text{Ce}^{3+}$ codoped $\text{TeO}_2\text{-WO}_3\text{-Na}_2\text{O-Nb}_2\text{O}_5$ glasses. *J Quant Spectrosc Radiat Transf* 2013;120:44–51.
- [83] Kumar MVV, Gopal KR, Reddy RR, Reddy GVL, Jamalaiah BC. Luminescence and gain characteristics of 1.53 μm broadband of Er^{3+} in lead telluroborate glasses. *J Lumin* 2013;142:128–34.
- [84] Reddy AA, Babu SS, Pradeesh K, Otton CJ, Prakash GV. Optical properties of highly Er^{3+} -doped sodium–aluminium–phosphate glasses for broadband 1.5 μm emission. *J Alloys Compd* 2011;509:4047–52.
- [85] Linganna K, Rathaiah M, Vijaya N, Basavapoornima Ch, Jayasankar CK, Ju S, et al. 1.53 μm luminescence properties of Er^{3+} -doped K–Sr–Al phosphate glasses. *Ceram Int* 2015;41:5765–71.
- [86] Basavapoornima Ch, Linganna K, Kesavulu CR, Ju S, Kim BH, Han W-T, et al. Spectroscopic and pump power dependent upconversion studies of Er^{3+} -doped lead phosphate glasses for photonic applications. *J Alloys Compd* 2017;699: 959–68.
- [87] Liao M, Hu L, Duan Z, Zhang L, Wen L. Spectroscopic properties of fluorophosphate glass with high Er^{3+} concentration. *Appl Phys B* 2007;86:83–9.
- [88] Rasool SkN, Jamalaiah BC, Suresh K, Moorthy LR, Jayasankar CK. Spectroscopic properties of Er^{3+} -doped phosphate based glasses for broadband 1.54 μm emission. *J Mol Struct* 2017;1130:837–43.
- [89] Ramachari D, Moorthy LR, Jayasankar CK. Gain properties and concentration quenching of Er^{3+} -doped niobium oxyfluorosilicate glasses for photonic applications. *Opt Mater* 2014;36:823–8.
- [90] Wei T, Chen F, Tian Y, Xu S. Broadband 1.53 μm emission property in Er^{3+} doped germa-silicate glass for potential optical amplifier. *Opt Commun* 2014;315:199–203.
- [91] Devarajulu G, Ravi O, Reddy CM, Ahamed SdZA, Raju BDP. Spectroscopic properties and upconversion studies of Er^{3+} -doped $\text{SiO}_2\text{-Al}_2\text{O}_3\text{-Na}_2\text{CO}_3\text{-SrF}_2\text{-CaF}_2$ oxyfluoride glasses for optical amplifier applications. *J Lumin* 2018;194:499–506.
- [92] Kesavulu CR, Sreedhar VB, Jayasankar CK, Jang K, Shin D-S, Yi SS. Structural, thermal and spectroscopic properties of highly Er^{3+} -doped novel oxyfluoride glasses for photonic application. *Mater Res Bull* 2014;51:336–44.
- [93] Yuliantini L, Djamal M, Hidayat R, Boonin K, Yasaka P, Kothan S, et al. IR emission of Er^{3+} ion-doped fluoroborotellurite glass for communication application. *J Non-Cryst Solids* 2021;566:120849.

P7

Wojciech A. Pisarski, Karolina Kowalska, Marta Kuwik, Joanna Pisarska, Dominik
Dorosz, Marcin Kochanowicz, Jacek Żmojda, Jan Dorosz,
Enhanced mid-IR luminescence of Er³⁺ ions at 2.7 μm
in TiO₂-GeO₂-BaO-Ga₂O₃ glasses
Journal of Luminescence 265 (2024) 120227



Contents lists available at ScienceDirect

Journal of Luminescence

journal homepage: www.elsevier.com/locate/jlumin

Full Length Article

Enhanced mid-IR luminescence of Er³⁺ ions at 2.7 μm in TiO₂-GeO₂-BaO-Ga₂O₃ glasses

Wojciech A. Pisarski^{a,*}, Karolina Kowalska^a, Marta Kuwik^a, Joanna Pisarska^a,
Dominik Dorosz^b, Marcin Kochanowicz^c, Jacek Żmojda^c, Jan Dorosz^c

^a University of Silesia, Institute of Chemistry, Szkolna 9 Street, 40-007, Katowice, Poland

^b AGH University of Science and Technology, Faculty of Materials Science and Ceramics, 30 Mickiewicza Avenue, 30-059, Krakow, Poland

^c Białystok University of Technology, Faculty of Electrical Engineering, Wiejska 45D Street, 15-351, Białystok, Poland

ARTICLE INFO

Keywords:

Glasses

Er³⁺ ions

Mid-infrared luminescence

Spectroscopic properties

ABSTRACT

Er³⁺-doped glass based on TiO₂-GeO₂-BaO-Ga₂O₃ has been examined for mid-IR luminescence applications. Mid-IR luminescence corresponding to the ⁴I_{11/2} → ⁴I_{13/2} transition of Er³⁺ is enhanced in the presence of TiO₂. These effects are stronger for mid-IR emission at 2727 nm than near-IR emission at 1533 nm related to the ⁴I_{13/2} → ⁴I_{15/2} transition of Er³⁺. The gain bandwidth for the ⁴I_{11/2} → ⁴I_{13/2} transition of Er³⁺ is relatively large (σ_{em} × FWHM = 8.14 × 10⁻²⁶ cm³), which imply that glass with TiO₂ might be a promising candidate for efficient sources emitting mid-IR radiation.

1. Introduction

Nowadays there is a great interest in compact lasers operating in the near-IR (up to 2 μm) and mid-IR (2–5 μm) spectral ranges for optical communications, medical and eye-safe light detecting. These aspects are really important in the field of infrared photonics and material engineering [1] and have been examined for numerous systems from luminescent materials [2] and fiber based sources [3] to their optical device applications. Among rare earth ions, the trivalent Er³⁺ seems to be an excellent candidate for diode-pumped lasers emitting near-IR (1500 nm) and mid-IR (2700 nm) radiation due to ⁴I_{13/2} → ⁴I_{15/2} [4] and ⁴I_{11/2} → ⁴I_{13/2} [5] transitions, respectively. The rapid development of optical telecommunication and data-transmitting services demands to increase the transmission capacity of wavelength division multiplexing (WDM) systems. It requires broadband optical amplification beyond the conventional window (1500 nm, C-band) of Er³⁺-doped fiber amplifiers (EDFA) in order to fully utilize low-loss band of silica based optical fibers (1300–1700 nm).

On the other hand, broadband and/or tunable laser source operated at the mid-infrared region 2–5 μm (atmospheric transmission window, where the Earth's atmosphere is relatively transparent) is especially strongly demanded for the atmospheric, security and industrial applications. However, the stretching vibrations of hydroxyl groups OH⁻ varying with the glass composition are located in the 2700–3000 nm

spectral region and they are usually difficult to eliminate. The relatively high concentration of hydroxyl groups effectively quench luminescence from excited states of rare earth ions and this effect is especially important for Er³⁺-doped glasses emitting mid-infrared radiation at about 2700 nm. It clearly indicates that technological conditions during all steps from synthesis of precursor glass to fiber fabrication should be extremely rigorous. For that reason an ultra-dry atmosphere filled glove-box is strongly recommended and, in fact, absolutely required for glass preparation (including chemical batching, glass melting, preform making and annealing) in order to obtain the appropriate low OH content (below 1 ppm in weight). Thus, it is possible to fabricate dehydrated active glass fibers with relatively low OH content (1 ppm in weight) and low OH-induced attenuation (10 dB/m level in 3–4 μm region) showing promise for 2–5 μm mid-IR nonlinear applications. It was well presented and discussed in the excellent work published recently [6]. In order to further reducing the OH content to the level 0.1 ppm weight and the OH-induced loss to 1 dB/m level, the glass-host matrices with different oxide and fluoride glass-modifiers are tested and all parameters during glass and fiber fabrication are still optimized due to restricted procedure and technological conditions necessary for mid-IR emitting fibers. The recent studies indicate that the choice of the glass-host matrix is very important in order to achieve efficient mid-IR radiation. It is generally accepted that inorganic glasses with relatively low phonon energies have lower rates of non-radiative multiphonon relaxation. Extended

* Corresponding author.

E-mail address: wojciech.pisarski@us.edu.pl (W.A. Pisarski).

<https://doi.org/10.1016/j.jlumin.2023.120227>

Received 14 August 2023; Accepted 24 September 2023

Available online 25 September 2023

0022-2313/© 2023 Elsevier B.V. All rights reserved.

transparency in the IR range and low phonon energy of the host makes these glasses attractive for mid-IR emission and active fiber applications.

In practice, the mid-IR luminescence investigations were limited to low-phonon oxide (tellurite, germanate, bismuthate) and non-oxide (fluoride, chalcogenide) glass systems [7–11], which are more transparent in the IR range than classical silica glasses. The previously published work suggests that the Er^{3+} -doped ZrF_4 -based fluoride glasses are attractive for 2.7 μm laser materials [12], in contrast to oxide glasses. However, the chemical and mechanical stability of fluoride fibers is still poor and limits their applications.

From accumulated experience it is well known that mixed oxy-fluoride glasses are quite good practical alternative to oxide and fluoride glass systems for mid-IR fiber applications, because they combine very good mechanical properties and thermal stability of oxide glasses and improved radiative luminescence properties of fluoride glasses. The addition of fluoride modifiers to oxide glasses starts to enhance contribution of radiative transitions and results in significant increasing spectroscopic parameters of rare earth ions such as luminescence lifetimes, quantum efficiencies and stimulated emission cross-sections. Thus, the Er^{3+} -doped fluoro-tellurite glass is considered as a new choice for 2.7 μm lasers [13]. The Er^{3+} doped tellurite fibers showing broadband 2.7 μm amplified spontaneous emission were also fabricated, which are really important in relation to practical mid-IR laser applications [14]. Compared with tellurite glasses having lower phonon energy, germanate glasses have relatively higher glass transition temperature as well as stronger chemical and mechanical stability. Consequently, it makes germanate glass have a good thermal stability to resist thermal damage at high pumping intensities. However, there have been only a few reports on the Er^{3+} doped germanate glasses for mid-infrared fiber applications. It was stated that mid-IR luminescence at 2700 nm depends critically on the population behavior between $^4I_{11/2}$ state and lower-lying $^4I_{13/2}$ state of Er^{3+} ions in germanate glasses [15]. Mid-infrared luminescence properties of Er^{3+} -doped germanate based glasses have been examined under 808 nm [16] and 980 nm [17] excitation. Further studies confirmed that the addition of various glass-modifiers to the base glass influenced significantly on mid-IR emission of erbium. The previously published works indicate that mid-IR luminescence of Er^{3+} ions in germanate glasses depends on the network-modifiers R_2O_3 , where $\text{R}=\text{La}$ or Y [18], Y_2O_3 and Nb_2O_5 [19], TeO_2 [20] and Bi_2O_3 [21]. These aspects were not yet examined for germanate based glass in the presence of titanium dioxide. Recently, near-IR luminescence properties of rare earth ions due to $^4F_{3/2} \rightarrow ^4I_{11/2}$ transition of Nd^{3+} at 1060 nm [22] and $^4I_{13/2} \rightarrow ^4I_{15/2}$ transition at 1500 nm [23] have been analyzed for germanate glass in function of TiO_2 content. Systematic investigations revealed that Er^{3+} -doped germanate glass with higher TiO_2 content (40 mol %) is suitable for broadband near-IR laser gain active media operating at 1.5 μm [23].

In this work, mid-IR emission of Er^{3+} in $\text{TiO}_2\text{-GeO}_2\text{-BaO-Ga}_2\text{O}_3$ glass has been examined in details. Based on luminescence spectra at 2700 nm and their decays, some spectroscopic parameters for Er^{3+} ions (the luminescence bandwidth and lifetime, the stimulated emission cross-section, the gain bandwidth) were determined for glasses with the absence and presence of TiO_2 . It is evidently seen that mid-IR emission of Er^{3+} ions is greatly enhanced with TiO_2 . Therefore, Er^{3+} -doped glass based on $\text{TiO}_2\text{-GeO}_2\text{-BaO-Ga}_2\text{O}_3$ is strongly recommended for broadband mid-IR luminescent sources operating at 2.7 μm .

2. Experimental

Glasses with the following molar compositions 40 TiO_2 -20 GeO_2 -30 BaO -9.5 Ga_2O_3 -0.5 Er_2O_3 denoted here as TGBG and 60 GeO_2 -30 BaO -9.5 Ga_2O_3 -0.5 Er_2O_3 (GBG) were prepared using melt quenching technique. The appropriate amounts of metal oxides of high purity (99.99%, Aldrich Chemical Co.) were mixed homogeneously together and then melted at 1200 $^\circ\text{C}$ for 0.45 h. Glass samples were polished for optical measurements. Next, they were characterized using by DSC, FT-IR and

luminescence methods. The DSC curves were acquired using a SETARAM Labsys thermal analyzer (SETARAM Instrumentation, Caluire, France) with heating rate of 10 $^\circ\text{C}/\text{min}$. Transmittance spectra were performed on the Nicolet iS50 ATR spectrometer in IR frequency region. Details for emission measurements (spectra and decays) are given in our previous work [23]. Measurements in wide range of 1000–3100 nm were carried out using an Acton 2300i monochromator equipped with a PbSe detector (Teledyne, Princeton Instruments, Acton, MA, USA) with a lock-in detection (Stanford Research Systems, Sunnyvale, CA, USA) setup and high power Roithner Lasertechnik GmbH (Vienna, Austria) laser diode ($\lambda_{\text{exc}} = 976$ nm, $P_{\text{opt(max)}} = 1$ W) as an excitation source. Resolution for spectral measurements was ± 0.1 nm. Decay curves were recorded with an accuracy of ± 0.5 μs .

3. Results and discussion

Fig. 1 presents DSC curves measured for glass samples without (GBG) and with TiO_2 (TGBG). From DSC curves the glass transition temperature T_g and the thermal stability parameter ($\Delta T = T_x - T_g$) were determined. They are also schematized on Fig. 1.

The glass transition temperature T_g increases from 620 $^\circ\text{C}$ to 705 $^\circ\text{C}$, whereas the thermal stability parameter is reduced from 187 $^\circ\text{C}$ to 80 $^\circ\text{C}$ in the presence of TiO_2 . Although the ΔT factor was decreased significantly, we suggest that our glass with TiO_2 exhibits still good thermal stability necessary for fiber drawing, when we compared to the values of ΔT (80 \div 85 $^\circ\text{C}$) obtained earlier for some mid-infrared emitting glasses based on AlF_3 [24] and $\text{PbO-PbF}_2\text{-Bi}_2\text{O}_3\text{-Ga}_2\text{O}_3$ glasses [25].

Further analysis for fluorotellurite glass systems [26–28] indicates that Er^{3+} -doped low-hydroxyl glasses are strongly demanded for laser applications at 2.7 μm . Our glass TGBG with TiO_2 also meets these requirements, because the residual absorption of OH^- groups is reduced drastically compared to GBG glass (without TiO_2). Fig. 2 presents transmittance spectra measured for glass samples without (GBG) and with TiO_2 (TGBG). Inset shows transmittance spectra registered in the range, where characteristic band due to hydroxyl groups occurs.

The IR absorption coefficient α_{OH} (given in cm^{-1}) was calculated using the following expression $\alpha_{\text{OH}} = (1/L) \ln(T_0/T)$, where: L is the thickness of the glass, T_0 and T are the transmission value of maximum and at 3 μm , respectively. The IR absorption coefficient for GBG glass is equal to 0.25 cm^{-1} , which is comparable to the value $\alpha_{\text{OH}} = 0.196$ cm^{-1} obtained for the $\text{Er}^{3+}/\text{Pr}^{3+}$ co-doped germanate glass without any hydroxyl removal process [29]. For TGBG glass with TiO_2 , the IR absorption coefficient is extremely low ($\alpha_{\text{OH}} < 0.05$ cm^{-1}) and its value is

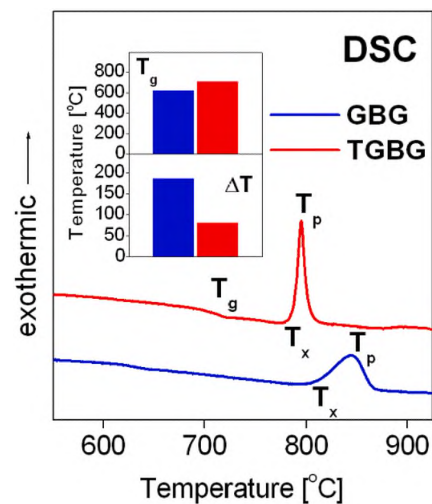


Fig. 1. DSC curves for glasses without (GBG) and with TiO_2 (TGBG).

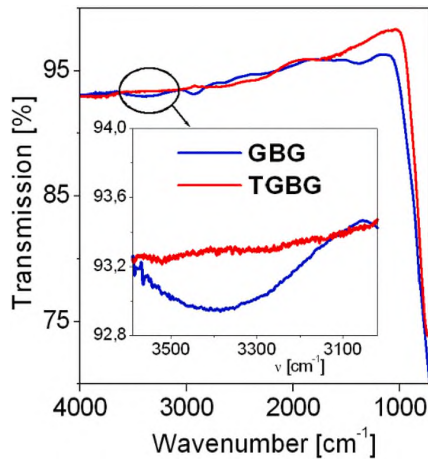


Fig. 2. Transmittance spectra for glasses without (GBG) and with TiO₂ (TGBG).

difficult to calculate with good accuracy. It is possible to obtain, because samples were prepared under rigorous technological conditions in glove-box, in a protective atmosphere of dried argon of high purity. The restrictive procedure has been also implemented for some Er³⁺-doped glasses [25–28]. The extremely low IR absorption coefficients (α_{OH} between 0.03 and 0.07 cm⁻¹) were achieved. This is an efficient way to fabricate precursor glasses attractive for optical fibers emitting mid-IR radiation.

Fig. 3 shows near-IR and mid-IR luminescence spectra of Er³⁺ ions centered at 1533 nm (on left) and 2727 nm (on right), which were measured for glass samples with the absence and presence of TiO₂. The infrared emission spectra were excited by 976 nm line. Luminescence bands correspond to the ⁴I_{13/2} → ⁴I_{15/2} (near-IR) and ⁴I_{11/2} → ⁴I_{13/2} (mid-IR) laser transitions of Er³⁺, respectively.

It is well evidenced that both near-IR and mid-IR emission lines are enhanced in the presence of TiO₂. The emission bandwidth referred as full width at half maximum (FWHM) increases from 48 nm (GBG) to 70 nm (TGBG) for ⁴I_{13/2} → ⁴I_{15/2} near-IR transition at 1533 nm, whereas the value of FWHM is reduced from 126 nm (GBG) to 118 nm (TGBG) for ⁴I_{11/2} → ⁴I_{13/2} mid-IR transition at 2727 nm, when GeO₂ is partially substituted by TiO₂ (40 mol%) in glass composition. Furthermore, the spectral bandwidths (FWHM) and the radiative transition probabilities A_J calculated using the Judd-Ofelt theory and adopted from Ref. [23] were applied to determine the peak stimulated emission cross-sections σ_{em} for the ⁴I_{11/2} → ⁴I_{13/2} transition of Er³⁺, which characterize the potential mid-IR laser performance of the glass-host. The values of σ_{em} were calculated using well-known relation given elsewhere [10]. The refractive indices *n* equal to 1.736 (GBG) and 1.998 (TGBG) were used

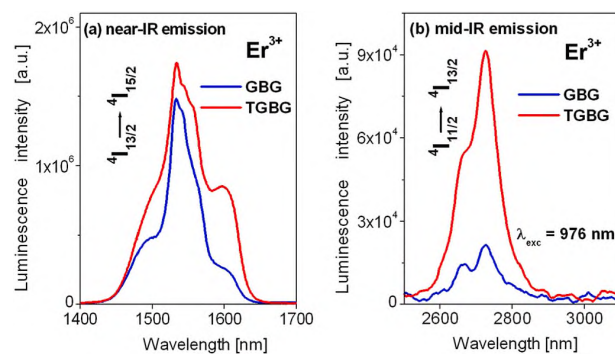


Fig. 3. Near-IR (a) and mid-IR (b) luminescence spectra of Er³⁺ ions for glasses without (GBG) and with TiO₂ (TGBG).

for calculation. The values of σ_{em} are compared to the results for some inorganic glasses emitting mid-IR radiation [29–36]. They are shown in Table 1.

For the studied glass GBG without TiO₂, the peak stimulated emission cross-section is close to $0.41 \times 10^{-20} \text{cm}^2$ and its value is similar to $0.45 \times 10^{-20} \text{cm}^2$ obtained for oxyfluoride tellurite glass [36]. The stimulated emission cross-section for the ⁴I_{11/2} → ⁴I_{13/2} transition of Er³⁺ at 2727 nm is increased from $0.41 \times 10^{-20} \text{cm}^2$ (GBG) to $0.69 \times 10^{-20} \text{cm}^2$ (TGBG) in the presence of TiO₂. You can see that the emission cross-section for the ⁴I_{11/2} → ⁴I_{13/2} mid-IR transition of Er³⁺ in glass with TiO₂ ($0.69 \times 10^{-20} \text{cm}^2$) is comparable with the values σ_{em} ranging between 0.57 and 0.77 (in 10^{-20}cm^2) for some inorganic glasses [29–35]. However, the values of σ_{em} can be much higher (σ_{em} above $0.7 \times 10^{-20} \text{cm}^2$) for fluoride glasses [37] or glass-ceramics [38] emitting mid-IR radiation at 2.7 μm .

Further spectroscopic analysis for glass TGBG with TiO₂ indicates that the integrated emission intensity for the ⁴I_{11/2} → ⁴I_{13/2} transition at 2727 nm is enhanced more significantly (3.4-fold increase) than for the ⁴I_{13/2} → ⁴I_{15/2} transition at 1533 nm (1.6-fold increase) compared to GBG glass. This situation is really promising for mid-IR emission. It is generally accepted that the upper state ⁴F_{7/2} (Er³⁺) is well populated through well-known ground state absorption (ESA) and excited state absorption (ESA) under 976 nm excitation [29]. The excitation energy transfers very fast to the ⁴I_{11/2} and ⁴I_{13/2} states of Er³⁺. Two energy transfer up-conversion processes ETU1 and ETU2 are responsible for depopulation of ⁴I_{11/2} and ⁴I_{13/2} states of Er³⁺. It was schematized on the energy level diagram (Fig. 4).

In particular, the most important is process ETU2, which depopulates state ⁴I_{13/2} giving important contribution to the enhanced probability of the radiative transition ⁴I_{11/2} → ⁴I_{13/2} and stronger mid-IR emission at 2.7 μm [29]. In our case, mid-IR emission originating from the ⁴I_{11/2} state of Er³⁺ in glass TGBG with TiO₂ increases much more rapidly than near-IR emission at 1.5 μm compared to the results obtained for glass GBG. Our luminescence investigations clearly indicate that the lower-lying state ⁴I_{13/2} (Er³⁺) is more efficiently depopulated than the higher-lying state ⁴I_{11/2} state. Luminescence decay curve analysis confirms this hypothesis.

Luminescence decays from the ⁴I_{13/2} and ⁴I_{11/2} states of Er³⁺ ions in glass samples without (GBG) and with TiO₂ (TGBG) are presented in Fig. 5. Based on decay curve measurements luminescence lifetimes for the ⁴I_{13/2} and ⁴I_{11/2} states of Er³⁺ ions were calculated. The ⁴I_{13/2} lifetime is slightly reduced from 5.35 ms (GBG) to 5.04 ms (TGBG), whereas two-fold increase from 69 μs (GBG) to 138 μs (TGBG) is observed for the ⁴I_{11/2} lifetime of Er³⁺ in glass with TiO₂. The ⁴I_{11/2} lifetime of Er³⁺ in glass with TiO₂ is comparable to the value of $\tau_m = 124 \mu\text{s}$ obtained for tellurite glass modified by GeO₂ [39]. Based on emission spectra and their decays it also suggests that TiO₂ modifies germanate glass-network and the local crystal field around the Er³⁺ ions influencing strongly on their luminescence properties. Similar effects were also observed earlier for Er³⁺ doped silica films modified by HfO₂ [40,41] giving important

Table 1

The peak stimulated emission cross-sections for the ⁴I_{11/2} → ⁴I_{13/2} transition of Er³⁺ ions in glass samples without (GBG) and with TiO₂ (TGBG). The values of σ_{em} are compared to the results obtained earlier for some inorganic glasses.

Glass host	$\sigma_{em} \times 10^{-21} \text{cm}^2$	Ref.
Germanate	7.00	[29]
Bismuthate germanate	7.73	[30]
Chalcohalide	6.60	[31]
Fluorophosphate	6.57	[32]
ZBLAN	6.10	[33]
Tungsten-tellurite	6.05	[34]
ZBSY	5.67	[35]
Oxyfluoride tellurite	4.50	[36]
GBG	4.10	this work
TGBG	6.90	this work

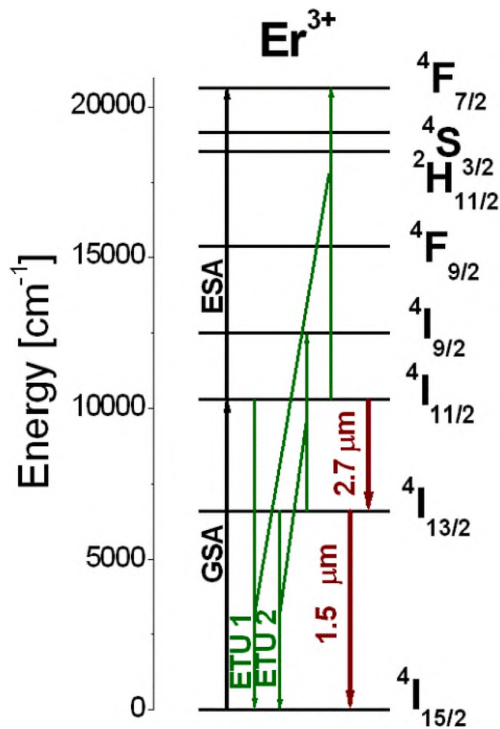


Fig. 4. Energy level scheme for Er^{3+} ions. All transitions are also indicated.

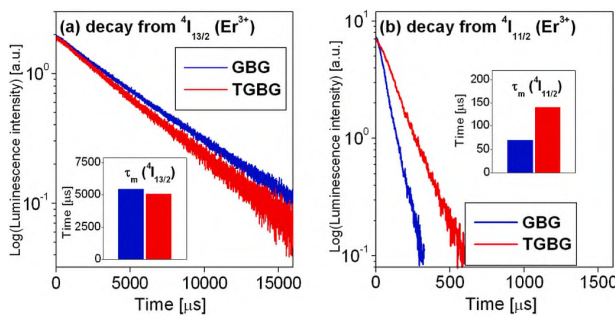


Fig. 5. Luminescence decays from the ${}^4I_{13/2}$ (a) and ${}^4I_{11/2}$ (b) states of Er^{3+} ions in glasses without (GBG) and with TiO_2 (TGBG).

contribution to their optical characteristics in relation to optical waveguides at 1.5 μm and spherical resonators.

Finally, the emission bandwidth and the peak stimulated emission cross-section were applied to calculate the gain bandwidth ($\sigma_{\text{em}} \times \text{FWHM}$) for the ${}^4I_{11/2} \rightarrow {}^4I_{13/2}$ mid-IR transition of Er^{3+} ions. The gain bandwidth belongs to important laser parameters, which identify the lasing in glass-hosts and mid-IR broadband amplification. High values of $\sigma_{\text{em}} \times \text{FWHM}$ are strongly required to generate laser action in glass. In our case, the gain bandwidth is changed from $5.17 \times 10^{-26} \text{cm}^3$ (GBG) to $8.14 \times 10^{-26} \text{cm}^3$ (TGBG), respectively. Previous investigations for Er^{3+} -doped germanate glass based on $\text{GeO}_2\text{-Ga}_2\text{O}_3\text{-BaF}_2\text{-La}_2\text{O}_3\text{-Li}_2\text{O}$ give interesting results. Owing to large peak stimulated emission cross-section equal to $1.484 \times 10^{-20} \text{cm}^2$ and relatively lower emission bandwidth (55 nm), the $\text{GeO}_2\text{-Ga}_2\text{O}_3\text{-BaF}_2\text{-La}_2\text{O}_3\text{-Li}_2\text{O}$ glass exhibited high gain performance close to $8.16 \times 10^{-26} \text{cm}^3$, which makes it an excellent candidate for mid-IR luminescence applications at 2.7 μm [17]. The gain bandwidth for our glass with TiO_2 is similar, but the values of peak stimulated emission cross-section and emission

bandwidth for the ${}^4I_{11/2} \rightarrow {}^4I_{13/2}$ mid-IR transition of Er^{3+} ions are completely different. Compared to the results obtained previously by Cai et al. [17], our glass based on $\text{TiO}_2\text{-GeO}_2\text{-BaO-Ga}_2\text{O}_3$ (TGBG) shows relatively lower peak stimulated emission cross-section ($\sigma_{\text{em}} = 0.69 \times 10^{-20} \text{cm}^2$) and higher emission bandwidth (118 nm) giving superior gain performance, i.e. the gain bandwidth is close to $8.14 \times 10^{-26} \text{cm}^3$. These results imply that Er^{3+} -doped glass based on $\text{TiO}_2\text{-GeO}_2\text{-BaO-Ga}_2\text{O}_3$ might be a promising candidate for mid-IR luminescence applications.

4. Conclusions

In summary, the enhanced mid-IR luminescence of Er^{3+} centered at 2727 nm was observed in $\text{TiO}_2\text{-GeO}_2\text{-BaO-Ga}_2\text{O}_3$ glasses under 976 nm excitation. Mid-IR luminescence corresponds to the ${}^4I_{11/2} \rightarrow {}^4I_{13/2}$ transition of Er^{3+} . The peak stimulated emission cross-section and emission bandwidth were determined and their values are close to $0.69 \times 10^{-20} \text{cm}^2$ and 118 nm, respectively. The results suggest that glass with TiO_2 exhibiting large gain bandwidth ($\sigma_{\text{em}} \times \text{FWHM} = 8.14 \times 10^{-26} \text{cm}^3$) could be attractive for mid-IR luminescence at 2.7 μm .

Credit author statement

W.A. Pisarski: Conceptualization, Writing - Original Draft, Writing - review & editing, Project administration, Funding acquisition, Supervision. K. Kowalska: Investigation, Data Curation, Visualization M. Kuwik: Investigation, Data Curation, Validation J. Pisarska: Methodology, Investigation, Resources, Supervision D. Dorosz: Investigation, Formal analysis M. Kochanowicz: Investigation J. Żmojda: Investigation J. Dorosz: Formal analysis.

Declaration of competing interest

The authors declare that they have no known competing financial interests or personal relationships that could have appeared to influence the work reported in this paper.

Data availability

Data will be made available on request.

Acknowledgments

This research was funded by National Science Centre (Poland), grant number 2018/31/B/ST8/00166.

References

- [1] S. Jackson, R. Vallee, M. Bernier, Mid-Infrared Fiber Photonics: Glass Materials, Fiber Fabrication and Processing, Laser and Nonlinear Sources, Woodhead Publishing, 2021.
- [2] J. Hu, L. Mawst, S. Moss, L. Petit, D. Ting, Feature issue introduction: mid-infrared optical materials and their device applications, *Opt. Mater. Express* 8 (2018) 2026–2034.
- [3] S.D. Jackson, R.K. Jain, Fiber-based sources of coherent MIR radiation: key advances and future prospects (invited), *Opt. Express* 28 (2020) 30964–31019.
- [4] Z. Zhou, Y. Li, Y. Jiang, Z. Wang, P. Yin, L. Zhang, L. Zhang, Broadband near-infrared luminescence in erbium ion single-doped tellurite glass for optical amplification, *Opt. Lett.* 48 (2023) 815–818.
- [5] R. Xu, Y. Tian, L. Hu, J. Zhang, Origin of 2.7 μm luminescence and energy transfer process of Er^{3+} : ${}^4I_{11/2} \rightarrow {}^4I_{13/2}$ transition in $\text{Er}^{3+}/\text{Yb}^{3+}$ doped germanate glasses, *J. Appl. Phys.* 111 (2012), 033525.
- [6] X. Feng, J. Shi, M. Segura, N.M. White, P. Kannan, W.H. Loh, L. Calvez, X. Zhang, L. Brilland, Halotellurite glass fiber with low OH content for 2.5- μm mid-infrared nonlinear applications, *Opt. Express* 21 (2013) 18949–18954.
- [7] H. Zhan, Z. Zhou, J. He, A. Lin, Intense 2.7 μm emission of Er^{3+} -doped water-free fluorotellurite glasses, *Opt. Lett.* 37 (2012) 3408–3410.
- [8] Y.Y. Guo, M. Li, Intense 2.7 μm emission and structural origin in Er^{3+} -doped bismuthate ($\text{Bi}_2\text{O}_3\text{-GeO}_2\text{-Ga}_2\text{O}_3\text{-Na}_2\text{O}$) glass, *Opt. Lett.* 37 (2012) 268–270.

- [9] G. Li, L. Li, X. Huang, J. Tang, S. Dai, G. Wang, T. Xu, Q. Jiao, Er³⁺ doped and Er³⁺/Pr³⁺ co-doped gallium-antimony-sulphur chalcogenide glasses for infrared applications, *Opt. Mater. Express* 6 (2016) 3849–3856.
- [10] Y. Liu, M. Liao, X. Wang, G. Chen, L. Hu, Mid-infrared spectroscopy of novel Er³⁺ doped indium modified chalcogenide glasses, *J. Lumin.* 187 (2017) 1–8.
- [11] W. Ding, X. Zhang, L. Li, Q. Ding, S. Wu, S. Yu, J. Zhang, Enhanced mid-infrared emission of erbium-doped fluoro-bromozirconate glass, *Appl. Opt.* 57 (2018) 5380–5384.
- [12] F. Huang, Y. Guo, Y. Ma, L. Zhang, J. Zhang, Highly Er³⁺-doped ZrF₄-based fluoride glasses for 2.7 μm laser materials, *Appl. Opt.* 52 (2013) 1399–1403.
- [13] Y. Guo, G. Gao, M. Li, L. Hu, J. Zhang, Er³⁺-doped fluoro-tellurite glass: a new choice for 2.7 μm lasers, *Mater. Lett.* 80 (2012) 56–58.
- [14] W.C. Wang, J. Yuan, L.X. Li, D.D. Chen, Q. Qian, Q.Y. Zhang, Broadband 2.7 μm amplified spontaneous emission of Er³⁺ doped tellurite fibers for mid-infrared laser applications, *Opt. Mater. Express* 5 (2015) 2964–2977.
- [15] T. Wei, Y. Tian, C. Tian, X. Jing, J. Zhang, L. Zhang, S. Xu, Optical spectroscopy and population behavior between ⁴I_{11/2} and ⁴I_{13/2} levels of erbium doped germanate glass, *Opt. Mater. Express* 4 (2014) 2150–2165.
- [16] M. Cai, B. Zhou, F. Wang, Y. Tian, J. Zhou, S. Xu, J. Zhang, Mid-infrared emission and quantitative analysis of energy transfer processes in Er³⁺ doped oxyfluorogermanate glasses, *J. Appl. Phys.* 117 (2015), 243106.
- [17] M. Cai, T. Wei, B. Zhou, Y. Tian, J. Zhou, S. Xu, J. Zhang, Analysis of energy transfer process based emission spectra of erbium doped germanate glasses for mid-infrared laser materials, *J. Alloys Compd.* 626 (2015) 165–172.
- [18] M. Cai, B. Zhou, F. Wang, T. Wei, Y. Tian, J. Zhou, S. Xu, J. Zhang, R₂O₃ (R = La, Y) modified erbium activated germanate glasses for mid-infrared 2.7 μm laser materials, *Sci. Rep.* 5 (2015), 13056.
- [19] T. Wei, F. Chen, Y. Tian, S. Xu, Efficient 2.7 μm emission and energy transfer mechanism in Er³⁺ doped Y₂O₃ and Nb₂O₅ modified germanate glasses, *J. Quant. Spectrosc. Radiat. Transf.* 133 (2014) 663–669.
- [20] Y. Lu, M. Cai, R. Cao, S. Qian, S. Xu, J. Zhang, Er³⁺ doped germanate-tellurite glass for mid-infrared 2.7 μm fiber laser material, *J. Quant. Spectrosc. Radiat. Transf.* 171 (2016) 73–81.
- [21] T. Ragin, J. Zmojda, M. Kochanowicz, P. Miluski, P. Jelen, M. Sitarz, D. Dorosz, Enhanced mid-infrared 2.7 μm luminescence in low hydroxide bismuth-germanate glass and optical fiber co-doped with Er³⁺/Yb³⁺ ions, *J. Non-Cryst. Solids* 457 (2017) 169–174.
- [22] W.A. Pisarski, K. Kowalska, M. Kuwik, J. Pisarska, J. Dorosz, J. Żmojda, M. Kochanowicz, D. Dorosz, Nd³⁺ doped titanate-germanate glasses for near-IR laser applications, *Opt. Mater. Express* 12 (2022) 2912–2926.
- [23] K. Kowalska, M. Kuwik, J. Pisarska, M. Leśniak, D. Dorosz, M. Kochanowicz, J. Żmojda, J. Dorosz, W.A. Pisarski, Influence of TiO₂ concentration on near-infrared luminescence of Er³⁺ ions in barium gallo-germanate glasses, *J. Mater. Res. Technol.* 21 (2022) 4761–4772.
- [24] F. Huang, Y. Ma, W. Li, X. Liu, L. Hu, D. Chen, 2.7 μm emission of high thermally and chemically durable glasses based on AlF₃, *Sci. Rep.* 4 (2014) 3607.
- [25] J. Yu, M. Zhang, X. Lu, Y. Du, G. Brambilla, S. Jia, S. Wang, P. Wang, Broadband 2.7 μm mid-infrared emissions in Er³⁺-doped PbO–PbF₂–Bi₂O₃–Ga₂O₃ glasses, *Opt. Lett.* 45 (2020) 4638–4641.
- [26] R. Wang, X. Meng, F. Yin, Y. Feng, G. Qin, W. Qin, Heavily erbium-doped low-hydroxyl fluorotellurite glasses for 2.7 μm laser applications, *Opt. Mater. Express* 3 (2013) 1127–1136.
- [27] T. Xue, Y. Li, Y. Liu, Z. Liu, S. Dai, M. Liao, L. Hu, High thermal stability and intense 2.71 μm emission in Er³⁺-doped fluorotellurite glass modified by GaF₃, *Opt. Mater.* 75 (2018) 367–372.
- [28] F. Qi, F. Huang, T. Wang, R. Ye, R. Lei, Y. Tian, J. Zhang, L. Zhang, S. Xu, Highly Er³⁺ doped fluorotellurite glass for 1.5 μm broadband amplification and 2.7 μm microchip laser applications, *J. Lumin.* 202 (2018) 132–135.
- [29] R. Xu, Y. Tian, L. Hu, J. Zhang, Enhanced emission of 2.7 μm pumped by laser diode from Er³⁺/Pr³⁺-codoped germanate glasses, *Opt. Lett.* 36 (2011) 1173–1175.
- [30] G. Zhao, S. Wang, H. Fan, L. Hu, Mid-infrared spectroscopic properties and energy transfer of Er³⁺/Yb³⁺ co-doped bismuth germanate glass, *Spectrochim. Acta* 101 (2013) 49–53.
- [31] H. Lin, A. Chen, Y. Yu, A. Yang, Y. Wang, Enhanced mid-infrared emissions of Er³⁺ at 2.7 μm via Nd³⁺ sensitization in chalcohalide glass, *Opt. Lett.* 36 (2011) 1815–1817.
- [32] Y. Tian, R. Xu, L. Zhang, L. Hu, J. Zhang, Observation of 2.7 μm emission from diode-pumped Er³⁺/Pr³⁺-codoped fluorophosphate glass, *Opt. Lett.* 36 (2011) 109–111.
- [33] Y. Guo, Y. Ma, F. Huang, Y. Peng, L. Zhang, J. Zhang, 2.7 μm emission properties of Er³⁺ doped tungsten-tellurite glass sensitized by Yb³⁺ ions, *Spectrochim. Acta* 111 (2013) 150–153.
- [34] H. Gan, K. Xia, Y. Gui, X. Zhang, N. Zeng, Z. Cao, X. Wang, S. Dai, Z. Liu, High content Er³⁺ doped ZBLAN glass: the spectral characteristics and high slope efficiency MIR laser investigation, *J. Alloys Compd.* 865 (2021), 159170.
- [35] S. Jia, C. Li, Z. Zhao, C. Yao, Z. Jia, G. Qin, Y. Ohishi, W. Qin, Er³⁺-doped ZnF₂-BaF₂-SrF₂-YF₃ fluoride glasses for 2.7 μm laser applications, *Mater. Lett.* 227 (2018) 97–99.
- [36] F.F. Zhang, W.J. Zhang, J. Yuan, D.D. Chen, Q. Qian, Q.Y. Zhang, Enhanced 2.7 μm emission from Er³⁺ doped oxyfluoride tellurite glasses for a diode-pump mid-infrared laser, *AIP Adv.* 4 (2014), 047101.
- [37] F. Huang, X. Liu, L. Hu, D. Chen, Spectroscopic properties and energy transfer parameters of Er³⁺ doped fluorozirconate and oxyfluoroaluminate glasses, *Sci. Rep.* 4 (2014) 5053.
- [38] S. Kang, X. Xiao, Q. Pan, D. Chen, J. Qiu, G. Dong, Spectroscopic properties in Er³⁺-doped germanotellurite glasses and glass ceramics for mid-infrared laser materials, *Sci. Rep.* 7 (2017), 43186.
- [39] Y. Tian, B. Li, R. Chen, J. Xia, X. Jing, J. Zhang, S. Xu, Thermal stability and 2.7 μm spectroscopic properties in Er³⁺ doped tellurite glasses, *Solid State Sci.* 60 (2016) 17–22.
- [40] L. Zampedri, G.C. Righini, H. Portales, S. Pelli, G. Nunzi Conti, M. Montagna, M. Mattarelli, R.R. Gonçalves, M. Ferrari, A. Chiasera, C. Armellini, Sol-gel-derived Er-activated SiO₂-HfO₂ planar waveguides for 1.5 μm application, *J. Non-Cryst. Solids* 345&346 (2004) 580–584.
- [41] G.C. Righini, S. Berneschi, G. Nunzi Conti, S. Pelli, E. Moser, R. Retoux, P. Féron, R. R. Gonçalves, G. Speranza, Y. Jestin, M. Ferrari, A. Chiasera, A. Chiappini, C. Armellini, Er³⁺-doped silica-hafnia films for optical waveguides and spherical resonators, *J. Non-Cryst. Solids* 355 (2009) 1853–1860.

P8

Joanna Pisarska, Karolina Kowalska, Marta Kuwik, Jan Dorosz, Marcin Kochanowicz,
Jacek Żmojda, Dominik Dorosz, Wojciech A. Pisarski,
Optical properties of titanate-germanate glasses containing Ho³⁺ ions
Materials Research Bulletin 166 (2023) 112353



Contents lists available at ScienceDirect

Materials Research Bulletin

journal homepage: www.elsevier.com/locate/matresbu

Research Papers

Optical properties of titanate-germanate glasses containing Ho³⁺ ions

Joanna Pisarska^{a,*}, Karolina Kowalska^a, Marta Kuwik^a, Jan Dorosz^b, Marcin Kochanowicz^b, Jacek Żmojda^b, Dominik Dorosz^c, Wojciech A. Pisarski^a

^a Institute of Chemistry, University of Silesia, Szkolna 9 Street, Katowice 40-007, Poland

^b Białystok University of Technology, Wiejska 45D Street, Białystok 15-351, Poland

^c AGH University of Science and Technology, 30 Mickiewicza Av., Krakow 30-059, Poland

ARTICLE INFO

Keywords:

Titanate-germanate glasses

Ho³⁺ ions

Optical properties

Near-infrared emission

ABSTRACT

Holmium-doped titanate-germanate glasses have been investigated for optical applications. Near-infrared luminescence at 2 μm due to ⁵I₇ → ⁵I₈ transition of holmium ions has been examined in function of TiO₂ concentration. Several spectroscopic parameters for holmium ions such as emission linewidth and lifetime, stimulated emission cross-section and quantum efficiency were determined based on absorption and luminescence experiments and calculated using the Judd-Ofelt theory. Systematic studies demonstrate that holmium-doped titanate-germanate glasses with higher TiO₂ concentration show excellent optical properties. Multicomponent glasses with molar ratios GeO₂:TiO₂ = 1:2 and 1:3 are recommended for near-infrared luminescence at 2 μm.

1. Introduction

Holmium-doped glasses are attractive optical materials due to several visible and infrared luminescent transitions [1]. Among others, trivalent holmium was used successfully as an efficient luminescence center because it produces two ⁵F₄, ⁵S₂ → ⁵I₈ and ⁵F₅ → ⁵I₈ emissive transitions giving primary (green and red) colors of light [2]. Luminescence bands and their intensities and spectral positions can be quite well modulated in inorganic glasses. These phenomena can be achieved using selective excitation wavelengths, power of the excitation source, changes of activator (Ho³⁺) concentration, chemical composition of glass matrices, glass components (network-formers and/or network-modifiers) and their relative molar ratios. Optical aspects were presented and discussed for holmium ions in several inorganic glasses like borate [3], phosphate [4], silicate [5] and tellurite [6–8] based glass systems. Borate [9] phosphate [10] and heavy metal glasses [11–13] containing holmium ions have been also proposed for green laser and luminescent device applications.

On the other hand, glasses belonging to low-phonon glass-family are excellent candidates for luminescent systems emitting near-infrared radiation (NIR) at 1.2 μm [14] and 2 μm [15], which correspond to ⁵I₆ → ⁵I₈ and ⁵I₇ → ⁵I₈ transitions of holmium. They can be applied to laser medical surgery, atmospheric monitoring, remote chemical sensing, eye-safe laser radars and other NIR luminescent devices. Optical properties with a special regard to near-infrared luminescence of Ho³⁺

ions at 2 μm have been examined for phosphate [16] and silicate [17] glasses containing lead as well as silicate [18], lanthanum-tungsten-tellurite [19], germanium-tellurite [20,21] and germanate based glass systems [22,23]. The later system, i.e. germanate glass is recommended for laser applications in ~2.1 μm spectral region, which has been well described in review article published the last year [24]. Further studies demonstrate that the enhanced NIR emission of Ho³⁺ at 2 μm is observed in germanate based glasses sensitized by transition metals [25–27] or rare earths [28–30]. Special attention has been paid to germanate double-clad optical fibers co-doped with Ho³⁺/Ln³⁺, where Ln = Yb [31] and Tm [32].

The recently published work for Ho³⁺:V⁴⁺ co-doped Na₂O–SiO₂–ZrO₂ glasses indicates that the influence of modifier oxide on their spectroscopic properties is significant [33]. The presence of higher concentration of V₂O₅ in this glass system is resulted in the high luminescence efficiency of Ho³⁺ ions especially in the red spectral region. Holmium-doped glasses with relatively high TiO₂ concentration have not yet been studied, to our knowledge. Optical and spectroscopic properties of Ho³⁺ ions have been examined for glass systems based on H₃BO₃–Li₂CO₃–CaF₂–PbO–TiO₂ [34], P₂O₅–BaF₂–CaF₂–TiO₂ [35], TeO₂–TiO₂–La₂O₃ [36] and TeO₂–Nb₂O₅–10TiO₂–Al₂O₃ [37], where amount of TiO₂ playing the role as glass-modifier did not exceed 10 mol %, only.

The aim of our work is concerned on the enhanced near-infrared luminescence of holmium ions in multicomponent germanate based

* Corresponding author.

E-mail address: joanna.pisarska@us.edu.pl (J. Pisarska).

<https://doi.org/10.1016/j.materresbull.2023.112353>

Received 12 March 2023; Received in revised form 14 May 2023; Accepted 20 May 2023

Available online 21 May 2023

0025-5408/© 2023 Elsevier Ltd. All rights reserved.

glasses varying with TiO₂ concentration. Experimental studies using absorption and luminescence spectroscopy and theoretical calculations using the Judd-Ofelt theory are presented and discussed for glass samples, where GeO₂:TiO₂ molar ratio was changed from 5:1 (10% TiO₂) to 1:5 (50% TiO₂). Thermal and structural aspects for titanate-germanate glasses evidenced by differential scanning calorimetry (DSC), X-ray diffraction (XRD), electron paramagnetic resonance (EPR), Raman and FT-IR spectroscopy were described in our previous work [38]. Theoretical and experimental results presented here suggest that the presence of higher concentration of TiO₂ in the multicomponent germanate based glass-host doped with holmium ions seems to be an excellent way to obtain amorphous systems emitting efficient near-infrared radiation at 2 μm.

2. Experimental

2.1. Glass preparation

Glasses with the following compositions xTiO₂-(60-x)GeO₂-30BaO-9.75Ga₂O₃-0.25Ho₂O₃ (x = 0, 10, 20, 30, 40, 45 and 50) were synthesized. The concentrations of components are given in mol%. In the first step, high purity components (99.99% Aldrich Chemical Co.) were mixed homogeneously together. Next, they were melted at T = 1200 °C for t = 0.45 h. Each glass sample was polished for optical measurements.

2.2. Glass characterization

The refractive index was determined using the Metricon 2010 prism coupler at a wavelength of 632.8 nm. The absorption spectra of glass samples were carried out using Cary 5000 UV-VIS-NIR spectrophotometer (Agilent Technology, USA). For measurements of near-infrared luminescence spectra and their decays, the appropriate laser equipment was used. It consists of PTI QuantaMaster QM40 spectrofluorometer with a xenon lamp (75 W), tunable pulsed optical parametric oscillator, Nd:YAG laser (OpotekOpolette 355 LD), double 200 mm monochromators, Hamamatsu H10330B-75 detector and PTI ASOC-10 USB-2500 oscilloscope. Resolution for spectral measurements was ±0.1 nm. Decay curves were recorded with an accuracy of ±0.5 μs.

3. Theoretical background

Bonding parameters (β and δ) were determined from the absorption spectra and calculated using the following equation:

$$\delta = ((1 - \beta) / \beta) \times 100\% \quad (1)$$

where $\beta = \Sigma_N = \beta^* / N$ and $\beta^* = \nu_c / \nu_a$ [39]. In the equation given above, β is the shift of energy level position (Nephelauxetic effect), whereas N denotes number of levels used for calculation of β-values. In order to calculate β*, the energies of the corresponding transitions in the investigated complex ν_c and free-ion ν_a are necessary [40]. Positive or negative sign for the values of δ suggests covalent or ionic bonding between Ho³⁺ and surrounding ligands.

The standard Judd-Ofelt theory [41,42] was used to calculate radiative transition probabilities for excited states of holmium ions in titanate-germanate glasses. At this moment it should be pointed out that the Judd-Ofelt calculations have been used previously not only for rare earth ions in amorphous systems [43], but they were also applied successfully to some inorganic phosphors. In particular, the Judd-Ofelt parameters for some crystalline compounds NaGd(WO₄)₂:Er³⁺, YLiF₄:Nd³⁺ and Y₂O₃:Er³⁺ were determined using the excitation spectrum [44]. Furthermore, a universal route for calculating the Judd-Ofelt parameters for powdered phosphors β-NaYF₄:Er³⁺/Yb³⁺ have been developed by Zhang et al. [45]. Also, Luo et al. [46] have proposed that the Judd-Ofelt parameters for inorganic phosphors NaYF₄:Er³⁺ can also be derived from the fluorescence decays.

The calculation procedure for holmium-doped titanate-germanate glasses was carried out using the commercially available software OriginPro (version 2018b). The Origin C was used in the calculations. According to the standard procedure, the x-axis of absorption spectrum was converted to wavenumbers given in cm⁻¹. Then, the baseline was fitted individually to the each absorption band of Ho³⁺ and the integrated areas were calculated.

The measured oscillator strengths of transitions were estimated by measuring the areas under the absorption bands of holmium ions using the following expressions:

$$P_{meas} = 4.18 \times 10^{-9} \int \epsilon(\nu) d\nu \quad (2)$$

$$\epsilon(\nu) = A / (c \times l) \quad (3)$$

where: ∫ε(ν) represents the area under the absorption line, A and l indicates the absorbance and the optical path length, whereas c is the concentration of Ho³⁺ ions (mol × l⁻¹).

The theoretical oscillator strengths for each absorption transition of Ho³⁺ ions were calculated using the relation, which was defined as follows:

$$P_{calc} = \frac{8\pi^2 m c (n^2 + 2)^2}{3h\lambda(2J + 1)9n} \times \sum_{t=2,4,6} \Omega_t (\langle 4f^N J \| U^t \| 4f^N J' \rangle) \quad (4)$$

In this relation, m, c, n, h and λ are the mass of the electron, the velocity of light, the refractive index of the medium, the Planck constant and the mean wavelength of the each transition, respectively. The values of ||U^t|| used for Ho³⁺ ions were adopted from Ref. [40] and represent the square of the matrix elements of the unit tensor operator U^t.

In the next step, the measured and theoretical oscillator strengths for Ho³⁺ were compared. The three phenomenological intensity parameters Ω_t (t = 2, 4, 6) were determined. The fit quality was expressed by the magnitude of the root-mean-square deviation rms, defined using the relation [11] given below:

$$rms = \left(\sum (P_{meas} - P_{calc})^2 / N \right)^{1/2} \quad (5)$$

where N denotes the total number of transitions involved in the fitting procedure.

The Judd-Ofelt intensity parameters Ω_t are necessary to calculate the radiative transition probabilities, the luminescence branching ratios, the peak stimulated emission cross-sections and the radiative lifetimes. The radiative transition probabilities A_J for the excited states of holmium ions were calculated as follows:

$$A_J = \frac{64\pi^4 e^2}{3h(2J + 1)\lambda^3} \times \frac{n(n^2 + 2)^2}{9} \times \sum_{t=2,4,6} \Omega_t (\langle 4f^N J \| U^t \| 4f^N J' \rangle) \quad (6)$$

The luminescence branching ratio β is due to the relative intensities of transitions from the excited state to all terminal states of holmium ions.

$$\beta = \frac{A_J}{\sum_i A_{Ji}} \quad (7)$$

The radiative transition probability A_J and the emission linewidth Δλ referred as full width at half maximum (FWHM) were applied to determine the peak stimulated emission cross-section σ_{em} using the following expression [47–49]:

$$\sigma_{em} = \frac{\lambda_p^4 A_J}{8\pi c n^2} \times \frac{\lambda_p I(\lambda)}{\int \lambda_p I(\lambda) \Delta\lambda} \quad (8)$$

where λ_p is the peak emission wavelength for the electronic transition of Ho³⁺ and I(λ) is the emission intensity.

The radiative lifetime τ_{rad} is the inverse of the total radiative transition probability defined as the sum of the A_J terms:

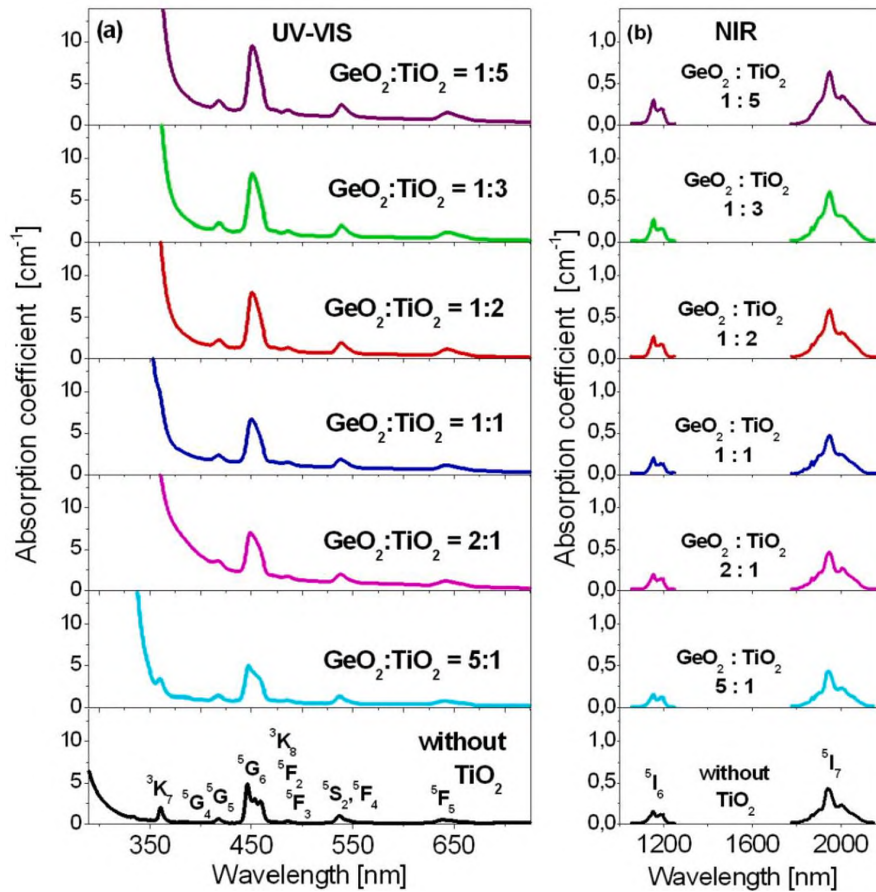


Fig. 1. Absorption spectra of Ho³⁺ ions in titanate-germanate glasses measured in the UV-VIS and NIR ranges.

$$\tau_{rad} = \frac{1}{\sum_i A_{ji}} = \frac{1}{A_T} \quad (9)$$

Finally, the radiative lifetime τ_{rad} calculated from the relation (9) and experimental lifetime from the luminescence decay measurements were used to determine the quantum efficiency η using the following

relation:

$$\eta = \tau_m / \tau_{rad} \times 100\% \quad (10)$$

4. Results and discussion

Fig. 1 shows absorption spectra of holmium ions in multicomponent

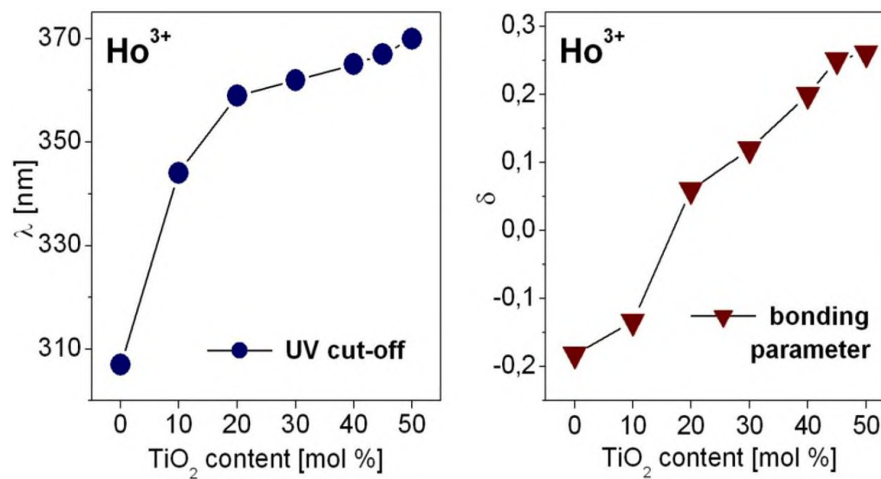


Fig. 2. UV cut-off and bonding parameters for glass samples varying with TiO₂ content.

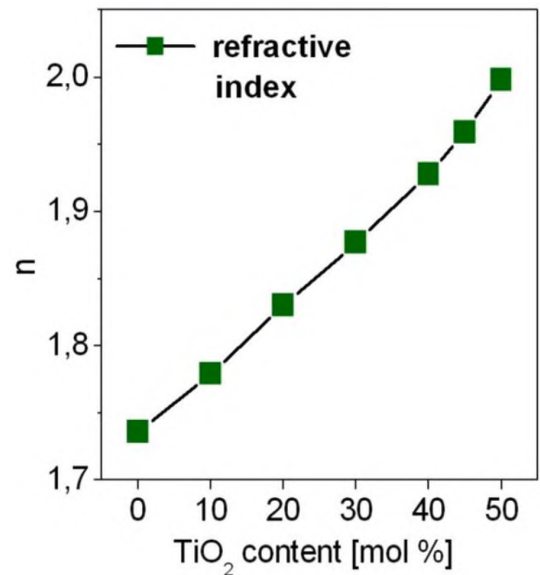
Table 1Glass composition, TiO₂ concentration, holmium ion concentration, UV cut-off and bonding parameter.

Glass composition [mol %]	TiO ₂ concentration [mol%]	GeO ₂ :TiO ₂	$N \times 10^{20}$ [ion/cm ³]	UV cut-off [nm]	δ
60GeO ₂ -30BaO-9.75Ga ₂ O ₃ -0.25Ho ₂ O ₃	0	–	1.07	307	-0.182
50GeO ₂ -10TiO ₂ -30BaO-9.75Ga ₂ O ₃ -0.25Ho ₂ O ₃	10	5:1	1.09	344	-0.133
40GeO ₂ -20TiO ₂ -30BaO-9.75Ga ₂ O ₃ -0.25Ho ₂ O ₃	20	2:1	1.11	359	0.060
30GeO ₂ -30TiO ₂ -30BaO-9.75Ga ₂ O ₃ -0.25Ho ₂ O ₃	30	1:1	1.12	362	0.120
20GeO ₂ -40TiO ₂ -30BaO-9.75Ga ₂ O ₃ -0.25Ho ₂ O ₃	40	1:2	1.13	365	0.200
15GeO ₂ -45TiO ₂ -30BaO-9.75Ga ₂ O ₃ -0.25Ho ₂ O ₃	45	1:3	1.15	367	0.251
10GeO ₂ -50TiO ₂ -30BaO-9.75Ga ₂ O ₃ -0.25Ho ₂ O ₃	50	1:5	1.17	372	0.261

titanate-germanate glasses. The spectra were measured in the UV-VIS (a) and NIR (b) ranges for glass without TiO₂ and glass samples, where the molar ratio GeO₂:TiO₂ is changed from 5:1 to 1:5. Several inhomogeneously broadened absorption lines characteristic for 4f¹⁰-4f¹⁰ electronic transitions of Ho³⁺ ions are observed. Absorption bands are assigned to transitions from the ⁵I₈ ground state to the higher-lying ⁵I₇, ⁵I₆, ⁵F₅, (⁵S₂, ⁵F₄), ⁵F₃, (⁵F₂, ³K₈), ⁵G₆, ⁵G₅, ⁵G₄ and ³K₇ excited states of trivalent holmium, respectively.

Detailed analysis for the spectra recorded in the UV-VIS range reveals that the intensity of absorption band located near 450 nm and assigned to transition ⁵I₈ → ⁵G₆ (Ho³⁺) is the highest and further increase with increasing TiO₂ concentration in glass composition. Moreover, the absorption band at about 360 nm due to transition ⁵I₈ → ³K₇ (Ho³⁺) is quite well detectable for glass without TiO₂. For glass with GeO₂:TiO₂ = 5:1, the band associated to transition ⁵I₈ → ³K₇ (Ho³⁺) is already lying on absorption edge, whereas for glasses containing higher TiO₂ content is completely invisible. This phenomenon clearly indicates the absorption edge of titanate-germanate glass is changed drastically with increasing TiO₂ concentration. For that reason, the ultraviolet (UV) cut-off wavelength defined as the intersection between the zero base line and the extrapolation of absorption edge was determined. The absorption edge is changed from 307 nm (glass without TiO₂) to 372 nm (glass with GeO₂:TiO₂ = 1:5) with increasing TiO₂ content. Furthermore, the absorption spectra of Ho³⁺ ions were also used to calculate bonding parameter δ using the relation (1) given in Part 3. It is interesting to notice that the value of $\delta = -0.182$ for glass without TiO₂ has a negative sign suggesting ionic bonding between holmium ions and surrounding ligands. Similar situation was observed earlier for germanate based glasses doped with neodymium [50] and erbium [51], where the negative values of δ were also obtained and the nature of ionic bonding has been determined. In our case, an introduction of TiO₂ to the germanate glass host influence strongly on bonding between Ho³⁺ and the nearest environments. The bonding parameter δ is changed strongly from -0.182 (glass without TiO₂) to +0.261 (glass with GeO₂:TiO₂ = 1:5). It suggests that the nature of bonding is changed from ionic to more covalent with increasing TiO₂ content. The results from the absorption spectra measurements clearly indicate that the covalent bonding between holmium ions and surrounding ligands increases whereas the absorption edge for the studied glass samples is shifted to longer wavelengths with increasing TiO₂ concentration in glass composition. It was schematized on Fig. 2.

Details including glass compositions as well as the UV cut-off and the bonding parameter δ varying with TiO₂ concentration are also given in Table 1. The estimated uncertainties for the Ho³⁺ concentration, the UV cut-off wavelength and the δ value are close to $\pm 0.01 \times 10^{20}$ ion/cm³, ± 0.5 nm and ± 0.001 , respectively.

Fig. 3. Refractive indices for glass samples varying with TiO₂ content.

In the next step, several spectroscopic parameters for holmium ions in titanate-germanate glasses were calculated using the appropriate relations from the Judd-Ofelt theory [41,42] given in Part 3. At this moment, it should be pointed out that the excited states of holmium ions are well separated and the energy distances between them are suitable and favorable for the Judd-Ofelt evaluation [52,53]. The measured oscillator strengths for electronic transitions originating from the ⁵I₈ ground state to the higher lying excited states of holmium ions were determined from the absorption spectra (Fig. 1) using relations (2) and (3). The theoretical oscillator strengths for each absorption transition within 4f¹⁰ electronic configuration of Ho³⁺, were calculated using relation (4). The refractive indices necessary to calculate the theoretical oscillator strengths are changed from 1.736 (glass without TiO₂) to 1.998 (GeO₂:TiO₂ = 1:5) with increasing TiO₂ concentration. They are schematized on Fig. 3.

The measured and theoretical oscillator strengths for holmium ions in titanate-germanate glasses were compared. They are presented in Table 2. It is found from Table 2 that measured (P_{meas}) and calculated (P_{calc}) oscillator strengths are close to each other, which suggests that the calculation procedure applied to Ho³⁺ ions in titanate-germanate glasses is reliable. In most cases, the differences between P_{meas} and P_{calc} for all absorption transitions of Ho³⁺ ions used for the Judd-Ofelt calculations are relatively small and their values did not exceed 10%. Furthermore, the absorption spectra were registered under the same experimental conditions. Thus, the measuring uncertainties of the spectral data are nearly the same for the studied series of glass samples and should be ignored. Also, Luo et al. [44] suggest that different calculation routes, different transitions used in the calculations or different transition numbers involved in the calculations influence drastically on the final results in performed Judd-Ofelt analysis. Here, the calculation procedure was identical for all Ho³⁺ doped glass samples and the values of P_{meas} and P_{calc} seems to be reliable. It was also confirmed by the root-mean-square (rms) deviation. The quality of the fit was expressed by the magnitude of rms deviation from relation (5). For the studied glass samples, relatively small rms values were achieved suggesting the reliability of our results. The rms deviations are changed between 0.35 to 0.69 ($\times 10^{-6}$) depending on TiO₂ concentration, which suggests that the error is within the acceptable range compared to similar holmium-doped glass systems, for example rms = 0.41×10^{-6} for Ho³⁺-doped lead bismuth gallate glass [54] and rms = 0.553×10^{-6}

Table 2

Measured and calculated oscillator strengths ($\times 10^{-6}$) for holmium ions in titanate-germanate glasses. The rms deviations ($\times 10^{-6}$) are also shown. Transitions are from the 5I_8 ground state to the levels indicated.

Levels	Energy [cm^{-1}]	0% TiO ₂		10% TiO ₂		20% TiO ₂		30% TiO ₂	
		P _{meas}	P _{calc}	P _{meas}	P _{calc}	P _{meas}	P _{calc}	P _{meas}	P _{calc}
5I_7	5150	1.340	1.445	1.240	1.257	1.460	1.484	1.410	1.437
5I_6	8580	0.680	1.030	0.670	0.895	0.790	1.053	0.730	1.014
5F_5	15,550	3.040	2.655	3.000	2.832	3.600	3.480	3.760	3.524
$^5G_2, ^5F_4$	18,600	4.020	3.760	3.680	3.334	4.500	4.019	4.410	3.964
$^5F_3, (^5F_2, ^3K_8), ^5G_6$	22,100	29.40	29.39	31.40	31.39	36.30	36.29	36.70	36.69
5G_5	23,950	3.040	3.285	2.930	3.278	3.800	4.156	3.900	4.372
rms deviation		0.41		0.35		0.44		0.56	

States	Energy [cm^{-1}]	40% TiO ₂		45% TiO ₂		50% TiO ₂	
		P _{meas}	P _{calc}	P _{meas}	P _{calc}	P _{meas}	P _{calc}
5I_7	5150	1.770	1.790	1.720	1.751	1.800	1.861
5I_6	8580	0.940	1.270	0.930	1.247	1.080	1.318
5F_5	15,550	4.200	4.159	3.970	3.907	4.470	4.360
$^5G_2, ^5F_4$	18,600	5.440	4.821	5.270	4.623	5.680	5.015
$^5F_3, (^5F_2, ^3K_8), ^5G_6$	22,100	44.70	44.69	44.90	44.89	49.00	48.99
5G_5	23,950	4.610	4.942	4.130	4.497	4.820	5.237
rms deviation		0.60		0.66		0.69	

Table 3

The Judd-Ofelt intensity parameters Ω_t ($t = 2, 4, 6$) $\times 10^{-20} \text{ cm}^2$ for holmium ions.

TiO ₂ concentration [mol %]	GeO ₂ : TiO ₂	Ω_2	Ω_4	Ω_6
0	–	6.32 ± 0.25	2.55 ± 0.38	1.45 ± 0.17
10	5:1	6.82 ± 0.21	2.46 ± 0.31	1.19 ± 0.11
20	2:1	7.41 ± 0.23	2.99 ± 0.35	1.34 ± 0.13
30	1:1	7.19 ± 0.25	3.02 ± 0.37	1.22 ± 0.14
40	1:2	8.50 ± 0.26	3.28 ± 0.39	1.49 ± 0.14
45	1:3	8.43 ± 0.26	2.88 ± 0.39	1.42 ± 0.14
50	1:5	8.90 ± 0.24	3.28 ± 0.36	1.45 ± 0.13

for Ho³⁺-doped aluminum germanate glass [55].

The three phenomenological Judd-Ofelt intensity parameters Ω_t ($t = 2, 4, 6$) were evaluated from the least-square fit of measured and calculated oscillator strengths for holmium ions. They are given in Table 3.

In all cases, the trend of the Judd-Ofelt intensity parameters Ω_t was found to be the same, i.e. $\Omega_2 > \Omega_4 > \Omega_6$, which is in a good agreement with the calculation results obtained previously for Ho³⁺-doped glass systems [52–55]. Furthermore, the Judd-Ofelt intensity parameter Ω_2 is connected with the asymmetry of the environment and the degree of covalency between holmium ions and surrounding ligands. The highest values of Ω_2 (above $8 \times 10^{-20} \text{ cm}^2$) exhibit glasses with relatively higher TiO₂ concentration suggesting that the bonds between holmium ions and the nearest surroundings are strongly covalent in character compared to series of the studied glass samples. According to previous works [52–55], the spectroscopic quality factor χ referred as Ω_4/Ω_6 deals with lasing efficiencies of transitions of Ho³⁺ and can be used to predict the stimulated emission of the laser materials. The higher values

Table 4

The calculated radiative transition probabilities and luminescence branching ratios for holmium ions in titanate-germanate glasses.

Transition	Average wavelength [nm]	0% TiO ₂		10% TiO ₂		20% TiO ₂		30% TiO ₂	
		A _J [s^{-1}]	β	A _J [s^{-1}]	β	A _J [s^{-1}]	β	A _J [s^{-1}]	β
$^5F_5 \rightarrow ^5I_5$	2247	10	0.003	10	0.003	12	0.003	13	0.003
5I_6	1429	125	0.041	118	0.039	150	0.038	156	0.037
5I_7	952	606	0.196	599	0.199	775	0.198	825	0.199
5I_8	643	2348	0.760	2284	0.759	2974	0.761	3162	0.761
$^5I_5 \rightarrow ^5I_6$	3922	8	0.044	8	0.049	10	0.049	11	0.053
5I_7	1653	100	0.553	90	0.549	112	0.549	111	0.536
5I_8	901	73	0.403	66	0.402	82	0.402	85	0.411
$^5I_6 \rightarrow ^5I_7$	1857	23	0.102	77	0.296	97	0.298	100	0.301
5I_8	1170	202	0.898	183	0.704	229	0.702	232	0.699
$^5I_7 \rightarrow ^5I_8$	2000	84	1.000	76	1.000	94	1.000	98	1.000

Transition	Average wavelength[nm]	40% TiO ₂		45% TiO ₂		50% TiO ₂	
		A _J [s^{-1}]	β	A _J [s^{-1}]	β	A _J [s^{-1}]	β
$^5F_5 \rightarrow ^5I_5$	2247	17	0.003	17	0.003	19	0.003
5I_6	1429	202	0.038	202	0.040	226	0.039
5I_7	952	1138	0.215	1018	0.200	1169	0.199
5I_8	643	3945	0.744	3862	0.757	4446	0.759
$^5I_5 \rightarrow ^5I_6$	3922	14	0.051	14	0.050	16	0.053
5I_7	1653	150	0.543	152	0.547	165	0.543
5I_8	901	112	0.406	112	0.403	123	0.404
$^5I_6 \rightarrow ^5I_7$	1857	131	0.297	132	0.296	146	0.299
5I_8	1170	310	0.703	314	0.704	342	0.701
$^5I_7 \rightarrow ^5I_8$	2000	128	1.000	132	1.000	140	1.000

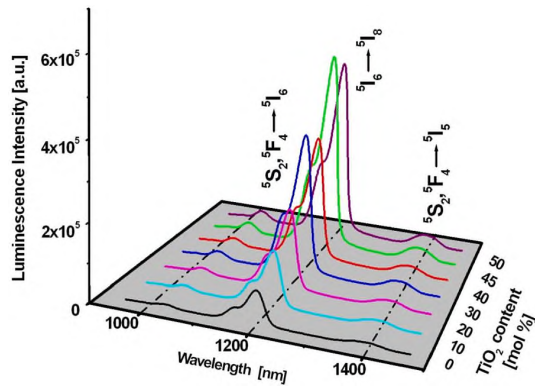


Fig. 4. Near-infrared luminescence spectra of Ho^{3+} ions in titanate-germanate glasses.

of χ would benefit the stimulated emission in a laser active media, thus implying a stronger near-infrared luminescence properties. In our case, the spectroscopic quality factor is relatively large ($\chi > 2$) independently on TiO_2 concentration, which seems to be favorable for development of solid-state lasers. The three Judd-Ofelt intensity parameters Ω_t ($t = 2, 4, 6$) were applied to calculate radiative transition probabilities and luminescence branching ratios using relations (6) and (7). The results are given in Table 4. The estimated uncertainties for the radiative transition probabilities are close to $\pm 1 \text{ s}^{-1}$. Unexpectedly, the radiative transition probabilities calculated for the main $^5\text{I}_7 \rightarrow ^5\text{I}_8$ NIR laser transition of Ho^{3+} ions at $2 \mu\text{m}$ are quite large ($128\text{--}140 \text{ s}^{-1}$) for glasses with higher TiO_2 concentrations (40–50 mol%), when we compare to the values of 88.19 s^{-1} and 103.38 s^{-1} obtained for low-phonon germanate-tellurite [56] and germanate [57] based glasses co-doped with

$\text{Ho}^{3+}/\text{Yb}^{3+}$.

Fig. 4 presents near-infrared luminescence spectra registered for holmium ions in titanate-germanate glasses under excitation of $^5\text{G}_6$ state by 450 nm line. The spectra were measured in the 950–1450 nm range. Luminescence bands at 1.03 μm and 1.4 μm correspond to transitions originating from the $^5\text{S}_2, ^5\text{F}_4$ states to the lower-lying $^5\text{I}_6$ and $^5\text{I}_5$ states, respectively. The most intense NIR emission band at 1.2 μm is related to $^5\text{I}_6 \rightarrow ^5\text{I}_8$ transition of holmium. Generally, their emission intensities enhance with increasing TiO_2 concentration.

Further investigations confirmed the improvement of near-infrared emission of holmium ions in glass samples varying with TiO_2 concentration. Near-infrared luminescence spectra at 2 μm were measured for holmium ions in titanate-germanate glasses under 450 nm excitation. They are presented in Fig. 5(a). Luminescence bands near 2 μm are assigned to the main $^5\text{I}_6 \rightarrow ^5\text{I}_8$ near-infrared laser transition of holmium. The maximum of emission peak is nearly independent on TiO_2 concentration and its value is close to $1969 \pm 3.5 \text{ nm}$. The intensities of emission bands became stronger with increasing TiO_2 concentration. Inset shows the photo of selected glass sample ($\text{GeO}_2:\text{TiO}_2 = 1:2$). The radiative transition rates (b), the emission linewidths (c) and the stimulated emission cross-sections (d) for the $^5\text{I}_7 \rightarrow ^5\text{I}_8$ (Ho^{3+}) transition varying with TiO_2 content are also illustrated. Interestingly, the radiative transition rates calculated for the main $^5\text{I}_7 \rightarrow ^5\text{I}_8$ NIR laser transition of Ho^{3+} ions at 2 μm (Table 4) increase significantly with increasing TiO_2 concentration, as mentioned above. Similar situation is also observed for the emission linewidth referred as full width at half maximum (FWHM), which increase from 160 nm (glass without TiO_2) to nearly 175 nm ($\text{GeO}_2:\text{TiO}_2 = 1:5$), respectively.

The emission linewidth and the radiative transition rate for the $^5\text{I}_7 \rightarrow ^5\text{I}_8$ near-infrared laser transition of Ho^{3+} at 2 μm were used to calculate the stimulated emission cross-section using relation (8). The values of σ_{em} are larger (above $0.4 \times 10^{-20} \text{ cm}^2$) for glasses with higher TiO_2 content (40–50 mol%) and consistent with the results obtained for Ho^{3+}

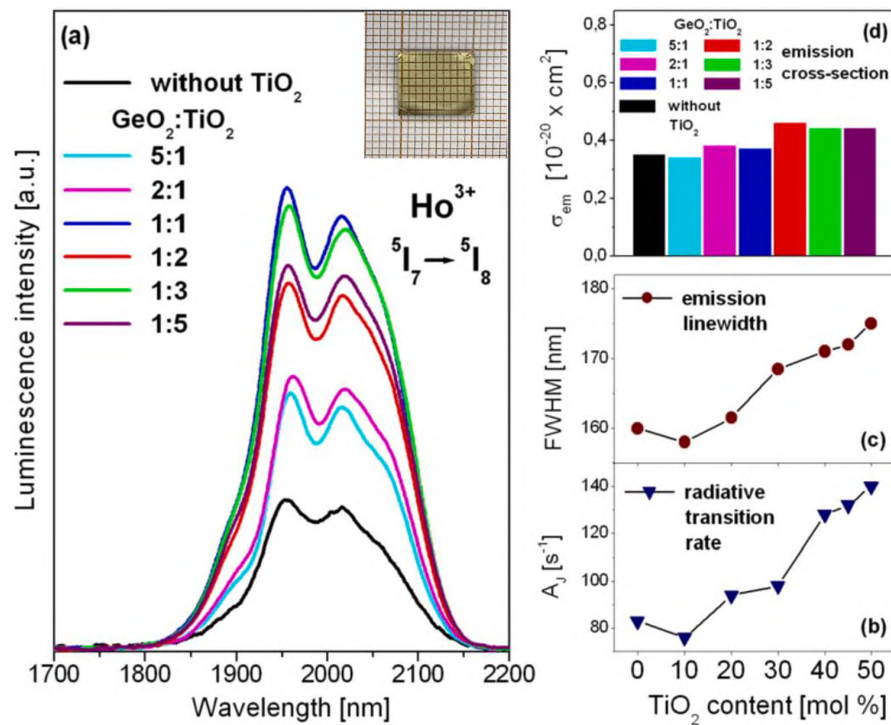


Fig. 5. Near-infrared luminescence spectra of Ho^{3+} ions in titanate-germanate glasses at 2000 nm (a). Inset shows the photo of glass with molar ratio $\text{GeO}_2:\text{TiO}_2 = 1:2$. The radiative transition rates (b), the emission linewidths (c) and the stimulated emission cross-sections (d) for near-infrared transition $^5\text{I}_7 \rightarrow ^5\text{I}_8$ (Ho^{3+}) varying with TiO_2 content are also indicated.

Table 5

The emission peak wavelength λ_p , the emission linewidth (FWHM), the stimulated emission cross-section σ_{em} , the radiative lifetime τ_{rad} , the measured lifetime τ_m and the quantum efficiency η for the NIR transition $^5I_7 \rightarrow ^5I_8$ (Ho^{3+}) varying with TiO_2 concentration.

TiO_2 concentration[mol%]	$GeO_2:TiO_2$	λ_p [nm]	FWHM [nm]	σ_{em} [$10^{-20} \times cm^2$]	τ_{rad} [ms]	τ_m [ms]	η [%]
0	–	1960	160	0.35	12.0	2.88	24
10	5:1	1960	158	0.34	13.2	3.26	25
20	2:1	1962.5	161.5	0.38	10.6	3.16	30
30	1:1	1955.5	168.5	0.37	10.2	4.40	43
40	1:2	1958.5	171	0.45	7.8	3.73	48
45	1:3	1958.5	172	0.44	7.6	3.87	51
50	1:5	1957	175	0.42	7.1	3.28	46

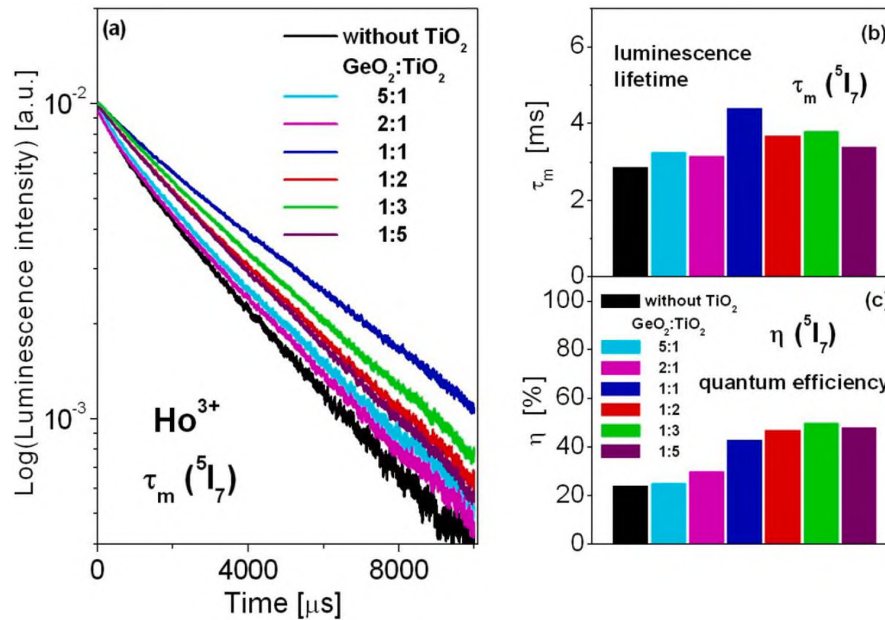


Fig. 6. Luminescence decays from the 5I_7 state of Ho^{3+} ions in titanate-germanate glasses (a). The luminescence lifetimes (b) and the quantum efficiencies (c) for the excited state 5I_7 (Ho^{3+}) varying with TiO_2 content are also schematized.

ions lead bismuth gallate glass with $\sigma_{em} = 0.475 \times 10^{-20} cm^2$ [54] and germanate based glasses with σ_{em} equal to $0.451 \times 10^{-20} cm^2$ [48] and $0.446 \times 10^{-20} cm^2$ [58]. The stimulated emission cross-sections for the $^5I_7 \rightarrow ^5I_8$ NIR transition of holmium ions in titanate-germanate glasses are given in Table 5.

Finally, luminescence decay curves for the 5I_7 state of holmium ions were also measured for glass samples in function of TiO_2 content. Luminescence decays from the upper 5I_7 laser state of Ho^{3+} ions in titanate-germanate glasses are shown in Fig. 6(a). The luminescence lifetimes (b) and the quantum efficiencies (c) for the excited state 5I_7 (Ho^{3+}) varying with TiO_2 concentration are also schematized.

Luminescence decay curves are nearly single-exponential because of the low activator concentration (0.25 mol%) and the lack of energy transfer processes between holmium ions. For higher activator content (usually above 0.5 mol% Ho^{3+}), the non-radiative relaxation processes become dominant and near-infrared luminescence is successfully quenched due to the increasing interactions between holmium ions. These phenomena depend significantly on activator concentration [23]. Based on decay curve measurements, luminescence lifetimes for the upper 5I_7 (Ho^{3+}) laser state of holmium ions in glasses varying with TiO_2 concentration were determined. Generally, the experimental values of τ_m become longer for glass samples in the presence of TiO_2 . However, the changes in luminescence lifetimes 5I_7 (Ho^{3+}) with TiO_2 content are non-linear. Details are given in Table 5.

The radiative lifetimes τ_{rad} obtained from the Judd-Ofelt theory

using Eq. (9) and the measured luminescence lifetimes τ_m were used to calculate the quantum efficiency η for the upper laser state 5I_7 (Ho^{3+}) from relation (10) given in Part 3. The values of η are enhanced rapidly with increasing TiO_2 concentration (Fig. 6).

The peak stimulated emission cross-section σ_{em} and the quantum efficiency η for the main $^5I_7 \rightarrow ^5I_8$ transition of holmium ions are important spectroscopic parameters to identify the potential of titanate-germanate glass for NIR emission and laser applications. Spectroscopic analysis (Table 5) clearly demonstrate that glasses with higher TiO_2 content are preferred for potential applications as an efficient sources emitting near-infrared radiation at 2 μm . Glass systems containing relatively higher TiO_2 concentration (40 and 45 mol%) exhibit the highest stimulated emission cross-sections and the quantum efficiencies equal to $\sigma_{em} = 0.45 \times 10^{-20} cm^2$ and $\eta = 48\%$ ($GeO_2:TiO_2 = 1:2$) and $0.44 \times 10^{-20} cm^2$ and $\eta = 51\%$ ($GeO_2:TiO_2 = 1:3$) among series of the studied glasses. They are comparable to the results obtained earlier for Ho^{3+} ions in multicomponent glass based on $GeO_2-SiO_2-PbO-CaO-K_2O$ [58], where the values of σ_{em} and η for the $^5I_7 \rightarrow ^5I_8$ transition are close to $0.446 \times 10^{-20} cm^2$ and 47.1%, respectively. The relatively large stimulated emission cross-sections and quantum efficiencies represent the probability of receiving more laser gain, signifying that holmium-doped titanate-germanate glasses with higher TiO_2 concentrations ($GeO_2:TiO_2 = 1:2$ and $1:3$) will be a competitive candidates for near-infrared luminescence and laser applications at 2 μm . Furthermore, it should also be mentioned that the optical properties of Ho^{3+} ions in

titanate-germanate glasses presented here are quite well correlated with theoretical and experimental results obtained by us for Er^{3+} ions in glass, where the presence of higher TiO_2 concentration ($\text{GeO}_2:\text{TiO}_2 = 1:2$) is strongly recommended for NIR emission associated to the $^4\text{I}_{13/2} \rightarrow ^4\text{I}_{15/2}$ laser transition of erbium at $1.5 \mu\text{m}$ [59]. Also, we believe that the optical results for titanate-germanate glasses containing holmium ions are attractive for near-infrared luminescence applications, giving an essential contribution to the development of photonic glasses [60].

5. Conclusions

In this work, the optical properties of titanate-germanate glasses containing holmium ions have been examined. The absorption and luminescence spectroscopy together with the Judd-Ofel't calculations were used to study multicomponent glasses, where molar ratio $\text{GeO}_2:\text{TiO}_2$ are changed from 5:1 to 1:5. Our investigations reveal that titanate-germanate glasses show strong near-infrared luminescence at $2 \mu\text{m}$, which corresponds to the $^5\text{I}_7 \rightarrow ^5\text{I}_8$ transition of holmium ions. Several spectroscopic parameters for Ho^{3+} ions in glasses varying with TiO_2 concentration were obtained. The stimulated emission cross-section (σ_{em}) and the quantum efficiency (η) are the highest for glasses with higher TiO_2 concentration (40 and 45 mol%). They are as follows: $\sigma_{\text{em}} = 0.45 \times 10^{-20} \text{ cm}^2$ and $\eta = 48\%$ ($\text{GeO}_2:\text{TiO}_2 = 1:2$) and $0.44 \times 10^{-20} \text{ cm}^2$ and $\eta = 51\%$ ($\text{GeO}_2:\text{TiO}_2 = 1:3$).

Based on theoretical and experimental results we conclude that glasses with higher TiO_2 content could be potentially useful for optical applications. In particular, holmium-doped glasses with $\text{GeO}_2:\text{TiO}_2 = 1:2$ and $1:3$ are suitable for near-infrared luminescence at $2 \mu\text{m}$.

CRedit authorship contribution statement

Joanna Pisarska: Methodology, Investigation, Resources, Supervision, Writing – original draft. **Karolina Kowalska:** Investigation, Data curation, Validation, Visualization. **Marta Kuwik:** Investigation. **Jan Dorosz:** Formal analysis. **Marcin Kochanowicz:** Investigation. **Jacek Żmojda:** Investigation. **Dominik Dorosz:** Investigation, Formal analysis. **Wojciech A. Pisarski:** Conceptualization, Writing – review & editing, Project administration, Funding acquisition, Supervision.

Declaration of Competing Interest

The authors declare that they have no known competing financial interests or personal relationships that could have appeared to influence the work reported in this paper.

Data availability

Data will be made available on request.

Acknowledgment

The National Science centre (Poland) supported this work under research project 2018/31/B/ST8/00166.

References

- Sk. Mahamuda, K. Swapna, P. Packiyaraj, A. Srinivasa Rao, G. Vijaya Prakash, Visible red, NIR and Mid-IR emission studies of Ho^{3+} doped zinc alumino bismuth borate glasses, *Opt. Mater.* 36 (2013) 362–371, <https://doi.org/10.1016/j.optmat.2013.09.023>.
- S. Babu, M. Seshadri, A. Balakrishna, V. Reddy Prasad, Y.C. Ratnakaram, Study of multicomponent fluoro-phosphate based glasses: ho^{3+} as a luminescence center, *Phys. B* 479 (2015) 26–34, <https://doi.org/10.1016/j.physb.2015.09.023>.
- A. Balakrishna, D. Rajesh, Y.C. Ratnakaram, Spectroscopic analysis of Ho^{3+} transitions in different modifier oxide based lithium–fluoro-borate glasses, *Phys. B* 450 (2014) 58–66, <https://doi.org/10.1016/j.physb.2014.05.052>.
- K. Linganna, M. Rathaiah, V. Venkatramu, C.K. Jayasankar, Spectroscopic properties of Ho^{3+} -doped K–Sr–Al phosphate glasses, *Appl. Phys. A* 115 (2014) 689–696, <https://doi.org/10.1007/s00339-013-7852-7>.
- T. Srikumar, M.G. Brik, Ch.Srinivasa Rao, N. Venkatramaiah, Y. Gandhi, N. Veeraiiah, Emission features of Ho^{3+} ion in Nb_2O_5 , Ta_2O_5 and La_2O_3 mixed $\text{Li}_2\text{O}-\text{ZrO}_2-\text{SiO}_2$ glasses, *Phys. B* 406 (2011) 3592–3598, <https://doi.org/10.1016/j.physb.2011.06.046>.
- S.B. Rai, A.K. Singh, S.K. Singh, Spectroscopic properties of Ho^{3+} ions doped in tellurite glass, *Spectrochim. Acta A* 59 (2003) 3221–3226, [https://doi.org/10.1016/S1386-1425\(03\)00178-1](https://doi.org/10.1016/S1386-1425(03)00178-1).
- C. Devaraja, G.V. Jagadeesha Gowda, B. Eraiah, K. Keshavamurthy, Optical properties of bismuth tellurite glasses doped with holmium oxide, *Ceram. Int.* 47 (2021) 7602–7607, <https://doi.org/10.1016/j.ceramint.2020.11.099>.
- P. Vani, G. Vinitha, R. Praveena, M. Durairaj, T.C. Sabari Girisun, N. Manikandan, Influence of holmium ions on the structural and optical properties of barium tellurite glasses, *Opt. Mater.* 136 (2023), 113438, <https://doi.org/10.1016/j.optmat.2023.113438>.
- C.R. Kesavulu, H.J. Kim, S.W. Lee, J. Kaewkhao, N. Wantana, S. Kothan, S. Kaewjaeng, Optical spectroscopy and emission properties of Ho^{3+} -doped gadolinium calcium silicoborate glasses for visible luminescent device applications, *J. Non Cryst. Solids* 474 (2017) 50–57, <https://doi.org/10.1016/j.jnoncrsol.2017.08.018>.
- V.R. Prasad, S. Damodaraiah, Y.C. Ratnakaram, Optical spectroscopy and luminescence properties of Ho^{3+} doped zinc fluorophosphate (ZFP) glasses for green luminescent device applications, *Opt. Mater.* 78 (2018) 63–71, <https://doi.org/10.1016/j.optmat.2018.02.007>.
- M. Venkateswarlu, Sk. Mahamuda, K. Swapna, M.V.V.K.S. Prasad, A.S. Rao, S. Shakya, A.M. Babu, G.V. Prakash, Holmium doped lead tungsten tellurite glasses for green luminescent applications, *J. Lumin.* 163 (2015) 64–71, <https://doi.org/10.1016/j.jlumin.2015.02.052>.
- B. Suresh, Ya. Zhidachevskii, M.G. Brik, A. Suchocki, M. Srinivasa Reddy, M. Piasecki, N. Veeraiiah, Amplification of green emission of Ho^{3+} ions in lead silicate glasses by sensitizing with Bi^{3+} ions, *J. Alloy. Compd.* 683 (2016) 114–122, <https://doi.org/10.1016/j.jallcom.2016.05.056>.
- P. Rekha Rani, M. Venkateswarlu, K. Swapna, Sk. Mahamuda, M.V.V.K.S. Prasad, A.S. Rao, Spectroscopic and luminescence properties of Ho^{3+} ions doped barium lead alumino fluoro borate glasses for green laser applications, *Solid State Sci.* 102 (2020), 106175, <https://doi.org/10.1016/j.solidstatesciences.2020.106175>.
- B.J. Chen, L.F. Shen, E.Y.B. Pun, H. Lin, $\sim 1.2\mu\text{m}$ near-infrared emission and gain anticipation in Ho^{3+} doped heavy-metal gallate glasses, *Opt. Commun.* 284 (2011) 5705–5709, <https://doi.org/10.1016/j.optcom.2011.08.067>.
- J. He, H. Zhan, Z. Zhou, A. Zhang, A. Lin, Study on $2.0\mu\text{m}$ fluorescence of Ho-doped water-free fluorotellurite glasses, *Opt. Mater.* 35 (2013) 2573–2576, <https://doi.org/10.1016/j.optmat.2013.07.031>.
- C.S. Rao, K. Upendra Kumar, P. Babu, C.K. Jayasankar, Optical properties of Ho^{3+} ions in lead phosphate glasses, *Opt. Mater.* 35 (2012) 102–107, <https://doi.org/10.1016/j.optmat.2012.07.023>.
- X. Liu, P. Kuan, D. Li, S. Gao, X. Wang, L. Zhang, L. Hu, D. Chen, Heavily Ho^{3+} -doped lead silicate glass fiber for $\sim 2\mu\text{m}$ fiber lasers, *Opt. Mater. Express* 6 (2016) 1093–1098, <https://doi.org/10.1364/OME.6.001093>.
- X. Wang, L. Hu, W. Xu, S. Wang, L. Zhang, Ch. Yu, D. Chen, Spectroscopic properties of Ho^{3+} and Al^{3+} co-doped silica glass for $2\mu\text{m}$ laser materials, *J. Lumin.* 166 (2015) 276–281, <https://doi.org/10.1016/j.jlumin.2015.05.055>.
- D. Li, W. Xu, P. Kuan, W. Li, Z. Lin, X. Wang, L. Zhang, Ch. Yu, K. Li, L. Hu, Spectroscopic and laser properties of Ho^{3+} doped lanthanum-tungsten-tellurite glass and fiber, *Ceram. Int.* 42 (2016) 10493–10497, <https://doi.org/10.1016/j.ceramint.2016.03.076>.
- B. Zhou, L. Tao, C.Y.Y. Chan, W. Jin, Y.H. Tsang, E.Y.B. Pun, Near- and mid-infrared photoluminescence in Ho^{3+} doped and $\text{Ho}^{3+}-\text{Yb}^{3+}$ codoped low-phonon-energy germano tellurite glasses, *J. Lumin.* 137 (2013) 132–137, <https://doi.org/10.1016/j.jlumin.2012.12.045>.
- Z.Q. Sui, B.J. Chen, E.Y.B. Pun, H. Lin, Infrared radiation properties of Ho^{3+} in multicomponent germanium tellurite glasses, *Appl. Opt.* 54 (2015) 5976–5982, <https://doi.org/10.1364/AO.54.005976>.
- R. Xu, M. Wang, Y. Tian, L. Hu, J. Zhang, $2.05\mu\text{m}$ emission properties and energy transfer mechanism of germanate glass doped with Ho^{3+} , Tm^{3+} , and Er^{3+} , *J. Appl. Phys.* 109 (2011), 053503 <https://doi.org/10.1063/1.3553877>.
- J. Pisarska, M. Kuwik, A. Górny, M. Kochanowicz, J. Żmojda, J. Dorosz, D. Dorosz, M. Sitarz, W.A. Pisarski, Holmium doped barium gallo-germanate glasses for near-infrared luminescence at 2000nm , *J. Lumin.* 215 (2019), 116625, <https://doi.org/10.1016/j.jlumin.2019.116625>.
- M. Khalid, M. Usman, I. Arshad, Germanate glass for laser applications in $\sim 2.1\mu\text{m}$ spectral region: a review, *Heliyon* 9 (2023) e13031, <https://doi.org/10.1016/j.heliyon.2023.e13031>.
- W. Cao, F. Huang, T. Wang, R. Ye, R. Lei, Y. Tian, J. Zhang, S. Xu, $2.0\mu\text{m}$ emission of Ho^{3+} doped germanosilicate glass sensitized by non-rare-earth ion Bi: a new choice for $2.0\mu\text{m}$ laser, *Opt. Mater.* 75 (2018) 695–698, <https://doi.org/10.1016/j.optmat.2017.11.033>.
- F.F. Zhang, J. Yuan, Y. Liu, W.C. Wang, D.C. Yu, M.Y. Peng, Q.Y. Zhang, Efficient $2.0\mu\text{m}$ fluorescence in Ho^{3+} -doped fluorogermanate glass sensitized by Cr^{3+} , *Opt. Mater. Express* 4 (2014) 1404–1410, <https://doi.org/10.1364/OME.4.001404>.
- J. Pisarska, M. Kuwik, A. Górny, J. Dorosz, M. Kochanowicz, J. Żmojda, M. Sitarz, D. Dorosz, W.A. Pisarski, Influence of transition metal ion concentration on near-infrared emission of Ho^{3+} in barium gallo-germanate glasses, *J. Alloy. Compd.* 793 (2019) 107–114, <https://doi.org/10.1016/j.jallcom.2019.04.154>.

- [28] R. Xu, J. Pan, L. Hu, J. Zhang, 2.0 μm emission properties and energy transfer processes of $\text{Yb}^{3+}/\text{Ho}^{3+}$ codoped germanate glass, *J. Appl. Phys.* 108 (2010), 043522, <https://doi.org/10.1063/1.3468726>.
- [29] G. Tang, X. Wen, Q. Qian, T. Zhu, W. Liu, M. Sun, X. Chen, Z. Yang, Efficient 2.0 μm emission in $\text{Er}^{3+}/\text{Ho}^{3+}$ co-doped barium gallo-germanate glasses under different excitations for mid-infrared laser, *J. Alloy. Compd.* 664 (2016) 19–24, <https://doi.org/10.1016/j.jallcom.2015.12.205>.
- [30] X. Gao, Y. Tian, Q. Liu, B. Li, W. Tang, J. Zhang, S. Xu, Broadband 2 μm emission characteristics and energy transfer mechanism of Ho^{3+} doped silicate germanate glass sensitized by Tm^{3+} ions, *Opt. Laser. Technol.* 111 (2019) 115–120, <https://doi.org/10.1016/j.optlastec.2018.09.043>.
- [31] M. Kochanowicz, J. Zmojda, P. Miluski, T. Ragin, W.A. Pisarski, J. Pisarska, R. Jadach, M. Sitarz, D. Dorosz, Structural and luminescent properties of germanate glasses and double-clad optical fiber co-doped with $\text{Yb}^{3+}/\text{Ho}^{3+}$, *J. Alloy. Compd.* 727 (2017) 1221–1226, <https://doi.org/10.1016/j.jallcom.2017.08.243>.
- [32] M. Kochanowicz, J. Zmojda, P. Miluski, A. Baranowska, M. Leich, A. Schwuchow, M. Jäger, M. Kuwik, J. Pisarska, W.A. Pisarski, D. Dorosz, $\text{Tm}^{3+}/\text{Ho}^{3+}$ co-doped germanate glass and double-clad optical fiber for broadband emission and lasing above 2 μm , *Opt. Mater. Express* 9 (2019) 1450–1458, <https://doi.org/10.1364/OME.9.001450>.
- [33] K. Neeraja, T.G.V.M. Rao, A. Rupesh Kumar, Influence of modifier oxide on spectroscopic properties of $\text{Ho}^{3+}:\text{V}^{4+}$ co-doped $\text{Na}_2\text{O}-\text{SiO}_2-\text{ZrO}_2$ glasses, *J. Alloy. Compd.* 586 (2014) 159–168, <https://doi.org/10.1016/j.jallcom.2013.10.038>.
- [34] K. Mariselvam, Juncheng Liu, Green emission and laser properties of Ho^{3+} doped titano lead borate (TLB) glasses for colour display applications, *J. Solid State Chem.* 293 (2021), 121793, <https://doi.org/10.1016/j.jssc.2020.121793>.
- [35] T. Jayachandra Prasad, G. Neelima, N. Ravi, N. Kiran, N.K.R. Nallabala, V. K. Kummara, K. Suresh, P. Gadige, Optical and spectroscopic properties of Ho^{3+} -doped fluorophosphate glasses for visible lighting applications, *Mater. Res. Bull.* 124 (2020), 110753, <https://doi.org/10.1016/j.materresbull.2019.110753>.
- [36] G. Gupta, S. Balaji, K. Biswas, K. Annapurna, Enhanced luminescence at 2.88 and 2.04 μm from $\text{Ho}^{3+}/\text{Yb}^{3+}$ codoped low phonon energy $\text{TeO}_2-\text{TiO}_2-\text{La}_2\text{O}_3$ glass, *AIP Adv.* 9 (2019), 045201, <https://doi.org/10.1063/1.5054190>.
- [37] J.J. Leal, E. Rodríguez, C.G. Nava-Dino, M.C. Maldonado-Orozco, F. Gaxiola, R. Narro-García, Effect of Ho^{3+} concentration on the luminescent and thermal stability of tellurite glasses, *Mater. Res. Bull.* 144 (2021), 111483, <https://doi.org/10.1016/j.materresbull.2021.111483>.
- [38] W.A. Pisarski, K. Kowalska, M. Kuwik, J. Polak, E. Pietrasik, T. Goryczka, J. Pisarska, Novel multicomponent titanate-germanate glasses: synthesis, structure, properties, transition metal, and rare earth doping, *Materials* 13 (2020) 4422, <https://doi.org/10.3390/ma13194422>.
- [39] S.P. Sinha, *Complexes of the Rare Earths*, Pergamon Press Ltd., Oxford, 1966.
- [40] W.T. Carnall, P.R. Fields, K. Rajnak, Electronic energy levels in the trivalent lanthanide aquo ions. I. Pr^{3+} , Nd^{3+} , Pm^{3+} , Sm^{3+} , Dy^{3+} , Ho^{3+} , Er^{3+} , and Tm^{3+} , *J. Chem. Phys.* 49 (1968) 4424–4442, <https://doi.org/10.1063/1.1669893>.
- [41] B.R. Judd, Optical absorption intensities of rare-earth ions, *Phys. Rev.* 127 (1962) 750–761, <https://doi.org/10.1103/PhysRev.127.750>.
- [42] G.S. Ofelt, Intensities of crystal spectra of rare-earth ions, *J. Chem. Phys.* 37 (1962) 511–520, <https://doi.org/10.1063/1.1701366>.
- [43] C. Yu, X. Zhang, X. Li, J. Zhang, S. Xu, X. Zhang, Y. Zhang, X. Wang, L. Wang, G. Sui, B. Chen, Determination of Judd-Ofelt parameters for Eu^{3+} -doped alkali borate glasses, *Mater. Res. Bull.* 120 (2019), 110590, <https://doi.org/10.1016/j.materresbull.2019.110590>.
- [44] W. Luo, J. Liao, R. Li, X. Chen, Determination of Judd-Ofelt intensity parameters from the excitation spectra for rare-earth doped luminescent materials, *Phys. Chem. Chem. Phys.* 12 (2010) 3276–3282, <https://doi.org/10.1039/B921581F>.
- [45] Y. Zhang, B. Chen, S. Xu, X. Li, J. Zhang, J. Sun, X. Zhang, H. Xia, R. Hua, A universal approach for calculating the Judd-Ofelt parameters of RE^{3+} in powdered phosphors and its application for the $\beta\text{-NaYF}_4:\text{Er}^{3+}/\text{Yb}^{3+}$ phosphor derived from auto-combustion-assisted fluoridation, *Phys. Chem. Chem. Phys.* 20 (2018) 15876–15883, <https://doi.org/10.1039/C8CP02317D>.
- [46] M. Luo, B. Chen, X. Li, J. Zhang, S. Xu, X. Zhang, Y. Cao, J. Sun, Y. Zhang, X. Wang, Y. Zhang, D. Gao, L. Wang, Fluorescence decay route of optical transition calculation for trivalent rare earth ions and its application for Er^{3+} -doped NaYF_4 phosphor, *Phys. Chem. Chem. Phys.* 22 (2020) 25177–25183, <https://doi.org/10.1039/D0CP04379F>.
- [47] F. Huang, J. Cheng, X. Liu, L. Hu, D. Chen, $\text{Ho}^{3+}/\text{Er}^{3+}$ doped fluoride glass sensitized by Ce^{3+} pumped by 1550nm LD for efficient 2.0 μm laser applications, *Opt. Express* 22 (2014) 20924–20935, <https://doi.org/10.1364/OE.22.020924>.
- [48] G. Tang, T. Zhu, W. Liu, W. Lin, T. Qiao, M. Sun, D. Chen, Q. Qian, Z. Yang, Tm^{3+} doped lead silicate glass single mode fibers for 2.0 μm laser applications, *Opt. Mater. Express* 6 (2016) 2147–2157, <https://doi.org/10.1364/OME.6.002147>.
- [49] G. Tang, D. Yang, W. Huang, L. Kuang, W. Lin, Y. Zhang, F. Zhang, Z. Nie, D. Chen, Q. Qian, Z. Yang, Nd^{3+} doped multi-component phosphate glass multi-material fiber for a 1.05 μm laser, *Opt. Mater. Express* 11 (2021) 3966–3973, <https://doi.org/10.1364/OME.442565>.
- [50] T. Wei, Y. Tian, C. Tian, X. Jing, M. Cai, J. Zhang, L. Zhang, S. Xu, Comprehensive evaluation of the structural, absorption, energy transfer, luminescent properties and near-infrared applications of the neodymium doped germanate glass, *J. Alloy. Compd.* 618 (2015) 95–101, <https://doi.org/10.1016/j.jallcom.2014.08.139>.
- [51] M. Cai, T. Wei, B. Zhou, Y. Tian, J. Zhou, S. Xu, J. Zhang, Analysis of energy transfer process based emission spectra of erbium doped germanate glasses for mid-infrared laser materials, *J. Alloy. Compd.* 626 (2015) 165–172, <https://doi.org/10.1016/j.jallcom.2014.11.077>.
- [52] S.A. Jupri, S.K. Ghoshal, M.F. Omar, N.N. Yusof, Spectroscopic traits of holmium in magnesium zinc sulfophosphate glass host: judd-Ofelt evaluation, *J. Alloy. Compd.* 753 (2018) 446–456, <https://doi.org/10.1016/j.jallcom.2018.04.218>.
- [53] A.S. Alqarni, R. Hussin, S.K. Ghoshal, S.N. Alamri, Y.A. Yamusa, S.A. Jupri, Intense red and green luminescence from holmium activated zinc-sulfo-boro-phosphate glass: judd-Ofelt evaluation, *J. Alloy. Compd.* 808 (2019), 151706, <https://doi.org/10.1016/j.jallcom.2019.151706>.
- [54] B. Zhou, E.Y.B. Pun, H. Lin, D. Yang, L. Huang, Judd-Ofelt analysis, frequency upconversion, and infrared photoluminescence of Ho^{3+} -doped and $\text{Ho}^{3+}/\text{Yb}^{3+}$ -codoped lead bismuth gallate oxide glasses, *J. Appl. Phys.* 106 (2009), 103105, <https://doi.org/10.1063/1.3256184>.
- [55] B.J. Chen, J.X. Yang, E.Y.B. Pun, X. Zhao, H. Lin, Gain anticipation of Ho^{3+} in ion-exchangeable germanate waveguide glasses, *Appl. Phys. B* 124 (2018) 226, <https://doi.org/10.1007/s00340-018-7085-8>.
- [56] Y.P. Peng, Y. Guo, J. Zhang, L. Zhang, $\text{Ho}^{3+}/\text{Yb}^{3+}$ -codoped germanate-tellurite glasses for 2.0 μm emission performance, *Appl. Opt.* 53 (2014) 1564–1569, <https://doi.org/10.1364/AO.53.001564>.
- [57] M. Cai, B. Zhou, F. Wang, Y. Tian, J. Zhou, S. Xu, J. Zhang, Highly efficient mid-infrared 2 μm emission in $\text{Ho}^{3+}/\text{Yb}^{3+}$ -codoped germanate glass, *Opt. Mater. Express* 5 (2015) 1431–1439, <https://doi.org/10.1364/OME.5.001431>.
- [58] X. Fan, P. Kuan, K. Li, L. Zhang, D. Li, L. Hu, Spectroscopic properties and quenching mechanism of 2 μm emission in Ho^{3+} doped germanate glasses and fibers, *Opt. Mater. Express* 5 (2015) 1356–1365, <https://doi.org/10.1364/OME.5.001356>.
- [59] K. Kowalska, M. Kuwik, J. Pisarska, M. Leśniak, D. Dorosz, M. Kochanowicz, J. Zmojda, J. Dorosz, W.A. Pisarski, Influence of TiO_2 concentration on near-infrared luminescence of Er^{3+} ions in barium gallo-germanate glasses, *J. Mater. Res. Technol.* 21 (2022) 4761–4772, <https://doi.org/10.1016/j.jmrt.2022.11.081>.
- [60] W. Blanc, Y.G. Choi, X. Zhang, M. Nalin, K.A. Richardson, G.C. Righini, M. Ferrari, A. Jha, J. Massera, S. Jiang, J. Ballato, L. Petit, The past, present and future of photonic glasses: a review in homage to the United Nations International Year of glass 2022, *Prog. Mater. Sci.* 134 (2023), 101084, <https://doi.org/10.1016/j.pmatsci.2023.101084>.

P9

Marta Kuwik, Karolina Kowalska, Joanna Pisarska, Wojciech A. Pisarski,

**Experimental and theoretical studies on NIR luminescence
of titanate-germanate glasses doped with Pr³⁺ and Tm³⁺ ions**

Journal of the American Ceramic Society 106 (2022) 7460-7472

RESEARCH ARTICLE

Experimental and theoretical studies on NIR luminescence of titanate-germanate glasses doped with Pr³⁺ and Tm³⁺ ions

Marta Kuwik  | Karolina Kowalska  | Joanna Pisarska  |
Wojciech A. Pisarski 

Institute of Chemistry, University of Silesia, Katowice, Poland

Correspondence

Marta Kuwik, Institute of Chemistry, University of Silesia, Szkolna 9, Katowice 40-007, Poland.
Email: marta.kuwik@us.edu.pl

Funding information

National Science Centre (Poland), Grant/Award Number: 2018/31/B/ST8/00166; Narodowe Centrum Nauki, Grant/Award Number: 2018/31/B/ST8/00166

Abstract

Near-infrared (NIR) luminescence of Pr³⁺ and Tm³⁺ ions in titanate-germanate glasses has been studied for laser and fiber amplifier applications. The effect of the molar ratio GeO₂:TiO₂ (from 5:1 to 1:5) on spectroscopic properties of glass systems was studied by absorption, luminescence measurements, and theoretical calculations using the Judd–Ofelt theory. It was found that independent of the TiO₂ concentration, intense NIR emissions at 1.5 and 1.8 μm were observed for glasses doped with Pr³⁺ and Tm³⁺ ions, respectively. Moreover, several spectroscopic and NIR laser parameters for Pr³⁺ and Tm³⁺ ions, such as emission bandwidth, stimulated emission cross-section, quantum efficiency, gain bandwidth, and figure of merit, were determined. The results were discussed in detail and compared to the different laser glasses. Systematic investigations indicate that Pr³⁺-doped system with GeO₂:TiO₂ = 2:1 and Tm³⁺-doped glass with GeO₂:TiO₂ = 1:2 present profit laser parameters and could be successfully applied to NIR lasers and broadband optical amplifiers.

KEYWORDS

Judd–Ofelt parameters, lasers, luminescence, rare earths

1 | INTRODUCTION

Optical sources such as glasses and glass ceramics doped with trivalent rare-earth ions (RE³⁺) operating in the near-infrared (NIR) spectral range are interesting systems due to their wide field of applications in the fabrication of fibers, waveguides, solid-state lasers, and amplifiers.^{1–7} Moreover, the significant progress in modern information technology and capacity in optoelectronics demands searching for new optical fiber amplifiers with broad and efficient gain bandwidth in the telecommunication windows.^{8–10} Therefore, inorganic materials doped with RE³⁺ ions, such as trivalent praseodymium (Pr³⁺) and thulium (Tm³⁺) ions, have been paid attention owing to their unique spectroscopic properties. In view of broadband NIR emission

covering a wide region of the optical telecommunication window (1.3–1.7 μm), the systems doped with Pr³⁺ ions have been widely investigated as potential materials for optical amplification.^{11–13} On the other hand, glasses containing Tm³⁺ ions can be useful in the production of fiber optic amplifiers (TDFAs) for S-band¹⁴ and infrared lasers due to the NIR luminescence at about 1.8 μm corresponding to ³F₄ → ³H₆ transition of thulium ions.¹⁵

It is well known that the luminescence properties of RE³⁺ ions are sensitive to the chemical composition of the glass matrix. The choice of the host material is an essential factor that needs to be considered when developing new optical glass materials. For that reason, the spectroscopic studies mainly focus on low phonon energy systems such as tellurite,^{16,17} fluoroindate,¹⁸ zinc fluoride,¹⁹ and

germanate^{20,21} glasses. Glass systems with low phonon energy are more suitable as host materials for the RE³⁺ because of the less probable non-radiative relaxation process. Consequently, those materials are characterized by higher quantum efficiency of photoluminescence and/or a longer luminescence lifetime of the excited state of RE³⁺ ions. Zhou et al.²² studied NIR luminescence properties of fluorotellurite glass systems doped with Er³⁺ ions in the relatively unexplored wavelength region (1.2 μm). It was stated that the observed intense emission corresponding to the $^4\text{S}_3 \rightarrow ^4\text{I}_{11/2}$ transition of Er³⁺ ions was mainly contributed by the relatively low phonon energy of the fluorotellurite glass host ($\sim 776\text{ cm}^{-1}$). The investigations of fluoroindate glasses co-doped with Pr³⁺ and Er³⁺ ions indicate that those systems with their phonon energies close to 510 cm^{-1} are promising materials for broadband optical amplifiers. The NIR luminescence (full width at half maximum [FWHM] = 278 nm) associated with the $^1\text{G}_4 \rightarrow ^3\text{H}_5$ (Pr³⁺), $^1\text{D}_2 \rightarrow ^1\text{G}_4$ (Pr³⁺), and $^4\text{I}_{13/2} \rightarrow ^4\text{I}_{15/2}$ (Er³⁺) transitions of rare-earth ions in glass system are successfully observed under direct excitation at 483 nm.²³ According to Wen et al.,²⁴ the lower phonon energy ($\sim 845\text{ cm}^{-1}$), as well as the smaller OH⁻ absorption coefficient of barium gallo-germanate glasses, could reduce the probability of non-radiative relaxation and thus enhance luminescence at 1.8 μm , corresponding to $^3\text{F}_4 \rightarrow ^3\text{H}_6$ transition of Tm³⁺ ions.

Furthermore, previously published results proved that the presence of modifier oxides has an important influence on the structural, thermal, and spectroscopic properties of low phonon glass systems containing rare-earth ions.^{25–27} Among metal oxides that are components of glasses emitting NIR luminescence, titanium(IV) oxide (TiO₂) deserves particular attention.^{28,29} The addition of TiO₂ increases the linear and non-linear refractive indices, increasing the radiative transition probabilities and improving the non-linear optical properties.³⁰ Thermal studies indicate that glasses with low TiO₂ content as a modifier exhibit high stability against crystallization.³¹ Moreover, small quantities of TiO₂ in the host matrices enhance the glass-forming ability and chemical durability of the glass systems.^{32,33} On the contrary, oxide modifiers TiO₂ added to some glass matrices effectively promotes crystallization.³⁴ Therefore, it is challenging to synthesize thermally stable and fully amorphous systems with high TiO₂ concentrations. To the best of our knowledge, the NIR luminescence properties of rare-earth ions in low phonon energy germanate glass matrices are not frequently examined in the function of TiO₂ at high concentration.

For that reason, in our study, titanate-germanate glass systems singly doped with Pr³⁺ and Tm³⁺ ions were

fabricated, and their properties were investigated. Spectroscopic properties of obtained materials were analyzed as a function of the molar ratio GeO₂:TiO₂ (from 5:1 to 1:5) in the glass compositions. The NIR emission spectra and luminescence decay curves for glass systems doped with Pr³⁺ and Tm³⁺ ions were registered and discussed in detail. Based on measurements, some spectroscopic parameters for rare-earth ions in glasses depending critically on the molar ratio GeO₂:TiO₂ were defined. Moreover, the optical properties of Pr³⁺ and Tm³⁺ ions in studied glass systems were characterized by standard Judd–Ofelt theory.

2 | EXPERIMENTAL

Titanate-germanate glasses with the following composition: $(60 - x)\text{GeO}_2 - x\text{TiO}_2 - 30\text{BaO} - 9.9\text{Ga}_2\text{O}_3 - 0.1\text{Ln}_2\text{O}_3$ (where $x = 0, 10, 20, 30, 40, 45, 50\text{ mol}\%$ and Ln = Pr, Tm) were synthesized using the melt-quenching technique. Appropriate amounts of metal oxides (99.99%, Aldrich Chemical Co.) were mixed homogeneously together in an agate ball mill. Then, the glass baths were placed in a corundum crucible (Łukasiewicz Research Network, Institute of Ceramics and Building Materials) and were melted at 1250°C for 60 min in an electric furnace (FCF 4/170 M produced by Czyłok). In order to eliminate internal mechanical stresses, each sample was quenched and annealed below the glass transition temperature (T_g). Finally, the samples were slowly cooled to room temperature and obtained transparent glass systems were shaped and polished for further optical measurements.

In the first step, the refractive indices for all titanate-germanate glasses were determined using the Model 2010/M prism coupler at 632.8 nm. Next, optical measurements were carried out for systems with different GeO₂:TiO₂ molar ratios at room temperature. The absorption spectra were recorded using a Cary 5000 UV–vis–NIR spectrophotometer (Agilent Technology). In contrast, Photon Technology International (PTI) QuantaMaster 40 (QM40) UV/VIS steady-state spectrofluorometer was used to perform the luminescence spectra and decay curves. The laser system was equipped with a tunable pulsed optical parametric oscillator, Nd:YAG laser, and xenon lamp as excitation sources and double 200 mm monochromators. A Hamamatsu H10330B-75 detector was used to record the NIR emission spectra. The resolution for spectral measurements was $\pm 0.5\text{ nm}$. Decay curves were registered and stored by a PTI ASOC-10 (USB-2500) oscilloscope with an accuracy of $\pm 1\ \mu\text{s}$.

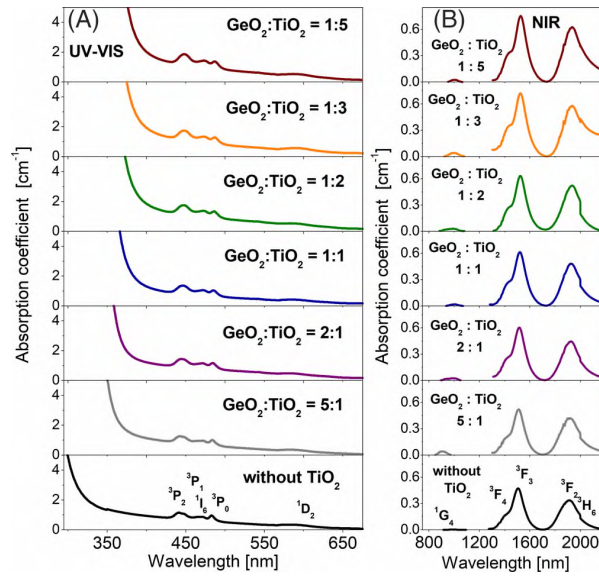


FIGURE 1 UV-vis (A) and near-infrared (NIR) (B) absorption spectra of Pr^{3+} ions in titanate-germanate glasses.

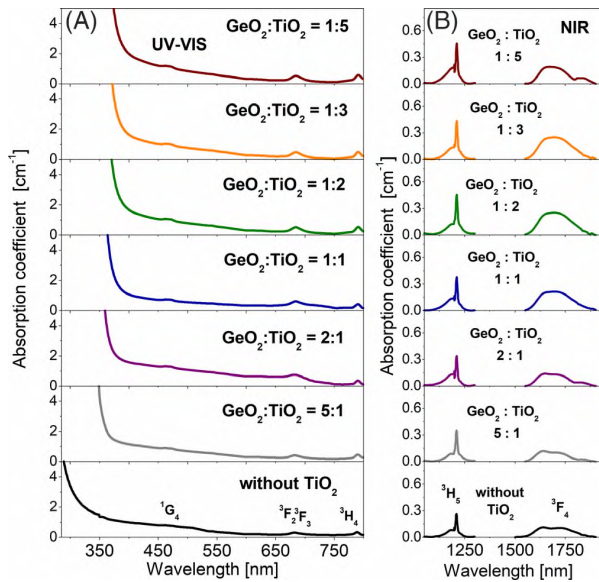


FIGURE 2 UV-vis (A) and near-infrared (NIR) (B) absorption spectra of Tm^{3+} ions in titanate-germanate glasses.

3 | RESULTS AND DISCUSSION

3.1 | Absorption spectra and Judd–Ofelt analysis

The absorption spectra of titanate-germanate glasses singly doped with Pr^{3+} and Tm^{3+} ions are presented in Figures 1 and 2, respectively. The spectra consist of

inhomogeneously broadened absorption lines characteristic of the $4f^2-4f^2$ (Pr^{3+}) and $4f^{12}-4f^{12}$ (Tm^{3+}) transitions of RE^{3+} . They are located in the visible and as well as NIR spectral ranges. These absorption lines of Pr^{3+} correspond to the transitions from the $^3\text{H}_4$ ground state to the $^3\text{H}_6$, $^3\text{F}_2$, $^3\text{F}_3$, $^3\text{F}_4$, $^1\text{G}_4$, $^1\text{D}_2$, $^3\text{P}_0$, $^3\text{P}_1$, $^1\text{I}_6$, and $^3\text{P}_2$ excited states. The absorption lines of Tm^{3+} are related to transitions originating from the $^3\text{H}_6$ ground state to the $^3\text{F}_4$, $^3\text{H}_5$, $^3\text{H}_4$, $^3\text{F}_3$, $^3\text{F}_2$, and $^1\text{G}_4$ excited states. In both cases, the absorption lines are shifted to longer wavelengths with increasing TiO_2 concentration. The UV cut-off derived from the absorption spectra of Pr^{3+} and Tm^{3+} ions and the refractive index of the glass host as a function of the molar ratio $\text{GeO}_2:\text{TiO}_2$ (from 5:1 to 1:5) are summarized in Table 1.

The experimental oscillator strengths for rare-earth ions were determined from the optical absorption spectra. In the next step, the theoretical oscillator strengths for each transition of Pr^{3+} and Tm^{3+} ions were calculated using the Judd–Ofelt theory.^{35,36} The theoretical oscillator strength is defined as follows:

$$P_{\text{calc}} = \frac{8\pi^2 mc(n^2 + 2)^2}{3h\lambda(2J + 1) \times 9n} \times \sum_{t=2,4,6} \Omega_t (\langle 4f^N J \| U^t \| 4f^N J' \rangle)^2 \quad (1)$$

where m is the mass of the electron, c is the velocity of light, h is the Planck constant, and λ is the mean wavelength of each transition. In order to perform the analysis, the refractive index of the medium (Table 1) and $\|U^t\|^2$ from,³⁷ representing the square of the matrix elements of the unit tensor operator U^t , were used for calculations. At this moment, it should be pointed out that $\|U^t\|^2$ are the doubly reduced matrix elements of the unit tensor operators of the rank $t = 2, 4, 6$ evaluated in the intermediate coupling approximation for each transition between the initial J and terminal J' states, which practically do not vary with different glass hosts.³⁸ This calculation procedure with the host insensitive reduced matrix elements $\|U^t\|^2$ taken from Carnall et al.³⁷ was applied for several glass systems doped with Pr^{3+} and Tm^{3+} ions.^{39–43} Next, the experimental and theoretical oscillator strengths were compared. They are given in Tables 2 and 3.

It should be pointed out that the $^3\text{H}_4 \rightarrow ^3\text{P}_2$ transition of Pr^{3+} was omitted from the Judd–Ofelt analysis due to the anomalous behavior of this transition.⁴⁴ Due to too high a discrepancy between the measured and calculated oscillator strengths, the $^3\text{H}_6 \rightarrow ^3\text{H}_5$ transition of Tm^{3+} was also excluded from the fitting. This transition is connected with the contributions of magnetic dipole line strengths strongly influencing the fitting procedure.

TABLE 1 Glass composition, GeO₂:TiO₂ molar ratio, rare-earth ions concentration, UV cut-off, and refractive index of glass host.

Glass composition (mol%) ^a	GeO ₂ :TiO ₂	N × 10 ¹⁹ (g/cm ³)		UV cut-off (nm)		n
		Pr ³⁺	Tm ³⁺	Pr ³⁺	Tm ³⁺	
60GeO ₂ -30BaO-9.9Ga ₂ O ₃ -0.1Ln ₂ O ₃	-	4.94	4.94	283	282	1.736
50GeO ₂ -10TiO ₂ -30BaO-9.9Ga ₂ O ₃ -0.1Ln ₂ O ₃	5:1	5.07	5.06	343	341	1.779
40GeO ₂ -20TiO ₂ -30BaO-9.9Ga ₂ O ₃ -0.1Ln ₂ O ₃	2:1	5.14	5.13	353	352	1.830
30GeO ₂ -30TiO ₂ -30BaO-9.9Ga ₂ O ₃ -0.1Ln ₂ O ₃	1:1	5.20	5.19	359	360	1.877
20GeO ₂ -40TiO ₂ -30BaO-9.9Ga ₂ O ₃ -0.1Ln ₂ O ₃	1:2	5.29	5.29	364	363	1.928
15GeO ₂ -45TiO ₂ -30BaO-9.9Ga ₂ O ₃ -0.1Ln ₂ O ₃	1:3	5.41	5.41	368	365	1.969
10GeO ₂ -50TiO ₂ -30BaO-9.9Ga ₂ O ₃ -0.1Ln ₂ O ₃	1:5	5.49	5.49	370	369	1.998

^aLn = Pr or Tm.TABLE 2 Measured and calculated oscillator strengths (×10⁻⁶) for Pr³⁺ ions in titanate-germanate glasses.

States	Energy (cm ⁻¹)	Glass composition													
		60GeO ₂		50GeO ₂ -10TiO ₂		40GeO ₂ -20TiO ₂		30GeO ₂ -30TiO ₂		20GeO ₂ -40TiO ₂		15GeO ₂ -45TiO ₂		10GeO ₂ -50TiO ₂	
		P _{meas}	P _{calc}	P _{meas}	P _{calc}	P _{meas}	P _{calc}	P _{meas}	P _{calc}	P _{meas}	P _{calc}	P _{meas}	P _{calc}	P _{meas}	P _{calc}
³ P ₁ , ¹ I ₆	21 400	4.510	4.867	4.380	4.764	5.630	5.805	5.520	5.718	5.760	5.932	5.210	5.512	6.260	6.570
³ P ₀	20 600	3.820	3.405	3.660	3.213	4.190	3.986	4.140	3.910	4.280	4.079	3.910	3.558	4.790	4.430
¹ D ₂	17 000	0.850	0.726	0.850	0.823	0.830	0.986	0.780	0.977	0.980	0.964	0.950	1.161	1.480	1.123
¹ G ₄	9900	0.200	0.202	0.250	0.231	0.330	0.276	0.260	0.274	0.300	0.269	0.300	0.329	0.330	0.315
³ F ₃ , ³ F ₄	6650	6.580	6.580	7.520	7.519	8.940	8.937	8.880	8.875	8.760	8.760	10.650	10.644	10.270	10.275
³ H ₆ , ³ F ₂	5200	3.650	3.649	5.020	5.019	4.920	4.919	5.100	5.099	5.220	5.219	7.310	7.309	7.020	7.019
rms deviation		0.053		0.058		0.017		0.022		0.012		0.043		0.059	

Transitions are from the ³H₄ ground state to the levels indicated. The root-mean-square (rms) deviation (×10⁻⁶) is also given.TABLE 3 Measured and calculated oscillator strengths (×10⁻⁶) for Tm³⁺ ions in titanate-germanate glasses.

States	Energy (cm ⁻¹)	Glass composition													
		60GeO ₂		50GeO ₂ -10TiO ₂		40GeO ₂ -20TiO ₂		30GeO ₂ -30TiO ₂		20GeO ₂ -40TiO ₂		15GeO ₂ -45TiO ₂		10GeO ₂ -50TiO ₂	
		P _{meas}	P _{calc}	P _{meas}	P _{calc}	P _{meas}	P _{calc}	P _{meas}	P _{calc}	P _{meas}	P _{calc}	P _{meas}	P _{calc}	P _{meas}	P _{calc}
¹ G ₄	21 900	6.500	6.304	5.500	5.140	5.500	5.640	1.200	1.170	1.110	1.087	1.100	1.082	0.700	0.687
³ F ₂ , ³ F ₃	14 650	1.680	1.680	2.230	2.230	2.840	2.840	3.890	3.890	3.390	3.390	3.310	3.310	3.630	3.630
³ H ₄	12 650	0.890	0.890	2.060	2.059	1.500	1.500	1.340	1.339	2.640	2.640	2.420	2.420	3.040	3.040
³ F ₄	5900	1.900	1.900	1.750	1.751	1.780	1.780	3.450	3.451	3.450	3.451	3.400	3.400	2.370	2.370
rms deviation		0.010		0.032		0.005		0.002		0.002		0.001		0.001	

Note: Transitions are from the ³H₆ ground state to the levels indicated. The root-mean-square (rms) deviation (×10⁻⁶) is also given.

The three Judd-Ofelt intensity parameters Ω_t ($t = 2, 4, 6$) for rare-earth ions in titanate-germanate glasses were evaluated (Tables 4 and 5). The fit quality was expressed by the magnitude of the root-mean-square (rms) deviation, which is defined by $\text{rms} = \Sigma(P_{\text{meas}} - P_{\text{calc}})^2$.

In the next step, the intensity parameters Ω_t ($t = 2, 4, 6$) were applied to calculate the radiative transition rates, luminescence branching ratios, and radiative lifetimes. The radiative transition rates A_J for excited states of Pr³⁺ and Tm³⁺ ions from an initial level J to a final ground level

J' were calculated using the following relation:

$$A_J = \frac{64\pi^4 e^2}{3h(2J+1)\lambda^3} \times \frac{n(n^2+2)^2}{9} \times \sum_{t=2,4,6} \Omega_t (\langle 4f^N J \| U^t \| 4f^N J' \rangle)^2 \quad (2)$$

The total radiative emission rate A_T involving all the intermediate terms is the sum of the A_J terms. The

TABLE 4 The Judd–Ofelt intensity parameters Ω_t ($t = 2, 4, 6$) $\times 10^{-2}$ cm² for Pr³⁺ ions.

TiO ₂ content (mol%)	GeO ₂ :TiO ₂	Ω_2	Ω_4	Ω_6
0	–	1.60 ± 0.27	4.93 ± 0.30	2.54 ± 0.11
10	5:1	4.09 ± 0.27	4.49 ± 0.30	2.96 ± 0.11
20	2:1	2.55 ± 0.16	5.35 ± 0.17	3.45 ± 0.06
30	1:1	2.87 ± 0.17	5.05 ± 0.18	3.29 ± 0.07
40	1:2	2.84 ± 0.11	5.05 ± 0.12	3.01 ± 0.01
45	1:3	6.14 ± 0.21	4.26 ± 0.23	3.90 ± 0.10
50	1:5	4.90 ± 0.25	5.17 ± 0.27	3.34 ± 0.10

TABLE 5 The Judd–Ofelt intensity parameters Ω_t ($t = 2, 4, 6$) $\times 10^{-2}$ cm² for Tm³⁺ ions.

TiO ₂ content (mol%)	GeO ₂ :TiO ₂	Ω_2	Ω_4	Ω_6
0	–	1.11 ± 0.03	2.35 ± 0.02	0.10 ± 0.01
10	5:1	2.87 ± 0.05	0.41 ± 0.04	0.88 ± 0.01
20	2:1	1.10 ± 0.02	1.71 ± 0.02	0.72 ± 0.01
30	1:1	0.53 ± 0.04	4.72 ± 0.03	0.25 ± 0.01
40	1:2	3.29 ± 0.03	2.29 ± 0.02	0.68 ± 0.01
45	1:3	2.84 ± 0.02	2.43 ± 0.02	0.57 ± 0.01
50	1:5	3.18 ± 0.02	0.43 ± 0.01	1.23 ± 0.01

radiative lifetime τ_{rad} of an excited level is the inverse of the total radiative emission rate. In contrast, the luminescence branching ratio β is due to the relative intensities of transitions from the excited state to all terminal states. The expressions for the radiative lifetime and luminescence branching ratio are given below:

$$\tau_{\text{rad}} = \frac{1}{\sum_i A_{Ji}} = \frac{1}{A_T} \quad (3)$$

$$\beta = \frac{A_J}{\sum_i A_{Ji}} \quad (4)$$

The calculated radiative transition rates A_J and luminescence branching ratios β for Pr³⁺ and Tm³⁺ ions in titanate-germanate glasses are shown in Tables 6–9. The calculation results are limited to transitions originating from the ¹D₂ state of Pr³⁺ as well as the ³H₄ and ³F₄ excited states of Tm³⁺, from which the main luminescence lines in the NIR range occur.

3.2 | Near-infrared luminescence spectra and decay

Figure 3a presents the NIR luminescence spectra registered under direct excitation at 450 nm (³P₂ state)

for titanate-germanate glasses doped with Pr³⁺ ions. Independent of the GeO₂:TiO₂ molar ratio, two emission bands were registered for all studied glass systems. The most intense band at 1040 nm corresponds to ¹D₂ → (³F₃, ³F₄) transition, whereas the broad NIR band covers a wavelength range from 1300 nm to about 1625 nm. For that reason, it was necessary to use deconvolution of this band for better understanding (Figure 3b). Based on the deconvolution procedure, it was stated that the broad-band emission consists of four luminescent bands, which are important for optical fiber amplifiers operating at the telecommunication window and cover E (1360–1460 nm), S (1460–1530 nm), and C + L (1530–1625 nm) bands. Among these bands, the most intense NIR luminescence band centered at about 1490 nm is attributed to the ¹D₂ → ¹G₄ transition of praseodymium ions.⁴⁵ On the other hand, bands at about 1358, 1565, and 1600 nm are due to ¹G₄ → ³H₅, ³F₄ → ³H₄, and ³F₃ → ³H₄ transitions of Pr³⁺ ions, respectively (Figure 3c). It was stated that the intensity of registered emission bands depends on glass composition, and the system with 40 mol% TiO₂ exhibits the greatest NIR luminescence. Moreover, the ¹D₂ → ¹G₄ transition of Pr³⁺ ions is shifted to shorter wavelengths from 1513 nm (glass without TiO₂) to 1491.5 nm (system with 50 mol% TiO₂). This relation is similar to the results of research in Pr³⁺-doped fluorotellurite glasses. Zhou et al.⁴⁶ reported that the maximum broadband emission covering the 1.30–1.67 μ m spectral region moves to short wavelengths with increasing rare-earth ions in the glass composition.

Also, the NIR emission spectra for titanate-germanate glass systems doped with Tm³⁺ ions were recorded under excitation at 808 nm (³H₄ state). Figure 4a shows two broad emission bands at about 1.47 and 1.8 μ m. It was observed that the intensity of these bands originating from ³H₄ → ³F₄ and ³F₄ → ³H₆ transitions of Tm³⁺ ions significantly increased with the change in the GeO₂:TiO₂ molar ratio. The most intensive NIR luminescence occurs for glass with 50 mol% TiO₂. Furthermore, the emission peak wavelength λ_p for the ³F₄ → ³H₆ transition of Tm³⁺ ions is shifted to shorter and then to longer wavelengths when GeO₂:TiO₂ molar ratio changes from 5:1 to 2:1 and from 1:1 to 1:5, respectively. According to Tang et al.,⁴⁷ introducing TiO₂ to tellurite systems causes a shift to longer wavelengths in the 1.8 μ m luminescence band position. The presence of TiO₂ in the glass host enhances the optical alkalinity of the system due to the increasing number of non-bridged oxygen bonds. Hence, the O²⁻ in the glass structure has a higher polarizability, giving good covalency and asymmetry to the system. Additionally, NIR emission observed when the glass samples were excited by 470 nm is due to the ³H₅ → ³H₆ transition of thulium ions.⁴⁸

Next, the influence of the GeO₂:TiO₂ molar ratio on the spectroscopic properties of a glass system doped with rare-earth ions was examined based on luminescence decay

TABLE 6 The calculated radiative transition probabilities A_J and luminescence branching ratios β for Pr^{3+} ions in germanate glass without TiO_2 and titanate-germanate glasses (0, 10, 20, and 30 mol% TiO_2).

Transition	Average wavelength (nm)	Glass composition							
		60GeO ₂		50GeO ₂ -10TiO ₂		40GeO ₂ -20TiO ₂		30GeO ₂ -30TiO ₂	
		A_J (s ⁻¹)	β	A_J (s ⁻¹)	β	A_J (s ⁻¹)	β	A_J (s ⁻¹)	β
¹ D ₂ → ³ H ₄	588	741	0.274	877	0.205	1116	0.265	1163	0.250
³ H ₅	683	23	0.009	25	0.006	31	0.007	32	0.007
³ H ₆	805	461	0.170	463	0.108	606	0.144	626	0.135
³ F ₂	844	504	0.186	545	0.127	672	0.159	703	0.151
³ F ₃	950	110	0.041	181	0.042	167	0.040	188	0.040
³ F ₄	995	628	0.232	1704	0.397	1193	0.282	1458	0.315
¹ G ₄	1480	237	0.088	494	0.115	429	0.102	475	0.102
A_{TOTAL} (s ⁻¹)		2705		4289		4214		4645	

TABLE 7 The calculated radiative transition probabilities A_J and luminescence branching ratios β for Pr^{3+} ions in titanate-germanate glasses (40, 45, and 50 mol% TiO_2).

Transition	Average wavelength (nm)	Glass composition					
		20GeO ₂ -40TiO ₂		15GeO ₂ -45TiO ₂		10GeO ₂ -50TiO ₂	
		A_J (s ⁻¹)	β	A_J (s ⁻¹)	β	A_J (s ⁻¹)	β
¹ D ₂ → ³ H ₄	588	1211	0.242	1514	0.191	1507	0.199
³ H ₅	683	35	0.007	34	0.004	41	0.005
³ H ₆	805	686	0.137	642	0.081	803	0.106
³ F ₂	844	773	0.154	797	0.101	952	0.125
³ F ₃	950	206	0.041	335	0.042	322	0.042
³ F ₄	995	1587	0.317	3655	0.462	3080	0.406
¹ G ₄	1480	512	0.102	940	0.119	884	0.117
A_{TOTAL} (s ⁻¹)		5008		7917		7589	

TABLE 8 The calculated radiative transition probabilities A_J and luminescence branching ratios β for Tm^{3+} ions in germanate glass without TiO_2 and titanate-germanate glasses (0, 10, 20, and 30 mol% TiO_2).

Transition	Average wavelength (nm)	Glass composition							
		60GeO ₂		50GeO ₂ -10TiO ₂		40GeO ₂ -20TiO ₂		30GeO ₂ -30TiO ₂	
		A_J (s ⁻¹)	β	A_J (s ⁻¹)	β	A_J (s ⁻¹)	β	A_J (s ⁻¹)	β
³ H ₄ → ³ H ₆	790	422	0.818	1032	0.918	792	0.877	749	0.777
³ F ₄	1460	60	0.116	84	0.075	81	0.090	126	0.131
³ H ₅	2353	34	0.066	8	0.007	30	0.033	89	0.092
A_{TOTAL} (s ⁻¹)		516		1124		903		964	
³ F ₄ → ³ H ₆	1800	164	1.000	159	1.000	170	1.000	348	1.000

TABLE 9 The calculated radiative transition probabilities A_J and luminescence branching ratios β for Tm^{3+} ions in titanate-germanate glasses (40, 45, and 50 mol% TiO_2).

Transition	Average wavelength (nm)	Glass composition					
		20GeO ₂ -40TiO ₂		15GeO ₂ -45TiO ₂		10GeO ₂ -50TiO ₂	
		A_J (s ⁻¹)	β	A_J (s ⁻¹)	β	A_J (s ⁻¹)	β
³ H ₄ → ³ H ₆	790	1550	0.881	1486	0.873	1920	0.911
³ F ₄	1460	160	0.091	159	0.093	152	0.072
³ H ₅	2353	50	0.028	58	0.034	35	0.017
A_{TOTAL} (s ⁻¹)		1760		1703		2107	
³ F ₄ → ³ H ₆	1800	367	1.000	378	1.000	271	1.000

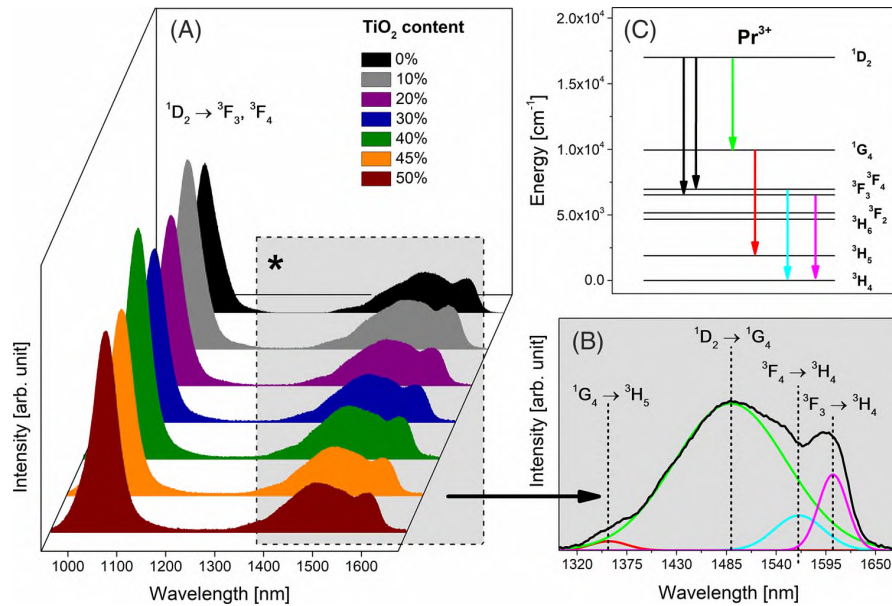


FIGURE 3 Near-infrared luminescence spectra (A), deconvoluted infrared spectra (B), and energy level scheme (C) for Pr³⁺ ions in titanate-germanate glasses.

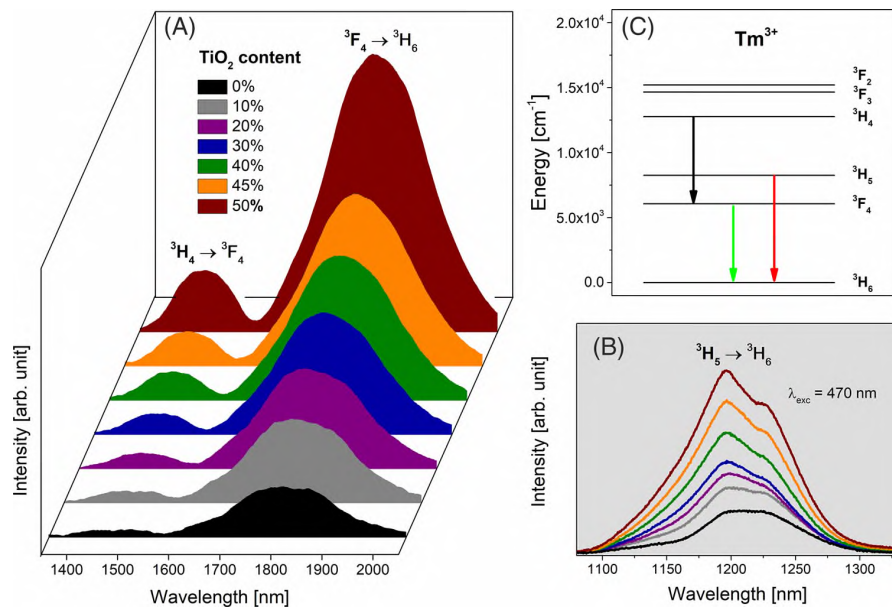


FIGURE 4 Near-infrared luminescence spectra (A), infrared band ($\lambda_{exc} = 470$ nm) (B), and energy level scheme (C) for Tm³⁺ ions in titanate-germanate glasses.

curve analysis. The luminescence decay curves for excited states of Pr³⁺ and Tm³⁺ ions in titanate-germanate glasses were registered and analyzed in detail. All decay curves were well fitted to a nearly singly exponential function (Figures 5a, 6a, and 7a). The luminescence lifetimes of ¹D₂ for Pr³⁺ and ³H₄ and ³F₄ for Tm³⁺ were evaluated in

function of different content of TiO₂ in the glass composition. Our results indicate that the concentration of titanium oxide influences luminescence lifetimes, and the values of the ¹D₂ lifetime of Pr³⁺ ions and ³F₄ lifetime of Tm³⁺ ions for investigated glass samples decrease (Figures 5b and 6b). On the contrary, the experimental

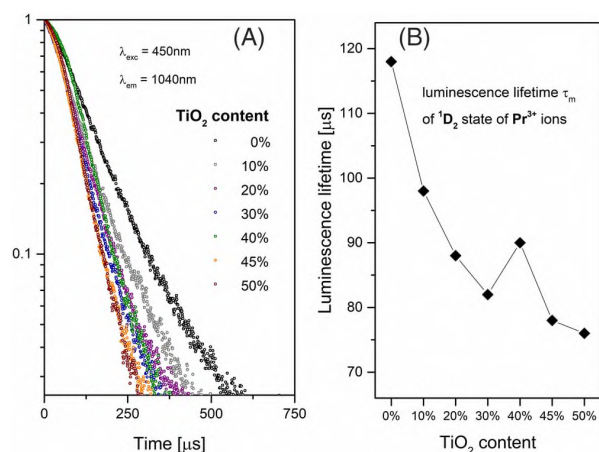


FIGURE 5 Luminescence decay curves (A) and luminescence lifetime of 1D_2 state of Pr^{3+} ions in titanate-germanate glasses (B).

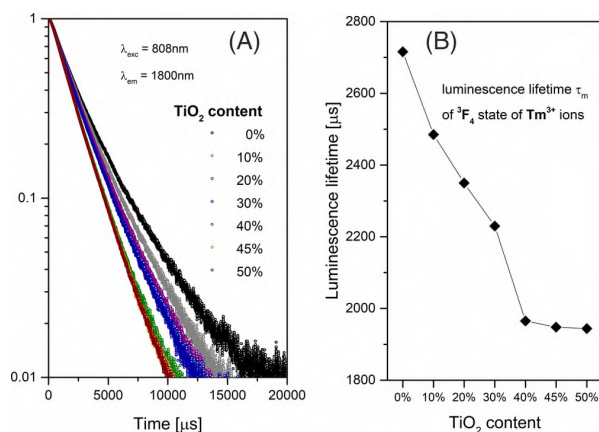


FIGURE 6 Luminescence decay curves (A) and luminescence lifetime of 3F_4 state of Tm^{3+} ions in titanate-germanate glasses (B).

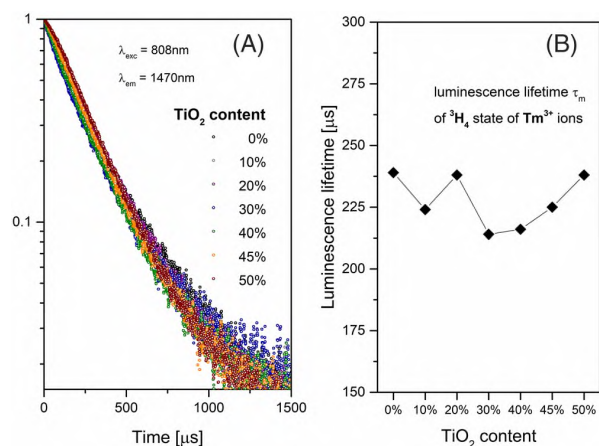


FIGURE 7 Luminescence decay curves (A) and luminescence lifetime of 3H_4 state of Tm^{3+} ions in titanate-germanate glasses (B).

TABLE 10 The calculated radiative lifetime τ_{rad} , the measured lifetime τ_m , and the quantum efficiency η for the 1D_2 state of Pr^{3+} ions varying with TiO_2 concentration.

TiO_2 content (mol%)	$GeO_2:TiO_2$	τ_{rad} (μs)	τ_m (μs)	η (%)
0	–	370	118	31.9
10	5:1	233	98	42.0
20	2:1	237	88	37.1
30	1:1	215	82	38.1
40	1:2	200	90	45.0
45	1:3	126	78	61.9
50	1:5	132	76	57.6

luminescence lifetime for the 3H_4 state of thulium ions practically does not change with increasing content of TiO_2 in germanate glasses (Figure 7b).

3.3 | Influence of $GeO_2:TiO_2$ ratio on spectroscopic parameters of Pr^{3+} and Tm^{3+}

From the literature, it is known that the analysis of spectroscopic parameters is crucial to characterize the relation between glass composition and properties of systems doped with RE^{3+} ions. Therefore, the investigation of the emission bandwidth (FWHM), peak stimulated emission cross-section (σ_{em}), and quantum efficiency (η) is an interesting way to prove the influence of $GeO_2:TiO_2$ molar ratio on spectroscopic properties of studied glasses doped with Pr^{3+} and Tm^{3+} ions. The results are summarized in Tables 10–13.

It is clearly seen that the emission bandwidth referred to as FWHM and determined for systems containing praseodymium and thulium ions is almost unchanged with increasing TiO_2 concentration. The FWHM values for the $^1D_2 \rightarrow ^1G_4$ (Pr^{3+}) and $^3F_4 \rightarrow ^3H_6$ (Tm^{3+}) NIR transitions of RE^{3+} ions are close to 201 ± 2.5 nm (Table 11) and 228.5 ± 2.5 nm (Table 13), respectively. Based on emission bandwidths and radiative transition probabilities for the $^1D_2 \rightarrow ^1G_4$ transition of Pr^{3+} ions and $^3F_4 \rightarrow ^3H_6$ transition of Tm^{3+} ions, the peak stimulated emission cross-sections σ_{em} were evaluated. This important radiative parameter can be calculated using the following expression:

$$\sigma_{em} = \frac{\lambda_p^4}{8\pi c n^2 \Delta\lambda} A_J \quad (5)$$

where λ_p is the peak emission wavelength, n is the refractive index, c is the velocity of light, $\Delta\lambda$ is the emission bandwidth (FWHM), and A_J is the calculated radiative transition probability from the Judd–Ofelt theory. It is generally

TABLE 11 The emission peak wavelength λ_p , the emission bandwidth full width at half maximum (FWHM) for the $^1D_2 \rightarrow ^1G_4$ near-infrared transition, the stimulated emission cross-section σ_{em} , the gain bandwidth $\sigma_{em} \times FWHM$, and figure of merit $\sigma_{em} \times \tau_m$ for Pr^{3+} ions varying with TiO_2 concentration.

TiO ₂ content (mol%)	GeO ₂ :TiO ₂	λ_p (nm)	FWHM (nm)	σ_{em} (10 ⁻²⁰ × cm ²)	$\sigma_{em} \times FWHM$ (10 ⁻²⁷ × cm ³)	$\sigma_{em} \times \tau_m$ (10 ⁻²⁶ × cm ² s)
0	–	1513	199.5	0.98	196	115
10	5:1	1511.5	203.5	1.10	224	108
20	2:1	1508	201	1.16	233	102
30	1:1	1497	199.5	1.15	229	94
40	1:2	1492	201	1.01	203	91
45	1:3	1493.5	198.5	1.10	218	86
50	1:5	1491.5	198.5	1.09	216	83

TABLE 12 The calculated radiative lifetime τ_{rad} , the measured lifetime τ_m , and the quantum efficiency η for the 3H_4 and 3F_4 states of Tm^{3+} ions varying with TiO_2 concentration.

TiO ₂ content (mol%)	GeO ₂ :TiO ₂	3H_4 (Tm ³⁺)			3F_4 (Tm ³⁺)		
		τ_{rad} (μ s)	τ_m (μ s)	η (%)	τ_{rad} (μ s)	τ_m (μ s)	η (%)
0	–	1938	239	12.3	6094	2716	44.6
10	5:1	890	224	25.2	6289	2485	39.5
20	2:1	1107	238	21.5	5882	2350	40.0
30	1:1	1037	214	20.6	2874	2230	77.6
40	1:2	568	216	38.0	2725	1965	72.1
45	1:3	587	225	38.3	2643	1948	73.7
50	1:5	475	238	50.1	3690	1944	52.7

TABLE 13 The emission peak wavelength λ_p , the emission bandwidth full width at half maximum (FWHM) for the $^3F_4 \rightarrow ^3H_6$ near-infrared transition, the stimulated emission cross-section σ_{em} , the gain bandwidth $\sigma_{em} \times FWHM$, and figure of merit $\sigma_{em} \times \tau_m$ for Tm^{3+} ions varying with TiO_2 concentration.

TiO ₂ content (mol%)	GeO ₂ :TiO ₂	λ_p (nm)	FWHM (nm)	σ_{em} (10 ⁻²¹ × cm ²)	$\sigma_{em} \times FWHM$ (10 ⁻²⁹ × cm ³)	$\sigma_{em} \times \tau_m$ (10 ⁻²⁴ × cm ² s)
0	–	1806	223	3.44	76.7	9.3
10	5:1	1796.5	228	3.04	69.3	7.6
20	2:1	1792	230.5	3.01	69.4	7.1
30	1:1	1795.5	231	5.90	136.3	13.2
40	1:2	1801.5	229	6.05	138.5	12.0
45	1:3	1802	227.5	5.99	136.3	11.7
50	1:5	1805.5	226	4.33	97.8	8.4

accepted that a relatively large value of σ_{em} is required for an efficient laser transition. Our results for titanate-germanate glasses containing Pr^{3+} ions indicated that the value of σ_{em} (1.16×10^{-20} cm²) is the highest for glass sample with molar ratio $GeO_2:TiO_2$ equal to 2:1 (Table 11). Contrary to Pr^{3+} -doped glass systems, the peak stimulated emission cross-section for the $^3F_4 \rightarrow ^3H_6$ (Tm^{3+}) transition is relatively large ($\sigma_{em} = 6.05 \times 10^{-21}$ cm²) for glass with 40 mol% TiO_2 content ($GeO_2:TiO_2$ equal to 1:2) compared to

the values calculated for other studied systems doped with thulium ions (Table 13).

In the next step, the radiative lifetime τ_{rad} calculated from the Judd–Ofelt theory and the measured luminescence lifetime τ_m were applied to calculate the quantum efficiency (η) for the $^1D_2 \rightarrow ^1G_4$ transition of Pr^{3+} ions and the $^3H_4 \rightarrow ^3F_4$ and $^3F_4 \rightarrow ^3H_6$ transitions of Tm^{3+} ions (Tables 10 and 12). It was observed that the value of this parameter is definitely larger for glasses with higher

TiO₂ content. However, it is more evident for Tm³⁺ than Pr³⁺ ions. In particular, the quantum efficiencies for the ³F₄ → ³H₆ NIR transition of Tm³⁺ ions at 1.8 μm are the highest (η above 70%) for glass samples, where molar ratio GeO₂:TiO₂ was changed from 1:1 to 1:3.

The supplementary spectroscopic parameters were verified for potential applications such as NIR lasers and fiber amplifiers. The stimulated emission cross-section (σ_{em}), the measured emission lifetime (τ_m), and the emission bandwidth (FWHM) were applied to calculate the following laser parameters: gain bandwidth (σ_{em} × FWHM product) and figure of merit (FOM) (σ_{em} × τ_m). The results for the ¹D₂ → ¹G₄ (Pr³⁺) and ³F₄ → ³H₆ (Tm³⁺) transitions of rare-earth ions in titanate-germanate glasses are given in Tables 11 and 13, respectively. Comparing the received data, it can be stated that the Pr³⁺-doped system with 20 mol% TiO₂ has the highest gain bandwidth and its value is close to 233 × 10⁻²⁷ cm³. Also, the parameter σ_{em} × τ_m for the ¹D₂ → ¹G₄ transition of Pr³⁺ ions is relatively high for glass with molar ratio GeO₂:TiO₂ = 2:1. On the other hand, the highest values of gain bandwidth (σ_{em} × FWHM = 138.5 × 10⁻²⁹ cm³) and FOM (σ_{em} × τ_m = 12.0 × 10⁻²⁴ cm² s) were determined for the ³F₄ → ³H₆ transition of Tm³⁺ ions in a glass system with 40 mol% TiO₂ (GeO₂:TiO₂ = 1:2).

It is interesting to see that the identical results were obtained earlier by us for multicomponent titanate-germanate glasses containing Nd³⁺⁴⁹ and Er³⁺⁵⁰ ions. Based on our previous measurements of NIR emission spectra and luminescence decays, it can be concluded that spectroscopic properties of systems with different molar ratios GeO₂:TiO₂ strongly depend on the ionic radius of RE³⁺. It should be noted that the ionic radius of Pr³⁺ is close to the ionic radius of Nd³⁺ ions. In both cases, the best laser parameters were evaluated for glasses with molar ratio GeO₂:TiO₂ = 2:1. For that reason, titanate-germanate glass (20 mol% TiO₂) containing Pr³⁺ ion-like system doped with Nd³⁺ ions can be successfully used for NIR laser applications. Furthermore, a similar dependence was observed for glasses doped with Tm³⁺ and Er³⁺ ions. The highest values of the stimulated emission cross-section, the gain bandwidth, and the FOM for ³F₄ → ³H₆ (Tm³⁺) and ⁴I_{13/2} → ⁴I_{15/2} (Er³⁺) transitions were calculated for systems with molar ratio GeO₂:TiO₂ = 1:2 due to the same ionic radius (89 pm). Therefore, Tm³⁺-doped titanate-germanate glass with 40 mol% can be a potential system for laser and fiber amplifier applications. We also postulate that multicomponent titanate-germanate glasses with lower (GeO₂:TiO₂ = 2:1) and higher (GeO₂:TiO₂ = 1:2) titanium dioxide concentrations are favored for NIR luminescence of RE³⁺ ions located at the beginning (Pr³⁺, Nd³⁺) and the end (Er³⁺, Tm³⁺) of lanthanide series, respectively.

Finally, Tables 14 and 15 present a comparison of spectroscopic parameters in various inorganic systems doped with praseodymium⁵¹⁻⁵⁴ and thulium.⁵⁵⁻⁶¹ It was found that the stimulated emission cross-section, gain bandwidth, and FOM for the ¹D₂ → ¹G₄ transition of Pr³⁺ ions are comparable to those of other germanate glasses.⁵¹ Additionally, values of σ_{em} × FWHM (233 × 10⁻²⁷ cm³) and FOM σ_{em} × τ_m (102 × 10⁻²⁶ cm² s) are greater than those obtained for tellurite⁴⁶ and borate⁵⁴ systems. Previously published studies for glass systems containing Tm³⁺ ions compared with presented data for titanate-germanate glasses give interesting results. It can be stated that the stimulated emission cross-section and the gain bandwidth for ³F₄ → ³H₆ transition of Tm³⁺ ions in the studied system (GeO₂:TiO₂ = 1:2) are similar to values reported by Gao et al.⁵⁶ for glass based on GeO₂-TeO₂-PbO-CaO. On the other hand, the values of laser parameters are large compared with borate⁶⁰ and phosphate glasses⁶¹ but are less than those calculated for another germanate⁵⁵ and tellurite glass systems.⁵⁷ The presented results clearly confirm that laser parameters depend significantly on glass composition.

4 | CONCLUSION

In summary, experimental and theoretical studies on the NIR luminescence properties of titanate-germanate glasses singly doped with Pr³⁺ and Tm³⁺ ions were examined for laser and fiber amplifier applications. The glass systems with different molar ratios GeO₂:TiO₂ were prepared, and then, based on absorption, luminescence spectroscopy, and calculations using the Judd-Ofelt theory, the spectroscopic and laser parameters were evaluated. Independent of the TiO₂ concentration, intense NIR emissions at 1.5 and 1.8 μm were observed for glasses doped with Pr³⁺ and Tm³⁺ ions, respectively. Systematic investigations indicate that the Pr³⁺-doped system with GeO₂:TiO₂ = 2:1 presents profit laser parameters for the main ¹D₂ → ¹G₄ transition of Pr³⁺ ions are as follows: the measured lifetime τ_m = 88 μs, the stimulated emission cross-section σ_{em} = 1.16 × 10⁻²⁰ cm², the gain bandwidth σ_{em} × FWHM = 233 × 10⁻²⁷ cm³, and FOM known as σ_{em} × τ_m product = 102 × 10⁻²⁶ cm² s. On the contrary, the excellent laser parameters such as the stimulated emission cross-section σ_{em} = 6.05 × 10⁻²¹ cm², the measured lifetime τ_m = 1.96 ms, the quantum efficiency η = 72.1%, and the gain bandwidth σ_{em} × FWHM = 138.5 × 10⁻²⁹ cm³ were determined for ³F₄ → ³H₆ transition of Tm³⁺ ions in glass with GeO₂:TiO₂ = 1:2 and this system is attractive compared with some reported laser glasses. Our results suggest that the systems with molar ratio GeO₂:TiO₂ equal to 2:1 (Pr³⁺) and 1:2 (Tm³⁺) show good NIR luminescence

TABLE 14 Comparison of the stimulated emission cross-section (σ_{em}), gain bandwidth ($\sigma_{em} \times FWHM$), and figure of merit ($\sigma_{em} \times \tau_m$) in different laser glasses doped with Pr^{3+} .

Glass host	σ_{em} ($10^{-20} \times cm^2$)	$\sigma_{em} \times FWHM$ ($10^{-27} \times cm^3$)	$\sigma_{em} \times \tau_m$ ($10^{-26} \times cm^2 s$)	Ref.
GeO ₂ :TiO ₂ = 2:1	1.16	233	102	This work
GeO ₂ -BaO-BaF ₂ -Ga ₂ O ₃	0.97	201	107	51
LaF ₃ -BaF ₂ -BaCO ₃ -ZnO-TeO ₂	0.90	174.6	83.1	46
Na ₂ O-MgO-Al ₂ O ₃ -P ₂ O ₅	1.14	128.8	-	52
Li ₂ O-CaO-BaO-Al ₂ O ₃ -La ₂ O ₃ -P ₂ O ₅	1.29	171.6	-	53
PbO-P ₂ O ₅ -Ga ₂ O ₃	1.28	165	77	54
B ₂ O ₃ -BaO-Ga ₂ O ₃	0.37	81	6	54

Abbreviation: FWHM, full width at half maximum.

TABLE 15 Comparison of the stimulated emission cross-section (σ_{em}) and figure of merit ($\sigma_{em} \times \tau_m$) in different laser glasses doped with Tm^{3+} .

Glass host	σ_{em} ($10^{-21} \times cm^2$)	$\sigma_{em} \times \tau_m$ ($10^{-24} \times cm^2 s$)	Ref.
GeO ₂ :TiO ₂ = 1:2	6.05	12	This work
GeO ₂ -BaO-BaF ₂ -Ga ₂ O ₃ -Na ₂ O-La ₂ O ₃	8.70	26.59	55
GeO ₂ -TeO ₂ -PbO-CaO	5.18	12.54	56
TeO ₂ -Nb ₂ O ₅ -ZnO-LiF	8.10	14	57
BaO-Ga ₂ O ₃ -GeO ₂ -La ₂ O ₃ -Y ₂ O ₃	4.92	-	58
Bi ₂ O ₃ -B ₂ O ₃ -Al ₂ O ₃ -BaF ₂	5.29	-	59
Li ₂ B ₂ O ₇ -BaO-CdO	1.90	-	60
P ₂ O ₅ -PbO-K ₂ O-Al ₂ O ₃ -Na ₂ O	1.41	-	61

properties and we can conclude that these multicomponent titanate-germanate glasses are promising materials for NIR photonic applications.

ACKNOWLEDGMENTS

The National Science Centre (Poland) supported this work under research project 2018/31/B/ST8/00166.

ORCID

Marta Kuwik  <https://orcid.org/0000-0002-7367-9486>

Karolina Kowalska  <https://orcid.org/0000-0003-0979-0478>

Joanna Pisarska  <https://orcid.org/0000-0002-9833-8944>

Wojciech A. Pisarski  <https://orcid.org/0000-0002-4147-8719>

REFERENCES

- Kassab LRP, Bell MJV. Rare-earth-doped germanate and tellurite glasses: laser, waveguide, and ultrafast device applications. In: Martin-Ramos P, Ramos Silva M, editors. Lanthanide-based multifunctional materials from OLEDs to SIMs. Elsevier Inc.; 2018. p. 263–89.
- Ferrari M, Righini GC. Glass-ceramic materials for guided-wave optics. *Int J Appl Glass Sci.* 2015;6:240–8.
- Marcondes LM, Ramos da Cunha C, Paula de Sousa C, Maestri S, Gonçalves RR, Cassanjes FC, et al. Thermal and spectroscopic properties studies of Er³⁺-doped and Er³⁺/Yb³⁺-codoped niobium germanate glasses for optical applications. *J Lumin.* 2019;205:487–94.
- Cao W, Huang F, Wang T, Ye R, Lei R, Tian Y, et al. 2.0 μ m emission of Ho³⁺ doped germanosilicate glass sensitized by non-rare-earth ion Bi: a new choice for 2.0 μ m laser. *Opt Mater.* 2018;75:695–8.
- Bhemarajam J, Syam Prasad P, Mohan Babu M, Prasad M. Spectroscopic and optical investigations on Er³⁺/Yb³⁺ co-doped bismuth-boroleadlithium glasses for solid state laser applications. *Opt Mater.* 2021;122:111657.
- Li M, Luan J, Zhang Y, Jiang F, Zhou X, Tang J, et al. Spectroscopic properties Er/Yb co-doped glass ceramics containing nanocrystalline Bi₂ZnB₂O₇ for broadband near-infrared emission. *Ceram Int.* 2019;45:18831–7.
- Lakshminarayana G, Bashar KhA, Baki SO, Lira A, Caldiño U, Meza-Rocha AN, et al. Er³⁺/Dy³⁺ codoped B₂O₃-TeO₂-PbO-ZnO-Li₂O-Na₂O glasses: optical absorption and fluorescence features study for visible and near-infrared fiber laser applications. *J Non-Cryst Solids.* 2019;503–504:366–81.
- Vijayatha D, Sujatha B, Chandrashekaraiiah G, Narayana Reddy C, Sivasankara Reddy N. Enhanced near-infrared luminescence at 1.07 μ m of Nd³⁺ doped PbCl₂-Li₂B₄O₇ glasses for solid state laser and optical fiber amplifier applications. *Opt Mater.* 2021;111:110543.

9. Hegde V, Devarajulu G, Pramod AG, Kolavekar SB, Aloraini DA, Almuqrin AH, et al. Analysis of optical and near-infrared luminescence for Er^{3+} and $\text{Er}^{3+}/\text{Yb}^{3+}$ co-doped heavy metal borate glasses for optical amplifier applications. *Photonics*. 2022;9:355.
10. Bhemarajam J, Swapna, Mohan Babu M, Syam Prasad P, Prasad M. Spectroscopic studies on Er^{3+} ions incorporated bismuth borolead lithium glasses for solid state lasers and fiber amplifiers. *Opt Mater*. 2021;113:110818.
11. Charfi B, Damak K, Maalej R, Alqahtani MS, Hussein KI, Alshehri AM, et al. Enhancement of optical telecommunication bands: Pr^{3+} -doped halide phosphate glasses display broadband NIR photoluminescence emission. *Materials*. 2022;15: 6518.
12. Herrera A, Balzaretta NM. Effect of gold nanoparticles in broadband near-infrared emission of Pr^{3+} doped B_2O_3 - PbO - Bi_2O_3 - GeO_2 glass. *J Lumin*. 2017;181:147-52.
13. Belançon M, Marconi JD, Ando MF, Barbosa LC. Near-IR emission in Pr^{3+} single doped and tunable near-IR emission in $\text{Pr}^{3+}/\text{Yb}^{3+}$ codoped tellurite tungstate glasses for broadband optical amplifiers. *Opt Mater*. 2014;36:1020-6.
14. Lakshminarayana G, Caldino U, Meza-Rocha AN, Lira A, Venkateswara Rao P, Singh V, et al. Fluorescence features of Tm^{3+} -doped multicomponent borosilicate and borotellurite glasses for blue laser and S-band optical amplifier applications. *Opt Mater*. 2019;96:109354.
15. Fang Y, Zhao G, Xu J, Zhang N, Ma Z, Hu L. Energy transfer and $1.8\mu\text{m}$ emission in $\text{Yb}^{3+}/\text{Tm}^{3+}$ co-doped bismuth germanate glass. *Ceram Int*. 2014;40:6037-43.
16. Hou G, Cao L, Zhang C, Yu X, Fu W, Li G, et al. Improvement of ultra-broadband near-infrared emission in Nd^{3+} - Er^{3+} - Pr^{3+} tri-doped tellurite glasses. *Opt Mater*. 2021;111:110547.
17. Balaji S, Ghosh D, Biswas K, Allu AR, Gupta G, Annapurna K. Insights into $\text{Er}^{3+} \leftrightarrow \text{Yb}^{3+}$ energy transfer dynamics upon infrared ~ 1550 nm excitation in a low phonon fluoro-tellurite glass system. *J Lumin*. 2017;187:441-8.
18. Kochanowicz M, Lesniak M, Zmojda J, Miluski P, Baranowska A, Ragin T, et al. Structure, luminescence and energy transfer of fluorindate glasses co-doped with $\text{Er}^{3+}/\text{Ho}^{3+}$. *Ceram Int*. 2020;46:26403-9.
19. Zhou L, Huang F, Dou B, Li Y, Ye R, Wang H, et al. Sensitization effect between Ln^{3+} ions in zinc fluoride glasses for MIR applications. *Ceram Int*. 2019;45:10640-5.
20. Carvalho EA, Freitas AM, Silva GH, Bell MJV, Kassab LRP, Anjos V. Thermal and structural analysis of germanate glass and thin films co-doped with silver nanoparticles and rare earth ions with insights from visible and Raman spectroscopy. *Vib Spectrosc*. 2016;87:143-8.
21. Kochanowicz M, Zmojda J, Miluski P, Ragin T, Pisarski WA, Pisarska J, et al. Structural and luminescent properties of germanate glasses and double-clad optical fiber co-doped with $\text{Yb}^{3+}/\text{Ho}^{3+}$. *J Alloys Compd*. 2017;727:1221-6.
22. Zhou B, Tao L, Yat-Yin Chan C, Tsang YH, Jin W, Yue-Bun Pun E. Intense near-infrared emission of $1.23\mu\text{m}$ in erbium-doped low-phonon-energy fluorotellurite glass. *Spectrochim Acta A Mol Biomol Spectrosc*. 2013;111:49-53.
23. Pisarski WA, Pisarska J, Kuwik M, Kochanowicz M, Zmojda J, Miluski P, et al. Fluoroindate glasses co-doped with $\text{Pr}^{3+}/\text{Er}^{3+}$ for near-infrared luminescence applications. *Sci Rep*. 2020;10:21105.
24. Wen X, Tang G, Yang Q, Chen X, Qian Q, Zhang Q, et al. Highly Tm^{3+} doped germanate glass and its single mode fiber for $2.0\mu\text{m}$ laser. *Sci Rep*. 2016;6:20344.
25. Jadach R, Zmojda J, Kochanowicz M, Miluski P, Pisarska J, Pisarski WA, et al. Investigation of the aluminium oxide content on structural and optical properties of germanium glasses doped with RE ions. *Spectrochim Acta A Mol Biomol Spectrosc*. 2018;201:143-52.
26. Zmojda J, Kochanowicz M, Miluski P, Golonko P, Baranowska A, Ragiń T, et al. Luminescent studies on germanate glasses doped with europium ions for photonic applications. *Materials*. 2020;13:2817.
27. Uma V, Marimuthu K, Muralidharan G. Effect of modifier oxides (SrO , Al_2O_3 , ZnO , CdO , PbO and Bi_2O_3) on the luminescence properties of Er^{3+} doped telluroborate glasses for laser and optical amplifier applications. *J Lumin*. 2019;207:534-44.
28. Alajerami YSM, Hashim S, Hassan WMSW, Ramli AT. The effect of titanium oxide on the optical properties of lithium potassium borate glass. *J Mol Struct*. 2012;1026:159-67.
29. Herrera A, Londoño F, Balzaretta NM. Structural and optical properties of Nd^{3+} doped GeO_2 - PbO glass modified by TiO_2 for applications in laser and fiber amplifier. *Opt Mater*. 2021;113:110884.
30. De M, Jana S, Mitra S. Structural and spectroscopic characteristics of Eu^{3+} embedded titanium lead phosphate glasses for red luminescence. *Solid State Sci*. 2021;114:106560.
31. Burtan-Gwizdala B, Reben M, Cisowski J, Szpil S, Yousef ES, Lisiecki R, et al. Thermal and spectroscopic properties of Er^{3+} -doped fluorotellurite glasses modified with TiO_2 and BaO . *Opt Mater*. 2020;107:109968.
32. Balaji Rao R, Krishna Rao D, Veeraiiah N. The role of titanium ions on structural, dielectric and optical properties of Li_2O - MgO - B_2O_3 glass system. *Mater Chem Phys*. 2004;87:357-69.
33. Maity A, Jana S. Excitation dependent tunable emission colour of Eu^{3+} - Tb^{3+} co-doped titanium zinc sodium phosphate glass. *Phys B: Condens*. 2021;619:413186.
34. Haily E, Bih L, Jerroudi M, Azrou M, El bouari A, Manoun B. Structural investigation of SrO - BaO - TiO_2 - B_2O_3 - P_2O_5 glass-ceramics. *Mater Today: Proc*. 2021;37:3798-802.
35. Judd BR. Optical absorption intensities of rare-earth ions. *Phys Rev*. 1962;127:750-61.
36. Ofelt GS. Intensities of crystal spectra of rare-earth ions. *J Chem Phys*. 1962;37:511-20.
37. Carnall WT, Fields PR, Rajnak K. Electronic energy levels in the trivalent lanthanide aquo ions. I. Pr^{3+} , Nd^{3+} , Pm^{3+} , Sm^{3+} , Dy^{3+} , Ho^{3+} , Er^{3+} and Tm^{3+} . *J Chem Phys*. 1968;49:4424-42.
38. Yu S, Yang Z, Xu S. Judd-Ofelt and laser parameterization of Tm^{3+} -doped barium gallo-germanate glass fabricated with efficient dehydration methods. *Opt Mater*. 2009;31:1723-8.
39. Florez A, Florez M, Messaddeq Y, Aegerter MA, Porcher P. Application of standard and modified Judd-Ofelt theories to thulium doped fluorindate glass. *J Non-Cryst Solids*. 1999;247:215-21.
40. Pisarski WA, Pisarska J, Dominiak-Dzik G, Ryba-Romanowski W. Visible and infrared spectroscopy of Pr^{3+} and Tm^{3+} ions in lead borate glasses. *J Phys Condens Matter*. 2004;16:6171-84.
41. Vijaya Kumar MV, Rama Gopal K, Reddy RR, Lokeswara Reddy GV, Sooraj Hussain N, Jamalaiah BC. Application of modified Judd-Ofelt theory and the evaluation of radiative properties

- of Pr³⁺-doped lead telluroborate glasses for laser applications. *J Non-Cryst Solids*. 2013;364:20–7.
42. Basavapoornima CH, Kesavulu CR, Maheswari T, Pecharapa W, Depuru SR, Jayasankar CK. Spectral characteristics of Pr³⁺-doped lead based phosphate glasses for optical display device applications. *J Lumin*. 2020;228:117585.
43. Falci RF, Guerineau T, Delarosbil J-L, Messaddeq Y. Spectroscopic properties of gallium-rich germano-gallate glasses doped with Tm³⁺. *J Lumin*. 2022;249:119014.
44. Peacock RD. The intensities of lanthanide f–f transitions. *Struct Bond*. 1975;22:83–122.
45. Naresh V, Ham BS. Influence of multiphonon and cross relaxations on ³P₀ and ¹D₂ emission levels of Pr³⁺ doped borosilicate glasses for broad band signal amplification. *J Alloys Compd*. 2016;664:321–30.
46. Zhou B, Tao L, Tsang YH, Jin W, Yue-Bun Pun E. Super broadband near-IR photoluminescence from Pr³⁺-doped fluorotellurite glasses. *Opt Express*. 2012;20:3803–13.
47. Tang W, Tian Y, Li B, Xu Y. Effect of introduction of TiO₂ and GeO₂ oxides on thermal stability and 2 μm luminescence properties of tellurite glasses. *Ceram Int*. 2019;45:16411–6.
48. Schweizer T, Samson BN, Hector JR, Brocklesby WS, Hewak DW, Payne DN. Infrared emission and ion–ion interactions in thulium- and terbium-doped gallium lanthanum sulfide glass. *J Opt Soc Am B*. 1999;16:308–16.
49. Pisarski WA, Kowalska K, Kuwik M, Pisarska J, Dorosz J, Żmojda J, et al. Nd³⁺ doped titanate-germanate glasses for near-IR laser applications. *Opt Mater Express*. 2022;7:2912–26.
50. Kowalska K, Kuwik M, Pisarska J, Leśniak M, Dorosz D, Kochanowicz M, et al. Influence of TiO₂ concentration on near-infrared luminescence of Er³⁺ ions in barium gallo-germanate glasses. *J Mater Res Technol*. 2022;21:4761–72.
51. Pisarska J, Kowal M, Kochanowicz M, Żmojda J, Dorosz J, Dorosz D, et al. Influence of BaF₂ and activator concentration on broadband near-infrared luminescence of Pr³⁺ ions in gallo-germanate glasses. *Opt Express*. 2016;24:2427–35.
52. Shen LF, Chen BJ, Lin H, Pun EYB. Praseodymium ion doped phosphate glasses for integrated broadband ion-exchanged waveguide amplifier. *J Alloys Compd*. 2015;622:1093–7.
53. Han X, Shen L, Pun EYB, Ma T, Lin H. Pr³⁺-doped phosphate glasses for fiber amplifiers operating at 1.38–1.53 μm of the fifth optical telecommunication window. *Opt Mater*. 2014;36:1203–8.
54. Pisarska J, Kuwik M, Pisarski WA. Spectroscopic properties of inorganic glasses doped with Pr³⁺: a comparative study. *Materials*. 2022;15:767.
55. Xu R, Xu L, Hu L, Zhang J. Structural origin and laser performance of thulium-doped germanate glasses. *J Phys Chem A*. 2011;115:14163–7.
56. Gao S, Fan X, Liu X, Liao M, Hu L. Mechanical and ~2 μm emission properties of Tm³⁺-doped GeO₂–TeO₂(or SiO₂)–PbO–CaO glasses. *Opt Mater*. 2015;45:167–70.
57. Lachheb R, Damak K, Assadi AA, Herrmann A, Yousef E, Rüssel C, et al. Characterization of Tm³⁺ doped TNZL glass laser material. *J Lumin*. 2015;161:281–7.
58. Wen X, Tang G, Wang J, Chen X, Qian Q, Yang Z. Tm³⁺ doped barium gallo-germanate glass single mode fibers for 2.0 μm laser. *Opt Express*. 2015;23:7722–31.
59. Song H, Zhou D, Xu P, Han K, Song C. ~2 μm fluorescence and energy transfer characteristics in a highly Tm³⁺-doped bis-muthate glass based on Al₂O₃ adjustment. *Opt Mater Express*. 2021;11:3755–67.
60. El-Maaref AA, Abdel Wahab EA, Shaaban KHS, Abdelawwad M, Koubisy MSI, Börcsök J, et al. Visible and mid-infrared spectral emissions and radiative rates calculations of Tm³⁺ doped BBLC glass. *Spectrochim Acta A Mol Biomol Spectrosc*. 2020;242:118774.
61. Basavapoornima Ch, Maheswari T, Deviprasad CJ, Kesavulu CR, Tröster Th, Jayasankar CK. Thermal, structural, mechanical and 1.8 μm luminescence properties of the thulium doped Pb–K–Al–Na glasses for optical fiber amplifiers. *J Non-Cryst Solids*. 2020;530:119773.

How to cite this article: Kuwik M, Kowalska K, Pisarska J, Pisarski WA. Experimental and theoretical studies on NIR luminescence of titanate-germanate glasses doped with Pr³⁺ and Tm³⁺ ions. *J Am Ceram Soc*. 2023;1–13. <https://doi.org/10.1111/jace.19378>

P10

Karolina Kowalska, Marta Kuwik, Joanna Pisarska, Wojciech A. Pisarski,

Thulium-doped titanate-germanate glasses for infrared photonics

Journal of Luminescence 272 (2024) 120649



Contents lists available at ScienceDirect

Journal of Luminescence

journal homepage: www.elsevier.com/locate/jlum

Full Length Article

Thulium-doped titanate-germanate glasses for infrared photonics

Karolina Kowalska^{*}, Marta Kuwik, Joanna Pisarska, Wojciech A. Pisarski^{**}

Institute of Chemistry, University of Silesia, Szkolna 9 Street, 40-007, Katowice, Poland

ARTICLE INFO

Keywords:

Titanate-germanate glasses
Rare-earth ions
Near-infrared luminescence
Inokuti-Hirayama model
Structure-property relationship

ABSTRACT

In this paper, we performed a comparative spectroscopic analysis of Tm³⁺-doped glasses based on GeO₂-BaO-Ga₂O₃ (GBG) and TiO₂-GeO₂-BaO-Ga₂O₃ (TGBG) to achieve broadband luminescence at 1.8 μm. Glasses were prepared at different doping concentrations (0.05 mol% and 1 mol%) in order to investigate the effect of Tm³⁺ ions as well as host composition (GeO₂:TiO₂ molar ratios) on near-IR luminescence properties. We report on the hypersensitivity of the transition ³H₆ → ³F₄ of Tm³⁺ in a series of titanate-germanate glasses, which was shifted to longer wavelengths with increasing TiO₂ concentration. The relative intensity of the main near-IR emission band corresponding to the ³F₄ → ³H₆ (1.8 μm) transition of Tm³⁺ was 4.8-fold enhanced for glass with molar ratio GeO₂:TiO₂ = 1:5 compared to GBG glass system. We observed the luminescence quenching phenomena for samples containing more than 0.5 mol% of Tm³⁺ ions. The calculated spectroscopic parameters, such as measured luminescence lifetime (τ_m) and the quantum efficiency (η), were discussed and compared to the different laser glasses. Importantly, luminescence decay curves have been examined using the Inokuti-Hirayama model. Additionally, the correlation between optical properties and local structure in glasses was well evidenced by Raman spectroscopy. The proposed strategy, in combination with various chemical composition of glass host activated by various Tm₂O₃ concentration, might be beneficial for modern near-infrared photonics.

1. Introduction

Glasses belong to important classes of engineering materials, which are useful in numerous industrial and medical applications. Since 1990 the discovery of the GeO₂-BaO-Ga₂O₃ system, referred as GBG, belongs to the low-phonon glass family, was characterized using various spectroscopic methods, and offers an ideal alternative to silicate-based glass [1,2]. Different metal oxides have been added to the GBG system in order to improve their properties, e.g. where GeO₂ was partially substituted by titanium dioxide. A new type host of barium gallo-germanate glass (TiO₂-GeO₂-BaO-Ga₂O₃) [3] has been investigated for near-IR application. Titanate-germanate glasses shows a fully amorphous character, good thermal stability, and excellent optical properties for modern photonics and laser technology. The experimental data clearly demonstrate that the enhanced near-infrared emission was realized for TGBG systems with predominantly TiO₂ singly doped with rare-earth ions (Nd³⁺ [4], Er³⁺ [5], Ho³⁺ [6]). Moreover [7], it can be concluded that higher titanium dioxide concentration is favored for NIR luminescence of rare-earth ions located at the end of the lanthanide series. From the wide family of luminescent rare-earth elements, the

thulium ion doped materials cover attention due to their near-IR emission. Thulium ion is classified as activators, generating radiation in the 1.4–2.0 μm range, respectively [8,9]. The luminescence properties of Tm³⁺ ions have been examined for numerous crystals [10–13], glass-ceramics [14–17], and glasses [18–23]. Systematic studies demonstrated that the type of host matrix and activator concentration influenced strongly on their spectral characteristics [24–26]. At present, the reported glass hosts exhibiting 1.8 μm emission are mainly involved silicate (~1050 cm⁻¹) [27], tellurite (~780 cm⁻¹) [28] lead-phosphate (~1120 cm⁻¹) [29], borate (~1400 cm⁻¹) [30] systems.

On the other hand, some interesting spectroscopic results for glasses singly doped with thulium ions were presented and focused on the optimal activator concentration. A high doping concentration is not achievable in e.g. silica glass due to its defined local structure. The multicomponent modifications of oxide glasses which allow higher Tm³⁺ ions solubility triggered great interest. The optical aspect for Tm³⁺-doped multicomponent borosilicate and borotellurite glasses for S-band optical amplifier applications was studied [31]. It was stated that the intensity of the band corresponding to the ³F₄ → ³H₆ transition of Tm³⁺ ions gradually increased up to 2 mol% content without

^{*} Corresponding author.^{**} Corresponding author.E-mail addresses: karolina.kowalska@us.edu.pl (K. Kowalska), wojciech.pisarski@us.edu.pl (W.A. Pisarski).<https://doi.org/10.1016/j.jlum.2024.120649>

Received 2 March 2024; Received in revised form 3 April 2024; Accepted 24 April 2024

Available online 26 April 2024

0022-2313/© 2024 Elsevier B.V. All rights reserved.

luminescence quenching phenomena. So et al. fabricated thulium-doped calcium aluminosilicate glasses [32] with dopant concentrations of up to 7 mol%. The material showed the most intensity band for the $^3F_4 \rightarrow ^3H_6$ transition doped with 1 mol% of Tm_2O_3 , Song et al. reported the optical properties for the Tm^{3+} -doped $Bi_2O_3-GeO_2-Ga_2O_3-Na_2O$. In the case of this glass system, in the function of Tm_2O_3 concentration the intensity corresponding to the strongest emission at 1.8 μm increased, while the intensity of 1.47 μm band fluorescence from $^3H_4 \rightarrow ^3F_4$ transition decreased [33]. The research showed that the distance between Tm^{3+} ions become smaller with the increase of the activator concentration, and increases the probability of cross-relaxation. Further evaluated near-IR optical features was realized for the multicomponent germanate glasses which offers a high rare-earth solubility. According to the previous researches, the highest Tm_2O_3 doping concentration in $GeO_2-BaO-Ga_2O_3$ system was 1 mol% [34,35].

In this work, correlation between optical properties and local structure of Tm^{3+} ions in two types of glass host belonging to low phonon glass family was well evidenced by luminescence and Raman spectroscopy. We propose an approach based on Tm^{3+} -doped $GeO_2-BaO-Ga_2O_3$ (GBG) and $TiO_2-GeO_2-BaO-Ga_2O_3$ (TGBG) glass systems. It is established that the insertion of TiO_2 as an intermediate oxide is suitable component for rare-earth ions in GBG host because of less probable non-radiative relaxation process, which may result in a higher lifetime of the excited state. Taking into account the potential applications of the developed glasses in laser and broadband amplifiers, the chemical composition was modified by gradually replacing the GeO_2 by TiO_2 and the activator concentration (from extremely low 0.05–1 mol%). Importantly, the absorbance spectra were applied to analyze the effect of TiO_2 on position the “hypersensitive transition”, which strongly depends on the local environment of the thulium ions. Special attention has been paid to achieve broadband near-IR luminescence properties around 1.8 μm corresponding to the $^3F_4 \rightarrow ^3H_6$ transition of Tm^{3+} ions. In particular, this work concerns on the enhanced near-IR luminescence $^3F_4 \rightarrow ^3H_6$ (1.8 μm) transition and luminescence decays from upper 3F_4 excited state of thulium ions in studied materials. Luminescence decay curves have been examined using the Inokuti-Hirayama model. Moreover, the structural changes that have occurred resulting from the change in glass composition were investigated through the Raman spectra. These results and the developed strategy show that the optimal molar concentration of luminescent Tm^{3+} ions and the presence of TiO_2 in GBG glass system play important roles in achieving near-IR emission for the modern photonics.

2. Material and methods

Tm^{3+} -doped $GeO_2-BaO-Ga_2O_3$ (GBG) and $TiO_2-GeO_2-BaO-Ga_2O_3$ (TGBG) glass system were synthesized using melt quenching technique. High purity powder chemicals purchased from Sigma-Aldrich (St. Louis, MO, USA) GeO_2 (99.99 %), TiO_2 (99.995 %, rutile), BaO (99.99 %), Ga_2O_3 (99.99 %), and Tm_2O_3 (99.99 %) were used as starting constituents for glass preparation. The compositions are $60GeO_2-30BaO-(10-y)Ga_2O_3$ (GBG glass system) and $xTiO_2-(60-x)GeO_2-30BaO-(10-y)Ga_2O_3$ (TGBG glass system), where $x = 10, 20, 30, 40, 45, 50$. Thulium ions was doped additively as 0.05, 0.1, 0.3, 0.5, 0.7, 1.0 mol% Tm_2O_3 . Each chemical constituent was weighed with a precision electronic balance and batches of 5 g were mixed homogeneously together in an agate mortar. Next, the corundum crucible was transferred to the electric furnace and melted at 1250 °C for 0.45 h. Finally, after cooling slowly to the room temperature, the prepared glasses were polished to meet the requirements for optical measurements.

As a part of near-IR luminescence investigations on the Tm^{3+} -doped GBG and TGBG glass systems were characterized using absorption (Cary 5000 UV-VIS-NIR spectrophotometer, Agilent Technology, USA) and photoluminescence spectroscopy. For luminescence measurements (spectra and decays) laser equipment was used, which consists of PTI QuantaMaster QM40 spectrofluorometer with a xenon lamp (75 W) as

an excitation source, tunable pulsed optical parametric oscillator (OPO), Nd:YAG laser (OpotekOpolette 355 LD), double 200 mm monochromators, Hamamatsu H10330B-75 detector and PTI ASOC-10 USB-2500 oscilloscope. Resolution for spectral measurements was ± 0.1 nm. Decay curves were recorded with an accuracy of ± 0.5 μs . In order to compare the emission intensity under the same experimental conditions, measurements of glass systems were carried out at the same slit settings. The structural properties and vibrations of groups were investigated using Raman spectroscopy. These spectra were recorded on an Thermo ScientificTM DXRTM2xi Raman imaging microscope. The appropriate laser source with an excitation wavelength of 633 nm was used to collect the data within 1200–400 cm^{-1} frequency range (120 scans, 0.1 cm^{-1} resolution). The laser was directly focused on the sample with an Olympus long-working-distance microscope objective (50 \times). Analysis of the registered data was carried out using Origin Pro 9.1 software. All optical and structural and measurements were carried out at room temperature.

3. Results and discussion

Fig. 1a presents near-infrared emission spectra for Tm^{3+} ions in $GeO_2-BaO-Ga_2O_3$ glasses. The spectra of this glass samples doped with various thulium ions concentration were recorded under excitation at 808 nm. Luminescence band at about 1.8 μm corresponds to transition from excited state 3F_4 to ground state 3H_6 of Tm^{3+} ions. To explain this behavior, we used a simplified scheme of Tm^{3+} energy-levels considered in Fig. 1 b. The near-infrared luminescence at about 1.45 μm due to the $^3H_4 \rightarrow ^3F_4$ transition of Tm^{3+} can be observed (not presented in this work). Next, the part of trivalent thulium ions passes directly through the 3H_5 state to the 3F_4 lower energy state due to the multi-phonon relaxation rates. The 3H_5 state is characterized by a short lifetime and its role in the relaxation process can be neglected. The 3F_4 state is long and it allows for reaching a high population density at this level. Additionally, by successive cross-relaxation (CR) channel between 3H_4 and 3H_6 states of Tm^{3+} ions contributes greatly to stronger near-infrared emissions at about 1.8 μm . The cross-relaxation process between pairs of Tm^{3+} : $^3H_4 + ^3H_6 \rightarrow ^3F_4 + ^3F_4$ may cause depopulation of the 3H_4 state. Consequently, the near-infrared emission at 1.45 μm due to the $^3H_4 \rightarrow ^3F_4$ transition of Tm^{3+} is quenched [36,37]. Luminescence properties of $GeO_2-BaO-Ga_2O_3$ glass singly doped with trivalent thulium ions were examined in 1600–2100 nm spectral range. Spectroscopic studies indicate that increased Tm^{3+} ions concentration in GBG glass system affects the rising the intensity of near-infrared luminescence band due to the $^3F_4 \rightarrow ^3H_6$ transition of Tm^{3+} . The intensity of luminescence band 1.8 μm of Tm^{3+} ions increase with increasing Tm_2O_3 concentration up to 0.3 mol %. According to available data, the higher concentration of Tm^{3+} ions contributes to increasing the probability of non-radiative transitions among cross-relaxation channels and the energy transfer process [38]. Indeed, the quenching of fluorescence intensity in fabricated glasses was observed with high dopant levels. Based on the collected spectra, analysis of luminescence linewidth referred to as full width at half maximum (FWHM) was calculated. The values of FWHM for barium gallo-germanate glasses are about 220 nm (0.05mol%), 223 nm (0.1 mol %), 228 nm (0.3 mol%), 226 nm (0.5 mol%), 224 nm (0.7 mol%), 224 nm (224 nm) and depend slightly on Tm^{3+} ions concentration.

In the next step, luminescence decay curves for the upper 3F_4 laser state of Tm^{3+} in barium gallo-germanate glasses were measured and analyzed (Fig. 1c). Luminescence decay curves were quite well fitted to nearly single-exponential function. Based on decay curve measurements, luminescence lifetimes for the upper 3F_4 state of thulium ions in glasses varying with Tm_2O_3 concentration were determined. Luminescence lifetime is an important parameter to estimate the rare-earth ions behavior of the excited state in various glass systems. Generally, the experimental values of τ_m obtained for the barium gallo-germanate glass samples are reduced with increasing Tm_2O_3 concentration. Additionally, the radiative lifetimes (τ_{rad}) obtained from the Judd-Ofelt theory

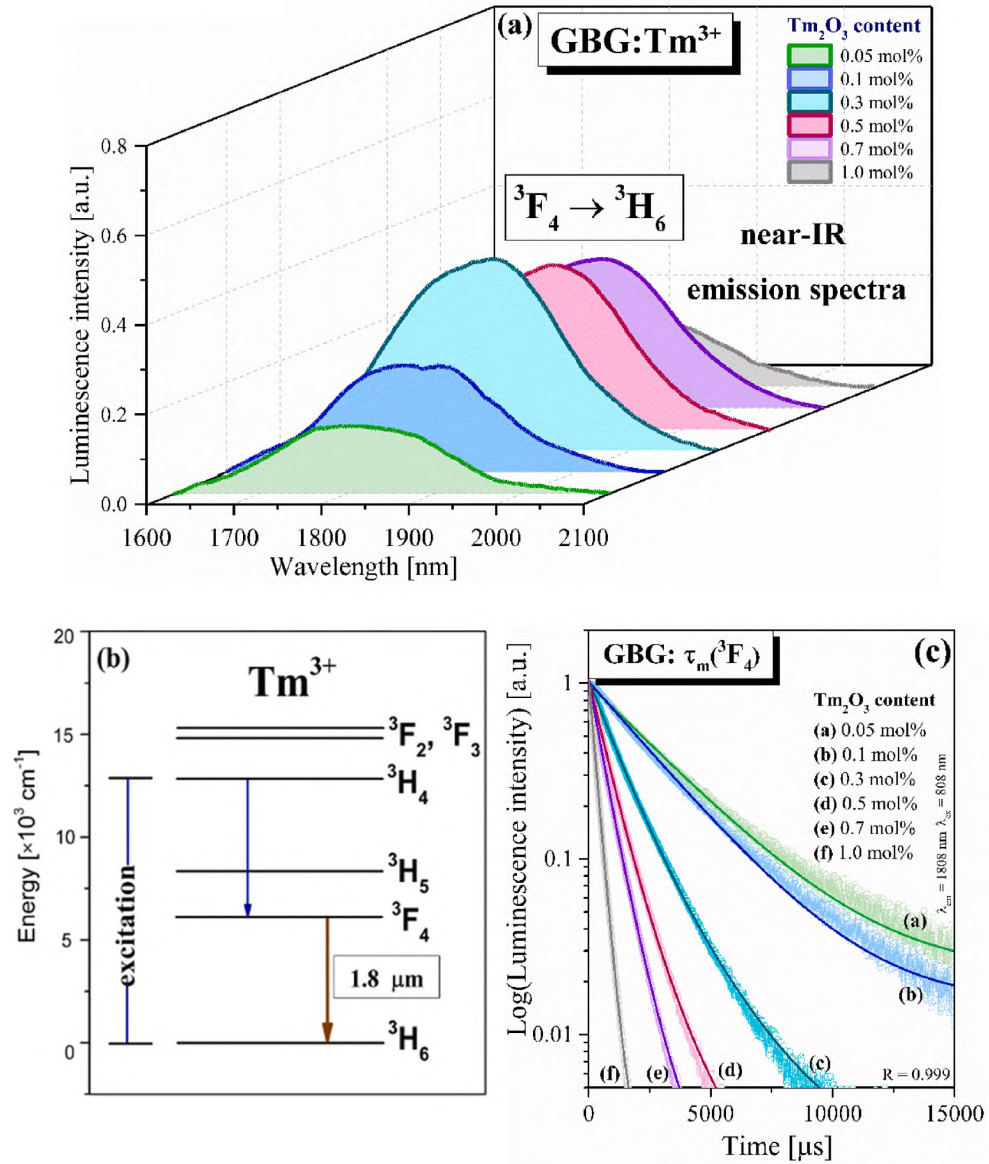


Fig. 1. Near-IR luminescence bands due to ${}^3F_4 \rightarrow {}^3H_6$ laser transition of Tm^{3+} ions (a), simplified energy level diagram for Tm^{3+} ions (b), luminescence decays from the upper 3F_4 laser state (c) of Tm^{3+} ions in barium gallo-germanate glasses.

using relation given in Ref. [39], and the measured luminescence lifetimes (τ_m) were used to calculate the quantum efficiency η for the upper laser state 3F_4 (Tm^{3+}). For rare-earth ions, the quantum efficiency (η) is another important parameter, which is used to predict the efficiency/quality of the laser host material. This can be evaluated by using following relation given below:

$$\eta = \tau_m / \tau_{rad} \times 100\% \quad (1)$$

Among the studied samples, the quantum efficiency for the upper laser state 3F_4 of Tm^{3+} ions in barium gallo-germanate glasses is the highest for sample doped with extremely low concentration (0.05 mol%) of thulium ions and its value is close to $\eta = 50\%$. Details are also given in Table 1. The luminescence lifetimes (τ_m) and the quantum efficiency (η) are compared to several Tm^{3+} -doped glasses published previously [40–51]. The results are summarized in Table 2.

To verify the effect of TiO_2 concentration on optical properties of

Table 1
The calculated luminescence lifetimes (τ_m), quantum efficiency (η) for Tm^{3+} ions in fabricated barium gallo-germanate (GBG) glass systems.

Chemical composition of glass-host [mol%]	τ_m [ms]	η [%]
60GeO ₂ -30BaO-9.95Ga ₂ O ₃ -0.05Tm ₂ O ₃	3.07	50
60GeO ₂ -30BaO-9.9Ga ₂ O ₃ -0.1Tm ₂ O ₃	2.70	44
60GeO ₂ -30BaO-9.7Ga ₂ O ₃ -0.3Tm ₂ O ₃	1.27	20
60GeO ₂ -30BaO-9.5Ga ₂ O ₃ -0.5Tm ₂ O ₃	0.77	13
60GeO ₂ -30BaO-9.3Ga ₂ O ₃ -0.7Tm ₂ O ₃	0.59	9
60GeO ₂ -30BaO-9.0Ga ₂ O ₃ -1.0Tm ₂ O ₃	0.27	4

GeO₂-BaO-Ga₂O₃ glass system, where the concentration of Tm^{3+} ions was the same (0.5 mol%) the absorption spectroscopy was used. Fig. 2 presents optical absorption spectra of Tm^{3+} ions in TGBG glass system with various GeO₂:TiO₂ molar ratios. The spectra consist of the inhomogeneously broadened absorption lines characteristic for $4f^{12}$ - $4f^{12}$

Table 2
Comparison of the luminescence lifetimes (τ_m), quantum efficiency (η) in different laser glasses doped with Tm^{3+} .

Glass host	Tm_2O_3 content [mol%]	τ_m [ms]	η [%]	Ref.
GeO-BaO-Ga ₂ O ₃	0.05	3.07	50	this work
TeO ₂ -Al ₂ O ₃ -BaF ₂	4.0	0.17	–	[40]
Ga ₂ O ₃ -GeO ₂ -BaO	1.0	5.55	–	[41]
GeO ₂ -BaO-K ₂ O	1.0	0.60	12	[42]
GeO ₂ -PbO-Nb ₂ O ₅	1.0	0.74	42	[43]
GeO ₂ -BaO/CaO-Na ₂ O/Li ₂ O	1.0	4.29	100	[43]
GeO ₂ -BaO/BaF ₂ -Ga ₂ O ₃ -Na ₂ O-La ₂ O ₃	1.0	3.06	71	[43]
BaO-GeO ₂	0.8	5.64	–	[43]
GeO ₂ -TeO ₂ -PbO-CaO	0.3	2.48	78	[44]
GeO ₂ -Ga ₂ O ₃ -BaO-Nb ₂ O ₅ -PbO	0.5	1.91	55	[45]
GeO ₂ -Ga ₂ O ₃ -BaO-Nb ₂ O ₅ -PbO	1.5	0.60	20	[45]
TeO ₂ -ZnF ₂ -Bi ₂ O ₃ -GeO ₂	0.5	5.25	–	[46]
TeO ₂ -ZnO-ZnF ₂	0.5	1.22	65	[47]
PbO-Bi ₂ O ₃ -Ga ₂ O ₃	1.5	1.03	69	[48]
TeO ₂ -Ga ₂ O ₃ -BaF ₂	1.0	0.57	–	[49]
BaO-Ga ₂ O ₃ -GeO ₂ -La ₂ O ₃ -Y ₂ O ₃	1.8	0.7	–	[50]
Bi ₂ O ₃ -GeO ₂ -Ga ₂ O ₃ -Na ₂ O	1.0	1.63	74	[51]
Bi ₂ O ₃ -GeO ₂ -Ga ₂ O ₃ -BaF ₂	1.0	2.25	91	[51]

electronic transitions of Tm^{3+} which are located in the visible range, respectively. Absorption bands correspond to transitions originating from the $^3\text{H}_6$ ground state to the higher-lying $^1\text{G}_4$ (472 nm), $^3\text{F}_2$, $^3\text{F}_3$ (686 nm) and $^3\text{H}_4$ (792 nm) excited states of Tm^{3+} ions. It could be observed that the intensities of individual absorption bands have grown with increasing $\text{GeO}_2:\text{TiO}_2$ molar ratio, confirming that there is no cluster formation in the glass medium. From the absorption spectra, the glass parameter i.e. UV cut-off wavelength defined as the intersection between the zero base line and the extrapolation of absorption edge was determined. In Fig. 2b the UV cut-off of glass host in function of TiO_2 content can be seen in more detail. The absorption edge is changed from 290 nm (glass without TiO_2) to 380 nm (glass with $\text{GeO}_2:\text{TiO}_2 = 1:5$) with increasing TiO_2 concentration. The UV absorption edge for the studied samples is shifted to longer wavelengths (red shift) with increasing TiO_2 concentration due to the presence of Ti^{3+} , as explained by Zikmund et al. [52]. It is in a good agreement with the previous results, which was obtained for modified barium gallo-germanate glass hosts [53]. The Judd theory propounded in 1966 has been of immense value in the quantitative interpretation of the intensities of the hypersensitive transitions in rare-earth [54], initiated a study of this aspect in optical materials. One of the most important concerns in glasses doped with luminescent rare-earth ions is to determine a dopant environment. Selected trivalent rare-earth ions have electronic transitions that are

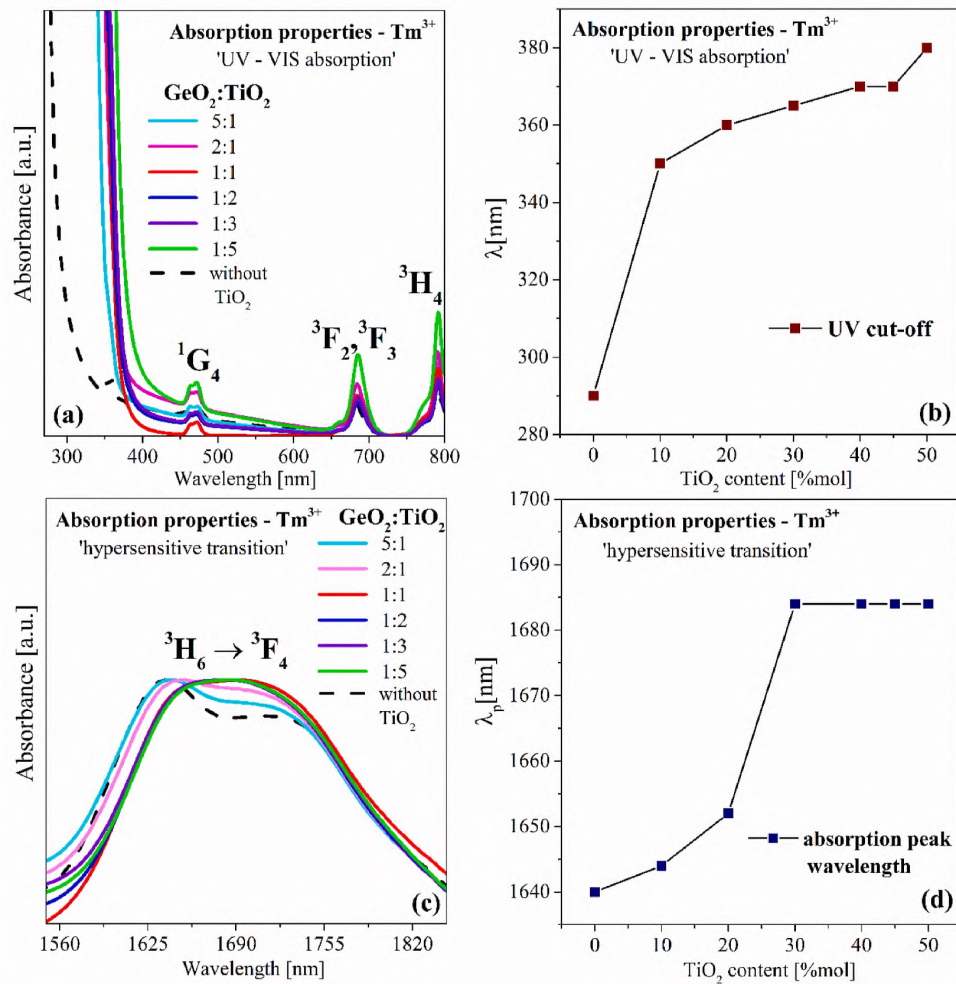


Fig. 2. Absorption properties for Tm^{3+} ions in titanate-germanate glasses with various molar ratios $\text{GeO}_2:\text{TiO}_2$ compared to $\text{GeO}_2\text{-BaO-Ga}_2\text{O}_3$ glass i.e. absorption spectra (a), UV cut-off (b), hypersensitive transition (c), absorption peak wavelength (d).

hypersensitive to the field of surrounding ligands. For example, glasses doped with Er^{3+} , Ho^{3+} and Nd^{3+} revealed hypersensitive $^4I_{15/2} \rightarrow ^2H_{11/2}$ [55], $^5I_8 \rightarrow ^5G_8$ [56], $^4I_{9/2} \rightarrow ^4G_{5/2}$, $^2G_{7/2}$ [4] transitions, respectively. In general, the hypersensitive transition is a useful probe because it is sensitive to small changes of the glass environment around rare-earth ions. Especially, the absorption band corresponding to the $^3H_6 \rightarrow ^3F_4$ transition [57] of Tm^{3+} located in a near-infrared range near 1700 nm follows well the selection rules: $|S| = 0$, $|\Delta L| \leq 2$ and $|\Delta J| \leq 2$. Fig. 2c shows the hypersensitive absorption band of Tm^{3+} varying with GeO_2 : TiO_2 molar ratios. In order to determine the absorption peak wavelength in the function of TiO_2 content, as shown in Fig. 2d—a detailed deconvolution process procedure for the $^3H_6 \rightarrow ^3F_4$ transition was performed using Origin Pro software. Notably, the findings presented in this work indicated that the spectral profile and position of this transition are changed during the modification of fabricated barium gallo-germanate glass-host in the function TiO_2 content. The absorption band related to

the hypersensitive transition of Tm^{3+} ions is shifted to longer wavelengths (red shift) with increasing TiO_2 concentration. B. So et al. [58] achieved similar spectroscopic behavior in the intensity and shape of the hypersensitive $^3H_6 \rightarrow ^3F_4$ transition in $\text{CaO-Al}_2\text{O}_3\text{-SiO}_2$ glass, which reflects the local environment surrounding Tm^{3+} ions. Interestingly, the hypersensitive $^3H_6 \rightarrow ^3F_4$ transition, turns out to reflect the modified chemical environments more significantly than other transitions of Tm^{3+} ions. According to H. Yang et al. [59] only some coordination shells surrounding a Tm^{3+} ion, within a few Å, are effectively modified when Ga and CsBr were added into Tm^{3+} -doped Ge-As-S glasses. Their investigation revealed that the crystal fields would be changed gradually with increased compositional modification and then become fixed for a sufficiently large modification. As such, the current experimental results confirm that the degree of covalency of the $\text{Tm}^{3+}\text{-O}$ bond increases with increasing TiO_2 concentration in glass composition. For this reason, the relationship between optical properties and local structure will be

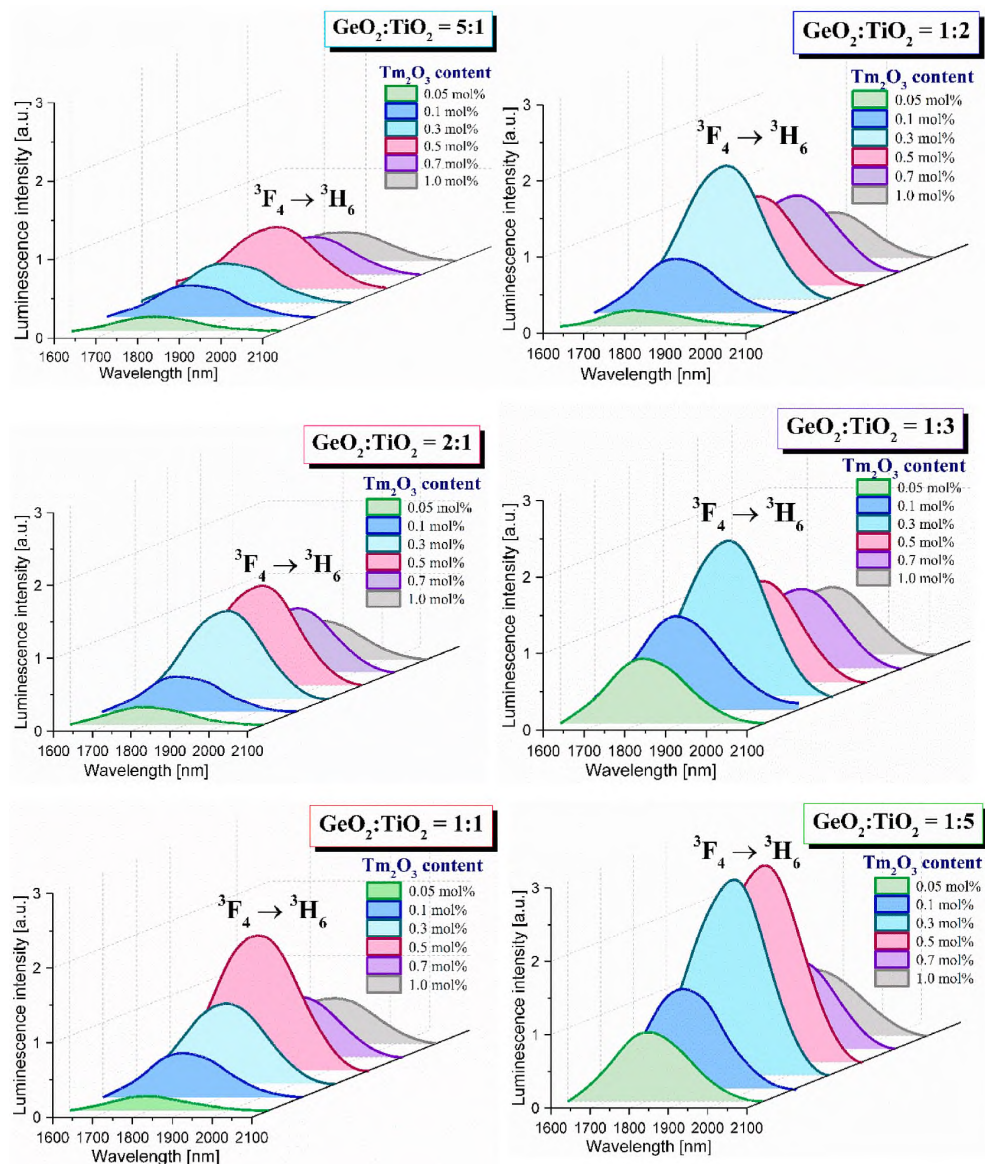


Fig. 3. Near-IR luminescence bands due to $^3F_4 \rightarrow ^3H_6$ laser transition of Tm^{3+} ions in titanate-germanate glass systems with various GeO_2 : TiO_2 molar ratio in function of Tm^{3+} ions concentration.

confirmed in the next part of this work.

The luminescence properties of Tm^{3+} -doped $\text{TiO}_2\text{-GeO}_2\text{-BaO-Ga}_2\text{O}_3$ glasses were investigated to determine the influence of TiO_2 on the luminescence intensity of thulium ions. Fig. 3 shows the near-IR luminescence spectra of Tm^{3+} ions in titanate-germanate glasses. As can be seen, there were significant differences between the intensity of the band corresponding to the ${}^3\text{F}_4 \rightarrow {}^3\text{H}_6$ transition of Tm^{3+} , and the chemical composition of the designed material. In general, the integrated emission intensity for the ${}^3\text{F}_4 \rightarrow {}^3\text{H}_6$ transition of Tm^{3+} is a 4.8-fold increase for glass systems with a molar ratio $\text{GeO}_2:\text{TiO}_2 = 1:5$

compared to the GBG glass system. However, the titanate-germanate system with a relatively high concentration of GeO_2 exhibited strong luminescence at $1.8 \mu\text{m}$ for samples activated with 0.5 mol% Tm^{3+} ions. The opposite situation has been observed for Tm -doped samples, where the $\text{GeO}_2:\text{TiO}_2$ ratio was changed from 1:2 to 1:5. In this case, the enhanced emission band associated to ${}^3\text{F}_4 \rightarrow {}^3\text{H}_6$ transition was observed for samples doped with 0.3 mol% of thulium ions. The quenching phenomenon is also observed for highly doping samples (0.7 and 1.0 mol% Tm_2O_3) the same as for GBG glass system. The emission linewidth for the ${}^3\text{F}_4 \rightarrow {}^3\text{H}_6$ transition of Tm^{3+} ions equal to 219 nm (0.05 mol% Tm^{3+})

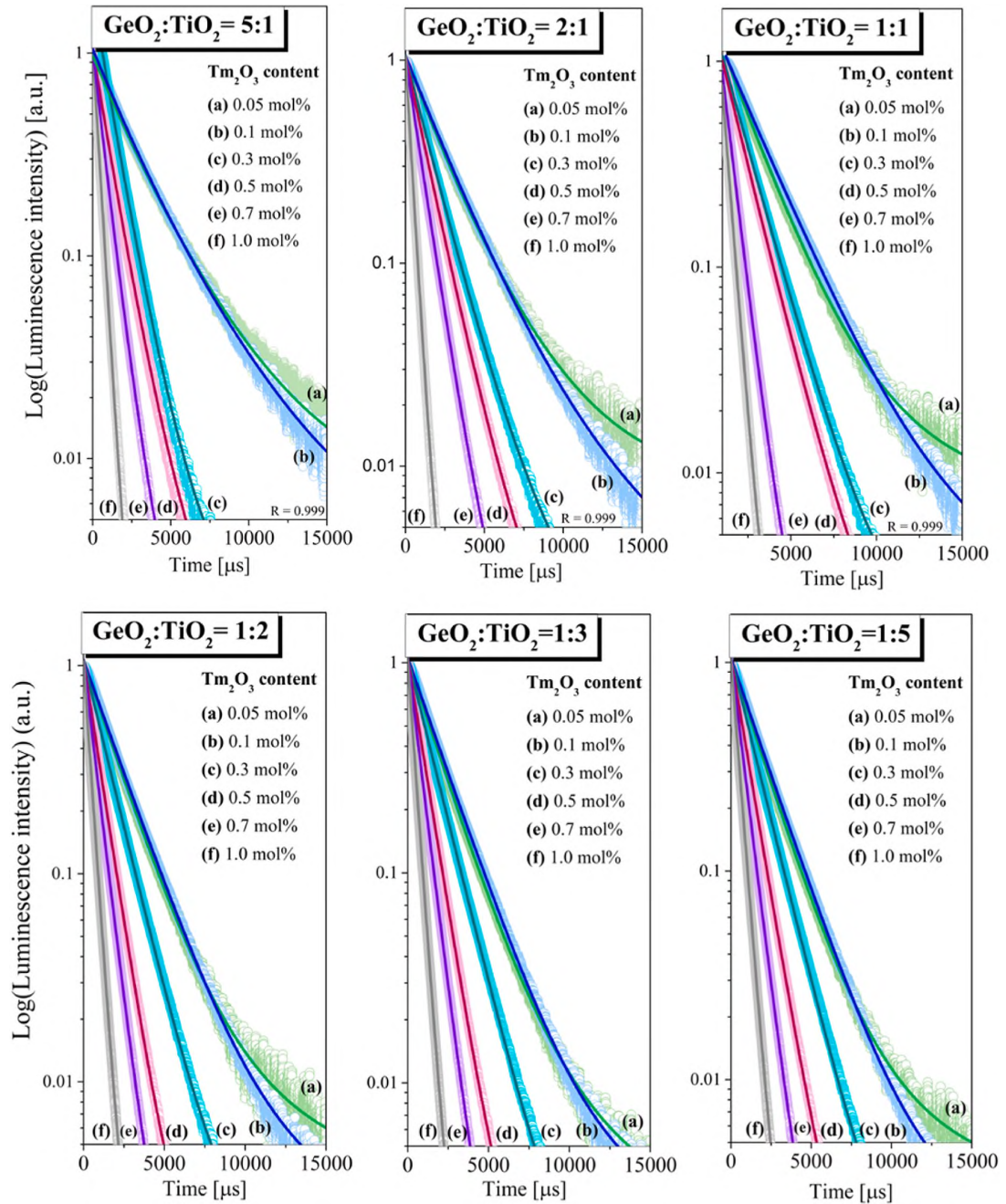


Fig. 4. Luminescence decays from the upper ${}^3\text{F}_4$ laser state of Tm^{3+} ions in titanate-germanate glass systems with various $\text{GeO}_2:\text{TiO}_2$ molar ratio in function of Tm^{3+} ions concentration.

and 248 nm (1.0 mol% Tm^{3+}) in system with molar ratio $\text{TiO}_2:\text{GeO}_2 = 5:1$, 238 nm (0.05 mol% Tm^{3+}) and 246 nm (1.0 mol% Tm^{3+}) in system with molar ratio $\text{TiO}_2:\text{GeO}_2 = 2:1$, 223 nm (0.05 mol% Tm^{3+}) and 253 nm (1.0 mol% Tm^{3+}) in system with molar ratio $\text{TiO}_2:\text{GeO}_2 = 1:1$, 224 nm (0.05 mol% Tm^{3+}), 246 nm (1.0 mol% Tm^{3+}) in system with molar ratio $\text{TiO}_2:\text{GeO}_2 = 1:2$, 222 nm (0.05 mol% Tm^{3+}), and 238 nm (1.0 mol% Tm^{3+}) in system with molar ratio $\text{TiO}_2:\text{GeO}_2 = 1:3$, 226 nm (0.05 mol% Tm^{3+}), and 241 nm (1.0 mol% Tm^{3+}) in system with molar ratio $\text{TiO}_2:\text{GeO}_2 = 1:5$ compared to 220 nm (0.05 mol% Tm^{3+}) and 224 nm (1.0 mol% Tm^{3+}) in GBG system without TiO_2 . This situation is really promising for near-IR applications. To confirm the validity of the postulated near-infrared emission properties after incorporation of the TiO_2 into to barium gallo-germanate network, we measured the luminescence decay curves for the system with various molar ratios $\text{GeO}_2:\text{TiO}_2$, excited at $\lambda_{\text{exc}} = 808$; monitored at $\lambda_{\text{em}} = 1808$, which are presented in Fig. 4. In our previous work [39], Tm^{3+} -doped titanate-germanate glasses have been examined using the Judd-Ofelt (J-O) theory. The radiative lifetimes for the $^3\text{F}_4$ state of Tm^{3+} ions calculated from the J-O theory were compared to the experimental lifetimes, and the quantum efficiencies were determined using the relation (1). The results for glass samples doped with 0.1 mol% are summarized in Table 3. The radiative lifetimes (*) for the studied glass samples were adopted from Ref. [39]. The same procedure was applied in the present work to all glass samples varying with activator concentration. Luminescence lifetimes and quantum efficiencies with various molar ratios $\text{GeO}_2:\text{TiO}_2$ and Tm^{3+} ions concentration are schematized in Fig. 5a and b. Luminescence decay curves analysis suggests that the $^3\text{F}_4$ lifetimes of thulium ions depends on the activator (Tm^{3+}) concentration and chemical composition of the glass host. Their values are shorter compared to glass samples without TiO_2 . Among the studied samples, the quantum efficiencies for the $^3\text{F}_4$ state of Tm^{3+} ions are the highest for glass systems with molar ratios $\text{GeO}_2:\text{TiO}_2 = 1:1$, 1:2, 1:3, and their values are above 70 %, respectively. The highest quantum efficiency for the $^3\text{F}_4$ state of Tm^{3+} ions was obtained for the glass system with $\text{GeO}_2:\text{TiO}_2 = 1:1$ M ratio. Details are given in Table 4. Independence on activator concentration, the quantum efficiencies are higher for multi-component titanate-germanate (TGBG) systems than for barium gallo-germanate (GBG) systems without TiO_2 (Table 1).

At this moment, it should be pointed out that luminescence decay curves are changed in character from nearly single-exponential to non-exponential, and the measured lifetimes for the $^3\text{F}_4$ state decrease with increasing activator (Tm^{3+}) concentration. For higher-concentrated thulium-doped glass samples, the interactions between rare-earth ions become prominent that the energy transfer process takes place from an excited Tm^{3+} ion playing the role as donor to a non-excited Tm^{3+} ion (acceptor), leading to a non-exponential shape of the luminescence

Table 3

The radiative (τ_{rad}) and measured (τ_{m}) luminescence lifetimes and the quantum efficiencies (η) for the $^3\text{F}_4$ state of Tm^{3+} ions in titanate-germanate glasses. The activator concentration was 0.1 mol% Tm_2O_3 .

Glass composition [mol%]	$\text{GeO}_2:\text{TiO}_2$ ratio	τ_{rad} [ms] ^a	τ_{m} [ms]	η [%]
50 GeO_2 -10 TiO_2 -30 BaO -9.9 Ga_2O_3 -0.1 Tm_2O_3	5:1	6.289	2.485	39.5
40 GeO_2 -20 TiO_2 -30 BaO -9.9 Ga_2O_3 -0.1 Tm_2O_3	2:1	5.882	2.350	40.0
30 GeO_2 -30 TiO_2 -30 BaO -9.9 Ga_2O_3 -0.1 Tm_2O_3	1:1	2.874	2.230	77.6
20 GeO_2 -40 TiO_2 -30 BaO -9.9 Ga_2O_3 -0.1 Tm_2O_3	1:2	2.725	1.965	72.1
15 GeO_2 -45 TiO_2 -30 BaO -9.9 Ga_2O_3 -0.1 Tm_2O_3	1:3	2.643	1.948	73.7
10 GeO_2 -50 TiO_2 -30 BaO -9.9 Ga_2O_3 -0.1 Tm_2O_3	1:5	3.690	1.944	52.7

^a Radiative lifetimes calculated from the Judd-Ofelt theory and their values adopted from [39].

decay curves [60]. Thus, the luminescence of Tm^{3+} is successfully quenched due to the increasing ion-ion interaction and the presence of the energy transfer processes. One of them is the cross-relaxation between pairs of rare-earths. This process can be observed for Tm^{3+} -doped glasses due to the favorable distribution of energy states of thulium ions. The transfer of excitation energy to the $^3\text{F}_4$ state is followed by an efficient pumping of the higher-lying $^3\text{H}_4$ state and cross-relaxation process between two neighboring Tm^{3+} ions: $^3\text{H}_4 + ^3\text{H}_6 \rightarrow ^3\text{F}_4 + ^3\text{F}_4$ [61]. Considering a non-exponential character of decays from the $^3\text{F}_4$ (Tm^{3+}) state, the ion-ion interactions in thulium-doped titanate-germanate glasses have been estimated using the Inokuti-Hirayama (I-H) model [62]. The time evolution of the emission intensity was fitted using by the following relation:

$$I(t) = A \exp \left[- \left(\frac{t}{\tau_0} \right) - \alpha \left(\frac{t}{\tau_0} \right)^{3/s} \right] \quad (2)$$

where 'A' is a constant, $I(t)$ is emission intensity after pulse excitation, τ_0 is the lifetime of donor in the absence of acceptor, $s = 6$ for a dipole-dipole type interaction between the ions, and the α parameter is given as follows:

$$\alpha = 4/3\pi\Gamma(1 - 3/s)N_aR_0^3 \quad (3)$$

where Γ is the Euler function, N_a is the concentration of acceptor ions and R_0 is the critical transfer distance. The values of critical transfer distance R_0 and measured lifetime τ_0 were applied to determine the donor-acceptor interaction parameter C_{da} and the energy transfer probability $W_{\text{D-A}}$. They are given by the following equations:

$$C_{\text{da}} = R_0^6 \tau_0^{-1} \quad (4)$$

$$W_{\text{D-A}} = C_{\text{da}} R_0^{-6} \quad (5)$$

The results for the studied thulium-doped glass systems using the Inokuti-Hirayama model are summarized in Tables 5–11.

For all studied glass samples, the critical transfer distance R_0 defined as donor-acceptor separation is reduced with increasing Tm^{3+} concentration. It suggests the ion-ion interaction increasing and the energy transfer processes between thulium ions become dominant. Consequently, the energy transfer probabilities $W_{\text{D-A}}$ for the $^3\text{F}_4$ excited state increase with increasing activator (Tm^{3+}) concentration. It was schematically illustrated on Fig. 6a. However, it is interesting to see that the trend of $W_{\text{D-A}}$ values is completely different for low and high activator concentrations. For low Tm^{3+} concentration, the values of $W_{\text{D-A}}$ increase in direction from glass without TiO_2 to titanate-germanate glass with the highest molar ratio $\text{GeO}_2:\text{TiO}_2 = 1:5$ (50 mol% TiO_2). Opposite situation is observed for titanate-germanate glass with higher activator concentration, especially visible for 1 mol% Tm^{3+} . In this case, the values of $W_{\text{D-A}}$ are reduced in direction from glass without TiO_2 to titanate-germanate glass with the highest molar ratio $\text{GeO}_2:\text{TiO}_2 = 1:5$ (50 mol% TiO_2). For better clarity, these effects are presented on the graph with the energy transfer probabilities $W_{\text{D-A}}$ plotted as a function of TiO_2 concentration (Fig. 6b). It worth to notice that the energy transfer probabilities $W_{\text{D-A}}$ increase with increasing TiO_2 concentration in glass samples containing low Tm^{3+} content. These effects are especially visible for glass samples with 0.05 and 0.1 mol% Tm^{3+} . The values of $W_{\text{D-A}}$ are the smallest for glass samples containing 0.1 mol% Tm^{3+} , except sample without TiO_2 and titanate-germanate glass with $\text{GeO}_2:\text{TiO}_2 = 5:1$ (10 mol% TiO_2). For highly concentrated Tm^{3+} -doped glass samples, the energy transfer probabilities $W_{\text{D-A}}$ are reduced with increasing TiO_2 concentration. This phenomenon is important for the glass systems varying with TiO_2 content, because the smaller $W_{\text{D-A}}$ parameters suggest low self-quenching luminescence from the excited states of rare-earth ions.

Based on the analysis using the Inokuti-Hirayama model we conclude that concentration-dependent luminescence self-quenching of Tm^{3+} is

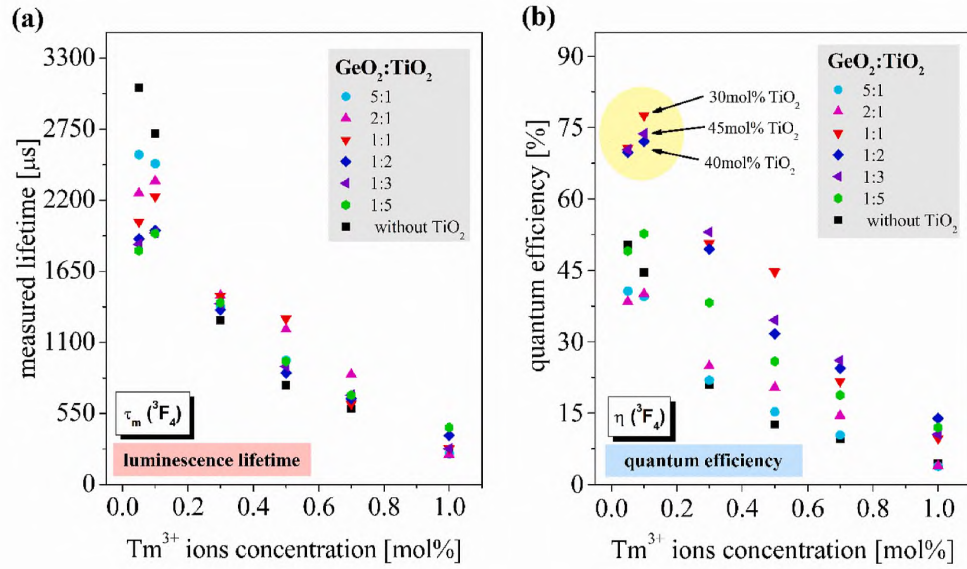


Fig. 5. The measured luminescence lifetime (a) and quantum efficiency (b) of titanate-germanate glass systems with various $\text{GeO}_2\text{:TiO}_2$ molar ratio in function of Tm^{3+} ions concentration.

Table 4

The calculated luminescence lifetimes (τ_m), quantum efficiency (η) for Tm^{3+} ions in fabricated multicomponent titanate-germanate (TGBG) glass systems. The molar ratio was $\text{GeO}_2\text{:TiO}_2 = 1:1$.

Chemical composition of glass-host [mol%]	τ_m [ms]	η [%]
$30\text{GeO}_2\text{-}30\text{TiO}_2\text{-}30\text{BaO}\text{-}9.95\text{Ga}_2\text{O}_3\text{-}0.05\text{Tm}_2\text{O}_3$	2.032	70.8
$30\text{GeO}_2\text{-}30\text{TiO}_2\text{-}30\text{BaO}\text{-}9.9\text{Ga}_2\text{O}_3\text{-}0.1\text{Tm}_2\text{O}_3$	2.230	77.6
$30\text{GeO}_2\text{-}30\text{TiO}_2\text{-}30\text{BaO}\text{-}9.7\text{Ga}_2\text{O}_3\text{-}0.3\text{Tm}_2\text{O}_3$	1.457	51.4
$30\text{GeO}_2\text{-}30\text{TiO}_2\text{-}30\text{BaO}\text{-}9.5\text{Ga}_2\text{O}_3\text{-}0.5\text{Tm}_2\text{O}_3$	1.284	45.2
$30\text{GeO}_2\text{-}30\text{TiO}_2\text{-}30\text{BaO}\text{-}9.3\text{Ga}_2\text{O}_3\text{-}0.7\text{Tm}_2\text{O}_3$	0.646	22.1
$30\text{GeO}_2\text{-}30\text{TiO}_2\text{-}30\text{BaO}\text{-}9.0\text{Ga}_2\text{O}_3\text{-}1.0\text{Tm}_2\text{O}_3$	0.278	10.3

Table 5

Molar ion concentration (N_a , 10^{20} ion/ cm^3), α value, critical transfer distance (R_0 , Å), donor-acceptor interaction (C_{da} , 10^{-52} m^6s^{-1}) and the energy transfer probability (W_{D-A} , s^{-1}) for various molar content of Tm^{3+} in germanate glass without TiO_2 .

Tm^{3+}	N_a	α	R_0	C_{da}	W_{D-A}
0.05	0.212	0.20	10.84	4.51	278
0.10	0.423	0.20	8.61	1.27	312
0.30	1.265	0.23	8.06	1.99	626
0.50	2.103	0.75	7.84	2.06	887
0.70	2.933	0.45	6.68	0.60	1375
1.00	4.174	0.50	5.45	0.74	2857

Table 6

Molar ion concentration (N_a , 10^{20} ion/ cm^3), α value, critical transfer distance (R_0 , Å), donor-acceptor interaction (C_{da} , 10^{-52} m^6s^{-1}) and the energy transfer probability (W_{D-A} , s^{-1}) for various molar content of Tm^{3+} in titanate-germanate glass with $\text{GeO}_2\text{:TiO}_2 = 5:1$ (10 % TiO_2).

Tm^{3+}	N_a	α	R_0	C_{da}	W_{D-A}
0.05	0.216	0.10	8.55	1.32	339
0.10	0.431	0.15	7.77	0.77	351
0.30	1.289	0.18	5.73	0.22	606
0.50	2.144	0.20	5.61	0.26	854
0.70	2.990	0.20	4.49	0.11	1370
1.00	4.255	0.25	4.30	0.16	2500

Table 7

Molar ion concentration (N_a , 10^{20} ion/ cm^3), α value, critical transfer distance (R_0 , Å), donor-acceptor interaction (C_{da} , 10^{-52} m^6s^{-1}) and the energy transfer probability (W_{D-A} , s^{-1}) for various molar content of Tm^{3+} in titanate-germanate glass with $\text{GeO}_2\text{:TiO}_2 = 2:1$ (20 % TiO_2).

Tm^{3+}	N_a	α	R_0	C_{da}	W_{D-A}
0.05	0.220	0.15	9.72	3.18	377
0.10	0.440	0.20	8.50	1.37	364
0.30	1.315	0.20	5.90	0.25	599
0.50	2.186	0.20	5.05	0.14	813
0.70	3.048	0.25	4.85	0.16	1266
1.00	4.337	0.25	4.27	0.15	2439

Table 8

Molar ion concentration (N_a , 10^{20} ion/ cm^3), α value, critical transfer distance (R_0 , Å), donor-acceptor interaction (C_{da} , 10^{-52} m^6s^{-1}) and the energy transfer probability (W_{D-A} , s^{-1}) for various molar content of Tm^{3+} in titanate-germanate glass with $\text{GeO}_2\text{:TiO}_2 = 1:1$ (30 % TiO_2).

Tm^{3+}	N_a	α	R_0	C_{da}	W_{D-A}
0.05	0.225	0.25	11.44	9.34	417
0.10	0.449	0.25	9.09	2.15	381
0.30	1.341	0.35	7.06	0.72	585
0.50	2.247	0.23	5.17	0.17	833
0.70	3.108	0.25	4.77	0.16	1389
1.00	4.422	0.25	4.24	0.13	2220

Table 9

Molar ion concentration (N_a , 10^{20} ion/ cm^3), α value, critical transfer distance (R_0 , Å), donor-acceptor interaction (C_{da} , 10^{-52} m^6s^{-1}) and the energy transfer probability (W_{D-A} , s^{-1}) for various molar content of Tm^{3+} in titanate-germanate glass with $\text{GeO}_2\text{:TiO}_2 = 1:2$ (40 % TiO_2).

Tm^{3+}	N_a	α	R_0	C_{da}	W_{D-A}
0.05	0.229	0.32	12.35	15.77	444
0.10	0.458	0.28	9.38	2.87	433
0.30	1.368	0.30	6.66	0.55	633
0.50	2.275	0.30	5.62	0.29	909
0.70	3.172	0.25	5.03	0.22	1351
1.00	4.513	0.23	4.48	0.18	2174

Table 10

Molar ion concentration (N_a , 10^{20} ion/cm³), α value, critical transfer distance (R_0 , Å), donor-acceptor interaction (C_{da} , 10^{-52} m⁶s⁻¹) and the energy transfer probability (W_{D-A} , s⁻¹) for various molar content of Tm³⁺ in titanate-germanate glass with GeO₂:TiO₂ = 1:3 (45 % TiO₂).

Tm ³⁺	N_a	α	R_0	C_{da}	W_{D-A}
0.05	0.232	0.32	12.30	15.53	448
0.10	0.463	0.28	9.34	2.87	434
0.30	1.382	0.25	6.25	0.37	621
0.50	2.299	0.30	5.60	0.27	877
0.70	3.205	0.20	4.38	0.10	1299
1.00	4.559	0.23	4.15	0.11	2083

Table 11

Molar ion concentration (N_a , 10^{20} ion/cm³), α value, critical transfer distance (R_0 , Å), donor-acceptor interaction (C_{da} , 10^{-52} m⁶s⁻¹) and the energy transfer probability (W_{D-A} , s⁻¹) for various molar content of Tm³⁺ in titanate-germanate glass with GeO₂:TiO₂ = 1:5 (50 % TiO₂).

Tm ³⁺	N_a	α	R_0	C_{da}	W_{D-A}
0.05	0.234	0.35	12.64	18.54	455
0.10	0.468	0.35	10.03	4.43	435
0.30	1.397	0.35	6.97	0.72	625
0.50	2.322	0.35	5.88	0.34	833
0.70	3.237	0.30	5.00	0.20	1250
1.00	4.605	0.30	4.45	0.15	1961

relatively smaller in titanate-germanate glasses with higher TiO₂ concentration. In another words, self-quenching of near-infrared luminescence is decreased with increasing TiO₂ concentration in glass samples containing higher Tm³⁺ content. It is quite well correlated with the luminescence spectra measurements. The relative intensities of luminescence bands of Tm³⁺ ions are increased with increasing TiO₂ concentration in glass composition. Near-IR emission corresponding to the ³F₄ → ³H₆ transition of Tm³⁺ ions at 1.8 μm was 4.8-fold enhanced for titanate-germanate glass with GeO₂:TiO₂ = 1:5 compared to glass sample without TiO₂.

The amorphous barium gallo-germanate glasses [63,64] possesses interesting physicochemical properties e.g. relatively large glass-forming region, quite strong chemical and mechanical stability, relatively high thermal stability, comparatively low phonon energy

promoting enhanced optical properties and superior IR transparency and it seems to be a host extensively applied in numerous fields of applications. Therefore, barium gallo-germanate glass doped with rare-earth ions playing the role of optically active ions it seems to be an excellent material for optical component testing, solid-state lasers, amplifiers, drawing the optical fibers, medical applications including laser surgery, and atmosphere pollution monitoring [65–67]. In our case, spectroscopic characterization for all these titanate-germanate glass systems doped with Tm³⁺ ions suggests the possibility of using these materials in the near-infrared region. As with other glasses, having a full understanding of the optical properties requires an in-depth spectroscopic characterization. Titanium dioxide (TiO₂) [68,69], playing the dual role of network-modifier or network-former, is a promising component for rare-earth ions to achieve excellent luminescence behavior. The evaluation of absorption and luminescence spectra, and decay curve measurements, several spectroscopic and laser parameters of Tm³⁺ ions in the presence of TiO₂ confirms the hypothesis given above and suggests that TiO₂ modifies GBG glass-network and the local crystal field around the Tm³⁺ ions influencing strongly on their luminescence properties. Firstly, in our experiment, the increase of titanium dioxide content in GBG glass leads to the red shift of the peak position of “hypersensitive transition” of thulium ions. This evidenced that the with TiO₂ incorporation in the glass host enhances the numbers of non-bridged oxygen bond, thereby enhancing the optical alkalinity of the glass. The increased glass optical alkalinity means that O²⁻ in the glass structure has a higher polarizability, giving good covalency and asymmetry for the glass. The correlation between the symmetry in the surroundings of the thulium ions, as well the degree of covalence of bonds of these ions in the function of TiO₂, was perfectly demonstrated based on Judd-Ofelt parameters. The Judd-Ofelt intensity parameters Ω_2 for glasses changes from 1.11 ± 0.03 (0%mol TiO₂) to 3.18 ± 0.02 (50% mol TiO₂) [39], suggesting that the bonds between Tm³⁺ ions and the nearest surroundings are strongly covalent in character in glass with relatively high TiO₂ content. Based on luminescence spectra measurements and calculated data, we suggest that higher concentrations of TiO₂ in GBG glass is strongly recommended. The integrated emission intensity for the main laser transition associated to the ³F₄ → ³H₆ of Tm³⁺ ions located in the optical telecommunication window is significant enhanced in systems containing 50 mol% TiO₂. Moreover, obtained high values of luminescence bandwidth (FWHM = 253 nm) is strongly

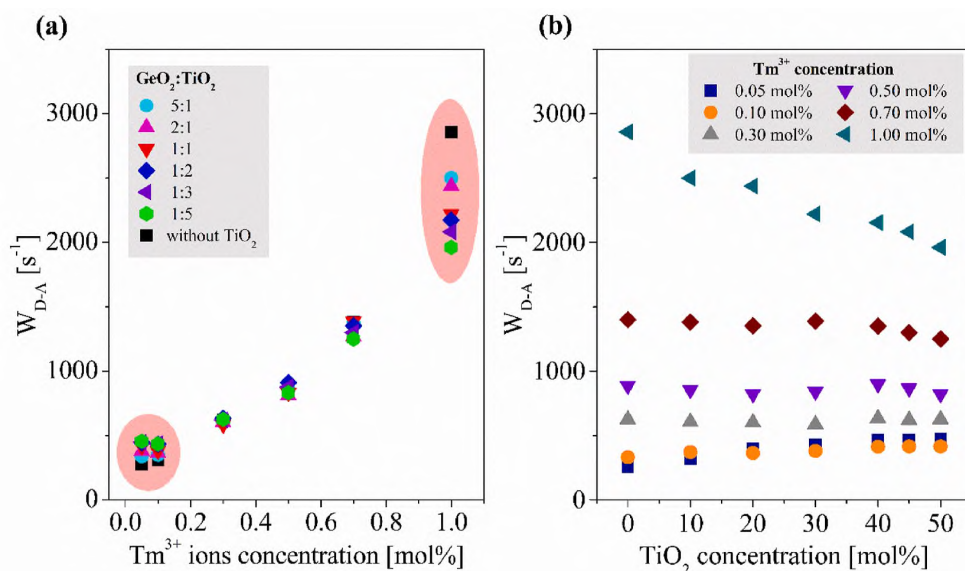


Fig. 6. The energy transfer probabilities as a function of Tm³⁺ (a) and TiO₂ (b) concentration.

required to generate laser action in glass. Previous studies have indicated that the increase in luminescence properties is on account of the influence of low phonon energy of glass primarily [70,71]. Glass host with low phonon energy is suitable material for the rare-earth doping because causes decrease the risk of non-radiative relaxation process. Consequently, this material can be characterized by a longer luminescence lifetime or/and higher quantum efficiency of the excited state of rare-earth ions and verifies its potential near-IR applications. It should be noted that the phonon energy of the fabricated glass host was reduced from 790 cm^{-1} (without TiO_2) to 765 cm^{-1} (with the presence of TiO_2) [3]. It was found that the quantum efficiencies for the ${}^3\text{F}_4 \rightarrow {}^3\text{H}_6$ NIR transition of Tm^{3+} ions are the highest (η above 70 %) for samples, where the molar ratio $\text{GeO}_2:\text{TiO}_2$ was changed from 1:1 to 1:3. The addition of TiO_2 increases the radiative transition, which is required to achieve lasing condition for the enhanced near-IR channel of Tm^{3+} ions. Previously published studies for modified germanate-based glasses containing Tm^{3+} ions [39] compared with presented experimental data in this work for a series of titanate-germanate glass systems give an important contribution. For example, the radiative transition probability A_j calculated for the main near-IR laser transition ${}^3\text{F}_4 \rightarrow {}^3\text{H}_6$ of Tm^{3+} ions in titanate-germanate increases from 164 s^{-1} (without TiO_2) to 378 s^{-1} for highly TiO_2 concentrated glass sample. Besides, the emission properties of Tm^{3+} ions in the presence of TiO_2 were limited only to $\text{TeO}_2\text{-ZnO-Na}_2\text{CO}_3$ (5mol% TiO_2) [72], $\text{GeO}_2\text{-K}_2\text{O}$ (20mol% TiO_2) [73] glasses.

Finally, it should also be pointed out that the relationship between optical and local structure is one of the essential aspects for rare earth-doped glasses to judge their suitability for device fabrication, e.g., laser applications or broadband optical amplifiers. In the paper published by Satyanarayana et al. [74], when TiO_2 was incorporated into glass alloys, the empty d orbital of this heavy metal oxide can imparted high oxygen hyperpolarizability of Ti-O pairs and large oxide ion electronic polarizabilities, which is beneficial to the improvement of optical properties. Indeed, for Tm^{3+} -doped titanate-germanate glasses described in this work, the substitution of TiO_2 at the expense of GeO_2 favors the near-infrared luminescence corresponding to ${}^3\text{F}_4 \rightarrow {}^3\text{H}_6$ (1.8 μm) transition. Therefore, to study the performance of the TGBT system in depth, their structures are analyzed from the Raman spectra in detail. Fig. 7 indicates the Raman spectra of titanate-germanate glasses (TGBG), where the $\text{GeO}_2/\text{TiO}_2$ ratio is changed from 5:1 to 1:5 were performed. The Raman spectra for the glass series change significantly as TiO_2 content increases. The observed three Raman signal peaks in the range of $400\text{-}1000\text{ cm}^{-1}$ are indicative of different types of vibrations. As reported in the literature, the low-frequency band located from 400 cm^{-1} to 600 cm^{-1} is due to GeO_4 structural units, which share their corners, where the germanium atom bending is covalently bonded to four bridging oxygens. The next high-frequency band between 700 cm^{-1} and 900 cm^{-1} is attributed to the GeO_6 structural units, where the central atom germanium is surrounded by six oxygen atoms. This is similar to the related research in the previous system of germanate-based glasses [75–78]. As shown in Fig. 7, with the addition of TiO_2 , a new band at around 650 cm^{-1} develops. This peak was very well observed for the glass systems containing 45mol% and 50mol% TiO_2 , respectively. In earlier studies, TiO_2 was present in the form of tetrahedral TiO_4 or as the network modifier in the form of octahedral TiO_6 and rarely with a tetragonal pyramid structure of TiO_5 [79,80]. According to a paper by Limbach et al. [81] that studied the structure of $\text{Na}_2\text{O-CaO-TiO}_2\text{-SiO}_2$ glasses, increasing TiO_2 concentrations up to 12mol% strongly affects the titanate network connectivity. The authors suggested that the band at 720 cm^{-1} most likely arises from Ti-O bridging oxygen vibrations of fully polymerized TiO_4 tetrahedra units. They also suggested that the particular behavior of TiO_2 on glass network is still not fully understood. Indeed, Reynard and Webb [82] attributed the band at 900 cm^{-1} to the presence of titanyl bonds Ti=O in TiO_5 polyhedra, while Mysen et al. [83] discussed this band in terms of Ti-O bridging oxygen vibrations associated with Ti atoms in tetrahedral

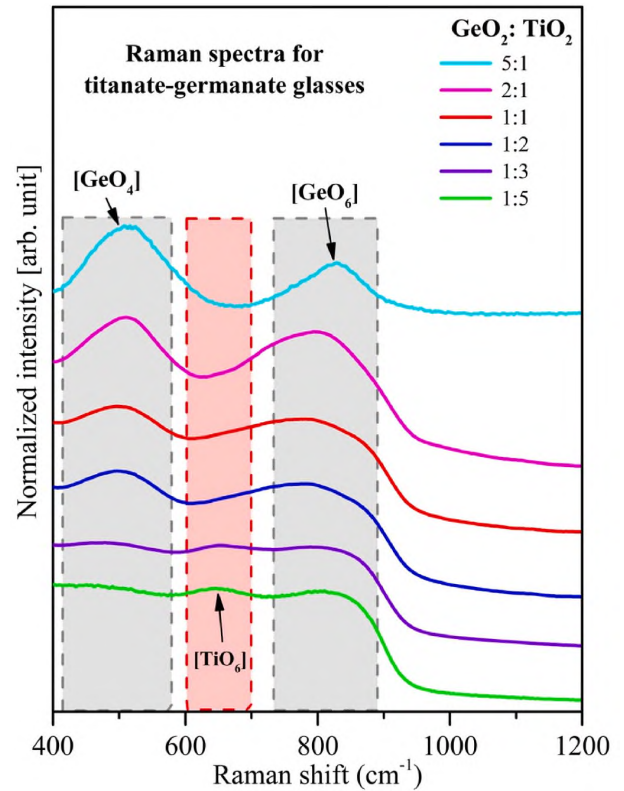


Fig. 7. Normalized Raman spectra of titanate-germanate glass host in function of TiO_2 content.

coordination. In our experiment, where the molar ratio $\text{GeO}_2:\text{TiO}_2$ was changed, we may speculate that indicated differences in intensity of the band at 650 cm^{-1} located in between the low- and high-frequency region of the Raman spectra are strictly associated with the dual role of TiO_2 in glass network depending on its concentration. This comparatively inconspicuous band seems to be increasing with gradual titanium dioxide addition. When TiO_2 acts as a network former, it promotes a more polymerized structure and increases the glass stability with respect to devitrification. Further, Kamitsos et al. [84] verified similar effects for rubidium germanate glasses, where the additional band located near 650 cm^{-1} was quite well observed. While the precise structural role of TiO_2 in inorganic glasses is still under debate, the herein-advocated structural role of the TiO_6 unit supports the suggestions of [85] of the dominance of stretching vibration of Ti-O in the TiO_6 unit. Similar effects were observed for early investigations of $\text{Na}_2\text{O-TiO}_2\text{-P}_2\text{O}_5$ [86], $\text{TiO}_2\text{-P}_2\text{O}_5\text{-CaO}$ [87], and $\text{TiO}_2\text{-P}_2\text{O}_5$ [88] glasses. Therefore, based on the performed Raman measurements, we could suppose that in samples containing $\text{TiO}_2 > 30\text{ M\%}$, where TiO_2 is a network former, the TiO_6 unit is present, and hence, these systems exhibited enhanced near-infrared luminescence properties.

Additionally, thulium-doped glasses, due to several near-infrared emission transitions, are interesting from the spectroscopic and application points of view. Our systematic investigations confirmed that Tm^{3+} -doped barium gallo-germanate glasses modified by TiO_2 can be successfully used for near-IR laser applications at 1.8 μm (this work) and 1.45 μm [39]. However, laser sources emitting at mid-infrared ($>2.1\text{ }\mu\text{m}$) range have gained interest in recent years due to their applications in atmosphere gas sensing, combustion studies, pollutant detection, and non-invasive glucose blood measurement. In this field, most published papers are related to the mid-infrared luminescence corresponding to the ${}^3\text{H}_4 \rightarrow {}^3\text{H}_5$ (at 2.3 μm) transition of Tm^{3+} in crystals [89–96].

Another strategy proposed in the literature to observe the luminescence of Tm^{3+} ions at 2.3 μm consists of using glasses characterized by low phonon energies, wide transmission window, and high solubility for rare earth ions. In 1988, L. Esterowitz et al. [97] reported for the first time laser emission for Tm^{3+} -doped $\text{ZrF}_4\text{-BaF}_2\text{-LaF}_3\text{-AlF}_3\text{-NaF}$ system which to this day is used commercially available Tm: ZBLAN fiber. Interestingly, the spectroscopic behavior of Tm^{3+} ions as 2.3 μm laser source in amorphous materials characterized and described in the current literature is limited to fluoride glasses [98–100]. Moreover, our preliminary study confirmed that titanate-germanate glasses modified by BaF_2 [101] with extremely low IR absorption coefficients represent a good starting point for further investigations focused on the mid-infrared band of thulium ions. We assume that the improved spectroscopic and laser parameters for Tm^{3+} ions for multicomponent titanate-germanate glasses with relatively higher TiO_2 content may be promising for mid-infrared emission associated with ${}^3\text{H}_4 \rightarrow {}^3\text{H}_5$ transition of thulium ions at 2.3 μm . These aspects will be examined in the future.

4. Conclusions

In this paper, Tm^{3+} -doped glasses based on $\text{GeO}_2\text{-BaO-Ga}_2\text{O}_3$ (GBG) and $\text{TiO}_2\text{-GeO}_2\text{-BaO-Ga}_2\text{O}_3$ (TGBG) have been synthesized. We have experimentally confirmed that the optical (absorption and near-IR luminescence) and structural properties of trivalent thulium ions in barium gallo-germanate glass, one of the representative low phonon glasses, are modified dramatically upon the introduction of titanium dioxide. We assumed that titanium dioxide in fabricated materials plays the role of glass-modifier ($\text{TiO}_2 < 30 \text{ mol}\%$) or glass-former ($\text{TiO}_2 > 30 \text{ mol}\%$). Some of the key findings are:

With increasing TiO_2 concentration in barium gallo-germanate glasses, the degree of covalency of the $\text{Tm}^{3+}\text{-O}$ bond increases, which was confirmed by the position of hypersensitive ${}^3\text{H}_6 \rightarrow {}^3\text{F}_4$ transition. Then, systematic investigations using near-infrared luminescence spectroscopy indicate that emission intensity for the main laser transition of Tm^{3+} ions was completely different for the barium gallo-germanate glasses containing relatively high concentrations of TiO_2 . Importantly, the integrated emission intensity assigned to ${}^3\text{F}_4 \rightarrow {}^3\text{H}_6$ transition at 1.8 μm was enhanced significantly (4.8-fold increase) compared to GBG glass without TiO_2 . Moreover, high values of luminescence bandwidth $\text{FWHM} = 253 \text{ nm}$ required to generate laser action was obtained for TiO_2 -rich GBG systems. Introducing TiO_2 increases the radiative transition, which is required to achieve the lasing condition for the enhanced near-IR channel of Tm^{3+} ions. The quantum efficiencies for the ${}^3\text{F}_4$ state of Tm^{3+} ions were the highest (η above 70 %) for glass systems with molar ratios $\text{GeO}_2:\text{TiO}_2 = 1:1, 1:2, \text{ and } 1:3$, respectively. For all studied glass samples, the critical transfer distance R_0 was reduced with increasing Tm^{3+} ions concentration. Based on the analysis using the Inokuti-Hirayama model, we observed that the self-quenching of near-infrared luminescence is reduced with increasing TiO_2 concentration in glass samples containing higher Tm^{3+} content. Further analysis of the Raman spectra confirmed that for higher TiO_2 contents ($\text{TiO}_2 > 30 \text{ mol}\%$), where TiO_2 plays a network-former role, a significant fraction of the Ti speciation involves TiO_6 unit.

Experimentally proven that when concentration of TiO_2 added to the glass a great change in the glass network occurs which induces measurable effects in the optical properties of the glasses. The study's findings are important in glass technology, materials engineering, and modern photonics. We suggest that Tm^{3+} -doped titanate-germanate (TGBG) glasses containing 30mol% TiO_2 ($\text{GeO}_2:\text{TiO}_2 = 1:1$), 40mol% TiO_2 ($\text{GeO}_2:\text{TiO}_2 = 1:2$), and 45 mol% TiO_2 ($\text{GeO}_2:\text{TiO}_2 = 1:3$) are suitable for luminescence at 1.8 μm . Based on these considerations, we believe that this study might provide useful information for the further development of oxide glassy systems based on $\text{TiO}_2\text{-GeO}_2\text{-BaO-Ga}_2\text{O}_3$ in both rare-earth optimization and composition modifications, giving an essential contribution to the development of modern near-infrared photonics applications. Thus, future research will be devoted to Tm^{3+} -

doped titanate-germanate glasses operating at mid-infrared range at 2.3 μm (${}^3\text{H}_4 \rightarrow {}^3\text{H}_5$) due to their broad range of potential applications such as optical metrology or non-invasive glucose blood measurement.

CRedit authorship contribution statement

Karolina Kowalska: Writing – original draft, Visualization, Software, Methodology, Investigation, Formal analysis, Data curation, Conceptualization. **Marta Kuwik:** Investigation. **Joanna Pisarska:** Conceptualization. **Wojciech A. Pisarski:** Writing – review & editing, Visualization, Project administration, Methodology, Investigation, Funding acquisition, Formal analysis, Conceptualization.

Declaration of competing interest

The authors declare that they have no known competing financial interests or personal relationships that could have appeared to influence the work reported in this paper.

Data availability

Data will be made available on request.

Acknowledgment

This work was supported by the National Science Centre (Poland) [2018/31/B/ST8/00166].

References

- [1] P. Miller, A. E. Rutgers University, 1991. Ph.D. thesis.
- [2] P.L. Higy, I.D. Aggarwal, Properties of barium gallium germanate glasses, *J. Non-Cryst. Solids* 163 (1993) 303–308, [https://doi.org/10.1016/0022-3093\(93\)91308-P](https://doi.org/10.1016/0022-3093(93)91308-P).
- [3] W.A. Pisarski, K. Kowalska, M. Kuwik, J. Polak, E. Pietrasik, T. Goryczka, J. Pisarska, Novel multicomponent titanate-germanate glasses: synthesis, structure, properties, transition metal, and rare-earth doping, *Materials* 13 (2020) 4422, <https://doi.org/10.3390/ma13194422>.
- [4] W.A. Pisarski, K. Kowalska, M. Kuwik, J. Pisarska, J. Dorosz, J. Żmojda, M. Kochanowicz, D. Dorosz, Nd^{3+} doped titanate-germanate glasses for near-IR laser applications, *Opt Express* 12 (2022) 2912–2926, <https://doi.org/10.1364/OME.463478>.
- [5] K. Kowalska, M. Kuwik, J. Pisarska, M. Leśniak, D. Dorosz, M. Kochanowicz, J. Żmojda, J. Dorosz, W.A. Pisarski, Influence of TiO_2 concentration on near-infrared luminescence of Er^{3+} ions in barium gallo-germanate glasses, *J. Mater. Res. Technol.* 21 (2022) 4761–4772, <https://doi.org/10.1016/j.jmrt.2022.11.081>.
- [6] J. Pisarska, K. Kowalska, M. Kuwik, J. Dorosz, M. Kochanowicz, J. Żmojda, D. Dorosz, W.A. Pisarski, Optical properties of titanate-germanate glasses containing Ho^{3+} ions, *Mater. Res. Bull.* 166 (2023) 112353, <https://doi.org/10.1016/j.materresbull.2023.112353>.
- [7] E.R. López, M. Morales-Luna, M.V. González, R. Aruna-Devi, F. de Moure-Flores, S.A.M. Hernández, J.S. Cruz, Bandgap modification of titanium dioxide doped with rare earth ions for luminescent processes, *J. Appl. Phys.* 128 (2020) 175106, <https://doi.org/10.1063/5.0021616>.
- [8] R. Lachheb, K. Damak, A.A. Assadi, A. Herrmann, E. Yousef, C. Rüsel, R. Maalej, Characterization of Tm^{3+} doped TNZL glass laser material, *J. Lumin.* 161 (2015) 281–287, <https://doi.org/10.1016/j.jlumin.2014.12.069>.
- [9] Y. Chu, Y. Yang, Y. Liu, S. Wang, C. Shi, D. Zhang, H. Li, J. Peng, N. Dai, J. Li, L. Yang, 1.8 μm fluorescence characteristics of Tm^{3+} doped silica glasses and fiber prepared by the glass phase-separation technology, *J. Non-Cryst. Solids* 529 (2020) 119704, <https://doi.org/10.1016/j.jnoncrysol.2019.119704>.
- [10] G.S. Shakurov, R.B. Zaripov, V.V. Badikov, D.V. Badikov, Wide-band EPR spectroscopy and relaxation study of Tm^{3+} ions in PbGa_2S_4 crystal, *Opt. Mater.* 121 (2021) 111555, <https://doi.org/10.1016/j.optmat.2021.111555>.
- [11] D. Kasprówicz, P. Gluchowski, M.G. Brik, M.M. Makowski, M. Chrunik, A. Majchrowski, Visible and near-infrared up-conversion luminescence of $\text{KGD}(\text{WO}_4)_2$ micro-crystals doped with Er^{3+} , Tm^{3+} , Ho^{3+} and Yb^{3+} ions, *J. All. Compd.* 684 (2016) 271–281, <https://doi.org/10.1016/j.jallcom.2016.05.136>.
- [12] A.V. Malakhovskii, I.S. Edelman, A.E. Sokolov, V.L. Temerov, S.L. Gnatchenko, I. S. Kachur, V.G. Piryatinskaya, Optical absorption spectrum and local symmetry of Tm^{3+} ion in $\text{TmAl}_3(\text{BO}_3)_4$ crystal, *Phys. Lett.* 371 (2007) 254–258, <https://doi.org/10.1016/j.physleta.2007.06.025>.
- [13] D. Wang, Y. Guo, Q. Wang, Z. Chang, J. Liu, J. Luo, Judd-Ofelt analysis of spectroscopic properties of Tm^{3+} ions in K_2YF_5 crystal, *J. Alloys Compd.* 474 (2009) 23–25, <https://doi.org/10.1016/j.jallcom.2008.06.075>.

- [14] M. Mattarelli, V.K. Tikhomirov, A.B. Seddon, M. Montagna, E. Moser, A. Chiasera, S. Chaussedent, G. Nunzi Conti, S. Pelli, G.C. Righini, L. Zampedi, M. Ferrari, Tm³⁺-activated transparent oxy-fluoride glass-ceramics: structural and spectroscopic properties, *J. Non-Cryst. Solids* 345–346 (2004) 354–358, <https://doi.org/10.1016/j.jnoncrysol.2004.08.043>.
- [15] T. Satyanarayana, I.V. Kityk, M.G. Brik, V. Ravi Kumar, N. Veeraiyah, Fluorescence features of Tm³⁺ ions in PbO-Sb₂O₃-B₂O₃ glass ceramics, *Phys. B Condens. Matter* 405 (2010) 1872–1880, <https://doi.org/10.1016/j.physb.2010.01.066>.
- [16] W.J. Zhang, J.P. Zhang, Z. Wang, W.C. Wang, Q.Y. Zhang, Spectroscopic and structural characterization of transparent fluorogermanate glass ceramics with LaF₃:Tm³⁺ nanocrystals for optical amplifications, *J. Alloys Compd.* 634 (2015) 122–129, <https://doi.org/10.1016/j.jallcom.2015.01.313>.
- [17] U.R. Rodríguez-Mendoza, F. Lahoz, NIR upconversion emission of Tm³⁺ doped glassceramics for solar cells applications, *J. Lumin.* 179 (2016) 40–43, <https://doi.org/10.1016/j.jlumin.2016.06.052>.
- [18] M.S. Al-Assiri, H. Algarni, M. Reben, E. Yousef, H.H. Hegazy, Y.M. AbouDeif, Ahmad Umar, UV-Vis-NIR and luminescent characterization of PZC:O:Tm laser oxide glasses, *Opt. Mater.* 73 (2017) 284–289, <https://doi.org/10.1016/j.optmat.2017.08.030>.
- [19] K. Damak, R. Maalej, E.S. Yousef, A.H. Qusti, Ch Rüssel, Thermal and spectroscopic properties of Tm³⁺ doped TZPPN transparent glass laser material, *J. Non-Cryst. Solids* 358 (2012) 2974–2980, <https://doi.org/10.1016/j.jnoncrysol.2012.07.027>.
- [20] X. Shen, Y. Zhang, L. Xia, J. Li, G. Yang, Y. Zhou, Broadband flat near-infrared emission from tellurite glass doped with Tm³⁺, Er³⁺ and Ag NPs, *Opt. Laser Technol.* 129 (2020) 106264, <https://doi.org/10.1016/j.optlastec.2020.106264>.
- [21] K. Mariselvam, J. Liu, Concentration effect of Tm³⁺ ions doped B₂O₃-Li₂CO₃-BaCO₃-CaF₂-ZnO glasses: blue laser and radiation shielding investigations, *Opt. Laser Technol.* 154 (2022) 108262, <https://doi.org/10.1016/j.optlastec.2022.108262>.
- [22] Karolina Milewska, Michał Maciejewski, Marcin Łapiński, Anna Synak, Mirosław Behrendt, Wojciech Sadowski, Barbara Kocińska, Structural and luminescence properties of B₂O₃-Bi₂O₃-AlF₃ glass doped with Eu³⁺, Tb³⁺ and Tm³⁺ ions, *J. Non-Cryst. Solids* 605 (2023) 122169, <https://doi.org/10.1016/j.jnoncrysol.2023.122169>.
- [23] Y. Cheng, Z. Wu, X. Hu, T. Wu, W. Zhou, Thermal stability and optical properties of a novel Tm³⁺ doped fluorotellurite glass, *J. Rare Earths* 32 (2014) 1154–1161, [https://doi.org/10.1016/S1002-0721\(14\)60197-6](https://doi.org/10.1016/S1002-0721(14)60197-6).
- [24] S. Cenik, B. Demirata, M.L. Öveçoglu, G. Özen, Thermal properties and optical transition probabilities of Tm³⁺ doped TeO₂-WO₃ glass, *Spect-Chim. Acta* 57 (2001) 2367–2372, [https://doi.org/10.1016/S1386-1425\(01\)00444-9](https://doi.org/10.1016/S1386-1425(01)00444-9).
- [25] Ch Zhang, K. Han, D. Zhou, Ch Song, P. Xu, T. Wu, Ch Huang, S. Qiang, Q. Wu, High concentration Tm³⁺ doped TeO₂-Al₂O₃-BaF₂ glass for ~2 μm fiber lasers, *J. Alloys Compd.* 901 (2022) 163592, <https://doi.org/10.1016/j.jallcom.2021.163592>.
- [26] S. Nishimura, S. Fuchi, Y. Takeda, Luminescence properties of Tm₂O₃-doped oxide glasses for NIR wideband light source, *J. Mater. Sci. Mater. Electron.* 28 (2017) 7157–7162, <https://doi.org/10.1007/s10854-017-6699-7>.
- [27] A.S. Yasukevich, G.E. Rachkovskaya, G.B. Zakharevich, E.E. Trusova, A. A. Kornienko, E.B. Dunina, V.E. Kisel, N.V. Kuleshov, Spectral-luminescence properties of oxyfluoride lead-silicate-germanate glass doped with Tm³⁺ ions, *J. Lumin.* 229 (2021) 117667, <https://doi.org/10.1016/j.jlumin.2020.117667>.
- [28] J. Cao, P. Xu, C. Song, D. Zhou, Y. Wu, Y. Bai, Y. Cong, Realization of broadband ~1.8 μm luminescence by level population inversion in Tm³⁺ doped tellurite glass for laser applications, *J. Non-Cryst. Solids* 617 (2023) 122445, <https://doi.org/10.1016/j.jnoncrysol.2023.122445>.
- [29] M. Kuwik, C.K. Jayasankar, W.A. Pisarski, J. Pisarska, Theoretical calculations and experimental investigations of lead phosphate glasses singly doped with Pr³⁺ and Tm³⁺ ions using luminescence spectroscopy, *J. All. Compd.* 842 (2020) 155801, <https://doi.org/10.1016/j.jallcom.2020.155801>.
- [30] G. Lakshminarayana, A.N. Meza-Rocha, O. Soriano-Romero, U. Caldiño, A. Lira, Dong-Eun Lee, J. Yoon, T. Park, Optical and visible and near-infrared fluorescence aspects of Er³⁺, Tm³⁺, and Nd³⁺-doped B₂O₃-rich glasses for fiber amplifiers and NIR lasers, *J. Mater. Res. Technol.* 18 (2022) 658–680, <https://doi.org/10.1016/j.jmrt.2022.02.115>.
- [31] G. Lakshminarayana, U. Caldiño, A.N. Meza-Rocha, A. Lira, P. Venkateswara Rao, V. Singh, A. Dahshan, I.V. Kityk, Dong-Eun Lee, J. Yoon, T. Park, Fluorescence features of Tm³⁺-doped multicomponent borosilicate and borotellurite glasses for blue laser and S-band optical amplifier applications, *Opt. Mater.* 96 (2019) 109354, <https://doi.org/10.1016/j.optmat.2019.109354>.
- [32] B. So, J. She, Y. Ding, J. Miyake, T. Atsumi, K. Tanaka, L. Wondraczek, Magnetic properties and photoluminescence of thulium-doped calcium aluminosilicate glasses, *Opt. Mater. Express* 9 (2019) 4348–4359, <https://doi.org/10.1364/OME.9.004348>.
- [33] X. Song, K. Han, D. Zhou, P. Xu, P. Zhang, Broadband ~1.8 μm emission characteristics of Tm³⁺-doped bismuthgermanate glass based on Ga₂O₃ modification, *J. Non-Cryst. Solids* 557 (2021) 120575, <https://doi.org/10.1016/j.jnoncrysol.2020.120575>.
- [34] T. Guérineau, S. Aouji, S. Morency, F. Calzavara, P. Laroche, J. Lapointe, S. Danto, T. Cardinal, E. Fargin, M. Bernier, R. Vallée, Y. Messaddeq, Toward low-loss mid infrared Ga₂O₃-BaO-GeO₂ optical fibers, *Sci. Rep.* 13 (2023) 3697, <https://doi.org/10.1038/s41598-023-30522-1>.
- [35] G. Tang, D. Zhang, F. Zhang, W. Zhao, Q. Qian, Z. Yang, Structure and luminescence properties of Tm³⁺ doped barium gallo-germanate glass tailored by Lu₂O₃, *J. Lumin.* 257 (2023) 119771, <https://doi.org/10.1016/j.jlumin.2023.119771>.
- [36] K. Pavani, L. Rama Moorthy, A. B. Suresh Kumar, A. Mohan Babu, Energy transfer and luminescence properties of Tm³⁺ ions in calcium fluoroborate glasses for fiber amplifiers, *J. Lumin.* 136 (2013) 383–388, <https://doi.org/10.1016/j.jlumin.2012.12.014>.
- [37] M. Taher, H. Gebavi, S. Taccheo, D. Milanese, R. Balda, Novel approach towards cross-relaxation energy transfer calculation applied on highly thulium doped tellurite glasses, *Opt Express* 19 (2011) 6269–26274, <https://doi.org/10.1364/OE.19.026269>.
- [38] K. Pavani, L. Rama Moorthy, J. Suresh Kumar, A. Mohan Babu, Energy transfer and luminescence properties of Tm³⁺ ions in calcium fluoroborate glasses for fiber amplifiers, *J. Lumin.* 136 (2013) 383–388, <https://doi.org/10.1016/j.jlumin.2012.12.014>.
- [39] M. Kuwik, K. Kowalska, J. Pisarska, W.A. Pisarski, Experimental and theoretical studies on NIR luminescence of titanate-germanate glasses doped with Pr³⁺ and Tm³⁺ ions, *J. Am. Ceram. Soc.* 106 (2023) 7460–7472, <https://doi.org/10.1111/jace.19378>.
- [40] C. Zhang, K. Han, D. Zhou, Ch Song, P. Xu, T. Wu, Ch Huang, S. Qiang, Q. Wu, High concentration Tm³⁺ doped TeO₂-Al₂O₃-BaF₂ glass for ~2 μm fiber lasers, *J. Alloys Compd.* 901 (2022) 163592, <https://doi.org/10.1016/j.jallcom.2021.163592>.
- [41] R.F. Falci, T. Guérineau, J.L. Delarosbil, Y. Messaddeq, Spectroscopic properties of gallium-rich germano-gallate glasses doped with Tm³⁺, *J. Lumin.* 249 (2022) 119014, <https://doi.org/10.1016/j.jlumin.2022.119014>.
- [42] S. Nishimura, Y. Nanai, S. Koh, S. Fuchi, Luminescence properties of Tm₂O₃-doped germanate glass phosphors for near-infrared wideband light-source, *J. Mater. Sci. Mater. Electron.* 32 (2021) 14813–14822, <https://doi.org/10.1007/s10854-021-06035-w>.
- [43] R. Xu, L. Xu, L. Hu, J. Zhang, Structural Origin and laser performance of thulium-doped germanate glasses, *J. Phys. Chem. A* 115 (2011) 14163–14167, <https://doi.org/10.1021/jp207574m>.
- [44] S. Gao, X. Fan, X. Liu, M. Liao, L. Hu, Mechanical and ~2 μm emission properties of Tm³⁺-doped GeO₂-TeO₂ (or SiO₂)-PbO-CaO glasses, *Opt. Mater.* 45 (2015) 167–170, <https://doi.org/10.1016/j.optmat.2015.03.028>.
- [45] S. Gao, X. Liu, X. Fan, X. Li, T. Xue, K. Li, M. Liao, L. Hu, 2 μm emission properties and non-radiative processes of Tm³⁺ in germanate glass, *J. Appl. Phys.* 116 (2014) 173108, <https://doi.org/10.1063/1.4900534>.
- [46] H. Cankaya, A.T. Gorgulu, A. Kurt, A. Speghini, M. Bettinelli, A. Sennaroglu, Comparative spectroscopic investigation of Tm³⁺:tellurite glasses for 2-μm lasing applications, *Appl. Sci.* 8 (2018) 333, <https://doi.org/10.3390/app8030333>.
- [47] Y. Ma, X. Wang, L. Zhang, F. Huang, L. Hu, Increased radiative lifetime of Tm³⁺:F₄ →³H₆ transition in oxyfluoride tellurite glasses, *Mater. Res. Bull.* 64 (2015) 262–266, <https://doi.org/10.1016/j.materresbull.2014.12.066>.
- [48] J. Heo, Y.B. Shin, J.N. Jang, Spectroscopic analysis of Tm³⁺ in PbO-Bi₂O₃-Ga₂O₃ glass, *Appl. Opt.* 34 (1995) 4284–4289, <https://doi.org/10.1364/AO.34.004284>.
- [49] J. Yuan, W. Wang, Y. Ye, T. Deng, D. Ou, J. Cheng, S. Yuan, P. Xiao, Effect of BaF₂ Variation of Tm³⁺ spectroscopic properties of Tm doped gallium tellurite glasses for efficient 2.0 μm laser, *Front. Chem.* 8 (2021) 628273, <https://doi.org/10.3389/fchem.2020.628273>.
- [50] X. Wen, G. Tang, Q. Yang, X. Chen, Q. Qian, Q. Zhang, Z. Yang, Highly Tm³⁺ doped germanate glass and its single mode fiber for 2.0 μm laser, *Sci. Rep.* 6 (2016) 20344, <https://doi.org/10.1038/srep20344>.
- [51] K. Han, P. Zhang, S. Wang, Y. Guo, D. Zhou, F. Yu, Optical characterization of Tm³⁺ doped Bi₂O₃-GeO₂-Ga₂O₃ glasses in absence and presence of BaF₂, *Sci. Rep.* 6 (2016) 31207, <https://doi.org/10.1038/srep31207>.
- [52] M. Zikmund, L. Štepnicková, Spectral study of chloro(tetrahydrofuran) titanium (III) complexes, *Chem. Pap. - Chem. Zvesti* 23 (1969) 850–855.
- [53] K. Kowalska, M. Kuwik, J. Pisarska, M. Sitarz, W.A. Pisarski, Raman and infrared spectroscopy of barium-gallo germanate glasses containing B₂O₃/TiO₂, *Materials* 16 (2023) 1516, <https://doi.org/10.3390/ma16041516>.
- [54] B.R. Judd, Hypersensitive transitions in rare-earth ions, *J. Chem. Phys.* 44 (1966) 839–840, <https://doi.org/10.1063/1.1726774>.
- [55] J. Pisarska, W.A. Pisarski, T. Goryczka, R. Lisiecki, W. Ryba-Romanowski, Thermal analysis and near-infrared luminescence of Er³⁺-doped lead phosphate glasses modified by PbF₂, *J. Lumin.* 160 (2015) 57–63.
- [56] Y.C. Ratnakaram, R.P.S. Chakradhar, K.P. Ramesh, J.L. Rao, J. Ramakrishna, Mixed alkali effect in borate glasses-optical absorption studies in Ho³⁺ doped x(Na₂O)·(30-x)(K₂O)·70(B₂O₃) glasses, *J. Math. Sci.* 38 (2003) 833–841.
- [57] J.C.G. Binzli, S.V. Eliseeva, Basics of lanthanide Photophysics, in: P. Hänninen, H. Härmä (Eds.), *Lanthanide Luminescence*, vol. 7, Springer Series on Fluorescence, 2010, https://doi.org/10.1007/4243_2010_3.
- [58] B. So, J. She, Y. Ding, J. Miyake, T. Atsumi, K. Tanaka, L. Wondraczek, Magnetic properties and photoluminescence of thulium-doped calcium aluminosilicate glasses, *Opt. Mater. Express* 9 (2019) 4348–4359, <https://doi.org/10.1364/OME.9.004348>.
- [59] Y.G. Choi, J.H. Song, Spectroscopic properties of Tm³⁺ ions in chalcogenide Ge-As-S glass containing minute amount of Ga and CsBr, *Opt Commun.* 281 (2008) 4358–4362, <https://doi.org/10.1016/j.optcom.2008.04.064>.
- [60] R. Praveena, K.H. Jang, C.K. Jayasankar, H.J. Seo, Optical absorption and fluorescence properties of Tm³⁺-doped K-Mg-Al phosphate glasses for laser applications, *J. Alloys Compd.* 496 (2010) 335–340, <https://doi.org/10.1016/j.jallcom.2010.02.007>.
- [61] Y.S. Han, J.H. Song, J. Heo, Analysis of cross relaxation between Tm³⁺ ions in PbO-Bi₂O₃-Ga₂O₃-GeO₂ glass, *J. Appl. Phys.* 94 (2003) 2817–2820, <https://doi.org/10.1063/1.1595148>.

- [62] M. Inokuti, F. Hirayama, Influence of energy transfer by the exchange mechanism on donor luminescence, *J. Chem. Phys.* 43 (1965) 1978, <https://doi.org/10.1063/1.1697063>.
- [63] G. Tanga, D. Zhanga, F. Zhanga, W. Zhao, Q. Qian, Z. Yang, Structure and luminescence properties of Tm^{3+} -doped barium gallo-germanate glass tailored by Lu_2O_3 , *J. Lumin.* 257 (2023) 119771, <https://doi.org/10.1016/j.jlumin.2023.119771>.
- [64] S.S. Bayya, G.D. Chin, J.S. Sanghera, I.D. Aggarwal, Germanate glass as a window for high energy laser systems, *Opt Express* 14 (2006) 11687–11693, <https://doi.org/10.1364/OE.14.011687>.
- [65] D.E. Zelman, S.S. Bayya, J.S. Sanghera, I.D. Aggarwal, Dispersion of barium gallogermanate glass, *Appl. Opt.* 41 (2002) 1366–1367, <https://doi.org/10.1364/AO.41.001366>.
- [66] J. Pisarska, M. Soltys, A. Górny, M. Kochanowicz, J. Zmojda, J. Dorosz, D. Dorosz, M. Sitarz, W.A. Pisarski, Rare earth-doped barium gallo-germanate glasses and their near-infrared luminescence properties, *Spectrochim. Acta, Part A* 201 (2018) 362–366, <https://doi.org/10.1016/j.saa.2018.05.027>.
- [67] M. Kochanowicz, J. Zmojda, P. Miluski, T. Ragin, W.A. Pisarski, J. Pisarska, R. Jadach, M. Sitarz, D. Dorosz, Structural and luminescent properties of germanate glasses and double-clad optical fiber co-doped with $\text{Yb}^{3+}/\text{Ho}^{3+}$, *J. All. Compd.* 727 (2017) 1221–1226, <https://doi.org/10.1016/j.jallcom.2017.08.243>.
- [68] M. Emili, L. Incoccia, S. Mobilio, G. Fagherazzi, M. Guglielmi, Structural investigations of $\text{TiO}_2/\text{SiO}_2$ glassy and glass-ceramic materials prepared by the sol-gel method, *J. Non-Cryst. Solids* 74 (1985) 129–146, [https://doi.org/10.1016/0022-3093\(85\)90407-7](https://doi.org/10.1016/0022-3093(85)90407-7).
- [69] S. Karlsson, L.G. Bäck, P. Kidkhunthod, K. Lundstedt, L. Wondraczek, Effect of TiO_2 on optical properties of glasses in the soda-lime-silicate system, *Opt. Mater. Express* 6 (2016) 1198–1216, <https://doi.org/10.1364/OME.6.001198>.
- [70] K. Yoshimoto, A. Masuno, M. Ueda, H. Inoue, H. Yamamoto, T. Kawashima, Low phonon energies and wideband optical windows of $\text{La}_2\text{O}_3\text{-Ga}_2\text{O}_3$ glasses prepared using an aerodynamic levitation technique, *Sci. Rep.* 7 (2017) 45600, <https://doi.org/10.1038/srep45600>.
- [71] A. Sennaroglu, I. Kabalci, A. Kurt, U. Demirbas, G. Ozen, Spectroscopic properties of $\text{Tm}^{3+}:\text{TeO}_2\text{-PbF}_2$ glasses, *J. Lumin.* 116 (2006) 79–86, <https://doi.org/10.1016/j.jlumin.2005.03.006>.
- [72] A. MarzukiRiyatun, M. Larasati, G.T. Singgih, Radiative properties of Tm^{3+} -doped $\text{TeO}_2\text{-ZnO-Na}_2\text{O-TiO}_2$ glasses studied using Judd-Ofelt Theory, *Conf. Ser.: Mater. Sci. Eng.* 675 (2019) 012070, <https://doi.org/10.1088/1757-899X/675/1/012070>.
- [73] G. Lakshminarayana, J. Qiu, M.G. Brik, I.V. Kityk, Photoluminescence of Eu^{3+} , Tb^{3+} , Dy^{3+} , and Tm^{3+} -doped transparent $\text{GeO}_2\text{-TiO}_2\text{-K}_2\text{O}$ glass ceramics, *J. Phys. Condens. Matter* 20 (2008) 335106, <https://doi.org/10.1088/0953-8984/20/33/335106>.
- [74] T. Satyanarayana, I.V. Kityk, K. Ozga, M. Piasecki, P. Bragiel, M.G. Brik, V. Ravi Kumar, A.H. Reshak, N. Veeraiyah, Role of titanium valence states in optical and electronic features of $\text{PbO-Sb}_2\text{O}_3\text{-B}_2\text{O}_3\text{-TiO}_2$ glass alloys, *J. All. Compd.* 482 (2009) 283–297, <https://doi.org/10.1016/j.jallcom.2009.03.185>.
- [75] J. Zmojda, M. Kochanowicz, P. Miluski, M. Leśniak, M. Sitarz, W. Pisarski, J. Pisarska, D. Dorosz, Effect of GeO_2 content on structural and spectroscopic properties of antimony glasses doped with Sm^{3+} ions, *J. Mol. Struct.* 1126 (2016) 207–212, <https://doi.org/10.1016/j.molstruc.2016.02.012>.
- [76] J. Alvarado-Rivera, D.A. Rodríguez-Carvajal, M. del C. Acosta-Enriquez, M. B. Manzanares-Martínez, E. Álvarez, R. Lozada-Morales, G.C. Díaz, A. de Leon, M. E. Zayas, Effect of CeO_2 on the glass structure of Sodium germanate glasses, *J. Am. Ceram. Soc.* 97 (2014) 3494–3500, <https://doi.org/10.1111/jace.13202>.
- [77] T. Furukawa, W.B. White, Raman spectroscopic investigation of the structure and crystallization of binary alkali germanate glasses, *J. Mater. Sci.* 15 (1980) 1648–1662, <https://doi.org/10.1007/BF00550581>.
- [78] O.N. Koroleva, N.M. Korobatoeva, M.V. Shtenberg, T.N. Ivanova, Structure of glasses of the $\text{Li}_2\text{O-K}_2\text{O-GeO}_2$ system: Raman spectroscopic data, *Geochem. Int.* 57 (2019) 331–340, <https://doi.org/10.1134/S0016702919030054>.
- [79] G. Scannell, S. Barra, L. Huang, Structure and properties of $\text{Na}_2\text{O-TiO}_2\text{-SiO}_2$ glasses: role of Na and Ti on modifying the silica network, *J. Non-Cryst. Solids* 448 (2016) 52–61, <https://doi.org/10.1016/j.jnoncrysol.2016.06.028>.
- [80] M. Farouk, Effect of TiO_2 on the structural, thermal and optical properties of $\text{BaO-Li}_2\text{O-diborate}$ glasses, *J. Non-Cryst. Solids* 402 (2014) 74–78, <https://doi.org/10.1016/j.jnoncrysol.2014.05.011>.
- [81] R. Limbach, S. Karlsson, G. Scannell, R. Mathew, M. Edén, L. Wondraczek, The effect of TiO_2 on the structure of $\text{Na}_2\text{O-CaO-SiO}_2$ glasses and its implications for thermal and mechanical properties, *J. Non-Cryst. Solids* 471 (2017) 6–18, <https://doi.org/10.1016/j.jnoncrysol.2017.04.013>.
- [82] B. Reynard, S.L. Webb, High-temperature Raman spectroscopy of $\text{Na}_2\text{TiSi}_2\text{O}_7$ glass and melt: coordination of Ti^{4+} and nature of the configurational changes in the liquid, *Eur. J. Mineral* 10 (1998) 49–58, <https://doi.org/10.1127/ejm/10/1/0049>.
- [83] B. Mysen, D. Neuville, Effect of temperature and TiO_2 content on the structure of $\text{Na}_2\text{Si}_2\text{O}_5\text{-Na}_2\text{Ti}_2\text{O}_5$ melts and glasses, *Geochem. Cosmochim. Acta* 59 (1995) 325–342, [https://doi.org/10.1016/0016-7037\(94\)00290-3](https://doi.org/10.1016/0016-7037(94)00290-3).
- [84] E.I. Kamitsos, Y.D. Yannopoulos, M.A. Karakassides, G.D. Chryssikos, H. Jain, Raman and infrared structural investigation of $\text{xRb}_2\text{O-(1-x)GeO}_2$ glasses, *J. Phys. Chem.* 100 (1996) 11755–11765, <https://doi.org/10.1021/jp960434+>.
- [85] M. Lu, F. Wang, Q. Liao, K. Chen, J. Qin, S. Pan, FTIR spectra and thermal properties of TiO_2 -doped iron phosphate glasses, *J. Mol. Struct.* 1081 (2015) 187–192, <https://doi.org/10.1016/j.molstruc.2014.10.029>.
- [86] S. Krimi, A.El Jazouli, L. Rabardel, M. Couzi, I.L. Mansouri, G. Flem, Glass Formation in the $\text{Na}_2\text{O-TiO}_2\text{-P}_2\text{O}_5$ system, *J. Solid State Chem.* 102 (1993) 400–407, <https://doi.org/10.1006/jssc.1993.1051>.
- [87] A.M.B. Silva, R.N. Correia, J.M.M. Oliveira, M.H.V. Fernandes, Structural characterization of $\text{TiO}_2\text{-P}_2\text{O}_5\text{-CaO}$ glasses by spectroscopy, *J. Eur. Ceram. Soc.* 30 (2010) 1253–1258, <https://doi.org/10.1016/j.jeurceramsoc.2009.11.001>.
- [88] D.A. Magdas, O. Cozar, V. Chis, I. Ardelean, N. Vedeanu, The structural dual role of Fe_2O_3 in some lead-phosphate glasses, *Vib. Spectrosc.* 48 (2008) 251–254, <https://doi.org/10.1016/j.vibspec.2008.02.016>.
- [89] H. Dupont, L. Guillemot, P. Loiko, R. Maria Solé, X. Mateos, M. Aguiló, F. Díaz, A. Braud, P. Camy, P. Georges, F. Druon, Cascade laser optimization for $^3\text{H}_4 \rightarrow ^3\text{H}_5$ and $^3\text{F}_4 \rightarrow ^3\text{H}_6$ sequent transitions in Tm^{3+} -doped materials, *Opt Express* 31 (2023) 34201, <https://doi.org/10.1364/OE.501585>.
- [90] R. Moncorge, Y. Guyot, C. Kränkel, K. Lebbou, A. Yoshikawa, Mid-infrared emission properties of the Tm^{3+} -doped sesquioxide crystals Y_2O_3 , Lu_2O_3 , Sc_2O_3 and mixed compounds $(\text{Y,Lu,Sc})_2\text{O}_3$ around 1.5-, 2- and 2.3- μm , *J. Lumin.* 241 (2022) 118537, <https://doi.org/10.1016/j.jlumin.2021.118537>.
- [91] X. Yu, Z. Pan, H. Chu, H. Pan, S. Zhao, D. Li, Diode-pumped efficient high-power cascade $\text{Tm}:\text{GdVO}_4$ laser simultaneously operating at $\sim 2 \mu\text{m}$ and $\sim 2.3 \mu\text{m}$, *Opt Express* 31 (2023) 26368, <https://doi.org/10.1364/OE.497230>.
- [92] X. Yu, Z. Pan, H. Chu, F. Zha, H. Pan, L. Ma, P. Loiko, P. Camy, D. Li, Cascade lasing at $\sim 2 \mu\text{m}$ and $\sim 2.3 \mu\text{m}$ in a diode-pumped $\text{Tm}:\text{YVO}_4$ laser, *Opt Express* 31 (2023) 13576, <https://doi.org/10.1364/OE.484647>.
- [93] L. Guillemot, P. Loikoa, E. Kiflea, J.L. Doualana, A. Brauda, F. Stareckia, T. Georges, J. Rouvillainb, A. Hideurc, P. Camya, Watt-level mid-infrared continuous-wave $\text{Tm}:\text{YAG}$ laser operating on the $^3\text{H}_4 \rightarrow ^3\text{H}_5$ transition, *Opt Express* 101 (2020) 109745, <https://doi.org/10.1016/j.optmat.2020.109745>.
- [94] P. Loiko, E. Kifle, L. Guillemot, J.L. Doualan, F. Starecki, A. Braud, M. Aguiló, F. Diaz, V. Petrov, X. Mateos, P. Camy, Highly efficient 2.3 μm thulium lasers based on a high-phonon-energy crystal: Evidence of vibronic-assisted emissions, *J. Opt. Soc. Am. B* 38 (2021) 482, <https://doi.org/10.1364/JOSAB.411075>.
- [95] L. Guillemot, P. Loiko, R. Soular, A. Braud, J.L. Doualan, A. Hideur, P. Camy, Close look on cubic $\text{Tm}:\text{KY}_3\text{F}_{10}$ crystal for highly efficient lasing on the $^3\text{H}_4 \rightarrow ^3\text{H}_5$ transition, *Opt Express* 28 (2020) 3451–3463, <https://doi.org/10.1364/OE.382650>.
- [96] H. Dupont, P. Loiko, A. Tyazhev, L. Giordano, Z. Pan, H. Chu, D. Li, B. Viana, A. Hideur, L. Guillemot, A. Braud, P. Camy, P. Georges, F. Druon, $\text{Tm}:\text{CALGO}$ lasers at 2.32 μm : cascade lasing and upconversion pumping, *Opt Express* 31 (2023) 18751–18764, <https://doi.org/10.1364/OE.487590>.
- [97] L. Esterowitz, R. Allen, I. Agarwal, Pulsed laser emission at 2.3 μm in a thulium-doped fluorozirconate fibre, *Electron. Lett.* 24 (1988) 1104, <https://doi.org/10.1049/el:19880749>.
- [98] J. Wang, Z. Jia, Y. Mei, Ch Zhang, F. Wang, Y. Sun, Y. Ohishi, W. Qin, G. Qin, 2.3 μm lasing in Tm^{3+} -doped fluoroaluminate glass fibers with an upconversion pumping scheme, *Opt. Mater. Express* 13 (2023) 64–770, <https://doi.org/10.1364/OME.482684>.
- [99] C. Jia, B.J. Shastri, P.R. Prucnal, M. Saad, L.R. Chen, Simultaneous Q-switching of a $\text{Tm}^{3+}:\text{ZBLAN}$ fiber laser at 1.9 μm and 2.3 μm using graphene, *IEEE Photonics Technol. Lett.* 29 (2017) 405–408.
- [100] X. Li, Y. Xu, L. Yang, Y. Cui, Z. Zhou, M. Wang, Z. Wang, 2.3- μm single-frequency $\text{Tm}:\text{ZBLAN}$ fiber amplifier with output power of 1.41 W, *Opt Express* 31 (2023) 40991–40999, <https://doi.org/10.1364/OE.508003>.
- [101] K. Kowalska, M. Kuwik, J. Pisarska, W.A. Pisarski, Introduction of BaF_2 to titanate-germanate glasses doped with rare-earth ions evidenced by NIR luminescence spectroscopy, *Mater. Lett.* 361 (2024) 136140, <https://doi.org/10.1016/j.matlet.2024.136140>.

P11

Karolina Kowalska, Marta Kuwik, Joanna Pisarska, Wojciech. A. Pisarski,
**Near-IR luminescence of rare-earth ions (Er^{3+} , Pr^{3+} , Ho^{3+} , Tm^{3+})
in titanate-germanate glasses under excitation of Yb^{3+}**

Materials 15 (2022) 3660

Article

Near-IR Luminescence of Rare-Earth Ions (Er^{3+} , Pr^{3+} , Ho^{3+} , Tm^{3+}) in Titanate–Germanate Glasses under Excitation of Yb^{3+}

Karolina Kowalska * , Marta Kuwik , Joanna Pisarska and Wojciech A. Pisarski *

Institute of Chemistry, University of Silesia, Szkolna 9 Street, 40-007 Katowice, Poland; marta.kuwik@us.edu.pl (M.K.); joanna.pisarska@us.edu.pl (J.P.)

* Correspondence: karolina.kowalska@us.edu.pl (K.K.); wojciech.pisarski@us.edu.pl (W.A.P.)

Abstract: Inorganic glasses co-doped with rare-earth ions have a key potential application value in the field of optical communications. In this paper, we have fabricated and then characterized multicomponent TiO_2 -modified germanate glasses co-doped with $\text{Yb}^{3+}/\text{Ln}^{3+}$ ($\text{Ln} = \text{Pr}, \text{Er}, \text{Tm}, \text{Ho}$) with excellent spectroscopic properties. Glass systems were directly excited at 980 nm (the ${}^2\text{F}_{7/2} \rightarrow {}^2\text{F}_{5/2}$ transition of Yb^{3+}). We demonstrated that the introduction of TiO_2 is a promising option to significantly enhance the main near-infrared luminescence bands located at the optical telecommunication window at 1.3 μm ($\text{Pr}^{3+}: {}^1\text{G}_4 \rightarrow {}^3\text{H}_5$), 1.5 μm ($\text{Er}^{3+}: {}^4\text{I}_{13/2} \rightarrow {}^4\text{I}_{15/2}$), 1.8 μm ($\text{Tm}^{3+}: {}^3\text{F}_4 \rightarrow {}^3\text{H}_6$) and 2.0 μm ($\text{Ho}^{3+}: {}^5\text{I}_7 \rightarrow {}^7\text{I}_8$). Based on the lifetime values, the energy transfer efficiencies (η_{ET}) were estimated. The values of η_{ET} are changed from 31% for $\text{Yb}^{3+}/\text{Ho}^{3+}$ glass to nearly 53% for $\text{Yb}^{3+}/\text{Pr}^{3+}$ glass. The investigations show that obtained titanate–germanate glass is an interesting type of special glasses integrating luminescence properties and spectroscopic parameters, which may be a promising candidate for application in laser sources emitting radiation and broadband tunable amplifiers operating in the near-infrared range.

Keywords: germanate glasses; ytterbium ions; energy transfer; luminescence property relationship



Citation: Kowalska, K.; Kuwik, M.; Pisarska, J.; Pisarski, W.A. Near-IR Luminescence of Rare-Earth Ions (Er^{3+} , Pr^{3+} , Ho^{3+} , Tm^{3+}) in Titanate–Germanate Glasses under Excitation of Yb^{3+} . *Materials* **2022**, *15*, 3660. <https://doi.org/10.3390/ma15103660>

Academic Editor: Gerhard Wilde

Received: 30 April 2022

Accepted: 18 May 2022

Published: 20 May 2022

Publisher's Note: MDPI stays neutral with regard to jurisdictional claims in published maps and institutional affiliations.



Copyright: © 2022 by the authors. Licensee MDPI, Basel, Switzerland. This article is an open access article distributed under the terms and conditions of the Creative Commons Attribution (CC BY) license (<https://creativecommons.org/licenses/by/4.0/>).

1. Introduction

Numerous inorganic glass materials are fabricated and widely applied industrially. Novel glass host matrices are still developed and must fulfill the rising demand for good-quality optical components and devices such as active optical fibers, solid-state laser sources, broadband near-IR fiber amplifiers, photonic integrated devices, and so on [1–4]. Systematic studies clearly demonstrate that positions and spectral linewidths for characteristic luminescence bands of lanthanides ions can be tuned according to the chemical compositions of glass and glass-ceramic matrices and dopant ions [5–9]. One of the most perspective options to remedy the drawbacks and improve the photoluminescence properties of lanthanide ions is a modification of the glassy network with suitable additives. In this context, TiO_2 -modified glasses [10,11] have gained much importance due to their interesting properties that make them promising candidates for luminescent sources and optical devices. The beneficial effect of these additives is the improvement of the thermal and chemical stability of glasses [12–14]. It is also assumed that presence of titanium dioxide in matrices with low phonon energy may significantly broaden and enhance the luminescence bands of lanthanides ions.

From the accumulated experience and literature data [15,16], it is known that the trivalent ytterbium ions have been extensively studied for use as efficient emitters of radiation in the infrared range. It should be noted that Yb^{3+} ions with a broad absorption band in the wavelength region of 860–1060 nm and a relatively long fluorescence lifetime (1–2 ms) can be excellent sensitizers to activate other lanthanide ions for luminescence [17,18]. For this reason, co-doping of materials with Yb^{3+} ions allows for the efficient pumping of around 980 nm using a commercially available diode [19,20]. From the experimental approach, it

can be concluded the near-IR radiative transitions of lanthanide ions are greatly dependent on the reduction of matrix phonons to achieve high luminescence efficiency. Indeed, in the past few years, subsequent research on germanate glass remains a perspective option as an oxide glass host matrix for lanthanide ions thanks to its favorable properties, such as smaller multiphonon relaxation probabilities due to relatively low phonon energy ($\sim 800\text{ cm}^{-1}$), high transparency from the visible to the infrared region and presence of non-linear optical effects [21,22]. One should remember that the following lanthanides Ln^{3+} ions such as Pr^{3+} , Er^{3+} , Tm^{3+} , and Ho^{3+} are proposed as co-activators for photoluminescence in $\text{Yb}^{3+}/\text{Ln}^{3+}$ -doubly doped glasses owing to their favorable location of energy levels and the possibility of radiative transitions at the infrared [23]. Among them, Tm^{3+} [24] has gained increasing attention because the near-IR emission associated with the ${}^3\text{F}_4 \rightarrow {}^3\text{H}_6$ transition at 1800 nm is useful as a medical light source. The Er^{3+} ions [25] are widely used in materials for optical applications. Main ${}^4\text{I}_{13/2} \rightarrow {}^4\text{I}_{15/2}$ near-IR transition of Er^{3+} at 1500 nm corresponds to the C + L telecommunication window. Next, Ho^{3+} ions [26] are one of the interesting dopants appropriate for laser sources operated at 2000 nm owing to the ${}^5\text{I}_7 \rightarrow {}^7\text{I}_8$ transition. Although such interesting observations, insufficient attention has been paid to the effects of TiO_2 on near-IR emission properties of low-phonon germanate glasses co-doped with lanthanides. From this point of view, it is interesting to find out how emission bands of selected lanthanide ions located in the near-IR range are changed with different $\text{GeO}_2:\text{TiO}_2$ molar ratios in chemical composition under Yb^{3+} ions excitation.

This paper concerns novel multicomponent titanate–germanate glasses belonging to the low-phonon oxide glass family. Glass samples were successfully synthesized using the conventional high-temperature melting technique. The optical properties of glass series containing two network-formers, TiO_2 and GeO_2 , were characterized using luminescence spectroscopy. In our studies, Yb^{3+} plays an important role, such as a sensitizer to activate selected lanthanide ions. Our attention has been paid to titanate–germanate glass systems co-doped with $\text{Yb}^{3+}/\text{Er}^{3+}$, $\text{Yb}^{3+}/\text{Ho}^{3+}$, $\text{Yb}^{3+}/\text{Tm}^{3+}$, $\text{Yb}^{3+}/\text{Pr}^{3+}$, and their energy transfer process. Near-infrared luminescence spectra and decay curves were examined for samples where GeO_2 was substituted by TiO_2 . In the studied glass systems, molar ratios are changed from $\text{GeO}_2:\text{TiO}_2 = 5:1$ up to $\text{GeO}_2:\text{TiO}_2 = 1:5$. Based on the measured values of luminescence lifetimes, the energy transfer efficiencies $\text{Yb}^{3+} \rightarrow \text{Ln}^{3+}$ ($\text{Ln} = \text{Pr}, \text{Er}, \text{Tm},$ and Ho) were determined for glass samples differing in TiO_2 content. The influence of TiO_2 on structural properties has already been carried out on the previous titanate–germanate glasses published recently [27].

2. Materials and Methods

The investigated TiO_2 -modified germanate glasses co-doped with lanthanides ions with chemical composition (given in mol%): $x\text{TiO}_2-(60-x)\text{GeO}_2-30\text{BaO}-9.5\text{Ga}_2\text{O}_3-0.5\text{Yb}_2\text{O}_3$ and $x\text{TiO}_2-(60-x)\text{GeO}_2-30\text{BaO}-9.4\text{Ga}_2\text{O}_3-0.5\text{Yb}_2\text{O}_3-0.1\text{Ln}_2\text{O}_3$, (where $\text{Ln} = \text{Er}, \text{Tm}, \text{Pr}, \text{Ho}$, and $x = 10, 20, 30, 40, 45, 50$) were obtained by traditional melt quenching technique. In present research, glasses containing various molar ratios $\text{GeO}_2:\text{TiO}_2$ are equal to 5:1, 2:1, 1:1, 1:2, 1:3, and 1:5 and glass codes are as follows: 5Ge-1Ti, 2Ge-1Ti, 1Ge-1Ti, 1Ge-2Ti, 1Ge-3Ti, and 1Ge-5Ti. All of the glass components used during synthesis were of high purity (99.99%) from Aldrich Chemical Co. (St. Louis, MO, USA). Appropriate precursor metal oxides were mixed in an agate mortar. After homogenization of the components, 5 g glass bathes were placed in a platinum crucible (Łukasiewicz Research Network, Institute of Ceramics and Building Materials, Cracow, Poland). In the present procedure, the melting conditions were $T = 1250\text{ }^\circ\text{C}$ for 60 min in an electric furnace. Finally, each glass sample was cooled to room temperature and polished to meet the requirements for optical measurements. A series of transparent glass samples with the dimensions $12\text{ mm} \times 12\text{ mm}$ and thickness $\pm 3\text{ mm}$ was successfully prepared to determine their optical properties. The luminescence measurements of glasses were performed on a Photon Technology International (PTI) Quanta-Master 40 (QM40) UV/VIS Steady State Spectrofluorometer (Photon Technology International, Birmingham, NJ, USA) supplied with a tunable pulsed optical parametric

oscillator (OPO) pumped by the third harmonic of an Nd:YAG laser (Opotek Opolette 355 LD, OPOTEK, Carlsbad, CA, USA). The laser system was coupled with a 75 W xenon lamp, a double 200 mm monochromator, and a Hamamatsu H10330B-75 detector (Hamamatsu, Bridgewater, NJ, USA). The emission spectra were recorded with a spectral resolution of 0.5 nm. Decay curves were recorded by a PTI ASOC-10 (USB-2500) oscilloscope with an accuracy of $\pm 2 \mu\text{s}$ and have been measured under excitation wavelengths 980 nm and monitoring emission wavelength 1030 nm. In order to compare the emission intensity under the same experimental conditions, measurements of glass systems were carried out at the same slit settings. Measurements were performed at room temperature.

3. Results and Discussion

3.1. Optical Absorption Properties

In this study, measurements of the absorption spectra of glass systems 1Ge:1Ti co-doped with $\text{Yb}^{3+}/\text{Ln}^{3+}$ ($\text{Ln} = \text{Er}, \text{Pr}, \text{Tm}, \text{Ho}$) were carried out and presented in Figure 1.

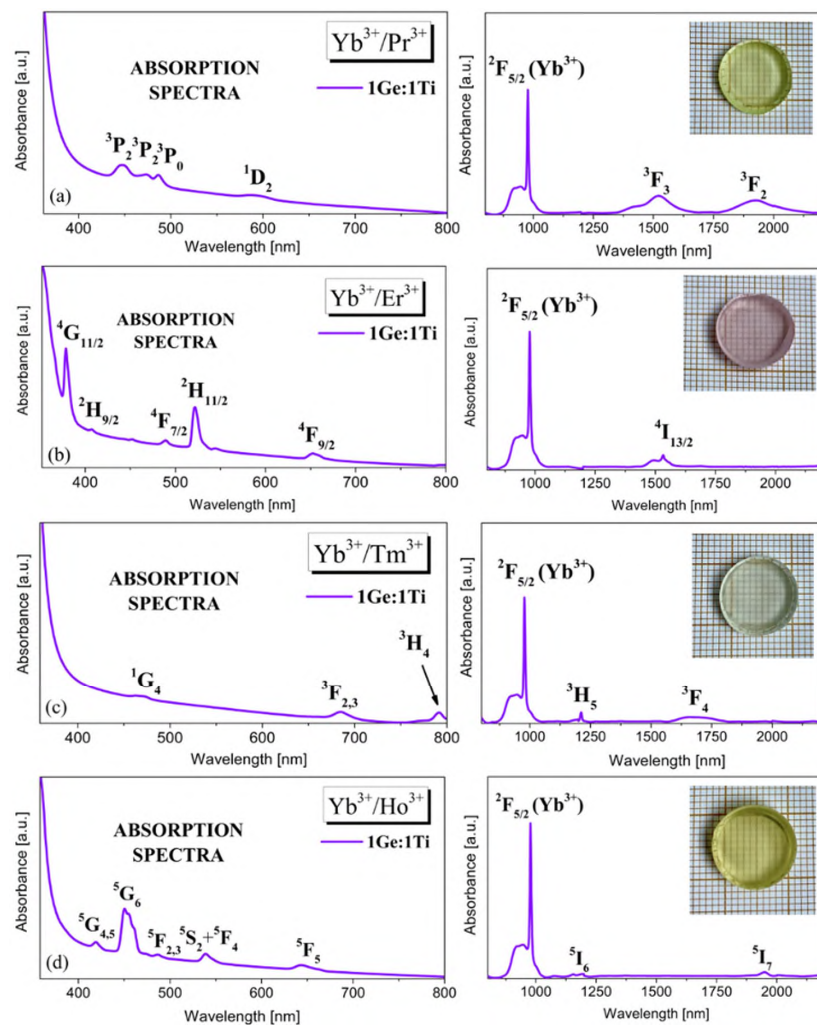


Figure 1. Typical absorption spectra of titanate–germanate glasses co-doped with $\text{Yb}^{3+}/\text{Pr}^{3+}$ (a), $\text{Yb}^{3+}/\text{Er}^{3+}$ (b), $\text{Yb}^{3+}/\text{Tm}^{3+}$ (c) and $\text{Yb}^{3+}/\text{Ho}^{3+}$ (d). Inset shows a photographic image of the glass sample.

Absorption spectra measured for representative titanate–germanate glasses consist of the characteristic bands corresponding to transitions originating from the ground state to

higher-lying excited states of selected lanthanide ions. The glass sample co-doped with $\text{Yb}^{3+}/\text{Pr}^{3+}$ ions (Figure 1a) shows four weakly intense absorption bands in the 350–800 nm range. The two most intense absorption bands due to ${}^3\text{H}_4 \rightarrow {}^3\text{F}_3$ and ${}^3\text{H}_4 \rightarrow {}^3\text{F}_2$ transitions are well observed in the infrared spectral range. Interestingly, literature data indicate that on the band edge, due to ${}^3\text{H}_4 \rightarrow {}^3\text{F}_3$, a weakly separated absorption band at about 1400 nm associated with the ${}^3\text{H}_4 \rightarrow {}^3\text{F}_4$ transition is detected [28]. Next, it is evidently seen for titanium germanium glass co-doped with $\text{Yb}^{3+}/\text{Er}^{3+}$ that the absorption bands (Figure 1b) due to the transition from the ${}^4\text{I}_{15/2}$ state of Er^{3+} are well observed at 380 nm (${}^4\text{G}_{11/2}$), 407 nm (${}^2\text{H}_{9/2}$), 489 nm (${}^4\text{F}_{7/2}$), 522 nm (${}^2\text{H}_{11/2}$), 652 nm (${}^4\text{F}_{9/2}$) and band centered in the near-infrared range at 1530 nm due to ${}^4\text{I}_{15/2} \rightarrow {}^4\text{I}_{13/2}$ transition [29]. Figure 1c shows the absorption spectrum of the $\text{Yb}^{3+}/\text{Tm}^{3+}$ co-doped titanate–germanate sample. The five absorption bands at 471 nm, 685 nm, 790 nm, 1210 nm, and 1690 nm correspond to the transitions from the ground state ${}^3\text{H}_6$ to excited states ${}^1\text{G}_4$, ${}^3\text{F}_2 + {}^3\text{F}_3$, ${}^3\text{H}_4$, ${}^3\text{H}_5$, and ${}^3\text{F}_4$, respectively [30]. In turn, the absorption spectrum measured for $\text{Yb}^{3+}/\text{Ho}^{3+}$ co-doped glass is shown in Figure 1d. The results show that the obtained glass characterizes seven absorption bands in the spectral region of 350–2200 nm. The spectrum exhibits the bands due to the following absorption transitions: ${}^5\text{I}_8 \rightarrow {}^5\text{G}_{4,5}$, ${}^5\text{I}_8 \rightarrow {}^5\text{G}_6$, ${}^5\text{I}_8 \rightarrow {}^5\text{F}_{2,3}$, ${}^5\text{I}_8 \rightarrow {}^2\text{S}_2 + {}^5\text{F}_4$, ${}^5\text{I}_8 \rightarrow {}^5\text{F}_5$ in the visible range and ${}^5\text{I}_8 \rightarrow {}^5\text{I}_6$, ${}^5\text{I}_8 \rightarrow {}^5\text{I}_7$ in the NIR region [31]. For all glass samples, note that the main peak in the absorption spectra was concentrated at 980 nm, defining the lowest Yb^{3+} : ${}^2\text{F}_{5/2}$ Stark splitting energy level is the most intense; therefore, in the following section, the excitation line at 980 nm had been selected to investigate the near-infrared luminescence properties of the fabricated glasses co-doped with $\text{Yb}^{3+}/\text{Pr}^{3+}$, $\text{Yb}^{3+}/\text{Er}^{3+}$, $\text{Yb}^{3+}/\text{Tm}^{3+}$, $\text{Yb}^{3+}/\text{Ho}^{3+}$, where Yb^{3+} plays an important role of emission sensitizer for lanthanides ions.

3.2. Near-Infrared Luminescence Properties

Trivalent ytterbium (Yb^{3+}) has a simple energy-level structure, i.e., the ${}^2\text{F}_{7/2}$ ground level and the ${}^2\text{F}_{5/2}$ excited level, with an energy separation between them of about $10,000 \text{ cm}^{-1}$ [32]. The Yb^{3+} ion has been demonstrated to be an excellent emission sensitizer for other lanthanides due to its effective absorption cross-section at 980 nm [33]. In the presented work, four titanate–germanate glass systems co-doped with $\text{Yb}^{3+}/\text{Pr}^{3+}$, $\text{Yb}^{3+}/\text{Er}^{3+}$, $\text{Yb}^{3+}/\text{Tm}^{3+}$, and $\text{Yb}^{3+}/\text{Ho}^{3+}$ varying with TiO_2 referred to as 5Ge-1Ti, 2Ge-1Ti, 1Ge-1Ti, 1Ge-2Ti, 1Ge-3Ti, and 1Ge-5Ti were selected and their near-IR emission properties under direct excitation of Yb^{3+} at wavelength 980 nm were compared. In addition, the interactions between Yb^{3+} and the second lanthanide ion and their mechanisms are discussed and presented schematically for each glass system on diagrams of the energy levels in order to understand the energy transfer processes. One of the interesting aspects of the ongoing research focusing on the properties of co-doped glasses is the observation of the sensitization of near-IR emission of Pr^{3+} at $1.35 \mu\text{m}$ under excitation Yb^{3+} . Figure 2 presents near-IR luminescence spectra for $\text{Yb}^{3+}/\text{Pr}^{3+}$ co-doped titanate–germanate glasses varying with TiO_2 .

The observed near-IR emission bands at about $1.35 \mu\text{m}$ correspond to ${}^1\text{G}_4 \rightarrow {}^3\text{H}_5$ transition of Pr^{3+} . It should be particularly pointed out that the emission intensities of Pr^{3+} ions increased significantly with increasing TiO_2 concentration from 5Ge-1Ti to 1Ge-5Ti. Hence, it could be suggested that the introduction of titanium dioxide to germanate glass favor near-infrared luminescence attributed to the ${}^1\text{G}_4 \rightarrow {}^3\text{H}_5$ transition of Pr^{3+} under direct excitation of Yb^{3+} . The observed ${}^1\text{G}_4 \rightarrow {}^3\text{H}_5$ transition of Pr^{3+} ions in titanate–germanate glass under excitation of Yb^{3+} is presented on the energy level diagram in Figure 2. It is clearly seen that both excited levels ${}^2\text{F}_{5/2}$ (Yb^{3+}) and ${}^1\text{G}_4$ (Pr^{3+}) lie close to each other and the energy gap between them is very small. Moreover, the absorption cross-section at around 980 nm is larger for Yb^{3+} than Pr^{3+} ions, which is crucial for the pumping efficiency of praseodymium-doped fiber amplifiers PDFA [34,35]. Due to this fact, the energy transfer process $\text{Yb}^{3+} \rightarrow \text{Pr}^{3+}$ is nearly resonant and supposed to be much more efficient in titanate–germanate glass. Thus, we observe near-IR emission at $1.35 \mu\text{m}$ due

to $^1G_4 \rightarrow ^3H_5$ transition of Pr^{3+} , which enhanced rapidly with increasing in TiO_2 content. Based on the above experiment analysis, it can be concluded that Yb^{3+}/Pr^{3+} co-doped germanate glass in the presence of TiO_2 is promising for near-IR emission and sample 1Ge-5Ti seems to be a potential precursor active glass material to realize a fiber laser operating at $1.35 \mu m$ [36,37].

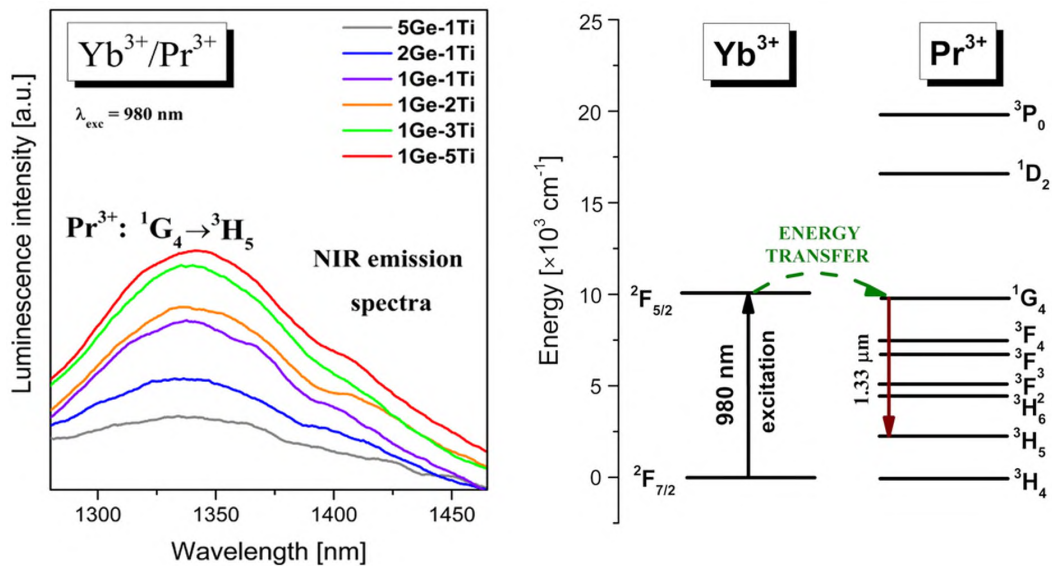


Figure 2. Near-infrared emission spectra and energy level diagram for titanate–germanate glasses co-doped with Yb^{3+}/Pr^{3+} .

From the literature [38–40], it is well known that broadband near-infrared emission bands of Er^{3+} ions in inorganic glasses depend strongly on their chemical compositions. The rapid development of optical telecommunications requires the broadening of the near-IR range for erbium-doped fiber amplifiers (EDFA), in which signal transmission occurs at about 1500 nm . In fact, the EDFA systems based on silicate glasses [41,42] exhibit relatively narrow bandwidth, which contributes to the limited near-infrared broadband transmission. For that reason, many precursor glass systems singly doped with Er^{3+} and co-doped with Yb^{3+}/Er^{3+} are still tested and selected in order to obtain enhanced near-IR luminescence in the so-called third telecommunication window. Figure 3 presents near-IR emission spectra measured in the wavelength range from 1400 nm to 1700 nm for Yb^{3+}/Er^{3+} co-doped titanate–germanate glasses under excitation by a 980 nm line. Near-IR emission bands centered at about $1.53 \mu m$ correspond to the $^4I_{13/2} \rightarrow ^4I_{15/2}$ transition of Er^{3+} .

The intensity of the near-IR emission band at $1.5 \mu m$ is reduced from 5Ge-1Ti to 1Ge-2Ti and then increased with further increasing TiO_2 concentration up to glass sample 1Ge-5Ti. The emission linewidth for the $^4I_{13/2} \rightarrow ^4I_{15/2}$ transition of Er^{3+} ions, referred to as the full width at half maximum, is larger for sample 1Ge-5Ti (FWHM = 55 nm) than 5Ge-1Ti (FWHM = 38 nm). Schematic representation of energy levels, possible energy transfer between Yb^{3+} and Er^{3+} ions and the main near-IR laser transition of Er^{3+} ions at $1.5 \mu m$ are presented in Figure 3. Similar to the Yb^{3+}/Pr^{3+} system, the excitation energy transfers resonantly very fast from the $^2F_{5/2}$ (Yb^{3+}) to the $^4I_{11/2}$ (Er^{3+}) due to a small energy mismatch between the interacting excited levels [43]. The absorption cross-section of Yb^{3+} ions at around 980 nm is higher by a factor of ten roughly than that of Er^{3+} [44], favoring an efficient $Yb^{3+} \rightarrow Er^{3+}$ energy transfer process. Next, the excitation energy relaxes nonradiatively to the $^4I_{13/2}$ state by multiphonon process and consequently, we observe $^4I_{13/2} \rightarrow ^4I_{15/2}$ near-IR transition of Er^{3+} .

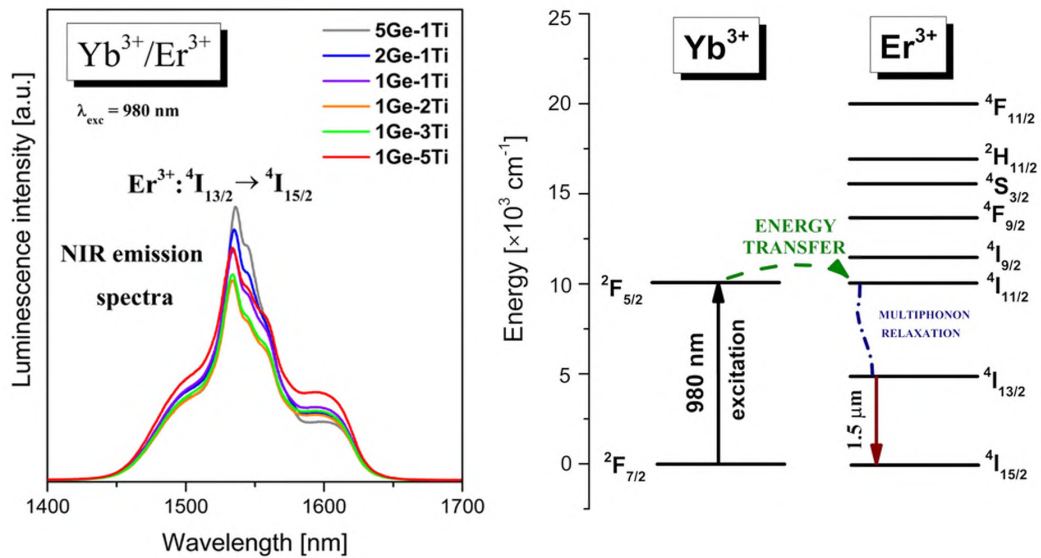


Figure 3. Near-infrared emission spectra and energy level diagram for titanate–germanate glasses co-doped with $\text{Yb}^{3+}/\text{Er}^{3+}$.

Our previous studies [27] indicate that the introduction of TiO_2 to germanate glass resulted in higher asymmetry and better covalent bonds between rare earth and oxygens. In addition, these structural changes led to the site-to-site variation of the crystal field strength in the local environment of rare earths. It resulted in the inhomogeneous broadening of spectral lines corresponding to the presence of various sites for the optically active ions. As a consequence, the profiles of emission spectra and their values of FWHM are dependent on the symmetry, the ligand field strength, and the site-to-site variation of the Ln^{3+} local environment. This is the main reason that the spectral profiles of Er^{3+} , i.e., the emission peak position, emission linewidth (FWHM), and the relative intensities of shoulders existing at about 1600 nm, are changed during the modification of glass matrices. In some cases, the glass modifiers have a minor influence on absorption properties but a strong impact on the emission cross-sections attributed to the ${}^4\text{I}_{13/2} \rightarrow {}^4\text{I}_{15/2}$ near-infrared transition of Er^{3+} ions. Recently, it was well demonstrated for Er^{3+} ions in silicate glass with various Al_2O_3 content [45] and $\text{Er}^{3+}/\text{Yb}^{3+}$ co-doped phosphate glass modified by Y_2O_3 [46].

Thulium is another well-known lanthanide dopant, which is introduced to various glass systems in order to generate near-IR luminescence at about 1.8 μm [47]. In particular, co-doping with Tm^{3+} and Yb^{3+} ions is an excellent way to achieve enhanced near-infrared emission by using a 980 nm wavelength as an excitation source [48]. Figure 4 shows near-IR emission spectra of series titanate–germanate glass samples co-doped with $\text{Yb}^{3+}/\text{Tm}^{3+}$. Near-IR emission bands centered at 1.8 μm are associated with ${}^3\text{F}_4 \rightarrow {}^3\text{H}_6$ transition of Tm^{3+} . The intensities of near-IR emission bands increase and then decrease with increasing TiO_2 concentration in the glass composition. The highest intensity of emission band related to the ${}^3\text{F}_4 \rightarrow {}^3\text{H}_6$ transition of Tm^{3+} was observed for sample 1Ge-1Ti, where the molar ratio GeO_2 to TiO_2 is close 1:1. The energy level diagram for $\text{Yb}^{3+}/\text{Tm}^{3+}$ co-doped titanate–germanate glasses is shown in Figure 4.

In contrast to the $\text{Yb}^{3+}/\text{Er}^{3+}$ system, the energy mismatch between interacting ${}^2\text{F}_{5/2}$ (Yb^{3+}) and ${}^3\text{H}_5$ (Tm^{3+}) excited levels is much higher [49] and thus, non-resonant $\text{Yb}^{3+} \rightarrow \text{Tm}^{3+}$ energy transfer process in titanate–germanate glasses occurs. The excitation energy is transferred nonradiatively by multiphonon relaxation from the ${}^3\text{H}_5$ level to the lower-lying ${}^3\text{H}_4$ level generating near-IR emission at 1.8 μm due to ${}^3\text{F}_4 \rightarrow {}^3\text{H}_6$ transition of Tm^{3+} . Nearly the same mechanism was proposed for $\text{Yb}^{3+}/\text{Ho}^{3+}$ co-doped glass systems, which are also interesting from the optical point of view [50].

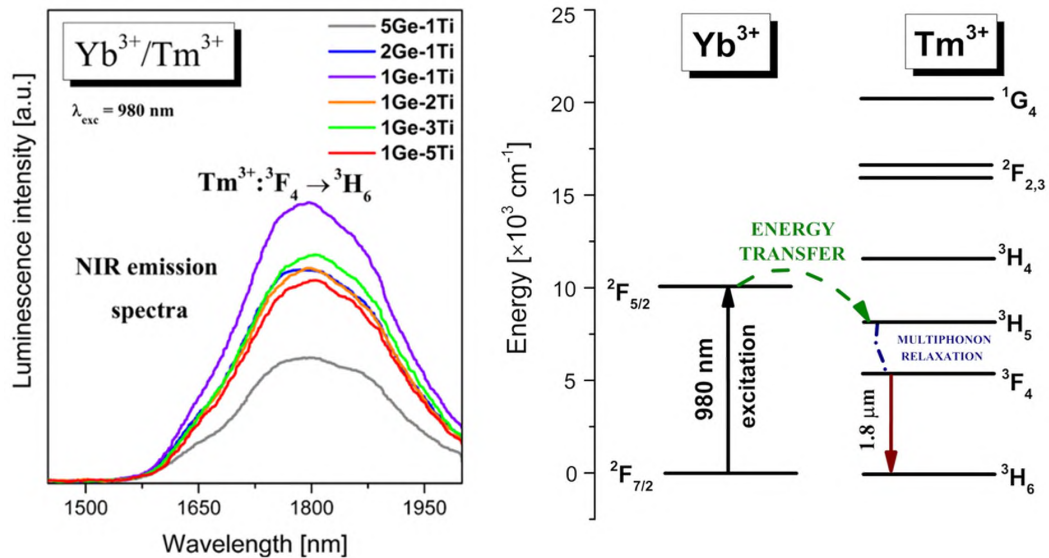


Figure 4. Near-infrared emission spectra and energy level diagram for titanate–germanate glasses co-doped with $\text{Yb}^{3+}/\text{Tm}^{3+}$.

These glass systems present near-IR emission at 2 μm due to the $^5\text{I}_7 \rightarrow ^5\text{I}_8$ transition of Ho^{3+} [51,52]. The energy transfer mechanism has been mentioned in the literature by Wang et al. [53]. Upon excitation wavelength at 980 nm, the excited level of Yb^{3+} is well populated and then the excitation energy is transferred from the $^2\text{F}_{5/2}$ state of Yb^{3+} to the $^5\text{I}_6$ state of Ho^{3+} . The energy transfer process $\text{Yb}^{3+} \rightarrow \text{Ho}^{3+}$ is non-resonant. In the next step, very fast multiphonon relaxation to the lower-lying $^5\text{I}_7$ level of Ho^{3+} is observed and consequently, we can observe near-IR emission at about 2000 nm associated with the $^5\text{I}_7 \rightarrow ^5\text{I}_8$ transition of Ho^{3+} [54,55]. Figure 5 presents near-IR luminescence spectra measured for titanate–germanate glasses co-doped with $\text{Yb}^{3+}/\text{Ho}^{3+}$. The emission bands are more intense for glass samples containing higher concentrations of TiO_2 . All transitions are also indicated in the energy level diagram, which is shown in Figure 5.

In order to achieve intense IR emission of rare-earth ions, the heavy doping of the activators such as Pr^{3+} , Er^{3+} , Ho^{3+} , and Tm^{3+} is usually required. Remarkably interesting results were presented in work by Tu et al. [56], where they successfully developed heavily Tm^{3+} -doped germanate glasses, promising for glass fibers. On the other hand, the concentrations of activators should be optimal and relatively low in order to reduce luminescence quenching. In our case, luminescence quenching in the studied glass samples is negligibly small because of the low concentrations of acceptors (Pr^{3+} , Er^{3+} , Ho^{3+} , Tm^{3+}) and the lack of energy transfer processes between pairs of Pr^{3+} - Pr^{3+} , Er^{3+} - Er^{3+} , Tm^{3+} - Tm^{3+} , and Ho^{3+} - Ho^{3+} ions, respectively. The non-radiative transfer processes become dominant for glass samples with higher Ln^{3+} concentrations. These effects are especially stronger for glass systems with diagrams of excited states favoring the presence of cross-relaxation processes. Thus, the probabilities of these non-radiative relaxation processes increase and the luminescence is quenched due to the increasing interaction among the Ln^{3+} ions at higher concentrations. Our spectroscopic investigations indicate that the relative intensities of emission bands of rare-earth ions in germanate glasses are changed drastically with the presence of TiO_2 . Figure 6 shows the integrated intensities of emission bands related to the main $^1\text{G}_4 \rightarrow ^3\text{H}_5$ (Pr^{3+}), $^4\text{I}_{13/2} \rightarrow ^4\text{I}_{15/2}$ (Er^{3+}), $^3\text{F}_4 \rightarrow ^3\text{H}_6$ (Tm^{3+}) and $^5\text{I}_7 \rightarrow ^5\text{I}_8$ (Ho^{3+}) near-IR transitions of rare-earth ions in the studied glass samples varying with TiO_2 content. For pairs $\text{Yb}^{3+}/\text{Pr}^{3+}$ and $\text{Yb}^{3+}/\text{Ho}^{3+}$, the integrated intensities of near-infrared emission bands located at 1.35 and 2 μm increase with increasing TiO_2 concentration. A completely different situation is observed for pairs of $\text{Yb}^{3+}/\text{Er}^{3+}$ and $\text{Yb}^{3+}/\text{Tm}^{3+}$ ions in titanate–germanate glasses. The integrated intensities of near-infrared emission bands

due to the $^4I_{13/2} \rightarrow ^4I_{15/2}$ transition of Er^{3+} ions are reduced from 5Ge-1Ti to 1Ge-2Ti and then increase with further increasing TiO_2 content. Contrary to $\text{Yb}^{3+}/\text{Er}^{3+}$, the emission intensities of near-infrared bands related to the $^3F_4 \rightarrow ^3H_6$ transition of Tm^{3+} ions are enhanced to the 1Ge-1Ti system and then start to decrease with increasing TiO_2 content in the glass composition; however, the changes in emission intensities with TiO_2 content are non-linear for pair $\text{Yb}^{3+}/\text{Tm}^{3+}$.

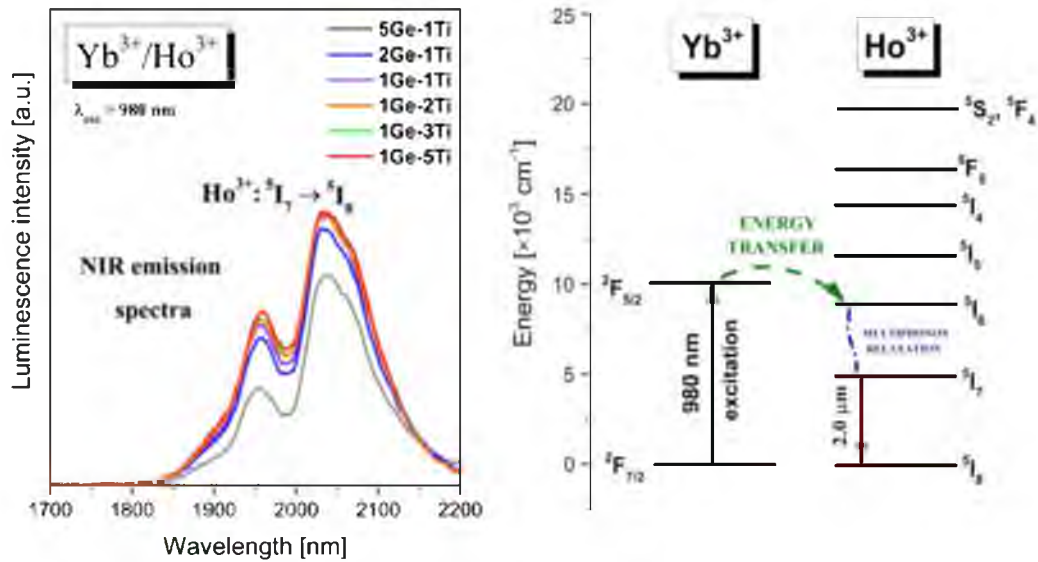


Figure 5. Near-infrared emission spectra and energy level diagram for titanate–germanate glasses co-doped with $\text{Yb}^{3+}/\text{Ho}^{3+}$.

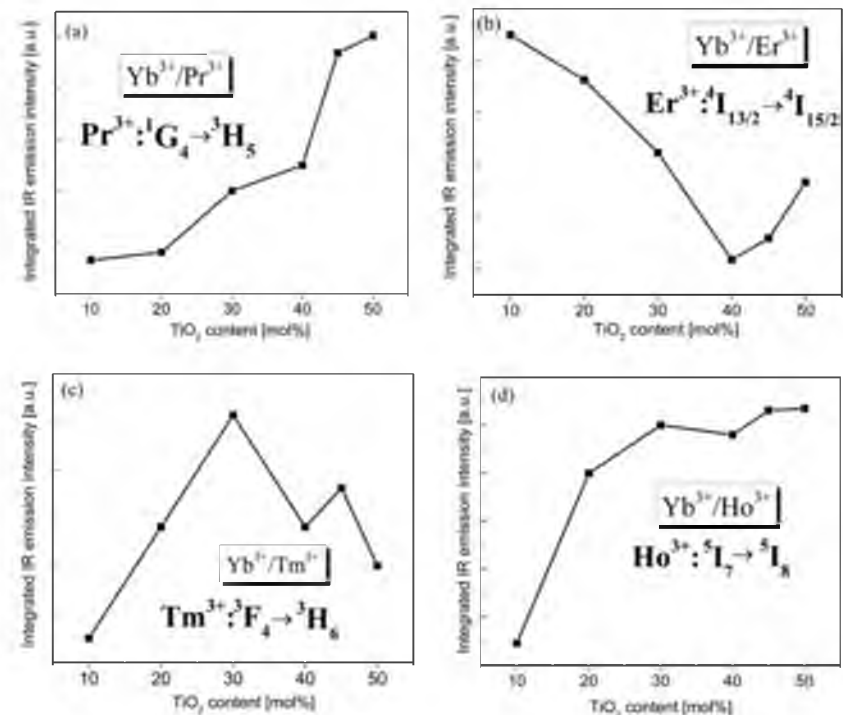


Figure 6. The integrated intensities of emission bands of rare-earth ions $\text{Yb}^{3+}/\text{Pr}^{3+}$ (a), $\text{Yb}^{3+}/\text{Er}^{3+}$ (b), $\text{Yb}^{3+}/\text{Tm}^{3+}$ (c) and $\text{Yb}^{3+}/\text{Ho}^{3+}$ (d) vary with TiO_2 .

To summarize this part of the research, the authors declare that near-IR emission studies will be devoted in the future to further optimization of the TiO₂ content of individual systems containing Yb³⁺/Ln³⁺ (Ln = Pr, Er, Tm, Ho). Obtained results for near-IR emission presented here will contribute to the fabrication of titanate–germanate optical fibers.

3.3. Luminescence Decays and Energy Transfer Efficiencies

The systematic studies indicate that luminescence lifetimes for excited states of Yb³⁺ in several low-phonon glass systems are completely different and depend significantly on the glass network-former and network-modifier added to the base composition [57,58]. To determine the efficiency of the energy transfer process between Yb³⁺ and Ln³⁺ ions (Ln = Pr, Er, Tm, Ho), the luminescence decays for titanate–germanate glasses were measured and analyzed. Figure 7 shows decay curves measured for co-doped samples under 980 nm excitation. Based on decays, luminescence lifetimes were determined and compared to Yb³⁺ singly doped glass samples. The results are given in Table 1.

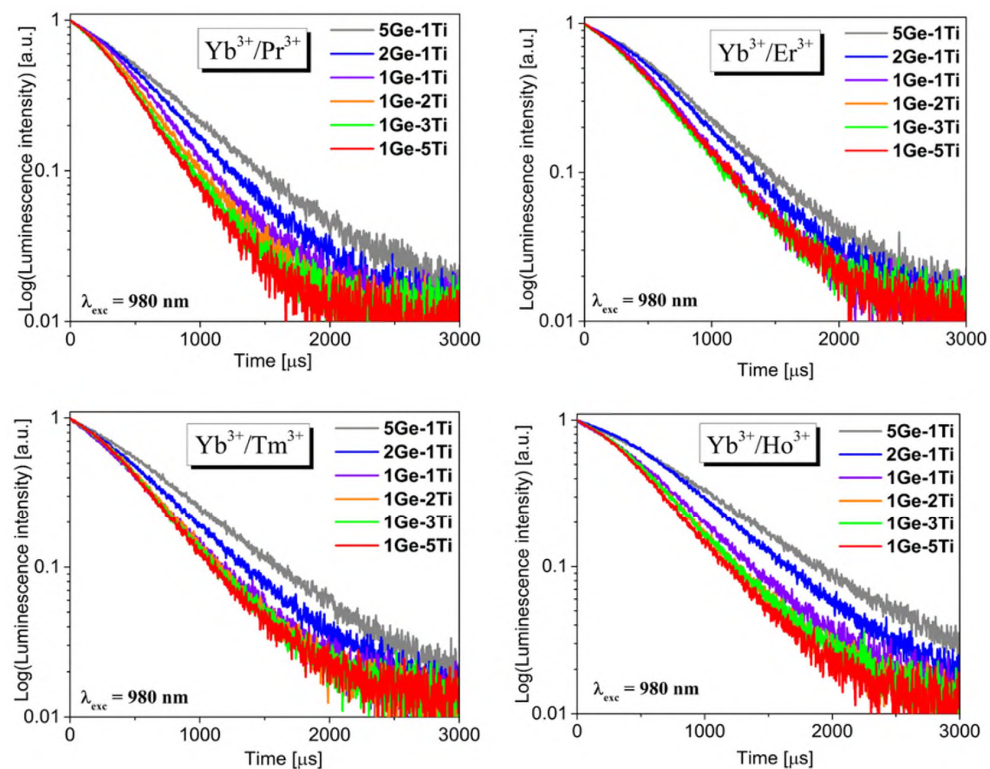


Figure 7. Luminescence decay curves for co-doped titanate–germanate glasses ($\lambda_{exc} = 980$ nm).

Table 1. Measured lifetimes for ⁵F₂ state of Yb³⁺ in single and co-doped titanate–germanate glasses.

TiO ₂ (mol%)	GeO ₂ :TiO ₂	τ_m (ms)				
		Yb ³⁺	Yb ³⁺ /Pr ³⁺	Yb ³⁺ /Er ³⁺	Yb ³⁺ /Tm ³⁺	Yb ³⁺ /Ho ³⁺
10	5:1	1.21	0.63	0.65	0.70	0.83
20	2:1	1.10	0.55	0.59	0.59	0.75
30	1:1	1.00	0.48	0.52	0.51	0.61
40	1:2	1.91	0.44	0.51	0.51	0.56
45	1:3	0.86	0.42	0.50	0.49	0.54
55	1:5	0.84	0.40	0.49	0.48	0.52

In general, measured lifetimes are reduced from 5Ge-1Ti to 1Ge-5Ti with increasing TiO_2 concentration in the glass composition. The experimental values of emission lifetimes decrease from 0.63 ms (5Ge-1Ti) to 0.40 ms (1Ge-5Ti) for $\text{Yb}^{3+}/\text{Pr}^{3+}$ co-doped glass systems, 0.65 ms (5Ge-1Ti) to 0.49 ms (1Ge-5Ti) for $\text{Yb}^{3+}/\text{Er}^{3+}$ systems, 0.70 ms (5Ge-1Ti) to 0.48 ms for $\text{Yb}^{3+}/\text{Tm}^{3+}$ systems, and 0.83 ms (5Ge-1Ti) to 0.52 ms (1Ge-5Ti) for $\text{Yb}^{3+}/\text{Ho}^{3+}$ systems, respectively. Luminescence lifetimes measured for Yb^{3+} singly doped glasses and samples co-doped with $\text{Yb}^{3+}/\text{Ln}^{3+}$ were applied to calculate the energy transfer efficiencies [59]. The energy transfer efficiency η_{ET} between Yb^{3+} and lanthanides ions in fabricated glasses was evaluated by calculations with the formula given below:

$$\eta_{\text{ET}} = 1 - \frac{\tau_{\text{Yb(Ln)}}}{\tau_{\text{Yb}}}$$

where $\tau_{\text{Yb(Ln)}}$ and τ_{Yb} are the measured lifetimes for the ${}^2\text{F}_{5/2}$ level of Yb^{3+} ions in the presence and absence of acceptor Ln (where Ln = Pr, Er, Tm, Ho), respectively. The results are presented schematically in Figure 8.

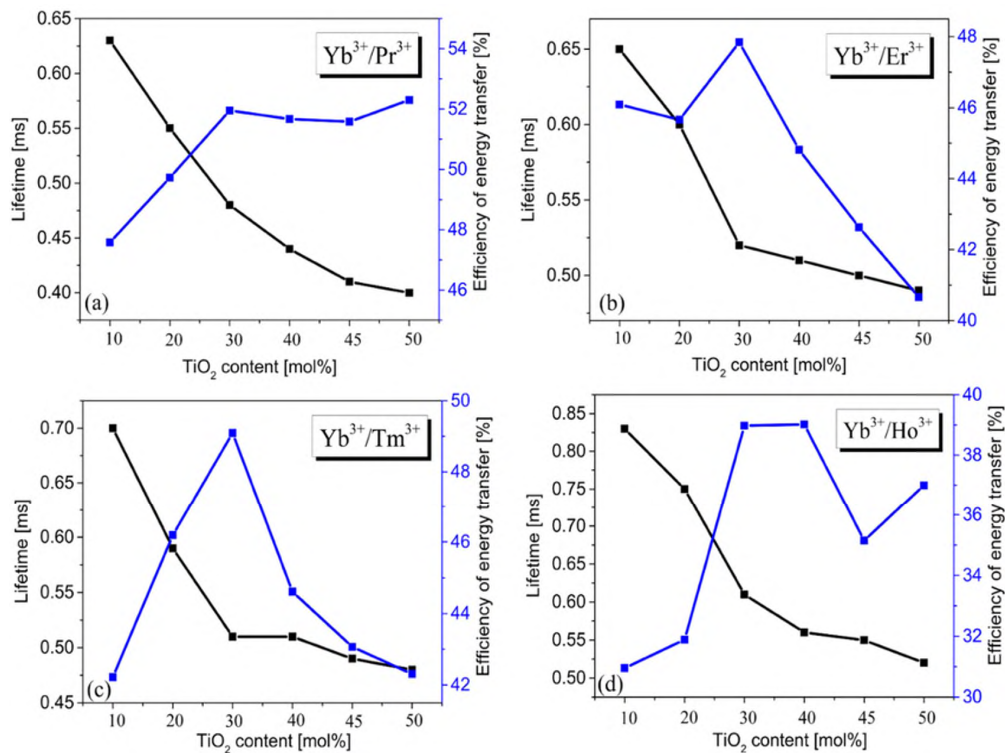


Figure 8. The measured luminescence lifetime and the energy transfer efficiency $\text{Yb}^{3+} \rightarrow \text{Ln}^{3+}$ (where Ln = Pr (a), Er (b), Tm (c), Ho (d)) in the function of TiO_2 content.

Our studies indicate that measured lifetimes decrease with increasing TiO_2 content, while changes in the energy transfer efficiency seems to be completely different. For all pairs of $\text{Yb}^{3+}/\text{Ln}^{3+}$ (Ln = Pr, Er, Tm, Ho), the energy transfer efficiency is the highest for the 1Ge-1Ti system, but the trend of η_{ET} values varying with TiO_2 content is not the same. For the pair of $\text{Yb}^{3+}/\text{Pr}^{3+}$, the values of η_{ET} increase to 1Ge-1Ti, whereas they are nearly independent for glasses with higher TiO_2 content. For pairs $\text{Yb}^{3+}/\text{Er}^{3+}$ and $\text{Yb}^{3+}/\text{Tm}^{3+}$, the energy transfer efficiency increases from 5Ge-1Ti to 1Ge-1Ti and then decreases to 1Ge-5Ti with further increasing TiO_2 concentration. For the pair of $\text{Yb}^{3+}/\text{Ho}^{3+}$, the values of η_{ET} are the highest for 1Ge-1Ti to 1Ge-2Ti glass systems, respectively; however, the changes of η_{ET} with TiO_2 content are non-linear. Our calculations indicate that the energy transfer effi-

ciencies are changed from 31% for Yb³⁺/Ho³⁺ glass (5Ge-1Ti) to nearly 53% for Yb³⁺/Pr³⁺ glass (1Ge-5Ti). At this moment, it should also be mentioned that the up-conversion luminescence pathways [60] make an important contribution to the energy transfer processes and their efficiencies in Yb³⁺/Ln³⁺ (Ln = Pr, Er, Ho, Tm) co-doped glasses.

4. Conclusions

Multicomponent titanate–germanate glasses co-doped with Yb³⁺/Ln³⁺ (Ln = Pr³⁺, Er³⁺, Tm³⁺, Ho³⁺) were synthesized and then studied their near-IR luminescence properties. The spectroscopic properties of glasses have been examined under the excitation of Yb³⁺ ions by 980 nm. Obtained results were discussed based on the energy level diagrams for sensitizer (Yb³⁺) and acceptors (Pr³⁺, Er³⁺, Tm³⁺, Ho³⁺) and interactions between them. The near-IR luminescence bands corresponding to the ¹G₄ → ³H₅ (Pr³⁺), ⁴I_{13/2} → ⁴I_{15/2} (Er³⁺), ³F₄ → ³H₆ (Tm³⁺) and ⁵I₇ → ⁵I₈ transitions of lanthanide ions have been examined with TiO₂ concentration. Our investigations indicate that the intensities of emissions are dependent on titanium dioxide content. The resonant Yb³⁺ → Pr³⁺ and Yb³⁺ → Er³⁺ and non-resonant Yb³⁺ → Tm³⁺ and Yb³⁺ → Ho³⁺ energy transfer process in co-doped titanate–germanate is observed. The analysis of decay profiles allowed for the deeper optical characterization of the energy transfer processes between Yb³⁺ and Ln³⁺ ions (Ln = Pr, Er, Tm, Ho) and for establishing the relation between luminescence lifetimes and the role of titanium dioxide in germanate glasses. Based on decay measurements and values of luminescence lifetimes, the efficiencies of energy transfer were estimated. The values of η_{ET} are changed from 31% for Yb³⁺/Ho³⁺ to nearly 53% for Yb³⁺/Pr³⁺. For all studied pairs Yb³⁺/Ln³⁺, the maximal values of η_{ET} are 53% (Yb³⁺/Pr³⁺), 48% (Yb³⁺/Er³⁺), 49%, (Yb³⁺/Tm³⁺), and 40% (Yb³⁺/Ho³⁺). Further studies revealed that the luminescence lifetimes are reduced with increasing TiO₂ content, whereas the energy transfer efficiencies are changed completely different, depending on pair Yb³⁺/Ln³⁺ (Ln = Pr³⁺, Er³⁺, Tm³⁺, Ho³⁺) in titanate–germanate glass.

Author Contributions: Conceptualization, J.P.; methodology, K.K., J.P. and M.K.; formal analysis, K.K. and W.A.P.; investigation, K.K. and M.K.; writing—original draft preparation, K.K.; writing—review and editing, W.A.P.; visualization, K.K.; project administration, W.A.P.; funding acquisition, W.A.P. All authors have read and agreed to the published version of the manuscript.

Funding: This research was funded by the National Science Centre (Poland), grant number 2018/31/B/ST8/00166.

Institutional Review Board Statement: Not applicable.

Informed Consent Statement: Not applicable.

Data Availability Statement: Not applicable.

Conflicts of Interest: The authors declare no conflict of interest.

References

- Zhang, Y.; Chen, B.; Zhang, X.; Zhang, J.; Xu, S.; Li, X.; Wang, Y.; Cao, Y.; Li, L.; Yu, H.; et al. Net Optical Gain Coefficients of Cu⁺ and Tm³⁺ Single-Doped and Co-Doped Germanate Glasses. *Materials* **2022**, *15*, 2134. [[CrossRef](#)] [[PubMed](#)]
- Marro Bellot, C.; Sangermano, M.; Olivero, M.; Salvo, M. Optical Fiber Sensors for the Detection of Hydrochloric Acid and Sea Water in Epoxy and Glass Fiber-Reinforced Polymer Composites. *Materials* **2019**, *12*, 379. [[CrossRef](#)] [[PubMed](#)]
- Lopez-Isooa, P.; Ojha, N.; Aryal, U.; Pugliese, D.; Boetti, N.G.; Milanese, D.; Petit, L. Spectroscopic Properties of Er³⁺-Doped Particles-Containing Phosphate Glasses Fabricated Using the Direct Doping Method. *Materials* **2019**, *12*, 129. [[CrossRef](#)] [[PubMed](#)]
- Cheng, Y.; Dong, H.; Yu, C.; Yang, Q.; Jiao, Y.; Wang, S.; Shao, C.; Hu, L.; Dai, Y. Temperature Dependence of Absorption and Energy Transfer Efficiency of Er³⁺/Yb³⁺/P⁵⁺ Co-Doped Silica Fiber Core Glasses. *Materials* **2022**, *15*, 996. [[CrossRef](#)]
- Yu, X.; Zhao, T.; Wang, T.; Bao, W.; Zhang, H.; Su, C. Up-conversion luminescence properties of Ho³⁺-Yb³⁺ co-doped transparent glass ceramics containing Y₂Ti₂O₇. *J. Non Cryst. Solids* **2021**, *574*, 121163. [[CrossRef](#)]
- Karaksina, E.V.; Kotereva, T.V.; Shiryaev, V.S. Luminescence properties of core-clap Pr-doped Ge-As-Se-Ga (In, I) glass fibers. *J. Lumin.* **2018**, *204*, 154–156. [[CrossRef](#)]
- Su, M.L.; Zhang, Q.; Gao, Y.J.; Wang, D.X.; Chen, C.; Wei, W. Enhanced luminescence of CsPbBr₃ nanocrystals-glass composite scintillators based on Ce³⁺-doped borosilicate glass. *J. Lumin.* **2022**, *242*, 118553. [[CrossRef](#)]

8. Yanes, A.C.; del-Castillo, J.; Luis, D.; Puentes, J. Novel Sr₂LuF₇-SiO₂ nano-glass-ceramics: Structure and up-conversion luminescence. *J. Lumin.* **2016**, *170*, 789–794. [[CrossRef](#)]
9. Secu, M.; Secu, C.; Bartha, C. Optical Properties of Transparent Rare-Earth Doped Sol-Gel derived Nano-Glass Ceramics. *Materials* **2021**, *14*, 6871. [[CrossRef](#)]
10. Zhang, B.; He, F.; Cao, X.; Wei, M.; Zheng, C.; Xie, J. The effect of TiO₂ and B₂O₃ on sintering behavior and crystallization behavior of SrO-BaO-B₂O₃-SiO₂ glass-ceramics. *Ceram. Int.* **2022**, *48*, 7013–7023. [[CrossRef](#)]
11. Farouk, M. Effect of TiO₂ on the structural, thermal, and optical properties of BaO-Li₂O-diborate glasses. *J. Non Cryst. Solids* **2014**, *402*, 74–78. [[CrossRef](#)]
12. Dharmar, S.; Gopalakrishnan, R.; Mohan, A. Environmental effect of denitrification of structural glass by coating TiO₂. *Mater. Today Proc.* **2021**, *45*, 6454–6458. [[CrossRef](#)]
13. Shafaghi, R.; Rodriguez, O.; Phull, S.; Schemitsch, E.H.; Zalzal, P.; Waldman, S.D.; Papini, M.; Towler, M.R. Effect of TiO₂ doping on degradation rate, microstructure and strength of borate bioactive glass scaffolds. *Mater. Sci. Eng. C* **2020**, *107*, 110351. [[CrossRef](#)] [[PubMed](#)]
14. Shirakawa, M.A.; John, V.M.; Mocelin, A.; Zilles, R.; Toma, S.H.; Araki, K.; Toma, H.E.; Thomaz, A.C.; Gaylarde, C.C. Effect of silver nanoparticle and TiO₂ coatings on biofilm formation on four types of modern glass. *Int. Biodeterior. Biodegrad.* **2016**, *108*, 175–180. [[CrossRef](#)]
15. Venkataiah, G.; Babu, P.; Martin, I.R.; Krishnaiah, K.V.; Suresh, K.; Lavin, V.; Jayasankar, C.K. Spectroscopic studies on Yb³⁺-doped tungsten-tellurite glasses for laser applications. *J. Non Cryst. Solids* **2018**, *479*, 9–15. [[CrossRef](#)]
16. Kassab, L.R.P.; Fukumoto, M.E.; Cacho, V.D.D.; Wetter, N.U.; Morimoto, N.I. Spectroscopic properties of Yb³⁺ doped PbO-Bi₂O₃-Ga₂O₃ glasses for IR laser applications. *Opt. Mater.* **2005**, *27*, 1576–1582. [[CrossRef](#)]
17. Fu, S.; Shi, W.; Feng, Y.; Zhang, L.; Yang, Z.; Xu, S.; Zhu, X.; Norwood, R.A.; Peyghambarian, N. Review of recent progress on single-frequency fiber lasers. *J. Opt. Soc. Am. B* **2017**, *34*, A49–A62. [[CrossRef](#)]
18. Zhang, L.Y.; Li, H. Lasing improvement of Yb³⁺: Phosphate glass with GeO₂ modification. *J. Lumin.* **2017**, *192*, 237–242. [[CrossRef](#)]
19. Zhang, L.; Xia, Y.; Shen, X.; Yang, R.; Wei, W. Investigations on the effects of the Stark splitting on the fluorescence behaviors in Yb³⁺-doped silicate, tellurite, germanate, and phosphate glasses. *Opt. Mater.* **2018**, *75*, 1–6. [[CrossRef](#)]
20. Krishnaiah, K.V.; Rajeswari, R.; Kumar, K.U.; Babu, S.S.; Martin, I.R.; Jayasankar, C.K. Spectroscopy and radiation trapping of Yb³⁺ ions in lead phosphate glasses. *J. Quant. Spectrosc. Radiat. Transf.* **2014**, *140*, 37–47. [[CrossRef](#)]
21. Calzavara, F.; Allix, M.; Dussauze, M.; Jubera, V.; Nalin, M.; Cardinal, T.; Fargin, E. Glass forming regions, structure and properties of lanthanum barium germanate and gallate glasses. *J. Non Cryst. Solids* **2021**, *571*, 121064. [[CrossRef](#)]
22. Yan, S.; Yue, Y.; Wang, Y.; Diao, Y.; Chen, D.; Zhang, L. Effect of GeO₂ on structure and properties of Yb³⁺: Phosphate glass. *J. Non Cryst. Solids* **2019**, *520*, 119455. [[CrossRef](#)]
23. Luo, Y.; Wen, J.; Zhang, J.; Canning, J.; Peng, G.D. Bismuth and erbium optical fiber with ultrabroadband luminescence across O-, E-, S-, C-, and L-bands. *Opt. Lett.* **2012**, *16*, 3447–3449. [[CrossRef](#)] [[PubMed](#)]
24. Lisiecki, R.; Ryba-Romanowski, W. Silica-based oxyfluoride glass and glass-ceramic doped with Tm³⁺ and Yb³⁺-VUV-VIS-NIR spectroscopy and optical thermometry. *J. Alloys Compd.* **2020**, *814*, 152304. [[CrossRef](#)]
25. Prasanth, M.; Thyagarajan, K.; Venkata Krishnaiah, K.; Ravi, N. 1.5 μm NIR emission property of erbium doped bismuth borate glasses for optical amplifier applications. *Mater. Today Proc.* **2022**, *56*, 1935–1938. [[CrossRef](#)]
26. Cai, M.; Zhou, B.; Wang, F.; Tian, Y.; Zhou, J.; Xu, S.; Zhang, J. Highly efficient mid-infrared 2 μm emission in Ho³⁺/Yb³⁺-codoped germanate glass. *Opt. Mater. Express* **2015**, *5*, 1431–1439. [[CrossRef](#)]
27. Pisarski, W.A.; Kowalska, K.; Kuwik, M.; Polak, J.; Pietrasik, E.; Goryczka, T.; Pisarska, J. Novel Multicomponent Titanate-germanate-Glasses: Synthesis, Structure, Properties, Transition Metal, and Rare Earth Doping. *Materials* **2020**, *13*, 4422. [[CrossRef](#)]
28. Ding, D.; Gao, J.; Zhang, S.; Duo, L. The photoluminescence properties of Pr³⁺-Yb³⁺ co-doped gallo-germanate glasses and glass ceramics as energy transfer. *J. Lumin.* **2020**, *226*, 117512. [[CrossRef](#)]
29. Lakshminarayana, G.; Ruan, J.; Qiu, J. NIR luminescence from Er-Yb, Bi-Yb and Bi-Nd codoped germanate glasses for optical amplification. *J. Alloys Compd.* **2009**, *476*, 878–883. [[CrossRef](#)]
30. Wang, W.C.; Yuan, J.; Liu, X.Y.; Chen, D.D.; Zhang, Q.Y.; Jiang, Z.H. An efficient 1.8 μm emission in Tm³⁺ and Yb³⁺/Tm³⁺ doped fluoride modifier germanate glasses for a diode-pump mid-infrared laser. *J. Non Cryst. Solids* **2014**, *404*, 19–25. [[CrossRef](#)]
31. Xia, J.; Tian, Y.; Li, B.; Zheng, L.; Jing, X.; Zhang, J.; Xu, S. Enhanced 2.0 μm emission in Ho³⁺/Yb³⁺ co-doped silica-germanate glass. *Infrared Phys. Technol.* **2017**, *81*, 17–20. [[CrossRef](#)]
32. Sun, Y.; Xin, W.; Meisong, L.; Lili, H.; Guzik, M.; Boulon, G.; Xia, L.; Kuan, P.W.; Weiqing, G.; Wang, T. Compositional dependence of Stark splitting and spectroscopic properties in Yb³⁺-doped lead silicate glasses. *J. Non Cryst. Solids* **2020**, *532*, 119890. [[CrossRef](#)]
33. Dai, N.; Hu, L.; Chen, W.; Boulon, G.; Yang, H.; Dai, S.; Lu, P. Spectroscopic and fluorescence decay behaviors of Yb³⁺-doped SiO₂-PbO-Na₂O-K₂O glass. *J. Lumin.* **2005**, *113*, 221–228. [[CrossRef](#)]
34. Krasteva, V.M.; Sigel, G.H.; Semjonov, S.L.; Bubnov, M.M.; Belovolov, M.I. Pr³⁺-Doped Ge-S-I Glasses and Fibers for PDFA Applications. In *Optical Amplifiers and Their Applications*; Paper FAW10; Optica Publishing Group: Victoria, BC, Canada, 1997. [[CrossRef](#)]
35. Medeiros Neto, J.A.; Taylor, E.R.; Samson, B.N.; Wang, J.; Hewak, D.W.; Laming, R.I.; Payne, D.N.; Tarbox, E.; Maton, P.D.; Roba, G.M.; et al. The application of Ga:La:S-based glass for optical amplification at 1.3 μm. *J. Non Cryst.* **1995**, *184*, 292–296. [[CrossRef](#)]

36. Taniguchi, M.M.; Zanuto, V.S.; Portes, P.N.; Malacarne, L.C.; Astrath, N.G.C.; Marconi, J.D.; Belancon, M.P. Glass engineering to enhance Si solar cells: A case study Pr^{3+} - Yb^{3+} codoped tellurite-tungstate as special converter. *J. Non Cryst. Solids* **2019**, *526*, 119717. [[CrossRef](#)]
37. Gonzalez-Perez, S.; Lahoz, F.; Caceres, J.M.; Lavin, V.; Dilva, I.; Gonzalez-Platas, J.; Martin, I.R. Energy transfer in Pr^{3+} - Yb^{3+} codoped oxyfluoride glass ceramics. *Opt. Mater.* **2007**, *29*, 1231–1235. [[CrossRef](#)]
38. Dan, H.K.; Qiu, J.; Zhou, D.; Jiao, Q.; Wang, R.; Thai, N.L. Super broadband near-infrared emission and energy transfer in Nd-Bi-Er co-doped transparent silicate glass-ceramics. *Mater. Lett.* **2019**, *234*, 142–147. [[CrossRef](#)]
39. Klinkov, V.A.; Semench, A.V.; Aseev, V.A.; Tsimerman, E.A.; Honcharenko, D. The influence of erbium additives on lead-bismuth-gallium glass matrix structure modification. *J. Non Cryst. Solids* **2020**, *547*, 120300. [[CrossRef](#)]
40. Lihui, H.; Xingreen, L.; Baojiu, C.; Jiuling, L. Near infrared emission for erbium-doped calcium aluminum silicate glass. *Chem. Phys. Lett.* **2001**, *345*, 235–238. [[CrossRef](#)]
41. Shen, S.; Naftaly, M.; Jha, A. Tungsten-tellurite-a host glass for broadband EDFA. *Opt. Commun.* **2002**, *205*, 101–105. [[CrossRef](#)]
42. Taherunnisa, S.K.; Krishna Reddy, D.V.; SambasivaRao, T.; Rudramamba, K.S.; Zhydashchevsky, Y.A.; Suchocki, A.; Piasecki, M.; Rami Reddy, M. Effect of up-conversion luminescence in Er^{3+} doped phosphate glasses for developing Erbium-Doped Fiber Amplifiers (EDFA) and G-LED's. *Opt. Mater. X* **2019**, *3*, 100034. [[CrossRef](#)]
43. Pisarski, W.A.; Grobelny, L.; Pisarska, J.; Lisiecki, R.; Ryba-Romanowski, W. Spectroscopic properties of Yb^{3+} and Er^{3+} ions in heavy metal glasses. *J. Alloys Compd.* **2011**, *509*, 8088–8092. [[CrossRef](#)]
44. Pisarski, W.A.; Janek, J.; Pisarska, J.; Lisiecki, R.; Ryba-Romanowski, W. Influence of temperature on up-conversion luminescence in $\text{Er}^{3+}/\text{Yb}^{3+}$ doubly doped lead-free fluorogermanate glasses for optical sensing. *Sens. Actuators B Chem.* **2017**, *253*, 85–91. [[CrossRef](#)]
45. Jiao, Y.; Guo, M.; Wang, R.J. Influence of Al/Er ratio on the optical properties and structures of $\text{Er}^{3+}/\text{Al}^{3+}$ co-doped silica glasses. *Appl. Phys.* **2021**, *129*, 053104. [[CrossRef](#)]
46. Veselsky, K.; Lahti, V.; Petit, L.; Prajzler, V.; Sulc, J.; Jelinkova, H. Influence of Y_2O_3 Content on Structural, Optical, Spectroscopic, and Laser Properties of Er^{3+} , Yb^{3+} Co-Doped Phosphate Glasses. *Materials* **2021**, *14*, 4041. [[CrossRef](#)] [[PubMed](#)]
47. Tang, D.; Liu, Q.; Liu, X.; Wang, X.; Yang, X.; Liu, Y.; Ying, T.; Renguang, Y.; Zhang, X.; Xu, S. High quantum efficiency of 1.8 μm luminescence in Tm^{3+} fluoride tellurite glass. *Infrared Phys. Techn.* **2022**; in press. [[CrossRef](#)]
48. Li, S.; Song, X.X.; Wang, Y.; Jia, C.L. Structural and photoluminescence properties of Yb/Tm co-implanted ZnO crystals. *Phys. B Condens. Matt.* **2017**, *527*, 57–60. [[CrossRef](#)]
49. Pisarska, J.; Lisiecki, R.; Ryba-Romanowski, W.; Dominiak-Dzik, G.; Pisarski, W.A. Up-converted luminescence in Yb-Tm co-doped lead fluoroborate glasses. *J. Alloys Compd.* **2008**, *451*, 226–228. [[CrossRef](#)]
50. Babu, P.; Martin, I.R.; Lavin, V.; Rodriguez-Mendoza, U.R.; Seo, H.J.; Krishanaiah, K.V.; Venkatramu, V. Quantum cutting and near-infrared emission in $\text{Ho}^{3+}/\text{Yb}^{3+}$ codoped transparent glass-ceramics. *J. Lumin.* **2020**, *226*, 117424. [[CrossRef](#)]
51. Reddy, A.S.S.; Purmachand, N.; Kostrzewa, M.; Nriak, M.G.; Venkatramaiah, N.; Ravi Kumar, V.; Veeraiah, N. The role of gold metallic particles in improving green and NIR emission of Ho^{3+} ions in non-conventional SeO_2 based glass ceramics. *J. Non Cryst. Solids* **2022**, *576*, 121240. [[CrossRef](#)]
52. Boyer, J.C.; Vetrone, F.; Capobianco, J.A.; Speghini, A.; Bettinelli, M. Optical transitions and up-conversion properties of Ho^{3+} doped ZnO- TeO_2 glass. *J. Appl. Phys.* **2003**, *93*, 9460–9465. [[CrossRef](#)]
53. Wang, M.; Yu, C.; He, D.; Feng, S.; Li, S.; Zhang, L.; Zhang, J.; Hu, L. Enhanced 2 μm emission of Yb-Ho doped fluorophosphate glass. *J. Non Cryst. Solids* **2011**, *357*, 2447–2449. [[CrossRef](#)]
54. Peng, B.; Izumitani, T. Optical properties, fluorescence mechanisms and energy transfer in Tm^{3+} , Ho^{3+} , and $\text{Tm}^{3+}/\text{Ho}^{3+}$ doped near-infrared laser glasses, sensitized by Yb^{3+} . *Opt. Mater.* **1995**, *4*, 797–810. [[CrossRef](#)]
55. Wang, M.; Yi, L.; Chen, Y.; Yu, C.; Wang, G.; Hu, L.; Zhang, J. Effect of Al (PO_3)₃ content on physical, chemical, and optical properties of fluorophosphate glasses for 2 μm supplication. *Mater. Chem. Phys.* **2009**, *114*, 295–299. [[CrossRef](#)]
56. Tu, L.; Tang, G.; Qian, Q.; Yang, Z. Controllable structural tailoring for enhanced ~2 μm emission in heavily Tm^{3+} -doped germanate glasses. *Opt. Lett.* **2021**, *46*, 310–313. [[CrossRef](#)]
57. Liang, Y.; Liu, F.; Chen, Y.; Wang, X.; Sun, K.; Pan, Z. Extending the applications for lanthanide ions: Efficient emitters in short-wave infrared persistent luminescence. *J. Mat. Chem. C* **2017**, *5*, 6488–6492. [[CrossRef](#)]
58. Lesniak, M.; Kochanowicz, M.; Baranowska, A.; Golonko, P.; Kuwik, M.; Zmojda, J.; Miluski, P.; Dorosz, J.; Pisarski, W.A.; Pisarska, J.; et al. Structure and Luminescence Properties of Transparent Germanate Glass-Ceramics Co-Doped with $\text{Ni}^{2+}/\text{Er}^{3+}$ for Near-Infrared Optical Fiber Application. *Nanomaterials* **2021**, *11*, 2115. [[CrossRef](#)]
59. Zheng, Y.; Chen, B.; Zhong, H.; Sun, J.; Cheng, L.; Li, X.; Zhang, J.; Tian, Y.; Lu, W.; Wan, J.; et al. Optical Transition, Excitation State Absorption, and Energy Transfer Study of Er^{3+} , Nd^{3+} Single-Doped, and $\text{Er}^{3+}/\text{Nd}^{3+}$ Codoped Tellurite Glasses for Mid-Infrared Laser Applications. *J. Am. Ceram. Soc.* **2011**, *94*, 1766–1772. [[CrossRef](#)]
60. Auzel, F. Upconversion and Anti-Stokes Processes with f and d Ions in Solids. *Chem. Rev.* **2004**, *104*, 139–173. [[CrossRef](#)]

P12

Karolina Kowalska, Marta Kuwik, Tomasz Goryczka, Joanna Pisarska,
Wojciech A. Pisarski,

**The impact of pair $\text{Er}^{3+}/\text{Yb}^{3+}$ on titanate-germanate glasses:
Physicochemical and near-infrared luminescence investigations**

Materials Science and Engineering: B 301 (2024) 117117



The impact of pair $\text{Er}^{3+}/\text{Yb}^{3+}$ on titanate-germanate glasses: Physicochemical and near-infrared luminescence investigations

Karolina Kowalska^{a,*}, Marta Kuwik^a, Tomasz Goryczka^b, Joanna Pisarska^a, Wojciech A. Pisarski^{a,*}

^a Institute of Chemistry, University of Silesia, Szkolna 9 Street, 40-007 Katowice, Poland

^b Institute of Materials Engineering, 75. Pułku Piechoty 1A Street, University of Silesia, 41-500 Chorzów, Poland

ARTICLE INFO

Keywords:

Glasses
Rare earth ions
Chemical composition-property relationship
Spectroscopic methods

ABSTRACT

This work combines photoluminescence methods, Raman spectroscopy, and X-ray diffraction (XRD) to expand the knowledge of the effects of pair rare earth ions doping on the physicochemical and near-IR properties of glasses. For this purpose, glass systems based on $\text{GeO}_2\text{-BaO-Ga}_2\text{O}_3$ (GBG) and $\text{TiO}_2\text{-GeO}_2\text{-BaO-Ga}_2\text{O}_3$ (TGBG) doped with Er^{3+} ions (0.1, 0.25, 0.5 mol%) and Yb^{3+} ions (0.5, 1.25, 2.5 mol%) were synthesized and analyzed. The near-IR luminescence band corresponding to $\text{Er}^{3+}:^4\text{I}_{13/2} \rightarrow ^4\text{I}_{15/2}$ is narrowed for germanate-based glasses (FWHM = 31 nm), whereas in the presence of TiO_2 is more intense and broadened (FWHM = 65 nm). The energy transfer efficiencies between Yb^{3+} and Er^{3+} ions in glass samples have been calculated. Notably, the absorption spectra showed the Stark splitting for the band due to the $^4\text{I}_{15/2} \rightarrow ^2\text{H}_{11/2}$ hypersensitive transition. Finally, we find the formation of $\text{Er}_2\text{Ti}_2\text{O}_7$ and $\text{Yb}_2\text{Ti}_2\text{O}_7$ crystalline phases in highly doping titanate-germanate samples. The results provide valuable ideas to evaluate the effect of the rare earths doping procedure on properties of designed glasses for near-IR luminescence applications.

1. Introduction

Glasses activated with luminescent rare earth ions are important classes of engineering materials, which are useful in numerous industrial applications in photonic devices. The first realization of erbium-doped optical fiber amplifier (EDFA system) was developed in 1987 by Mears et al. at Optical Fibre Group [1]. From that time, the spectroscopy of trivalent Er^{3+} and Yb^{3+} ions have been intensively investigated for various kinds of glass-host matrix. Especially, the spectral profile of luminescence band corresponding to the $^4\text{I}_{13/2} \rightarrow ^4\text{I}_{15/2}$ transition of Er^{3+} and their relative intensity ratio is especially interesting from the spectroscopic and applications points of view [2,3].

Among inorganic glasses, a lot of work has been done on the spectroscopic properties of Er^{3+} and $\text{Er}^{3+}/\text{Yb}^{3+}$ co-doped silica glasses. Many advantages of silica glass host matrix, such as the lowest propagation losses (0.2 dB/km), can withstand high temperatures and shows exceptional mechanical strength and chemical durability, making them important active centers. However, due to strong Si-O-Si covalent bonds, a major drawback of silica glass permits only a relatively small concentration of rare earth ions [4,5]. Systematic studies demonstrate that a

lower concentration of trivalent Er^{3+} ions result in a narrow $^4\text{I}_{13/2} \rightarrow ^4\text{I}_{15/2}$ line width, which limits broadband near-infrared transmission. On the other hand, the high rare earth ions concentration often leads to the formation of clusters, which results in luminescence quenching [6]. This causes deleterious effects on the spectroscopic properties of silica-based glasses. Since then, many excellent papers [7–10] have been published on glasses activated with Er^{3+} and Yb^{3+} ions concerning on crucial aspects: from synthesis procedure, physicochemical and near-infrared optical properties to their potential applications. These phenomena are necessary for knowledge about optical glasses. The optimal way to fabricate the titanate-germanate glasses for near-infrared applications such as optical fiber is still the appropriate compromise between chemical composition of glass-network modifier/former, rare earth ions content and structural, luminescence properties.

Since the fabricated of amorphous and thermal stable material based on $\text{GeO}_2\text{-TiO}_2\text{-BaO-Ga}_2\text{O}_3$ system by Pisarski and his group [11], titanate-germanate as a novel glass host is ideally suitable to photonic application. According to our previous results, the incorporation of titanium dioxide (TiO_2) into barium gallo-germanate network significantly enhanced and broadened the main NIR luminescence band of rare

* Corresponding authors.

E-mail addresses: karolina.kowalska@us.edu.pl (K. Kowalska), wojciech.pisarski@us.edu.pl (W.A. Pisarski).

<https://doi.org/10.1016/j.mseb.2023.117117>

Received 31 October 2023; Received in revised form 4 December 2023; Accepted 14 December 2023
0921-5107/© 2023 Elsevier B.V. All rights reserved.

earth ions. Further, the authors reported the recommended molar ratio $\text{GeO}_2:\text{TiO}_2$ for Nd^{3+} [12], Er^{3+} [13] and Ho^{3+} [14] doped titanate-germanate glasses. Nevertheless, an introduction various concentration rare earth ions to inorganic glass host matrices influenced strongly on the local structure and their optical properties. Indeed, a clear correlation was observed for $\text{Yb}^{3+}/\text{Er}^{3+}$ co-doped phosphate [15], telluroborate [16], and phosphosilicate [17] glasses. A study by Z. Zhao et al. [15] showed that the high-concentration $\text{Er}^{3+}/\text{Yb}^{3+}$ co-doped phosphate glasses with the optimized $\text{Er}^{3+}/\text{Yb}^{3+}$ ratio of 0.5/12, gives the highest luminescence intensity at 1535 nm under 980 nm excitation. By analyzing the results of the study by Annapoorani et al. [16], it can be seen that in the case of $\text{Er}^{3+}/\text{Yb}^{3+}$ co-doped lithium telluroborate glasses luminescence quenching was observed beyond 0.5 wt% of Yb_2O_3 and Er_2O_3 . Further, Melkumov et al. [17] stated that the excitation transfer efficiency is determined by the ytterbium concentration and is essentially independent of erbium concentration. Hence, based on spectroscopic results for heavy metal systems [18] the authors assumed that the optimized rare earth doping ratio of Er^{3+} and Yb^{3+} will be equal 1:5 to necessary enhance pumping efficiency. These observations became the motivation for investigating the impact of $\text{Er}^{3+}/\text{Yb}^{3+}$ ions content on germanate-based glasses modified by TiO_2 presented in this article.

In this work, we focus on the synthesis and characterization of Er^{3+} and Yb^{3+} co-doped glass system based on $\text{GeO}_2\text{-BaO-Ga}_2\text{O}_3$ (GBG) and $\text{TiO}_2\text{-GeO}_2\text{-BaO-Ga}_2\text{O}_3$ (TGBG). The molar ratio $\text{Er}^{3+}/\text{Yb}^{3+}$ was 1:5, when concentration of Er^{3+} and Yb^{3+} used during synthesis was changed from 0.1/0.5 mol% to 0.5/2.5 mol% in the glass composition. The impact of pair rare earths, as well as the influence of glass-host matrix on near-infrared luminescence and physicochemical properties was discussed. Based on emission spectra and their decays, the $^4\text{I}_{13/2} \rightarrow ^4\text{I}_{15/2}$ line widths, luminescence lifetimes, energy transfer efficiencies were determined. The absorption band related to hypersensitive transition of Er^{3+} ions have been examined. Thus, prepared optical materials were characterized by Raman spectroscopy and X-ray diffraction.

2. Material and methods

The subject of this study is $\text{Er}^{3+}/\text{Yb}^{3+}$ co-doped glass synthesized by the high-temperature melt quenching-technique of the multicomponent systems $60\text{GeO}_2\text{-}30\text{BaO}\text{-}(10\text{-}x\text{-}y)\text{Ga}_2\text{O}_3\text{-}x\text{Yb}_2\text{O}_3\text{-}y\text{Er}_2\text{O}_3$ and $30\text{TiO}_2\text{-}30\text{GeO}_2\text{-}30\text{BaO}\text{-}(10\text{-}x\text{-}y)\text{Ga}_2\text{O}_3\text{-}x\text{Yb}_2\text{O}_3\text{-}y\text{Er}_2\text{O}_3$, where x and y denote concentrations of ytterbium oxide and erbium oxide, respectively. The concentration of Yb_2O_3 was 0.5, 1.25, and 2.5 mol%, and Er_2O_3 was 0.1, 0.25, and 0.5 mol%. The Yb^{3+} singly doped glasses were also prepared to determine the energy transfer efficiencies. In our synthesis procedure, the metal oxides GeO_2 (99.99 %), TiO_2 (99.995 %, rutile), BaO (99.99 %), Ga_2O_3 (99.99 %), and optical active dopants Yb_2O_3 (99.99 %), Er_2O_3 (99.99 %) were used from Sigma-Aldrich Chemical Company. Each batch composition of 5 g was weighed and mixed homogeneously together in an agate mortar. Then, the samples were placed in a corundum crucible (Łukasiewicz Research Network, Institute of Ceramics and Building Materials, Kraków, Poland) and were melted at 1250°C for 0.45 h in an electric furnace (FCF 4/170 M produced by Czyłok, Jastrzębie Zdrój, Poland). Glass samples were polished for measurements.

The physicochemical and near-infrared properties characterization of synthesized materials was performed using optical spectroscopy, Raman spectroscopy and X-ray diffraction. Luminescence measurements (spectra and decay curves) were carried out by the laser equipment, which consists of PTI QuantaMaster QM40 spectrofluorometer, tunable pulsed optical parametric oscillator (OPO), Nd:YAG laser (Opotek Opolette 355 LD), double 200 nm monochromators, Hamamatsu H10330B-75 detector and PTI ASOC-10 USB-2500 oscilloscope. The resolution for spectral measurements was ± 0.1 nm. Decay curves were recorded and stored by a PTI ASOC-10 [USB-2500] oscilloscope with an accuracy of ± 0.5 μs . Glass samples were characterized using absorption measurements (Varian Cary 5000 UV-Vis-NIR Spectrophotometer,

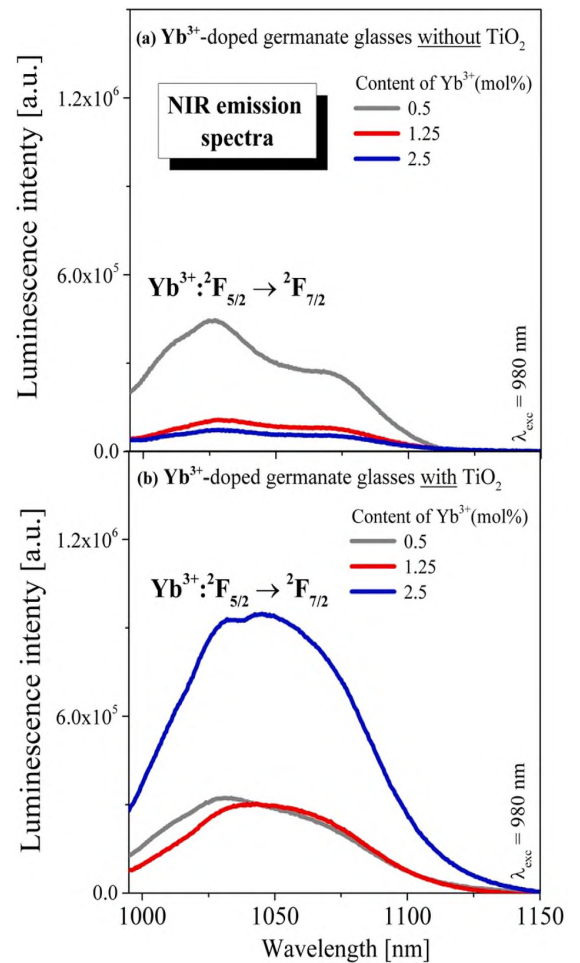


Fig. 1. Near-infrared luminescence spectra for Yb^{3+} ions in barium gallio-germanate glasses without (a) and with (b) titanium dioxide under 980 nm laser excitation.

Agilent Technology, Santa Clara, CA, USA). To examine the structural changes, the Raman spectra were registered using Thermo ScientificTM DXRTM2xi spectrometer (Waltham, MA, USA) in the frequency region 400 cm^{-1} — 1400 cm^{-1} with the resolution of 4 cm^{-1} and 128 scans. The appropriate laser source with an excitation wavelength of 633 nm was used to obtain the Raman spectra. To get more information about the nature of fabricated highly doping glass samples, the X-ray diffraction (XRD) analysis was carried out using an X'Pert Pro diffractometer supplied by PANalytical (Almelo, The Netherlands) with $\text{CuK}\alpha$ radiation (line $\lambda = 1.54056\text{ \AA}$). All optical and structural measurements were performed at room temperature.

3. Results and discussion

To analyze the effect of pair rare earth ions on the optical properties of fabricated glass samples, luminescence measurements were performed. Fig. 1 presents the near-IR luminescence spectra of Yb^{3+} ions in $\text{GeO}_2\text{-BaO-Ga}_2\text{O}_3$ (GBG) and $\text{TiO}_2\text{-GeO}_2\text{-BaO-Ga}_2\text{O}_3$ (TGBG) glass systems. Ytterbium ion is one of the important glass components due to its simple energy level scheme, with the $^2\text{F}_{7/2}$ being the ground state and the $^2\text{F}_{5/2}$ being the excited state. It is also important in terms of doubly doped glass systems, as will be demonstrated in the next part of this paper. The recorded spectra consist of an emission band assigned to the

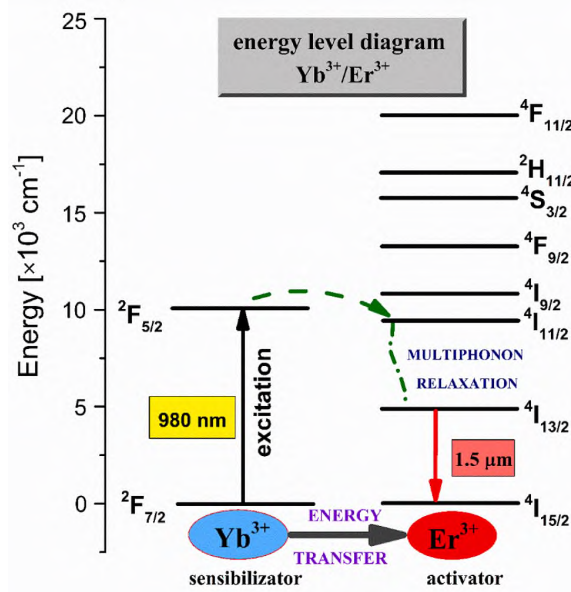


Fig. 2. A simplified energy level diagram of $\text{Yb}^{3+}/\text{Er}^{3+}$ ions in modified germanate glass.

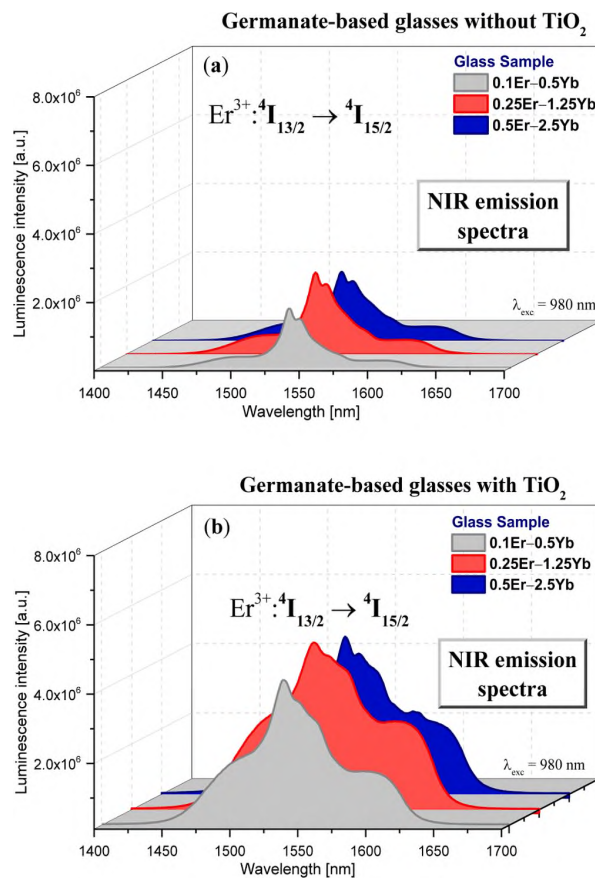


Fig. 3. Near-infrared luminescence spectra for $\text{Er}^{3+}/\text{Yb}^{3+}$ ions in barium gallate glasses without (a) and with (b) titanium dioxide under 980 nm laser excitation.

transition ${}^2\text{F}_{5/2} \rightarrow {}^2\text{F}_{7/2}$ of Yb^{3+} ions. Since the luminescence profile of the Yb^{3+} emission band is strictly dependent on the chemical composition of the host matrix, the near-IR emission spectra gave valuable information about the optical behavior of Yb^{3+} ions. It was observed that for the $\text{GeO}_2\text{-TiO}_2\text{-BaO-Ga}_2\text{O}_3$ system, a luminescence band assigned to the ${}^2\text{F}_{5/2} \rightarrow {}^2\text{F}_{7/2}$ transition was more intense compared to the $\text{GeO}_2\text{-BaO-Ga}_2\text{O}_3$ system. It is noticed that increasing of Yb_2O_3 content above 0.5 mol% leads to strong decreasing of luminescence (Fig. 1a), which confirms the concentration quenching phenomenon [19,20]. A completely different situation is observed for germanate-based glasses in the presence of titanium dioxide (TiO_2). According to the resulting luminescence spectra shown in Fig. 1(b), the integrated emission intensity for the ${}^2\text{F}_{5/2} \rightarrow {}^2\text{F}_{7/2}$ transition is enhanced more significantly in the function of Yb^{3+} ions compared to glasses without TiO_2 . This situation was also observed silicate glasses in the function of Yb^{3+} ions [21]. Based on this observation, we could conclude that the suitable Yb^{3+} ions concentration, which the strongest and broadened near-IR luminescence requires, can be satisfied in the titanate-germanate glasses. The obtained results were interpreted based on the emission spectra measurements because Yb^{3+} plays an important role as an excellent sensitizer for other rare earth ions [22–24]. Further analysis will be devoted to optical and structural aspects of co-doped two various glass systems in the function of Yb^{3+} ions (from 0.5 mol% to 2.5 mol%) and Er^{3+} ions (0.1, 0.25, 0.5 mol%). To explain the mechanism of the energy transfer from Yb^{3+} to Er^{3+} and the sensitization of near-IR emission of Er^{3+} ions at 1.5 μm for germanate-based samples with the absence and presence of TiO_2 the simplified energy level diagram is illustrated in Fig. 2. When co-doped material is excited by 980 nm, the ytterbium ions initially absorb the energy because the absorption cross-section is much higher for ${}^2\text{F}_{5/2}$ (Yb^{3+}) than ${}^4\text{I}_{11/2}$ (Er^{3+}). Thus, the energy relaxes from the ground state ${}^2\text{F}_{7/2}$ to the excited state ${}^2\text{F}_{5/2}$, respectively. Then, the excitation energy is quickly transferred to the Er^{3+} . The energy transfer process is usually very efficient due to the small energy gap between ${}^2\text{F}_{5/2}$ (Yb^{3+}) and ${}^4\text{I}_{11/2}$ (Er^{3+}) excited states. In the next step, the excitation energy relaxes nonradiatively to the upper ${}^4\text{I}_{13/2}$ state of erbium ions by multiphonon process [25–27].

Fig. 3 presents the NIR luminescence spectra registered under direct excitation at 980 nm for $\text{GeO}_2\text{-BaO-Ga}_2\text{O}_3$ (GBG), and $\text{TiO}_2\text{-GeO}_2\text{-BaO-Ga}_2\text{O}_3$ (TGBG) glass systems doped with $\text{Yb}^{3+}/\text{Er}^{3+}$ ions. Independent of the rare earth ions content, emission bands were registered for all studied samples. The emission spectra were measured under the same experimental conditions to compare the intensities of the band. The characteristic emission band corresponding to the main ${}^4\text{I}_{13/2} \rightarrow {}^4\text{I}_{15/2}$ laser transition of Er^{3+} is located in the eye-safe spectral region [28,29]. Spectroscopic studies indicate that the profile of emission bands of Er^{3+} ions depend strongly on chemical composition. It was stated that the integrated emission intensity for the ${}^4\text{I}_{13/2} \rightarrow {}^4\text{I}_{15/2}$ transition of Er^{3+} ions in $\text{TiO}_2\text{-GeO}_2\text{-BaO-Ga}_2\text{O}_3$ is significantly enhanced (2.0-fold increase) compared to $\text{GeO}_2\text{-BaO-Ga}_2\text{O}_3$ glass. Spectroscopic parameter such as the emission bandwidth for the ${}^4\text{I}_{13/2} \rightarrow {}^4\text{I}_{15/2}$ transition of Er^{3+} ions were determined and illustrated in Fig. 4. The emission bandwidth of Er^{3+} ions at 1.5 μm is an important parameter for EDFA, which is used in the WDM network system of optical communication. The commercial $\text{Er}^{3+}/\text{Yb}^{3+}$ -doped fiber amplifiers (EDFA) based on silica glass exhibit a relatively narrow linewidth that limits broadband NIR transmission. In order to meet the requirements, i.e. higher information transmission capacity and to improve the performance of the WDM network, a medium with a wide and flat gain at 1.5 μm , which is related to the width of the ${}^4\text{I}_{13/2} \rightarrow {}^4\text{I}_{15/2}$ emission band, is required for the EDFA [30–33]. Our studies clearly indicate that the spectral width defined as the full width at half maximum (FWHM) is about two times broader for 30 $\text{TiO}_2\text{-30GeO}_2\text{-30BaO-7Ga}_2\text{O}_3\text{-0.5Er}_2\text{O}_3\text{-2.5Yb}_2\text{O}_3$ sample ($\Delta\lambda = 65 \text{ nm} \pm 1$) than 60 $\text{GeO}_2\text{-30BaO-7Ga}_2\text{O}_3\text{-0.5Er}_2\text{O}_3\text{-2.5Yb}_2\text{O}_3$ ($\Delta\lambda = 31 \pm 1 \text{ nm}$) sample. These values are larger than that in other glass hosts used for optical fiber amplifiers, such as 26 nm in silicate glasses [34], 43 nm in phosphate glasses [35], 46 nm in niobium germanate glasses [36], and

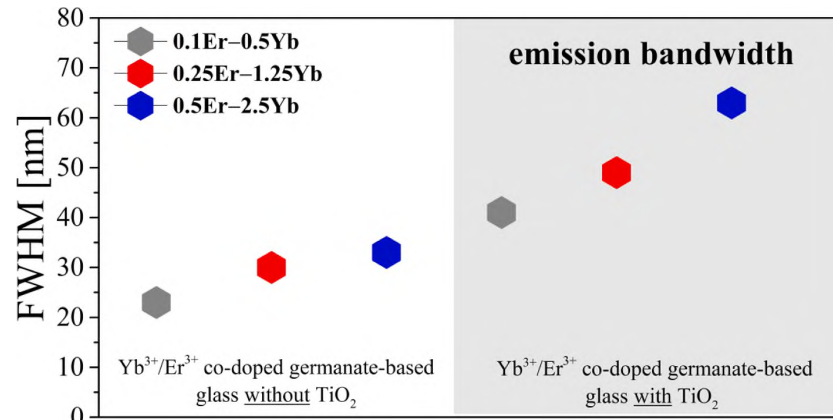


Fig. 4. FWHM values vs. $\text{Er}_2\text{O}_3/\text{Yb}_2\text{O}_3$ content in barium gallo-germanate glasses without/with titanium dioxide.

54 nm in tellurite glasses [37]. The understanding of optical properties and their relation to composition has been extensively reviewed by ElBatal [38]. It has been shown that many of the properties of glass relate to valence states of titanium ions as the trivalent (Ti^{3+}) and the tetravalent (Ti^{4+}). The ratio of each oxidation state in glass depends on the glass host matrix, chemical composition, and condition during the melting process. Notable work has been performed on the optical properties of titanium dioxide in silicate, borate, and phosphate glasses, culminating in the pioneering work by Moringa et al. [39]. Importantly, titanium ions were identified in a trivalent oxidation state for titanate-germanate glass, where the molar ratio was $\text{GeO}_2:\text{TiO}_2 = 1:1$ [40]. According to previous works [41,42], enhancement luminescence properties were observed after the introduction of TiO_2 to the germanate glass host because this component slightly reduces the phonon energy and strongly influences bonding between rare earth ions and the nearest environments. The large emission bandwidth of the $^4\text{I}_{13/2} \rightarrow ^4\text{I}_{15/2}$ transition of Er^{3+} can be explained by the local structure and bonding of trivalent erbium ions in titanate-germanate glasses confirmed by theoretical calculations using the Judd-Ofelt framework in our previous work [13]. Among Judd-Ofelt parameters, Ω_2 indicates the degree of covalency between Er^{3+} ions and surrounding ligands. The parameter Ω_2 increased from 4.77 ± 0.23 (BGG without TiO_2) to 5.94 ± 0.23 ($\text{GeO}_2:\text{TiO}_2 = 1:1$). It suggests that the bonds between Er^{3+} ions and surrounding ligands existing in the glass sample in the presence of TiO_2 are highly covalent. This study confirmed that the profiles of luminescence bands and their values of emission linewidth (FWHM) are dependent on the symmetry and the site-to-site variation of the rare earth local environment changes during the modification of the glass host. Moreover, the radiative transition probabilities calculated using Judd-Ofelt theory for the main infrared transition of rare earth ions increased significantly in the presence of TiO_2 , which is required for an efficient laser transition. For example, the radiative transition probability A_J calculated for the main NIR laser transition $^4\text{F}_{3/2} \rightarrow ^4\text{I}_{11/2}$ (Nd^{3+}) at 1060 nm increases from 1317 s^{-1} for glass sample without TiO_2 to 2105 s^{-1} for glass sample with 50 mol% TiO_2 . The highest value ($A_J = 2787 \text{ s}^{-1}$) was obtained for Nd^{3+} ions in a titanate-germanate glass containing 20 mol% TiO_2 [12]. A similar situation was also observed for titanate-germanate glasses singly doped with Ho^{3+} [14] and Tm^{3+} [42]. The radiative transition probabilities for the main $^3\text{F}_4 \rightarrow ^3\text{H}_6$ NIR laser transition of Tm^{3+} at 1800 nm increase from 164 s^{-1} (0 % TiO_2) to 348 s^{-1} (30 % TiO_2), 367 s^{-1} (40 % TiO_2) and 378 s^{-1} (45 % TiO_2), whereas the values of A_J for the main NIR laser transition $^5\text{I}_7 \rightarrow ^5\text{I}_8$ (Ho^{3+}) at 2000 nm increase from 84 s^{-1} (0 % TiO_2) to 98 s^{-1} (30 % TiO_2), 128 s^{-1} (40 % TiO_2) and 132 s^{-1} (45 % TiO_2) in the presence of TiO_2 . In particular, we observe a nearly two-fold increase in radiative transition probabilities calculated for the $^4\text{I}_{13/2} \rightarrow ^4\text{I}_{15/2}$ (near-IR) and $^4\text{I}_{11/2} \rightarrow$

Table 1

Glass composition, measured lifetimes for the $^2\text{F}_{5/2}$ (Yb^{3+}) state, and the energy transfer efficiencies for $\text{Er}^{3+}/\text{Yb}^{3+}$ co-doped glass samples without/with TiO_2 .

Chemical composition of glass samples (%mol)	τ_m (ms)	η_{ET} (%)
$60\text{GeO}_2\text{-}30\text{BaO}\text{-}9.4\text{Ga}_2\text{O}_3\text{-}0.1\text{Er}_2\text{O}_3\text{-}0.5\text{Yb}_2\text{O}_3$	0.99	22
$60\text{GeO}_2\text{-}30\text{BaO}\text{-}8.5\text{Ga}_2\text{O}_3\text{-}0.25\text{Er}_2\text{O}_3\text{-}1.25\text{Yb}_2\text{O}_3$	0.30	64
$60\text{GeO}_2\text{-}30\text{BaO}\text{-}7.0\text{Ga}_2\text{O}_3\text{-}0.5\text{Er}_2\text{O}_3\text{-}2.5\text{Yb}_2\text{O}_3$	0.19	73
$30\text{GeO}_2\text{-}30\text{TiO}_2\text{-}30\text{BaO}\text{-}9.4\text{Ga}_2\text{O}_3\text{-}0.1\text{Er}_2\text{O}_3\text{-}0.5\text{Yb}_2\text{O}_3$	0.59	24
$30\text{GeO}_2\text{-}30\text{TiO}_2\text{-}30\text{BaO}\text{-}8.5\text{Ga}_2\text{O}_3\text{-}0.25\text{Er}_2\text{O}_3\text{-}1.25\text{Yb}_2\text{O}_3$	0.40	39
$30\text{GeO}_2\text{-}30\text{TiO}_2\text{-}30\text{BaO}\text{-}7.0\text{Ga}_2\text{O}_3\text{-}0.5\text{Er}_2\text{O}_3\text{-}2.5\text{Yb}_2\text{O}_3$	0.42	36

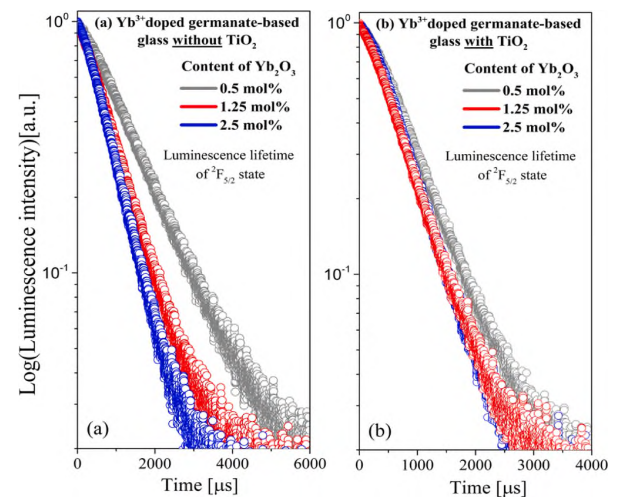


Fig. 5. Luminescence decay curves of Yb^{3+} -doped germanate glasses without (a) and with (b) titanium dioxide ($\lambda_{\text{exc}} = 980 \text{ nm}$).

$^4\text{I}_{13/2}$ (mid-IR) laser transitions of Er^{3+} ions in titanate-germanate glasses. For the near-IR transition $^4\text{I}_{13/2} \rightarrow ^4\text{I}_{15/2}$ (Er^{3+}) at 1500 nm the value of A_J increase from 110 s^{-1} (0 % TiO_2) to 215 s^{-1} (50 % TiO_2), whereas for the mid-IR transition $^4\text{I}_{11/2} \rightarrow ^4\text{I}_{13/2}$ (Er^{3+}) at 2700 nm the value of A_J is changed from 21 s^{-1} (0 % TiO_2) to 40 s^{-1} (50 % TiO_2), respectively [13]. At a consequence, near-IR [13] and mid-IR [43] emission of Er^{3+} ions is enhanced greatly in the presence of TiO_2 .

The lifetime is an important parameter since it reflects the mechanisms of depopulation of energy levels. The luminescence decay curves for the $^2\text{F}_{5/2}$ state of ytterbium in fabricated glasses singly doped with Yb^{3+} ions and doubly doped with $\text{Yb}^{3+}/\text{Er}^{3+}$ ions were analyzed. The

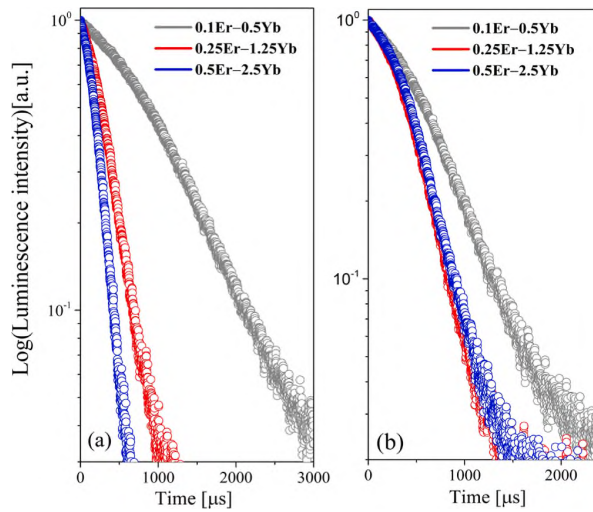


Fig. 6. Luminescence decay curves of $\text{Er}^{3+}/\text{Yb}^{3+}$ -doped germanate glasses without (a) and with (b) titanium dioxide ($\lambda_{\text{exc}} = 980 \text{ nm}$).

$^2\text{F}_{5/2}$ luminescence lifetime of Yb^{3+} was determined. Its value is reduced from $\tau = 1.28 \text{ ms}$ to $\tau = 0.72 \text{ ms}$ ($\text{GeO}_2\text{-BaO-Ga}_2\text{O}_3$) with increasing Yb^{3+} ions. For $\text{TiO}_2\text{-GeO}_2\text{-BaO-Ga}_2\text{O}_3$, the lifetimes decrease from $\tau = 0.78 \text{ ms}$ to $\tau = 0.65 \text{ ms}$ and then slightly increase to $\tau = 0.66 \text{ ms}$ with further increasing Yb_2O_3 concentration. Based on these data (Table 1), the energy transfer efficiency (η_{ET}) was calculated using the following relation:

$$\eta_{\text{ET}} = 1 - \frac{\tau(\text{Yb} - \text{Er})}{\tau(\text{Yb})} \quad (1)$$

where: $\tau_{(\text{Yb-Er})}$ and $\tau_{(\text{Yb})}$ are luminescence lifetimes for the $^2\text{F}_{5/2}$ state of Yb^{3+} ions in the presence and absence of Er^{3+} ions. In addition, the decay curves follow by single-exponential behavior (Figs. 5, 6). The luminescence lifetimes calculated for Yb^{3+} singly doped samples are longer than glass samples co-doped with $\text{Er}^{3+}/\text{Yb}^{3+}$, confirming the presence of the energy transfer process from ytterbium to erbium ions. The energy transfer efficiency η_{ET} is close to 22 % for germanate-based glass sample doped with 0.1 mol% Er_2O_3 and 0.5 mol% Yb_2O_3 , and its value drastically increases up to 73 % with increasing rare earth content, indicating efficient sensitization of the erbium ions by ytterbium. It is in good agreement with the results obtained for the $\text{GeO}_2\text{-NaO-NbO}$ glass system [44]. In contrast, our calculations indicate that the energy transfer efficiencies for $\text{Er}^{3+}/\text{Yb}^{3+}$ co-doped titanate-germanate glasses are significantly lower. The energy transfer efficiency increases from 24 % to 39 % and then decreases to 36 % with further increasing Er^{3+} and

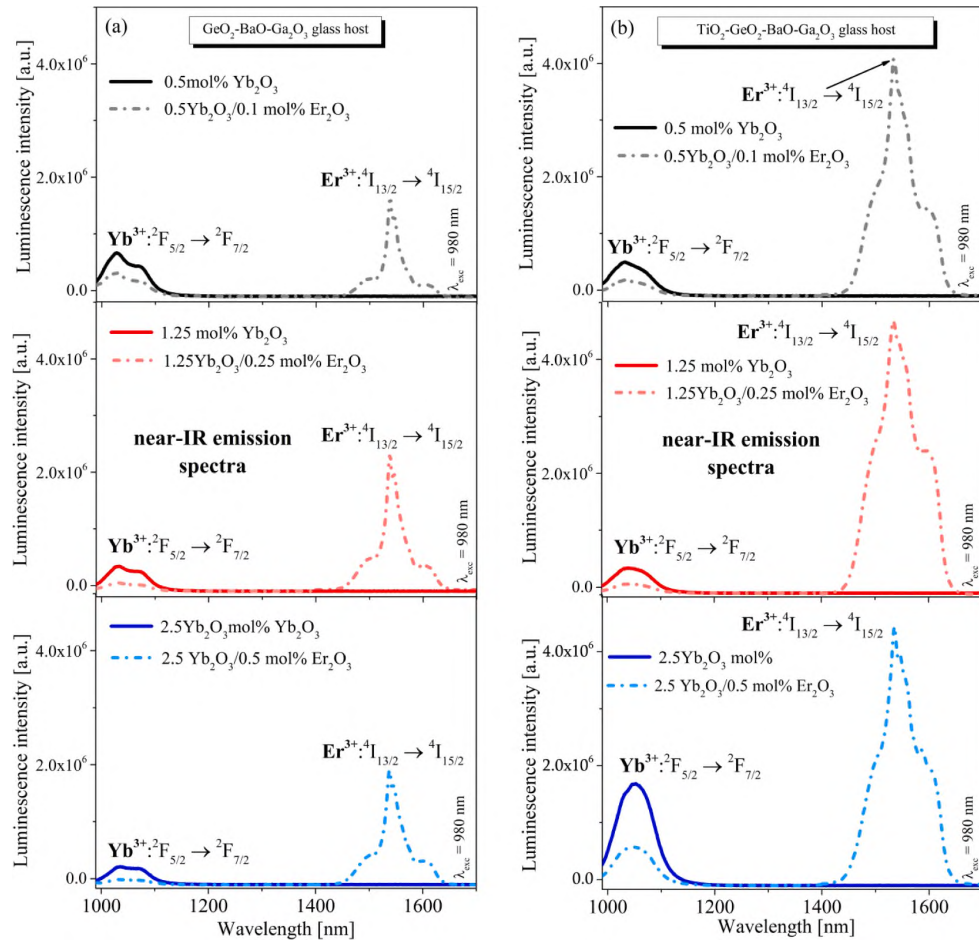


Fig. 7. Near-infrared emission spectra of Yb^{3+} singly (straight line) and $\text{Er}^{3+}/\text{Yb}^{3+}$ co-doped (dashed line) barium gallo-germanate glasses with/without TiO_2 ($\lambda_{\text{exc}} = 980 \text{ nm}$).

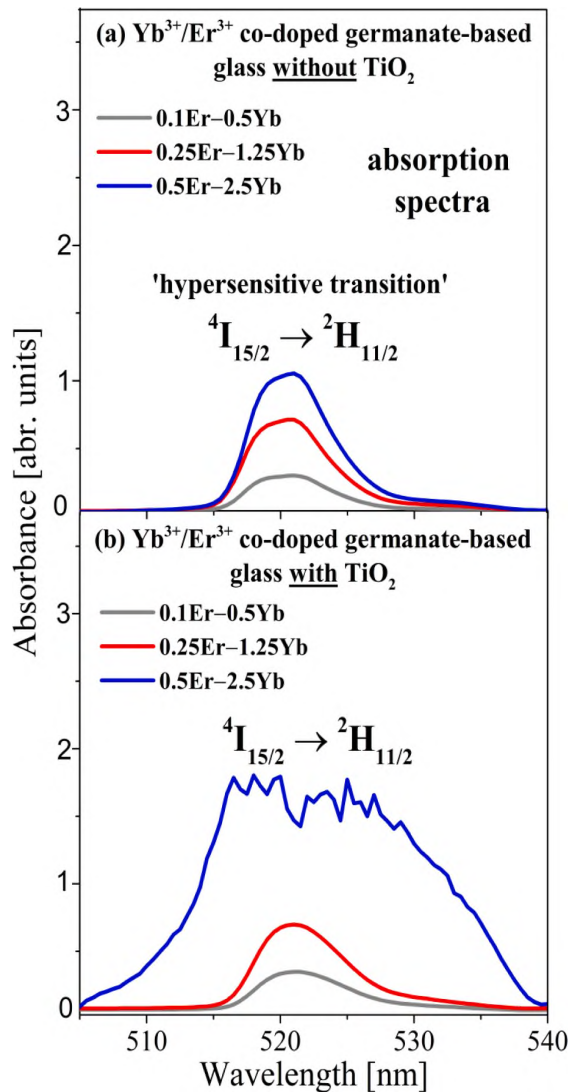


Fig. 8. Hypersensitive transition of erbium ions in $\text{Er}^{3+}/\text{Yb}^{3+}$ co-doped germanate samples without/with titanium dioxide.

Yb^{3+} ions concentration. Trends in luminescence lifetimes and energy transfer efficiency varying with Yb^{3+} and Er^{3+} ions concentration in fabricated glasses are significant from the spectroscopic point of view. Fig. 7 presents near-infrared luminescence spectra of barium gallogermanate glasses with/without TiO_2 doped with Yb^{3+} ions and co-doped with $\text{Yb}^{3+}/\text{Er}^{3+}$ ions under 980 nm excitation wavelength in the wide spectral range from 990 nm to 1700 nm. This experiment motivated us to demonstrate the changes in profiles of emission bands corresponding to the main laser transition of rare earth ions in fabricated two various matrices. Optical changes in their relative intensity confirmed resonant $\text{Yb}^{3+} \rightarrow \text{Er}^{3+}$ energy transfer are quite well observed. The energy transfer efficiency in this paper has a positive correlation with the trend observed in rare earth-doped germanate-based glasses modified by TiO_2 [45].

In the next, the absorption spectra for $\text{Er}^{3+}/\text{Yb}^{3+}$ co-doped samples were measured in the 500–540 nm range, where the band centered at about 520 nm corresponds to the ${}^4\text{I}_{15/2} \rightarrow {}^2\text{H}_{11/2}$ transition, so-called ‘hypersensitive transition’ of Er^{3+} ions [46]. This transition confirms the selection rule $\Delta J \leq 2$, $\Delta L \leq 2$, and $\Delta S = 0$. It is generally accepted that

the Stark splitting is quite well observed for the hypersensitive transition of Er^{3+} , when the sample is not fully amorphous. The absorption result obtained for titanate-germanate sample containing higher concentrations of Yb^{3+} and Er^{3+} ions confirms this hypothesis. For 0.5Er-2.5Yb system with TiO_2 , the absorption band due to the ${}^4\text{I}_{15/2} \rightarrow {}^2\text{H}_{11/2}$ hypersensitive transition of Er^{3+} is unusually intense and broadened as well as the stark splitting is well evidenced (Fig. 8). To summarize this part of the research, the Authors declare that this phenomenon is attributed to semi-crystalline nature of highly-concentrated $\text{Er}^{3+}/\text{Yb}^{3+}$ co-doped sample with titanium dioxide. Based on this conception, Raman spectroscopy was used to study the local structure of the fabricated materials. Fig. 9 shows experimental Raman spectra of titanate-germanate glasses doped with trivalent rare earth ions over the frequency range from 400 cm^{-1} to 1400 cm^{-1} . The photos of obtained Yb^{3+} -doped and $\text{Er}^{3+}/\text{Yb}^{3+}$ -co-doped titanate-germanate samples are presented in Fig. 9a and b. Fig. 9c illustrates the structural evolutions of Yb^{3+} -doped titanate-germanate glasses. The data analysis showed that all samples exhibited two domains at the (1) 400 cm^{-1} – 600 cm^{-1} range and (2) 650 cm^{-1} – 950 cm^{-1} range, respectively. Band in the lower frequency region is characteristic of GeO_4 structural units sharing their corners, where the germanium atom bending is covalently bonded to four bridging oxygens [47–49]. The high-frequency band could be assigned to a GeO_6 structural unit, where the central atom is germanium surrounded by six oxygen atoms [50–52]. Moreover, in the low-frequency region, the sharp band at 460 cm^{-1} is quite well observed for material doped with 2.5 mol% Yb^{3+} ions. Elkhoshkhany et al. [53] observed similar effects for tellurite glasses in the function of Yb_2O_3 . This band is due to the stretching vibrations mode of Yb^{3+} . In general, every material system presents a unique Raman spectrum. Indeed, Fig. 9d very well demonstrates the evolution of structure. Titanium dioxide acts as a network modifier or network former. Due to the small ionic radius of Ti^{4+} ion, it can easily penetrate into the glass network and thus lead to drastic changes in the local structure of the host glass [54]. Structural changes are evidently stronger for $\text{Er}^{3+}/\text{Yb}^{3+}$ co-doped titanate-germanate samples than for Yb^{3+} -doped titanate-germanate. In the analyzed case, the Raman spectra for co-doped titanate-germanate samples containing 0.1Er/0.5Yb and 0.25Er/1.25Yb show a band in the 600 – 800 cm^{-1} range. Based on previous studies, titanium dioxide in the germanate-based glass host generated the destruction of germanate tetrahedra and octahedra units [40]. The broad band at 650 cm^{-1} is attributed to the stretching vibration of Ti-O in the TiO_6 unit. However, more interesting is the fact that further increasing the Er_2O_3 and Yb_2O_3 content causes a significant structural evolution of the obtained material. Interestingly, the Raman spectrum for the sample containing 0.5 mol% Er^{3+} ions and 2.5 mol% Yb^{3+} ions is typical of glass-ceramics. Tiwari et al. [55] observed similar phenomena for alkaline earth based silicate systems. At this moment it should be pointed out that high doping activator concentration (0.5 % Er^{3+} /2.5 % Yb^{3+}) lead to significant changes in the Raman spectra, which are due to modification of glass-network by the presence of TiO_2 and its local structure symmetry breaking. These phenomena are not observed for glass samples without TiO_2 . In our opinion, it could be a disruption role of the TiO_2 on the glass-network with modification of the local crystal field around the rare earth ions playing the role as the optical dopants. It was also well confirmed by the absorption spectra measurements (hypersensitive transitions) presented and discussed here. Similar effects were observed and demonstrated earlier in the case of HfO_2 by Raman and luminescence measurements [56,57]. To further verify the proposed approach to the determination of the partial crystallization phenomena of the synthesized highly-concentrated titanate-germanate samples, an X-ray diffraction analysis has been undertaken.

The literature data shows that ionic size plays a dominant role in determining the chemical durability of lanthanide titanates. A strong correlation is established among chemical composition/structural variation [58]. Fig. 10 shows the X-ray diffraction patterns of GeO_2 - BaO - Ga_2O_3 and TiO_2 - GeO_2 - BaO - Ga_2O_3 singly doped with Yb^{3+} and co-doped

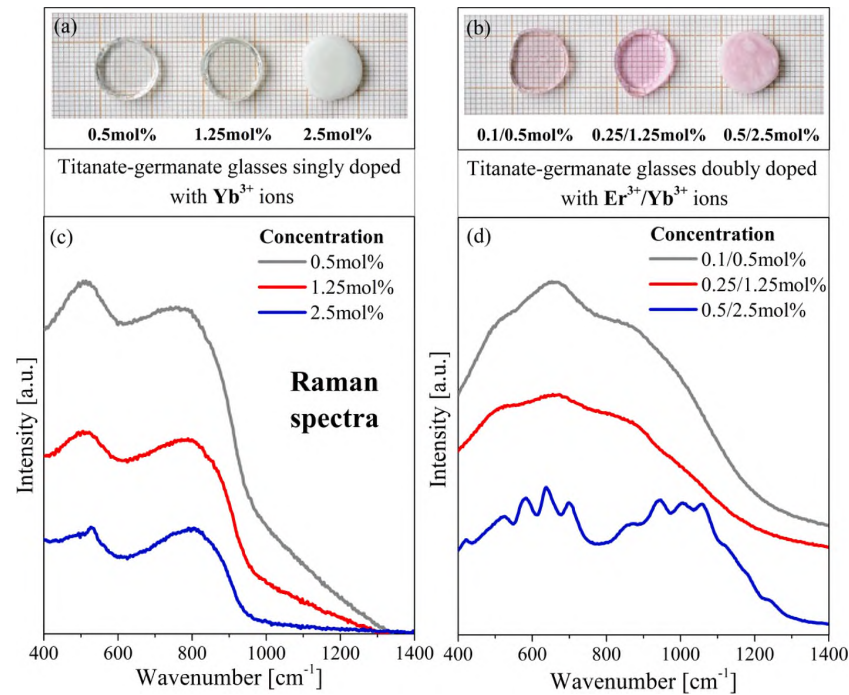


Fig. 9. Room temperature measured Raman spectra of Yb^{3+} and $\text{Er}^{3+}/\text{Yb}^{3+}$ co-doped titanate-germanate samples. Excitation: 633-nm laser line.

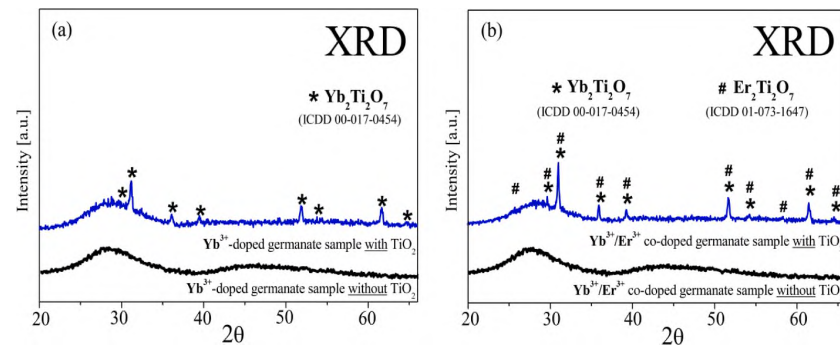


Fig. 10. X-ray diffraction patterns of Yb^{3+} doped (a) and $\text{Yb}^{3+}/\text{Er}^{3+}$ co-doped samples with and without TiO_2 with high content of luminescent rare earths (2.5 mol% Yb_2O_3 and 2.5 mol% $\text{Yb}_2\text{O}_3/0.5$ mol% Er_2O_3).

with $\text{Yb}^{3+}/\text{Er}^{3+}$, where the activator concentrations are the highest. X-ray diffraction patterns for barium gallo-germanate glasses without TiO_2 doped with 2.5 mol% Yb_2O_3 and co-doped with 2.5 mol% $\text{Yb}_2\text{O}_3/0.5$ mol% Er_2O_3 confirmed the absence of the crystalline phase because only two broad humps are observed, which corroborates the amorphous character of the fabricated glasses. Moreover, significant structural changes in the XRD patterns have been observed for samples after introduction 30 mol% TiO_2 to germanate-based glass host. The X-ray diffraction patterns of the titanate-germanate samples doped with 2.5 mol% Yb_2O_3 and co-doped with 2.5 mol% $\text{Yb}_2\text{O}_3/0.5$ mol% Er_2O_3 , in addition to the two maxima characteristics for an amorphous state, presents narrow diffraction lines with half-widths characteristic of the crystalline material. For Yb^{3+} doped sample, the narrow diffraction lines correspond to $\text{Yb}_2\text{Ti}_2\text{O}_7$ crystalline phase (PDF-2, card no 00-017-0454). For $\text{Er}^{3+}/\text{Yb}^{3+}$ co-doped sample, diffraction lines are related to the $\text{Yb}_2\text{Ti}_2\text{O}_7$ (PDF-2, card no 00-017-0454) and $\text{Er}_2\text{Ti}_2\text{O}_7$ (PDF-2, card no 01-073-1647) crystalline phases, respectively. Similar effects were observed previously for highly-concentrated lead borate glasses co-

doped with rare earth ions [59]. In this work, adding 0.5 mol% Er_2O_3 and 2.5 mol% Yb_2O_3 in the $\text{GeO}_2\text{-TiO}_2\text{-BaO-Ga}_2\text{O}_3$ glass shows that designed material is more prone to crystallization, which is unfavorable from the point of view of drawing optical fibers. Experimental results for fabricated glasses suggest that the proper choice of glass host is a critical factor in the success of $\text{Er}^{3+}/\text{Yb}^{3+}$ co-doped glass systems for near-infrared applications. Nevertheless, our results indicated that rare earth ions have a strong impact on the structural properties of titanate-germanate glasses. Considering all the above arguments, further investigations are needed to determine if glass based on $\text{GeO}_2\text{-TiO}_2\text{-BaO-Ga}_2\text{O}_3$ ($\text{GeO}_2\text{:TiO}_2 = 1\text{:}1$) activated with 0.25 mol% Er_2O_3 and 1.25 mol% Yb_2O_3 might be qualified as an attractive candidate for near-infrared photonics applications such as optical amplifier operated in the C (1530–1565 nm) band region in the optical communication window.

4. Conclusions

This paper presents novel results for luminescent $\text{Er}^{3+}/\text{Yb}^{3+}$ co-

doped GeO₂-BaO-Ga₂O₃ (GBG) and TiO₂-GeO₂-BaO-Ga₂O₃ (TGBG) glass systems synthesized by melt quenching technique, which offer important contributions in the field of materials sciences, glass technology, and near-infrared photonic. Particular attention was focused on the influence of pair Er³⁺/Yb³⁺ on physicochemical and near-infrared luminescence properties of fabricated materials evidenced using different experimental techniques. The obtained results which are necessary for knowledge about optical glasses, can be concluded as follows:

1. The optical investigations for fabricated materials indicate that luminescence properties strongly depend on the rare-earth concentration and kind of glass matrix. The integrated emission intensity for Yb³⁺: ²F_{5/2} → ²F_{7/2} transition was reduced in the GBG system, whereas it increases in the presence of TiO₂. For Er³⁺/Yb³⁺ co-doped TGBG glasses, the intensity for Er³⁺: ⁴I_{13/2} → ⁴I_{15/2} transition is about 2-fold enhanced compared to GBG glasses. The emission bandwidth was determined, and their value is close to 31 nm (GBG) and 65 nm (TGBG), co-doped with 2.5 mol% Yb₂O₃ and 0.5 mol% Er₂O₃ respectively. The energy transfer mechanisms between Yb³⁺ to Er³⁺ ions were discussed in detail, and the energy transfer efficiency was calculated to be 64 % for GBG glass and 39 % for TGBG glass. It is clearly seen that intensity of Er³⁺: ⁴I_{15/2} → ²H_{11/2} hypersensitive transition of Er³⁺ ions increased with increasing rare earth ions concentration. The Stark splitting was observed for titanate-germanate sample co-doped with 0.5 mol% Er₂O₃ and 2.5 mol% Yb₂O₃ indicated on structural changes.

2. The second part was concerned on the impact of pair Er³⁺/Yb³⁺ ions on the local structure of synthesized luminescent glasses. The registered Raman spectrum for the highly doped sample was typical for glass-ceramic. Furthermore, the structural characterization showed that the increasing concentration of the rare-earth ions (above 1.25 mol% Yb₂O₃ and 0.25 mol% Er₂O₃) leads to the partial crystallization of titanate-germanate systems. It is consistent with X-ray diffraction analysis, where the formation of Yb₂Ti₂O₇ and Er₂Ti₂O₇ crystalline phases was confirmed.

In consequence, based on theoretical and experimental results we indicated that titanate-germanate glasses (TiO₂:GeO₂ = 1:1) co-doped with 0.25 mol% Er₂O₃ and 1.25 mol% Yb₂O₃ with better near-IR optical properties could be potentially useful in constructing broadband optical fiber amplifiers and tunable fiber lasers in the optical telecommunication window operating at 1.5 μm.

CRedit authorship contribution statement

Karolina Kowalska: Conceptualization; Data curation; Formal analysis, Investigation; Methodology; Software; Validation; Visualization; Writing - original draft. **Marta Kuwik:** Investigation. **Tomasz Goryczka:** Investigation. **Joanna Pisarska:** Conceptualization, Formal analysis. **Wojciech A. Pisarski:** Conceptualization, Formal analysis, Funding acquisition, Project administration, Supervision, Writing - review & editing.

Declaration of competing interest

The authors declare that they have no known competing financial interests or personal relationships that could have appeared to influence the work reported in this paper.

Data availability

Data will be made available on request.

Acknowledgment

This work was supported by the National Science Centre (Poland) [2018/31/B/ST8/00166].

References

- [1] R.J. Mears, L. Reekie, I.M. Jauncey, D.N. Payne, Low-noise erbium-doped fibre amplifier at 1.54 μm, *Electr. Lett.* 23 (1987) 1026–1028, <https://doi.org/10.1049/el:19870719>.
- [2] S. Tanabe, Rare-earth-doped glasses for fiber amplifiers in broadband telecommunication, *Compt Rend. Chim.* 5 (2002) 815–824., [https://doi.org/10.1016/S1631-0748\(02\)01449-2](https://doi.org/10.1016/S1631-0748(02)01449-2).
- [3] N. Luevarasirikul, S. Sarachai, M. Djamal, J. Kaewkhao, Er³⁺-doped barium sodium borate glasses development for 1.54 μm broadband amplifier and optical laser, *Optik* 266 (2022) 169557, <https://doi.org/10.1016/j.ijleo.2022.169557>.
- [4] J.A. Johnson, C.J. Benmore, D. Holland, J. Du, B. Beunee, A. Mekki, Influence of rare-earth ions on SiO₂-Na₂O-RE₂O₃ glass structure, *J. Phys.: Condens. Matter* 23 (2011), 065404, <https://doi.org/10.1088/0953-8984/23/6/065404>.
- [5] W. Zhang, J. Liu, G. Zhou, C. Xia, S. Liang, Y. Chen, Z. Hou, Optical properties of the Yb/Er co-doped silica glass prepared by laser sintering technology, *Opt. Mater. Express* 7 (2017) 1708–1715, <https://doi.org/10.1364/OME.7.001708>.
- [6] S. Hraiech, M. Ferid, Y. Guyot, G. Boulon, Structural and optical studies of Yb³⁺, Er³⁺ and Er³⁺/Yb³⁺ co-doped phosphate glasses, *J. Rare Earths* 31 (2013) 685–693, [https://doi.org/10.1016/S1002-0721\(12\)60343-3](https://doi.org/10.1016/S1002-0721(12)60343-3).
- [7] R.A. Talewar, Sk. Mahamuda, K. Swapna, M. Venkateswarlu, A.S. Rao., Sensitization of Er³⁺ NIR emission using Yb³⁺ ions in alkaline-earth chloro borate glasses for fiber laser and optical fiber amplifier applications, *Mat. Res. Bull.* 136 (2021), 111144, <https://doi.org/10.1016/j.materresbull.2020.111144>.
- [8] Q. Nie, L. Lu, T. Xu, S. Dai, X. Shen, X. Liang, X. X. Zhang, X. Zhang, Upconversion luminescence of Er³⁺/Yb³⁺-codoped sodium-germanium-bismuth glasses, *J. Phys. Chem. Solids* 67 (2006) 2345–2350, <https://doi.org/10.1016/j.jpcs.2006.05.047>.
- [9] F. Tan, P. Xu, D. Zhou, L. Wang, Q. Yang, X. Song, K. Han, 1.53 μm luminescent properties and energy transfer processes of Er³⁺/Yb³⁺ co-doped bismuth germanate glass laser material, *J. Lumin.* 239 (2021), 118300, <https://doi.org/10.1016/j.jlumin.2021.118300>.
- [10] E. Kolobkova, A. Alkhlef, A. Yasukevich, A. Babkina, Spectroscopic and lasing properties of Er³⁺/Yb³⁺-doped fluorophosphate glass with small additives of phosphates, *Opt. Mater. Express* 9 (2019) 3666–3679, <https://doi.org/10.1364/OME.9.003666>.
- [11] W.A. Pisarski, K. Kowalska, M. Kuwik, J. Polak, E. Pietrasik, T. Goryczka, J. Pisarska, Novel Multicomponent Titanate-Germanate Glasses: Synthesis, Structure, Properties, Transition Metal, and Rare Earth Doping, *Materials* 13 (2020) 4422. Doi: 10.3390/ma13194422.
- [12] W.A. Pisarski, K. Kowalska, M. Kuwik, J. Pisarska, J. Dorosz, J. Żmojda, M. Kochanowicz, D. Dorosz, Nd³⁺ doped titanate-germanate glasses for near-IR laser applications, *Opt. Mat. Expr.* 12 (2022) 2912–2926, <https://doi.org/10.1364/OME.463478>.
- [13] K. Kowalska, M. Kuwik, J. Pisarska, M. Leśniak, D. Dorosz, M. Kochanowicz, J. Żmojda, J. Dorosz, W.A. Pisarski, Influence of TiO₂ concentration on near-infrared luminescence of Er³⁺ ions in barium gallo-germanate glasses, *J. Mat. Res. Technol.* 21 (2022) 4761–4772, <https://doi.org/10.1016/j.jmrt.2022.11.081>.
- [14] J. Pisarska, K. Kowalska, M. Kuwik, J. Dorosz, M. Kochanowicz, J. Żmojda, D. Dorosz, W.A. Pisarski, Optical Properties of titanate-germanate glasses containing Ho³⁺ ions, *Mat. Res. Bull.* 166 (2023), 112353, <https://doi.org/10.1016/j.materresbull.2023.112353>.
- [15] Z. Zhao, B. Zhang, Y. Gong, Y. Ren, M. Huo, Y. Wang, Concentration effect of Yb³⁺ ions on the spectroscopic properties of high-concentration Er³⁺/Yb³⁺ co-doped phosphate glasses, *J. Mol. Struct.* 1216 (2020), 128322, <https://doi.org/10.1016/j.molstruc.2020.128322>.
- [16] K. Annapoorani, K. Maheshwaran, S. ArunKumar, N. Suriya Murthy, T. Soukka, K. Marimuthu, Structural and spectroscopic behavior of Er³⁺/Yb³⁺ co-doped lithium telluroborate glasses, *Phys. B. Cond. Mat.* 457 (2015) 66–77, <https://doi.org/10.1016/j.physb.2014.09.043>.
- [17] M.A. Melkumov, A.Y. Laptsev, M.V. Yashkov, A.N. Guryanov, I.A. Bufetov, Effects of Yb³⁺ and Er³⁺ concentrations and doping procedure on excitation transfer efficiency in Er-Yb doped phosphosilicate fibers, *Inorg. Mater.* 46 (2010) 299–303, <https://doi.org/10.1134/S0020168510030167>.
- [18] W.A. Pisarski, L. Grobelny, J. Pisarska, R. Lisiecki, W. Ryba-Romanowski, Spectroscopic properties of Yb³⁺ and Er³⁺ ions in heavy metal glasses, *J. All. Compd.* 509 (2011) 8088–8092, <https://doi.org/10.1016/j.jallcom.2011.05.056>.
- [19] M.J.V. Bell, W.G. Quirino, S.L. Oliveira, D.F. de Sousa, L.A.O. Nunes, Cooperative luminescence in Yb³⁺-doped phosphate glasses, *J. Phys.: Condens. Matter* 15 (2003) 4877, <https://doi.org/10.1088/0953-8984/15/27/319>.
- [20] F. Auzel, P. Goldner, G.F. de Sa, Weak clustering and self-quenching in a fluorophosphate glass doped by Yb³⁺ and Er³⁺ organic precursors, *J. Non. Cryst. Solids* 265 (2000) 185–188, [https://doi.org/10.1016/S0022-3093\(99\)00960-6](https://doi.org/10.1016/S0022-3093(99)00960-6).
- [21] K. Linganna, S. Ju, B. Kim, W.T. Han, V. Venkatramu, C.K. Jayasankar, Spectroscopic Properties of Yb³⁺-Doped Silicate Glasses, *Z. Phys. Chem.* 232 (2018) 51–60, <https://doi.org/10.1515/zpch-2017-0941>.
- [22] A. Ali, Y.S. Rammah, M.H. Shaaban, The influence of TiO₂ on structural, physical and optical properties of B₂O₃-TeO₂-Na₂O-CaO glasses, *J. Non. Cryst. Solids* 514 (2019) 52–59, <https://doi.org/10.1016/j.jnoncrysol.2019.03.030>.
- [23] C.h. Basavapoornima, T. Maheswari, S.R. Depuru, C.K. Jayasankar, Sensitizing effect of Yb³⁺ ions on photoluminescence properties of Er³⁺ ions in lead phosphate glasses: Optical fiber amplifiers, *Opt. Mat.* 86 (2018) 256–269, <https://doi.org/10.1016/j.optmat.2018.09.027>.
- [24] M. Liao, L. Wen, H. Zhao, Y. Fang, H. Sun, L. Hu, Mechanisms of Yb³⁺ sensitization to Tm³⁺ for blue upconversion luminescence in fluorophosphate glass, *Mat. Lett.* 61 (2007) 470–472, <https://doi.org/10.1016/j.matlet.2006.04.090>.

- [25] N. Rakov, A.R. Terto, G.S. Maciel, Yb³⁺ sensitized Er³⁺ doped Gd₂SiO₅ powders prepared by combustion synthesis: Up-conversion fluorescence emission at visible from near-infrared, *Ceram. Int.* 41 (2015) 13348–13353, <https://doi.org/10.1016/j.ceramint.2015.07.120>.
- [26] N. Rakov, G.S. Maciel, Enhancement of 1.5 μm fluorescence signal from Er³⁺ due to Yb³⁺ in yttrium silicate powders pumped at 975 and 808 nm, *Methods Appl. Fluoresc.* 7 (2018), 015003, <https://doi.org/10.1088/2050-6120/aae475>.
- [27] X. Shi-Qing, F. Da-Wei, Z. Zai-Xuan, Z. Shi-Long, Z. Li-Yan, W. Bao-Ling, J. Zhong-Hong, Host Dependent Thermal Stability and Frequency Upconversion of Er³⁺-Doped Heavy Metal Oxyfluoride Germanate Glasses, *Chin. Phys. Phys.* 14 (2005) 2246–2250, <https://doi.org/10.1088/1009-1963/14/11/018>.
- [28] S. Balaji, D. Ghosh, K. Biswas, A.R. Allu, G. Gupta, K. Annapurna, Insights into Er³⁺ ↔ Yb³⁺ energy transfer dynamics upon infrared ~1550 nm excitation in a low phonon fluoro-tellurite glass system, *J. Lumin.* 187 (2017) 441–448, <https://doi.org/10.1016/j.jlumin.2017.03.059>.
- [29] C.H. Yeh, C.W. Chow, J.H. Chen, K.H. Chen, S.S. Lu, Broadband C-plus L-band CW wavelength-tunable fiber laser based on hybrid EDFA and SOA, *Opt. Fib. Techn.* 19 (2013) 359–361, <https://doi.org/10.1016/j.yofte.2013.04.006>.
- [30] A.S. Sadik, F.E. Durak, A. Altuncu, Widely tunable erbium doped fiber ring laser based on loop and double-pass EDFA design, *Opt. Las. Techn.* 124 (2020), 105979, <https://doi.org/10.1016/j.optlastec.2019.105979>.
- [31] T.S. Goncalves, R.J. Moreira Silva, M. de Oliveira Junior, C.R. Ferrari, G.Y. Poirier, H. Eckert, Structure-property relations in new fluorophosphate glasses singly and co-doped with Er³⁺ and Yb³⁺, *Mater. Chem. Phys.* 157 (2015) 45–55, <https://doi.org/10.1016/j.matchemphys.2015.03.012>.
- [32] G. Lakshminarayana, A.N. Meza-Rocha, O. Soriano-Romero, U. Caldino, A. Lira, D. E. Lee, J. Yoon, T. Park, Assessment of optical and fluorescence aspects of Er³⁺-doped multicomponent B₂O₃ glasses as active media for 1.532 μm near-infrared optical amplifiers, *J. Mat. Res. Techn.* 18 (2022) 3457–3477.
- [33] L.M. Marcondes, C.R. de Cunha, B.P. de Sousa, S. Maestri, R.R. Goncalves, F. C. Cassanjes, G.Y. Poirier, Thermal and spectroscopic properties studies of Er³⁺-doped and Er³⁺/Yb³⁺-codoped niobium germanate glasses for optical applications, *J. Lumin.* 205 (2019) 487–494, <https://doi.org/10.1016/j.jlumin.2018.09.046>.
- [34] S.F. Li, Q.Y. Zhang, Y.P. Lee, Absorption and photoluminescence properties of Er-doped and Er/Yb codoped soda-silicate laser glasses, *Appl. Phys.* 96 (2004) 4746–4540, doi.org/10.1063/1.1792388.
- [35] A. Langar, C. Bouzidi, H. Elhouichet, M. Férid, Er-Yb codoped phosphate glasses with improved gain characteristics for an efficient 1.55 μm broadband optical amplifiers, *J. Lumin.* 148 (2014) 249–255, <https://doi.org/10.1016/j.jlumin.2013.12.008>.
- [36] L.M. Marcondes, C.R.D. Cunha, B.P.D. Sousa, S. Maestri, R.R. Gonçalves, F. C. Cassanjes, G.Y. Poirier, Thermal and spectroscopic properties studies of Er³⁺-doped and Er³⁺/Yb³⁺-codoped niobium germanate glasses for optical applications, *J. Lumin.* 205 (2019) 487–494, <https://doi.org/10.1016/j.jlumin.2018.09.046>.
- [37] I. Jlassi, H. Elhouichet, M. Férid, C. Barthou, Judd-Ofelt analysis and improvement of thermal and optical properties of tellurite glasses by adding P₂O₅, *J. Lumin.* 130 (2010) 2394–2401, <https://doi.org/10.1016/j.jlumin.2010.07.026>.
- [38] F.H. ElBatal, M.A. Marzouk, H.A. ElBatal, Optical and crystallization studies of titanium dioxide doped sodium and potassium silicate glasses, *J. Mol. Struct.* 1121 (2016) 54–59, <https://doi.org/10.1016/j.molstruc.2016.05.052>.
- [39] K. Morinaga, H. Yoshida, H. Takebe, Compositional Dependence of Absorption Spectra of Ti³⁺ in Silicate, Borate, and Phosphate Glasses, *J. Am. Ceram. Soc.* 77 (1994) 3113–3118, <https://doi.org/10.1111/j.1151-2916.1994.tb04557.x>.
- [40] K. Kowalska, M. Kuwik, J. Pisarska, M. Sitarz, W.A. Pisarski, Raman and Infrared Spectroscopy of Barium-Gallo Germanate Glasses Containing B₂O₃/TiO₂, *Materials* 16 (2023) 1516, <https://doi.org/10.3390/ma16041516>.
- [41] M. Kuwik, K. Kowalska, J. Pisarska, M. Kochanowicz, J. Żmójda, J. Dorosz, D. Dorosz, W. A. Pisarski, Influence of TiO₂ concentration on near-infrared emission of germanate glasses doped with Tm³⁺ and Tm³⁺/Ho³⁺ ions, *Ceram. Int.* (2023) In press. <https://doi.org/10.1016/j.ceramint.2023.03.305>.
- [42] M. Kuwik, K. Kowalska, J. Pisarska, W.A. Pisarski, Experimental and theoretical studies on NIR luminescence of titanate-germanate glasses doped with Pr³⁺ and Tm³⁺ ions, *J. Am. Ceram. Soc.* 106 (2023) 7460–7472, <https://doi.org/10.1111/jace.19378>.
- [43] W.A. Pisarski, K. Kowalska, M. Kuwik, J. Pisarska, D. Dorosz, M. Kochanowicz, J. Żmójda, J. Dorosz, Enhanced mid-IR luminescence of Er³⁺ ions at 2.7 μm in TiO₂-GeO₂-BaO-Ga₂O₃ glasses, *J. Lumin.* 265 (2024) 120227. <https://doi.org/10.1016/j.jlumin.2023.120227>.
- [44] M. Ajroud, M. Haouari, H. Ben Ouada, H. Maaref, A. Brenier, B. Champagnon, Energy transfer processes in (Er³⁺-Yb³⁺)-codoped germanate glasses for mid-infrared and up-conversion applications, *Mat. Sci. Eng. C* 26 (2006) 523–529, <https://doi.org/10.1016/j.msec.2005.10.015>.
- [45] K. Kowalska, M. Kuwik, J. Pisarska, W.A. Pisarski, Near-IR Luminescence of Rare-Earth Ions (Er³⁺, Pr³⁺, Ho³⁺, Tm³⁺) in Titanate-Germanate Glasses under Excitation of Yb³⁺, *Materials* 15 (2022) 3660, <https://doi.org/10.3390/ma15103660>.
- [46] J. Pisarska, W.A. Pisarski, T. Goryczka, R. Lisiecki, W. Ryba-Romanowski, Thermal analysis and near-infrared luminescence of Er³⁺-doped lead phosphate glasses modified by PbF₂, *J. Lumin.* 160 (2015) 57–63, <https://doi.org/10.1016/j.jlumin.2014.11.029>.
- [47] F. Calzavara, M. Allix, M. Dussauze, V. Jubera, M. Nalin, M.T. Cardinal, E. Fargin, Glass forming regions, structure and properties of lanthanum barium germanate and gallate glasses, *J. Non Cryst. Solids* 571 (2021), 121064, <https://doi.org/10.1016/j.jnoncrysol.2021.121064>.
- [48] J.M. Jewell, P.L. Higby, I.D. Aggarwal, Properties of BaO-R₂O₃-Ga₂O₃-GeO₂ (R = Y, Al, La, and Gd) glasses, *J. Am. Ceram. Soc.* 77 (1994) 697–700, <https://doi.org/10.1111/j.1151-2916.1994.tb05351.x>.
- [49] S.S. Bayya, B.B. Harbison, J.S. Sanghera, I.D. Aggarwal, BaO-Ga₂O₃-GeO₂ glasses with enhanced properties, *J. Non-Cryst. Solids* 212 (1997) 198–207, [https://doi.org/10.1016/S0022-3093\(96\)00658-8](https://doi.org/10.1016/S0022-3093(96)00658-8).
- [50] G. Tang, D. Zhang, F. Zhang, W. Zhao, Q. Qian, Z. Yang, Structure and luminescence properties of Tm³⁺ doped barium gallo-germanate glass tailored by Lu₂O₃, *J. Lumin.* 257 (2023) 119771, <https://doi.org/10.1016/j.jlumin.2023.119771>.
- [51] E.I. Kamitsos, Y.D. Yiannopoulos, M.A. Karakassides, G.D. Chryssikos, H. Jain, Raman and Infrared Structural Investigation of xRb₂O(1-x)GeO₂ Glasses, *J. Phys. Chem.* 100 (1996) 11755–11765, <https://doi.org/10.1021/jp960434a>.
- [52] D.A. Mc Keown, C.I. Merzbacher, Raman spectroscopic studies of BaO-Ga₂O₃-GeO₂ glasses, *J. Non-Cryst. Solids* 183 (1995) 61–72, [https://doi.org/10.1016/0022-3093\(94\)00648-2](https://doi.org/10.1016/0022-3093(94)00648-2).
- [53] N. Elkhoshkhany, S. Marzouk, M. El-Sherbiny, A. Ahmed, Properties of tellurite glass doped with ytterbium oxide for optical applications, *J. Mat. Sci. Mat. Elect.* 30 (2019) 6963–6976, <https://doi.org/10.1007/s10854-019-01013-9>.
- [54] M. Kaur, A. Singh, V. Thakur, L. Singh, Effect of TiO₂ substitution on optical and structural aspects of phosphate glasses, *J. Mol. Struct.* 1089 (2015) 95–101, <https://doi.org/10.1016/j.molstruc.2015.02.012>.
- [55] B. Tiwari, M. Pandey, S.C. Gadgari, G.P. Kothiyal, Synthesis and structural studies of multi-component strontium zinc silicate glass-ceramics, *AIP Conf. Proc.* 1512 (2013) 568–569, <https://doi.org/10.1063/1.4791164>.
- [56] L. Zampedri, G.C. Righini, H. Portales, S. Pelli, G. Nunzi Conti, M. Montagna, M. Mattarelli, R.R. Gonçalves, M. Ferrari, A. Chiasera, C. Armellini, Sol-Gel-Derived Er-activated SiO₂-HfO₂ Planar Waveguides for 1.5 μm application, *J. Non-Cryst. Solids* 345&346 (2004) 580–584, <https://doi.org/10.1016/j.jnoncrysol.2004.08.088>.
- [57] G.C. Righini, S. Berneschi, G. Nunzi Conti, S. Pelli, E. Moser, R. Retoux, P. Féron, R. R. Gonçalves, G. Speranza, Y. Jestin, M. Ferrari, A. Chiasera, A. Chiappini, C. Armellini, Er³⁺-doped silica-hafnia films for optical waveguides and spherical resonators, *J. Non-Cryst. Solids* 355 (2009) 1853–1860. <https://doi.org/10.1016/j.jnoncrysol.2008.12.022>.
- [58] K. Yang, P. Lei, T. Yao, B. Gong, Y. Wang, M. Li, J. Wang, J. Lian, A systematic study of lanthanide titanates (A₂Ti₂O₇) chemical durability: corrosion mechanisms and control parameters, *Corr. Sci.* 185 (2021), 109394, <https://doi.org/10.1016/j.corsci.2021.109394>.
- [59] L. Zur, A. Kos, A. Górny, M. Sotys, E. Pietrasik, J. Pisarska, T. Goryczka, W. A. Pisarski, Influence of acceptor concentration on crystallization behavior and luminescence properties of lead borate glasses co-doped with Dy³⁺ and Tb³⁺ ions, *J. All. Compd.* 749 (2018) 561–566, <https://doi.org/10.1016/j.jallcom.2018.03.282>.

8. Podsumowanie

Wyniki przedstawione w rozprawie doktorskiej wskazują, że odpowiedni dobór składu chemicznego matrycy szklistej oraz aktywnych domieszek jonów ziem rzadkich, optymalizacja procesu syntezy pozwala na uzyskanie nowego materiału optycznego o specyficznych parametrach luminescencyjnych w zakresie podczerwieni. Dzięki szczegółowym i wnikliwym pracom eksperymentalnym udało się znacznie poszerzyć i uzupełnić wiedzę na temat szkieł nieorganicznych, zawierających w składzie TiO_2 . Wiedza ta pozwoliła na przezwycięzenie silnej tendencji do krystalizacji szkieł tytanowych i otrzymanie szkieł w pełni amorficznych.

Celem rozprawy było otrzymanie i zbadanie właściwości fizykochemicznych szkieł tytanowo-germanianowych, ze szczególnym uwzględnieniem właściwości luminescencyjnych w podczerwieni. Celem było w szczególności wykazanie wpływu stężenia TiO_2 na budowę oraz właściwości szkieł zawierających jony ziem rzadkich i emitujących promieniowanie podczerwone. W opracowanych wieloskładnikowych szklach tlenkowych, dwutlenek tytanu TiO_2 w zależności od stężenia nie tylko pełni rolę składnika szkłotwórczego, ale również modyfikuje właściwości fizykochemiczne matrycy. Realizacja założeń i celów rozprawy obejmowała wiele etapów: opracowanie składu chemicznego, dobór aktywnych optycznie domieszek i syntezę nowych szkieł, potwierdzenie amorficznej budowy wewnętrznej, zbadanie właściwości termicznych, strukturalnych i optycznych. Wyboru aktywnych optycznie domieszek dokonano z uwzględnieniem ich schematów energetycznych, sprzyjających emisji w zakresie podczerwieni.

Na podstawie analizy zgromadzonych danych eksperymentalnych i opracowanego na ich podstawie cyklu publikacji naukowych **P1-P12** wchodzących w skład rozprawy doktorskiej do najważniejszych osiągnięć można zaliczyć:

- Otrzymanie serii nowych w pełni amorficznych, wieloskładnikowych szkieł tytanowo-germanianowych $\text{TiO}_2\text{-Ga}_2\text{O}_3\text{-BaO-Ga}_2\text{O}_3$ pojedynczo/podwójnie aktywowanych jonami ziem rzadkich i/lub jonami metali przejściowych (synteza całkowicie amorficznych materiałów zawierających znaczne stężenie TiO_2 jest niezwykle ważnym osiągnięciem z punktu widzenia technologicznego, ponieważ takie układy cechuje duża skłonność do krystalizacji),

- Przeprowadzenie pełnej charakterystyki strukturalnej, termicznej i optycznej szkieł tytanowo-germanianowych. Określono między innymi, nieznanym dotychczas w literaturze, wpływ stężenia TiO_2 na otrzymywanie, budowę, stabilność termiczną oraz właściwości szkieł przy użyciu różnorodnych technik eksperymentalnych: DSC, XRD, EPR, IR, Ramana i spektroskopii optycznej,
- Wykazanie zmian lokalnego otoczenia wokół domieszki optycznie aktywnej oraz wzrostu charakteru kowalencyjnego wiązania w funkcji zawartości TiO_2 w szklach z wykorzystaniem jonów pełniących rolę sond spektroskopowych,
- Uzyskanie znacznego poszerzenia i wzmocnienia pasm emisyjnych jonów ziem rzadkich w zakresie bliskiej i średniej podczerwieni w badanych szklach w wyniku obecności TiO_2 , który może pełnić rolę składnika szkłotwórczego lub modyfikującego w zależności od jego stężenia,
- Poznanie procesów relaksacji promienistej i niepromienistej zachodzących w szklach tytanowo-germanianowych,
- Określenie parametrów spektroskopowych i laserowych jonów ziem rzadkich w funkcji stężenia TiO_2 , związanych z następującymi przejściami: ${}^4\text{F}_{3/2} \rightarrow {}^4\text{I}_{9/2}$ (Nd^{3+}) przy $1,06 \mu\text{m}$, ${}^4\text{I}_{13/2} \rightarrow {}^4\text{I}_{15/2}$ (Er^{3+}) przy $1,5 \mu\text{m}$, ${}^1\text{D}_2 \rightarrow {}^1\text{G}_4$ (Pr^{3+}) przy $1,5 \mu\text{m}$ i ${}^3\text{F}_4 \rightarrow {}^3\text{H}_6$ (Tm^{3+}) przy $1,8 \mu\text{m}$ oraz ${}^5\text{I}_7 \rightarrow {}^5\text{I}_8$ (Ho^{3+}) przy $2 \mu\text{m}$, na podstawie badań eksperymentalnych wykorzystując pomiary widm absorpcji, luminescencji i kinetyki ich zaniku oraz obliczeń z teorii Judda-Ofelta i modelu Inokuti-Hirayama,
- Uzyskanie wzmocnionej szerokopasmowej luminescencji w zakresie bliskiej i średniej podczerwieni przy $1,5 \mu\text{m}$, $1,8 \mu\text{m}$, $2 \mu\text{m}$ i $2,7 \mu\text{m}$ w układach szkieł tytanowo-germanianowych z dużą zawartością TiO_2 , związanej z przejściami jonów ziem rzadkich: ${}^4\text{I}_{13/2} \rightarrow {}^4\text{I}_{15/2}$ (Er^{3+}), ${}^3\text{F}_4 \rightarrow {}^3\text{H}_6$ (Tm^{3+}), ${}^5\text{I}_7 \rightarrow {}^5\text{I}_8$ (Ho^{3+}) oraz ${}^4\text{I}_{11/2} \rightarrow {}^4\text{I}_{13/2}$ (Er^{3+}),
- Wyjaśnienie mechanizmu procesu transferu energii wzbudzenia oraz określenie jego wydajności w funkcji stężenia TiO_2 w układach tytanowo-germanianowych domieszkowanych podwójnie jonami ziem rzadkich: $\text{Yb}^{3+}/\text{Pr}^{3+}$, $\text{Yb}^{3+}/\text{Tm}^{3+}$, $\text{Yb}^{3+}/\text{Er}^{3+}$, $\text{Yb}^{3+}/\text{Ho}^{3+}$, określenie wpływu stężenia jonów donora (Yb^{3+}) oraz akceptora (Er^{3+}) na budowę i właściwości luminescencyjne szkieł,

- Dokonanie wyboru szkieł tytanowo-germanianowych z jonami ziem rzadkich o najlepszych parametrach spektroskopowych i laserowych oraz wskazanie ich potencjalnego zastosowania w fotonice (realizacja badań w ramach rozprawy doktorskiej pozwoliła na wskazanie układów szkieł, z których możliwe będzie wyciąganie włókien szklanych do zastosowań światłowodowych).

9. Załączniki

9.1. Dorobek naukowy

Wykaz publikacji wchodzących w skład rozprawy doktorskiej

1. Wojciech A. Pisarski, **Karolina Kowalska**, Marta Kuwik, Justyna Polak, Ewa Pietrasik, Tomasz Goryczka, Joanna Pisarska, Novel multicomponent titanate-germanate glasses: synthesis, structure, properties, transition metal, and rare earth doping, *Materials* 13 (2020) 4422
2. **Karolina Kowalska**, Marta Kuwik, Justyna Polak, Joanna Pisarska, Wojciech A. Pisarski, EPR and optical spectroscopy of Cr³⁺ ions in barium gallo-germanate glasses containing B₂O₃/TiO₂, *Journal of Luminescence* 245 (2022) 118775
3. **Karolina Kowalska**, Marta Kuwik, Joanna Pisarska, Maciej Sitarz, Wojciech A. Pisarski, Raman and infrared spectroscopy of barium-gallo germanate glasses containing B₂O₃/TiO₂, *Materials* 16 (2023) 1516
4. **Karolina Kowalska**, Ewa Pietrasik, Marta Kuwik, Joanna Pisarska, Tomasz Goryczka, Wojciech A. Pisarski, Influence of titanium dioxide concentration on thermal properties of germanate based glasses, *Journal of Thermal Analysis and Calorimetry* (2024)
5. Wojciech A. Pisarski, **Karolina Kowalska**, Marta Kuwik, Joanna Pisarska, Jan Dorosz, Jacek Żmojda, Marcin Kochanowicz, Dominik Dorosz, Nd³⁺ doped titanate-germanate glasses for near-IR laser applications, *Optical Materials Express* 12 (2022) 2912-2926
6. **Karolina Kowalska**, Marta Kuwik, Joanna Pisarska, Magdalena Leśniak, Dominik Dorosz, Marcin Kochanowicz, Jacek Żmojda, Jan Dorosz, Wojciech A. Pisarski, Influence of TiO₂ concentration on near-infrared luminescence of Er³⁺ ions in barium gallo-germanate glasses, *Journal of Materials Research and Technology* 21 (2022) 4761-4772
7. Wojciech A. Pisarski, **Karolina Kowalska**, Marta Kuwik, Joanna Pisarska, Dominik Dorosz, Marcin Kochanowicz, Jacek Żmojda, Jan Dorosz, Enhanced mid-IR luminescence of Er³⁺ ions at 2.7 μm in TiO₂-GeO₂-BaO-Ga₂O₃ glasses, *Journal of Luminescence* 265 (2024) 120227
8. Joanna Pisarska, **Karolina Kowalska**, Marta Kuwik, Jan Dorosz, Marcin Kochanowicz, Jacek Żmojda, Dominik Dorosz, Wojciech A. Pisarski, Optical properties of titanate-germanate glasses containing Ho³⁺ ions, *Materials Research Bulletin* 166 (2023) 112353
9. Marta Kuwik, **Karolina Kowalska**, Joanna Pisarska, Wojciech A. Pisarski, Experimental and theoretical studies on NIR luminescence of titanate-germanate glasses doped with Pr³⁺ and Tm³⁺ ions, *Journal of the American Ceramic Society* 106 (2022) 7460-7472

10. **Karolina Kowalska**, Marta Kuwik, Joanna Pisarska, Wojciech A. Pisarski, Thulium-doped titanate-germanate glasses for infrared photonics, *Journal of Luminescence* 272 (2024) 120649

11. **Karolina Kowalska**, Marta Kuwik, Joanna Pisarska, Wojciech. A. Pisarski, Near-IR luminescence of rare-earth ions (Er^{3+} , Pr^{3+} , Ho^{3+} , Tm^{3+}) in titanate-germanate glasses under excitation of Yb^{3+} , *Materials* 15 (2022) 3660

12. **Karolina Kowalska**, Marta Kuwik, Tomasz Goryczka, Joanna Pisarska, Wojciech A. Pisarski, The impact of pair $\text{Er}^{3+}/\text{Yb}^{3+}$ on titanate-germanate glasses: Physicochemical and near-infrared luminescence investigations, *Materials Science and Engineering: B* 301 (2024) 117117

Wykaz pozostałych publikacji

1. **Karolina Kowalska**, Marta Kuwik, Joanna Pisarska, Dominik Dorosz, Wojciech A. Pisarski, Wieloskładnikowe szkła tytanowo-germanianowe dla podczerwonej fotoniki, *PRZEGLĄD ELEKTROTECHNICZNY* 98 (2022) 186-189

2. **Karolina Kowalska**, Marta Kuwik, Justyna Polak, Joanna Pisarska, Wojciech A. Pisarski, Transition metals (Cr^{3+}) and lanthanides (Eu^{3+}) in inorganic glasses with extremely different glass-formers B_2O_3 and GeO_2 , *Materials* 14 (2021) 7156

3. **Karolina Kowalska**, Marta Kuwik, Joanna Pisarska, Wojciech A. Pisarski, Introduction of BaF_2 to titanate-germanate glasses doped with rare earth ions evidenced by NIR luminescence spectroscopy, *Materials Letters* 361 (2024) 136140

4. Marta Kuwik, **Karolina Kowalska**, Joanna Pisarska, Wojciech A. Pisarski, Spectroscopic properties of Pr^{3+} , Tm^{3+} , and Ho^{3+} in germanate-based glass systems modified by TiO_2 , *Materials* 16 (2023) 61

5. Marta Kuwik, **Karolina Kowalska**, Joanna Pisarska, Marcin Kochanowicz, Jacek Żmojda, Jan Dorosz, Dominik Dorosz, Wojciech A. Pisarski, Influence of TiO_2 concentration on near-infrared emission of germanate glasses doped with Tm^{3+} and $\text{Tm}^{3+}/\text{Ho}^{3+}$ ions, *Ceramics International* 49 (2023) 41090-41097

Wykaz komunikatów konferencyjnych

1. Wojciech A. Pisarski, **Karolina Kowalska**, Marta Kuwik, Joanna Pisarska, Jan Dorosz, Marcin Kochanowicz, Jacek Żmojda, Dominik Dorosz, New multicomponent titanate-germanate glasses and their luminescence properties, *Optical Fibers and Their Applications 2020, Proceedings of SPIE*, Białowieża, Polska, 12.07.2020

2. **Karolina Kowalska**, Marta Kuwik, Joanna Pisarska, Wojciech A. Pisarski, Thulium doped titanate-germanate glasses for infrared photonics, *VIII International School and Conference on Photonics PHOTONICA 2021*, online, 23-27.08.2021 r.

3. **Karolina Kowalska**, Marta Kuwik, Joanna Pisarska, Wojciech A. Pisarski, Badania luminescencyjne nowych szkieł tytanowo-germanianowych: jony Eu^{3+} jako sonda spektroskopowa, II Ogólnopolska Studencka Konferencja Naukowa Bliżej Chemii, online, 8-9.01.2022 r.
4. **Karolina Kowalska**, Marta Kuwik, Joanna Pisarska, Wojciech A. Pisarski, Właściwości luminescencyjne szkieł germanianowych zawierających TiO_2 aktywowanych jonami Eu^{3+} oraz Cr^{3+} pełniącymi rolę sond spektroskopowych, VII Szczecińskie Sympozjum Młodych Chemików, online 23-27.05.2022 r.
5. **Karolina Kowalska**, Marta Kuwik, Joanna Pisarska, Wojciech A. Pisarski, Wpływ dwutlenku tytanu na właściwości luminescencyjne szkieł germanianowych domieszkowanych jonami europu oraz iterbu, XV Kopernikańskie Seminarium Doktoranckie, Toruń, 20-22.06.2022 r.
6. **Karolina Kowalska**, Marta Kuwik, Joanna Pisarska, Wojciech A. Pisarski, Yb^{3+} doped titanate-germanate glasses for near-IR luminescence applications, International Workshop on Advanced Spectroscopy and Optical Materials (IWASOM'2022), Gdańsk, 10-15.07.2022 r.
7. **Karolina Kowalska**, Marta Kuwik, Joanna Pisarska, Wojciech A. Pisarski, Influence of TiO_2 concentration on near-infrared luminescence of barium gallo-germanate glasses doped with Pr^{3+} and co-doped with $\text{Pr}^{3+}/\text{Yb}^{3+}$, 21st International Conference on Dynamical Processes in Excited States of Solids, Wrocław 4-9.09.2022 r.
8. **Karolina Kowalska**, Marta Kuwik, Joanna Pisarska, Wojciech A. Pisarski, Spectroscopy of $\text{Ti}^{3+}/\text{Ti}^{4+}$ doped germanate glasses, XVIth International Conference on Molecular Spectroscopy ICMS 2022, Szczawnica, 11-14.09.2022 r.
9. **Karolina Kowalska**, Marta Kuwik, Joanna Pisarska, Wojciech A. Pisarski, Wieloskładnikowe szkła tytanowo-germanianowe dla podczerwonej fotoniki, XXI Krajowa Konferencja Elektroniki, Darłowo, 5-9.06.2022 r.
10. **Karolina Kowalska**, Joanna Pisarska, Marta Kuwik, Jan Dorosz, Marcin Kochanowicz, Jacek Żmojda, Dominik Dorosz, Maciej Sitarz, Wojciech A. Pisarski, Near-infrared luminescence of Nd^{3+} , Er^{3+} and Ho^{3+} ions in multicomponent titanate-germanate glasses, XVIth International Conference on Molecular Spectroscopy ICMS, Photoluminescence in Rare Earths: Photonics Materials, PRE'22-Poland (satellite symposium), Szczawnica, 11-14.09.2022 r.

11. **Karolina Kowalska**, Joanna Pisarska, Marta Kuwik, Jan Dorosz, Marcin Kochanowicz, Jacek Żmojda, Dominik Dorosz, Maciej Sitarz, Wojciech A. Pisarski, Influence of TiO_2 concentration on spectroscopic properties of lanthanide ions in barium gallo-germanate glasses, XVIth International Conference on Molecular Spectroscopy ICMS, Szczawnica, 11-14.09.2022 r.
12. Marta Kuwik, **Karolina Kowalska**, Joanna Pisarska, Marcin Kochanowicz, Jacek Żmojda, Jan Dorosz, Dominik Dorosz, Wojciech A. Pisarski, *Influence of TiO_2 concentration on near-infrared emission of germanate glasses doped with Tm^{3+} and $\text{Tm}^{3+}/\text{Ho}^{3+}$ ions*, XVIth International Conference on Molecular Spectroscopy ICMS, Szczawnica, 11-14 września 2022 r.
13. **Karolina Kowalska**, Marta Kuwik, Joanna Pisarska, Wojciech A. Pisarski, *Wpływ stężenia jonów aktywatora Tm^{3+} na właściwości luminescencyjne szkieł tytanowo-germanianowych w zakresie bliskiej podczerwieni (NIR)*, V Pomorskie Studenckie Sympozjum Chemiczne, online, 25-26.03.2023 r.
14. **Karolina Kowalska**, Marta Kuwik, Joanna Pisarska, Wojciech A. Pisarski, *Synteza i właściwości emisyjne szkieł germanianowych modyfikowanych TiO_2 w funkcji zawartości jonów Pr^{3+} dla technologii optycznych*, VIII Szczecińskie Sympozjum Młodych Chemików, Szczecin, 16.05.2023 r.
15. **Karolina Kowalska**, Marta Kuwik, Joanna Pisarska, Wojciech A. Pisarski, *Low-phonon titanate-germanate glass co-doped with $\text{Er}^{3+}/\text{Yb}^{3+}$ ions for near-infrared luminescence applications*, Baltic Chemistry Conference (online) 27-28.05.2023 r.
16. **Karolina Kowalska**, Marta Kuwik, Joanna Pisarska, Wojciech A. Pisarski, *Thulium-doped barium gallo-germanate glasses modified by titanium dioxide: optical investigations for near infrared application*, Eleventh International Conference on Radiation, Natural Sciences, Medicine, Engineering, Technology and Ecology RAD2023, Herceg Novi, Czarnogóra, 19-23.06.2023 r.
17. Marta Kuwik, **Karolina Kowalska**, Joanna Pisarska, Wojciech A. Pisarski, *Near-infrared luminescence properties of germanate based glasses as a function of glass modifier TiO_2* , Eleventh International Conference on Radiation, Natural Sciences, Medicine, Engineering, Technology and Ecology RAD2023, Herceg Novi, Czarnogóra, 19-23.06.2023 r.
18. **Karolina Kowalska**, Ewa Pietrasik, Marta Kuwik, Joanna Pisarska, Tomasz Goryczka, Wojciech A. Pisarski, *Influence of titanium dioxide concentration on thermal properties of germanate based glasses*, 3rd Journal of Thermal Analysis and Calorimetry Conference and 9th V4 (Joint Czech- Hungarian-Polish-Slovakian) Thermoanalytical Conference (JTACC+V4 2023), Balatonfüred, Węgry, 20-23.06.2023 r.

19. **Karolina Kowalska**, Marta Kuwik, Joanna Pisarska, Dominik Dorosz, Jan Dorosz, Jacek Żmojda, Marcin Kochanowicz, Wojciech A. Pisarski, *Spectroscopic properties of rare earths in titanate-germanate glass*, 11th International Conference on f-Elements (ICFE-11), Strasbourg, Francja, 22-26.08.2023 r.
20. **Karolina Kowalska**, Marta Kuwik, Joanna Pisarska, Dominik Dorosz, Marcin Kochanowicz, Jacek Żmojda, Jan Dorosz, Wojciech A. Pisarski, *Właściwości optyczne szkieł tytanowo-germanianowych*, IX Kongres Metrologii, Ryn, 10-14.09.2023 r.
21. **Karolina Kowalska**, *Nowe szkła tytanowo-germanianowe dla luminescencji w zakresie podczerwieni*, Inicjatywa Doskonałości Badawczej PRIORYTETOWE OBSZARY BADAWCZE (POB) Uniwersytetu Śląskiego w Katowicach, POB 2 - Nowoczesne materiały i technologie oraz ich społeczno-kulturowe implikacje, Katowice, 16.11.2023 r.
22. **Karolina Kowalska**, Marta Kuwik, Joanna Pisarska, Wojciech A. Pisarski, *Fabrication of titanate-germanate glasses co-doped with Pr³⁺/Er³⁺: From synthesis to near-IR luminescence properties for optical applications*, Natural Science Baltic Conference, online, 20-21.04.2024 r.
23. **Karolina Kowalska**, Marta Kuwik, Joanna Pisarska, Tomasz Goryczka, Wojciech A. Pisarski, *Wpływ stężenia tlenu tytanu (IV) na właściwości luminescencyjne jonów ziem rzadkich w szklach germanianowych dla podczerwonej fotoniki*, XIV Seminarium Naukowe „Aktualne Problemy Chemii Analitycznej”, Katowice, 17.05.2024 r.
24. **Karolina Kowalska**, Marta Kuwik, Joanna Pisarska, Wojciech A. Pisarski, *Titanate-germanate glasses doped with rare earth ions for infrared photonics*, The 8th International Workshop on Advanced Spectroscopy and Optical Materials (IWASOM'2024), Gdańsk, 7-12.07.2024 r.
25. **Karolina Kowalska**, Marta Kuwik, Joanna Pisarska, Wojciech A. Pisarski, *Luminescence in Yb³⁺-doped titanate-germanate glass*, The 7th International Conference on the Physics of Optical Materials and Devices (ICOM2024) & the 4th International Conference on Phosphor Thermometry (ICPT2024), Budva, Becici, Montenegro, 26-30.08.2024 r.

Udział w projekcie badawczym

Szkła tytanowo-germanianowe i ich zastosowania jako włókna optyczne emitujące promieniowanie w zakresie bliskiej i średniej podczerwieni - Projekt NCN (OPUS16) Nr 2018/31/B/ST8/00166 - Stypendysta (od 1.10.2020 do 30.09.2022 r.). Kierownik projektu: prof. dr hab. Wojciech A. Pisarski.

Wykaz staży naukowych

Katedra Fotoniki, Elektroniki i Techniki Światłnej, Wydział Elektryczny, Politechnika Białostocka, Polska, 15.05.2024 – 15.06.2024, Krótkoterminowy staż naukowy dla doktorantki – mgr inż. Karoliny Kowalskiej finansowany ze środków w ramach Inicjatywy Doskonałości Badawczej POB2 - Nowoczesne materiały i technologie oraz ich społeczno-kulturowe implikacje

Wykaz ważniejszych nagród i osiągnięć

1. III miejsce w konkursie na najlepszą prezentację wyników badań naukowych pt.: „Właściwości luminescencyjne szkieł germanianowych zawierających TiO_2 aktywowanych jonami Eu^{3+} oraz Cr^{3+} pełniącymi rolę sond spektroskopowych”, Karolina Kowalska, Marta Kuwik, Joanna Pisarska, Wojciech A. Pisarski, VII Szczecińskie Sympozjum Młodych Chemików (on-line), Zachodniopomorski Uniwersytet Technologiczny, 23-27.05.2022 r.
2. III miejsce w konkursie na najlepszy komunikat ustny pt.: „Synteza i właściwości emisyjne szkieł germanianowych modyfikowanych TiO_2 w funkcji zawartości jonów Pr^{3+} dla technologii optycznych”, Karolina Kowalska, Marta Kuwik, Joanna Pisarska, Wojciech A. Pisarski, ogłoszony w ramach VIII Szczecińskiego Sympozjum Młodych Chemików, Zachodniopomorski Uniwersytet Technologiczny, 16.05.2023 r. Szczecin
3. Nagroda w konkursie na najlepszy poster naukowy pt.: Titanate-germanate glasses doped with rare earth ions for infrared photonics, Karolina Kowalska, Marta Kuwik, Joanna Pisarska, Wojciech A. Pisarski, The 8th International Workshop on Advanced Spectroscopy and Optical Materials (IWASOM'2024), Gdańsk, 7-12.07.2024 r.
4. Wyróżnienie Rektora Uniwersytetu Śląskiego w XVI edycji konkursu za osiągnięcia naukowe jako doktorantka w dyscyplinie nauki chemiczne w Szkole Doktorskiej UŚ, 7.06.2024, Katowice
5. Tytuł Doktorantki Roku w XVI edycji konkursu Wyróżnień Rektora Uniwersytetu Śląskiego, 7.06.2024, Katowice

9.2. Oświadczenia

Katowice, 4.07.2024

mgr inż. Karolina Kowalska
Uniwersytet Śląski w Katowicach
Wydział Nauk Ścisłych i Technicznych
Instytut Chemii

W przedstawionym cyklu publikacji **P1-P12** wchodzących w skład rozprawy doktorskiej mój udział polegał na: syntezie wieloskładnikowych układów szkieł tytanowo-germanianowych, wykonaniu pomiarów spektroskopowych (widm absorpcji, emisji, Ramana i w podczerwieni), ich analizie oraz identyfikacji przejść jonów lantanowców. Mój udział polegał też na analizie porównawczej właściwości strukturalnych, termicznych i optycznych w funkcji stężenia TiO_2 .

W pracach **P2-P4** oraz **P10-P12** mój udział polegał ponadto na: opracowaniu wyników badań, a także na współtworzeniu manuskryptu (przeprowadzenie przeglądu literaturowego, przygotowanie przygotowaniu tekstu manuskryptu i rysunków, dyskusji wyników, formułowaniu odpowiedzi na uwagi recenzentów oraz korekcie manuskryptu po otrzymanych recenzjach).

Karolina Kowalska

Prof. dr hab. Wojciech Pisarski
Uniwersytet Śląski w Katowicach
Wydział Nauk Ścisłych i Technicznych
Instytut Chemii

OŚWIADCZENIE WSPÓŁAUTORA

Oświadczam, że w niżej wymienionych 12 pracach naukowych wchodzących w skład rozprawy doktorskiej Pani mgr inż. Karoliny Kowalskiej mój udział polegał na opracowaniu koncepcji i założeń badań, konsultacji i interpretacji otrzymanych wyników oraz kierowaniu projektem naukowym obejmującym badania opisane częściowo w wymienionych pracach. Mój udział w pracach P1 i P5-P7 polegał również na napisaniu manuskryptu.

- [P1] W.A. Pisarski, K. Kowalska, M. Kuwik, J. Polak, E. Pietrasik, T. Goryczka, J. Pisarska, Novel multicomponent titanate-germanate glasses: synthesis, structure, properties, transition metal, and rare earth doping, *Materials* 13 (2020) 4422.
- [P2] K. Kowalska, M. Kuwik, J. Polak, J. Pisarska, W.A. Pisarski, EPR and optical spectroscopy of Cr³⁺ ions in barium gallo-germanate glasses containing B₂O₃/TiO₂, *Journal of Luminescence* 245 (2022) 118775.
- [P3] K. Kowalska, M. Kuwik, J. Pisarska, M. Sitarz, W.A. Pisarski, Raman and infrared spectroscopy of barium-gallo germanate glasses containing B₂O₃/TiO₂, *Materials* 16 (2023) 1516.
- [P4] K. Kowalska, E. Pietrasik, M. Kuwik, J. Pisarska, T. Goryczka, W.A. Pisarski, Influence of titanium dioxide concentration on thermal properties of germanate-based glasses, *Journal of Thermal Analysis and Calorimetry* (2024)
- [P5] W.A. Pisarski, K. Kowalska, M. Kuwik, J. Pisarska, J. Dorosz, J. Żmojda, M. Kochanowicz, D. Dorosz, Nd³⁺ doped titanate-germanate glasses for near-IR laser applications, *Optical Materials Express* 12 (2022) 2912-2926.
- [P6] K. Kowalska, M. Kuwik, J. Pisarska, M. Leśniak, D. Dorosz, M. Kochanowicz, J. Żmojda, J. Dorosz, W.A. Pisarski, Influence of TiO₂ concentration on near-infrared luminescence of Er³⁺ ions in barium gallogermanate glasses, *Journal of Materials Research and Technology* 21 (2022) 4761-4772.
- [P7] W.A. Pisarski, K. Kowalska, M. Kuwik, J. Pisarska, D. Dorosz, M. Kochanowicz, J. Żmojda, J. Dorosz, Enhanced mid-IR luminescence of Er³⁺ ions at 2.7 μm in TiO₂-GeO₂-BaO-Ga₂O₃ glasses, *Journal of Luminescence* 265 (2024) 120227.
- [P8] J. Pisarska, K. Kowalska, M. Kuwik, J. Dorosz, M. Kochanowicz, J. Żmojda, D. Dorosz, W.A. Pisarski, Optical properties of titanate-germanate glasses containing Ho³⁺ ions, *Materials Research Bulletin* 166 (2023) 112353.
- [P9] M. Kuwik, K. Kowalska, J. Pisarska, W.A. Pisarski, Experimental and theoretical studies on NIR luminescence of titanate-germanate glasses doped with Pr³⁺ and Tm³⁺ ions, *Journal of the American Ceramic Society* 106 (2023) 7460-7472.
- [P10] K. Kowalska, M. Kuwik, J. Pisarska, W.A. Pisarski, Thulium-doped titanate-germanate glasses for infrared photonics, *Journal of Luminescence* 272 (2024) 120649.
- [P11] K. Kowalska, M. Kuwik, J. Pisarska, W.A. Pisarski, Near-IR Luminescence of Rare-Earth Ions (Er³⁺, Pr³⁺, Ho³⁺, Tm³⁺) in Titanate-Germanate Glasses under Excitation of Yb³⁺, *Materials* 15 (2022) 3660.
- [P12] K. Kowalska, M. Kuwik, T. Goryczka, J. Pisarska, W.A. Pisarski, The impact of pair Er³⁺/Yb³⁺ on titanate-germanate glasses: Physicochemical and near-infrared luminescence investigations, *Materials Science and Engineering B* 301 (2024) 117117.

Stwierdzam jednocześnie jako promotor, że udział Pani mgr inż. Karoliny Kowalskiej w wyżej wymienionych publikacjach jest bardzo istotny dla realizacji tematyki badawczej zawartej w niniejszej rozprawie doktorskiej.



prof. dr hab. inż. Joanna Pisarska
Uniwersytet Śląski w Katowicach
Wydział Nauk Ścisłych i Technicznych
Instytut Chemii

OŚWIADCZENIE WSPÓŁAUTORA

Oświadczam, że w 12 pracach naukowych wchodzących w skład rozprawy doktorskiej Pani mgr inż. Karoliny Kowalskiej:

- [P1] W.A. Pisarski, K. Kowalska, M. Kuwik, J. Polak, E. Pietrasik, T. Goryczka, J. Pisarska, Novel multicomponent titanate-germanate glasses: synthesis, structure, properties, transition metal, and rare earth doping, *Materials* 13 (2020) 4422.
- [P2] K. Kowalska, M. Kuwik, J. Polak, J. Pisarska, W.A. Pisarski, EPR and optical spectroscopy of Cr³⁺ ions in barium gallo-germanate glasses containing B₂O₃/TiO₂, *Journal of Luminescence* 245 (2022) 118775.
- [P3] K. Kowalska, M. Kuwik, J. Pisarska, M. Sitarz, W.A. Pisarski, Raman and infrared spectroscopy of barium-gallo germanate glasses containing B₂O₃/TiO₂, *Materials* 16 (2023) 1516.
- [P4] K. Kowalska, E. Pietrasik, M. Kuwik, J. Pisarska, T. Goryczka, W.A. Pisarski, Influence of titanium dioxide concentration on thermal properties of germanate-based glasses, *Journal of Thermal Analysis and Calorimetry* (2024)
- [P5] W.A. Pisarski, K. Kowalska, M. Kuwik, J. Pisarska, J. Dorosz, J. Żmojda, M. Kochanowicz, D. Dorosz, Nd³⁺ doped titanate-germanate glasses for near-IR laser applications, *Optical Materials Express* 12 (2022) 2912-2926.
- [P6] K. Kowalska, M. Kuwik, J. Pisarska, M. Leśniak, D. Dorosz, M. Kochanowicz, J. Żmojda, J. Dorosz, W.A. Pisarski, Influence of TiO₂ concentration on near-infrared luminescence of Er³⁺ ions in barium gallogermanate glasses, *Journal of Materials Research and Technology* 21 (2022) 4761-4772.
- [P7] W.A. Pisarski, K. Kowalska, M. Kuwik, J. Pisarska, D. Dorosz, M. Kochanowicz, J. Żmojda, J. Dorosz, Enhanced mid-IR luminescence of Er³⁺ ions at 2.7 μm in TiO₂-GeO₂-BaO-Ga₂O₃ glasses, *Journal of Luminescence* 265 (2024) 120227.
- [P8] J. Pisarska, K. Kowalska, M. Kuwik, J. Dorosz, M. Kochanowicz, J. Żmojda, D. Dorosz, W.A. Pisarski, Optical properties of titanate-germanate glasses containing Ho³⁺ ions, *Materials Research Bulletin* 166 (2023) 112353.
- [P9] M. Kuwik, K. Kowalska, J. Pisarska, W.A. Pisarski, Experimental and theoretical studies on NIR luminescence of titanate-germanate glasses doped with Pr³⁺ and Tm³⁺ ions, *Journal of the American Ceramic Society* 106 (2023) 7460-7472.
- [P10] K. Kowalska, M. Kuwik, J. Pisarska, W.A. Pisarski, Thulium-doped titanate-germanate glasses for infrared photonics, *Journal of Luminescence* 272 (2024) 120649.
- [P11] K. Kowalska, M. Kuwik, J. Pisarska, W.A. Pisarski, Near-IR Luminescence of Rare-Earth Ions (Er³⁺, Pr³⁺, Ho³⁺, Tm³⁺) in Titanate-Germanate Glasses under Excitation of Yb³⁺, *Materials* 15 (2022) 3660.
- [P12] K. Kowalska, M. Kuwik, T. Goryczka, J. Pisarska, W.A. Pisarski, The impact of pair Er³⁺/Yb³⁺ on titanate-germanate glasses: Physicochemical and near-infrared luminescence investigations, *Materials Science and Engineering B* 301 (2024) 117117.

mój udział polegał na analizie dynamiki zaniku luminescencji z poziomów wzbudzonych jonów lantanowców w szklach. Mój udział w publikacji P8 polegał również na napisaniu manuskryptu. W pracach P5-P10 mój udział polegał ponadto na obliczeniu wybranych parametrów radiacyjnych z wykorzystaniem teorii Judda-Ofelta i modelu Inokuti-Hirayama.



Białystok, 4.07.2024

Prof. dr hab. inż. Jan Dorosz

Politechnika Białostocka

Wydział Elektryczny

OŚWIADCZENIE WSPÓŁAUTORA

Oświadczam, że w pracy naukowej wchodzącej w skład rozprawy doktorskiej Pani mgr inż. Karoliny Kowalskiej:

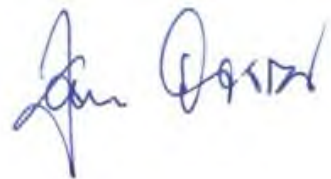
[P5] W.A. Pisarski, K. Kowalska, M. Kuwik, J. Pisarska, J. Dorosz, J. Żmojda, M. Kochanowicz, D. Dorosz, Nd³⁺ doped titanate-germanate glasses for near-IR laser applications, *Optical Materials Express* 12 (2022) 2912-2926.

[P6] K. Kowalska, M. Kuwik, J. Pisarska, M. Leśniak, D. Dorosz, M. Kochanowicz, J. Żmojda, J. Dorosz, W.A. Pisarski, Influence of TiO₂ concentration on near-infrared luminescence of Er³⁺ ions in barium gallogermanate glasses, *Journal of Materials Research and Technology* 21 (2022) 4761-4772.

[P7] W.A. Pisarski, K. Kowalska, M. Kuwik, J. Pisarska, D. Dorosz, M. Kochanowicz, J. Żmojda, J. Dorosz, Enhanced mid-IR luminescence of Er³⁺ ions at 2.7 μm in TiO₂-GeO₂-BaO-Ga₂O₃ glasses, *Journal of Luminescence* 265 (2024) 120227.

[P8] J. Pisarska, K. Kowalska, M. Kuwik, J. Dorosz, M. Kochanowicz, J. Żmojda, D. Dorosz, W.A. Pisarski, Optical properties of titanate-germanate glasses containing Ho³⁺ ions, *Materials Research Bulletin* 166 (2023) 112353.

mój udział polegał na konsultacjach wyników badań szkieł tytanowo-germanianowych emitujących promieniowanie podczerwone pod kątem możliwości wyciągania włókien optycznych.



Prof. dr hab. Dominik Dorosz
Akademia Górniczo – Hutnicza w Krakowie
Wydział Inżynierii Materiałowej i Ceramiki

OŚWIADCZENIE WSPÓŁAUTORA

Oświadczam, że w pracy naukowej wchodzącej w skład rozprawy doktorskiej Pani mgr inż. Karoliny Kowalskiej:

[P5] W.A. Pisarski, K. Kowalska, M. Kuwik, J. Pisarska, J. Dorosz, J. Żmojda, M. Kochanowicz, D. Dorosz, Nd³⁺ doped titanate-germanate glasses for near-IR laser applications, *Optical Materials Express* 12 (2022) 2912-2926.

[P6] K. Kowalska, M. Kuwik, J. Pisarska, M. Leśniak, D. Dorosz, M. Kochanowicz, J. Żmojda, J. Dorosz, W.A. Pisarski, Influence of TiO₂ concentration on near-infrared luminescence of Er³⁺ ions in barium gallogermanate glasses, *Journal of Materials Research and Technology* 21 (2022) 4761-4772.

[P7] W.A. Pisarski, K. Kowalska, M. Kuwik, J. Pisarska, D. Dorosz, M. Kochanowicz, J. Żmojda, J. Dorosz, Enhanced mid-IR luminescence of Er³⁺ ions at 2.7 μm in TiO₂-GeO₂-BaO-Ga₂O₃ glasses. *Journal of Luminescence* 265 (2024) 120227.

[P8] J. Pisarska, K. Kowalska, M. Kuwik, J. Dorosz, M. Kochanowicz, J. Żmojda, D. Dorosz, W.A. Pisarski, Optical properties of titanate-germanate glasses containing Ho³⁺ ions, *Materials Research Bulletin* 166 (2023) 112353.

mój udział polegał na analizie i dyskusji wyników badań luminescencyjnych szkieł w zakresie podczerwieni.



Kraków, 5.07.2024

Prof. dr hab. inż. Maciej Sitarz

Akademia Górniczo-Hutnicza im. Stanisława Staszica w Krakowie

Wydział Inżynierii Materiałowej i Ceramiki

OŚWIADCZENIE WSPÓŁAUTORA

Oświadczam, że w pracy naukowej wchodzącej w skład rozprawy doktorskiej
Pani mgr inż. Karoliny Kowalskiej:

[P3] K. Kowalska, M. Kuwik, J. Pisarska, M. Sitarz, W.A. Pisarski, Raman and infrared spectroscopy of barium-gallo germanate glasses containing B_2O_3/TiO_2 , *Materials* 16 (2023) 1516.

mój udział polegał na analizie i dyskusji wyników badań uzyskanych przy użyciu spektroskopii Ramana i w podczerwieni.

Sitarz Maciej

Białystok, 4.07.2024

Prof. dr hab. inż. Marcin Kochanowicz

Politechnika Białostocka

Wydział Elektryczny

OŚWIADCZENIE WSPÓŁAUTORA

Oświadczam, że w pracy naukowej wchodzącej w skład rozprawy doktorskiej Pani mgr inż. Karoliny Kowalskiej:

[P5] W.A. Pisarski, K. Kowalska, M. Kuwik, J. Pisarska, J. Dorosz, J. Żmojda, M. Kochanowicz, D. Dorosz, Nd³⁺ doped titanate-germanate glasses for near-IR laser applications, *Optical Materials Express* 12 (2022) 2912-2926.

[P6] K. Kowalska, M. Kuwik, J. Pisarska, M. Leśniak, D. Dorosz, M. Kochanowicz, J. Żmojda, J. Dorosz, W.A. Pisarski, Influence of TiO₂ concentration on near-infrared luminescence of Er³⁺ ions in barium gallogermanate glasses, *Journal of Materials Research and Technology* 21 (2022) 4761-4772.

[P7] W.A. Pisarski, K. Kowalska, M. Kuwik, J. Pisarska, D. Dorosz, M. Kochanowicz, J. Żmojda, J. Dorosz, Enhanced mid-IR luminescence of Er³⁺ ions at 2.7 μm in TiO₂-GeO₂-BaO-Ga₂O₃ glasses, *Journal of Luminescence* 265 (2024) 120227.

[P8] J. Pisarska, K. Kowalska, M. Kuwik, J. Dorosz, M. Kochanowicz, J. Żmojda, D. Dorosz, W.A. Pisarski, Optical properties of titanate-germanate glasses containing Ho³⁺ ions, *Materials Research Bulletin* 166 (2023) 112353.

mój udział polegał na dyskusji wyników badań, szczególnie parametrów spektroskopowych uzyskanych dla jonów lantanowców w zakresie bliskiej i średniej podczerwieni.



Białystok, 4.07.2024

Dr hab. inż. Jacek Żmojda, prof. PB

Politechnika Białostocka

Wydział Elektryczny

OŚWIADCZENIE WSPÓŁAUTORA

Oświadczam, że w pracy naukowej wchodzącej w skład rozprawy doktorskiej Pani mgr inż. Karoliny Kowalskiej:

[P5] W.A. Pisarski, K. Kowalska, M. Kuwik, J. Pisarska, J. Dorosz, J. Żmojda, M. Kochanowicz, D. Dorosz, Nd³⁺ doped titanate-germanate glasses for near-IR laser applications, *Optical Materials Express* 12 (2022) 2912-2926.

[P6] K. Kowalska, M. Kuwik, J. Pisarska, M. Leśniak, D. Dorosz, M. Kochanowicz, J. Żmojda, J. Dorosz, W.A. Pisarski, Influence of TiO₂ concentration on near-infrared luminescence of Er³⁺ ions in barium gallogermanate glasses, *Journal of Materials Research and Technology* 21 (2022) 4761-4772.

[P7] W.A. Pisarski, K. Kowalska, M. Kuwik, J. Pisarska, D. Dorosz, M. Kochanowicz, J. Żmojda, J. Dorosz, Enhanced mid-IR luminescence of Er³⁺ ions at 2.7 μm in TiO₂-GeO₂-BaO-Ga₂O₃ glasses, *Journal of Luminescence* 265 (2024) 120227.

[P8] J. Pisarska, K. Kowalska, M. Kuwik, J. Dorosz, M. Kochanowicz, J. Żmojda, D. Dorosz, W.A. Pisarski, Optical properties of titanate-germanate glasses containing Ho³⁺ ions, *Materials Research Bulletin* 166 (2023) 112353.

mój udział polegał na przeprowadzeniu pomiarów i analizy współczynnika załamania światła wytworzonych szkieł emitujących promieniowanie podczerwone w funkcji stężenia TiO₂.



Katowice, 4.07.2024

Dr hab. Tomasz Goryczka, Prof. UŚ
Uniwersytet Śląski w Katowicach
Wydział Nauk Ścisłych i Technicznych
Instytut Inżynierii Materiałowej

OŚWIADCZENIE WSPÓLAUTORA

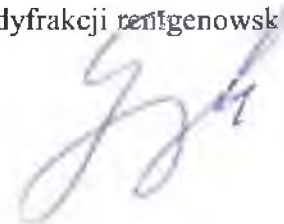
Oświadczam, że w trzech pracach naukowych wchodzących w skład rozprawy doktorskiej Pani mgr inż. Karoliny Kowalskiej:

[P1] W.A. Pisarski, K. Kowalska, M. Kuwik, J. Polak, E. Pietrasik, T. Goryczka, J. Pisarska, Novel multicomponent titanate-germanate glasses: synthesis, structure, properties, transition metal, and rare earth doping, *Materials* 13 (2020) 4422.

[P4] K. Kowalska, E. Pietrasik, M. Kuwik, J. Pisarska, T. Goryczka, W.A. Pisarski, Influence of titanium dioxide concentration on thermal properties of germanate-based glasses, *Journal of Thermal Analysis and Calorimetry* (2024)

[P12] K. Kowalska, M. Kuwik, T. Goryczka, J. Pisarska, W.A. Pisarski, The impact of pair $\text{Er}^{3+}/\text{Yb}^{3+}$ on titanate-germanate glasses: Physicochemical and near-infrared luminescence investigations, *Materials Science and Engineering B* 301 (2024) 117117.

mój udział polegał na wykonaniu pomiarów próbek szkieł metodą dyfrakcji rentgenowskiej.



Kraków, 4.07.2024

dr inż. Magdalena Leśniak
Akademia Górniczo – Hutnicza w Krakowie
Wydział Inżynierii Materiałowej i Ceramiki

OŚWIADCZENIE WSPÓŁAUTORA

Oświadczam, że w pracy naukowej wchodzącej w skład rozprawy doktorskiej
Pani mgr inż. Karoliny Kowalskiej:

[P6] K. Kowalska, M. Kuwik, J. Pisarska, M. Leśniak, D. Dorosz, M. Kochanowicz,
J. Zmojda, J. Dorosz, W.A. Pisarski, Influence of TiO₂ concentration on near-infrared
luminescence of Er³⁺ ions in barium gallogermanate glasses, *Journal of Materials Research
and Technology* 21 (2022) 4761-4772.

mój udział polegał na wyznaczeniu wybranych parametrów fizykochemicznych szkieł
tytanowo-germanianowych.

Magdalena Leśniak

Katowice, 4.07.2024

Dr Marta Kuwik
Uniwersytet Śląski w Katowicach
Wydział Nauk Ścisłych i Technicznych
Instytut Chemii

OŚWIADCZENIE WSPÓŁAUTORA

Oświadczam, że w pracach naukowych wchodzących w skład rozprawy doktorskiej Pani mgr inż. Karoliny Kowalskiej:

- [P1] W.A. Pisarski, K. Kowalska, M. Kuwik, J. Polak, E. Pietrasik, T. Goryczka, J. Pisarska, Novel multicomponent titanate-germanate glasses: synthesis, structure, properties, transition metal, and rare earth doping, *Materials* 13 (2020) 4422.
- [P2] K. Kowalska, M. Kuwik, J. Polak, J. Pisarska, W.A. Pisarski, EPR and optical spectroscopy of Cr³⁺ ions in barium gallo-germanate glasses containing B₂O₃/TiO₂, *Journal of Luminescence* 245 (2022) 118775.
- [P3] K. Kowalska, M. Kuwik, J. Pisarska, M. Sitarz, W.A. Pisarski, Raman and infrared spectroscopy of barium-gallo germanate glasses containing B₂O₃/TiO₂, *Materials* 16 (2023) 1516.
- [P4] K. Kowalska, E. Pietrasik, M. Kuwik, J. Pisarska, T. Goryczka, W.A. Pisarski, Influence of titanium dioxide concentration on thermal properties of germanate-based glasses, *Journal of Thermal Analysis and Calorimetry* (2024)
- [P5] W.A. Pisarski, K. Kowalska, M. Kuwik, J. Pisarska, J. Dorosz, J. Żmojda, M. Kochanowicz, D. Dorosz, Nd³⁺ doped titanate-germanate glasses for near-IR laser applications, *Optical Materials Express* 12 (2022) 2912-2926.
- [P6] K. Kowalska, M. Kuwik, J. Pisarska, M. Leśniak, D. Dorosz, M. Kochanowicz, J. Żmojda, J. Dorosz, W.A. Pisarski, Influence of TiO₂ concentration on near-infrared luminescence of Er³⁺ ions in barium gallogermanate glasses, *Journal of Materials Research and Technology* 21 (2022) 4761-4772.
- [P7] W.A. Pisarski, K. Kowalska, M. Kuwik, J. Pisarska, D. Dorosz, M. Kochanowicz, J. Żmojda, J. Dorosz, Enhanced mid-IR luminescence of Er³⁺ ions at 2.7 μm in TiO₂-GeO₂-BaO-Ga₂O₃ glasses, *Journal of Luminescence* 265 (2024) 120227.
- [P8] J. Pisarska, K. Kowalska, M. Kuwik, J. Dorosz, M. Kochanowicz, J. Żmojda, D. Dorosz, W.A. Pisarski, Optical properties of titanate-germanate glasses containing Ho³⁺ ions, *Materials Research Bulletin* 166 (2023) 112353.
- [P9] M. Kuwik, K. Kowalska, J. Pisarska, W.A. Pisarski, Experimental and theoretical studies on NIR luminescence of titanate-germanate glasses doped with Pr³⁺ and Tm³⁺ ions, *Journal of the American Ceramic Society* 106 (2023) 7460-7472.
- [P10] K. Kowalska, M. Kuwik, J. Pisarska, W.A. Pisarski, Thulium-doped titanate-germanate glasses for infrared photonics, *Journal of Luminescence* 272 (2024) 120649.
- [P11] K. Kowalska, M. Kuwik, J. Pisarska, W.A. Pisarski, Near-IR Luminescence of Rare-Earth Ions (Er³⁺, Pr³⁺, Ho³⁺, Tm³⁺) in Titanate-Germanate Glasses under Excitation of Yb³⁺, *Materials* 15 (2022) 3660.
- [P12] K. Kowalska, M. Kuwik, T. Goryczka, J. Pisarska, W.A. Pisarski, The impact of pair Er³⁺/Yb³⁺ on titanate-germanate glasses: Physicochemical and near-infrared luminescence investigations, *Materials Science and Engineering B* 301 (2024) 117117.

mój udział polegał na wykonaniu pomiarów krzywych zaniku luminescencji z poziomów wzbudzonych jonów lantanowców w szklach. Ponadto mój udział w publikacji P9 polegał na opracowaniu wyników badań i napisaniu manuskryptu.

Marta Kuwik

Katowice, 15.07.2024

Dr inż. Ewa Pietrasik
Uniwersytet Śląski w Katowicach
Wydział Nauk Ścisłych i Technicznych
Instytut Chemii

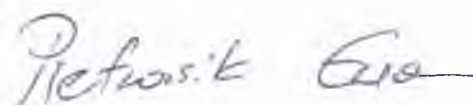
OŚWIADCZENIE WSPÓLAUTORA

Oświadczam, że w dwóch pracach naukowych wchodzących w skład rozprawy doktorskiej Pani mgr inż. Karoliny Kowalskiej:

[P1] W.A. Pisarski, K. Kowalska, M. Kuwik, J. Polak, E. Pietrasik, T. Goryczka, J. Pisarska, Novel multicomponent titanate-germanate glasses: synthesis, structure, properties, transition metal, and rare earth doping, *Materials* 13 (2020) 4422.

[P4] K. Kowalska, E. Pietrasik, M. Kuwik, J. Pisarska, T. Goryczka, W.A. Pisarski, Influence of titanium dioxide concentration on thermal properties of germanate-based glasses, *Journal of Thermal Analysis and Calorimetry* (2024)

mój udział polegał na wykonaniu badań metodą różnicowej kalorymetrii skaningowej (DSC).



Katowice, 4.07.2024

Dr Justyna Polak
Uniwersytet Śląski w Katowicach
Wydział Nauk Ścisłych i Technicznych
Instytut Chemii

OŚWIADCZENIE WSPÓŁAUTORA

Oświadczam, że w dwóch pracach naukowych wchodzących w skład rozprawy doktorskiej Pani mgr inż. Karoliny Kowalskiej:

[P1] W.A. Pisarski, K. Kowalska, M. Kuwik, J. Polak, E. Pietrasik, T. Goryczka, J. Pisarska, Novel multicomponent titanate-germanate glasses: synthesis, structure, properties, transition metal, and rare earth doping, *Materials* 13 (2020) 4422.

[P2] K. Kowalska, M. Kuwik, J. Polak, J. Pisarska, W.A. Pisarski, EPR and optical spectroscopy of Cr³⁺ ions in barium gallo-germanate glasses containing B₂O₃/TiO₂, *Journal of Luminescence* 245 (2022) 118775.

mój udział polegał na wykonaniu badań metodą spektroskopii elektronowego rezonansu paramagnetycznego (EPR).

Polak
Justyna